GEOMORPHOLOGY AND GEOTECHNICAL CHARACTERIZATION OF THE QUEENSTOWN HILL LANDSLIDE

A thesis submitted in partial fulfilment of the requirements
for the Degree of

Master of Science in Engineering Geology

University of Canterbury
School of Earth and Environment

By Laura Gnesko

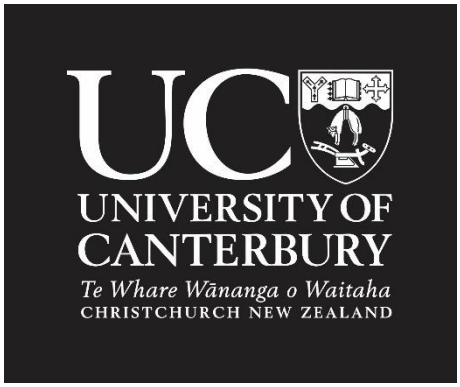

September 2020

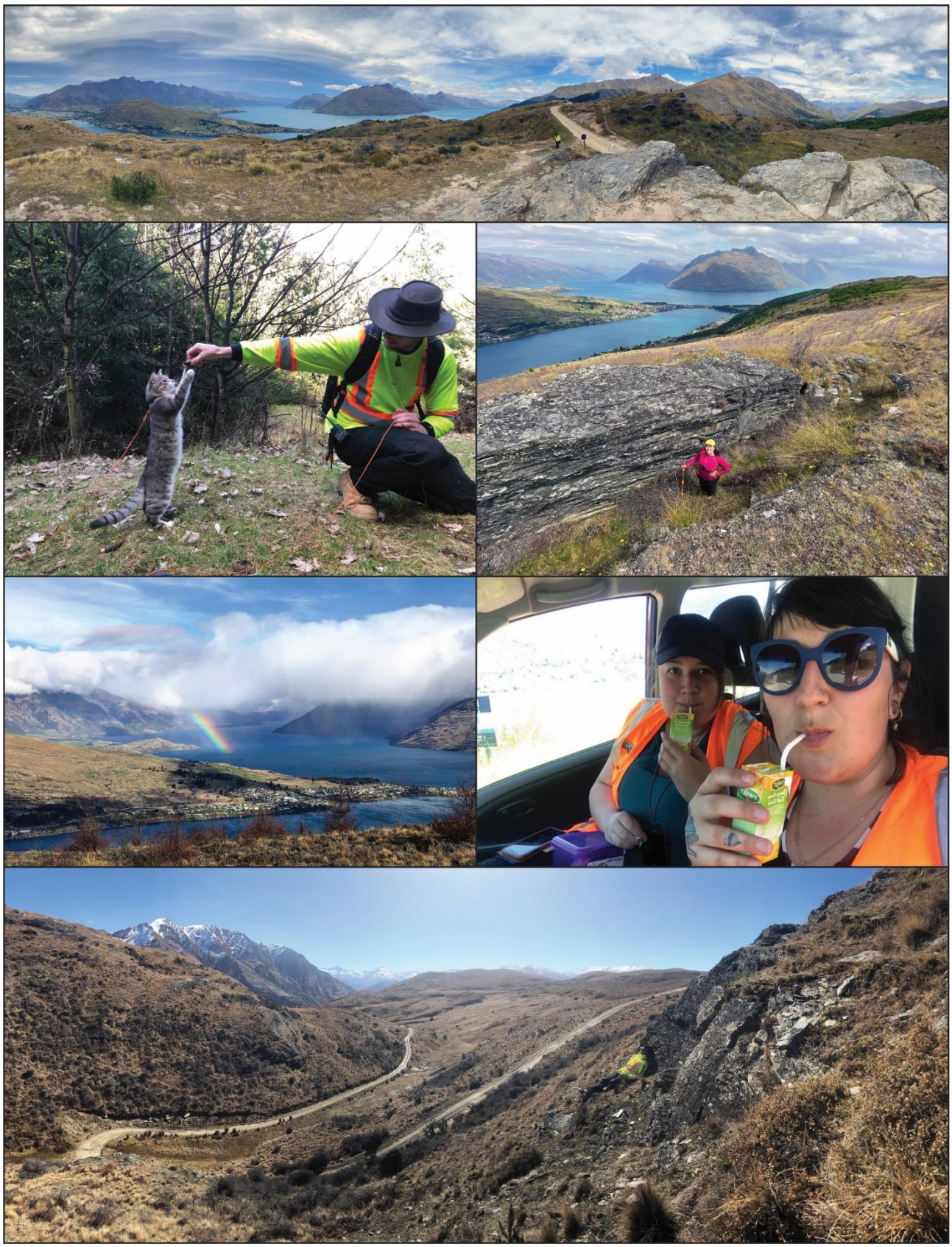

“I saw that I’d get nowhere on the straight path, and that to go crookedly was straighter.” - Nikolai Gogol

Abstract

The Queenstown Area is a major tourist destination in the lower South Island and has approximately 16,000 permanent residents. Residential development occurs predominantly on flat-lying alluvial terraces, and elsewhere on steep till-covered bedrock slopes modified by glacial ice and freeze-thaw processes. The steep slopes surrounding the Queenstown area are predisposed to instability due to inherent weakness of the Otago Schist due to lithotype variation, foliation attitude, foliation shears, and rock mass discontinuities. Pressure for residential expansion has resulted in an increasing number of development proposals on the lower slopes of Queenstown Hill.

The primary aims of this research were to develop a detailed geomorphic and geotechnical characterization of the schist within the Queenstown Hill Landslide, in response to increased development in the surrounding area. This study investigates the geomorphology and geotechnical properties of the landslide through mapping, paired with rock mechanics testing of the underlying schist. Four 25 m boreholes drilled into the landslide provided an opportunity to characterize recovered rock material and to evaluate the rock mass within landslide, as subsurface investigations were not previously available to inform investigations along the Frankton Arm.

The Queenstown Hill Landslide is a 50-75 m deep compound translational rockslide comprising interlayered quartzofeldspathic and semi-pelitic schist having an average foliation attitude dipping subparallel to the slope at 15-25° SSW. The main landslide body is interpreted as a compound rockslide with a bi-linear rupture surface, while the geometry of the eastern reactivation zone suggests a planar rockslide. The failure surface is interpreted as being subparallel to foliation, structurally controlled along foliation shears, and with block release defined by the intersection of steep to subvertical joint sets with multiple pre-existing foliation shear zones 0.1 to 1.5 m thick.

Geomorphic mapping identified five zones within the landslide from distinct surface morphologies: (1) a joint controlled headscarp; (2) the main landslide body with a subdued hummocky topography and well established drainage; (3) an extensional zone characterized by a graben and large tension cracks > 5 m deep, up to 100 m long; (4) a reactivation zone interpreted as a separate phase of movement; (5) a complex undulating toe zone bounded by compressional features but with no clear breakout.

Two interlayered schist lithotypes were mapped across the landslide and logged in the boreholes, these being a medium grey quartzofeldspathic schist and a dark green-grey semi-pelitic schist. Both lithotypes belong to the chlorite zone of the greenschist facies but exhibit variations in mineral assemblage, textural zone and weathering. A general predominance of the more micaceous dark green-grey semi-pelitic schist was recognized in the boreholes; although an uneven distribution was not observed in the field as the lithotypes are interlayered.

Laboratory testing of the physical and mechanical properties of the schist lithotypes showed significant variations in geotechnical properties and demonstrated a clear relationship between mineralogy and texture. On average, the medium grey quartzofeldspathic schist, with moderately developed foliation (Textural Zone III) is 1.5 times stronger than the dark grey-green semi-pelitic schist, with well-developed foliation (Textural Zone IV). Laboratory results indicate a low porosity (3.0 %) and a weak to moderately strong compressive strength (11.3 - 61.8 MPa) with low deformation modulus (0.9 - 41.1 GPa).

Lithological variations of the schist and geomorphic setting are likely to have a direct geotechnical influence on slope stability and foundation design, this is supported by kinematic analysis. Kinematic analysis demonstrates that failure is unlikely in moderately inclined (20°-35°) areas, other than localized toppling along foliation with subvertical joints acting as a releasing surface. In areas where the slope angle or cutback exceeds 50°, the number of potential planar and wedge failures increases and continue to increase as the

angle approaches 70-85°. Kinematic analysis has identified that the reactivation and extensional zones of the landslide are most susceptible to failure, especially planar failure along foliation and joint sets orientated parallel to the reactivation headscarp.

A detailed ground model developed from the results in this study suggests present movement within the landslide is unlikely. However, the complexity of the landslide warrants site-specific geotechnical investigations to avoid failures during construction. Future development within/surrounding the extension and reactivation zones should be avoided until further investigations are undertaken to refine our current understanding of stability.

Acknowledgements

First and foremost, I would like to thank my husband Jonathan Acton for his endless support, as I live life flying by the seat of my pants. Thank you for being an amazing field assistant, lab assistant, coffee maker and always having a great sense of humour. Thank you to my senior supervisor David “Palpatine” Bell for his words of wisdom, encouragement, essential sarcasm, infinite boxes of red pens, and most importantly, for converting me to the dark side (engineering geology); and thank you to my amazing supervisory team Tim Stahl, Marlene Villeneuve and Peter Forrest for their ongoing support, guidance and reviews throughout my thesis.

Considerable thanks to Sophie Hill for helping me in the field and taking me out of the house for a walk; Jessica Fensom for being my rock; Romy Ridl for her amazing checklists, conversations and death metal growl; Tania Salas for always being just a phone call away; Christine Prasad for always being there when you need a reality check; and Li-Jen (Ray) Hsu for helping me in the lab. I would also like to thank Colin Bloom and Corinne Singeisen for helping me with my painfully basic ArcGIS questions, without you the 10,000 maps in this thesis would not have been possible.

Many thanks to the university technical staff particularly Cathy Higgins, Sarah Pope, Rob Spiers and Sacha Baldwin for their help organizing field/lab equipment and tolerating me leaving my schist lying around everywhere. Thank you, Cathy and Sarah, for always being available to fix Clifford the big bad red dog, and Rob for cutting all those thin sections - for science! Thank you to the Mason Trust Fund for providing support with fieldwork expenses.

This research greatly benefitted from help from Dr. David Shelley, in identifying minerals in thin section, and indulging my curiosity about feldspars and random minerals. Thank you, Dr. Dave Craw, for helping put in context the “vast sea” of grey schist across Central Otago. Thank you, Dr. Stefan Winkler for sharing your invaluable knowledge about Quaternary geomorphology, extensive database maintenance, geomorphic symbol selection and for making me a much-needed cup up coffee at the Cass field station.

A special thank you to my adoptive family, Ruby and Shailesh, for their love, support, and wonderful cooking. Last, but most importantly (because you always save the best for last) I would like to thank my parents for their unconditional love, moral support, and care packages. Я вас так люблю і дякую. Without them, this wonderful adventure would not have been possible.

Table of Contents

List of Figures

List of Tables

Chapter 1: Introduction

1.1 Thesis Context

The Queenstown Area is an important tourist destination in the lower South Island that has approximately 16,000 permanent residents and receives 3.0 million visitors annually (Queenstown Lakes District Council, 2018; Turnbull, 2000b). Residential development occurs predominantly on flat-lying alluvial terraces, and elsewhere on steep till-covered schist bedrock slopes carved by ice during the Last Glacial Maximum (Barrell et al., 1994). Due to population growth and increased tourism, pressure to expand urban development and infrastructure onto more geotechnically difficult sites continues to increase.

The slopes surrounding the Queenstown area are predisposed to instability, as shown by several deep-seated bedrock landslides (Figure 1.1). Proposals to develop along the landslide margins is increasing, as many existing developments on the landslides have not experienced damage relating to slope movement (Bell, 1996a, b, 2018; Bell and Riddolls, 1992). For example, the Coronet Peak Skifield has been developed on the hummocky upper slopes of the Coronet Peak Landslide, as well as the associated infrastructure (including roads, buildings, chairlift towers and snowmaking ponds) (Bell, 2007a, b, 2008a, b, 2009; Philp, 2011). However, the pressure for residential expansion has led to more intensive subdivision development proposals on the lower slopes of the Queenstown Hill Landslide (Bell, 2018; Bell and Pettinga, 1985; Bell and Riddolls, 1992).

Within the Queenstown urban area, pressure for both residential and commercial developments on the steep schist bedrock slopes is necessitating careful geotechnical investigation and foundation design. Along the Frankton Arm, glacial till injection into hydraulically jacked schist bedrock required extensive rock-bolting to ensure long-term security of the building site (Bell, 2007c). Elsewhere, the Queenstown Hill Landslide has been identified as having formed as a consequence of ice retreat from the LGM, but the feature is now considered inactive and there is pressure for residential expansion onto the toe area (Cunningham, 1994;

Figure 1.1: Landslides mapped in the Queenstown Area (Otago Regional Council, 2020).

Stossel, 1999).

Foliation dip in the schist bedrock, specifically out of the slope at 15°-30°, is the most problematic given the low frictional strength along the mica layering (Stossel, 1999). However, there is little data available on the geotechnical properties of schist on Queenstown Hill, and this is essential in order to adequately assess viability of site development. The geology and geotechnical characteristics of the area must be better understood for safe development to proceed (Bell and Pettinga, 1985).

The aim of this thesis is to investigate the geomorphology and geotechnical properties of the Queenstown Hill landslide. Detailed mapping on lidar and in the field, paired with geotechnical characterization of the underlying schist will be used to produce a detailed ground model that allows us to better understand the implications for land development. The data obtained through detailed field mapping and laboratory testing help address the primary research questions.

1.2 Study Area and Existing Land-use

The Queenstown Hill landslide is located along the northwest edge of Frankton Arm, approximately 5 km east of Queenstown and has a peak height of 907 m and the lowest elevation of 309 m.a.s.l at Frankton Arm (Figure 1.2). Land-use in the area is shared between residential subdivisions, recreational purposes (4WD track) and rural farming. Currently, urban development is concentrated on the edge of Lake Wakatipu, where subdivisions extend up to 150 m above the lake level. There is no history of slope failures affecting residential properties, other than very localized foliation controlled features in excavated schist batters (Bell, 1996a; Bell and Riddolls, 1992). However, pressures for expansion have resulted in continued residential development proposals on some of the very large dormant landslide complexes in the District, notably the Queenstown Hill landslide.

Figure 1.2: Field Area and location of the Queenstown Hill Landslide 1:50,000 Series Topographical Map (Land Information New Zealand, 2019).

In the Queenstown area, there are two overarching elected bodies responsible for land-use planning, these being the Otago Regional Council (ORC) and the Queenstown Lakes District Council (QLDC). In 2018, the ORC released a 10-year plan where the main vision and strategies are directed at a proactive approach to maintaining and enhancing the natural environment. The Otago Regional Council Long Term Plan 2018-2028 projects a 2.4% and 2.6% growth, respectively, in annual visitors and resident population growth for the next 10 years. The plan acknowledges that this will increase the pressures on urban development and local farming practices, but no formal regional plan or strategy has been included in the Council's reports (Otago Regional Council, 2018).

The QLDC also has a 10-year plan and set of strategies to manage growth, infrastructure, structure plans, sustainable building, sustaining tourism growth, and urban design. The plan to accommodate growth encourages higher density developments in the urban area of Queenstown/Frankton and some existing zones outside of this area, but the council is discouraging growth beyond the planned boundaries in the Wakatipu Basin and in rural areas (Queenstown Lakes District Council, 2019).

Development is subject to a renewed code of practice for land development and subdivision set out by the QLDC, this includes strict engineering controls for earthworks investigations, compaction, drainage, foundation slab reinforcement and batter retention. Reports must also include information on land suitability, stability assessments, hazards, foundation considerations and other related matters (Queenstown Lakes District Council, 2019). Dwellings have been successfully constructed on the dormant landslide but there is a risk of renewed movement in the longer term if the schist is poorly interpreted and understood.

1.2.1 Previous investigations along Frankton Arm

Several schist landslides have been mapped along the Frankton arm, of which the Queenstown Hill Landslide was the largest (Stossel, 1999). These landslides have been interpreted as being triggered during the last glaciation 10,000-15,000 years ago. The predominant surface materials found beneath the Queenstown area are periglacial and glaciofluvial overlying schist bedrock. The landslide composition is predominantly quartzofeldspathic with bands of pelitic and greenschist (Bell and Riddolls, 1992).

The Queenstown Hill Landslide has an estimated total volume of 240 Mm^3 and has been interpreted as a translational landslide with a shallow compressional bulge from mid-slope to toe. Previous mapping and interpretations by Stossel (1999) proposed that the landslide underwent three phases of movement. The first phase of movement occurred during the final glaciation, initiated by ice scour and oversteepening. Glacial retreat removed lateral support resulting in increased pore pressures and reduced shear strength of the slope. The initial landsliding is characterized as a translational movement with slow rock mass creep along foliation shear zones and a stepped failure surface in fractured schist. The second and third phases of movement were initiated by removal of support at the toe of the landslide causing another translational slide and retrogressive failure. The third phase resulted in a toe bulge forming by gravitational creep down slope (Stossel, 1999).

1.3 Basement Terranes

A number of studies have been conducted on the provenance and structure of the basement terranes found in Central Otago (Adams et al., 2009; Adams and Graham, 1997; Bishop et al., 1976; Brown, 1963, 1967; Cooper, 1995; Cox, 1991; Craw, 1984; Forster and Lister, 2003; Graham and Mortimer, 1992; Hutton and Turner, 1936; Johnson, 1990; Kawachi, 1974; Mackenzie and Craw, 2005; Mortimer, 1993; Mortimer, 2000; Mortimer, 2003; Mortimer, 2004; Mortimer et al., 1993; Mortimer and Roser, 1992; Mortimer et al., 2001; Norris and Bishop, 1990; Park, 1906; Turnbull, 1979a, b, 2000b; Turnbull et al., 2001; Weinberger et al., 2010;

Wood, 1963, 1978). The most recent geological map for the region, which compiles much of the above work, is the 1:250,000 Geology of the Wakatipu area (Figure 1.3) (Turnbull, 2000b).

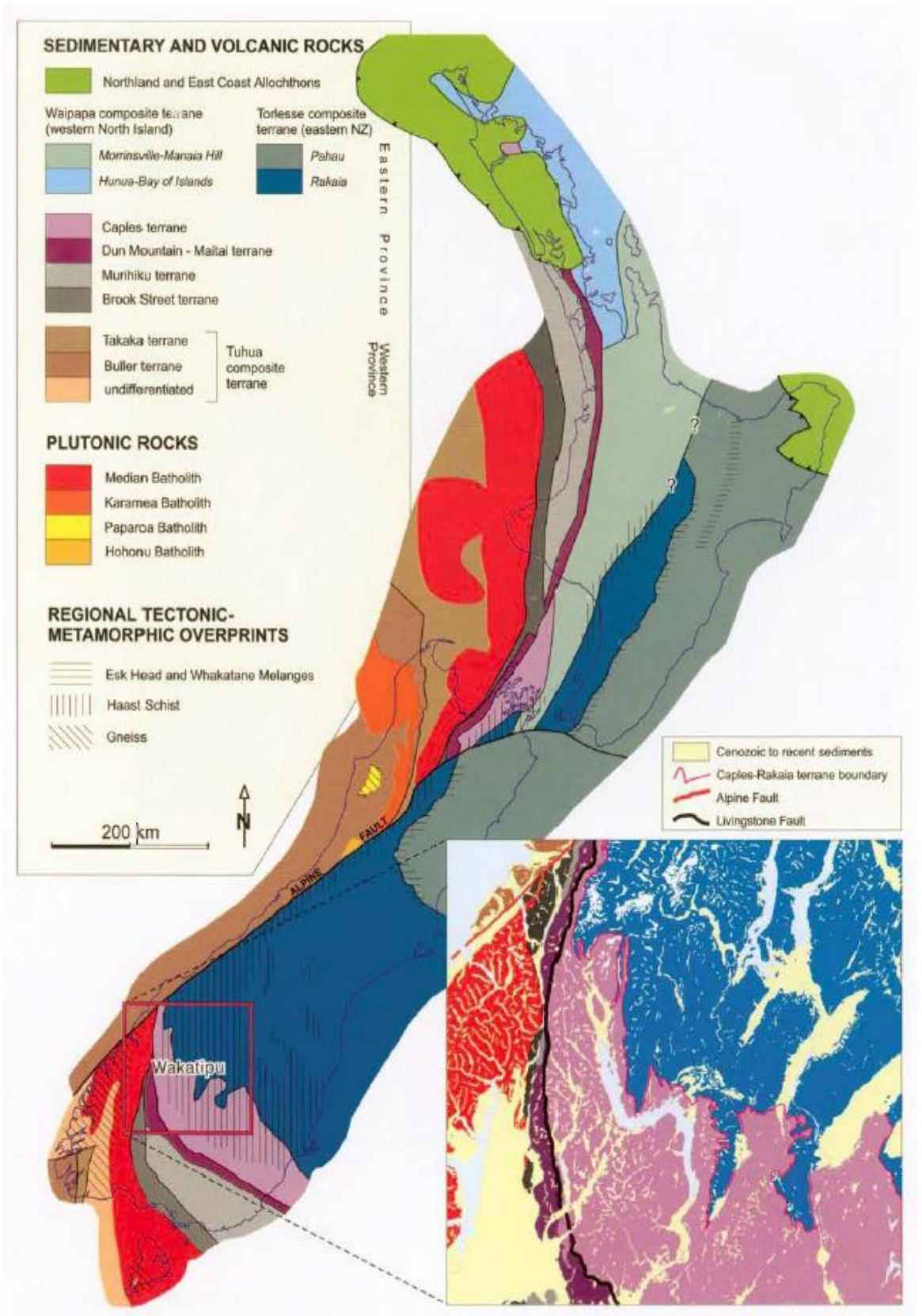

Figure 1.3: Tectonostratigraphic terranes within New Zealand. The Wakatipu map sheet covers the area outlined in red (Turnbull, 2000b).

The basement terrane underlying Central Otago is predominantly made up of Otago Schist. The Otago Schist is a subset of the Haast Schist that extends approximately 30,000 km^2 across Central Otago and comprises low metamorphic grade pelitic and psammitic schist with traceable horizons of greenschist and metacherts. The schist is bound by the Livingstone Fault to the west, the Alpine Fault to the northwest and the volcanic sequence in Dunedin to the east. Along the centre of the region is a cryptic suture, trending northwest, representing the Caples and Rakaia Terrane boundary, where the contact between the two terranes is overprinted by the Haast Schist (Figure 1.4) (Johnson, 1990).

The Haast Schist formed as a result of the Caples Terrane over thrusting the Rakaia Terrane from the south and west, during the Rangitata Orogeny 200 mya (Figure 1.5), and is defined as a northwest-trending schist belt that extends ~150km across the South Island (Gray and Foster, 2004). The Haast Schist is a broad term which includes the Kaimanawa, Malborough, Alpine, Chatham and Otago Schist (Norris and Bishop, 1990) - the schists along the Otago Region belong to the Otago Schist.

Predominant regional structures include a series of reverse faults trending north to northeast with a conjugate set trending northwest paired with antiform/synform structures promoting vertical offset between basin and ranges (Turnbull, 2000a). Macroscopic folds and lineations trend north-west to east plunging subparallel to the dip of the foliations. In Central Otago, folding, warping, fractures and crush zones have been interpreted as multiple generations of deformation responsible for the structures occurring within the terranes at various intensities (Forster and Lister, 2003; Mortimer, 1993; Turnbull, 1980; Wood, 1963).

The geotechnical behaviour of schist varies across the Otago region due to protolith (i.e. original parent rock), which are derived from materials sourced from the Caples and Rakaia terranes. The Caples terrane forms an arcuate shaped belt extending from the east Otago coast to the Alpine Fault and is mainly composed of late Permian to Triassic volcaniclastic sandstones, pillow lavas and cherts deposited in a submarine environment; while the Rakaia Terrane is dominated by early Permian cherts and pillow lavas sourced from an active continental arc overlain by quartzofeldspathic sandstones and mudstones deposited in an accretionary complex (Mortimer, 2004; Turnbull and Forsyth, 1988). Psammitic schists are derived from the Caples volcaniclastic sandstones, while pelitic schists are derived from Rakaia sandstones and mudstones. From either side of the Otago Schist, each terrane grades inward from prehnite-pumpellyite, pumpellyite-actinolite to greenschist facies in the biotite-garnet albite zone in the centre. More specifically, in the Queenstown area, the terranes grade from the Rakaia quartzofeldspathic greywacke and argillite in the northeast towards a quartzofeldspathic greyschist in the chlorite zone of the Greenschist Facies and back towards a volcaniclastic greywacke and argillite sourced from the Caples Terrane to the southwest (Mortimer and Roser, 1992). Table 1.1 highlights the differences in the Caples and Rakaia Terranes.

The collision of both terranes resulted in thickening of the crust and subjected the buried rock to high temperature and pressure conditions - forming the boundary of the metamorphosed Otago Schist. Folding of the schist continued until the early Cretaceous, which marked a period of crustal extension as New Zealand split from Gondwana. This allowed for a long period of exhumation and subaerial erosion of the schist from the Cretaceous to the Miocene. Within the literature, this erosional period that truncates the Caples and Rakaia terrane was formally referred to as the Otago Peneplain, now more recently the Waipounamu Erosion Surface (Bishop, 1994; Coates and Cox, 2002; Mortimer, 1993; Turnbull, 2000a).

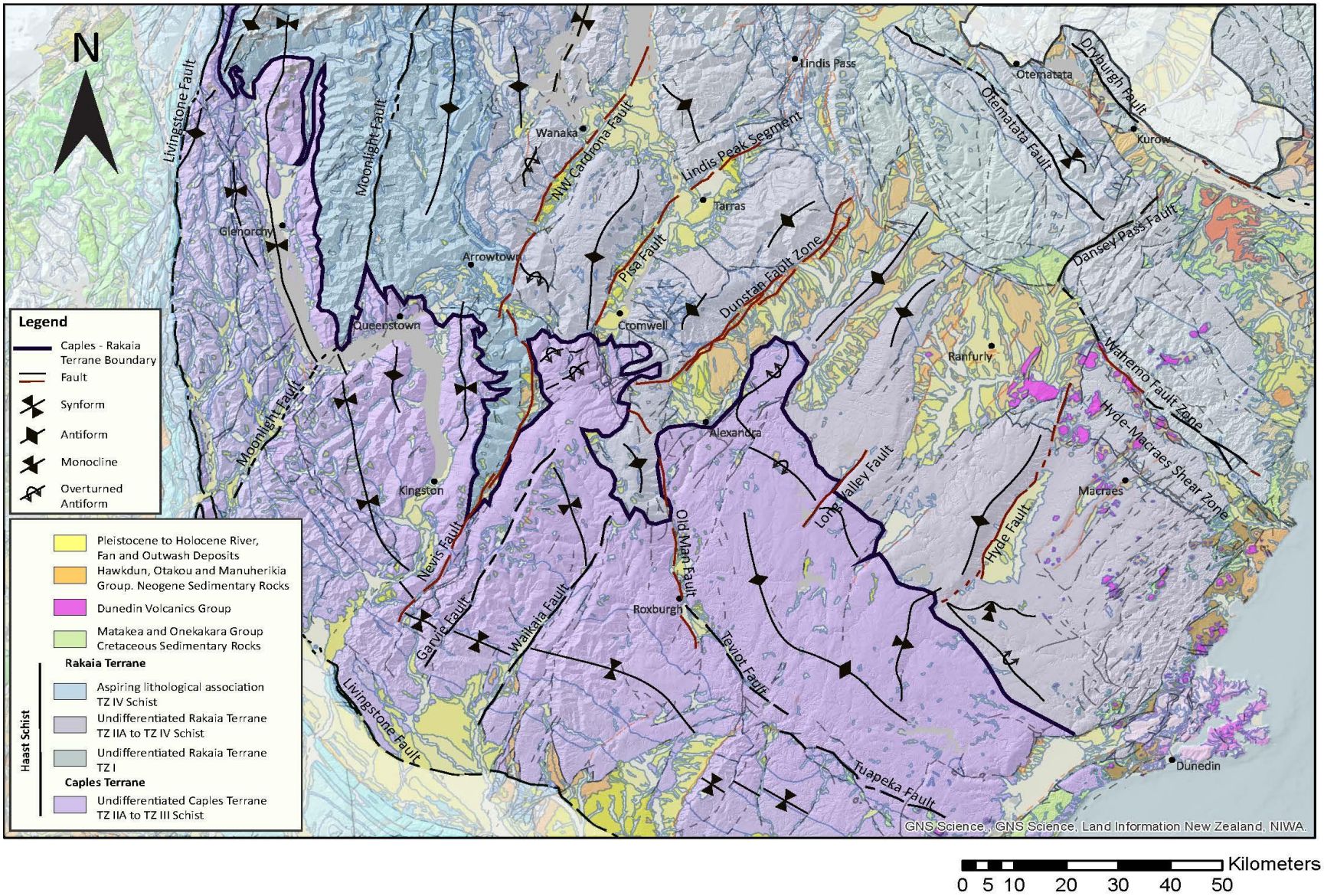

Figure 1.4: Simplified QMAP of the Otago Schist and regional structures. Redrawn from the 1:250,000 GNS Webmap, and the Wakatipu Geology map (GNS Science, 2018; Turnbull, 2000b).

Geologic Timescale of the Queenstown Area					
Eon	**Era**	**Period**	**Epoch**		
Phanerozoic	Cenozoic	Quaternary	Holocene	11,700	• Beer can deposition marked the onset of tourism.
			Pleistocene		• Fault traces formed on the Moonlight Fault at Mt Nicholas and on the Nevis-Cardrona Fault System in the Kawarau Gorge.
					• River-bed gravels and modern beaches forming. • The Kawarau River began draining Lake Wakatipu c. 10,000-12,000 years ago
					• High level of Lake Wakatipu (~50m above present lake level) and the formation of the Shotover delta. • Lake silts and beach gravels formed between 10,000-15,000 years ago. • End of the last glacial period approximately 15,000 years ago.
					• Episodes of ice advance 50,000 years ago; 35,000 years ago, 28,000 years ago and 18,000 years ago. • Valleys eroded and moraines formed.
				2.588 Ma	• Onset of Ice Age, global cooling and approximately 20 episodes of worldwide glacial and interglacial periods
		Tertiary – Neogene	Pliocene	5.332 Ma	• Kaikoura Orogeny: Faulting and upligt produced the regional basin and range topography. • Episodic movement on the Nevis-Cardrona and Moonlight Fault Systems.
			Miocene	23.03 Ma	• Moonlight Sea retreats • Uplift from faulting to the west of Lake Wakatipu.
		Tertiary – Paleogene	Oligocene	33.9 Ma	• Sediment deposition [Bobs Cove Beds]: sandstone, limestone, mudstone and breccia. • Intermittent movement on the Moonlight Fault.
			Eocene	55.8 Ma	• Deposition of fluvial sediments
			Paleocene	65.5 Ma	• Erosion of the Rangitata Orogeny • Schists exposed at the surface • Formation of the Otago Peneplain/Waiponamu Erosional surface
	Mesozoic	Cretaceous	Upper/Late	99.6 Ma	• Crustal extension led to the opening of the Tasman Sea and Southern Ocean. New Zealand split from Gondwana. • Cooling and exhumation of the Otago Schists begins.
			Lower/Early	145.5 Ma	
		Jurassic	Upper/Late	161.2 Ma	• Crustal thickening and metamorphism continue, forming the Otago Schist. • Convergence of the Gondwana Lower/Earlymargin continues to develop thrust-nappes.
			Middle	175.6 Ma	
			Lower/Early	199.6 Ma	• Formation of schists and semi-schists. • Rangitata Orogeny • Onset of metamorphism: folding of schists, followed by uplift and mountain building.
		Triassic	Upper/Late	228.7 Ma	
			Middle	245.0 Ma	
			Lower/Early	251.0 Ma	
	Paleozoic	Permian		260.4 Ma	• Parent sediments of schists • Oceanic trench infilling with sandstone, mudstone, etc. from volcanogenic sources.
				270.6 Ma	

Figure 1.5: Geological Timescale of the Queenstown area. Adapted from (Bell, 1976; Bishop, 1994; Johnson, 1990; McSaveney et al., 1992; Mortimer, 1993; Mortimer et al., 1993; Turnbull, 2000a; Turnbull and Forsyth, 1988)

Basement Terrane	Description
Rakaia Terrane	• Dominated by quartzofeldspathic sandstone and mudstone from a granitic source. Commonly interbedded. Bulk composition is granitic - 68-72% silica. • Deformed by early recumbent folds - usually refolded. • Series of antiforms mapped across the Terrane. • Fit a submarine fan model with turbidite sequences. • Repeated successions around flat line folds. • Steep cleavage with crenulations cuts earlier folds. • In the SW, greywacke grades into schists metamorphosed in the Jurassic (Otago Schist). • Currently 30km thick due to metamorphism but was likely twice as thick when deposited. • Four dominant schist types recognized: layered and massive quartzofeldspathic schist composed of alternating quartz-albite and mica-rich laminae, greenschist and quartz-spessartine schist. The contact between each type can be sharp or gradational. • Low grade metamorphic rocks, includes textural zones I-IV.
Caples Terrane	• Dominated by thick bedded massive grey-green volcanic sandstones, red and green sandstones with pillow lavas at the base. Subordinate black mudstone, red and green mudstone and conglomerates occur throughout. • Significantly lower in detrital quartz and mica than Rakaia derived sandstones. Predominantly andesitic-dacitic volcanic source. • Regional synform recorded in the western part of the Terrane • Has a complex structure with two or more phases of folding, tectonic slide zones. Overturned beds were later folded. • Caples terrane sediments are deformed into gently plunging or horizontal folds with steep dipping axial planes. • Interpreted as a deep submarine fan complex formed in a frontal arc and trench-slope/trench-floor environment. • Schistosity becomes the dominant structure to the east. The Caples is overprinted and grades into the Otago Schist. The schist cuts across the stratigraphy. • Low grade metamorphic rocks, includes textural zones I-III. In Otago, schists in the Caples terrane range from the prehnite-pumpellyite to lower greenschist facies

Table 1.1: Summary of the original lithological and structural features of the Caples and Rakaia Terrane (Adams et al., 2009; Adams & Graham, 1997; E. H. Brown, 1963; Gray & Foster, 2004; Kawachi, 1974; Turnbull, 1979b, 1980, 2000a; Turnbull & Forsyth, 1988)

1.4 Cenozoic Deposits

The basement rocks in Central Otago are overlain by a discontinuous cover of Paleogene to Neogene sediments derived from the long period of exhumation and erosion of schist from the Cretaceous to Cenozoic, including the submergence of almost all of New Zealand in the Oligocene. This period was followed by uplift, warping, faulting and thrusting during the Kaikoura Orogeny (5 Ma), which formed the current basin and range topography of Central Otago (Bishop, 1994).

The onset of global glacial and interglacial cycles in the Pleistocene (~2.6 Ma) followed by at least 4 periods of ice advance incised valleys into the Otago peneplain. The deepening valleys progressively downcut into the bedrock and eroded/undercut the toe of slopes resulting in glacial oversteepening and/or fluvial undercutting of slopes. Evidence of LGM is well preserved in thick beds of glacio-fluvial gravels, moraines, lake beaches and river gravels across the region (Bell, 1992).

1.5 Landslides in Schist

1.5.1 Landslides in Central Otago

Landslides are ubiquitous in the Central Otago Region (Figure 1.6). Both deep-seated and more surficial landslides occur in the schist bedrock and in loose materials. Deep-seated landslides are common across Central Otago and predominantly occur in schist bedrock. They developed as a result of tectonic uplift, erosion, fluvial downcutting and glaciation. While many deep-seated landslides were initially triggered by uplift and incision, other larger features (i.e Queenstown Hill Landslide, Coronet Peak Landslide, Arthur's Point Landslide) are proposed to be triggered by glacial undercutting and retreat; later reactivated by glacial over-steepening (Bell, 1976).

The landslides and slope geometries are influenced by the structures and lithologies of the basement terranes. The pronounced anisotropy of the schist introduces weakness and movement into the bedrock material creating an asymmetrical valley profile. Landslides in Otago Schist are largely controlled by their composition, foliation orientation and dip angle out of the slope. Previous investigations have shown that the lithological variations of the Otago schist have a direct geotechnical influence on slope stability and foundation design (Bell, 1976; Bell and Riddolls, 1992; Halliday, 2010; Paterson et al., 1983), and this is clearly relevant to the Queenstown Area. The schist-derived landslide debris in the region is predominantly weak with little internal strength, but studies conducted on the larger deep-seated landslides across Central Otago have shown that they are extremely variable in their engineering properties, ranging from large intact blocks separated by shear zones to internally chaotic masses (Macfarlane, 2009; Macfarlane et al., 1991b). Deep-seated landslides in Central Otago are triggered by a combination of stress-relief and progressive translational failure along low-angle foliation planes resulting in buckling at the toe (Gillon and Hancox, 1991; Macfarlane, 2009; Macfarlane et al., 1991b).

A significant amount of research has been conducted across Central Otago to map and monitor the rate of movement of schist landslides (Gillon et al., 1991a; Gillon et al., 1991b; Macfarlane, 2009). Due to cessation of active erosion at the toe of the landslides in the Queenstown area, the landslides have slowed to a creep (< 5 mm/year) or show no recorded movement (Bell and Riddolls, 1992; Cunningham, 1994; Stossel, 1999; Willetts, 2000). In areas where the toe has been excavated or inundated (i.e the Cromwell Gorge, Kawarau Gorge, Lake Dunstan and Gibbston), movement has been recorded and stabilization measures have been implemented to maintain slope stability (Brown et al., 1980; Gillon et al., 1991c; Jennings et al., 1991; Macfarlane, 2009; Newton and Smith, 1991).

The stability and engineering properties of individual landslides can usually only be assessed by site-specific investigations, including drilling and piezometric monitoring because of the importance of perched water controlling stability (Belcher, 2009; Macfarlane et al., 1991a; Macfarlane, 2009). Inadequate understanding of the schist behaviour led to failure at Maniototo (Moody, 1985; Paterson, 1979; Paterson et al., 1983; Paterson et al., 1988) - highlighting the importance of understanding the geotechnical behaviour of schist and especially weak zones, such as foliation shears within the rock mass.

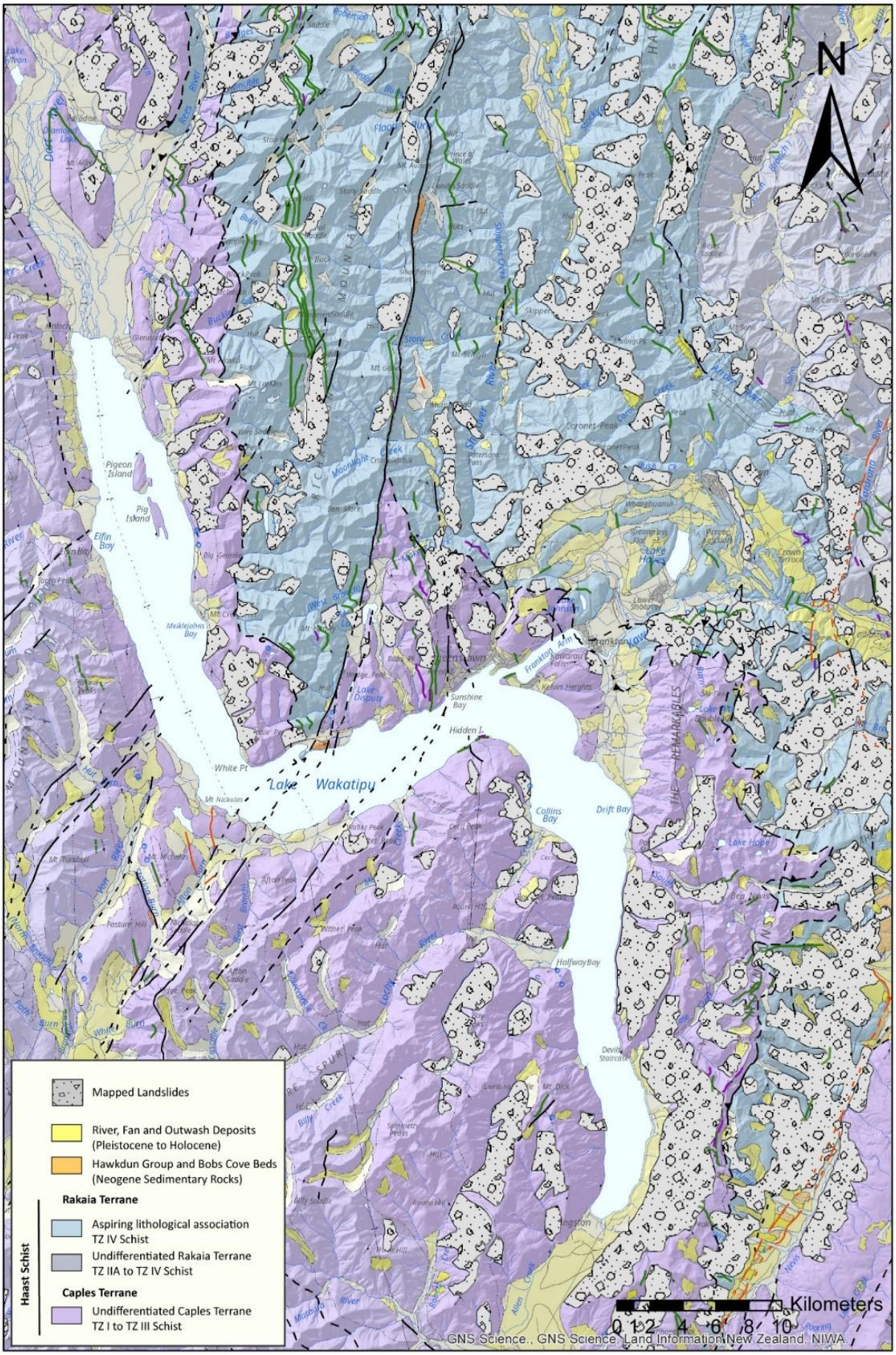

Figure 1.6: Mapped landslide distribution in the Queenstown Area. Map redrawn from GNS Webmap (GNS Science, 2018).

1.5.2 International Landslide Case studies

Rock-slope failures in anisotropic materials such as schist and gneiss are well documented internationally (Agliardi et al., 2012; Agliardi et al., 2014; Behrestaghi et al., 1996; Braathen et al., 2004; Kalenchuk et al., 2012; Loew et al., 2012; Malone et al., 2008) including investigations detailing the effects of multiple glaciations on slope stability (Glueer et al., 2020; Glueer et al., 2019; Grämiger et al., 2017; Grämiger et al., 2018; Imrie et al., 1991; Kalenchuk et al., 2012). The landslide geometries, surface expression, triggering mechanisms, failure surfaces and factors controlling stability were reviewed to compare with observations made on the Queenstown Hill landslide.

1.6 Motivation and Contributions

Development in the Queenstown area occurs on both the Rakaia and Caples derived schist, as well as along the boundary between the two terranes. Seeing how the geotechnical issues relate to the variability of the schist (i.e mineralogy, orientation of the foliation, increased pore pressures due to perched water bodies, etc.), this variability creates the need for characterization and zonation of the schist materials based on their geotechnical properties.

Currently, few subsurface investigations by drilling have been conducted in the Queenstown area, and there is limited data on the mechanical properties of schist due to challenges related to testing the material. This research will build on previous investigations undertaken along Frankton Arm (Stossel, 1999) and on the current understanding of schist landslides elsewhere in Central Otago. In 1999, access to lidar data and subsurface drilling were unavailable. This thesis provides a unique opportunity to map on new lidar and to supplement mapping with borehole data and testing. A primary objective of this thesis is to characterize schist lithotypes, so that important differences are understood numerically, and the data can be used to facilitate planning and development. It is also anticipated that the results will benefit future development and hazard assessments by:

- Filling knowledge gaps and recognizing factors that may predispose a site to slope failure.
- Providing parameters to enable modelling of future slope behaviour and identify problem areas considered for development.
- Providing additional parameters for empirical landslide hazard modelling and risk assessment, which in turn increases infrastructure and community resilience.

1.7 Thesis Format and Organization

Following the introduction and regional overview in this chapter, **Chapter 2** includes a literature review of the geological history and previous work undertaken in the Queenstown area. Lithological variations mapped in the field and logged from drillcores across the landslide are presented at the macro-scale and micro-scale along with the structural domains derived from data collected in the field.

Chapter 3 reviews the geomorphic setting in the Queenstown area, the influence of glaciation on the Wakapitu Basin and Quaternary deposits in the study area. A series of geomorphic maps are presented at various scales, from 1:2,000 to 1:15,000 including discussions on morphological zones, major landslide features, distribution and description of surficial deposits logged in the field.

Chapter 4 examines local and international laboratory testing results derived from engineering geology investigations of schist and presents the results obtained from borehole samples tested from the Queenstown Hill landslide. This includes physical parameters: moisture content, density, porosity, sound velocity and slake durability; and strength parameters: uniaxial compressive strength (UCS), indirect tensile

strength, point load strength and results from triaxial testing point load strength. In addition to testing, quality indexes derived from rock mass classification are evaluated.

Chapter 5 presents the engineering geology ground model constructed from the results and interpretations in this thesis. The ground model includes an overview of the geology and geomorphology of the Queenstown Hill landslide, structural controls on surface morphology, and kinematic analysis. This is followed by a discussion on the preferred landslide classification, failure mechanisms and evolution of the landslide.

Chapter 6 summarizes the key findings of this thesis and provides suggestions for future work.

Appendices referenced in text are separated by chapter and included at the end of this thesis. It should be noted that all maps and plans in this thesis have been projected in the New Zealand Transverse Mercator (NZTM 2000) national grid.

This thesis aims to answer the following questions (Table 1.2):

Objective/Contribution	Research Questions	Relevant Chapter
• Document lithological variations in the field and in drillcores. • Derive physical and strength parameters through laboratory testing.	How do the mineralogical and physical properties vary within the different schist types, and is this reflected within the mechanical properties of the different schist types?	**Chapter 2 & 4**
• Establish structural domains across the study site. • Produce geomorphic maps of the study site.	What are the main structural domains across the landslide, and how is this reflected in the geomorphology of the landslide?	**Chapter 2 & 3**
• Produce an engineering geology ground model. • Use kinematic analysis to identify possible failure modes.	How does the improved understanding of geomorphology and geotechnical characterization of the Queenstown Hill landslide be applied to future land development?	**Chapter 3 & 5**

Table 1.2: Research Questions

Chapter 2: Geology of Queenstown Hill

2.1 Introduction

This chapter includes a summary of the geological history, including a series of maps showing the distribution of the geological units in the Queenstown area and a summary of previous work undertaken along the Caples-Aspiring boundary. More specifically, sections 2.2 and 2.3 present our current understanding of the local geological history, lithologies, structures, metamorphic facies and textural zones. The scope of the literature review was expanded to include the Queenstown Area for context, as a limited number of studies have been undertaken on Queenstown Hill.

Methods used during field campaigns for borehole logging, field descriptions and petrographic analysis carried out as part of this study are presented in section 2.4. Results, structural domains and synthesis are in sections 2.5, 2.6 and 2.7, respectively.

The main objectives of the investigations were to:

1. Identify and describe various lithotypes present within and adjacent to the Queenstown Hill Landslide, both at the macro-scale and micro scale. The macro-scale descriptions were obtained during the field investigations and borehole logging, while the micro-scale analysis was completed through petrographic analysis.
2. Produce full logs and summary logs of lithologies from four 25 m boreholes drilled within the landslide.
3. Map the structural features within and surrounding the landslide, to subdivide the area into structural domains.

2.2 Geology of the Queenstown Area

The earliest records of geological maps of the Queenstown area date back to Hector (1863) and by Park (1906, 1908 and 1909). The maps included descriptions of glacial features, as well as lithological descriptions of the schist. Further structural mapping and interpretations were undertaken by Wood (1963). Bishop et al. (1976) refined the boundaries of the Haast Schist and described the lithological differences between the Caples and Rakaia Terranes. Turnbull (1979 a,b) used stratigraphic correlations and sedimentology to conclude that both terranes were sourced from separate accretionary complexes. The most recent geological maps (Figure 2.1) and timescale of the Otago Schist (Section 1.2) were completed by Mortimer et al. (1993) and Turnbull (1988, 2000).

The Otago Schist in the Queenstown area spans the boundary between the Caples Terrane (to the south west) and the Aspiring lithological association (to north east) of the Rakaia Terrane (Figure 2.2) (Craw, 1984). A brief summary of the geological evolution of the Rakaia and Caples basement terrane is included in Chapter 1. The boundary between the terranes is characterized by recumbent isoclinal folds, as a result of the Caples terrane being thrust over the Rakaia and later thoroughly re-crystallized. The boundary is flat to low dipping and cut by a series of faults. The boundary between the schist types has been defined by shear zones and schist lithotypes mapped at a regional scale, but generally the exact extent of the boundary is poorly defined (Craw, 1984). Cox (1991), Cooper (1995), and Gray and Foster (2004) identify the Caples-Aspiring boundary as a high strain zone of transposed psammitic and pelitic schist, with meta-volcanics containing rare biotite of the Aspiring association.

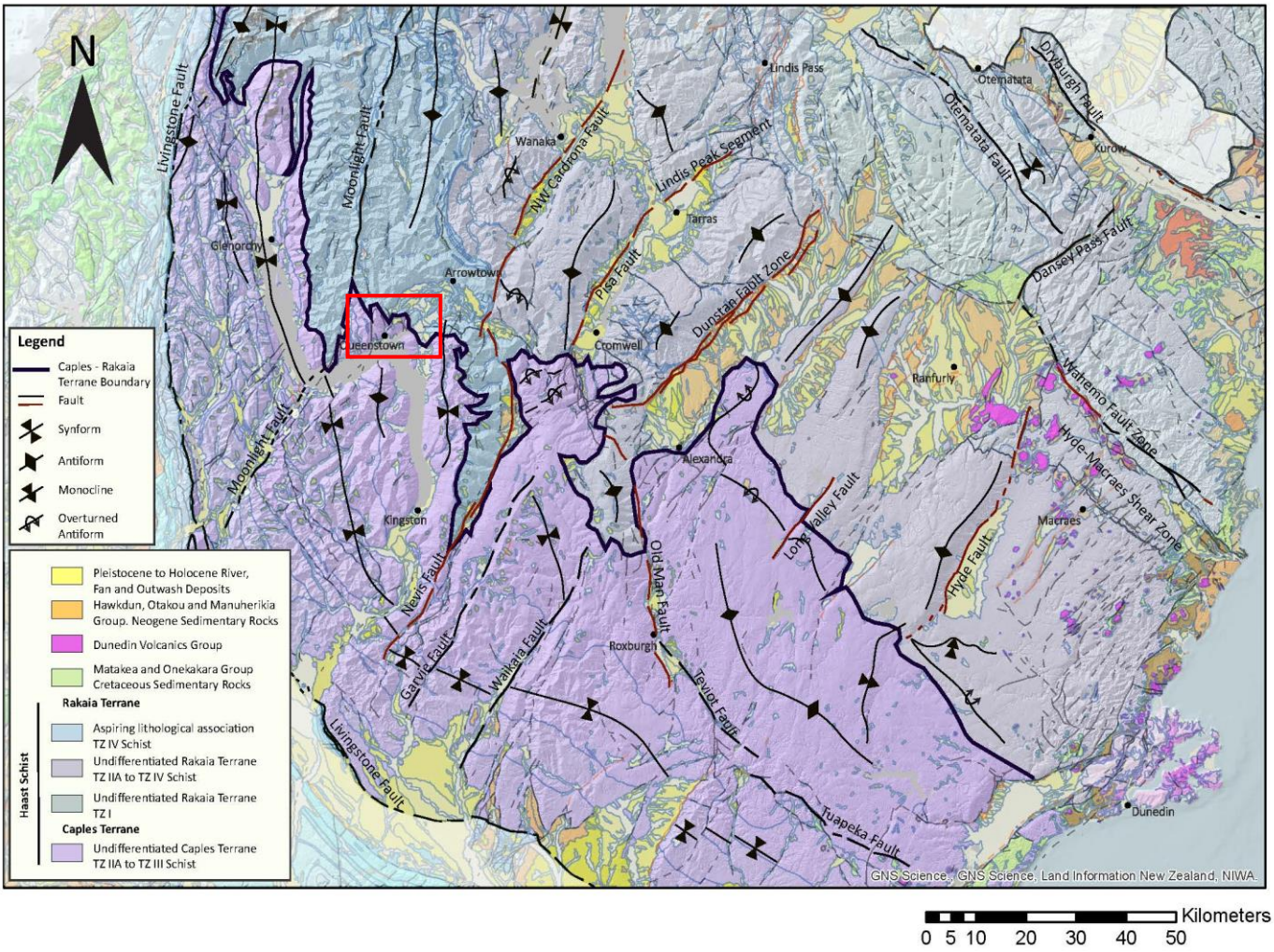

Figure 2.1: Adapted QMAP drawn at 1:900,000 showing the major regional structures and the extent of the Caples Terrane and Rakaia Terrane. The red box has been placed around the Queenstown Area (study area). (GNS Science, 2018)

The Queenstown area is cross-cut by two major north-east trending faults: the Moonlight Fault and the Nevis-Cardrona Fault System. The Moonlight Fault has been described as a steep and narrow east dipping reverse fault marked by a wedge of Oligocene sediments from Bobs Cove Beds (Turnbull, 2000b). Three periods of movement have occurred along the Moonlight Fault Zone during the pre-Oligocene, Oligocene and post-Oligocene. Movement across the fault has resulted in uplift of the Northwest side of Lake Wakatipu. Local kink folding has been mapped in the pelitic schists of the Aspiring lithologic association along the fault (Turnbull, 1980).

The Nevis-Cardrona Fault system separates the basin and range topography to the southeast and a series of conjugate north-trending faults are also mapped within the area. Other local faults such as the Two Mile Creek Fault, Von Fault, Gilbert Fault, Kennada Fault and Toothpeak Fault, etc. faults are described in detail in Turnbull (1980). Numerous splinter faults, crush zones and kink fold bands occur within these schists suggesting that the faults in this area may have young histories (Turnbull, 1980). Data associated with faults located within 5-6 km of the Queenstown Hill Landslide have been summarized in the table accompanying Figure 2.3.

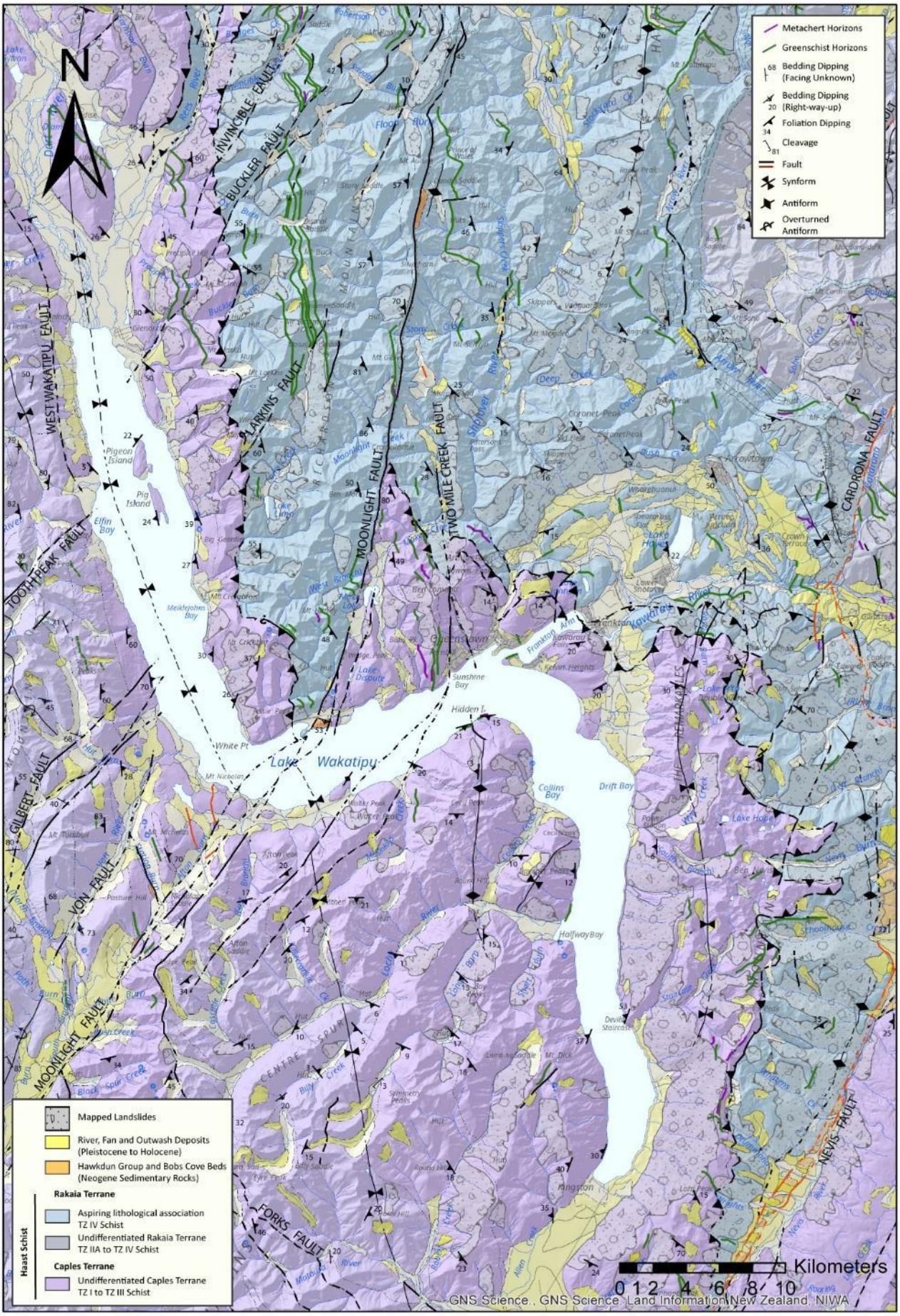

Figure 2.2: QMAP showing the geology and structures surrounding the Queenstown area. Map redrawn from GNS Webmap (GNS Science, 2018)

Post metamorphic folds defined by foliation are largely related to Miocene to Pliocene deformation. In the the Queenstown area, only mesoscopic folds are readily visible. One of the most prominent folds is the Taieri-Wakatipu synform, which is described as an enigmatic regional fold trending northwest across the map area. Other locally concentrated deformational structures are kink folds, which have been observed in foliation and span multiple generations, commonly associated with Cenozoic faults (Turnbull, 2000b).

2.2.1 Bedrock Lithologies

Various methods have been used to describe the schist lithotypes in the Queenstown Area (Brown, 1967; Craw, 1984; Graham and Mortimer, 1992; Mortimer and Roser, 1992; Turnbull, 1979a, 1981; Wood, 1963). Originally Wood (1963), Brown (1967) and Turnbull (1981) subdivided the schist into 4 broad lithotypes: layered or massive quartzofeldspathic rock, greenschist and metachert (Table 2.1). This classification was later refined by Craw (1984) into 2 major lithotypes, further subdivided to be recognizable at outcrop scale in the field (Table 2.2).

<table>
<tr><th>Lithotype</th><th colspan="2">Description</th></tr>
<tr><td>Layered quartzofeldspathic rock</td><td>• Alternating light and dark laminae, mica-rich, thinly laminated (2-15 mm thick), undulating, discontinuous. Well foliated.
• Contains 40-60% quartz and albite. Muscovite, chlorite, biotite, epidote and graphite make up the remaining constituents.
• Generally, pelitic.
• Can include interlayered greenschist and metachert bodies.
• Derived from argillaceous sediments.
• Unit thickness varies from 1 cm to over 100 m and traceable for tens of metres to kilometres.</td><td rowspan="2">• Predominate over the other lithologies.
• Most within the chlorite zone of the greenschist facies
• Mineralogy:
Quartz and Albite: 40-70%
Epidote: 12-32%
Muscovite: 10-30%
Chlorite, stilpnomelane and actinolite: < 15%
Biotite: 3-5%
Garnet: < 1%
Accessory: apatite, tourmaline, zircon, graphite, pyrite, marcasite, and chalcopyrite.
The most common opaque is finely divided graphite.
• Common assemblages:
1) quartz-albite-epidote-muscovite-stilpnomelane ± actinolite
2) quartz-albite-epidote-muscovite-chlorite± stilpnomelane and actinolite
3) quartz-albite-muscovite-chlorite ± epidote-actinolite-titanite-calcite-biotite-garnet-opaques</td></tr>
<tr><td>Massive quartzofeldspathic rock</td><td>• Light to medium grey, quartz-rich, thickly laminated with evenly distributed minerals. Poorly foliated *exception of irregularly spaced 0.5-2 mm quartz/albite laminae.
• Contain 45-80% quartz and albite. Muscovite, biotite, stilpnomelane, epidote and chlorite make up the remaining constituents.
• Derived from siliceous sandstone and mudstone.</td></tr>
<tr><td>Greenschist</td><td colspan="2">• Alternating light and dark green layers of metavolcanics.
• Range from massive poorly foliated (very dark green) to laminated well foliated (pale grey-green to yellow green meta-tuffs)
• Containing predominantly albite, chlorite, epidote and some muscovite and calcite. All lack graphite.
• Often grade into other schists.
• Iron-rich epidotes only occur in greenschist and quartzose schists.</td></tr>
<tr><td>Metacherts</td><td colspan="2">• Massive to thinly laminated metachert and/or quartzite units.
• Range in thickness from <1 cm to 4 m.
• Found as float in less continuous patches occurring in irregular masses or in vein-like segments.
• Composed mainly of quartz and spessartine in subequal proportions with minor albite and muscovite.
• Commonly associated with greenschist.
• Common Assemblage: > 90% quartz ± albite-chlorite-muscovite-actinolite-epidote-piemonite-spessartine-magnetite-hematite and calcite.</td></tr>
</table>

Table 2.1: Summary of the 4 schist lithotypes in the Queenstown area. Table adapted from Wood (1963), Brown (1967) and Turnbull (1981).

Major Lithotypes	General Description	Subdivision	Description
Greyschist	• Metamorphosed sedimentary rocks. • Consist mainly of quartz, albite, muscovite, chlorite and sphene with minor epidote, pyrite, tourmaline, apatite, calcite and graphite. • Commonly interlayered on a scale of 30 cm to many meters.	**Grey Pelitic**	• Textural zone (TZ) IV. • Well laminated and foliated lithology with up to 70% phyllosilicates. • Detrital minerals have not been recognized in the totally recrystallized TZ III and IV pelites. • Pelitic schists have segregations several millimetres wide (up to 1 cm).
		Porphyroblastic Pelitic	• Contains porphyroblastic albite (up to 3 mm) with associated finer grained quartz, in a matrix of phyllosilicates (mainly muscovite). The albite porphyroblasts are "coated" with fine black opaques giving the rock a distinctive grey spotted appearance. • Few laminations or segregation • Commonly the 2 types of pelite are interlayered, with sharp boundaries • The textural difference is not due to metamorphic grade.
		Psammitic Schist	• Quartz and albite dominate over phyllosilicates. • In TZ IV, segregation laminae are very pronounced - although a foliation is not always well developed, as phyllosilicate layers are often thin, distorted, discontinuous, thickened and thinned by folding. • The quartz-albite/phyllosilicate ratio is variable - especially in TZ IV • Interlayering of psammite and pelite on a scale of cm is not uncommon. • There are 2 psammitic schist end member types. **Eastern quartz-rich and western quartz poor.** Western psammitic schists have affinities to the volcanogenic Caples Terrane rather than the quartz-rich rocks on the eastern side of the schist belt.
Greenschist	• Metavolcanic material. • Mainly consists of albite-epidote-chlorite-titanite with minor magnetite, pyrite, pyrrhotite, actinolite, stilpnomelane, biotite, quartz, muscovite, calcite, and apatite. • Form layers from 1 cm to hundreds of m's thick • Interlayered with greyschists. • Lenses or layers are commonly found within greenschist horizons.	**Light Greenschist**	• Very pale green, well-foliated. • Thin < 2 m, continuous layers interlayered with grey pelite. • In addition to albite, contains low iron mafic minerals.
		Foliated Greenschist	• Dark green chloritic greenschist with high carbonate can give a pitted outcrop appearance. • Foliation is well developed, and layers are typically 20 cm-2 m thick. • Albite is essential but grains are not prominent in hand specimen. • Quartz and muscovite are very rare.
		Spotted Greenschist	• Distinctive spotted appearance. Poorly foliated. • Lithologic variation of lighter and darker layers on a 1 cm-1 m scale and sharp boundaries between layers. • Contains small amounts of quartz and muscovite, particularly as inclusions in albite porphyroblasts. Albite porphyroblasts up to 3 mm - set in a dark green matrix of chlorite (+- epidote and actinolite)
		Epidote Greenschist	• Poorly foliated greenschist with epidote-rich banding and lenses. • Variation is very prominent, with sharp boundaries between layers. • May contain concentric epidote-chlorite structures. Round "knots" or clusters of epidote grains are commonly seen in thin section. Epidotes may have dusty hematite inclusions in their cores and the matrix contains magnetite.
Metachert	• Hard white rocks with up to 95% quartz. • Form prominent layers up to 100 m thick. Rarely traceable for more than a few hundred metres. • Commonly found with greenschist horizons, occurring as layers. Rarely found interlayered with pelitic greyschists.		

Table 2.2: Summary of the refined lithotypes in the Queenstown area mapped by Craw (1984).

More than 95% of the schist identified in the Queenstown area is locally known as greyschist derived from low-grade metamorphic processes. Greyschist is a generalized term used to describe massive or layered schist derived from sedimentary rocks. The majority of Caples derived psammitic schists have a distinct "greenish" hue due to the large amount of chlorite and epidote. They are poorly foliated with segregation lamellae < 1 mm thick (Textural Zone III) and have a grainy appearance under the hand lens. In comparison, the Torlesse derived psammitic schist is typically darker grey, on account of it being muscovite-rich, with segregation lamellae > 1 mm thick (Kawachi, 1974; Mortimer and Roser, 1992).

Based on the current QMAP data, the Queenstown Hill Landslide is mapped within the Undifferentiated Caples Terrane Schist TZI-III, approximately 2 km west of the Caples-Aspiring Terrane boundary. The Aspiring Lithologic Association is mapped to the east of the Queenstown Hill Landslide and is distinguished from the Caples terrane by its abundant and pelitic greenschist (Figure 2.3). The schist associated with the Queenstown Hill Landslide is described as *well foliated psammitic and pelitic schist with incipient segregation; minor greenschist and metachert. Quartz veins are common. Schist overprints undifferentiated volcaniclastic sediments* (Turnbull, 2000).

However, it has been noted that rock units located in proximity to the Caples-Aspiring boundary and schists in textural zone (TZ) IV tend to have poorly defined boundaries and the contacts between lithological units can be either sharp or gradational (Craw, 1984). Samples collected from the Queenstown area by Graham & Mortimer (1992) have been described as "*massive, centimeter-thick quartz segregations/veins parallel to the foliation. Segregations show pinch and swell structures within the surrounding psammitic greyschist and contain mica-rich selvedges*. The schists mineral assemblage was quartz-albite-muscovite-chlorite-clinozoisite (epidote)-titanite. "Establishing a TZ proved difficult as the schist between the veins is a TZ III but the thick segregations indicate TZ IV. Most samples collected were found to be derived from the Caples Terrane, with some exceptions falling within the Torlesse Range" (Graham and Mortimer, 1992).

2.2.2 Caples-Rakaia Boundary

Many studies provide a broad description or geochemical analyses of the Caples-Rakaia boundary (Adams and Graham, 1996, 1997; Bishop et al., 1976; Cooper, 1995; Cox, 1991; Craw, 1984; Gray and Foster, 2004; Mortimer, 2000; Mortimer, 2003; Mortimer et al., 1993b; Turnbull, 1979b; Turnbull et al., 2000). However, previous investigations undertaken by Cox (1991) and Cooper (1995) were dedicated to characterizing the boundary between the Caples and Rakaia Terranes. Locally, the boundary has been mapped across the Remarkables Range extending across to Queenstown Hill and curves towards Glenorchy in the northwest.

Along the Remarkables Range and in the surrounding area, a combination of deep ductile structures superimposed with shallow brittle faults indicate that the boundary is likely a flat to low dipping feature cut by a series of faults, where the Caples terrane has been thrust over the Rakaia terrane. The estimated total displacement is 2 km - 150 km. Mesoscopic folds deformed east-west striking, vertically dipping surfaces over a wide area. Folds adjacent to the boundary are near isoclinal and more asymmetric, forming tight folds with short thick limbs and are commonly boudinaged. A change in deformation of quartz and albite grains was also recoded over the transitional zone (Cox, 1991).

In the Queenstown area, the Caples-Aspiring boundary is described as a 300-500 m thick transition zone of overlying psammitic schists derived from the Caples terrane (TZ III) onto psammitic and pelitic schists of the Aspiring Lithological Association (TZ III/IV). In this zone, an increase in thickness of segregation lamellae in psammitic schist from < 2 mm to > 2 mm was recorded. Geochemical analysis of samples collected along the boundary suggest affinities to both the Caples and Torlesse terranes (Cooper, 1995; Cox, 1991; Craw, 1984; Mortimer and Roser, 1992).

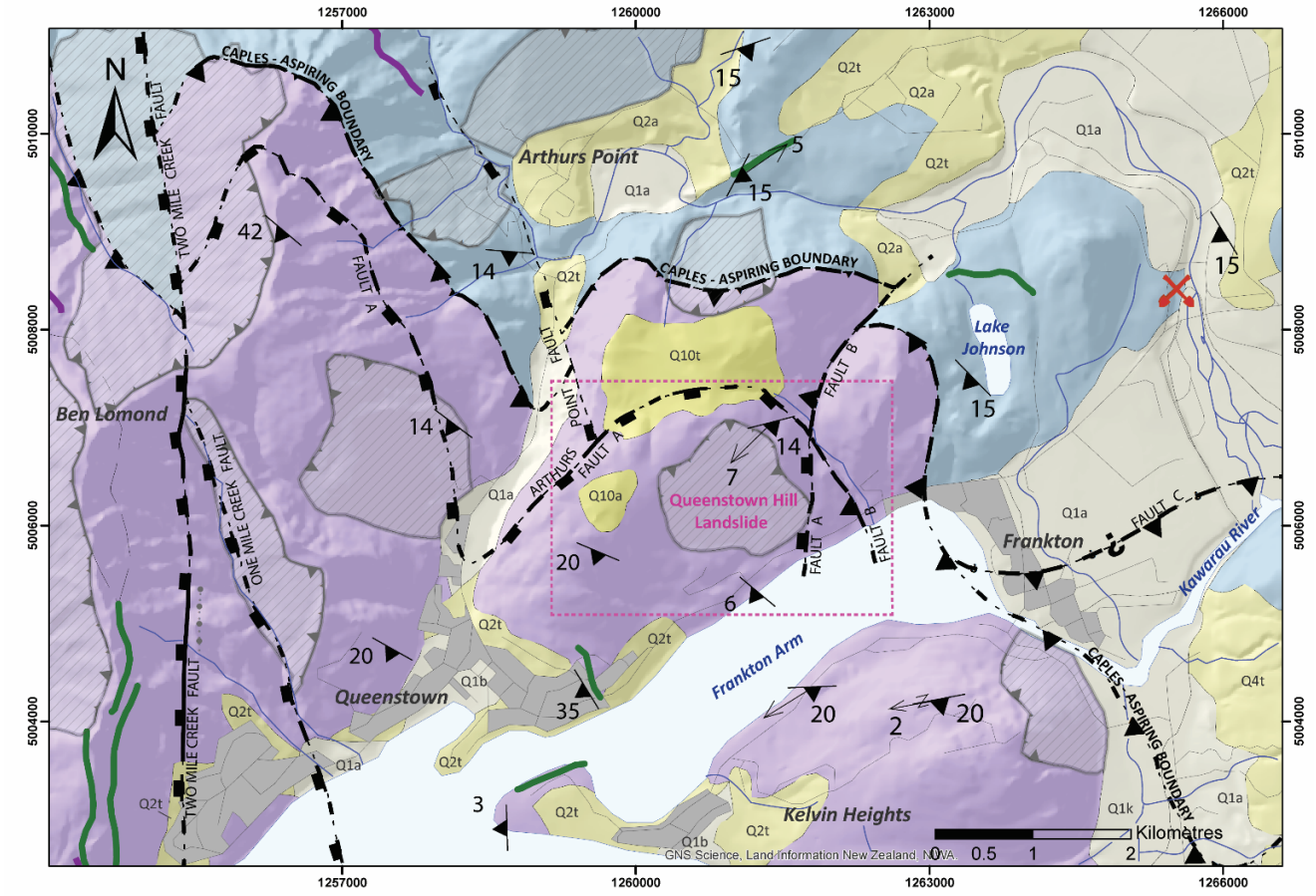

OIS 1 (Holocene) Fan and Lake Deposits [0 - 0.014 Ma]*
Q1a: Holocene gravel, sand, mud and minor peat of modern to postglacial flood plains; may be terraced. Loose, commonly angular, boulders, gravel, sand, and silt forming alluvial fans; grades into scree (upslope) & valley alluvium.
Q1b: Well sorted, fresh, rounded, fine to medium gravels in benches and storm beach ridges around major lakes.
Q1k: Laminated micaceous silt, mud and sand in old lake deposits.

OIS 2 (Late Pleistocene) Glacier Deposits [0.012 - 0.024 Ma]**
Q2a: Undifferentiated outwash gravel from valley glaciers; associated fan gravels and alluvium in low terraces in non-glaciated catchments. Generally unweathered, well sorted, loose, sandy to bouldery gravel forming large terraces and outwashplains.
Q2t: Undifferentiated till from valley glaciers. Generally unweathered, unsorted to sorted, loose sandy gravel, silt and sand in terminal and ground moraines.

OIS 10 (Middle Pleistocene) Glacier Deposits [0.339 - 0.362 Ma]***
Q10a: Slightly to moderately weathered alluvium and outwash gravels in terrace remnants; alluvium in non-glaciated catchments. Sandy to bouldery clayey gravel in outwash terrace remnants.
Q10t: Till in terrace remnants. Slightly to moderately weathered bouldery sandy gravel (till) in moraine remnants.

Haast Schist

Rakaia Terrane

Aspiring lithological association - TZ IV Schist [199.6 - 270.6 Ma] :
Variably schistose quartzofeldspathic sandstone ("greywacke") interbedded with mudstone ("argillite"). Variably segregated, veined and foliated; abundant laminated pelitic greyschist, and subordinate psammitic greyschist; minor greenschist bands and thinner horizons. Mixed pelitic and psammitic schist, distinctive porphyroblastic schist and thin chert horizons.

Caples Terrane

Undifferentiated Caples Terrane - TZ I to TZ III Schist [220.0 - 275.6 Ma] :
Undifferentiated, well foliated psammitic and pelitic schist with incipient segregation; minor greenschist and metachert. Quartz veins are common. Schist overprints undifferentiated volcaniclastic sandstone and siltstone, conglomerate, mudstone, sandstone, volcanics with rare limestone, rare chert, marble, interbedded red and green sandstone, black mudstone and granular conglomerate.

Undifferentiated Pleistocene to Holocene landslide deposits.

Residential Area

Pit Working (Aggregates)

Metachert Horizons

Greenschist Horizons

Bobs Cove Beds

34 Foliation strike, dip direction and dip angle

5 Trend and Plunge, angle of a lineation.

20 / 2 Minor folds plunging Z-vergence, Foliation

Fault, solid where known, dashed where inferred, dotted when covered.

Thrust fault with triangles on the hanging wall.

Reverse fault with rectangles on the hanging wall.

FAULT DETAILS

Fault Name	Fault Type	Subordinate Movement	Activity	Age	Deformation	Displacement (Total Slip)	Down Quadrant	Dip/ Dip Direction	Movement Type
Two Mile Creek Fault	High Angle Reverse Fault	n/a	Inactive	CZ - Cenozoic (0 - 66Ma)	Brittle	1-10km	E	80°/265°	Dip slip
One Mile Creek Fault	High Angle Reverse Fault	n/a	Inactive	CZ - Cenozoic (0 - 66 Ma)	Brittle	1-10km	E	85°/250°	Dip slip
Caples – Aspiring Boundary	Thrust Fault	n/a	Inactive	K - Cretaceous (66 - 145 Ma)	Ductile	10-100km	NE	25°/000°	Dip Slip/ Ductile Shear
Unknown (Labelled A)	High Angle Reverse Fault	Reverse Sinistral	Inactive	Mi, Pl - Miocene, Pliocene (2.58 - 23.03 Ma)	Brittle	0.1-1km	N	75°/185°	Oblique Slip
Unknown (Labelled B)	Thrust Fault	n/a	Inactive	Mi, Pl - Miocene, Pliocene (2.58 - 23.03 Ma)	Brittle	1-10km	NW	25°/135°	Dip Slip
Unknown (Labelled C)	Thrust Fault	n/a	Inactive	K - Cretaceous (66 - 145 Ma)	Brittle	n/a	N	33°/099°	Dip Slip

* Age based on geomorphology ** Age based on C14 dating and stratigraphic correlation *** Age based on stratigraphic correlation

Figure 2.3: Geological map of the study area, including a table summarizing local fault details. The magenta dashed rectangle represents the thesis study area. Map redrawn and fault data taken from GNS Webmap (GNS Science, 2018; Turnbull, 2000a).

The terrane boundary is a broad complex zone rather than a discrete narrow structure making a consensus on the exact location of the boundary difficult. This is likely due to a number of constraints such as: mapping scale/local variation, low dipping schist making lateral position hard to locate, and/or an increase in strain does not always develop a change in structural style resulting in thoroughly crystallized, indistinguishable structures. At present time, the most clearly defined boundary area is located at the Remarkables Range and between Queenstown and the Barrier Range (Mortimer, 2004; Mortimer and Roser, 1992).

2.3 Metamorphic Facies and Textural Zones

Due to the extensive distribution of schist across Central Otago, many attempts were made to subdivide the schist into zones that could easily be identified in the field at a 1:50,000 scale or smaller. The concept of mapping by metamorphic zone was introduced by Turner (1935), Hutton and Turner (1936). The original zones were established through petrographic studies of psammitic, pelitic and greenschist in Otago. The schists were later grouped by metamorphic facies, mineral assemblage and recorded transition from greywacke to quartz-albite-epidote-chlorite schist. In Otago, four divisions were designated by increasing metamorphic grade (Chl. 1 to Chl. 4) and predominant mineralogical assemblages were recorded (Hutton and Turner, 1936). By the 1970's, these zones had expanded to include metamorphic facies in the zeolite, prehnite-pumpellyite to greenschist facies. The metamorphic grade in Central Otago decreases both to the NE and SW (Figure 2.4) (Brown, 1967; Kawachi, 1974).

In 1972, Bishop redefined the petrographic system into a field-based mapping system of textural zones (TZ), which were adopted in favour of metamorphic zones, to classify the monotonous grey schist in Central Otago (Bishop, 1972; Turnbull et al., 2001). The baseline for the new textural zones were based on the observed variations from medium-grained quartzofeldspathic sandstone, combined with the knowledge that different protoliths resulted in various textures within the same metamorphic grade. Turnbull et al. (2001), revised the textural zones, because recognizing protoliths, identifying deformation structures and mapping large areas in higher textural grades proved inconsistent.

Under the revised classification, each zone represents a stage in schistosity development separated by isotects, which encompass rocks with an equal development of tectonic fabric (Martin et al., 2013; Turnbull et al., 2001). The textural grade is based on describing aspects of the rock fabric: degree of development of the foliation, segregation and the grain size of metamorphic minerals - specifically, white micas. A table of revised TZ definitions and field identification methods is included in Appendix A.1. Figure 2.4 shows the mapped extent of the revised TZ and Figure 2.5 is a summary of each zone. In the semi-schist and schist TZ, rock strength decreases as foliation develops into a significant rock defect. With increasing textural grade, rock strength decreases due to the increasing mica grain size, while jointing typically occurs perpendicular to foliation.

The descriptive nature of textural zones has been used as a basic field mapping/identification tool to inform geology models. Under the new revised textural zones, many previously mapped areas along the Caples Rakaia boundary that were mapped as TZ IIB-TZ IV have been revised, such as segments of the Remarkables that had a pelitic protoliths mapped as TZ IV are now TZIII. (Mortimer, 2000; Turnbull et al., 2001).

The schist along Queenstown Hill is foliated, veined by quartz and metamorphosed to the chlorite/chlorite2 zone of the greenschist facies and has been mapped as textural zones III and IV (Figure 2.6). Textural and metamorphic grade increases from TZ III in the west to IV at the terrane boundary. The rock properties associated with TZ III and IV are highly variable and the rocks are strongly anisotropic (Turnbull, 2000a).

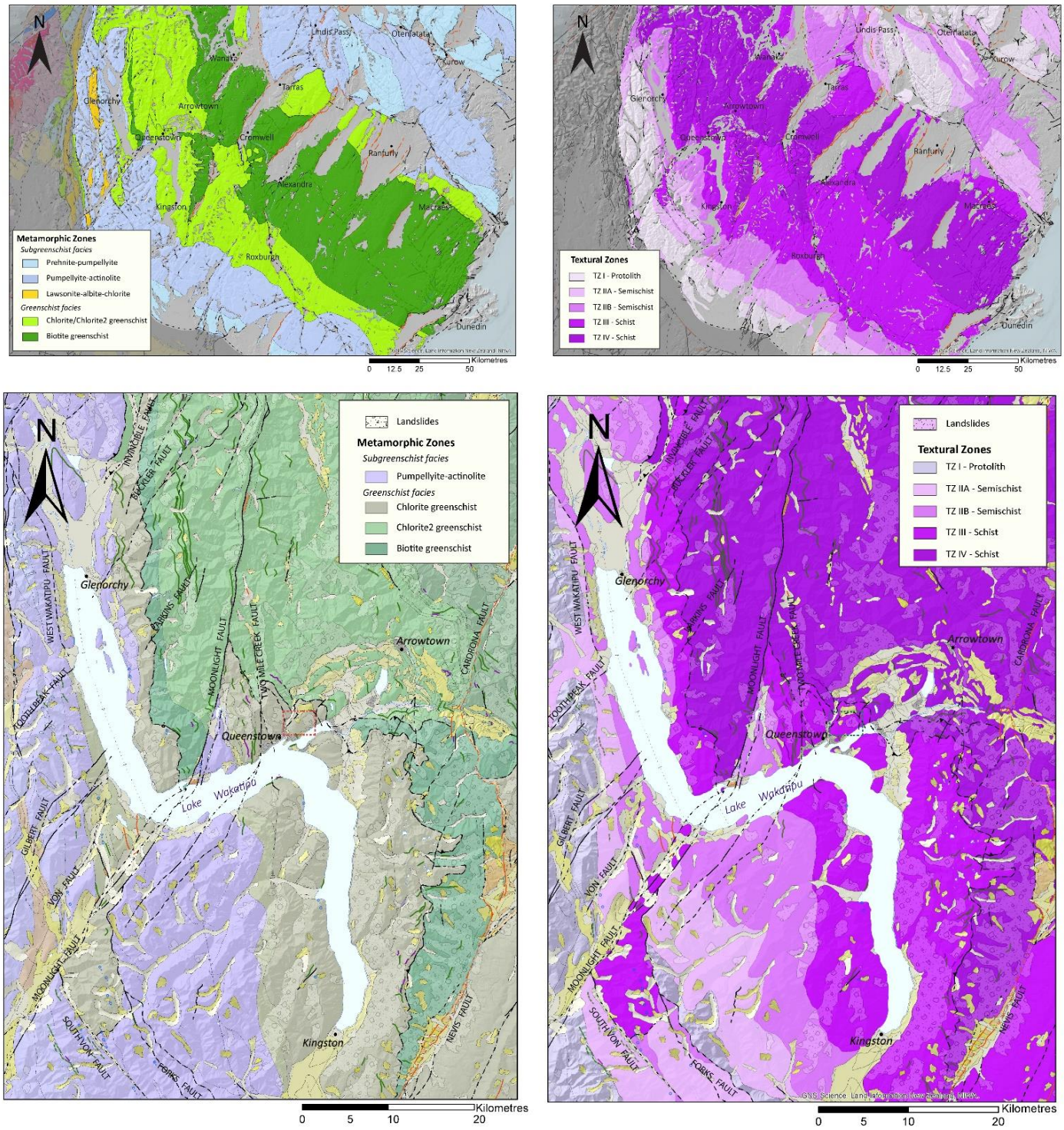

Figure 2.4:Distribution of Metamorphic Zones and Textural Zones across Central Otago and in the Queenstown area. Redrawn from Turnbull (2000) and GNS Webmap (2019).

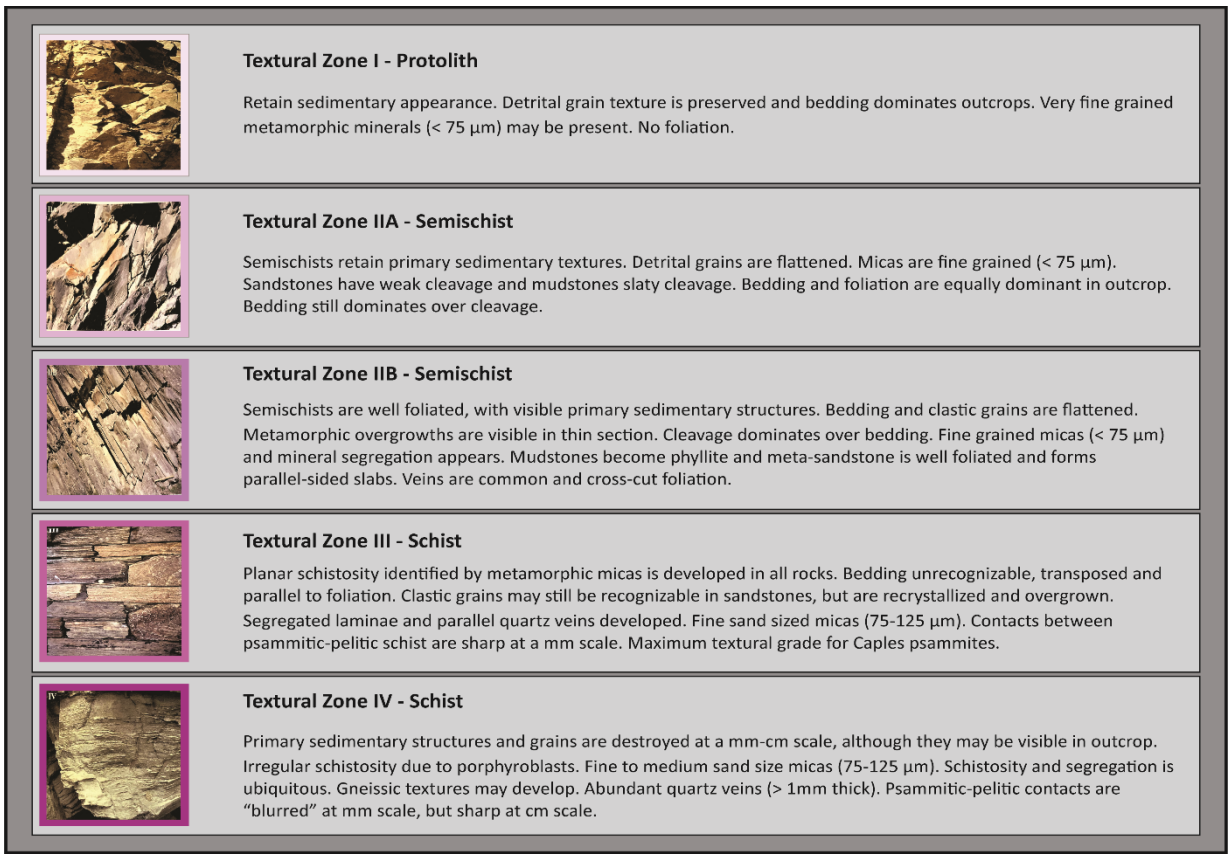

Figure 2.5: Summary of the revised textural zones (Turnbull et al., 2001).

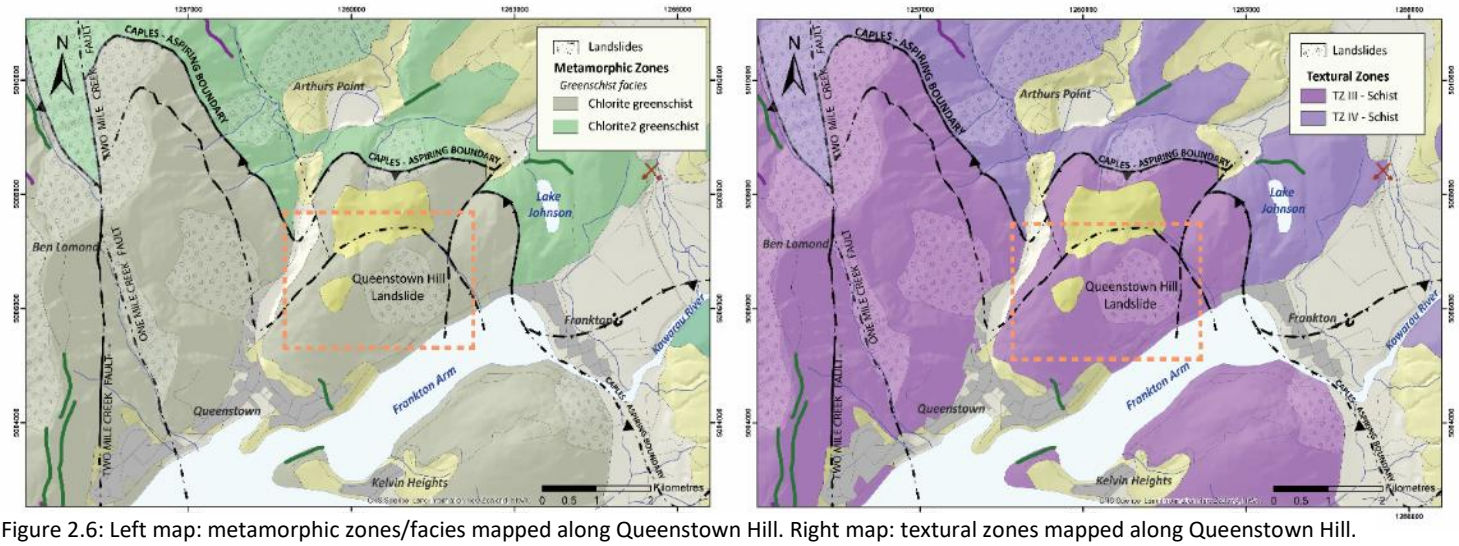

Figure 2.6: Left map: metamorphic zones/facies mapped along Queenstown Hill. Right map: textural zones mapped along Queenstown Hill. The study area is shown in the orange dashed box. Maps redrawn from GNS Webmap (GNS Science, 2018; Turnbull, 2000a).

2.4 Methodology

2.4.1 Field Investigation

The focus of the geological mapping was to record physical descriptions and structural measurements (foliation, joints, and discontinuities) of outcropping material (within the landslide body and outside), to identify lithological variations in the field and to establish structural domains within the Queenstown Hill Landslide Three field campaigns were undertaken to provide detailed descriptions of the bedrock material within the Queenstown Hill Landslide. Preliminary field investigations determined study feasibility, subsequently followed by detailed mapping and geological data collection in order to produce a series of maps and cross sections for an engineering geology model of the landslide.

2.4.2 Boreholes

Four 25 m, vertical boreholes were drilled into the lower half of the Queenstown Hill landslide (Figure 2.7) by Ground Consulting Limited for preliminary geotechnical investigations for subdivision expansion along Goldfield Heights. A rotary drill was used during several campaigns between April and May 2019, to obtain 63 mm diameter core (HQ). The core was logged independently by both myself and GCL. The logs presented in this thesis are my own. Information captured in the borehole logs include:

- A lithological description of the core: colour, mineralogy visible in hand sample, thickness, spacing, orientation and formation name.
- Weathering, hardness and moisture. These were determined based on the New Zealand Geotechnical Society (NZGS) field guide.
- RQD: RQD was calculated between each marker in the core box.
- Rock structures: defects, joints and foliation. Attitude, thickness, spacing, roughness, aperture and infill of these features were described as per the NZGS field guide.
- A graphic log: illustrated in Adobe Illustrator.

Once logging was completed, samples required for testing were sealed, to retain as much of their in-situ moisture content as possible and transported back to the laboratory at the University of Canterbury for testing.

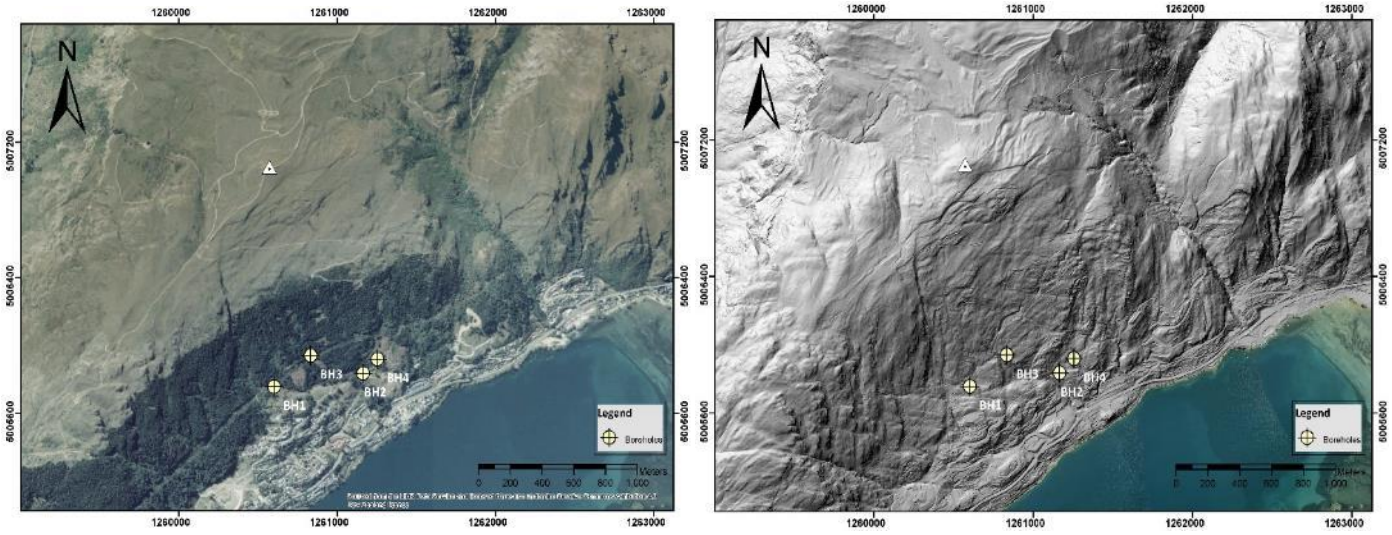

Figure 2.7: Borehole location map. Boreholes plotted on the aerial map (left) and on hillshade lidar (right) (LINZ,2019).

2.4.3 Petrography

60 thin sections were made using representative samples, cut in various orientations to foliation, from each core sample used for subsequent strength testing. The thin sections were analyzed to ascertain their mineral assemblage and textures. To avoid bias when estimating mineral percentages, a petrographic microscope with a Pelcon Point Counter were used to ascertain the mineral composition through point counting. 300 counts were selected per slide using a raster scan, at a step count of 1 mm (Higgins, 2006).

2.5 Results

2.5.1 Field Descriptions of Schist

During mapping, three distinct areas were identified by changes in colour, intensity of rock defects and rock structures such as foliation shape, attitude, thickness (Figure 2.8). The main area encompassing the Queenstown Hill Landslide and surrounding features to the north and west, consists of two predominant schist lithotypes recorded in outcrops. To the southeast of the landslide, the schist is highly deformed by foliation shears and kink banding. A laterally continuous area between ~380-400 masl, contained along the southern margin of the Queenstown Hill Landslide is very weak, fissile, and highly weathered.

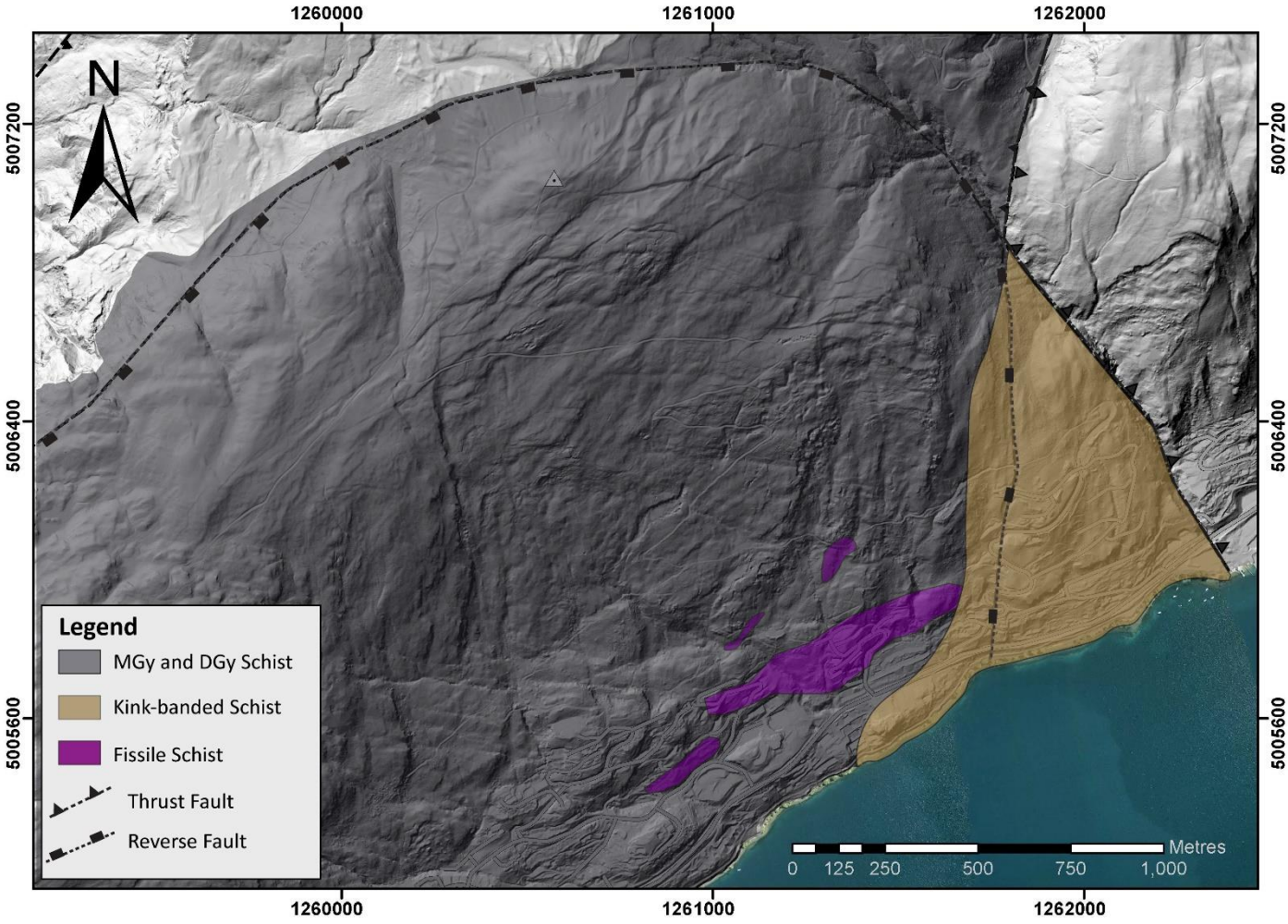

Figure 2.8: Mapped locations of the 2 main lithotypes, the kink banded area and the fissile schist across the study area. Lidar base map sourced from LINZ, 2019.

Two lithotypes were mapped across the Queenstown Hill Landslide and surrounding areas: a medium grey and a dark green-grey schist. A description of each lithotype is included in Table 2.3 and photos in Figure 2.9. In the field, the differences between the two schists can be subtle. Weathering and moss often obscure the lithotype in outcrop. Both lithotypes appear grey in the field, however in unweathered to slightly weathered outcrops mm-scale olive green and black laminae are visible giving the DGy schist its darker colour. When outcrops are moderately weathered or are highly iron-stained, the difference in foliation and smoothness of the discontinuities cause the MGy schist to be much smoother in outcrop, while the DGy has a more rough, undulating appearance. The DGy schist is also more friable in weathered outcrops than the MGy.

	Medium Grey Schist (MGy)	Dark Green-Grey Schist (DGy)
Weathering	Unweathered to moderately weathered	Slightly weathered to highly weathered
Colour	Medium Grey, homogeneous colour.	Dark grey with mm-scale dark green laminae giving it a dark green-grey appearance.
Fabric	Poorly foliated	Well foliated
Mafic content	~75-85% Mafic content	~ 65-75% Mafic content
Strength	Moderately strong to very strong	Weak to very strong
Foliation	• Poor to moderately developed, planar. Very thin laminae (<1mm). • Quartz segregations are generally 2-5mm thick but can be up to 25mm thick, spaced 15-200mm apart. In some outcrops, segregations are laterally continuous and occur in 0.5- 1.0m bands of closely spaced (10mm), thick (10 - 20mm) segregations. • Symmetric and asymmetric pinch and swell structures are common in the thicker quartz segregations. • Occasional 1-2mm thick green (chlorite/epidote?) segregations adjacent to 15-25mm thick quartz. • Foliation dips at 10°-30°	• Well developed, planar and undulating. Laminae generally 1-2mm, up to 5mm. • Quartz segregations are generally 3-7mm thick but can be up to 40mm thick, spaced 2-40mm apart. In some outcrops, segregations are laterally continuous and occur in 0.5-1.5m bands of very closely spaced (5mm), thick (10-35mm) segregations. • Symmetric and asymmetric pinch and swell structures are common throughout. • 1-3mm thick dark green (chlorite/epidote?) segregations occur throughout. • Foliation dips at 10°-40°
Quartz Veins	Quartz veins appear throughout the outcrops with various persistence (from 0.2-1.5m). Quartz veins are generally 1-5mm thick, oriented at 70°-85°.	Quartz veins, excluding laterally continuous segregations, are less frequent and less persistent (0.5-1m) than in the medium grey schist. Quartz veins are generally 1-3mm thick, oriented at 65°-70°.
Discontinuities	Joint sets are generally smooth undulating to planar, moderately wide to very widely spaced. Joint sets are commonly: • Along foliation (~20°-25°) • Very steeply inclined (65°-70°) • Sub-vertical (85°-88°)	Joint sets are generally rough stepped to smooth undulating, moderately wide to very widely spaced. Joint sets are commonly: • Along foliation (~20°-25°) • Steeply inclined (50°-60°) • Sub-vertical (85°-88°)
Other Metamorphic Features	• Symmetric, asymmetric, isoclinal, ptygmatic and refolded folds visible. • Felsic layers contain boudins • Texural Zone III	• Symmetric, asymmetric, isoclinal, sheath and refolded folds visible. • Felsic layers contain boudins • Textural Zone IV
NZGS Description	*Unweathered to moderately weathered medium grey foliated SCHIST; moderately strong to very strong; poor to moderately developed foliation, planar with thin < 1 mm laminae, laterally continuous 2-25 mm thick quartz segregations, spaced 15-200 mm, foliation dips 10°-30°; discontinuities are very steeply inclined (60°-70°) to sub-vertical (80°-88°). [Otago Schist, Textural Zone III]*	*Slightly weathered to highly weathered dark green-grey foliated SCHIST; weak to very; well-developed foliation, planar and undulating with 1-5 mm laminae, laterally continuous 3-40 mm thick quartz segregations, spaced 2-40 mm, foliation dips 10°-40°; discontinuities are very steeply inclined (50°-60°) to sub-vertical (80°-88°). [Otago Schist, Textural Zone IV]*

Table 2.3: Summary of the rock characteristics and defects recorded in the field for both schist lithotypes.

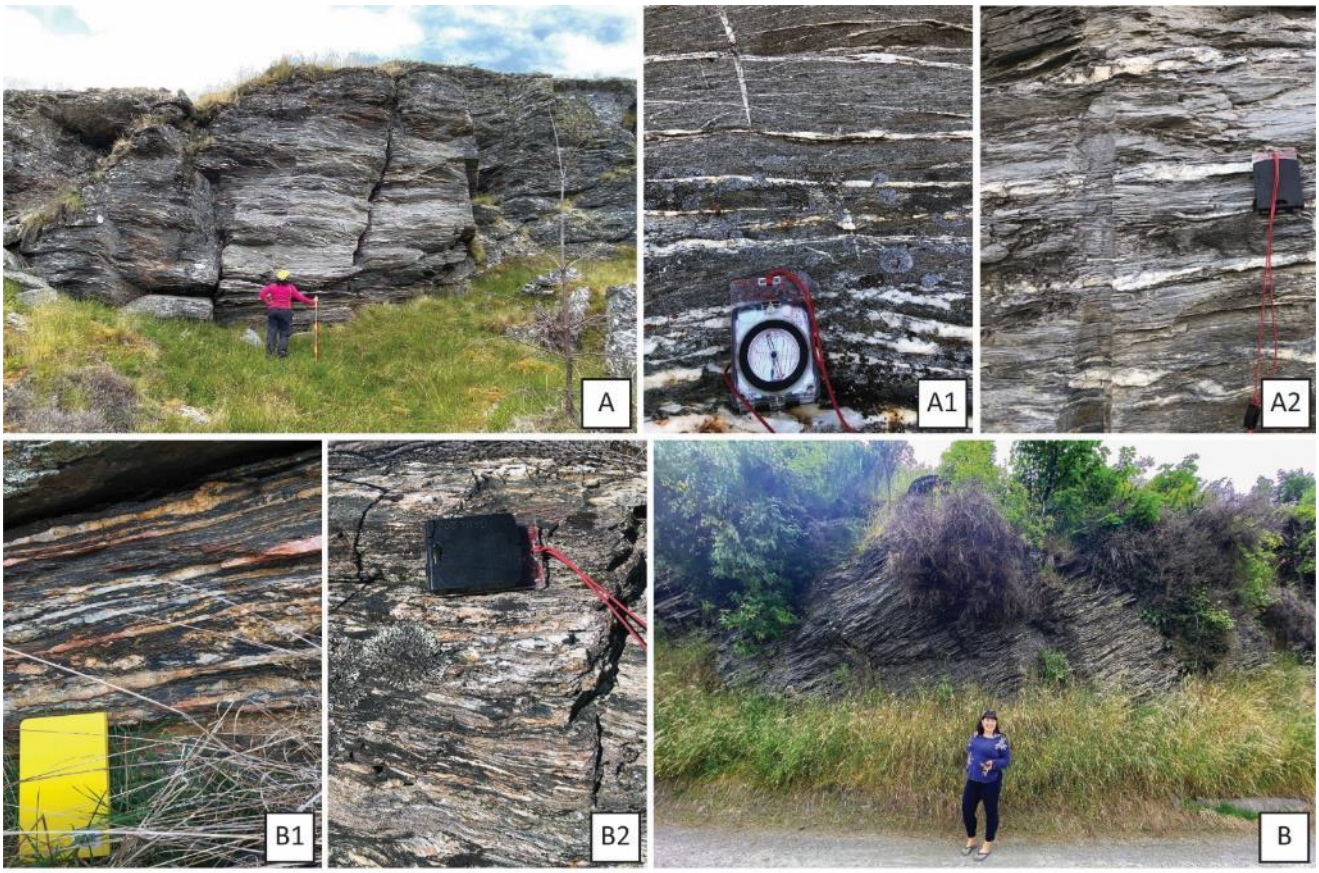

Figure 2.9: Photos of the medium grey (A, A1, A2) and dark green-grey (B, B1, B2) schist at outcrop scale. A: typical appearance of the medium grey schist in outcrop. The schist is relatively smooth, with well formed discontinuities. A1,A2) A1 was taken within the landslide. A2 is outside the landslide boundary in a subdivision road cutting - note drill hole from blasting. The thick quartz segregations are visible between the homogenous <1mm thin mafic foliations. B) typical appearance of the dark green-grey schist in outcrop. The schists surface roughness is due to preferential weathering of mafic layers in the undulating foliation. B was taken outside the landslide boundary along the Frankton Walkway. B1, B2) Both photos were taken within the landslide. The mm-cm scale undulating dark and light segregations are visible. Discontinuities are not as well developed and stepped/rough.

Seven end members were derived from the distribution of both lithotypes across the study site (Figure 2.10). Outcrops are not always exclusively represented by MGy or DGy schist. Various combinations of these lithotypes occur in the field and presumably in the subsurface. Unit thickness of the MGy and the DGy are typically 3-4 m but can extend up to 10 m. At outcrop scale, the contact between the two schists can be either sharp or gradational. Often when the contact is sharp, the DGy schist tends to be more intensely fractured and/or weathered than the MGy schist. Where the contact is gradational a 0.5-2 m interlayered sequence of both lithotypes is observed and the contact is nearly always preferentially eroded in the field.

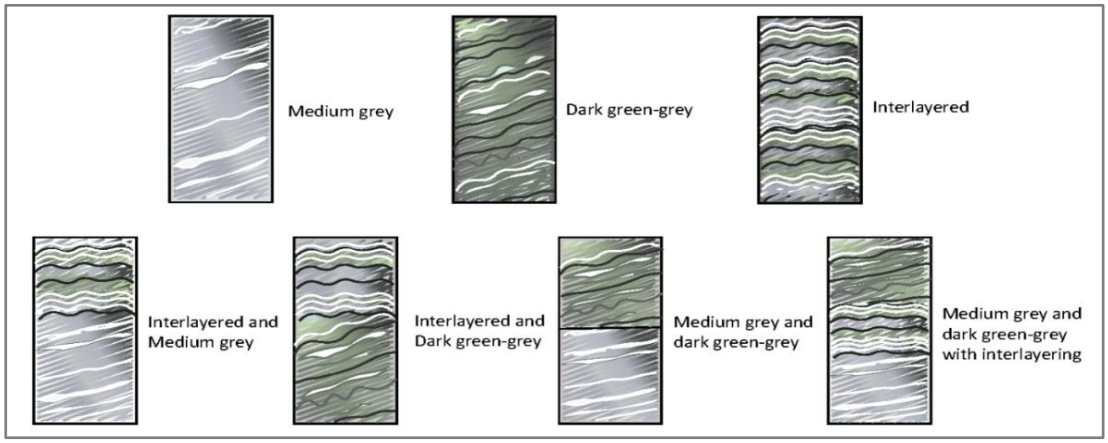

Figure 2.10: Schematic representation of the end members of the two schist lithotypes.

2.5.1.1 Kink Banded Schist

The schist outcrops recorded to the east of the landslide, between the two faults, are accessible via Middleton Rd. A description of the schist found in the subdivisions along Middleton Rd are included in Table 2.4 and annotated photographs of foliation shears along Florence Close, and kink bands along Middleton Rd can be found in Figure 2.11 and Figure 2.12.

The schist in this area is deformed and fissile in comparison to the schist located within the Queenstown Hill Landslide and to the north and west of the landslide. The southern end of the subdivision, towards SH6, are a series of grassed over mounds with few outcrops. However, as you progress further up the subdivision to the north, schist exposures increase in road cuttings up the hill. The outcrops along Middleton Road are moist, especially at the lower end of the subdivision towards SH6. No obvious seepage was recorded, but both summer and winter campaigns noted moist and wet outcrops in this area. Due to the fissile nature of the schist along Middleton Rd, stabilization measures (i.e shotcrete and schist bricks) have been implemented along the road cuttings due to raveling and localized failures.

	Kink banded Schist
Weathering	Unweathered to slightly weathered
Colour	Medium grey
Fabric	Well foliated, crenulation cleavage and kink banded.
Mafic content	~75-85% Mafic content
Strength	Very weak to moderately strong
Foliation	• Well developed, planar, undulating and kink banded. Laminae thickness is variable, from < 1 mm to 1-3 mm. • Quartz segregations are generally 3-7 mm thick but can be up to 20 mm thick, spacing is variable between 2-100 mm apart. Segregations are laterally continuous. • Symmetric and asymmetric pinch and swell structures are common throughout. • 100-300 mm lenses of “greenschist” occur sporadically throughout the outcrops. • Foliation dips at 25°-35°
Quartz Veins	Quartz veins are infrequent and generally not persistent (0.2-0.5 m). Most are 1-3 mm thick, oriented at 60°-70°, or occur en echelon. A rare number of veins are 10-40 mm thick and cross-cut foliation at 30°-40°.
Discontinuities	• Foliation shears are common throughout the outcrops, oriented NE-SW. Shears observed in the field are part of the granular end member and range in thickness from 0.06-1.5 m wide. The shears are both lensoidal and laterally continuous, their persistence ranges from 0.3 m segments to 2 m+ in length. Extensive raveling and localized failures were often observed within these areas. Average orientation of shears (32°/263°) Joint sets are generally smooth stepped to planar, wide to very widely spaced. Joint sets are commonly: • Steeply to Very steeply inclined (60°-73°) • Sub-vertical (85°-88°)
Other Metamorphic Features	• Symmetric, asymmetric, isoclinal, sheath and refolded folds visible. • Prominent kink banded deformation at outcrop scale. • Crenulation cleavage • Textural zone IIB or III.
NZGS Description	*Unweathered to slightly weathered medium grey foliated SCHIST; very weak to moderately strong; well-developed foliation, kink banded with < 1 up to 3 mm laminae, lensoidal 3-7 mm thick quartz segregations, pinch and swell structures common, foliation dips 25°-35°; discontinuities are widely spaced, moderately inclined (along foliation) to steep (60°-73°) to sub-vertical (85°-88°) with narrow to moderately wide apertures, sometimes infilled with sand to gravel sized schist fragments; moist to wet, seepage common. [Otago Schist, Textural Zone IIB or III].*

Table 2.4: Summary of the rock characteristics and defects recorded in the kink banded area along Middleton Rd.

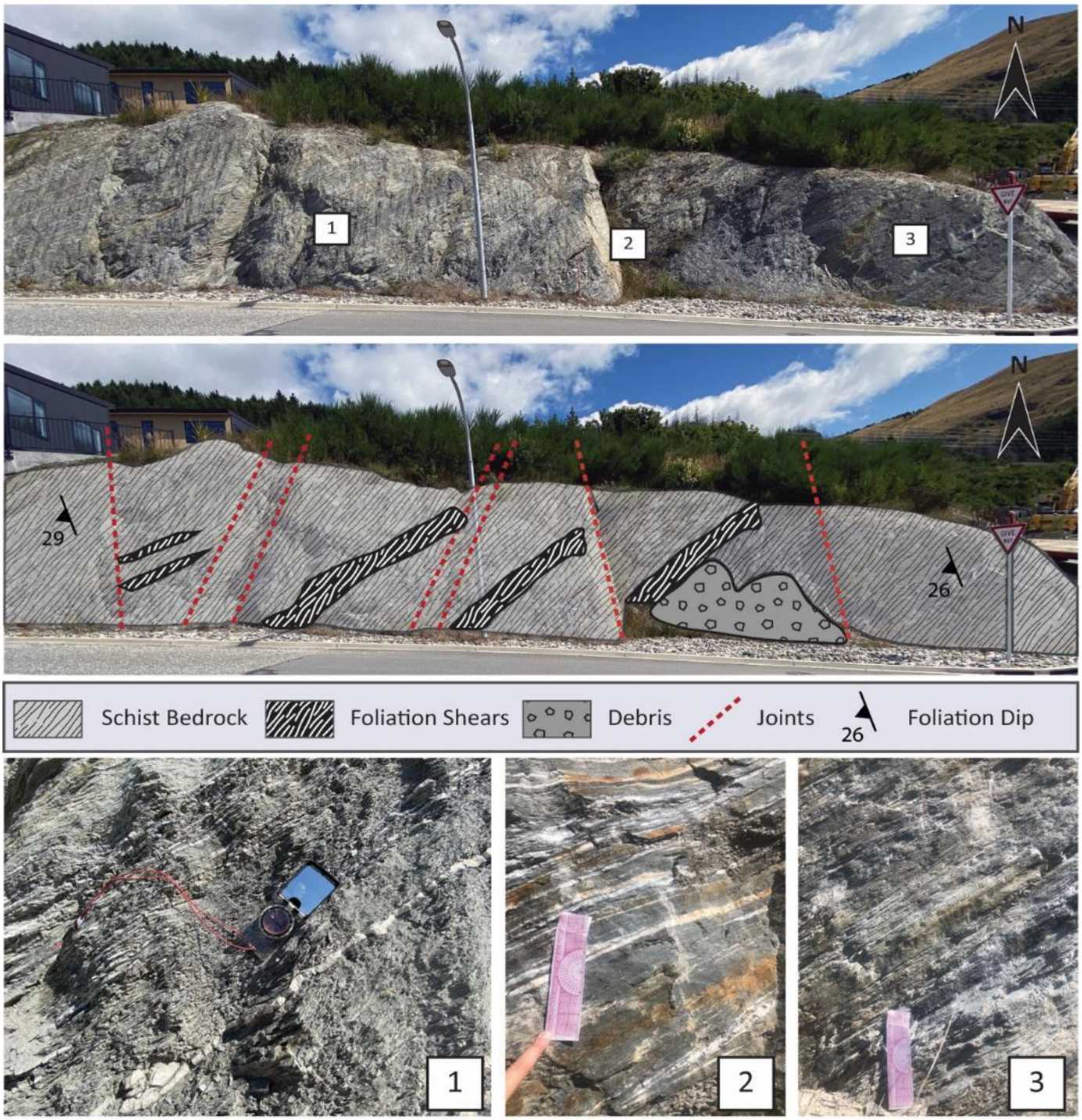

Figure 2.11: Foliation shears recorded in the road cutting along Florence Close. The schist is UW-SW with a series of NE-SW trending foliation shears (32°/263°) and three joint sets. A small debris talus at the base of the cutting is caused by ravelling of shears on the east end. Photos 1,2 and 3 highlight the variability of the rock quality over a short distance.
1) Close up photo of foliation shears. 2) UW-SW, strong schist along the face of a joint set. 3) UW-SW, moderately strong schist with small kink banded deformation and minor crenulation cleavage.

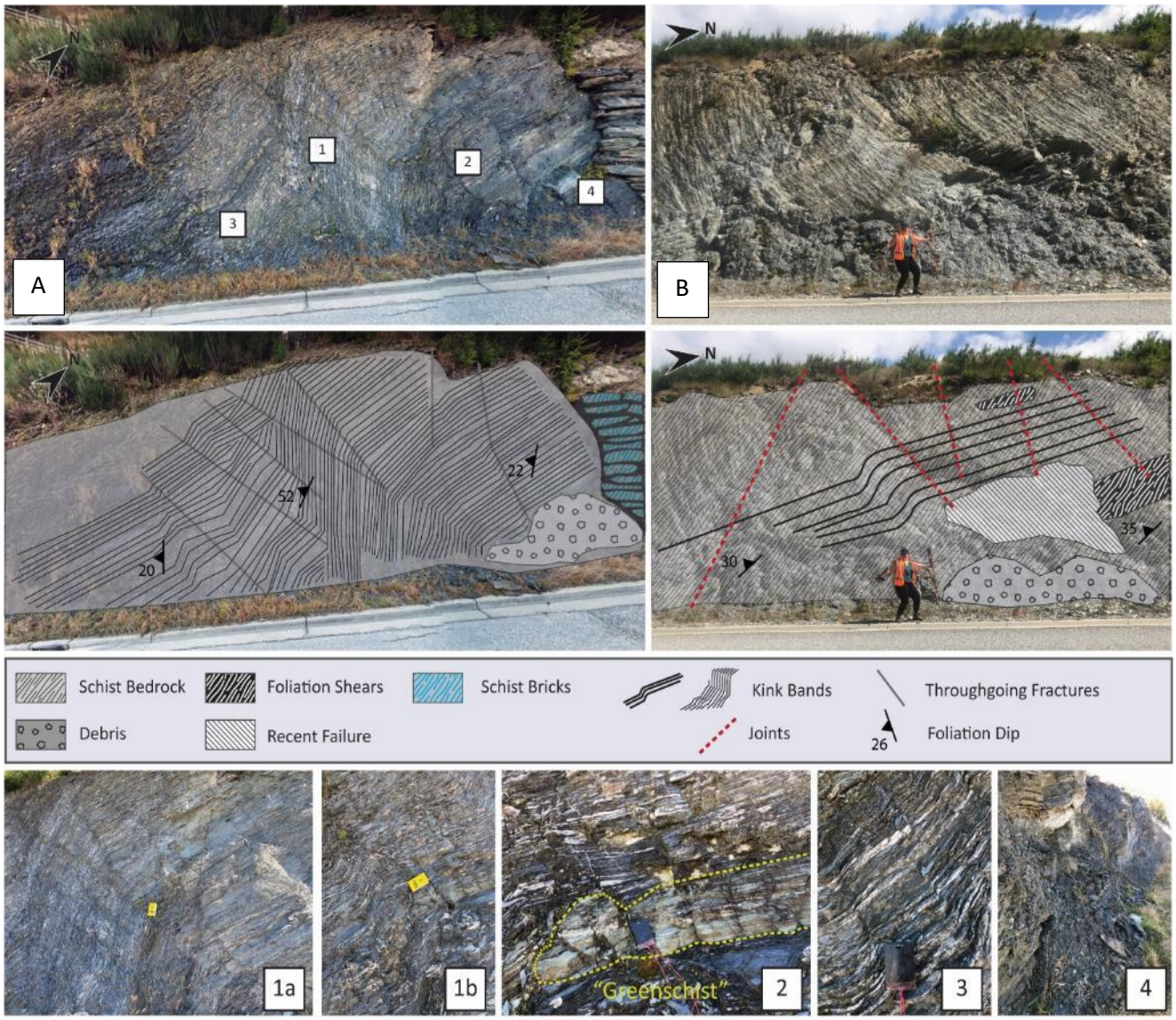

Figure 2.12: Kink bands in road cuttings along Middleton Road. Photos of road cuttings A and B show kink banding at outcrop scale. The series of throughgoing fractures (light grey lines where kink banding changes directions) in the rock mass at outcrop A hosts a series of vertical shears between closely spaced (< 50 mm) fractures. There is a measurable change in orientation of the foliation across the outcrop. Schist bricks were laid in similar orientations to joint sets measured in road cuttings. Shears and kink bands are visible in photos 1a and 1b. Crenulation cleavage and "greenschist" are visible at outcrop scale (Photo 1b, 2, 3) Ravelling and localized failures in proximity to intersection of throughgoing fractures and shears are common (Outcrop B and Photo 4).

2.5.1.2 Fissile Schist

The schist outcropping along Potters Hill Drive and Goldrush Way is very weak and fissile. The schist can easily be peeled by hand. A description of the outcropping material is included in Table 2.5 and annotated photographs can be found in Figure 2.13. The fissile schist is laterally continuous, but it is hard to determine its exact extent due to cross cutting drainage and subdivision development. Similar to the outcrops along Middleton Road, the schist in road cuttings is moist. No obvious seepage was recorded, but both summer and winter campaigns noted moist and wet outcrops in this area. Due to the fissile nature of the schist in these subdivisions, stabilization measures (i.e shotcrete, rock bolts, and mesh) have been implemented along road cuttings and in cut back slopes.

	Fissile Schist
Weathering	Moderately weathered to highly weathered
Colour	Grey brown to orange brown
Fabric	Well foliated
Mafic content	~75-90% Mafic content
Strength	Extremely weak to weak
Foliation	• Well-developed and undulating. Laminae thickness is variable, from < 1 mm to 1-3 mm. • Quartz segregations are difficult to see because of peeling material but are generally 1-3 mm thick, spacing is variable between 2-100 mm apart. Segregations are laterally continuous and lensoidal. • Symmetric and asymmetric pinch and swell structures are common throughout. • Foliation dip was difficult to ascertain due to the fissile nature of the material. (~20°-30°/172°-188°)
Quartz Veins	Quartz veins are rare and generally not persistent (0.2-0.5 m). The occasional vein is 1-2 mm thick, oriented at 60°-70°.
Discontinuities	Joint sets are generally smooth stepped to planar, wide to very widely spaced. Joint sets are commonly: • Steeply inclined (35°-40°) • Very steeply inclined (70°-75°)
Other Metamorphic Features	• Symmetric, asymmetric, isoclinal folds visible in moderately weathered material. • Possible crenulation cleavage. • Textural Zone III or IV
NZGS Description	*Moderately to highly weathered grey-brown to orange-brown foliated SCHIST; extremely weak to weak; well-developed foliation, undulating and/or kink banded with < 1 up to 3 mm laminae, laterally continuous and lensoidal 1-3 mm thick quartz segregations, spaced 2-100 mm, pinch and swell structures common, foliation dips 20°-30°; discontinuities are extremely closely to very closely spaced, moderately inclined (along foliation) to sub-vertical (80°-88°) with narrow to moderately wide apertures infilled with sand to gravel sized schist fragments; moist to wet, seepage common. [Otago Schist, Textural Zone IV].*

Table 2.5: Summary of the rock characteristics and defects recorded in the fissile areas along Goldrush Way and Potters Hill Drive.

Figure 2.13: Weak fissile schist at outcrop scale. Top photo shows an outcrop with a MW schist block in the centre surrounded by MW-HW (orange-brown) schist. Two joint sets are still visible across the outcrop. Remedial measures such as shotcrete are commonly used. A) Unit thickness measured up to 8 m. B) Close up photo of the weak and friable nature of the schist. C) Examples of remedial measures used in road cuttings and cut back slopes. Rock bolts, shotcrete and mesh were seen.

2.5.2 Borehole and Petrographic Descriptions

A summary log for each drillhole is presented below. Detailed logs were created on site and photos were taken of each borehole. Full detailed logs and accompanying photos are included in Appendix A.2 and A.3. Lithotypes, weathering, mineralogy and rock defects are presented after the summary logs.

Summary Log of Drill Hole

Project: MSc Thesis - Schist Characterization
Address: Queenstown Hill Landslide
Logged by: L. Gnesko
Date Drilled: April 15-16, 2019
Date Logged: April 29, 2019

Coordinate System: NZTM2000
Coordinates: 1260602.934, 5005756.898
Elevation: 499.266m (a.s.l)
Total meterage: 0.0 - 25.0m
Total Core Recovery:

Borehole ID: BH1
Drilling Method: Rotary Drilling
Core Diameter: 63mm
Angle from horizontal: 90°
Sheet No.: 1 of 1

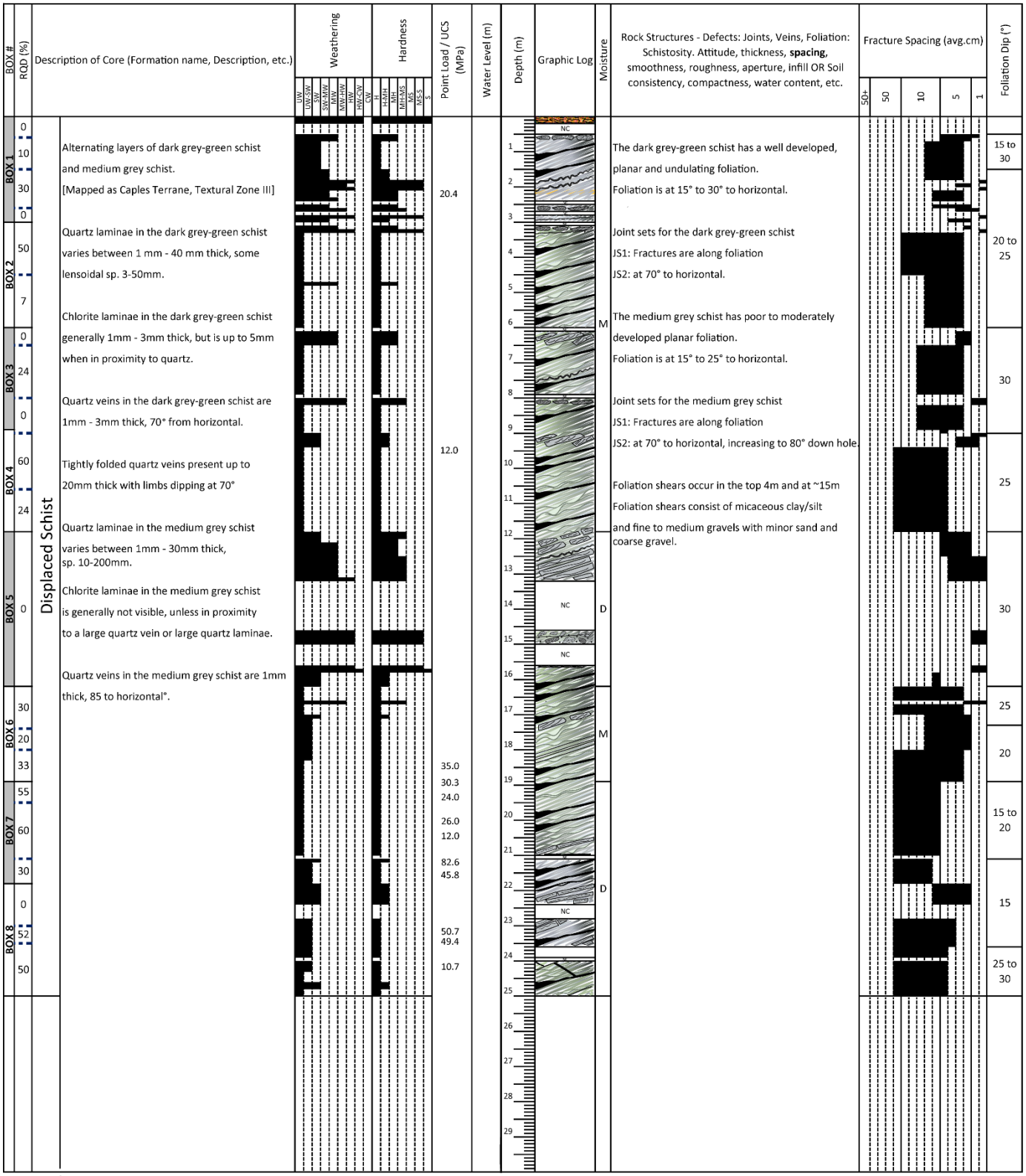

Legend

UW-MW, foliated dark grey-green SCHIST; strong; foliation dips 15-30° to horizontal, well developed, planar and undulating. Joints are steep to sub-vertically inclined and moderately wide spaced. [Mapped as Caples Terrane, Textural Zone 3 Schist]

UW-MW, foliated medium grey SCHIST; strong; foliation dips 15-25° to horizontal, poorly to moderately developed, planar. Joints are steep to sub-vertically inclined and moderately wide spaced. [Mapped as Caples Terrane, Textural Zone 3 Schist]

Clayey SILT with vf sand and rootlets; orange-brown. Soft, moist, moderate plasticity, poorly graded. Grades into angular, thin coarse gravel schist fragments. [TOPSOIL]

Fine to coarse GRAVEL schist fragments with minor sand and traces of clay and silt; light sparkly grey. Very loosely packed, gap graded, angular to sub-rounded, no plasticity.

Fracture or Joint
Foliation Shear
Cobble sized schist fragments
NC Core loss/No Recovery

Weathering
UW: Unweathered
SW: Slightly Weathered
MW: Moderately Weathered
HW: Highly Weathered
CW: Completely Weathered

Hardness
H: Hard
MH: Moderately Hard
MS: Moderately Soft
S: Soft

Summary Log of Drill Hole

Project: MSc Thesis - Schist Characterization
Address: Queenstown Hill Landslide
Logged by: L. Gnesko
Date Drilled: April 17, 2019
Date Logged: April 30, 2019

Coordinate System: NZTM2000
Coordinates: 1261164.975, 5005835.904
Elevation: 427.832m (a.s.l)
Total meterage: 0.0 - 26.5m
Total Core Recovery:

Borehole ID: BH2
Drilling Method: Rotary Drilling
Core Diameter: 63mm
Angle from horizontal: 90°
Sheet No.: 1 of 1

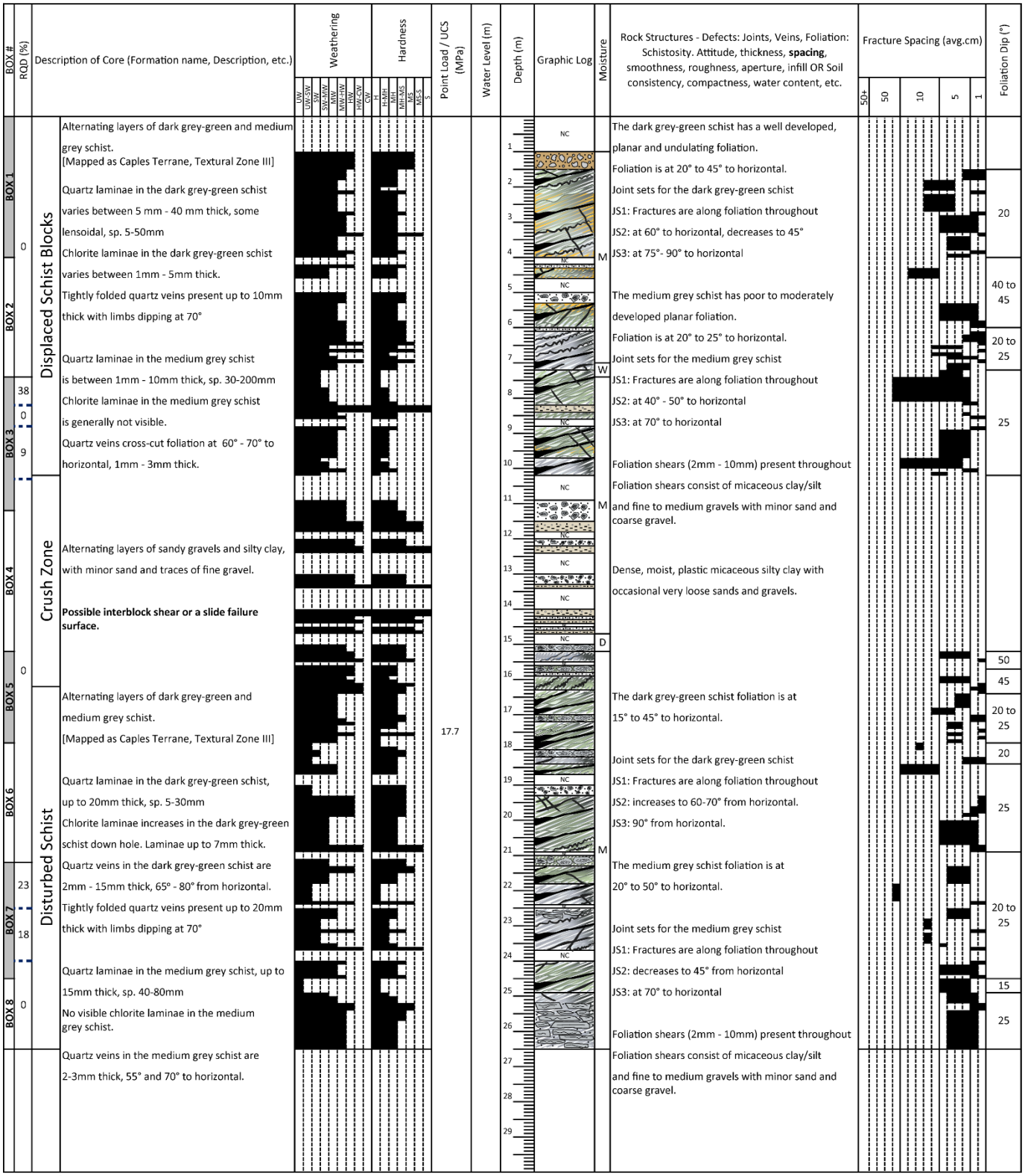

Legend

UW-MW, foliated dark grey-green SCHIST; strong; foliation dips 15-50° to horizontal, well developed, planar and undulating. Joints are steep to sub-vertically inclined and moderately wide spaced. [Mapped as Caples Terrane, Textural Zone 3 Schist]

UW-MW, foliated medium grey SCHIST; strong; foliation dips 20-25° to horizontal, poorly to moderately developed, planar. Joints are steep to sub-vertically inclined and moderately wide spaced. [Mapped as Caples Terrane, Textural Zone 3 Schist]

Sandy fine to coarse GRAVEL with minor organics, silt/clay; grey-brown.

Sandy SILTY CLAY with minor gravels; taupe. Medium density, firm, high plasticity.

Fine to coarse GRAVEL with minor sand; silver.

Sandy fine to coarse GRAVEL; medium grey.

Fracture or Joint

Iron Staining/ Weathering

Foliation Shear

Cobble sized schist fragments

NC Core loss/No Recovery

Weathering
UW: Unweathered
SW: Slightly Weathered
MW: Moderately Weathered
HW: Highly Weathered
CW: Completely Weathered

Hardness
H: Hard
MH: Moderately Hard
MS: Moderately Soft
S: Soft

Summary Log of Drill Hole

Project: MSc Thesis - Schist Characterization
Address: Queenstown Hill Landslide
Logged by: L. Gnesko
Date Drilled: April 18-29, 2019
Date Logged: May 1, 2019

Coordinate System: NZTM2000
Coordinates: 1260833.914, 5005941.35
Elevation: 517.732m (a.s.l)
Total meterage: 0.0 - 25.0m
Total Core Recovery:

Borehole ID: BH3
Drilling Method: Rotary Drilling
Core Diameter: 63mm
Angle from horizontal: 90°
Sheet No.: 1 of 1

BOX #	RQD (%)	Description of Core (Formation name, Description, etc.)	Weathering	Hardness	Point Load / UCS (MPa)	Water Level (m)	Depth (m)	Graphic Log	Moisture	Rock Structures - Defects: Joints, Veins, Foliation: Schistosity. Attitude, thickness, **spacing**, smoothness, roughness, aperture, infill OR Soil consistency, compactness, water content, etc.	Fracture Spacing (avg.cm)	Foliation Dip (°)
BOX 1	30	Displaced Schist Alternating layers of dark grey-green and medium grey schist. [Mapped as Caples Terrane, Textural Zone III]	UW, UW-SW, SW, SW-MW, MW, MW-HW, HW, HW-CW, CW	H, H-MH, MH, MH-MS, MS, MS-S, S	38.3		1			The dark grey-green schist has a well developed, planar and undulating foliation. Foliation is at 15° to 25° to horizontal.	50+, 50, 10, 5, 1	15
BOX 2	0 52 0	Quartz laminae in the dark grey-green schist varies between 4mm - 35mm thick, some lensoidal, sp. 4-70mm. Chlorite laminae in the dark grey-green schist varies between 1mm - 2mm thick.			52.6 58.3		2 3 4 5			Joint sets for the dark grey-green schist JS1: Fractures are along foliation JS2: at 60-65° to horizontal, decreases to 45-55° down hole.		20
BOX 3	58 27 55	Quartz laminae in the medium grey schist varies between 1mm - 25mm thick, some lensoidal, sp. 15-150mm. Chlorite laminae in the medium grey schist is generally not visible, unless it is adjacent to thick quartz laminae.			53.8		6 7 8 9	D NC NC		The medium grey schist has poor to moderately developed planar foliation. Foliation is at 15° to 20° to horizontal. Joint sets for the medium grey schist JS1: Fractures are along foliation JS2: at 45-50° to horizontal developed planar foliation.		25
BOX 4	86 52	Occasional quartz veins cross-cut foliation at 70° to horizontal in both dark grey-green and medium grey schist. Quartz veins up to 10mm thick.			38.4 41.3 38.9		10 11 12			Foliation shears (2mm - 20mm) present throughout In the top 10m, foliation shears consist of fine to coarse gravel schist fragments. Starting at 10m, shears consist of silty/clayey GRAVEL with sand.		20 to 25 15
BOX 5	68 95	Tightly folded quartz veins present up to 10mm th with limbs dipping at 70°			44.5		13 14 15					15 to 20
BOX 6	24 35	starting at 18.0m _ _					16 17 18	M				20
BOX 7	0 33 0	Iron staining and weathering increases down hole.			24.7 27.4 45.5		19 20 21	NC				20 to 25
BOX 8	55 29 9 0				36.4 38.4		22 23 24 25	M NC				
							26 27 28 29					

Legend

- UW-MW, foliated dark grey-green SCHIST; strong; foliation dips 10-30° to horizontal, well developed, planar and undulating. Joints are steep to sub-vertically inclined and moderately wide spaced. [Mapped as Caples Terrane, Textural Zone 3 Schist]
- UW-MW, foliated medium grey SCHIST; strong; foliation dips 10-30° to horizontal, poorly to moderately developed, planar. Joints are steep to sub-vertically inclined and moderately wide spaced. [Mapped as Caples Terrane, Textural Zone 3 Schist]
- Fracture or Joint
- Iron Staining/ Weathering
- Foliation Shear
- Cobble sized schist fragments
- Gravel sized schist fragments
- NC — Core loss/No Recovery

Weathering
UW: Unweathered
SW: Slightly Weathered
MW: Moderately Weathered
HW: Highly Weathered
CW: Completely Weathered

Hardness
H: Hard
MH: Moderately Hard
MS: Moderately Soft
S: Soft

Summary Log of Drill Hole

Project: MSc Thesis - Schist Characterization
Address: Queenstown Hill Landslide
Logged by: L. Gnesko
Date Drilled: May 23-24, 2019
Date Logged: June 19, 2019

Coordinate System: NZTM2000
Coordinates: 1261255.897, 5005919.899
Elevation: 432m (a.s.l)
Total meterage: 0.0 - 25.0m
Total Core Recovery:

Borehole ID: BH4
Drilling Method: Rotary Drilling
Core Diameter: 63mm
Angle from horizontal: 90°
Sheet No.: 1 of 1

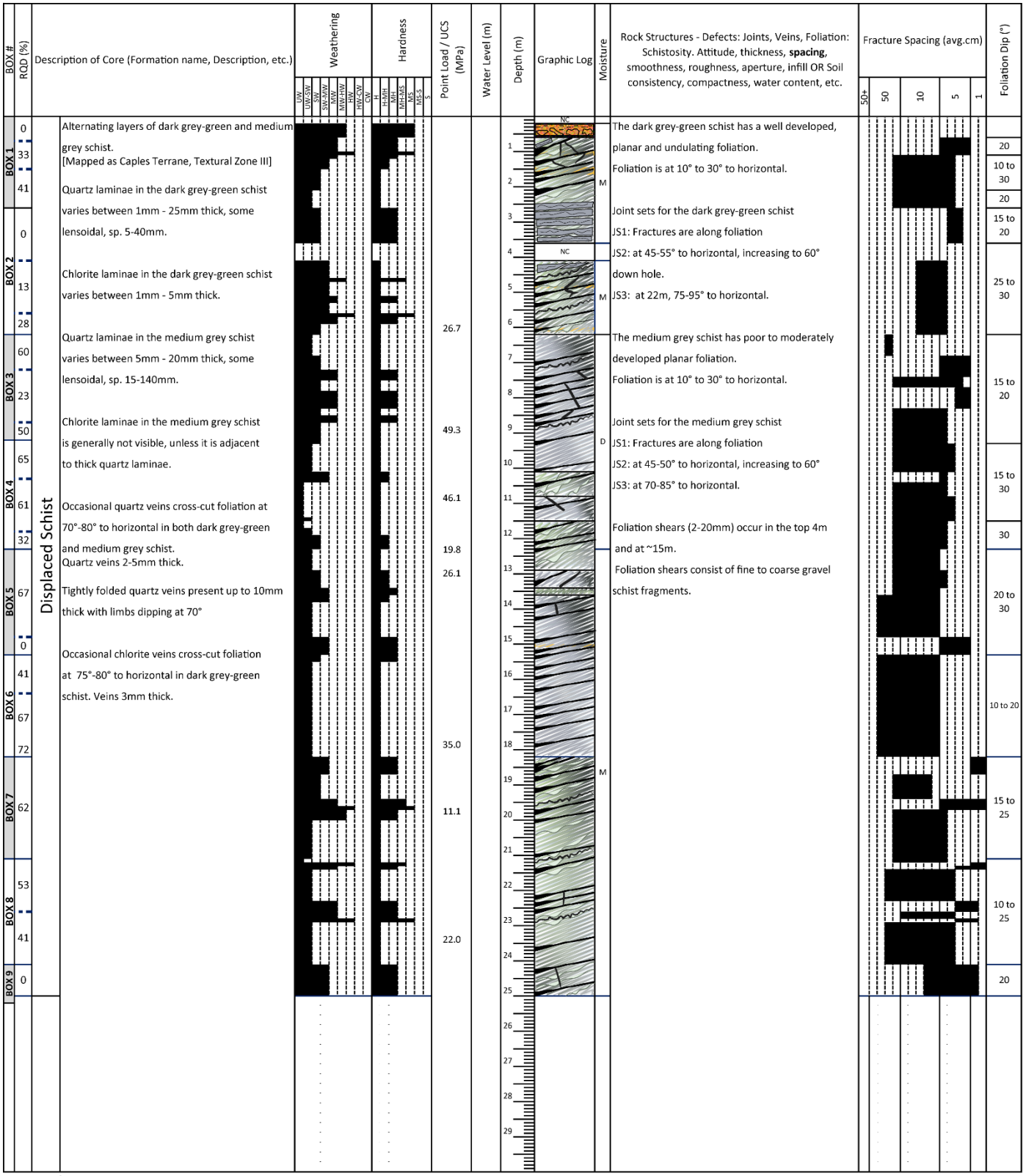

Legend

UW-MW, foliated dark grey-green SCHIST; strong; foliation dips 15-30° to horizontal, well developed, planar and undulating. Joints are steep to sub-vertically inclined and moderately wide spaced.
[Mapped as Caples Terrane, Textural Zone 3 Schist]

UW-MW, foliated medium grey SCHIST; strong; foliation dips 15-25° to horizontal, poorly to moderately developed, planar. Joints are steep to sub-vertically inclined and moderately wide spaced.
[Mapped as Caples Terrane, Textural Zone 3 Schist]

Sandy fine to coarse GRAVEL with silt/clay and rootlets; orange-brown. Soft, moist, no plasticity, well graded. Grades into subrounded, coarse gravel schist fragments.

Fracture or Joint
Iron Staining/ Weathering
Foliation Shear
Cobble sized schist fragments
NC Core loss/No Recovery

Weathering
UW: Unweathered
SW: Slightly Weathered
MW: Moderately Weathered
HW: Highly Weathered
CW: Completely Weathered

Hardness
H: Hard
MH: Moderately Hard
MS: Moderately Soft
S: Soft

2.5.2.1 Lithotypes

Two schist lithotypes, similar to the ones recorded from field descriptions, were identified in all four boreholes during logging: a medium grey schist (MGy) and a dark green-grey schist (DGy) (Figure 2.14). Both schists are predominantly grey in colour, however the contrasting foliation and mineral segregation give one a homogenous medium grey appearance, while the other is darker with olive green and black segregations. Based on their visual appearance, the MGy schist was estimated to be ~80-85% mafic, and the DGy 60-75%.

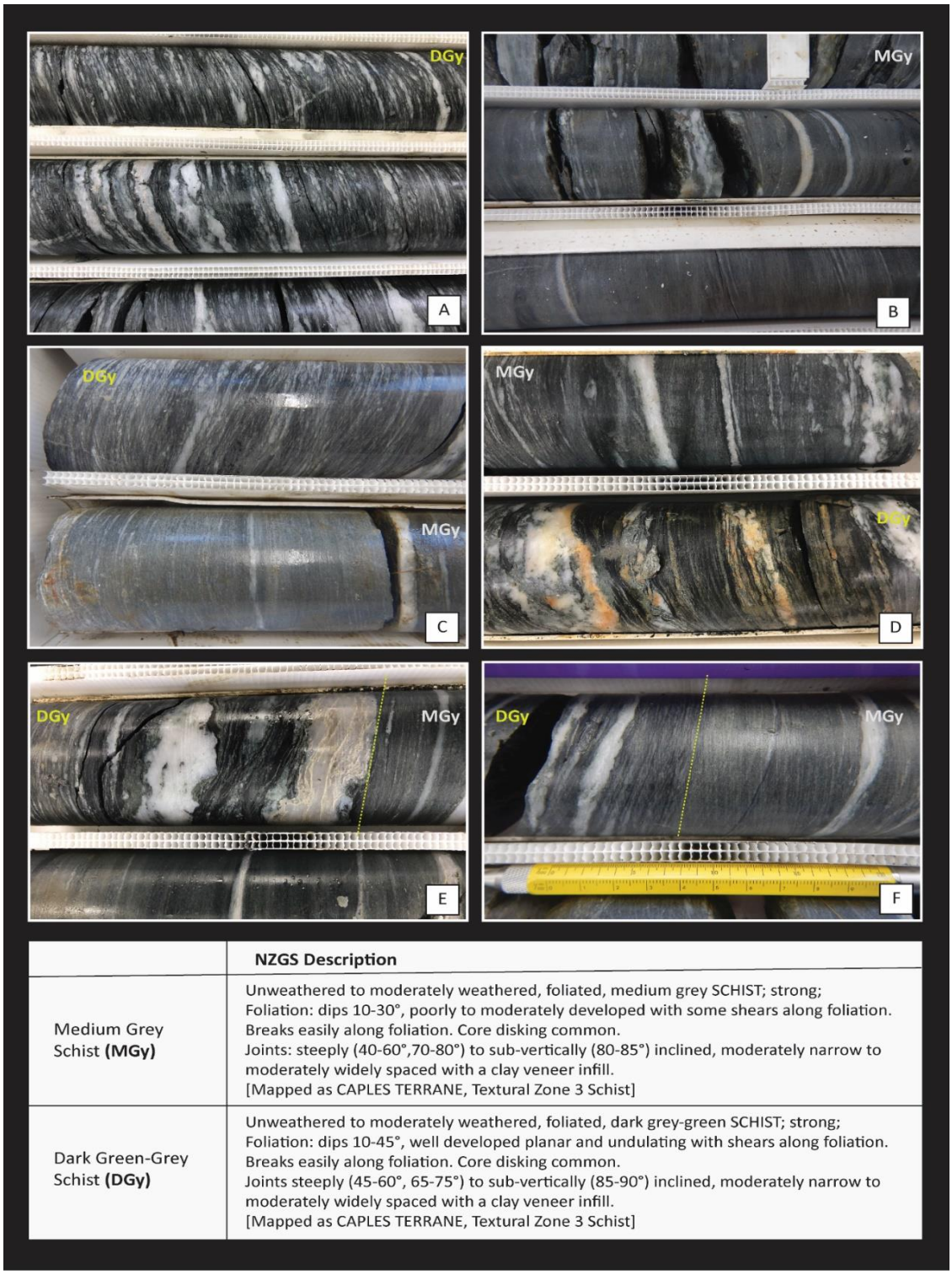

	NZGS Description
Medium Grey Schist **(MGy)**	Unweathered to moderately weathered, foliated, medium grey SCHIST; strong; Foliation: dips 10-30°, poorly to moderately developed with some shears along foliation. Breaks easily along foliation. Core disking common. Joints: steeply (40-60°,70-80°) to sub-vertically (80-85°) inclined, moderately narrow to moderately widely spaced with a clay veneer infill. [Mapped as CAPLES TERRANE, Textural Zone 3 Schist]
Dark Green-Grey Schist **(DGy)**	Unweathered to moderately weathered, foliated, dark grey-green SCHIST; strong; Foliation: dips 10-45°, well developed planar and undulating with shears along foliation. Breaks easily along foliation. Core disking common. Joints steeply (45-60°, 65-75°) to sub-vertically (85-90°) inclined, moderately narrow to moderately widely spaced with a clay veneer infill. [Mapped as CAPLES TERRANE, Textural Zone 3 Schist]

Figure 2.14: Two lithotypes identified during borehole logging. A) DGy core with well-developed undulating foliation and quartz segregation throughout. B) MGy core with poorly developed planar foliation, < 1mm. C and D show a gradational change and interlayered lithotypes. E and F are sharp contacts between both lithotypes.

Average measured foliation dip in the MGy schist is 15°-20° from horizontal and occasionally increases up to 30°. Foliation is poorly developed, < 1mm thick and planar with ~5-20 mm thick quartz-rich segregations oriented sub-parallel to foliation, spaced ~5-100 mm apart throughout. Occasionally, 1-2 mm thick green chlorite and plagioclase laminae were observed adjacent to and/or within the quartz-rich layers and <1 mm thick black laminae within the grey homogeneous layers (Figure 2.15).

Foliation orientation in the DGy is more variable than in the MGy. The average measured dip is 20°-25° from horizontal, however the dip ranges from 10-50° across all four boreholes. Foliation is well developed, 1-5 mm thick, undulating with ~5-40 mm thick quartz-rich segregations oriented parallel to foliation, spaced ~1-70 mm apart. 1-2 mm thick chlorite and 1-3 mm dark mafic foliations are observed throughout, while plagioclase segregations are infrequent and occur adjacent to quartz-rich layers (Figure 2.15).

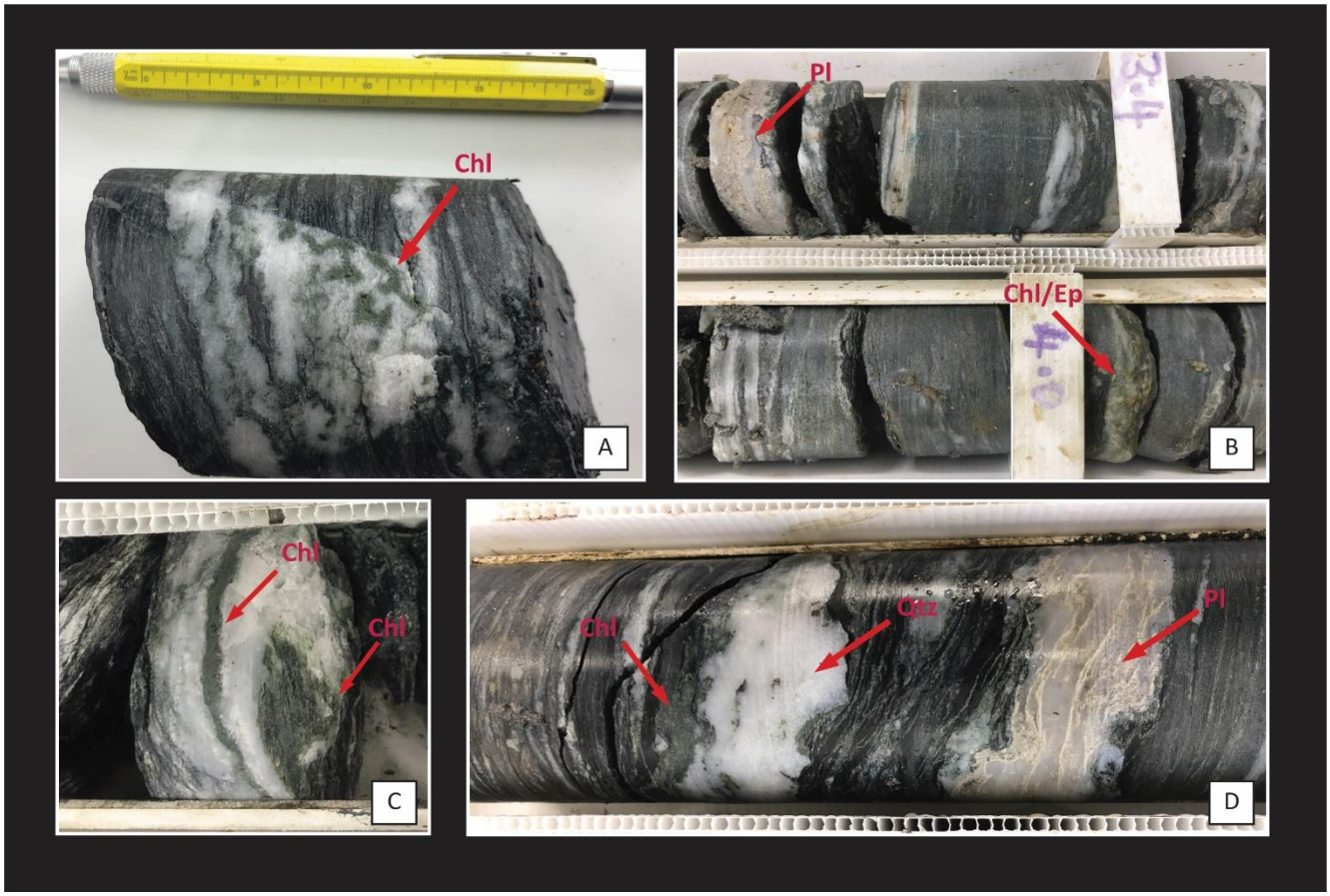

Figure 2.15: A and C: 2-4 mm chlorite segregations and folds in quartz veins (visible in hand sample). In B and D: Plagioclase occurs as an undulating 1-3mm thick beige/cream coloured segregation intermixed with quartz. B) Thin veneers of epidote/chlorite (yellow green) can occasionally be seen in fractures along foliation in the MGy. D) DGy sample - Chlorite (olive green), mafic (black), quartz and plagioclase are all visible in hand sample.

Quartz veins occur in both lithotypes with an average thickness of 2-5 mm but can range anywhere between 1-15 mm. Although infrequent, 1-3 mm chlorite veins were observed. All veins were measured at various orientations between 55°-80°. Other common metamorphic textures were recorded in all four boreholes: upright tight isoclinal folds, asymmetrical folds, mm-scale sheath folds and mm-scale boudins (Figure 2.16).

The average unit thickness of each lithotype is 4 m but ranges from 0.5-7 m. The contact between them is predominantly sharp, but on occasion 0.5-3 m gradational zones between them are observed (Figure 2.14).

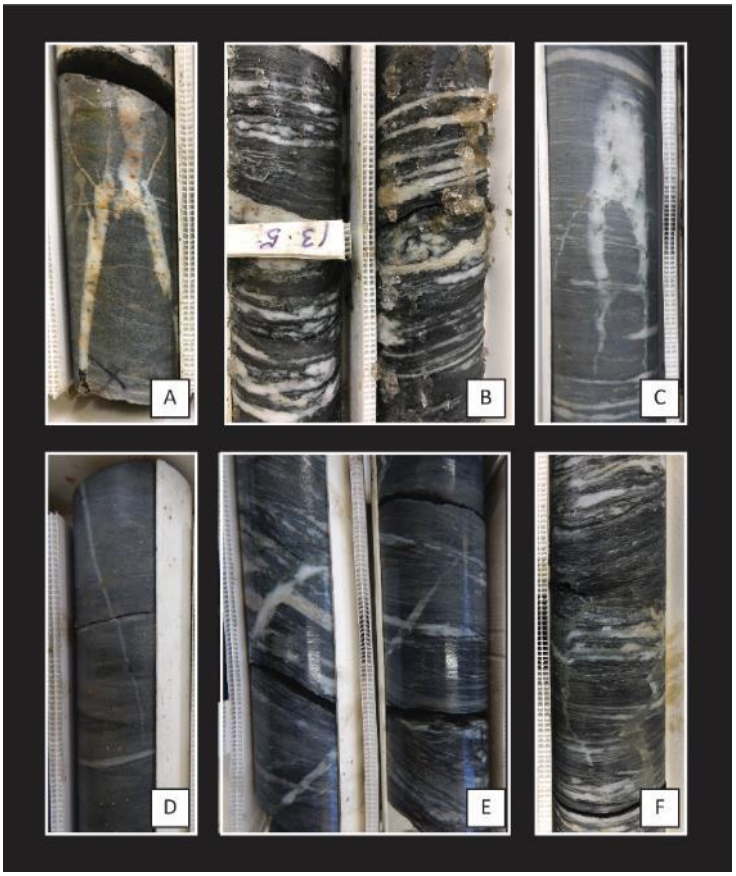

Figure 2.16: A) Upright, symmetric similar fold with limbs dipping at 70°. B) Multiple folds visible in the quartz/plagioclase veins. Photo C) Folded quartz with chlorite. D) Very steeply inclined (70°) 1-3mm quartz vein in MGy schist. E) 55° Quartz vein cross cutting quartz/plagioclase segregation and foliation. F) 1-5mm thick upright folded chlorite.

The lithotypes were analyzed to ascertain their mineral composition and textures, then presented in Table 2.6 and Table 2.7 respectively. A series of thin section photos were then stitched together to show the difference in compositional layering (Figure 2.17).

	MGy		DGy	
	Mean % (± σ)	Range (%)	Mean % (± σ)	Range (%)
Quartz	**22.0** ± 4.5	15.7 - 35.3	**23.6** ± 5.3	14.3 - 36.3
Albite	**20.6** ± 4.1	11.0 - 8.3	**24.2** ± 5.1	15.0 - 34.3
Muscovite	**11.2** ± 3.8	3.0 - 18.0	**19.0** ± 7.0	1.3 - 29.3
Chlorite	**17.8** ± 3.5	12.7 - 25.3	**13.3** ± 3.8	7.7 - 21.0
Epidote	**21.1** ± 4.3	13.7 - 31.3	**9.1** ± 4.2	2.7 - 18.3
Opaques	**2.7** ± 2.0	0.0 - 7.0	**6.4** ± 3.1	0.3 - 12.4
Calcite	**1.9** ± 2.8	0.0 - 10.3	**3.5** ± 4.0	0.0 - 12.3
Titanite	**2.6** ± 1.2	0.0 - 4.7	**0.6** ± 0.7	0.0 - 2.0
Stilpnomelane	**0.1** ± 0.2	0.0 - 1.0	**0.3** ± 0.7	0.0 - 2.7
Garnet	-	-	**0.1** ± 0.1	0.0 - 0.3
No. of thin sections	25		27	

Table 2.6: Summary of mineral composition of both schist lithotypes (DGy and MGy) derived through point counting.

	Medium Grey Schist (MGy)	Dark Green-Grey Schist (DGy)
Mineral Assemblage	• Quartz-albite-epidote-chlorite ± muscovite-titanite-calcite Accessory: stilpnomelane and graphite • Name: Chlorite epidote albite schist	• Albite-quartz-muscovite-chlorite ± epidote-calcite Accessory: titanite, stilpnomelane, garnet and graphite • Name: Chlorite muscovite albite schist
Mineral Description	• **Fine grained:** average grain size is 100 µm and increases to 250-300 µm in veins and segregations. • **Albite:** Subhedral. Generally, no twinning present (Becke Line needed to distinguish between quartz and albite). Twinning mostly present in detrital "relict" grains. • **Epidote:** Two types present: Clinozoisite (zoned) and Zoisite (anomalous blue and yellow). Epidote-rich thin sections have a higher percentage of plagioclase relicts. • **Micas:** Euhedral to subhedral. Overlapping, platy, prismatic and elongated. Stipnomelane and muscovite are acicular. • **Chlorite:** Euhedral to anhedral. Anomalous blue and brown • **Titanite:** Euhedral, up to 350 µm. • **Calcite:** Euhedral to anhedral, ~800 µm, occurs within quartz-rich segregations. • **Opaques** are crystal/platey shaped (likely magnetite, illminite, or pyrite). Minimal clay	• **Fine grained:** average grain size is 150 µm and increases to 250-400 µm in veins and segregations. • **Albite:** Subhedral. Generally, no twinning present (Becke Line needed to distinguish between quartz and albite). Twinning mostly present in detrital "relict" grains. • **Micas:** Euhedral to subhedral. Parallel and randomly oriented, interlocking, platy, prismatic and elongated. • **Chlorite:** Euhedral to anhedral. Predominantly anomalous blue and minor brown • **Epidote:** Euhedral to subhedral Zoisite (anomalous blue and yellow) • **Titanite:** Euhedral, up to 250 µm • **Calcite:** Euhedral to anhedral, 500-2000 µm, occurs within quartz-rich segregations. • **Opaques** occur as a shapeless dusting of flakey material (possibly graphite) AND in crystal/platey shapes (likely to be magnetite, illminite or pyrite)
Foliation	• Fine-scale foliation: mineral segregation poorly developed, a lot of overlapping minerals. More homogeneous appearance. • Compositional layering: alternating layers of aligned minerals Thickness: from 150-800 µm Composition: alternating layers of epidote + chlorite + muscovite and albite + quartz. Occasionally layers solely containing epidote or chlorite present. • Thicker segregations are quartz-rich, thinner segregations are albite-rich	• Intense foliation: mineral segregation well developed, parallel, heterogenous layered appearance - similar to gneissose texture. • Compositional layering: alternating layers of aligned minerals Thickness: from 300-4000 µm Composition: alternating layers of chlorite + muscovite + epidote and albite + quartz. • Thicker segregations are quartz-rich, thinner segregations are albite-rich • Relicts of the original bedding present • Foliation wraps around porphyroblasts.
Metamorphic Textures	• Sieve texture common in epidote and plagioclase • Poikiloblastic textures in albite with epidote inclusions. • Mosaic granoblastic texture is common in albite segregations. • Zoning and inequigranular texture commonly observed in epidote • Pressure shadows, boudinage and embayment textures are common. • Decussate textures, folding and warping common within micas. • Albite, titanite and epidote porphyroblasts present • Brittle fragmentation observed in folded chlorite veins. • Ribbon texture surrounding titanite porphyroblasts • Quartz and albite have irregular and sutured boundaries	• Crenulation cleavage • Sieve texture in epidote and plagioclase • Poikiloblastic textures in albite with epidote inclusions. • Mosaic granoblastic texture is common in albite segregations. • Zoning commonly observed in epidote. • Pressure shadows, boudinage and embayment textures are common. • Decussate textures, folding and warping common within micas. • Brittle fragmentation observed in folded chlorite veins. • Albite, titanite, chlorite and epidote porphyroblasts present • Quartz and albite have irregular and sutured boundaries

Table 2.7: Summary of textures observed in thin sections

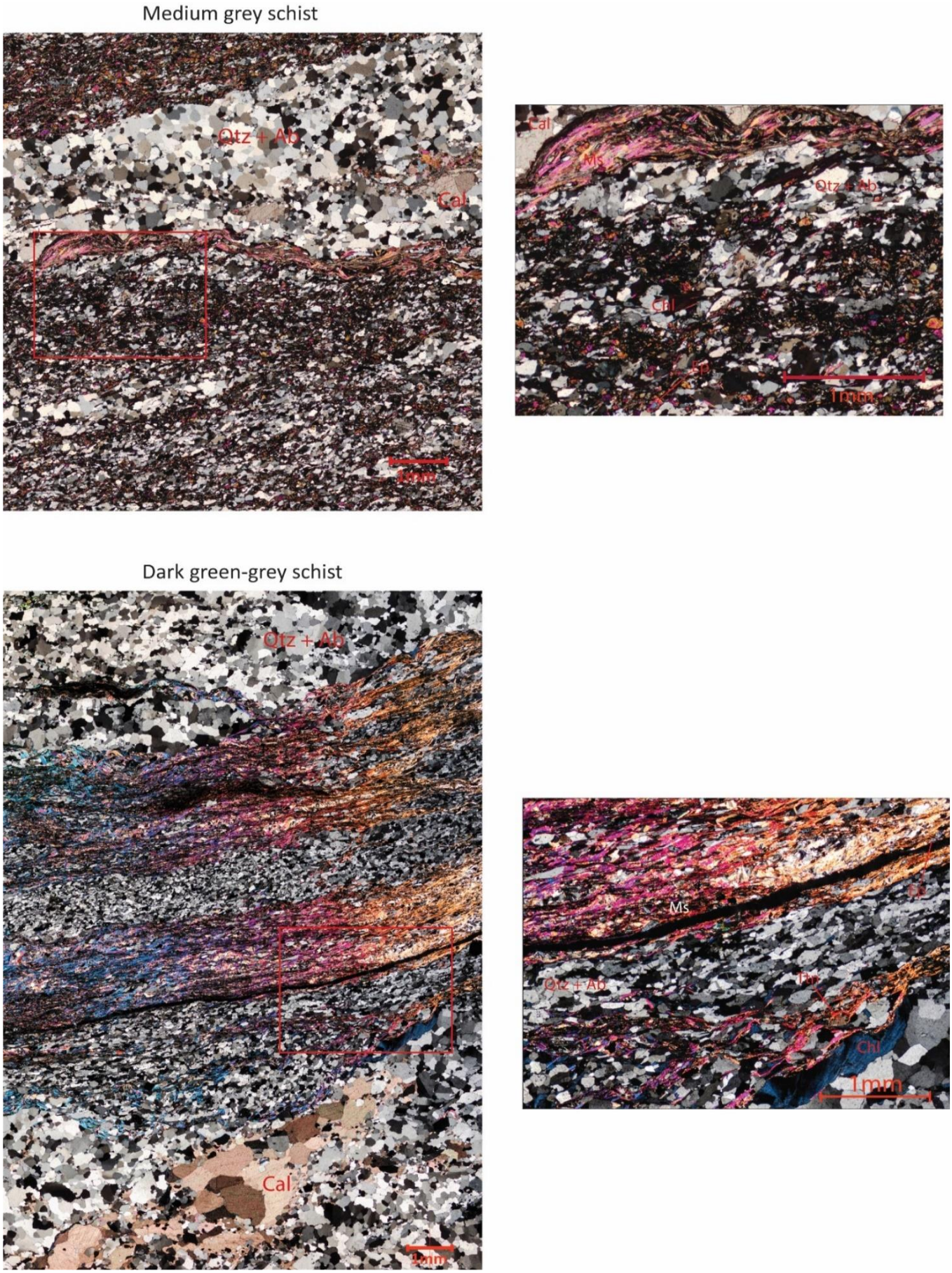

Figure 2.17: Stitched XPL photos of multiple thin section showing the differences in compositional layering and segregation thickness between the MGy and DGy lithotypes. (Photo credit: Kamen Engel)

Based on their mineral composition, the MGy and DGy schist lithotypes are part of the chlorite zone of the greenschist facies (Hollocher, 2014; Raymond, 1995; Yardley, 1989). Two distinct assemblages were recognized: (1) quartz-albite-epidote-chlorite ± muscovite-titanite-calcite (MGy) and (2) albite-quartz-muscovite-chlorite ± epidote-calcite (DGy). Based on the proportions of quartz, mica and carbonate minerals, the MGy schist can be identified as a quartzofeldspathic psammitic schist, and the DGy schist a semi-pelitic schist according to the ternary diagram from Barker (1998) (Figure 2.18). The metamorphic textures present in both lithotypes share many similarities, but they can be clearly identified by their differing fabric and compositional layering. The MGy schist has a poorly developed foliation with a more homogenous appearance. Many minerals are overlapping, compositional bands rarely exceed 800 µm, mm-scale bands are more likely to be infilled quartz-albite veins. The DGy schist is intensely foliated with a compositional layering that resembles gneissose texture. The compositional bands are parallel, mm-scale, well segregated with relicts of the original bedding present.

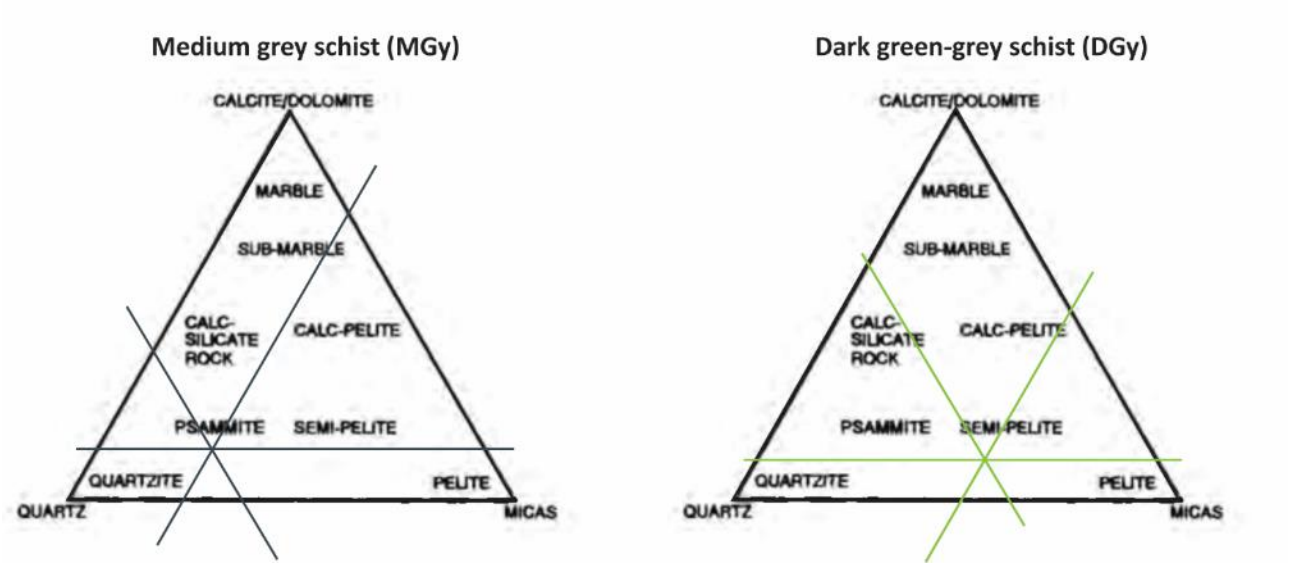

Figure 2.18: Ternary diagram from Barker (1998), to determine the nomenclature for metasedimentary rocks based on the relative proportions of quartz, mica and carbonate minerals.

2.5.2.2 Rock Defects

Joint sets, fractures and foliation shears are the most common rock defects logged in all four boreholes. Joint sets (JS) recorded for each lithotype are compiled in Figure 2.19. Fracture spacing is highly variable in each borehole and limited to the vertical orientation of the core. Fractures along foliation are the most common observed rock defect in all lithotypes and boreholes. The average spacing for all joint sets range between 5-50 cm, however spacing does range from < 1 cm - 110 cm (see full logs in Appendix A.3).

Foliation shears were logged in each borehole and were recorded predominantly in the DGy lithotype. Granular shears occur more frequently than clay-rich shears, are often confined between > 1 cm quartz segregations and are 10-100 mm thick. Foliation shears are described as follows (Figure 2.20):

- **Granular shears:** Are 100% composed of loose, angular gravel to cobble sized fragments.

  Fine to coarse GRAVEL with cobbles; grey, fissile. Loosely packed; gap graded, dry and moist no plasticity; gravel angular to subangular, unweathered to slightly weathered.

- **Granular shears with fines and clay:** The shears are made up of mostly gravel sized fragments but have a sand a gravel matrix. The material is typically loose, well graded, angular to subangular schist gravels with no plasticity. On occasion when clay, silt sized particles exceed 25% the shears can be

moderately plastic. The composition is variable: 5-30% clay/silt, 5-30% sand, 45-80% gravel sized schist fragments.

Sandy fine to coarse GRAVEL with minor silt and clay; grey-brown; Loosely packed; well graded, moist, no to moderate plasticity; gravel angular to subangular, slightly to moderately weathered.

- **Clay shears:** Contain > 50% micaceous clay, 25-30% sand sized pieces, and < 25% sub-rounded gravel and cobble fragments. Clay shears are relatively homogeneous, moderately dense packed; soft, high plasticity and well graded.

  Sandy CLAY with gravels; silver; Moderately dense; well graded, moist, high plasticity, soft; gravels are subangular, slightly weathered.

	Joint Set	Roughness	Aperture	Infill
MGy	JS1: Along Foliation *Fractures generally occur in proximity to qtz segregations	Rough and smooth stepped. Occasionally planar.	Very narrow to narrow. Occasionally moderately narrow.	Predominantly clay veneer infill but also SW-HW crushed micaceous schist fragments, micaceous clay and quartz sand.
	JS2: 45-50	Smooth and rough Stepped.	Narrow	Clay veneer with minor fine gravel schist fragments.
	JS3: 70-75	Rough and smooth stepped.	Narrow	< 2 mm micaceous clay or clay veneer.
	JS4: 80-85	Rough and smooth stepped.	Narrow to moderately narrow	< 2 mm micaceous clay with minor fine gravel schist fragments or clay veneer.
DGy	JS1: Along Foliation	Rough and smooth stepped. Rough and smooth undulating.	Very narrow to narrow. Occasionally moderately narrow to moderately wide.	Ranges from < 2 mm micaceous clay with minor fine gravel schist fragments, clay veneer to none.
	JS2: 40-55	Smooth stepped and rough undulating.	Narrow	< 2 mm micaceous clay with minor fine sand to fine gravel schist fragments.
	JS3: 80-85	Rough stepped.	Very narrow to narrow.	< 1 mm micaceous clay
	JS4: 60-65	Smooth and rough stepped	Very narrow to narrow. Occasionally moderately narrow.	< 1 mm micaceous clay with minor fine sand.
	JS5: 70	Rough stepped	Very narrow	Ranges from < 2 mm thick micaceous clay to none.

Figure 2.19: Summary of the joint sets logged for each lithotype. A) Fractures along foliation (MGy) Smaller spacing occurs in proximity to quartz segregations B) Fractures along foliation (DGy) Fractures occur throughout C) 45° Smooth undulating (MGy and DGy) D and E) 60°-75° stepped (DGy) F) subvertical (80°-88°) Rough stepped (DGy).

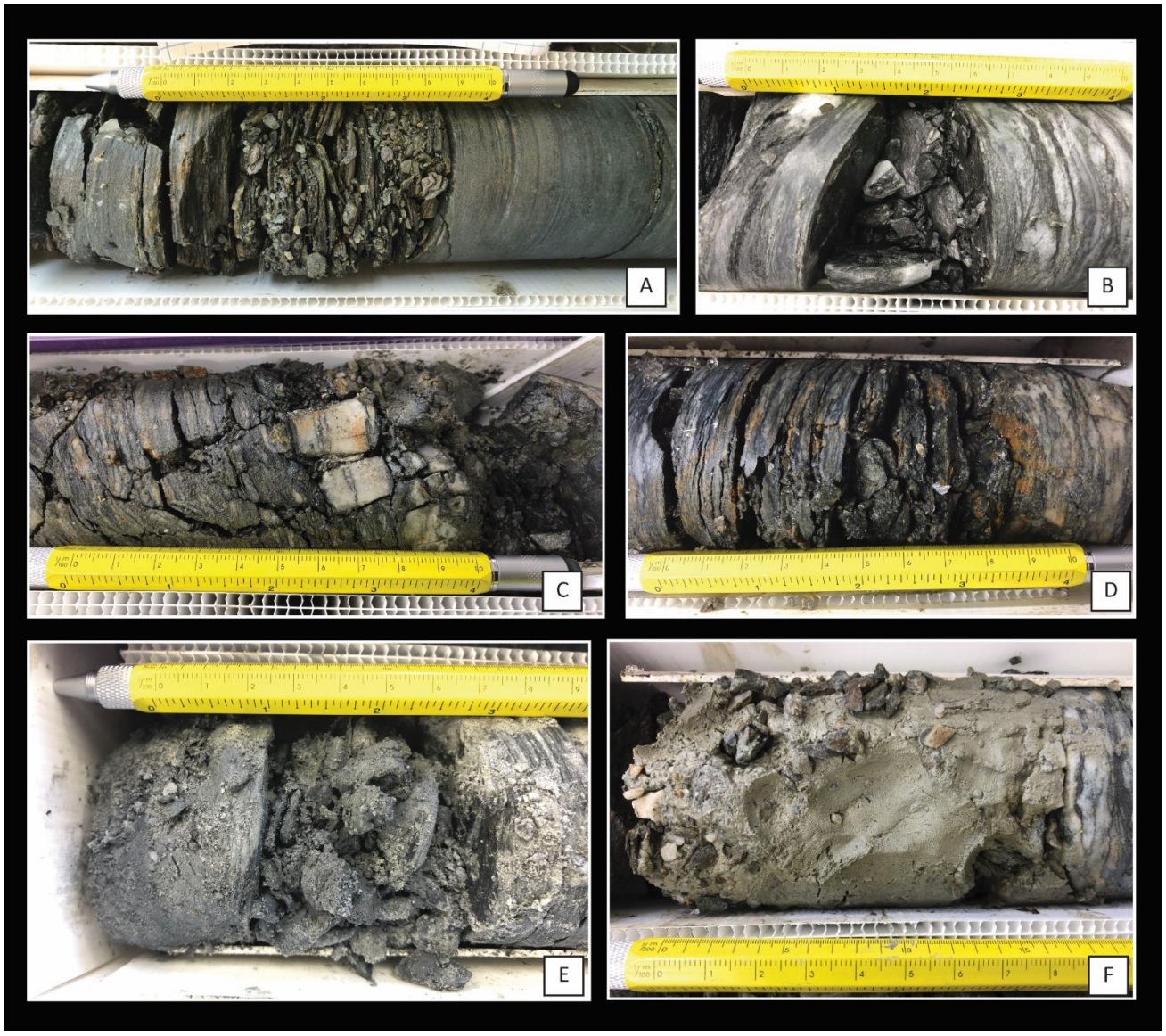

Figure 2.20: Examples of recovered foliation shears. A) Granular end member in MGy B, C and D) Granular in DGy. B is small and localized. C is > 100mm in length. D is granular but smaller fragments are beginning to disintegrate to fine sand and silt sized particles. E) Granular and clay combined end member F) Clay end member.

2.5.2.3 Weathering

Weathering in boreholes 1-4 was assessed through colour and fracture frequency. At least 60% of the material recovered in Boreholes 1, 3 and 4 was recorded as either unweathered (UW), unweathered to slightly weathered (UW-SW) or slightly weathered (SW), meaning only minor iron staining (that did not penetrate the rock) or no discolouration were visible and relatively low fracture frequency (> 10 cm). Moderately weathered (MW) core, was more prevalent in the DGy schist than in the MGy; iron staining was more extensive, darker and penetrated further into the DGy schist. Fractures along foliation were often closely spaced (< 5cm) and showed signs of weathering. Highly weathered (HW) material was generally used to describe zones with poor core recovery, loss of fines and presence of foliation shears. HW zones were evenly distributed in boreholes 1, 3 and 4 and amongst both lithotypes (Figure 2.21).

A single term was used as often as possible to designate a scale of weathering. However, at times this proved difficult, especially when trying to distinguish fractures that may have been induced through drilling and the ones that were already present prior to drilling. If a logged sample had no discolouration with a relatively

high fracture frequency and thin infilling veneer, making it hard to determine the source of the fracture, then the sample would have been recorded as unweathered (UW) to slightly weathered (SW).

Some important changes in weathering were recorded during logging in boreholes 1,3 and 4 (weathering in borehole 2 is discussed in section 2.5.2.4):

- In boreholes 1, 3 and 4, a 0.5-1 m thick, heavily iron stained and fractured zone was noted between 1-3 m bgl.
- In borehole 3, at 15.3 m the fracture intensity increases significantly from 50 cm spacing to <1 cm- 5 cm. Then at 18.0 m iron staining increases and the original rock mass begins decomposition to a soil-like material.

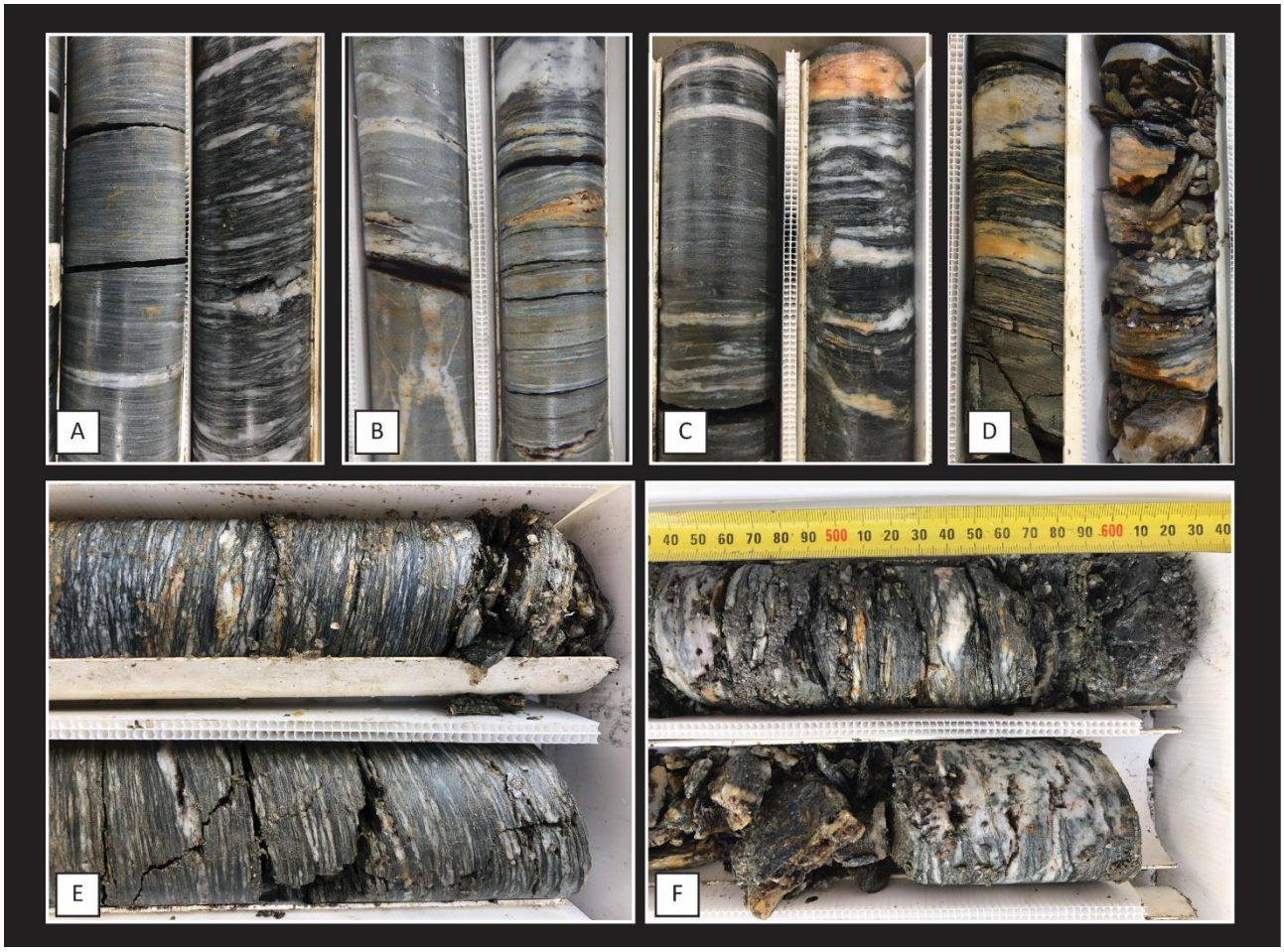

Figure 2.21: Degree of weathering in drilled samples. A) Unweathered core. Left: MGy, Right: DGy. B) Slightly weathered. Minor iron staining along the surface (MGy). C) Slightly weathered. Minor iron staining (DGy). D) Heavily iron stained and fractured zone noted between 1-3m bgl in BH1, BH3, BH4. E) Moderately weathered F) Moderately to highly weathered, the schist is partially turned into a soil-like material.

2.5.2.4 Borehole 2: Crush Zone

Of the four boreholes drilled into the Queenstown Hill Landslide, borehole 2 (BH2) was unlike the other three boreholes. Although fracturing and degrees of weathering varied across the other boreholes, they all had a relatively good rock quality (RQD ~45). However, BH2 had a low rock quality (RQD ~5), a disproportionately large amount of core loss during drilling, a high fracture frequency (average < 1 cm to 8 cm spacing) and was predominantly moderately to highly weathered.

Of particular note is box 4 (Figure 2.22), the total core recovery in box 4 was 56%. No rock was recovered, only soil. The soils consisted of 10-30cm sequences of silty clay with minor sand and fine to coarse gravels.

The silty clay was either silver or taupe, homogeneous, moderately densely packed, soft, moderately graded and highly plastic. Adjacent to the clay layers were 10-30cm sequences of loose sandy gravels with traces of sand and clay.

Silty CLAY with minor sand and gravels; silver-grey, homogeneous. Soft to firm; moist; moderate plasticity; gravels subangular to subrounded schist fragments.

If this soil sequence had been fully recovered, it would have extended a total length of 3.8m. During logging, it was assumed that many of the loosely packed materials in this box and the unrecovered sequences were likely washed out.

Figure 2.22: 10-30 cm sequences of silty clay with minor sand and fine to coarse gravels. The silty clay is silver and taupe, homogeneous, moderately densely packed, soft, moderately graded and highly plastic. Adjacent to the clay layers are 10-30 cm sequences of loose sandy gravels with traces of sand and clay.

2.6 Structural Domains

To provide quantitative data for kinematic analysis in Chapter 5, rock defects and foliation orientation were mapped within and outside of the landslide boundaries. Local structures were identified using lidar images, QMap data and through field mapping of schist outcrops in the study area.

The study area includes, from west to east, in situ bedrock, displaced landslide material and a deformed schist area bound by 2 inactive faults. Schist bedrock outcrops west of the Queenstown Hill Landslide, at the top of the Queenstown Hill walking track (~780 masl), behind the headscarp from the peak to the west in a north-south drainage, behind the headscarp to the east along the deeply incised drainage and throughout road cuttings in the lower subdivisions. Within the landslide, schist outcrops were recorded along the west lateral scarp, the western edge of the headscarp, and in large (10+ m) displaced blocks throughout the landslide. In the area bound by inactive faults, outcrops were recorded in road cuttings, recent subdivision excavation and along the Frankton Walkway.

A general overview of the structures recorded across the study area are set out in Figure 2.23 followed by map of structural domains determined by grouping local discontinuities with similar orientations (Figure 2. 24).

Foliation attitude across the study area is highly variable, ranging from 12°- 50° SE to NW, likely reflecting local deformation and previous slope movement. However, on average the intact schist dips downslope at 15°- 25°/192° (SSW). Locally, major joint sets were grouped along four azimuths represented by dashed coloured lines in Figure 2.23. Along these, seven major joint sets were identified:

- The red lines represent joint sets with a dip direction between 170°-190°or 350°-005°.
  JS1: 79°/358°
  JS2: 55°/359°
  JS3: 50°/181°
- The blue lines represent joint sets with a dip direction between 240°-260° or 060°-080°.
  JS4: 82°/069°
- The green lines represent joint sets with a dip direction between 125°-145° or 305°-325°.
  JS5: 84°/130°
- The golden yellow lines represent joint sets with a dip direction between 265°-285° or 085°-105°.
  JS6: 57°/097°
  JS7: 79°/097°

The major joint sets along Queenstown Hill are predominantly sub-vertical (82°-88°). The sub-vertical joints are well developed, smooth and persistent throughout outcrops at various scales. They are typically spaced 0.5-2m apart with moderate to open apertures. Dilation and relaxation of the rock mass often results in opposing dip directions in the sub vertical joint sets, meaning a subvertical joint dipping 79°-88° can be recorded dipping either north or south within the same joint set.

Fractures also propagate in steeply inclined (40°-60°) joint sets and along foliation. Fractures along foliation are the most common defect observed in the field. However, although they are the most common, the are the most variable in terms of persistence, spacing, roughness and aperture. Steeply inclined joints are stepped, 0.3-5m in length, spaced 0.3-7m apart with moderate to open apertures. Silt, sand, and gravel sized schist fragments infill some of the joints. However, unless recorded in narrow joints, infill was seldomly observed in the field, this is likely due to fines being washed away during storm events.

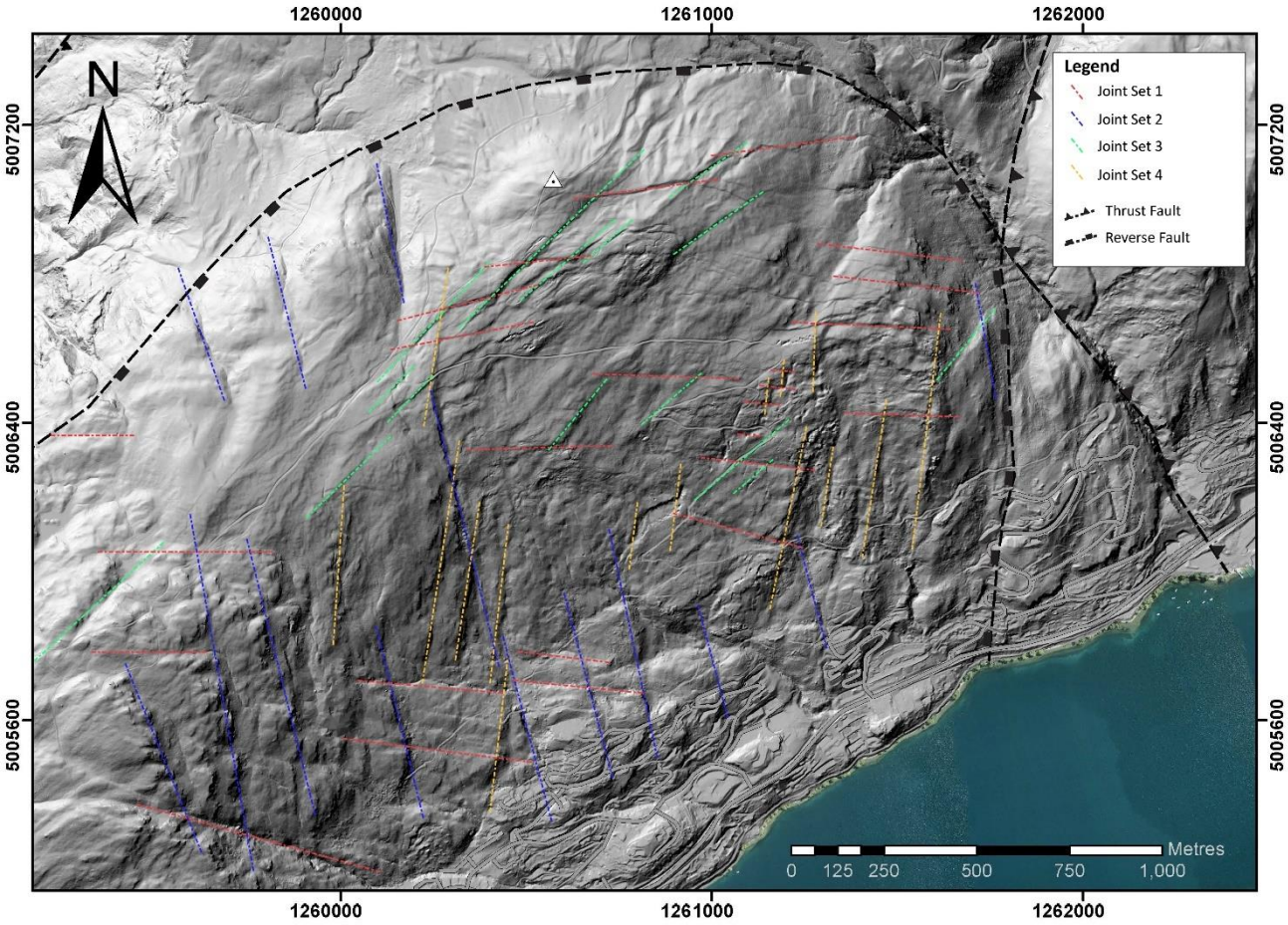

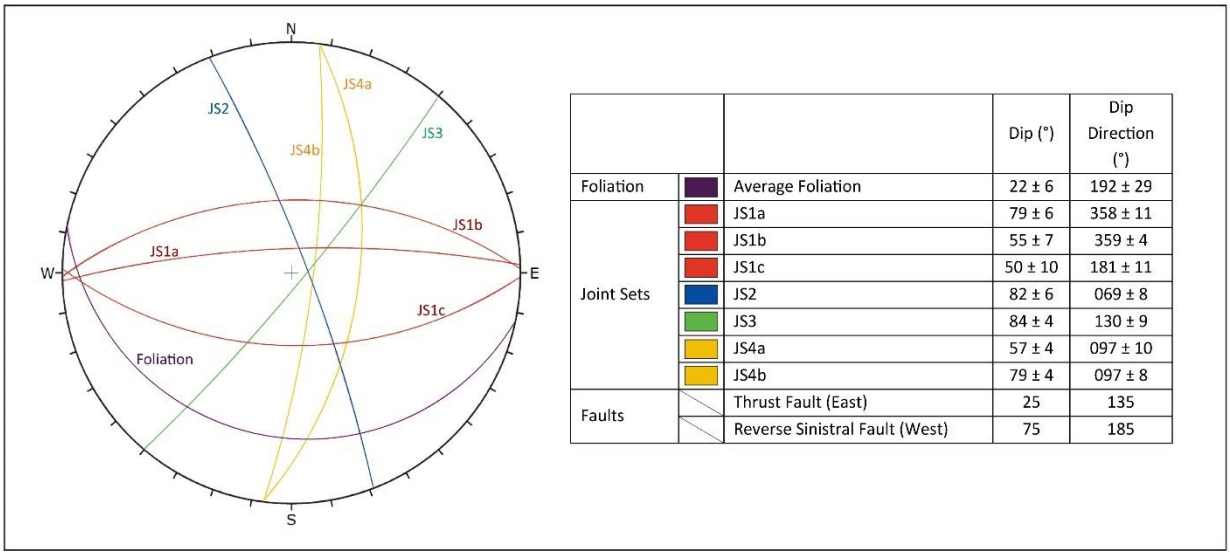

			Dip (°)	Dip Direction (°)
Foliation		Average Foliation	22 ± 6	192 ± 29
Joint Sets		JS1a	79 ± 6	358 ± 11
		JS1b	55 ± 7	359 ± 4
		JS1c	50 ± 10	181 ± 11
		JS2	82 ± 6	069 ± 8
		JS3	84 ± 4	130 ± 9
		JS4a	57 ± 4	097 ± 10
		JS4b	79 ± 4	097 ± 8
Faults		Thrust Fault (East)	25	135
		Reverse Sinistral Fault (West)	75	185

Figure 2.23: Major joint sets mapped across the study site using lidar, QMap and field measurements. Joint sets occur along four azimuths - coloured: red, blue, green, and yellow. Three joint sets occur along the red azimuth, one along the blue and green respectively and two along the yellow. Lidar basemap sourced from LINZ, 2019 and the stereonet was created using Dips by RocScience.

Analysis of the measurements taken during field investigations revealed a wide distribution of values with clustered groups of similar foliation and joint orientation values. The values were plotted on a map revealing five foliation trends across the study area. In each area, joint set measurements and surface geomorphic features were used to further constrain boundaries to establish zones for structural domains. In total, five structural domains were established (Figure 2.24):

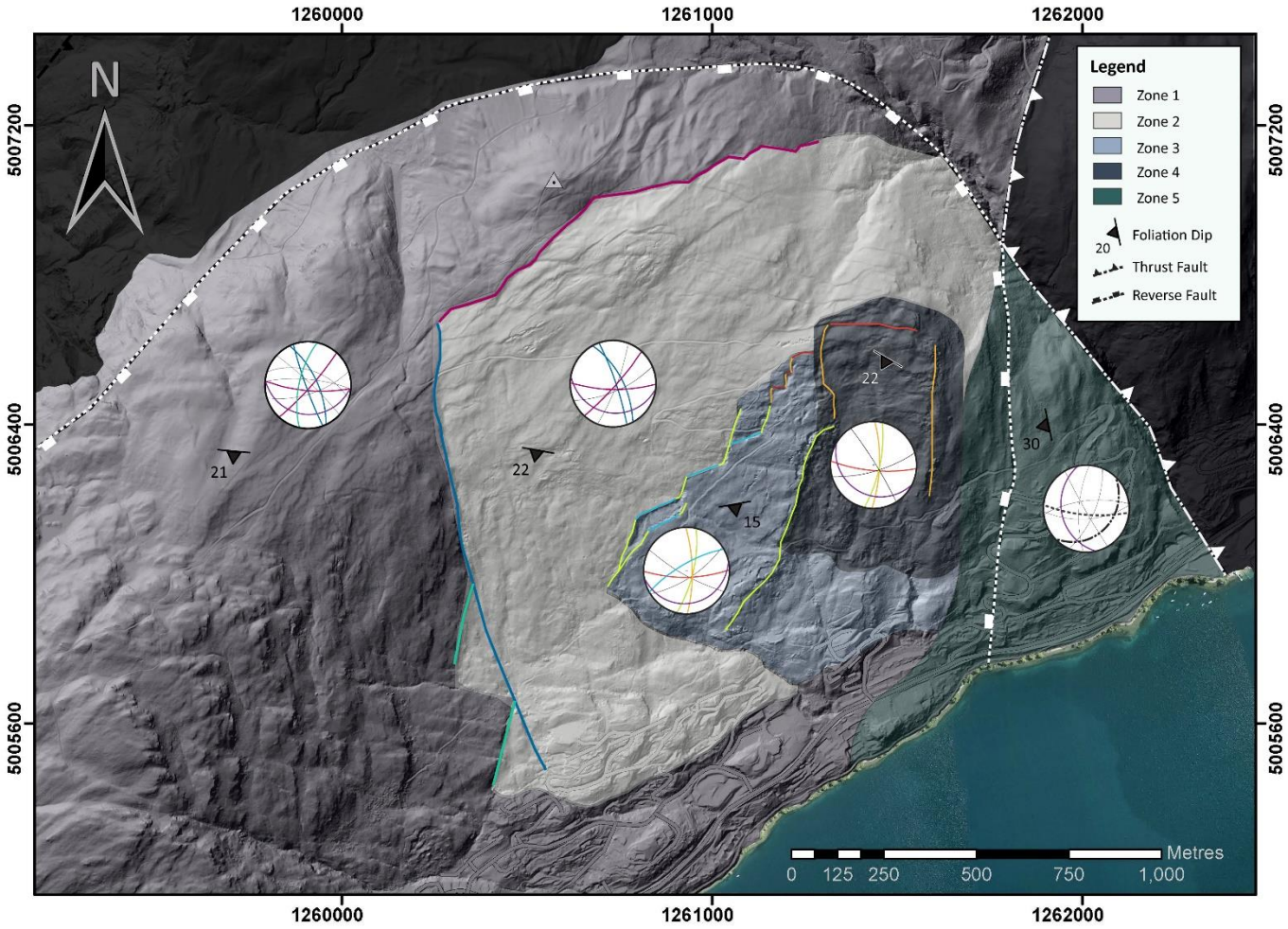

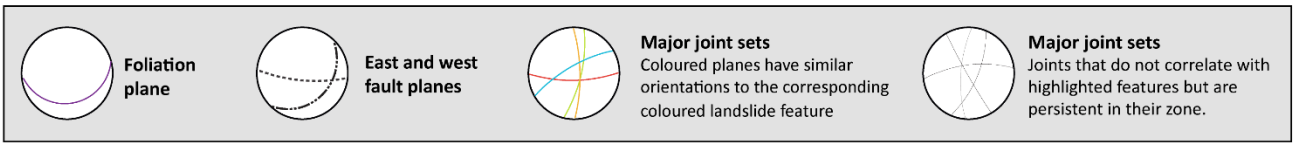

		Zone 1		Zone 2		Zone 3		Zone 4		Zone 5	
		Dip (°)	Dip Direction (°)	Dip (°)	Dip Direction (°)	Dip (°)	Dip Direction (°)	Dip (°)	Dip Direction (°)	Dip (°)	Dip Direction (°)
Foliation	**Average Foliation**	21 ± 5	184 ± 15	22 ± 5	189 ± 15	15 ± 8	169 ± 24	22 ± 4	209 ± 24	30 ± 10	259 ± 14
Joint Sets	**JS1**	84 ± 3	250 ± 8	75 ± 8	181 ± 6	72 ± 4	103 ± 2	74 ± 5	092 ± 4	67 ± 5	113 ± 3
	JS2	65 ± 7	065 ± 10	82 ± 5	071 ± 8	75 ± 5	089 ± 6	75 ± 4	185 ± 2	86 ± 2	240 ± 2
	JS3	83 ± 4	043 ± 7	82 ± 5	132 ± 7	73 ± 3	179 ± 12	73 ± 4	164 ± 3	69 ± 2	353 ± 2
	JS4	66 ± 6	162 ± 6	64 ± 4	062 ± 7	72 ± 10	330 ± 4	73 ± 4	102 ± 3	70 ± 4	274 ± 3
	JS5	75 ± 6	005 ± 14	80 ± 9	111 ± 8	70 ± 8	147 ± 8	84 ± 5	058 ± 8	63 ± 3	176 ± 7
	JS6	66 ± 5	282 ± 8	69 ± 7	157 ± 3	78 ± 8	209 ± 4	-	-	-	-
	JS7	52 ± 3	018 ± 9	-	-	-	-	-	-	-	-
Faults	**Thrust Fault (East)**	-	-	-	-	-	-	-	-	25	135
	Reverse Sinistral Fault (West)	75	185	75	185	-	-	75	185	75	185

Figure 2.24: Structural Domain map. Lidar basemap sourced from LINZ, 2019 and the stereonet was created using Dips by RocScience.

2.6.1 Zone 1: Area Surrounding the Queenstown Hill Landslide

This zone extends from the top of the Queenstown Hill walking track in the west, to behind the headscarp of the Queenstown Hill Landslide and is located outside of the Queenstown Hill Landslide boundaries. The west fault mapped by GNS cuts through the northern end of the site above the headscarp. This zone is primarily made up of in situ bedrock schist dipping at 21°/184°. The outcrops in this area are slightly weathered with well-formed major joint sets. The spacing between sets is wide and ranges between 1-10m+ apart and the aperture is narrow to moderately narrow (1-10mm). Seven joint sets were measured in this area (Figure 20). Of those, JS1 and JS2 are oriented along the same azimuth as the "blue" major joints identified in Figure 19. JS5 have a similar direction to the red and JS6 is oriented in the same direction as the golden yellow set. Although the joints are oriented along the same azimuths as the major joint sets, the subvertical discontinuities measured in situ bedrock tend to dip northwest to north east rather than downslope. This is likely because the discontinuities are less dilated in this zone.

2.6.2 Zone 2: Main Landslide Body

This zone lies solely within the boundaries of the Queenstown Hill Landslide. It extends from the headscarp to the west lateral scarp and includes only the upper portion of the east scarp (deeply incised drainage). The west fault is mapped by GNS through the deeply incised drainage to the east. This zone is primarily made up of large (6m +) displaced schist blocks dipping 22°/189°. The outcrops in this area are slightly to moderately weathered with well-formed major joint sets in large scarps, otherwise the area is largely grassed over. The spacing between sets is moderate, ranging between 0.5-7m with a moderately narrow to wide aperture (10-200mm). Six joint sets were measured in this area (Figure 20). Of those, JS1 and JS4 are oriented in the same direction as the main landslide headscarp - highlighted in magenta. JS2 and JS3 have a similar orientation to the west lateral scarp - highlighted in medium blue. The discontinuities share a dip direction, but one is subvertical (82°) and the other is very steeply inclined (64°). JS5 and JS6 are not linked to the highlighted landslide features but are locally persistent.

2.6.3 Zone 3: Centre of Landslide

This zone occupies the central part of the Queenstown Hill Landslide and includes the extensional feature at the centre of the slide down to a compressional bulge. This zone is primarily made up of large (6m +) displaced schist blocks dipping 15°/169°. This area is less exposed, as it is densely forested. Outcrops, when available, are slightly weathered with well-formed major joint sets in large tension cracks and scarps. The spacing between sets is moderate, ranging between 0.3-5m with a moderately narrow to very wide aperture (10mm - open). Six joint sets were measured in this area (Figure 20). Of those, JS1 and JS4 are oriented similarly to the stepped lines along the western end of the extensional area - highlighted in bright green and electric blue. JS2 and JS3 are oriented in the same direction as "zigzag" at the top of the extensional feature-highlighted in red and golden yellow. JS5 is oriented along the same azimuth as the "green" set identified in Figure 19 and JS6 is locally persistent.

2.6.4 Zone 4: Landslide Reactivation Zone

This zone encompasses the incipient failure within the Queenstown Hill Landslide and is bound to the east by the west fault mapped by GNS. The area is made up of both moderate (4-6m) and large (6m+) displaced schist blocks dipping 22°/209°. This area is topographically steep and densely forested. Outcrops are predominantly concentrated on the outer edges of this zone, and were recorded as moderately weathered with a high number of discontinuities relative to the previous zones. There are few outcrops throughout the centre of this zone. The spacing between joint sets are variable, ranging between 0.1-2m with a narrow to

wide aperture (5-150mm). Five major joint sets were recorded in this area (Figure 20). Of those, JS1 and JS4 correlate with the lateral scarps of the incipient failure - highlighted in golden yellow and bright green. JS2 is oriented in the same direction as the west fault mapped by GNS and the headscarp of the incipient failure. JS5 is oriented along the same azimuth as the "blue" set identified in Figure 19 and JS3 is locally persistent.

2.6.5 Zone 5: Kink Banded Schist Area

This zone is bound by the east and west faults mapped by GNS and does not have any obvious surface features or joint sets on the lidar image. This area is dominated by kink banded schist and foliation shears with an average foliation attitude of 30°/259° and shears dipping at 32°/263°. The outcrops in this area are unweathered to moderately weathered with well-formed major joint sets. The spacing between sets is wide and ranges between 2-7m apart and the aperture is very narrow to very wide (2mm-open). Five joint sets were measured in this area (Figure 20). Of those, JS2 is oriented along the same azimuth as the "blue" set identified in Figure 19. JS3 and JS5 have a similar attitude to the red, JS4 as the golden yellow set and JS1 is locally persistent.

2.7 Synthesis

2.7.1 Lithotypes

Assessment of the field and borehole data confirmed two schist lithotypes were recorded in the field and logged in the core from the Queenstown Hill Landslide: a medium grey schist (MGy) and a dark green-grey (DGy) schist. The fabric, structures and rock defects observed in each lithotype has a similar appearance at outcrop scale, especially when weathered, but appear different in hand sample. The lithotypes can be described as:

Unweathered to moderately weathered medium grey foliated SCHIST; moderately strong to very strong; poor to moderately developed foliation, planar with thin < 1mm laminae, laterally continuous 2-25mm quartz segregations, spaced 2-200mm, pinch and swell structures common, foliation dips 10°-30°; quartz veins and discontinuities are very steeply inclined (60°-70°) to sub-vertical (80°-88°).

Slightly weathered to highly weathered dark green-grey foliated SCHIST; weak to very strong; well developed foliation, planar and undulating with 1-5mm laminae, laterally continuous 3-40mm quartz segregations, spaced 2-40mm, pinch and swell as well as folded structures common, foliation dips 10°-40°; discontinuities are very steeply inclined (50°-60°) to subvertical (80°-88°).

Petrographic analysis confirms that the two lithotypes are distinct based on their composition and micro-scale textures. These findings reflect the previous work undertaken by Wood (1963), Brown (1967) and Turnbull (1981), Craw (1984), and by Stossel (1999). Table 2.8 summarizes the petrographic findings from this chapter and compares them to previous investigations.

Both lithotypes belong to the chlorite zone of the greenschist facies and can be characterized as psammitic or quartzofeldspathic (MGy) and semi-pelitic (DGy) (Barker, 1998). The mineral assemblage for the medium grey schist is quartz-albite-epidote-chlorite ± muscovite-titanite-calcite with accessory stilpnomelane and graphite and albite-quartz-muscovite-chlorite ± epidote-calcite with accessory titanite, stilpnomelane, garnet and graphite for the dark green-grey schist. The percentage of quartz, epidote, micas and felsic minerals in each lithotype paired with the intensity of compositional layering suggests that the DGy lithotype protolith may have been sourced from the Torlesse Terrane, whereas the MGy lithotype has more affinities to the Caples Terrane (Craw, 1984; Kawachi, 1974; Mortimer and Roser, 1992).

The field observations paired with the petrographic analysis indicate that the MGy schist is mappable as Textural Zone III and the DGy as Texural Zone IV (Appendix A.1). Due to intense deformation, it is difficult to confirm lithotypes and textural zones in the kink banded and highly fissile schist areas.

	Medium Grey Schist (MGy)	Dark Green-Grey Schist (DGy)
Mineral Assemblage	Quartz-albite-epidote-chlorite ± muscovite-titanite-calcite Accessory: stilpnomelane and graphite	Albite-quartz-muscovite-chlorite ± epidote-calcite Accessory: titanite, stilpnomelane, garnet and graphite
Metamorphic Facies	Chlorite zone of the greenschist facies	Chlorite zone of the greenschist facies
Nomenclature from index minerals	Chlorite epidote albite schist	Chlorite muscovite albite schist
Nomenclature from protolith	Psammitic schist	Semi-pelitic schist
Lithotype from Wood (1963), Brown (1967) and Turnbull (1981)	Massive quartzofeldpathic rock	Layered quartzofeldspathic rock
Lithotype from Craw (1984)	Greyschist: Psammitic schist	Greyschist: Grey pelitic schist
Textural Zone	Textural Zone III	Textural Zone IV

Table 2.8: Summary of the mineral assemblage, metamorphic facies and nomenclature for the MGy and DGy schist.

2.7.2 Structural Domains

A combination of lidar and field mapping confirmed revealed seven well developed, persistent major joint sets contained within four azimuths along Queenstown Hill:

JS1: 79° ± 6/358° ± 11
JS2: 55° ± 7/359° ± 4
JS3: 50° ± 10/181° ± 11
JS4: 82° ± 6/069° ± 8
JS5: 84° ± 4/130° ± 23
JS6: 57° ± 4/097° ± 10
JS7: 79° ± 4/097° ± 8

At first glance, the discontinuities presented in this thesis do not appear to share similarities with the values obtained by Stossel (1999) (Table 2.9). The scanline results presented in Stossel's thesis were measured in in situ schist in the commonage subdivision. In comparison the joint sets measured in this thesis were recorded within the landslide and in outcrops of relaxed schist at the base of the slope. Dilation and relaxation of subvertical joint sets can results in similar dips with opposing dip directions. A comparison of both datasets confirms that subvertical joints identified by Stossel (1999) dip in the opposing direction to the ones in this thesis.

	Thesis Results	Stossel (1999)	Opposite Dip direction
Foliation	22° ± 6/192° ± 29°	25° ± 5/197° ± 25	-
Joint Sets	79° ± 6/358° ± 11	85° ± 5/235° (Frankton Arm/QHL)	85°/055°
	55° ± 7/359° ± 4	90° ± 5/310° (Frankton Arm)	85°/130°
	50° ± 10/181° ± 11	88° ± 5/243° (QHL) (063)	88°/063°
	82° ± 6/069° ± 8	85° ± 5/307° (QHL) (127)	85°/127°
	84° ± 4/130° ± 23		
	57° ± 4/097° ± 10		
	79° ± 4/097° ± 8		

Table 2.9: Table comparing the results in this thesis to previous work undertaken by Stossel (1999). The third column shows the similarities in joint sets identified by changing the strike direction to accommodate for dilation and relaxation of joint sets. QHL: Queenstown Hill Landslide.

The study site was further subdivided into five structural domains that shared similar foliation measurements and rock defects. The structural domains will be used in Chapter 5 for kinematic analysis. Table 2.10 summarizes the orientation of the discontinuities and Table 2.11 summarizes the average discontinuity characteristics for each zone.

		Zone 1		Zone 2		Zone 3		Zone 4		Zone 5	
		Dip (°)	Dip Direction (°)	Dip (°)	Dip Direction (°)	Dip (°)	Dip Direction (°)	Dip (°)	Dip Direction (°)	Dip (°)	Dip Direction (°)
Foliation	Average Foliation	21 ± 5	184 ± 15	22 ± 5	189 ± 15	15 ± 8	169 ± 24	22 ± 4	209 ± 24	30 ± 10	259 ± 14
Joint Sets	JS1	84 ± 3	250 ± 8	75 ± 8	181 ± 6	72 ± 4	103 ± 2	74 ± 5	092 ± 4	67 ± 5	113 ± 3
	JS2	65 ± 7	065 ± 10	82 ± 5	071 ± 8	75 ± 5	089 ± 6	75 ± 4	185 ± 2	86 ± 2	240 ± 2
	JS3	83 ± 4	043 ± 7	82 ± 5	132 ± 7	73 ± 3	179 ± 12	73 ± 4	164 ± 3	69 ± 2	353 ± 2
	JS4	66 ± 6	162 ± 6	64 ± 4	062 ± 7	72 ± 10	330 ± 4	73 ± 4	102 ± 3	70 ± 4	274 ± 3
	JS5	77 ± 6	005 ± 14	80 ± 9	111 ± 8	70 ± 8	147 ± 8	84 ± 5	058 ± 8	63 ± 3	176 ± 7
	JS6	66 ± 5	282 ± 8	69 ± 7	157 ± 3	78 ± 8	209 ± 4	-	-	-	-
	JS7	53 ± 3	018 ± 9	-	-	-	-	-	-	-	-
Faults	Thrust Fault (East)	-	-	-	-	-	-	-	-	25	135
	Reverse Sinistral Fault (West)	75	185	75	185	-	-	75	185	75	185

Table 2.10: Foliation and joint orientation in each structural domain.

		Weathering	Spacing	Persistence	Roughness	Aperture	Infill
Foliation	MGy	UW-MW	< 1 mm	> 5 m	Smooth planar	n/a	Occasional shears
	DGy	SW-HW	1-3 mm	> 5 m	Smooth Undulating	n/a	Occasional shears
Zone 1		SW	1-10 m	1-5 m	Rough to smooth stepped, rough undulating	1-10 mm	None to gravel schist fragments
Zone 2		SW-MW	0.5-7 m	0.3-5 (<8) m	Rough to smooth stepped and undulating	10-200 mm	None to gravel schist fragments
Zone 3		SW	0.3-5 m	0.5-2 (<5) m	Smooth stepped, rough to smooth undulating	10 mm-open	None to sand/gravel schist fragments
Zone 4		MW-HW	0.1-2 m	0.5-3 (<8) m	Smooth stepped to undulating	5-150 mm	None to sand/gravel schist fragments
Zone 5		UW-MW	2-7 m	0.3-2 (<5) m	Rough to smooth stepped	2 mm-open	None to sand/silt

Table 2.11: Discontinuity characteristics in each structural zone

Chapter 3: Geomorphology of Queenstown Hill

3.1 Introduction

Chapter 3 reviews the geomorphic setting of the Queenstown area and the influence of glaciation on the Wakatipu Basin and surrounding slopes followed by a description of surficial deposits mapped locally, and a summary of previous work undertaken on landslides in the area. Preliminary investigations and field methods for this study are outlined in section 3.5.

The main focus of this chapter is to present a series of geomorphological maps of the Queenstown Hill landslide and to highlight key features. This chapter includes:

- A 1:10,000 scale plan of the landslide geomorphology, subdivided into five zones, based on their distinct morphology.
- Four 1:5,000 scale maps of the morphological zones.
- A 1:15,000 scale plan including the major features of Queenstown Hill, distribution of surficial deposits and a description of surficial deposits logged in the field.

The series of geomorphology maps highlights features and defects of the landslide at various scales, from 1:2,000 and 1:15,000. The data is later used to inform cross sections and engineering geology ground model in Chapter 5.

3.2 Geomorphological Setting

The Queenstown Hill landslide is located in a low-lying basin in the northwestern part of Otago, New Zealand in the Queenstown-Lakes District. The region is characterized by NE-SW trending faults forming a series of basin and ranges, with associated asymmetrical anticlinal-synclinal folds: these are the result of extension beginning in the Miocene followed by a reversal of movement and compression during modern oblique

Figure 3.1: Image showing the morphology of the immediate Queenstown Area. The pink map marker is placed on the Queenstown Hill landslide. (Google Earth Pro 7.3.3.7699 (November 11, 2019) Queenstown, New Zealand. 45°01’22.41” S, 168°42’15.46” E, Eye alt 7.49 km Google 2020, CNES/Airbus 2020, Maxar Technologies 2020 https://earth.google.com [June 16, 2020])

continental collision in the South Island (Kaikoura Orogeny). The Queenstown area itself is bounded by Ben Lomond, Coronet Peak, Crown Range, The Remarkables and Lake Wakatipu (Figure 3.1).

The Queenstown area occupies approximately 9000 km^2. The lowest topographic feature, Lake Wakatipu, is located at 309 masl, whilst the surrounding mountain ranges reach up to 2000 masl. The regional topography is largely due to intense folding, faulting and uplift related to the convergence of the Caples and Rakaia basement terranes (McSaveney and Stirling, 1992), followed by the onset of an extended erosional period (Adams et al., 2009; Adams and Graham, 1997; Bishop et al., 1994; Landis et al., 2008; Turnbull, 2000a) and ongoing uplift originating from the Kaikoura Orogeny (Barrell et al., 1994; Mortimer, 2004). Erosion related to uplift, and glactiation during the Quaternary resulted in very few Eocene and Pliocene sediments remaining in the Queenstown area, other than at Bob's Cove (Turnbull et al., 1975; Turnbull et al., 1988), where Tertiary sediments have been infaulted. As a result, the Queenstown area is characterized by flat-lying alluvial terraces, glacio-fluvial deposits, glacial till, and lake beaches surrounded by steep schist mountains with asymmetric valley profiles.

3.3 Glaciation in the Wakatipu area

Early investigations of New Zealand's glacial history, summarized by Gage (1985), Suggate (1990) and Barrell (2011), identified nine periods of glaciation starting in the Early Pleistocene (Table 3.1).

MIS Stage	Glaciation	Interglaciation	Approximate Age (cal.ka)
1		Aranui	0-11.5 (by definition, Aranui includes LGIT, and Spans 0-18)
2	"Last Glacial/Interglacial transition - LGIT" (Including "Late-glacial" events - e.g. Antarctic Cold Reversal (ACR))		11.5-18
	Late Otira (Last Glacial Maximum - LGM)		18-30
3	Mid-Otira (mid Last Glacial)		30-50
4	Early Otira (early Last Glacial)		~65
5		Kaihinu	Little direct age control in NZ - refer to published MIS stage boundaries
6	Waimea (Penultimate)		
7		Karoro	
8	Waimaunga		
9		(Not named)	
10	Nemona		
11		(Not named)	
12	Kawhaka		
(Preceding glaciations and interglaciations not assigned formal names)			
	Porika		> 1.8 Ma, ? < 2.6 Ma
	Ross		? < 2.6 Ma

Table 3.1: New Zealand Names for Glaciations and Interglaciations (Suggate, 1990; Suggate and Waight, 1999) (Barrell, 2011).

The Queenstown area is known to have experienced at least four periods of ice advance and retreat, with the most recent culminating approximately 18,000 years ago (Barrell, 2011; Barrell et al., 1994; Bell, 1992; Turnbull and Forsyth, 1988). The extent of glaciation and chronology has been interpreted by Gage (1985), Suggate (1990), Bell (1992), Turnbull and Forsyth (1988), Turnbull (2000) and Barrell (2011) based on a combination of dating methods and stratigraphic correlations. A summary of the interpreted ice extents can be seen in Figure 3.2, and the original mapped extents are in Appendix B.1.

Although there is no consensus regarding ice extent and deposit ages, glaciation has had a significant effect on the morphology of the Queenstown area. There is extensive evidence of Quaternary glaciation in the

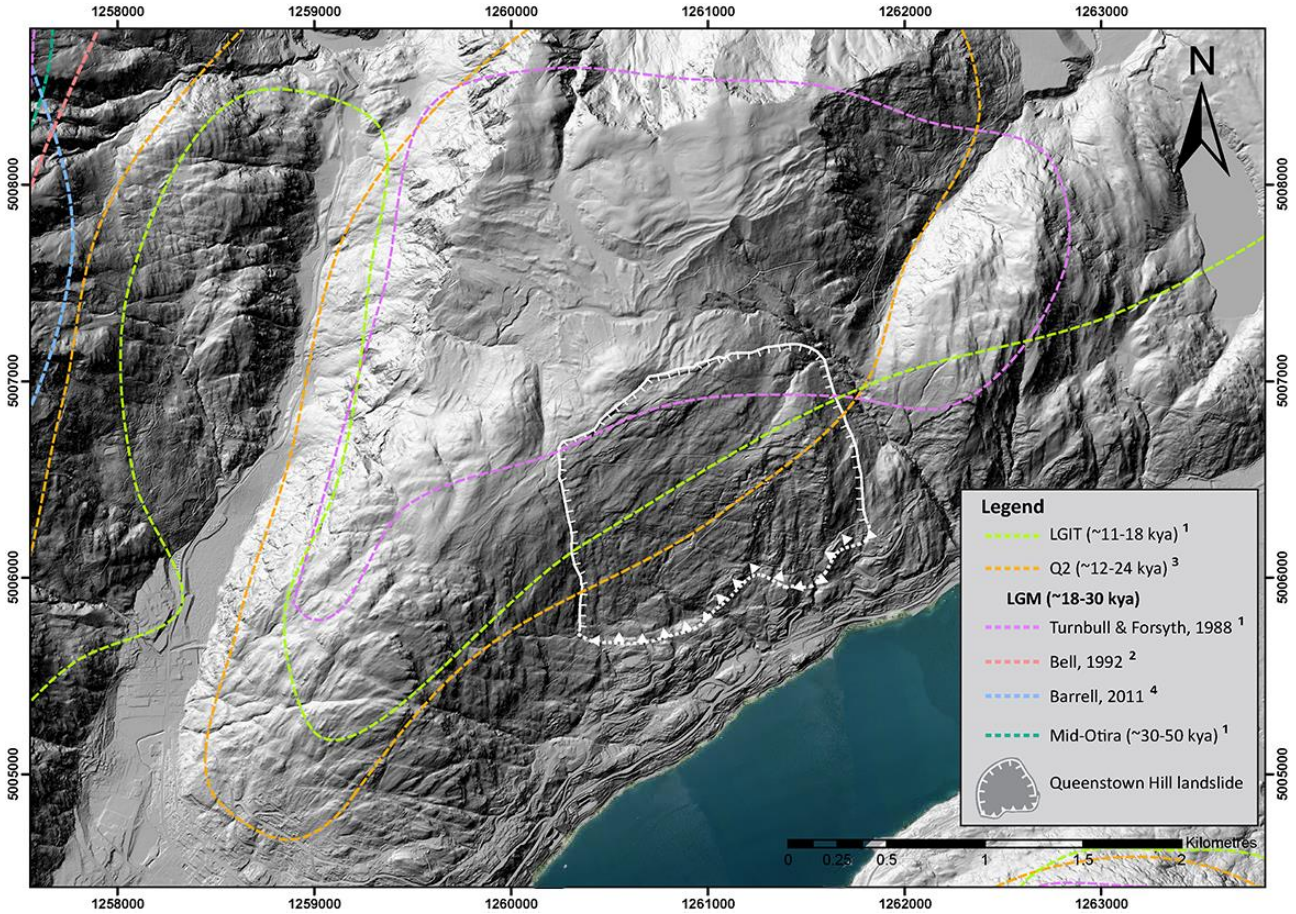

Figure 3.2: Summary of mapped Otira glacial ice extents surrounding Queenstown Hill. The light green dashed line represents the ice extent during the Last Glacial/Interglacial transition (LGIT) - the ice does not reach the upper portion of Queenstown Hill. Various authors show different mapped extents for the Last Glacial Maximum (LGM). Based on the interpretation by Turnbull & Forsyth (1998) and Turnbull (2000), the Wakatipu Glacier did not reach the upper portion of the Queenstown Hill during the LGM, while Bell (1992) and Barrell (2011) show the glacier covering Queenstown Hill. All glacial periods prior to the LGM map glacial ice covering Queenstown Hill.
Map redrawn/adapted from (Turnbull & Forsyth, 1988 [1] ; Bell, 1992 [2] ; Turnbull, 2000 [3] ; and Barrell, 2011 [4])
*it is important to note that the mapped extents are only approximates. Errors may have been introduced from georeferencing maps at various scales.

Wakatipu Basin: U-shaped valleys, cirques and glacial Lake Wakatipu are prime examples of regional landforms formed during episodic glaciation (Barrell et al., 1994; Bell, 1976, 1992; Bell and Riddolls, 1992; Cunningham, 1994; Turnbull, 2000a). Evidence for glaciation is especially prominent in the ice overridden Arrowtown Basin and the roches moutonnées along Queenstown Hill, Peninsula Hill, Ferry Hill and Mt Nicholas. During each advance, glaciers formed in the mountain ranges and extended across the valley floors, progressively scouring, and deepening them (Turnbull and Forsyth, 1988). The base of the slopes and valley floors are often infilled with Late Pleistocene outwash deposits and terraces (Barrell et al., 1994; Bell, 1992; McSaveney et al., 1991; Turnbull, 2000a).

During the various glacial periods, Lake Wakatipu ice had various outlets. The main outlet has been via the Mataura Valley, linking with Oreti River prior to major landsliding blocking that outlet (Bell, 1992). Subsidiary ice discharge has been via the Mavora lakes to the Mararoa catchment, and also via the Kawarau Valley draining into the Clutha River at Cromwell (Barrell, 2011). The Kingston outlet of Lake Wakatipu was abandoned, approximately 15,000 years ago, as a result of lake lowering, and the present Kawarau outlet was re-established (Bell, 1992; Stahl, 2014). Due to drainage derangement, alluvial fans and gravels are predominantly found along the Frankton Arm (Bell, 1982, 1992; Cotton et al., 1991). Episodic lake lowering and wave action formed beach ridges and lake strandlines (wave cut benches) around Lake Wakatipu, with a prominent shoreline recognized at 45 m above present lake level (Cunningham, 1994; Stahl, 2014; Turnbull

et al., 1988).

3.3.1 Surficial deposits

The glacial deposits in the Queenstown area are mapped based on age dating, local geomorphology, and lithology. When absolute ages were unavailable, ages were inferred from geomorphic correlation with dated sequences, from degree of weathering and from preservation of landforms through glacial events. They are currently mapped on the QMap as Oxygen Isotope stage 10 (OIS 10), OIS 2 and OIS 1 (Turnbull, 2000a).

During the glacial and interglacial periods, ice advance and retreat promoted a series of widespread surficial deposits (glacial, fan delta, lake, and beach) extending across the Queenstown area. These deposits have been mapped/described by Barrell et al. (1994), Cunningham (1994), Stossel (1999) and Turnbull (2000). A summary map and description of the deposits is shown in Figure 3.3. Individually authored maps are in Appendix B.2.

3.4 Landslides in the Queenstown Area

3.4.1 Principal Landslides

Landslides are common along the schist slopes in the Queenstown Area (Beetham et al., 1991; Bell, 1976, 1992; Bell and Pettinga, 1985; Cunningham, 1994; Fell, 2015; Gillon and Hancox, 1991; Glastonbury and Fell, 2010; Macfarlane et al., 1991; McSaveney et al., 1991; Stossel, 1999; van Woerden, 2018; Willetts, 2000). Many of these landslides occurred as a result of extension, warping, uplift, faulting, and glaciation. The landslides have been mapped at various scales and are available to view in the Otago Regional Council's Hazards Database (Otago Regional Council, 2020).

Local slope instability ranges from rockfalls and shallow (< 3 m deep), small scale (< 10,000 m^3 in volume) surficial landslides through to large volume (> 100 Mm^3) deep-seated failures. The largest landslides in the Queenstown Area (the Queenstown Hill landslide, the Coronet Peak landslide and the Arthurs Point landslide) have been interpreted as translational, foliation-controlled landslides with a basal failure surface within schist bedrock, dominated by psammitic and pelitic schist with subordinate greenschist and chlorite schist. Chaotic schist-derived blocks and finely crushed rock debris are the predominant slide materials. Although large-scale failure occurs mostly along foliation on the dip-slope, a significant rock fall hazard exists on the scarp-slope of the pelitic schist slopes caused by toppling (Halliday, 2010). Rock mass defects controlling slope stability are foliation, schistosity, foliation shears and jointing (Cunningham, 1994; Stossel, 1999; Willetts, 2000).

3.4.2 Previous Investigations of the Queenstown Hill Landslide

As part of her thesis, Cunningham (1994) produced a 1:25,000 geomorphological map detailing the surficial deposits and a 1:10,000 engineering geology map of the Wakatipu Basin. The main objectives of her thesis were to produce large scale maps as a guide for land use planning that identifies physical constraints of the Queenstown area. The Queenstown Hill landslide was included in her thesis, however, was not the focus of the study.

Stossel (1999) produced detailed engineering geology maps of the landslides along the Frankton Arm, including the Queenstown Hill landslide (Figure 3.4), mapped at a 1:5,000 scale and proposed failure models for seven landslides. Sensitivity analysis and field testing was also part of her scope of work.

Several site-specific geotechnical investigations have been undertaken along the Frankton Arm by various consultants. Consultancy report are generally unpublished and minimal data is currently available in the New Zealand Geotechnical Database (NZGD) for the Queenstown area. However, a number of reports have been

reviewed as part of this thesis (Bell, 1985a, b, 1989, 1994, 1995, 1997a, b, 2018; Salt and Yetton, 1985). These investigations were predominantly focused on developments in the area beneath the landslide but they provide valuable insight with respect to surficial deposits, bedrock structures and considerations for development.

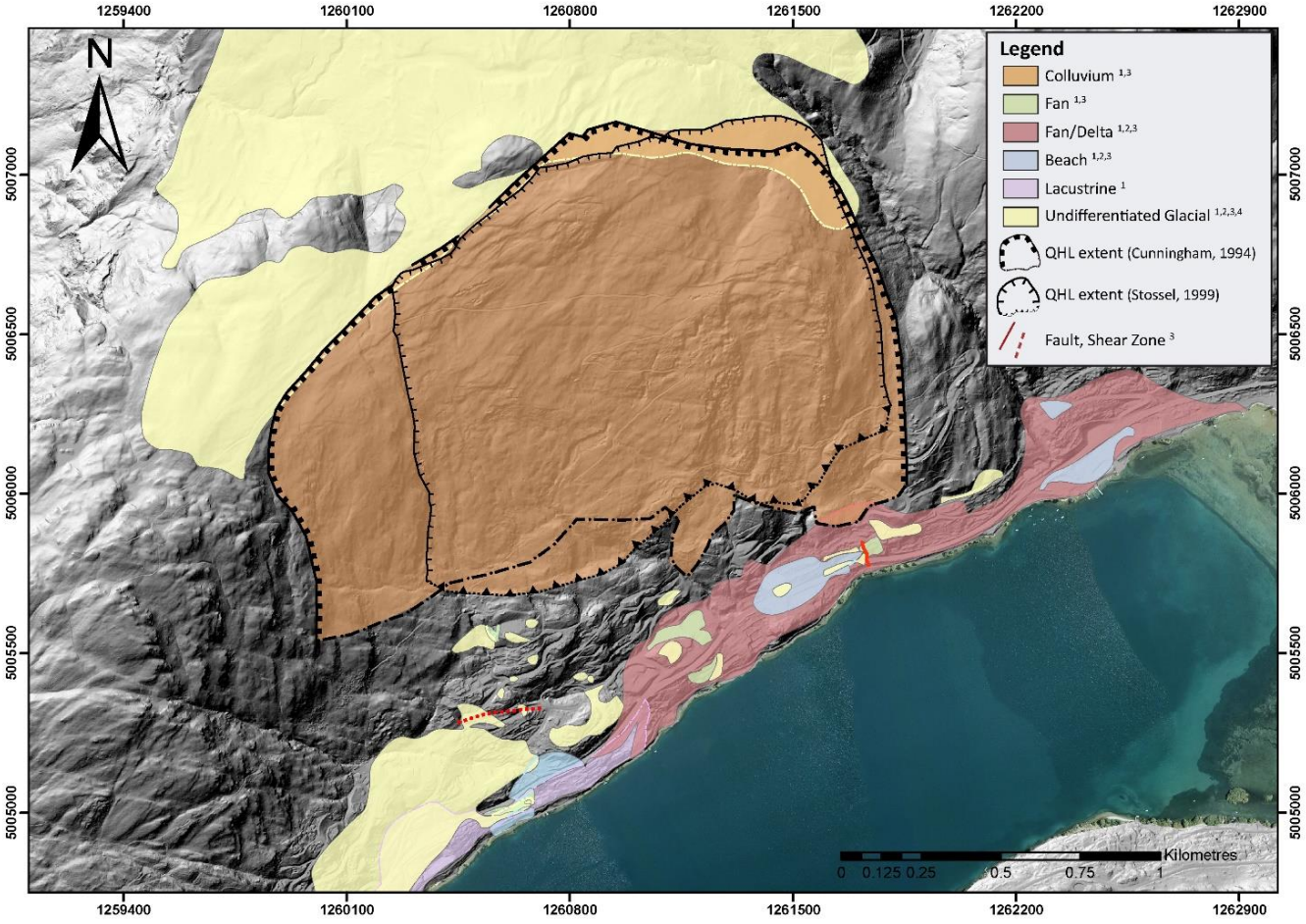

Deposit Type	QMap Symbol	Description
Colluvium (Landslide)	**Grey hatched patterned polygon**	Gravitationally displaced material. Characterized by hummocky terrain. Predominantly made up of schist debris, scree, rockfall deposits and other schist derived materials. Consist of layered gravelly and silty deposits. Thickness ranges from a few metres to hundreds of metres. Accumulated on > 20° slopes.
Fan/Delta	**Q1a, Q1b**	Formed where fans have built out into lakes. The deposits are dominated by loose, angular boulders and bedded sandy gravels near the head of the fan. With increasing distance from the old shoreline, the deposits fine to layered sand and silt. The deposits tend to dip towards the lake between 10°- 30°.
Lake	**Q1k**	Consist of grey, sub-horizontal thinly bedded and laminated micaceous silts, with interbedded fine sand and fine to coarse gravel.
Beach	**Q1a, Q1b**	Overlying gently sloping wave cut benches, deposits consist of well sorted, layered sandy, gravelly, and silty sediments. Units range in thickness from 10s of cm to m. Linear storm beach ridges are present around Lake Wakatipu. Beach deposits have been mapped at various heights up to 400m a.s.l.
Glacial	**Q2a, Q2t, Q10a, Q10t**	Undifferentiated unit including till, outwash and ice-margin sediments. Outwash plains are typically unweathered, well sorted, loose sandy to boulder gravels. Younger tills are typically unweathered, unstratified and are made up of either compact, gravelly, sandy, silt-clay, or loose clayey and sandy gravel. Ice-margin sediments include layered sandy gravel, sand and silt, typically with contorted or deformed layers. Older glacier deposits are slightly to moderately weathered, sandy to boulder clayey gravels.

Figure 3.3: Summary combining the surficial deposits mapped in the study area. Map also includes the Queenstown Hill Landslide extent mapped by Cunningham (1994) and Stossel (1999). Map and table adapted from (Cunningham, 1994 [1]; Barrell et al., 1994 [2] ; Stossel, 1999 [3] ; and Turnbull (2000) [4]).
*it is important to note that the mapped extents are only approximates as errors may have been introduced from georeferencing maps at various scales.

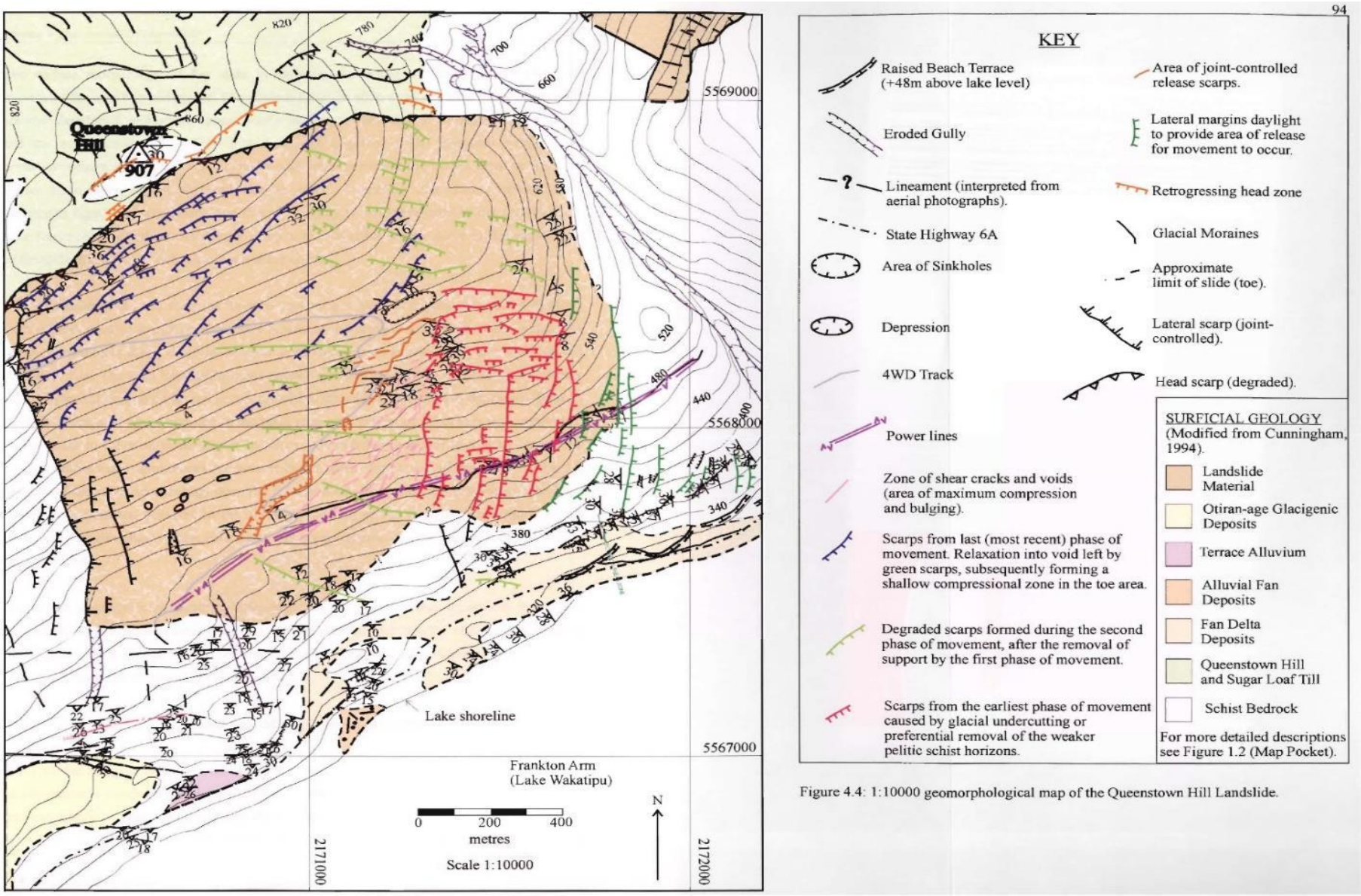

Figure 4.4: 1:10000 geomorphological map of the Queenstown Hill Landslide.

Figure 3.4: 1:10,000 geomorphological map of the Queenstown Hill Landslide drawn by Stossel (1999).

3.5 Methodology

A combination of field observations, remote sensing, and data analysis with Geographic Information Systems (GIS) were used to produce a geomorphic map of the landslide. Mapping guidelines and principles from Hutchinson (2001), Griffiths (2002) and Hearn (2019) were applied, and symbology from Otto & Dikau (2004) and GMK 25 (Leser and Stäblein, 1985) were used. High resolution topographic maps, aerial photos and lidar images were used for preliminary assessment of landform features and to identify the extent of the landslide. Two field campaigns were later undertaken to validate features mapped during the initial reconnaissance and to increase the level of mapping detail.

3.5.1 Topographic data and aerial photography

Aerial photographs were obtained from historical image archives for stereopair interpretation. Four photos (232500, 232501, 232502, 232503) taken on March 22, 1956 were used from survey number SN884, Run C, elevation 14,000, scale 1:20,300. The images were interpreted manually using stereopairs and digitally. The aerial photographs were downloaded from Retrolens, stitched, blended (Adobe Photoshop 2020) and georeferenced (ArcMap 10.7) to allow for comparison with more recent imagery (Figure 3.5). Imagery from 1956 was used to identify morphological changes over time and to map features in areas currently obscured by vegetation and subdivision development.

Three sets of orthophotos were downloaded from LINZ and imported into ArcGIS (Table 3.2).

	Type	Coordinate System	Resolution	Accuracy	Scale	Client
NZ Orthophotos 2000-2001	Orthophotos	NZGD49/New Zealand Map Grid	2.5 m pixel	-	1:25,000	LINZ
NZTA State Highway 2008-2009 Aerial Imagery, 0.15 m	Orthophotos	NZGD2000/NZTM 2000	15 cm pixel	± 2 m (within 400m of State Highway) ± 5 m (outside State Highway area)	-	NZTA
Otago 0.3 m Rural Aerial photos (2017-2019)	Orthophotos	NZGD2000/NZTM 2000	30 cm pixel	± 0.5 m	1:5,000	Otago Regional Council

Table 3.2: Orthophotos downloaded from Koordinates/LINZ.

Airborne Light Detection and Ranging (lidar) of the Queenstown area was captured for Otago Regional Council by aerial surveys in March and April 2016 at a 1:1,000 scale and vertical datum NZVD2016. The datasets were downloaded from Land Information New Zealand (LINZ) and processed to a 1 m grid digital elevation model (DEM) projected into NZTM2000 using ESRI's ArcMap 10.7 GIS software. Three terrain maps were created and used for interpretation: hillshade, slope and aspect. The hillshade is rendered with azimuth is 315° with an altitude of 45° (Figure 3.5).

3.5.2 Field Investigations

Two field mapping campaigns were undertaken to record detailed descriptions of geomorphic features and landforms of the landslide and surrounding area to produce a series of maps that can be integrated into the engineering geology ground model in Chapter 5. Aerial and lidar imagery were uploaded to Collector for ArcGIS to validate preliminary interpretations and to map features in the field. Geomorphology mapping was carried out on a 1:2,000 scale. The main objectives were to obtain physical descriptions of surficial material and to record landform features, such as scarps, tension cracks, breaks in slope, depressions, rockfall, drainage, seepage and ridges.

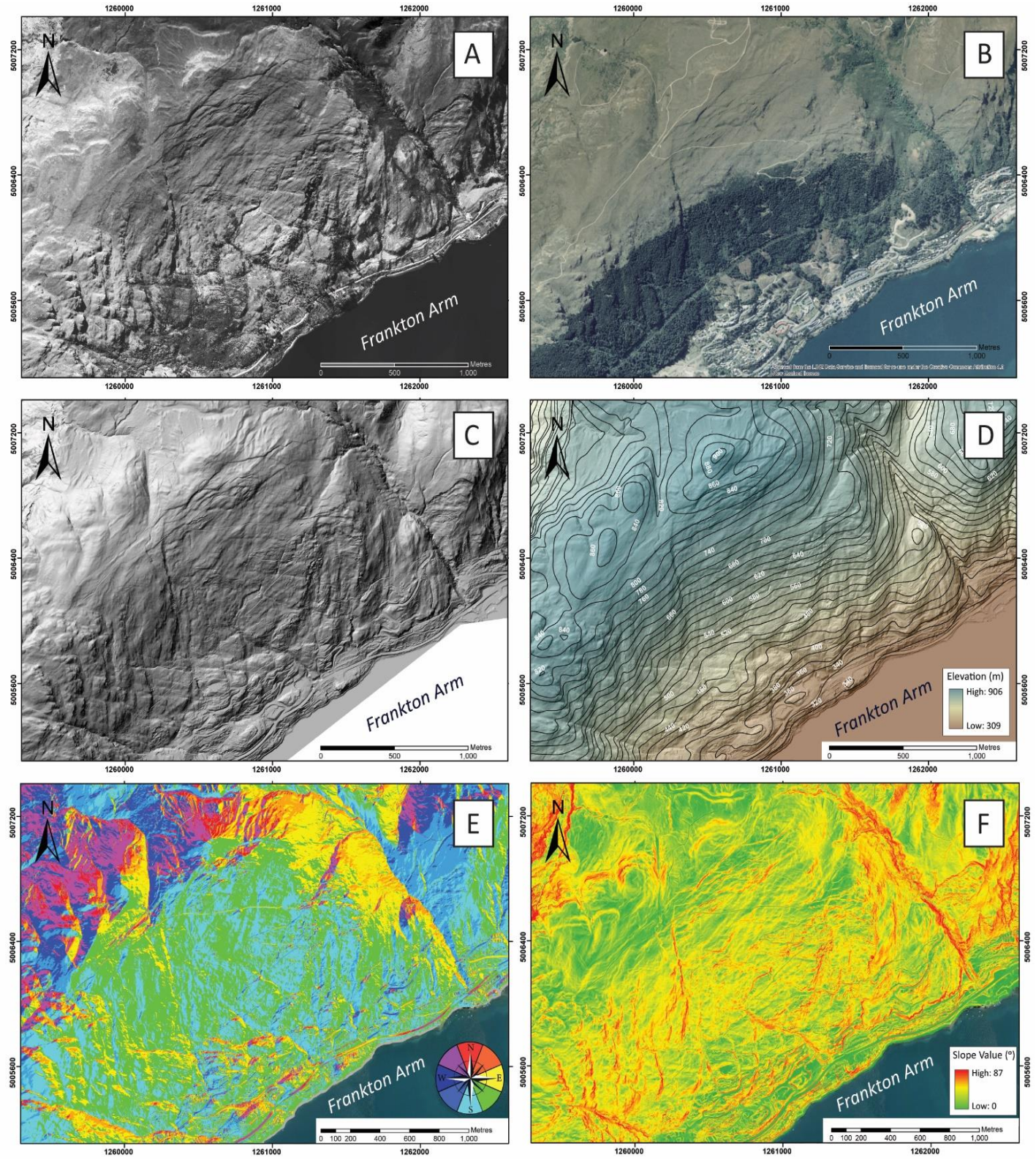

Figure 3.5: Queenstown Hill landslide terrain maps. Coordinate system: NZTM 2000, Scale 1:12,000. (A) 1956 Aerial photo, prior to subdivision development (Retrolens, 2020) (B) 2008 -2009 Aerial photo (LINZ, 2020) (C) 2016 lidar Hillshade (LINZ, 2019) (D) 2016 coloured DEM with 20m topographic contours. (E) Aspect map. (F) Slope map.

3.5.3 Map Scales

Following field investigations, six detailed geomorphic maps were drawn at three different scales: 1 x 1:15,000, 1 x 1:10,000 and 4 x 1:5,000 . These scales were selected to represent varying levels of detail at each scale (Table 3.3).

Map Scale	Map Content:
1:15,000	Major and moderate geomorphic features of the southwest side of Queenstown Hill. Approximate landslide boundaries, surrounding schist bedrock, and surficial deposits. Representative structural measurements. Faults mapped in Webmap by GNS (GNS Science, 2018). Borehole locations. *This map will later be used to reference cross section lines for the ground model.
1:10,000	Major and moderate landslide features. Borehole locations. Tracks, roads and the motorway (SH6A) Faults mapped in Webmap by GNS (GNS Science, 2018). Five geomorphic zones characterized by surface morphology (1) Headscarp (2) Upper-mid main landslide body (3) Extensional zone (4) Reactivation zone; and (5) Toe zone.
1:5,000	Four maps detailing the major, moderate and minor geomorphic features in the five zones listed above. Representative structural measurements. Rockfall and debris cover detail. Borehole locations. Tracks, roads and motorway.

Table 3.3: Summary of map scales and content.

3.6 Geomorphology Maps and Zones

The Queenstown Hill landslide is located on the southeast side of Queenstown Hill, along the Frankton Arm (1,260,804 m E, 5,006,653 m N, NZTM2000) with a peak elevation of 907 masl, and the lowest elevation at Frankton Arm is 309 masl. Based on statistical data derived from the slope and aspect maps, the landslide has an average slope angle and direction of 26°± 12/148°± 051 (SSE). The slope distance measures approximately 1425 m from headscarp to toe, with a maximum width of 1600 m and a vertical elevation of 400-500 m covering an area of approximately 2.28 km^2.

The surface expression of the landslide mass is rectangular and blocky, with a prominent headscarp and a western lateral scarp. The landslide is bound to the east by deeply incised drainage, which also coincides with a set of intersecting faults mapped by GNS (GNS Science, 2018). In the upper portion of the landslide, hummocky terrain dominates the landscape. The rockslide then transitions into an extensional zone marked by tension cracks, grabens and scarps suggesting the rock mass moved downdip towards the lake. The landscape features are well defined in the lidar imagery however, the extent of the landslide to the east and at the toe are not clearly defined.

The rockslide was subdivided into five major zones based on mapped surface morphology (Figure 3.6):

- Zone A: Headscarp zone of the landslide.
- Zone B: Main landslide body.
- Zone C: Extensional zone mid-slope.
- Zone D: Reactivation from mid-slope to the east boundary of the landslide.
- Zone E: Toe zone of the landslide.

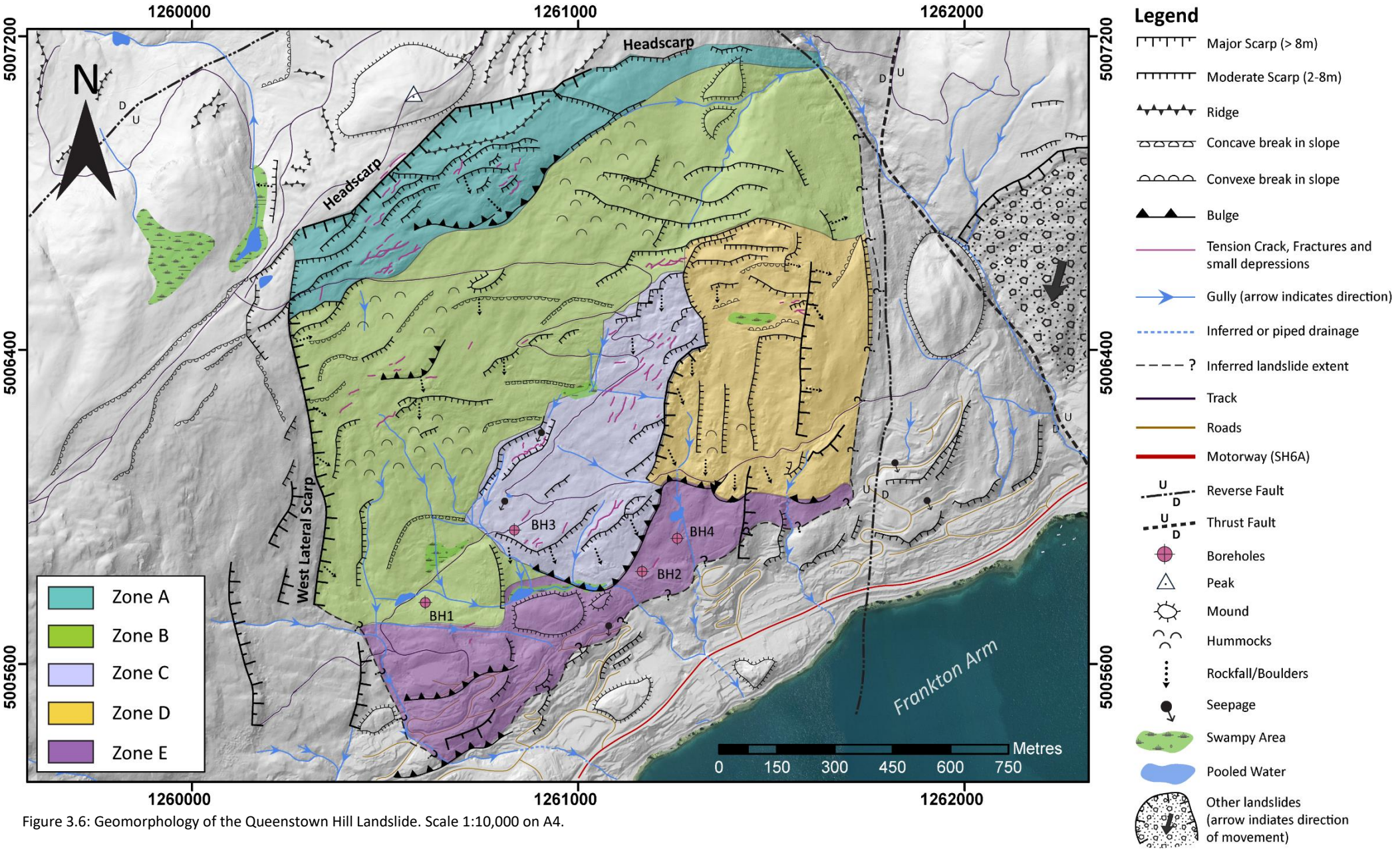

Figure 3.6: Geomorphology of the Queenstown Hill Landslide. Scale 1:10,000 on A4.

3.6.1 Zone A: Headscarp Zone

Zone A encompasses the area extending from the main headscarp at 890 masl (including small scarps above the main scarp) and a portion of the west lateral scarp to the base of a compressional bulge at 800 masl (Figure 3.6). The zone is 250-350 m wide, with the narrowest section at only 140 m wide to the east, trends NE-SW, and has an average slope inclination of approximately 22°. It is characterized by a steep (53°-70°) joint-controlled major scarp, and a series of NE-SW scarps stepping downslope, closely spaced extensional zones marked by tension cracks and a large compressional bulge at 820 masl (Figure 3.7).

The main headscarp measures 1450 m in length and is controlled by two major joint sets oriented 82° ±5/132° ±7 (SE) and 75° ±8/181° ±6 (S). The measured height along the main scarp is varies between 10-15 m, with the largest vertical offset measured towards the centre of the scarp. The scarp height decreases to 4 m to the west and flattens to <1 m in the east. There are few outcrop exposures in the headscarp, due to the level of degradation and erosion over time. However, steep (65°), dilated, fractured schist outcrops were recorded in scarps in the west (Figure 3.8).

To the west, the main headscarp transitions into a series of forward stepping scarps and two < 100 m long 5 m wide tension cracks at 800 and 820 masl. At 865 masl, an arcuate ridge/scarp structure is parallel to the centre of the headscarp. The western portion of the back-tilted feature has a clear downhill facing scarp with a sub-vertical edge. In contrast, the eastern limb is rounded with a visible crest. In the lidar image, it appears that the east ridge may be linked to the glacial ridges mapped to the north and east, and was later crosscut by the headscarp. The area between the headscarp and arcuate upslope facing landform is a 300 m long, 70 m wide depression, resembling a graben structure. There are small, 1 m, mounds in the depression area, which are likely grassed over blocky debris sourced from the headscarp (Figure 3.8).

The graben structure transitions into a series of moderate scarps, depressions, and 0.5-3 m deep tension cracks on top of a compressional bulge. The lower portion of the compressional zone hosts many medium (2-10 m) and large (> 10 m) rotated blocks thrusted over the existing ground. To the east of the graben and compressional zone, the headscarp and subordinate scarps are much smaller (< 1 m) than in the west and are predominantly oriented NW-SE (see disturbed area in Figure 3.7). The slope inclination is consistent, at 15°-20°, but orientation changes from south facing to facing east towards the large drainage gully. There is a visible increase in localized debris mantle in small drainage channels. The debris consists of small (< 1 m) subrounded schist fragments and gravelly material.

Finally, above the main headscarp to the north, and to the west of the headscarp and lateral scarp, the presence of moderate scarps (2-8 m) suggest possible retrogression of the main rockslide. The surface expression of the scarps above the headscarp are approximately 2-3 m and grassed over, but show no indication of recent movement (in the last 70 years). The scarps to the west of the headscarp following the shape of the headscarp and lateral scarp are raised 1-2 m but also form a 5 m wide gap and extend 1-2 m below the surface (Figure 3.8).

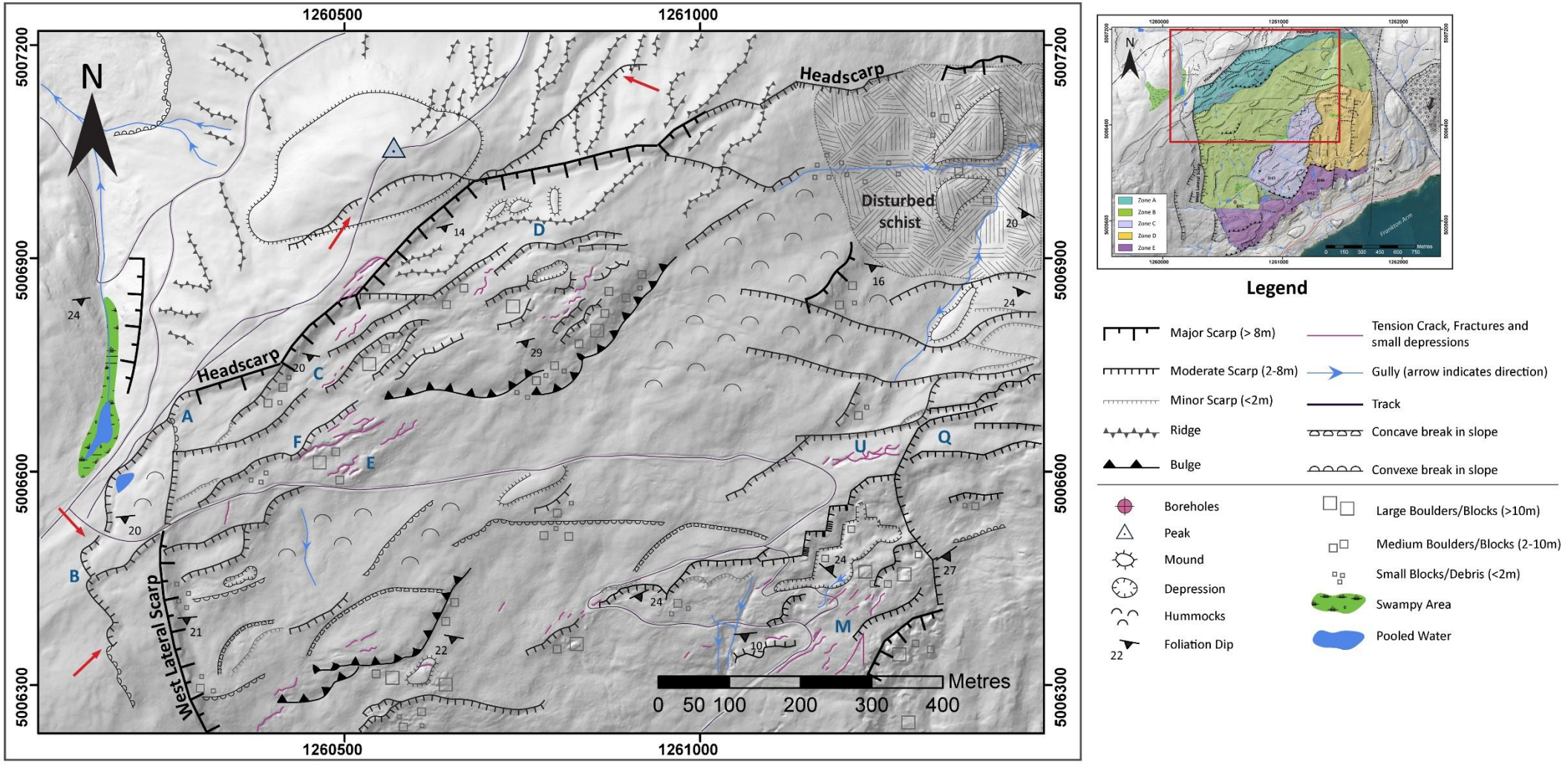

Figure 3.7: Geomorphology of the headscarp zone (Zone A), including a portion of the main landslide body (Zone B). Scale 1:5,000 on A4. Red arrows point to 2-3m high scarps extending beyond the main headscarp, possibly indicating continuing regression. Disturbed schist area has minimal vertical offset (< 2 m) and drainage flows NE towards the incised gully.
Notes: Letters on the map correspond to photo locations from later figures in this subsection. Representative structural measurements were plotted.

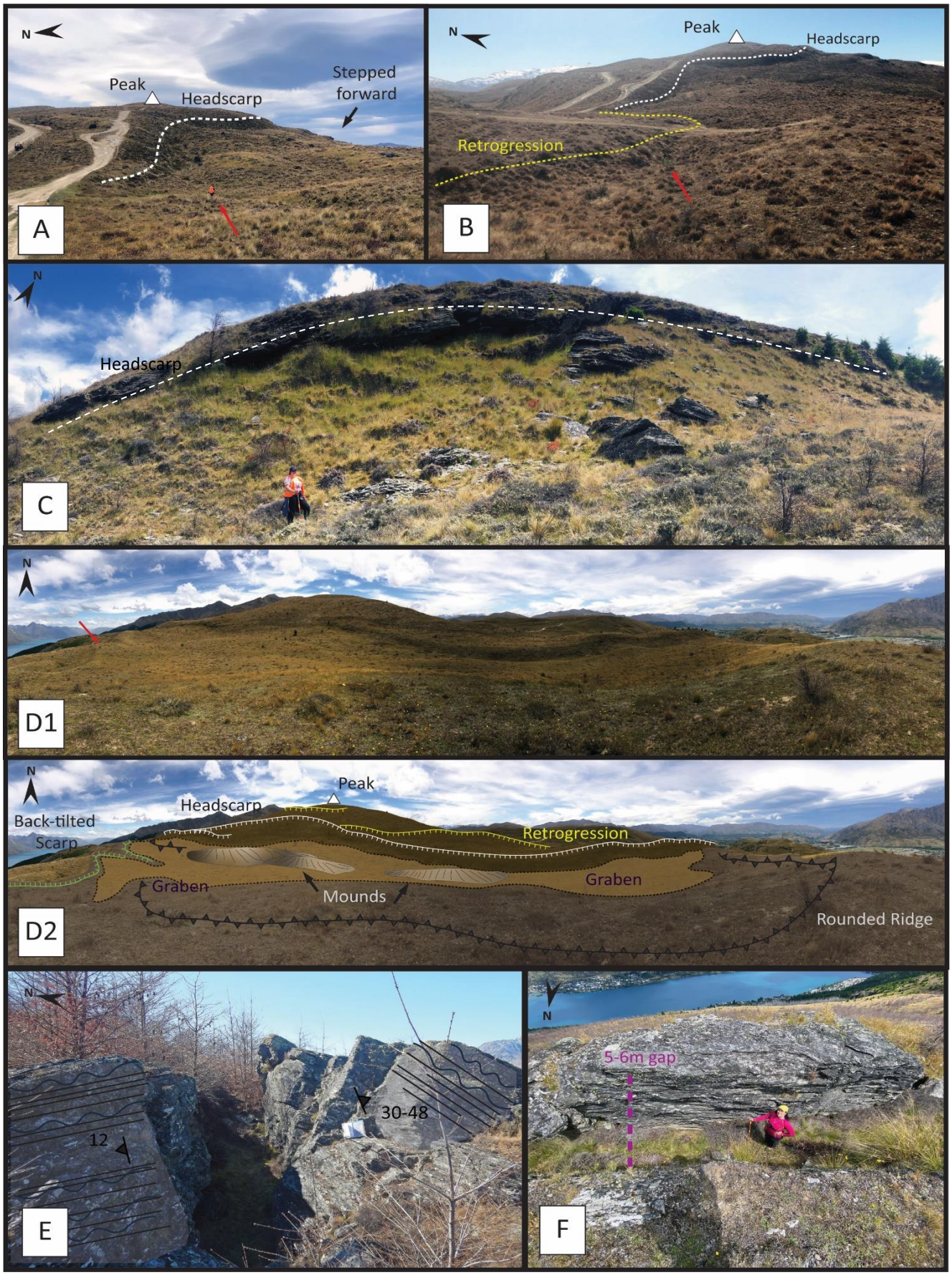

Figure 3.8: (A) Photo showing the degraded main headscarp and subsequent scarps stepping forward. (B) Eroded and grassed over scarps extending beyond the intersection of the headscarp and lateral scarp. Possibly retrogression. (C) The most exposed segment of the main headscarp. Fretting of small (<2 m) schist blocks continues progressively over time. (D1, D2) Sketch depicting the small graben beneath the headscarp. The photo was taken from the top of the graben looking up towards the headscarp. (E, F) Degraded tension cracks and relaxation of schist at the upper end of the landslide. Cracks are up to 3.5m deep, up to 6m wide and individual blocks were measured up to 30m in length. *The red arrows point to a person standing in the field for scale. (May require use of a magnifying glass)

3.6.2 Zone B: Main Landslide Body and Lateral Scarps

The upper-mid portion of the main landslide body extends from 460-800 masl and has an inclination of 23-27° SE. The zone is characterized by a prominent, steep (50°-83°), joint-controlled west lateral scarp, hummocky topography, NE-SW trending tension cracks, a complex drainage network and scattered boulder field across the main slide (Figure 3.9). The west lateral scarp is the most distinguishable feature of the landslide and can be clearly identified on aerial photos, lidar and in the field. The scarp is at least 970 m long, ranges from 3-15 m in height and has an orientation of 82°± 5/071°± 8 (ENE). Three joint sets were recorded along the lateral scarp at 45°/179° (JS1), 40°/004° (JS2) and 18°/209° (JS3, along foliation) (Figure 3.10).

Schist in the upper 180 m of the scarp is not well exposed, as the scarp is relatively degraded and covered in vegetation. Schist exposures in the upper-mid scarp are closely fractured with additional minor joint sets, resulting in a debris talus containing smaller (< 1 m) schist fragments accumulating beneath the scarp. A series of successive breaks in slope occur perpendicular to the northern part of the lateral scarp, from 660-790 masl. The schist exposed in the mid to lower slope is blocky and has a lower fracture frequency than the schist above. Large boulders (2-15 m) were mapped more frequently at the base of the scarp than small debris talus (Figure 3.10). To the south, the lateral scarp becomes poorly defined between 485-555 masl as it transitions to the toe zone.

Hummocks are ubiquitous in the main landslide body; however, a larger proportion are found in the southwest section of the slide. The relief observed in the centre and upper east section is largely attributed to a series of curved degraded scarps oriented from NW-SE, and breaks in slope follow a similar orientation to the major joint sets in the main headscarp. Tension cracks in this zone were mostly mapped in the western half of the landslide and are shorter (< 30 m) and much shallower (< 2 m) than elsewhere on the landslide.

The landslide body has an intricate drainage network, largely promoted by joint sets and faulting. Larger gullies are oriented parallel to the lateral scarps, and smaller incised streams weave across following smaller joint sets or zones of weaker material. A deeply incised drainage (up to 40 m deep) flows from the top of Queenstown Hill into Frankton arm, on the eastern edge of the landslide (Figure 3.10). The drainage orientation coincides with the reverse fault mapped by GNS (GNS Science, 2018). The upper reaches of the drainage are inferred to be part of the east lateral scarp of the landslide. However, the full extent of the landslide boundary to the east remains unclear, as it hard to differentiate between damage caused by landslide displacement or by the intersecting faults. As a result, the schist in this area is likely highly disturbed but minimal vertical offset was recorded in the field (Figure 3.7). The southwest section of the landslide is a good example of the complex rectangular drainage network, where the major gullies share the same orientation with the lateral scarp and are intersected by smaller incised streams. (Figure 3.10).

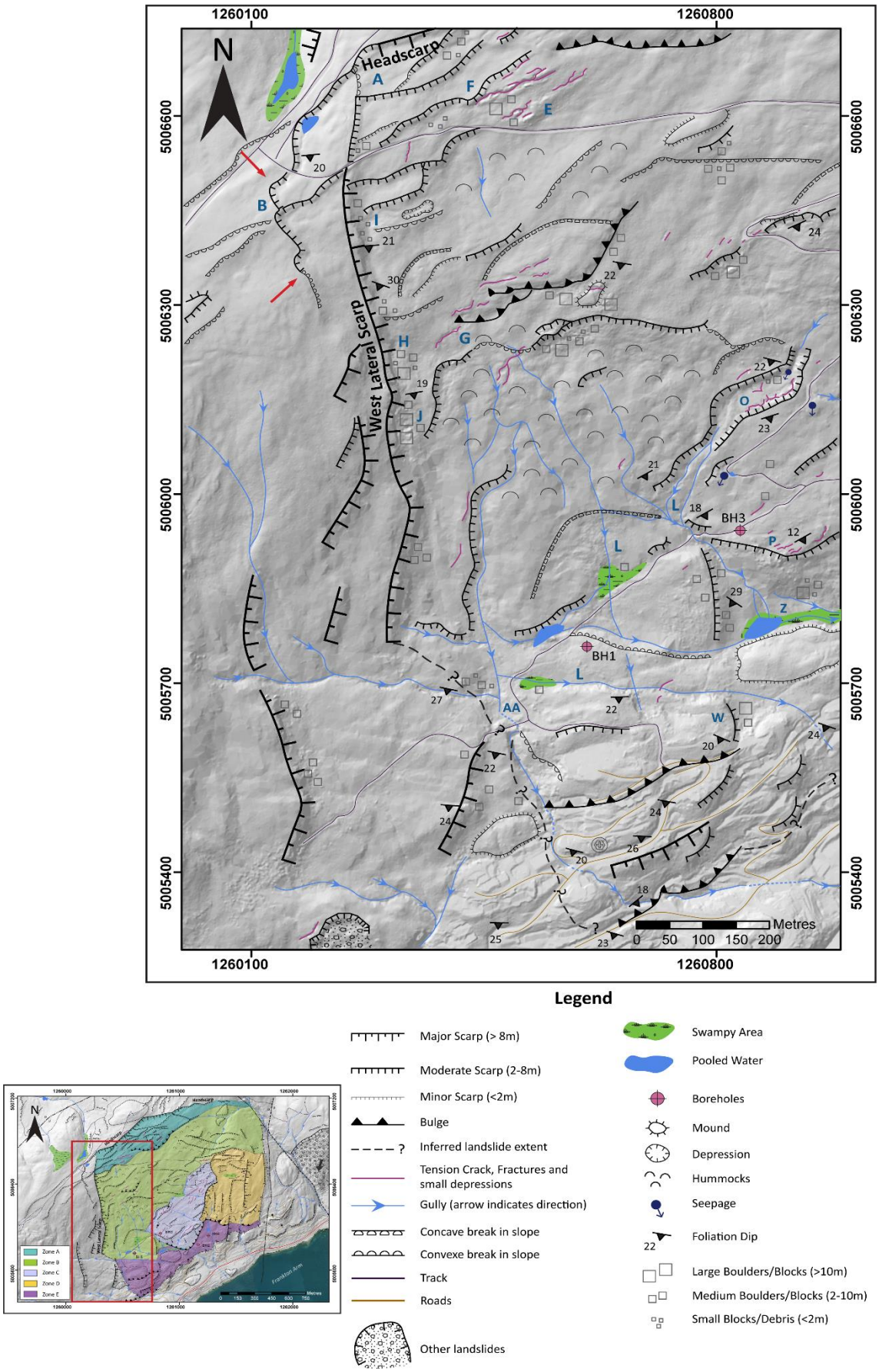

Figure 3.9: Geomorphology of the lateral scarp (east part of Zone B) of the landslide. Scale 1:5,000 on A4. Red arrows point to 2-3m high scarps extending beyond the main headscarp, possible retrogression.
Notes: Letters on the map correspond to photo locations from later figures in this subsection. Representative structural measurements were plotted.

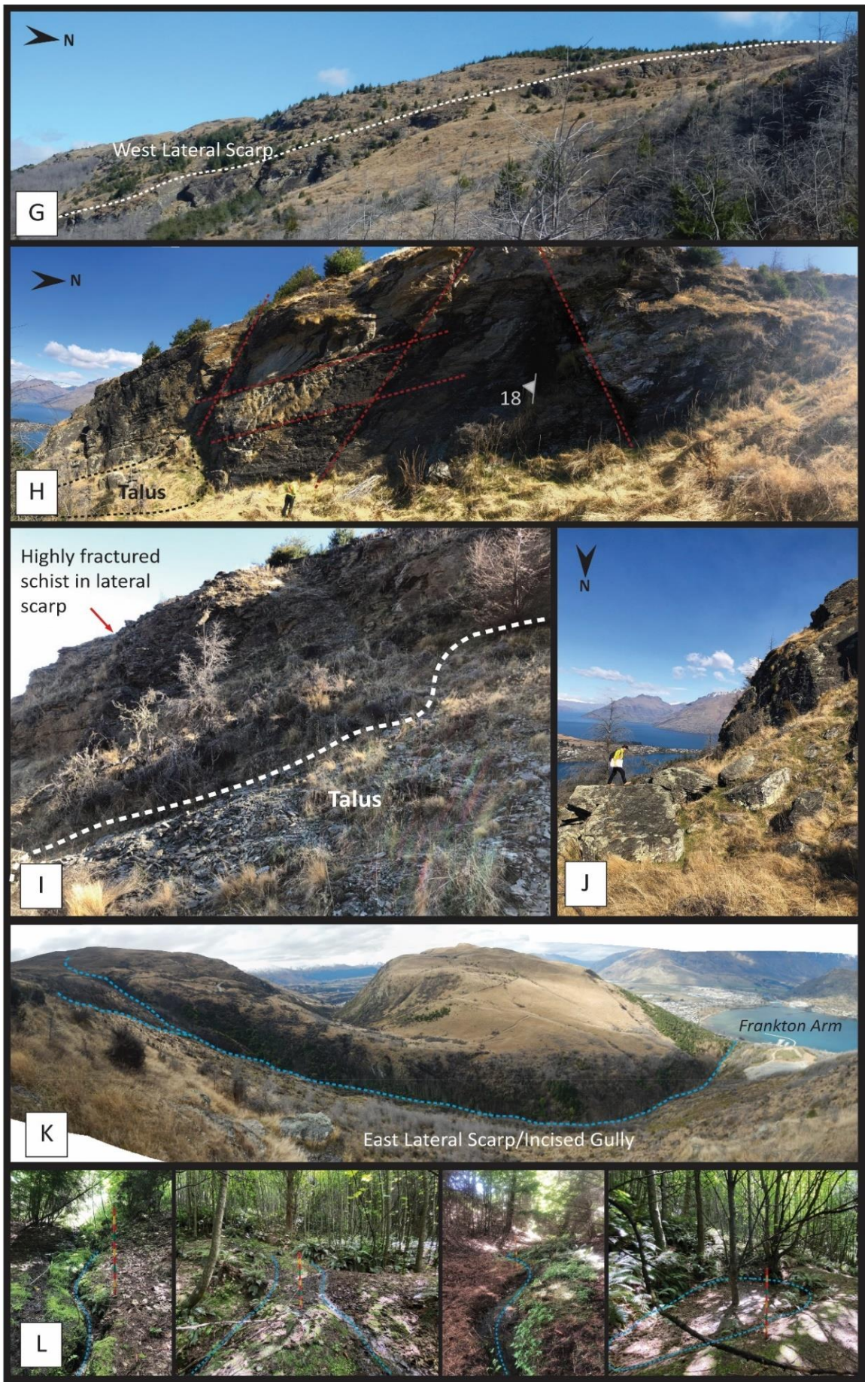

Figure 3.10: (G) Photo showing the west lateral scarp (H) Foliation and joint sets measured along the lateral scarp mid-slope (I) Closely fractured schist dominates the upper portion of the lateral scarp with small debris accumulating at the base of the scarp (J) The debris talus progresses to large rockfall at the base of the lateral scarp downslope. (K) Deeply incised gully extends from the top of Queenstown Hill to Frankton Arm. The gully coincides with the reverse fault along the eastern boundary of the landslide. (L) Various active streams and pooling water from the complex network mid-slope.

3.6.3 Zone C and D: Extensional Zone and Reactivation

3.6.3.1 Zone C: Extensional Zone

The extensional zone of the main landslide body is largely contained within a 250,000 m^2 triangular area mapped in the centre of the landslide from 431-710 masl. The overall slope angle steepens from 23° to 30° and is oriented further south (SSE) in comparison to the main landslide body. Zone C is characterized by steep (60°) joint-controlled stepped scarps, a pull-apart graben, a dense network of deep subvertical NE-SW trending tension cracks, boulder fields and a compressional bulge at the toe (Figure 3.11).

A zigzag scarp pattern extends across the upper boundary of the zone from the northeast to the southwest. The scarps have a vertical offset of 15-25m and are oriented at 73°± 3/179°± 12 (S) and 75°± 5/089°± 6 (E). The slope beneath the scarp steepens to 40°-55° before it transitions into a flat grass-covered depression mantled with blocky debris from forward-toppling blocks released by the joint controlled scarp above. The scarps branch off towards the west and along drainage gullies downslope until they reach the top of a large graben structure at 600 masl (Figure 3.12).

The graben structure measures 70 m long by 180 m wide and is oriented NE-SW. The northwest downhill facing scarp is 5-10 m high and the southeast scarp measures 1-4 m in height. Small scarps (< 2 m), mounds, forward tilted blocks, rockfall along the upper edge, seepage, drainage gullies and subvertical tension cracks measuring 10-60 m in length and up to 8 m deep were mapped in the central collapsed area of the graben.

A high fracture density was recorded in the upper section of the zone, beneath the zigzag scarp, with the frequency decreasing mid-slope. Mid-slope, from 495-505 masl, tension cracks were mapped in proximity to or on top of the compressional bulge and often formed a radial pattern downslope. Fracture length ranged between 0.3-2.5 m in width, 0.5-125 m in length, and with varying depths from a few metres to > 8 m deep. Cracks are predominantly subvertical (80-89°), striking NE-SW, dipping SE with slightly to moderately weathered exposures. Tension cracks and fractures are often controlled by joint sets and discontinuities within the rock (Figure 3.13, 3.14).

Mounds of large (> 8m), rotated blocks were mapped across and at the base of the compressional feature (Figure 3.11). Part of the drainage network flowing above the extensional area (from Zone B) merges and flows along the edges of the toe bulge. Disaggregated material and angled/rotated blocks were recorded where a small portion of the compressional area was exposed by the drainage and through cuttings made as part of the ongoing subdivision development

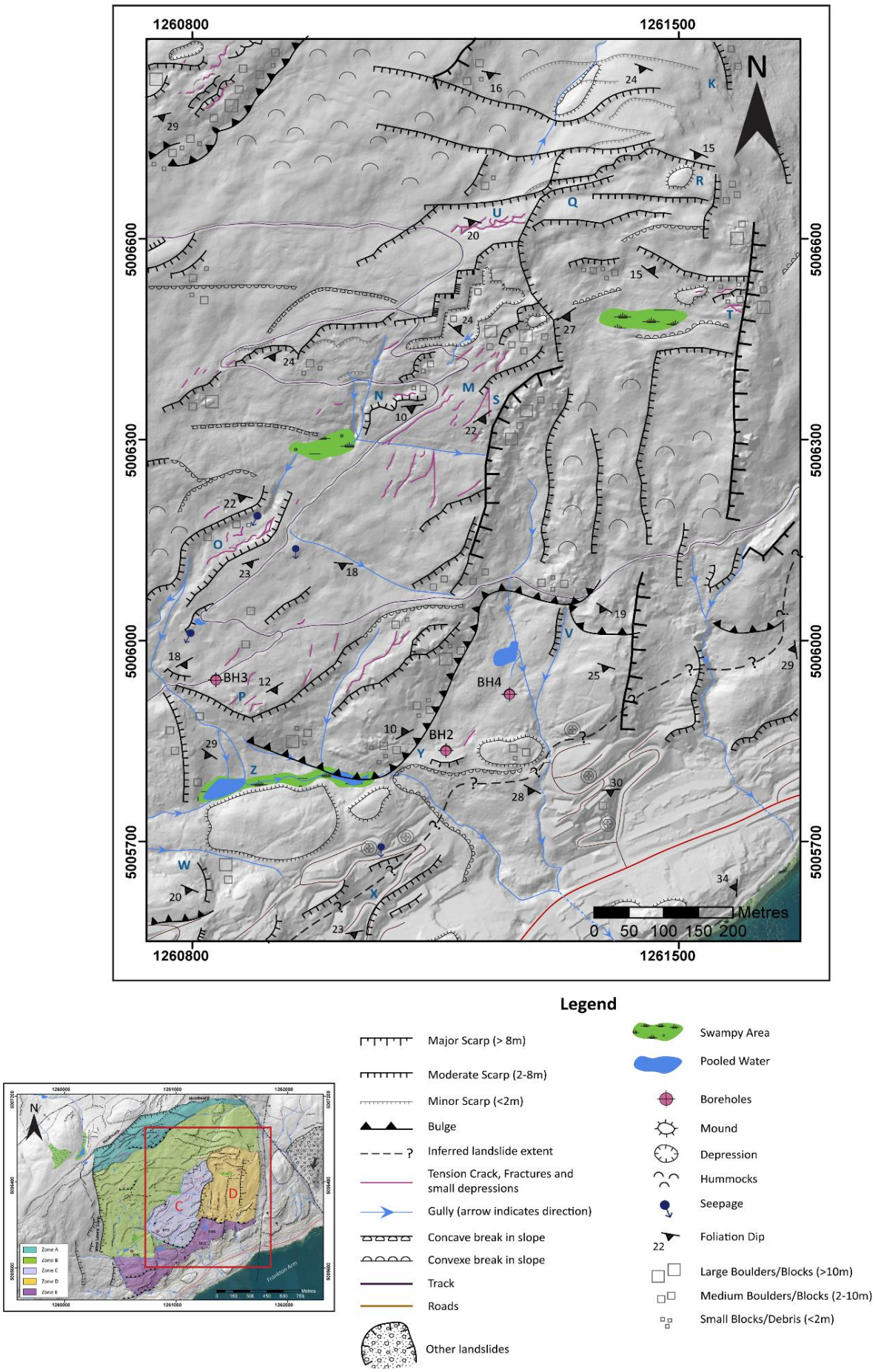

Figure 3.11: Geomorphology of Zone C and D. Scale 1:5,000 on A4. Note: Letters on the map correspond to photo locations from figures in this subsection. Representative structural measurements were plotted.

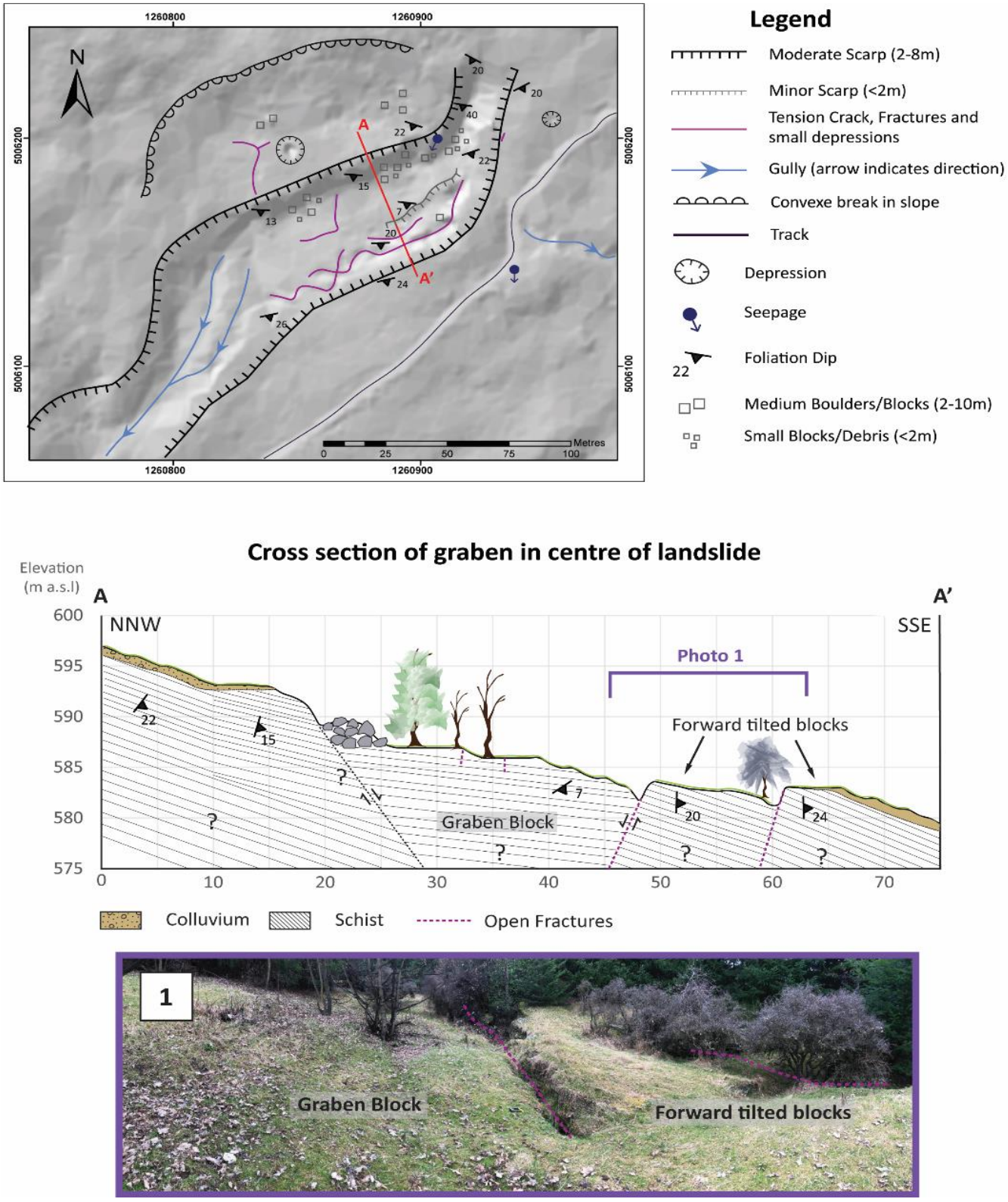

Figure 3.12: Cross section through the graben in the centre of the landslide (Scale: 1:2,000).

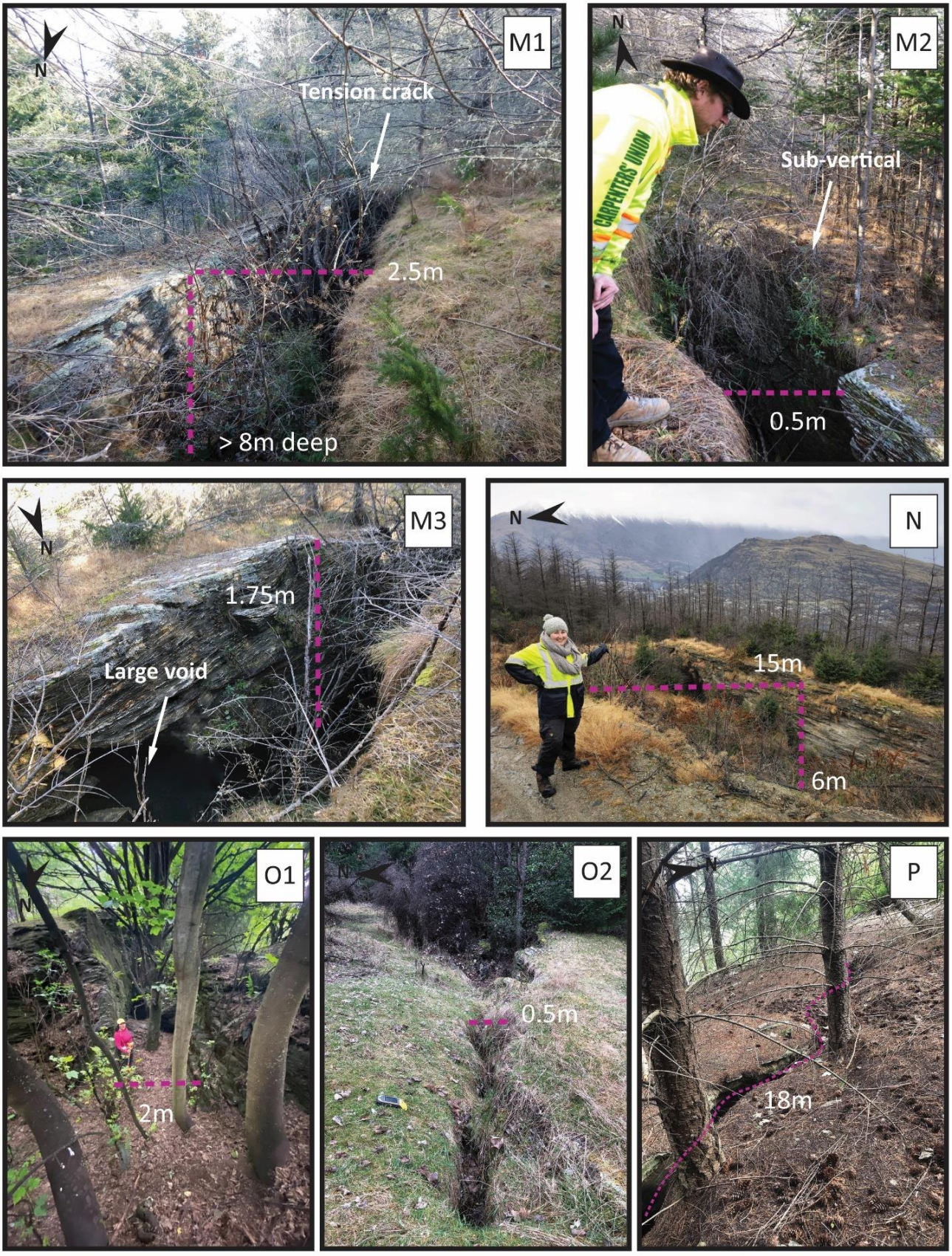

Figure 3.13: (M1, M2, M3) Large tension cracks strike parallel (~NNE-SSW) to the east facing scarps. Cracks are up to 10 m deep and voids are common. Photos were taken in the winter. During the summer months, this area is inaccessible as the cracks become overgrown and are no longer visible. (N) North facing scarp and tension crack along the transition towards the graben downslope (O) Large fractures propagating across the graben structure (P) Uppermost tension crack in the treed area below BH3. Parallel fractures occur further downslope in a radial pattern.

Figure 3.14: (P1) Alternate view of (P) from Figure 3.13. (P2) is the third fracture in a series of parallel fractures that continue downslope. (P3, P4) The released block slid along foliation and the identified joint sets provided a releasing surface.

3.6.3.2 Zone D: Reactivation

Zone D encompasses a 300,000 m^2 area extending from 450 to 700 masl along the eastern edge of the landslide body, with an average overall slope inclination of 32° (similar to Zone C) facing southeast (Figure 3.11). This area is characterized by a series of en echelon scarps facing to the north, two large (< 10 m) east-facing scarps to the east and west (Figure 3.15), two compressional lobes of over-thrusted material to the south, hummocky ground and large (< 10 m) rockfall areas. The pine tree and vegetation density increases from the base of the slope to 610 masl, resulting in a combination of lidar, 1956 aerial imagery and ground truthing being necessary to derive the mid-slope mapping data.

The upper 170 m of Zone D is defined by a series of en echelon scarps, stepping forward downslope with the main scarps measuring 8 m in height, and the smaller scarps varying between and 2-5 m. The scarps are steep (45°-60°), planar and occur along the joint set oriented at 73°± 3/179°± 12 (S) with flat (5°-12°) wide transitions between scarps. The scarps are rounded and grassed over with some outcropping schist blocks to the northeast, where groups of blocks detached from a larger scarp (Figure 3.16). Smaller scarps (1-5 m) mid-slope, at 615 masl, mimic the scarp pattern directly and mark the onset hummocky ground. Rockfall comprised of small to medium boulders (1-5 m) are concentrated beneath rounded scarps mid-slope, where exposure is minimal. Visible blocks are dilated, rotated, subangular and releasing progressively over time.

The east and west boundaries of the reactivation zone consist of large (< 10 m) east-facing scarps, trending North-South. The scarps are 400 m in length, sharp and subvertical (60°-80°) with extensive schist exposures (Figure 3.15). The base of the scarps are littered with large boulders (> 5 m), while smaller blocks (< 5 m) travelled further downslope. Tension cracks and fractures in this zone predominantly occur adjacent to and above the large scarps. Fractures are oriented both parallel and perpendicular to scarps (Figure 3.17).

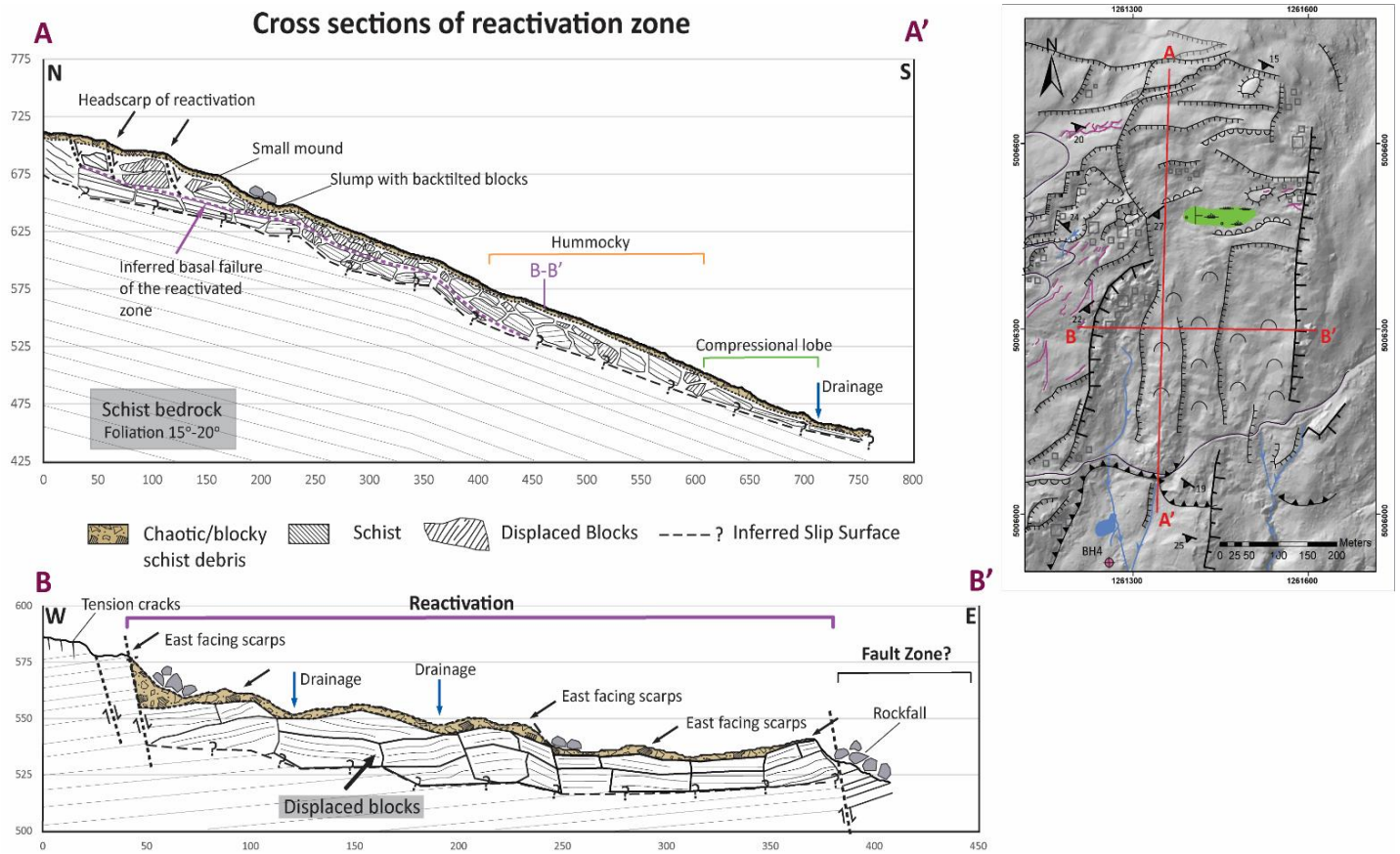

Figure 3.15: Cross sections through the reactivation zone showing a series of east facing scarps. The failure surface is inferred.

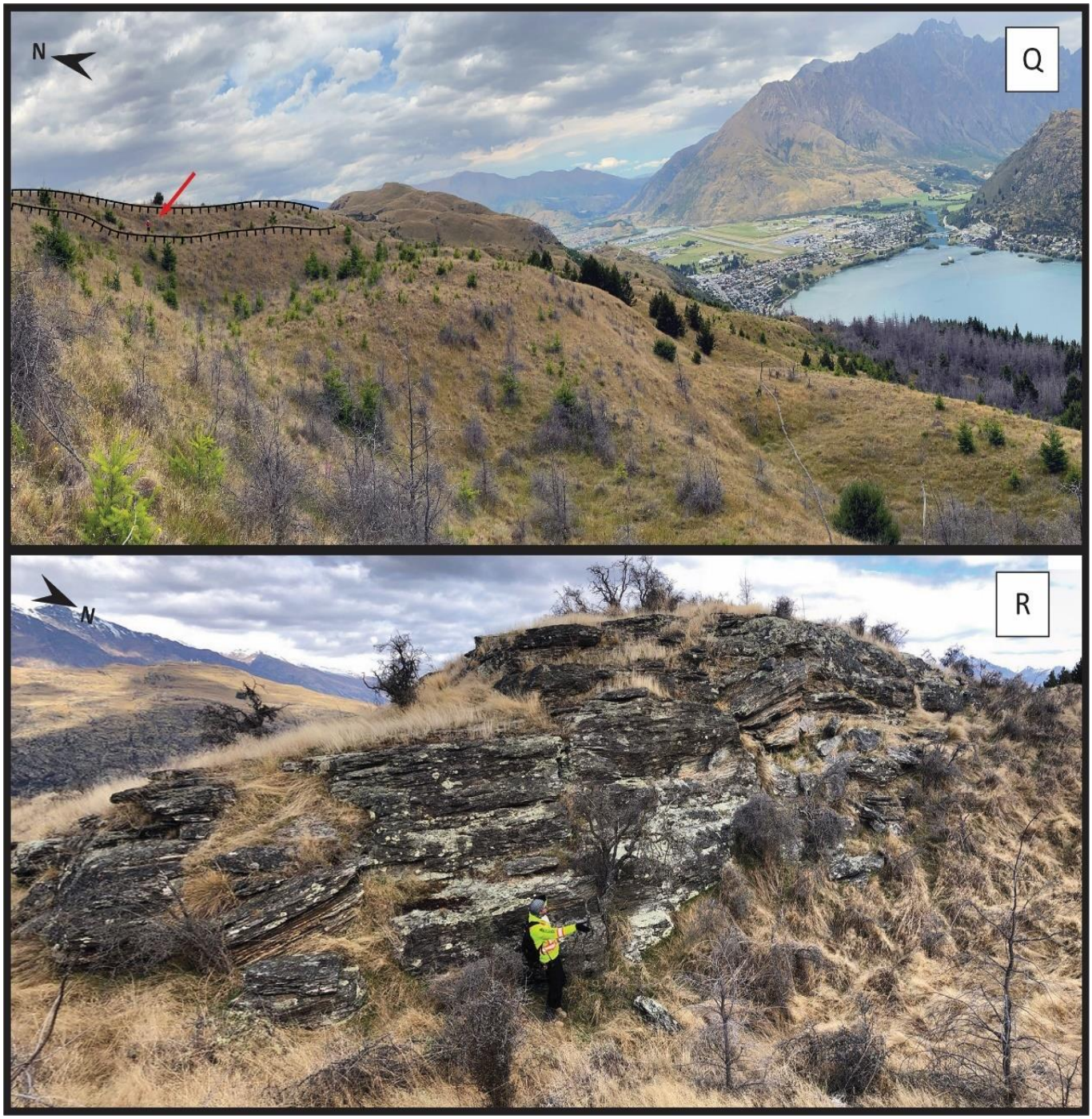

Figure 3.16: (Q) View (facing east) of the reactivation headscarp. > 5 m, steep scarps with wide flat transitions between (R) Group of detached blocks above the main reactivation scarp to the northeast. The blocks are oriented similarly to the major scarp in Photo Q *The red arrows point to a person standing in the field for scale. (May require use of a magnifying glass)

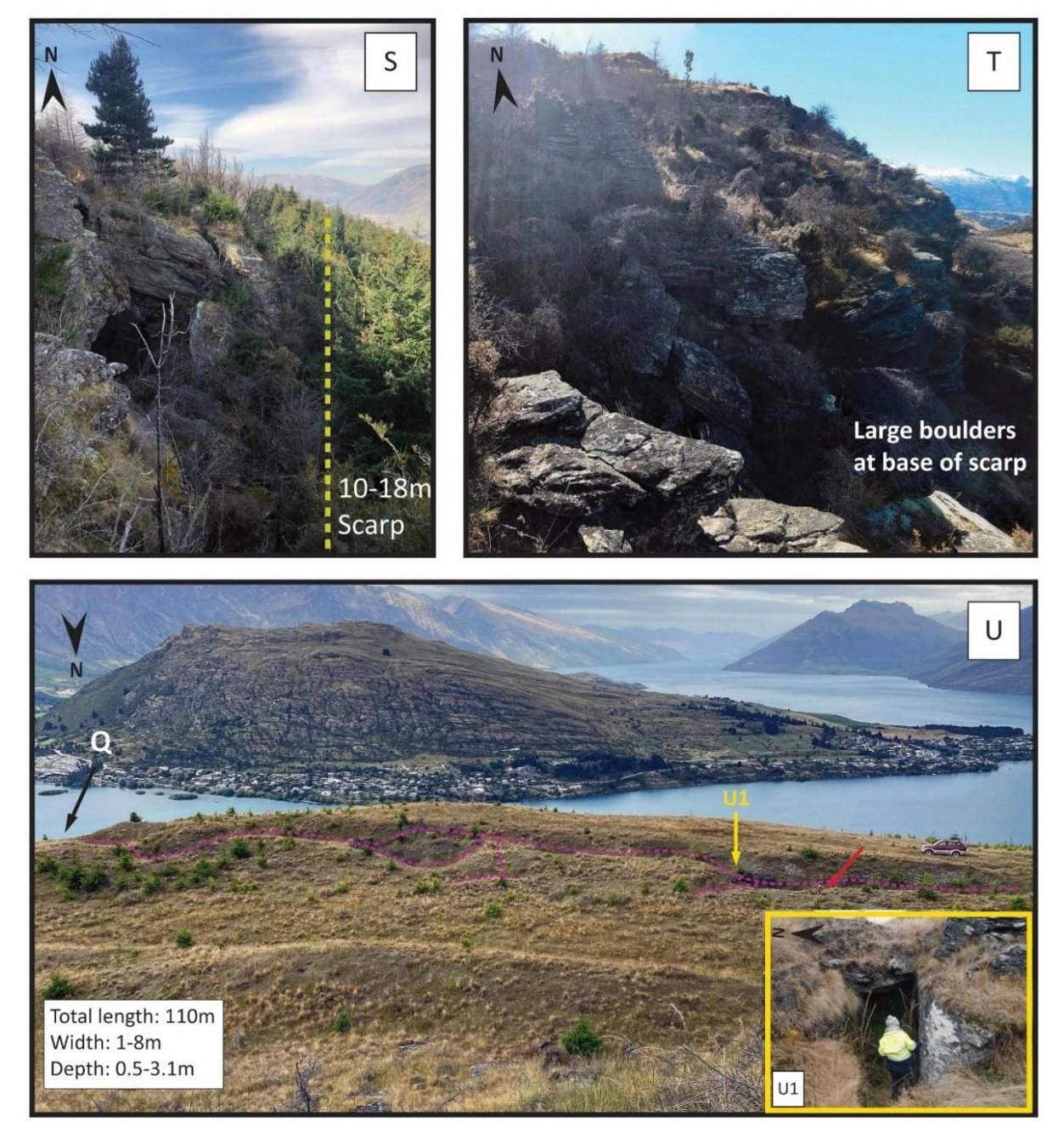

Figure 3.17: (S) Western boundary of Zone D marked by an east-facing subvertical, slightly to moderately weathered, fractured scarp with large (> 10 m) boulders at the base. (T) Eastern boundary of Zone D marked by an east-facing steeply inclined, weathered scarp with large mounds of medium to large (2-10 m) sized subangular boulders at the base. (U) Photo of a 110 m long tension crack connected to the main scarp of the reactivation zone. The tension crack shares a similar orientation to the reactivation headscarp. The opening could be interpreted as retrogression of Zone D. (U1) Wandering inside the tension crack for scale. The red arrow in photo U points to the top of the person's head - for scale and for science!

450-525 masl marks the transition from extensional to compressional features followed by an increased presence of hummocks between the N-S trending scarps, at 505 m-525 masl. Along the lower margins of Zone D, three prominent lobes comprised of over-thrusted large (> 8 m) displaced schist blocks are overlain by slightly to moderately weathered, medium subangular rotated blocks (2-8 m) and fragmented schist debris. The mounds are predominantly grassed over with the exception of recently excavated exposures (Figure 3.18).

The excavated exposure includes 2.5 m of weak fissile schist dipping at 19°/224° and is overlain by 2.5 m high x 10 m+ long displaced schist blocks. The displaced blocks are moderately weathered, fractured, and dilated. The foliation dip is similar to the fissile schist with a noticeable change in strike. Along the margins of the displaced blocks and fissile schist, there are large piles of schist fragments and debris. The debris is dry and moist with rotated schist blocks up to 1.5 m in a matrix of schist fragments ranging from 0.5 - 300 mm and minor silts (Figure 3.18). These chaotic debris piles are mapped along the base of all compressional features across the landslide with active drainage flowing along the outer edges and gullies oriented N-S along scarp bases.

Figure 3.18: (V1,V2) Cross section view of an excavated portion into the compressional lobe at the base of Zone D. This area is also included as part of the overall toe zone, due to its compressional nature at the base of the slope. Chaotic debris piles are mapped along the base of all compressional features across the landslide with drainage flowing along the outer edges. (V3) Displaced blocks on top of a compressional lobe exposed by tree clearing and excavation. (V4) Chaotic block mound along the margins of a compressional lobe.

3.6.4 Zone E: Toe Zone

The toe area of the landslide is a broad undulating zone across the base of the slope, between approximately 400-500 masl. The slope angle is highly variable (5°-80°) with an average slope inclination of 25° SSE. The zone is characterized by undulating topography (bulges, mounds, and boulders), a complex drainage network, swampy areas, a series of moderate scarps, and subdivision development (Figure 3.19). Subdivision development has both obscured large-scale geomorphic features as well as increased local outcrop exposure at the base of the slope. As a result, this area was mapped using a combination of aerial imagery (1956) and field mapping to delineate the possible toe zone.

The upper extent of the zone is bound by compressional features and drainage, while the lateral margins are constrained by major scarps (> 10 m) and drainage. Two compressional lobes, which were also identified as part of the lower boundary of Zones C and D, are mapped as the upper boundary of the toe zone. These bulges are characterized by large (> 10 m) dilated displaced schist blocks with small to moderate (1 m - 8 m) subangular rotated blocks on top and schist fragments (<1 m) along the margins (Figure 3.20).

The western margin of the zone is bound by deeply incised drainage along the lateral scarp. Drainage and gullies within the toe zone trend along the margins of compressional features, and along N-S and NW-SE joint sets. As a result of the extensive and complex drainage network, swampy ground and pooling water were mapped across this zone (Figure 3.21).

The lower extent of the toe zone is within subdivision developments along the Frankton Arm. Development currently extends up to 450 masl and recent excavation for future development up to ~500 masl. There is an increased number of short (50-80 m), steep scarps, piped drainage, minor seepage in road cuttings, and exposed moderately to highly weathered fissile schist. The base of the toe zone is poorly defined, but has been tentatively mapped along a semi-continuous band of weak, fissile schist at ~390 masl, coinciding with an increase in stability measures in road cuttings.

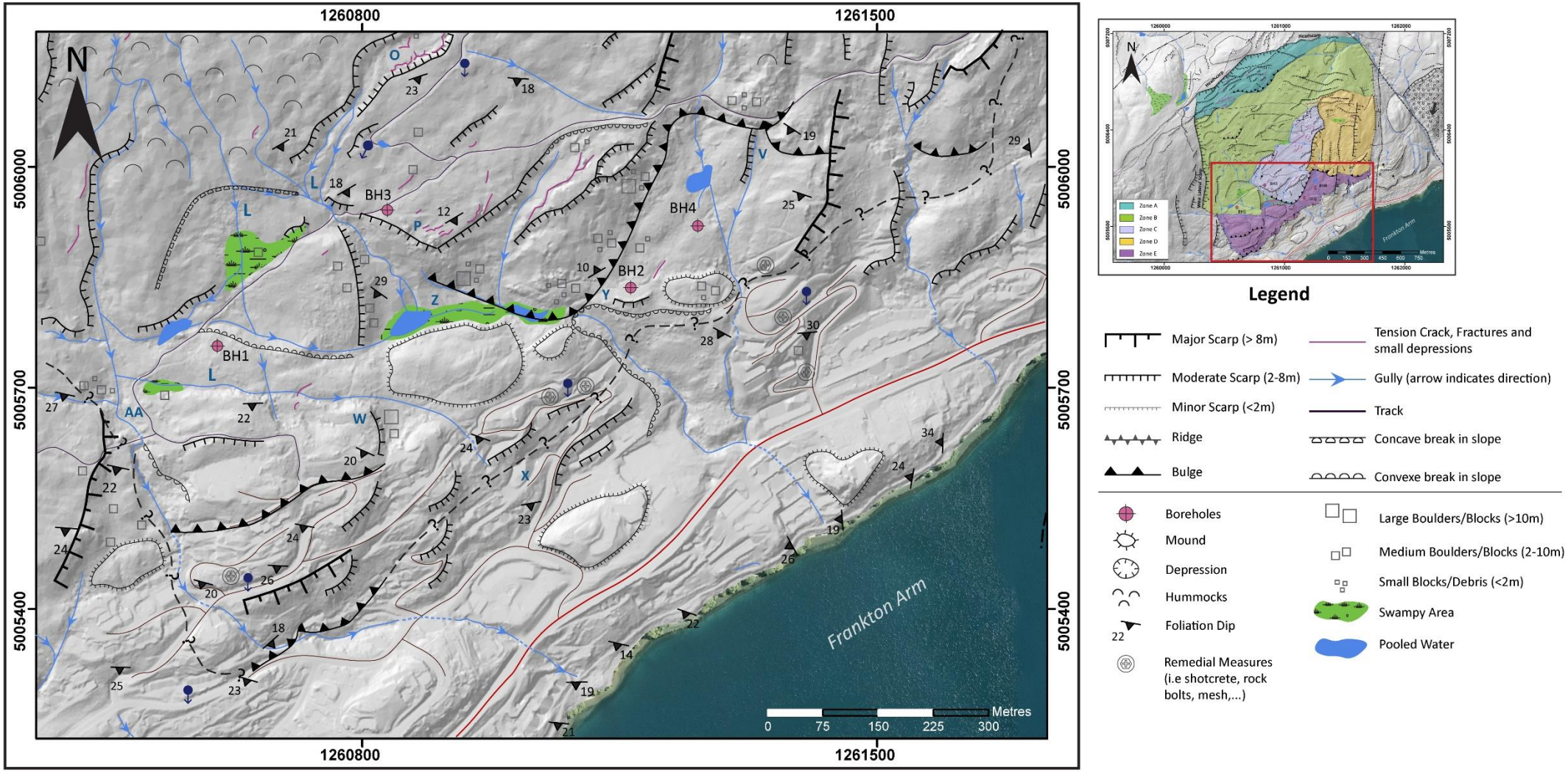

Figure 3.19: Geomorphology of Zone E. Scale 1:5,000 on A4.
Note: Letters on the map correspond to photo locations from subsequent figures in this subsection. Representative structural measurements were plotted.

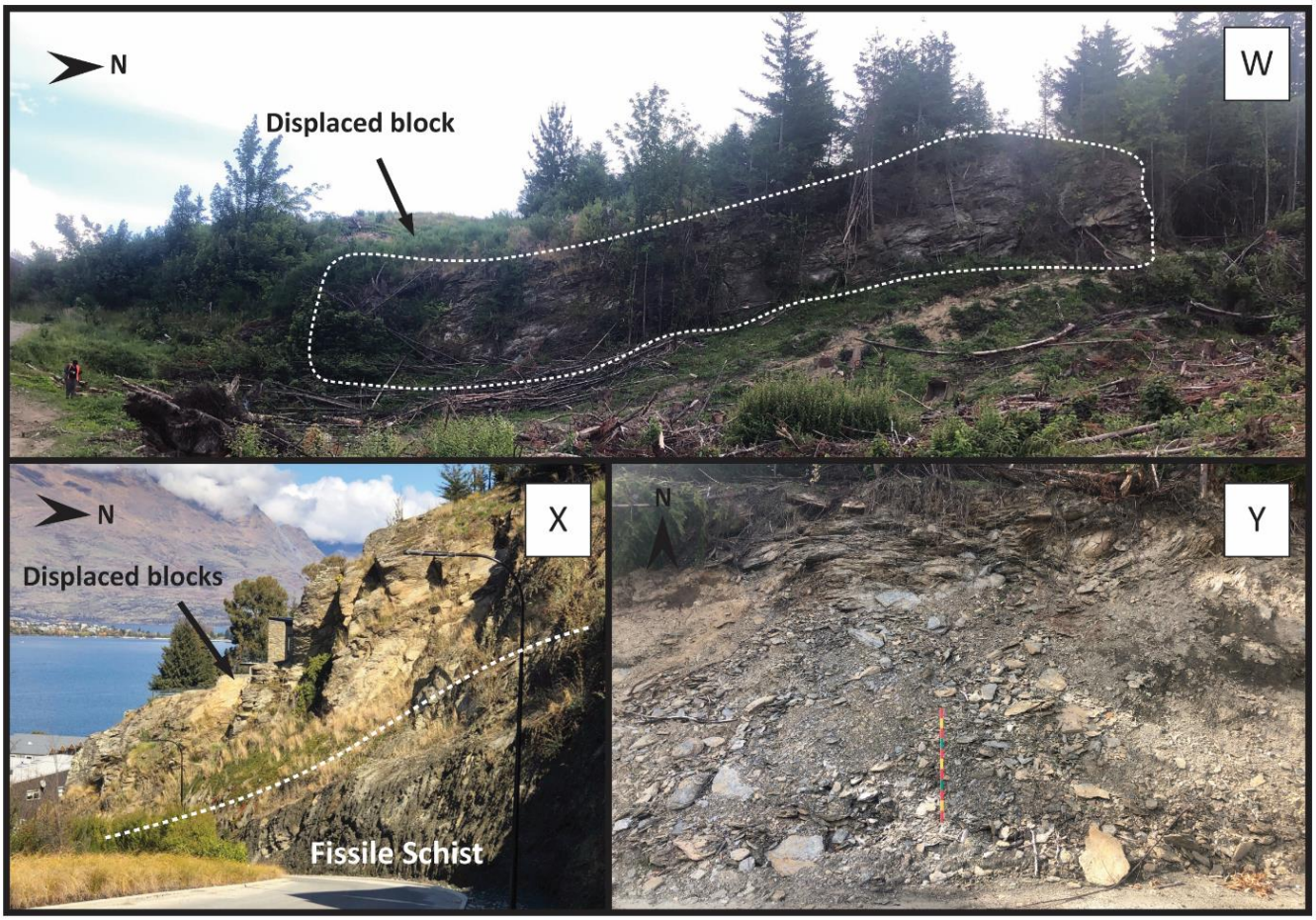

Figure 3.20: (W) Photo of a 35 m long displaced schist block (X) Similar sequence to the one recorded in Figure 3.18 V. Photo taken at the lower boundary of the toe zone in proximity to the semi-continuous band of weak fissile schist. (Y) Chaotic schist debris exposed in recent excavation of the base of the large compressional bulge at 425 masl. Composition identical to the debris in Figure 3.17 V.

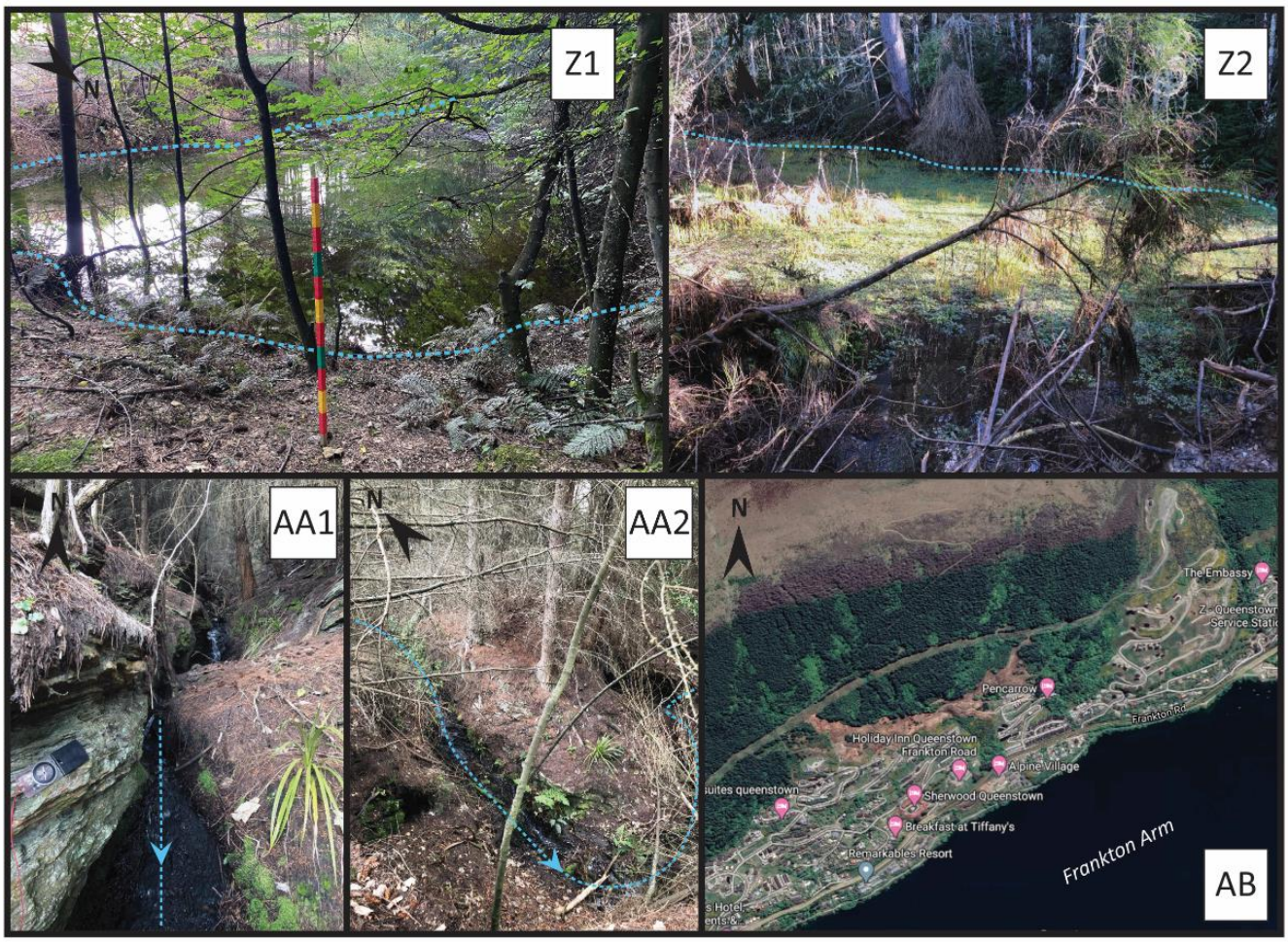

Figure 3.21: (Z1, Z2) Photos of pooling water and swampy ground. Ponds are fed by multiple converging streams with water retained behind mounds. The pooled water drains out through a small stream. (AA1, AA2) Deeply incised drainage along the west lateral scarp in toe zone (AB) Most recent satellite photo from Google Earth showing the extent of subdivision development at the base of the slope. The orange-brown area beneath the trees marks recent clearing for new development.

3.7 Surficial Deposits: Field Descriptions

Quarternary deposits surrounding the Queenstown Hill landslide and schist within the landslide boundaries were mapped by previous investigations (Figure 3.3). Material descriptions were interpreted as beach, fan, fan/delta, undifferentiated glacial deposits and colluvium (Barrell et al., 1994; Cunningham, 1994; Stossel, 1999). Mapping the extent of surficial deposits or confirming the current mapped extents exceeds the scope of this thesis. However, descriptions of surficial materials were recorded in the field when exposed in outcrop. This data was used to collate and compare data from previous investigations with this investigation (Figure 3.22) as well as to annotated cross sections and diagrams in Chapter 5. Summary descriptions of the units are compiled below for reference, but will not be further discussed.

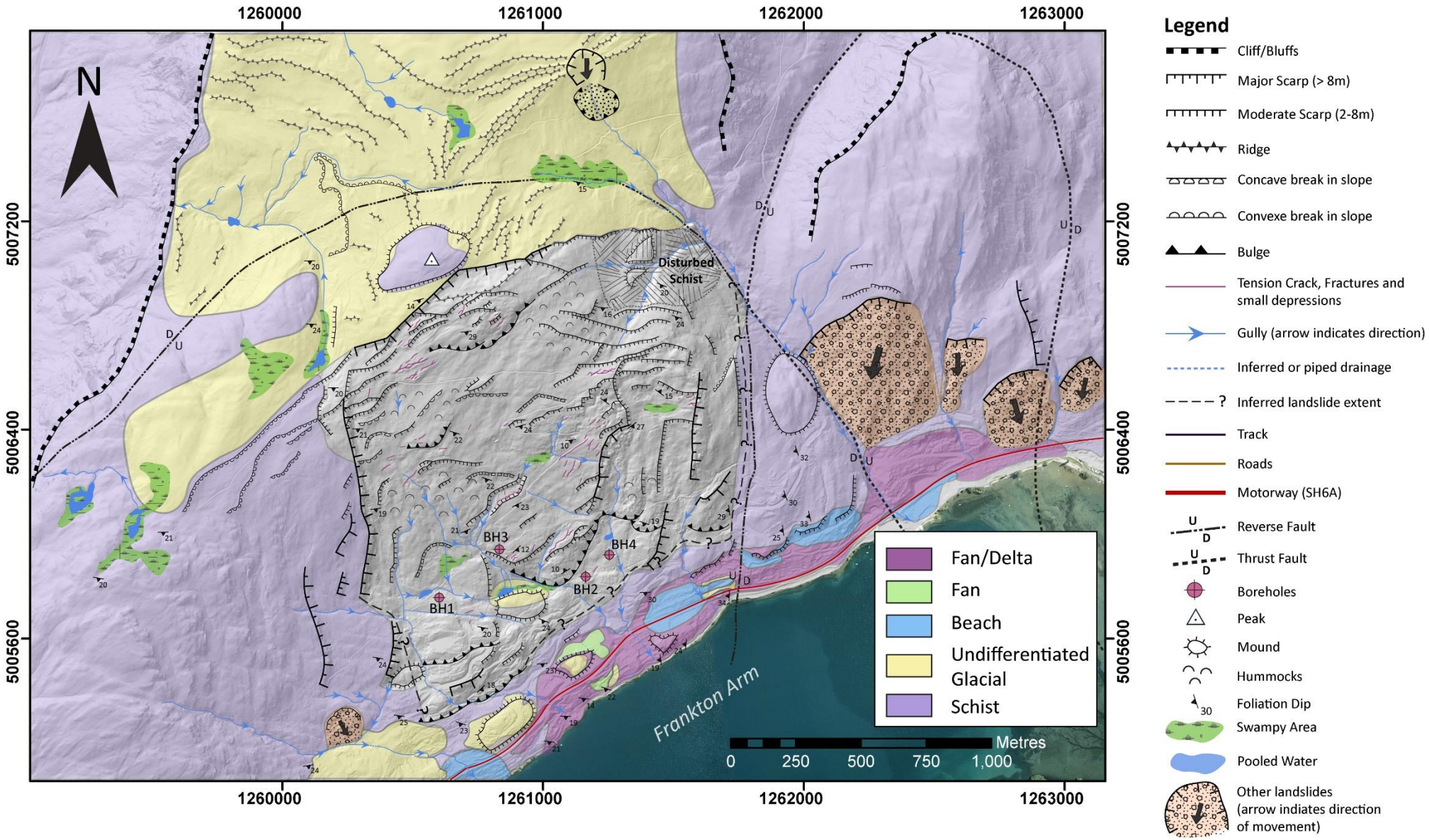

Figure 3.22: Surficial deposits from Figure 3.3 superimposed onto the geomorphic map of the Queenstown Hill landslide (grey). Scale 1:15,000 on A4. Refer to chaotic/blocky schist debris (3.7.1.2) for a description of the landslide material. Disturbed schist area shows minimal vertical displacement (< 1 m).

3.7.1 Undifferentiated Glacial Deposits

Glacial deposits in the study area vary in thickness, up to 4 m, and are predominantly made up of sandy gravels and gravelly sands and silts. Large 0.5-2 m erratic boulders were recorded on the top of Queenstown Hill. In other areas, an orange-brown post glacial weathering profile is present in the upper 1-2 m. Glacial deposits outcropping in track cuttings on top of Queenstown Hill (Figure 3.23) are described, using NZGS, as:

Silty sandy GRAVEL with cobbles and boulders; dark brownish grey, massive. Medium densely packed; firm; moist; well graded; no plasticity; thick; gravels and boulders, subrounded to rounded, slightly to moderately weathered

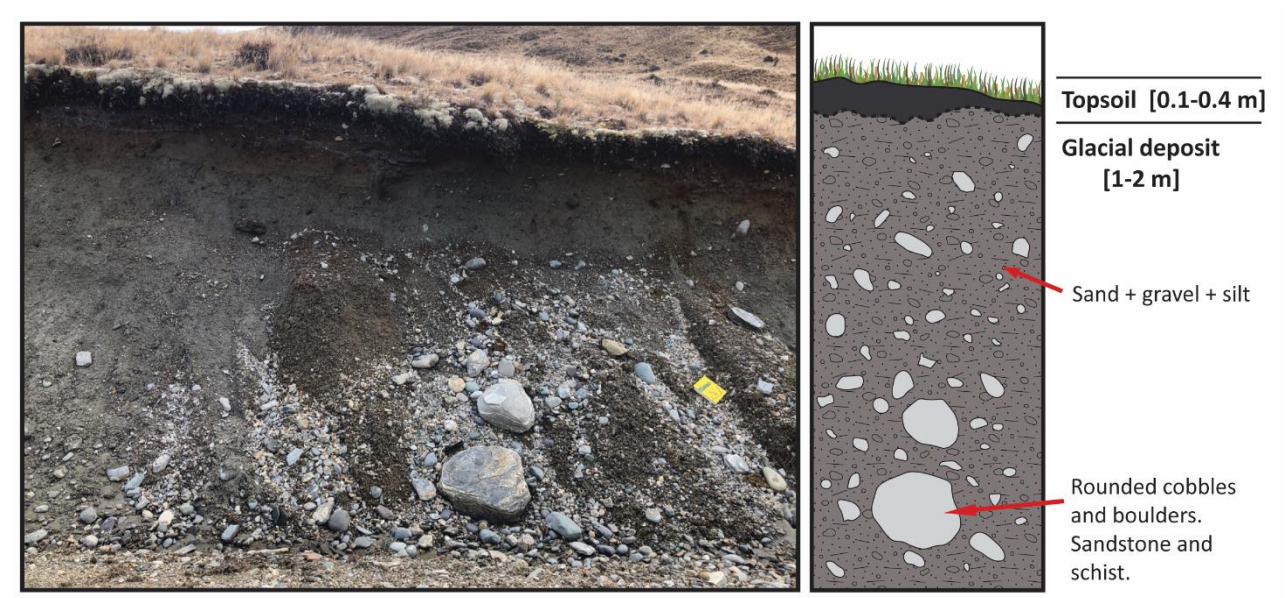

Figure 3.23: 1-2 m exposed glacial deposits in track cuttings along the top of Queenstown Hill. Silty sandy GRAVEL with cobbles and boulders. Cobbles and boulders up to 0.8 m in diameter are made up of Caples group sandstone and schist.

In the lower margins of the slope, two types of glacial deposits were exposed during excavation. A weathered orange-brown sandy gravel with subordinate silt and a blue-grey silty gravel overlain by weathered glacial deposits with a gradational contact. Weathered glacial deposits exposed in recently excavated ground, between 415-500 masl, (Figure 3.24) are described, using NZGS, as:

Figure 3.24: 1 m exposed glacial deposits in excavated area along the lower portion of the landslide. Gravelly SAND with silt with exposed post glacial weathering profile.

gravelly SAND with silt; orange-brown, massive. Densely packed; firm; moist; moderately graded; no plasticity; thick; gravels, subrounded, moderately weathered.

Unweathered silt and clay-rich glacial deposits (Figure 3.25) were recorded at 490 masl, and described as:

clayey GRAVEL with traces of sand; blue-grey, massive. Medium densely packed; firm; wet; well graded; moderate plasticity; thick; gravels, rounded to subgrounded; slightly weathered.

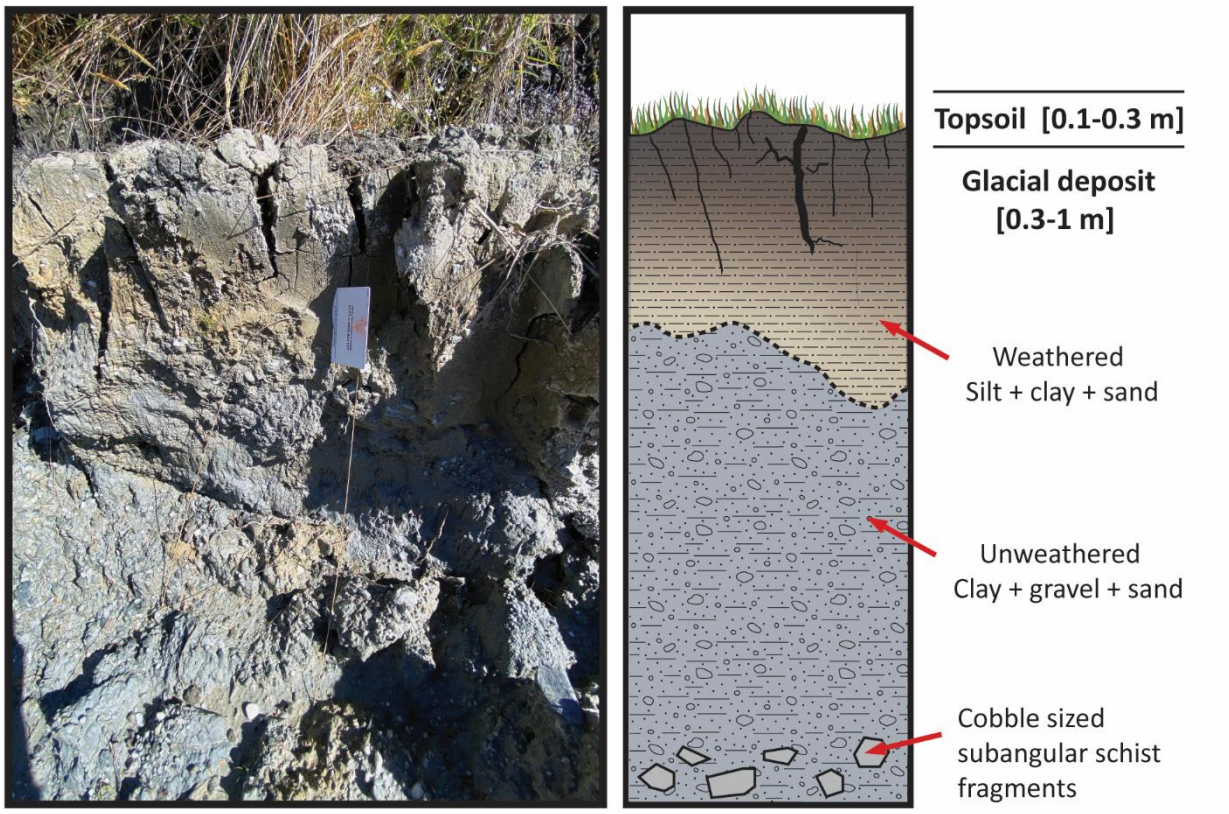

Figure 3.25: 1 m exposed shiny micaceous clay containing subangular schist gravels. Gravels not solely sourced from landslide material, other schist lithotypes and sandstones visible. This unit sits above and below a swampy, peaty layer mapped further downslope. Less than 5% of this deposit contains fragments larger than gravels.

3.7.2 Chaotic/Blocky Schist Debris

Chaotic/Blocky schist debris (mapped as colluvial deposits in Figure 3.3) are exposed in road/track cuttings, recent excavations and along large scarps within the landslide (Figure 3.26 and 3.27). Mapped deposits range in thickness from 0.3 m to 3 m and are sourced from schist bedrock. They can generally be described as:

cobbly BOULDERS with fine to coarse gravels and minor sand; grey, massive. Densely packed; firm to hard; dry; well graded; no plasticity; thick; boulders, dilated and fractured, subangular to angular, displaced and/or rotated, slightly weathered to moderately weathered; cobbles, subrounded to angular, slightly to moderately weathered

Figure 3.26: 2 m exposed chaotic/blocky schist debris in track cutting at the top of the landslide. Large displaced fractured block in a matrix of angular cobbles and sandy gravel.

The fractured, displaced/rotated blocks range in size from 0.3-3.5 m, are slightly to moderately weathered and can include large voids between blocks. The matrix is predominantly made up of gravel to cobble schist fragments and some fines (silt and sand), however 0.3-1.5 m thick pockets of glacial deposits have been identified adjacent to or within the colluvium.

Figure 3.27: 3 m exposed chaotic/blocky schist debris in track cutting within the landslide. Large (2m) rotated schist blocks in a matrix of angular cobbles, sandy gravel, and glacial material.

3.7.3 Beach/Shoreline deposits

Beach deposits (Figure 3.28) were mapped outside of the landslide area, along Frankton arm and in road cuttings at Kelvin Heights. Beach deposits consist of discoidal schist fragments and interlayered sand and gravel deposited at higher shorelines of Lake Wakatipu. The deposits were described as:

sandy GRAVEL with minor silt and cobbles; light grey and taupe, interlayered with planar gravels. Densely packed; stiff to hard; dry; gap graded; no plasticity; thick; gravels, angular to subrounded, slightly to moderately weathered

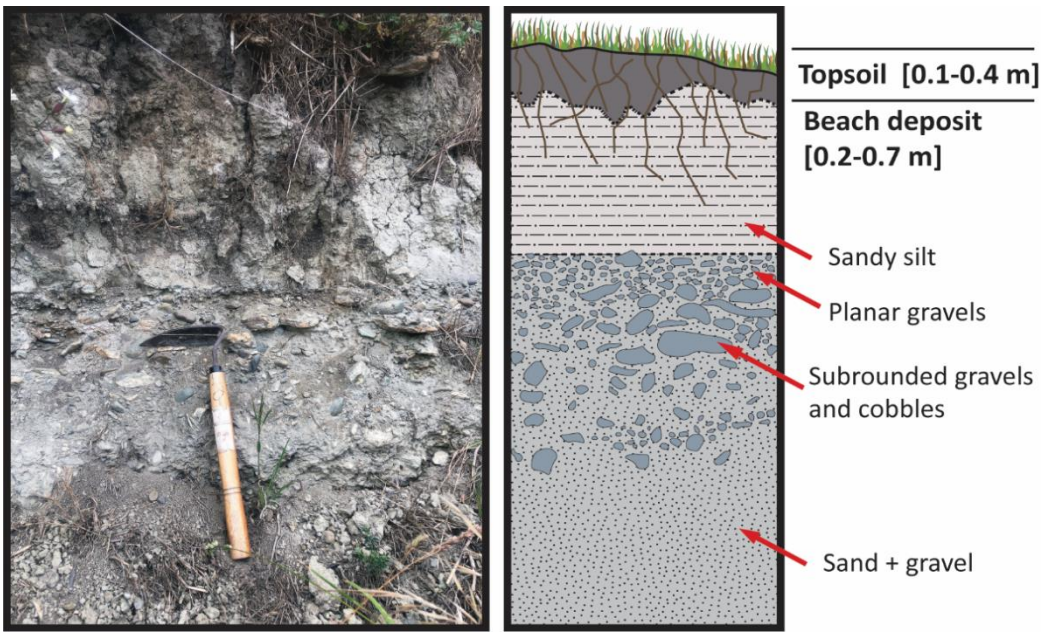

Figure 3.28: 1 m exposed beach shoreline deposit. Identified by the combination of pea gravels mixed with angular gravels and cobbles. The angular gravel fragments are imbricated along the contact between sandy silt and the beach deposit.

3.7.4 Lake deposits

Lake deposits (lake bottom sediments) (Figure 3.29) were mapped in the road cutting, along State Highway 6 (Kingston Rd.), on the south side of the Kawarau River. The deposit is made up of horizontal layered, interbedded micaceous silt and clay. Laminae thickness ranges from > 1mm to 70 mm, increasing with depth. Oxidation occurs predominantly along clay beds and is 1-11 mm thick. The deposit is described as :

clayey SILT with traces of sand; light and dark grey, subhorizontal and interbedded. Densely packed; firm to very stiff; dry; uniformly graded; no plasticity; thick; slightly to moderately weathered

Figure 3.29: 3 m bench of exposed lake deposit in road cutting along SH6.

3.8 Minor Structures

Very few fresh/recent features were mapped within the landslide. Of note, minor erosional features were measured in September 2019 and again in January 2020. These features are oriented in a similar direction as tension cracks and fractures in close proximity. Finer material is being eroding either between displaced blocks or along joint sets beneath the veneered surface leaving small cavities/holes at the surface (Figure 3.30).

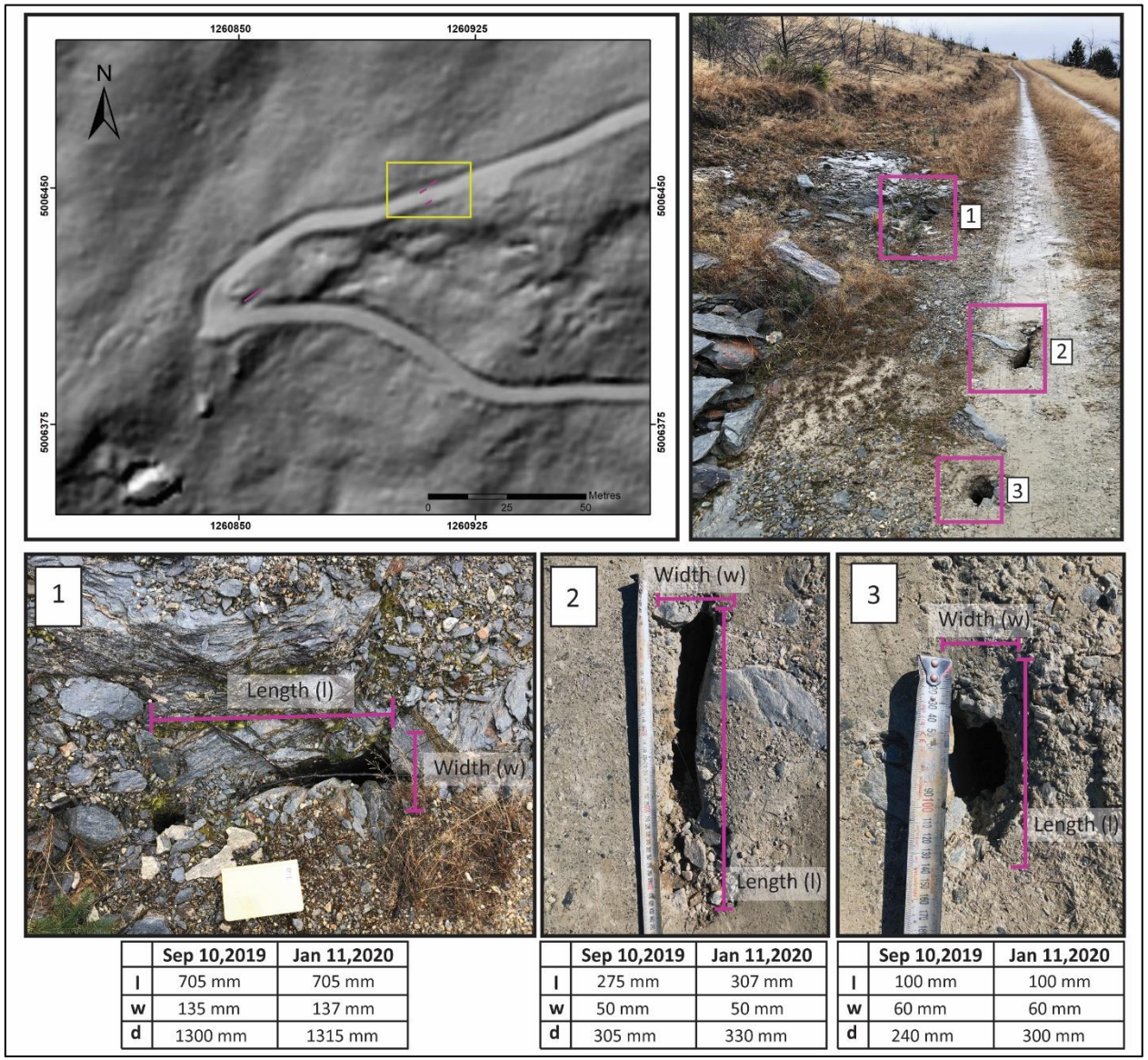

	Sep 10,2019	Jan 11,2020
l	705 mm	705 mm
w	135 mm	137 mm
d	1300 mm	1315 mm

	Sep 10,2019	Jan 11,2020
l	275 mm	307 mm
w	50 mm	50 mm
d	305 mm	330 mm

	Sep 10,2019	Jan 11,2020
l	100 mm	100 mm
w	60 mm	60 mm
d	240 mm	300 mm

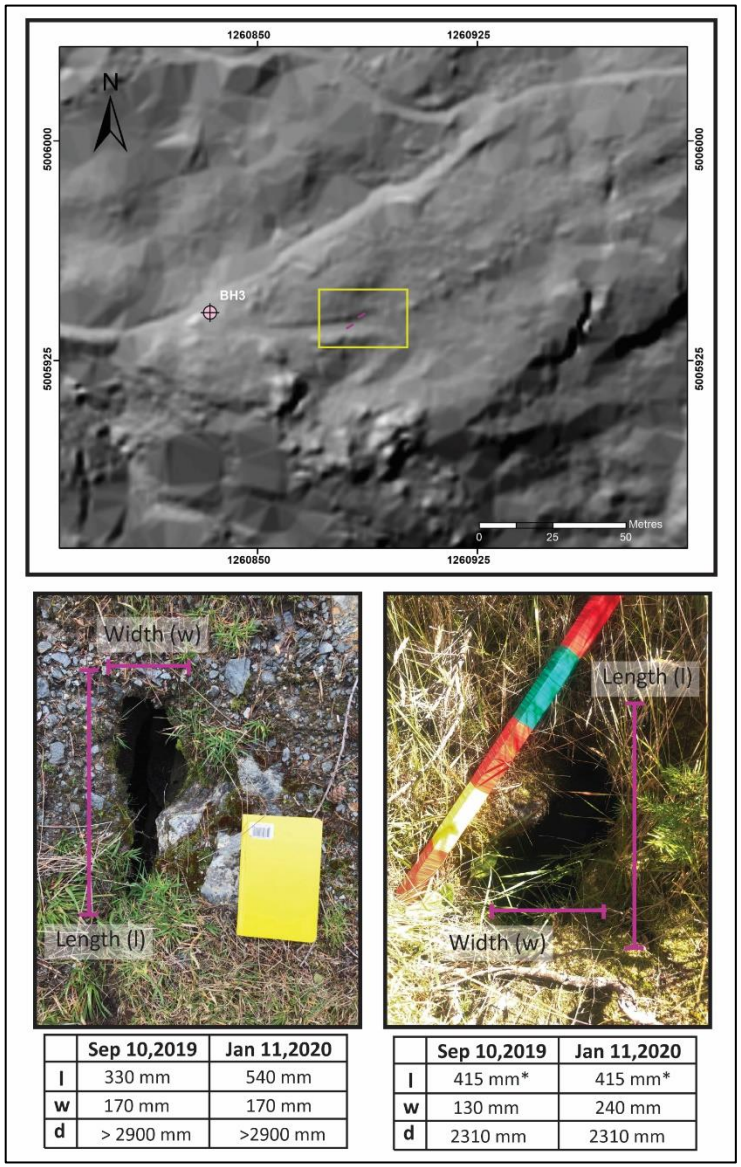

	Sep 10,2019	Jan 11,2020
l	330 mm	540 mm
w	170 mm	170 mm
d	> 2900 mm	>2900 mm

	Sep 10,2019	Jan 11,2020
l	415 mm*	415 mm*
w	130 mm	240 mm
d	2310 mm	2310 mm

Figure 3.30: The series of photos on the left were taken on the upper-mid section of the farm track up Queenstown Hill. The series of photos on the right were taken off the farm track ESE of BH3. Both photo series show small voids beginning to form as part of regular erosional processes. Very minor changes were recorded between September and January.

3.9 Discussion and Synthesis

The geometry of the Queenstown Hill landslide is decribed as a rectangular, blocky joint-controlled landslide with clearly defined margins at the crown (north), along the west lateral scarp, while the eastern boundary and the toe area are poorly defined. Geomorphic mapping identified five zones (Figure 3.3) based on distinct surface morphologies: (1) a joint controlled headscarp; (2) the main landslide body with a subdued hummocky topography and well established drainage; (3) an extensional zone characterized by a graben and large tension cracks (> 5 m deep, up to 100 m long); (4) a reactivation zone interpreted as a separate phase of movement; (5) a complex undulating toe zone bound by compressional features and subdivision development.

Although the northern and western boundaries of the landslide are clearly defined, the eastern boundary and toe area are poorly defined. The eastern boundary is currently inferred as originating from the upper east corner in the headscarp zone, where a zone of disturbed material showing minimal (< 1 m) vertical offset was recorded. The margin then likely coincides with the incised gully to the east and continues along the reverse fault mapped by GNS.

In previous investigations, the landslide toe was inferred along a NW-SE drainage transitioning to the base of the compressional lobes from 430-490 masl (Cunningham, 1994; Stossel, 1999). However, field, and subsurface investigations during this study revealed a semi-continuous band of moderately to highly weathered shears and fissile schist daylighting the slope along the 380-400 m elevation contour. This weak and fissile material coincided with a thick gravelly clay layer logged at 11-15 m depth in BH2. A fault was mapped by Bell (1985b) at a similar elevation to the west, and was described as a 3 m wide exposure in a stream bed that could be traced to the NW, for more than 1km across the lower slopes of Queenstown Hill. The fault was composed of “intensively folded and sheared schist, with clay-rich “pug” zones up to 150mm wide: considered to form part of the same fault zone, which trends in a general NW-SE direction and controls stream alignment along the property” (Bell (1985b),p.3). Apart from surface and groundwater flows related to faulting, its’ surface expression was minimal, as the fault zone was concealed beneath glacial till and/or high-level beach gravels (Bell, 1985b).

It is possible that there is a concealed inactive fault in proximity to the base of the landslide. However, the similar topographic elevation, geometry, and material description of the fault, when compared to borehole and mapping data suggest it may be part of the landslide toe. As a result, it was determined that it would be more appropriate to expand the toe boundary into a toe zone (Zone E) to include the results derived from mapping, borehole logging and previous investigations.

Within the landslide body, major scarps (> 8 m) are steep (> 50°) with evident vertical displacement up to 10-15 m in the headscarp, 10-20m in the lateral scarp and a 45-60 m compressional bulge. Hummocky topography dominates the upper portion of the landslide, while many features are subdued due to weathering and erosion. Although hummocks are mapped across the landslide body, they are much smaller, narrower, and more localized than those mapped in other schist landslides in Otago (e.g Coronet Peak, Arthurs Point, K9, Nine Mile, etc.). Moderate (2-8 m) and minor scarps (> 2 m) are mostly rounded and grassed over, this is especially true in the north east quadrant of the landslide. Active streams and abandoned drainage form a complex rectangular network across the landslide body. Streams flow in the same orientation as joint sets and along erodible pathways of weaker material. Active well-established drainage is more abundant on the lower half of the slope but is able to infiltrate through fractures in the upper to mid part of the slope.

Mid-slope, the landslide transitions into an extensional zone (Zone C) marked by a zigzag patterned scarp linking to a graben and large open fractures (0.3-2.5 m wide). This zone hosts a series of long (10-125 m), deep (up to 10 m) NE-SW trending fractures adjacent to a large (> 10 m) slightly weathered steep scarp. To the west of the extension, a series of large (> 8 m) and steep (> 50°) on echelon scarps across the upper area make up the headscarp of the reactivation zone. The reactivation zone is characterized by a series of east facing scarp along the lateral margins and within the zone. The base of the scarps are littered with boulders exceeding 5 m in diameter. Evidence suggests that occasional loose blocks continue to be released from dilated joints in scarps progressively over time. Above the reactivation zone, the profile of the NW-SE trending scarps in the northeast quadrant increases and the scarps change orientation from NW-SE to W-E, matching the headscarp of the reactivated zone.

None of the landscape or landslide features on Queenstown Hill have been dated, but relative ages can be inferred based on intensity and extent of geomorphic features mapped within the landslide. Mapping suggests the landslide underwent at least 2 phases of movement (Figure 3.31). The first phase of movement involved the entire landslide body, resulting in approximately 50 m of translational movement downslope. The second phase of movement reactivated landslide material along the eastern portion of the landslide only (Zone D). This reactivation resulted in an increased intensity of pre-existing fractures adjacent to the western scarp of Zone D, a slight change in scarp orientation along the graben in Zone C and a change in intensity and orientation of the smaller scarps above Zone D.

There are indications of retrogression along the headscarp of the main landslide body. Scarps with up to 1-3 m of vertical displacement and dilation were observed extending beyond the main headscarp, predominantly to the west and towards the peak of Queenstown Hill to the north (Figure 3.31). However, it remains unknown whether retrogression is part of the reactivation of Zone D, if it was a caused by a separate event or if it occurred gradually over time. The order presented in this thesis is opposite to the order interpreted by Stossel (1999).

No significant changes were identified between the 1956 aerial photo and 2016 lidar imagery, and no unweathered fractures, lichen-free scarps or recent propagation were mapped in the field. This suggests there hasn't been any significant movement in the past 60 years. Minor cracks and voids were identified in section 3.8, but can be attributed to regular erosional processes and slope evolution. In addition to aerial photos and field observations, the lower portion of the landslide was surveyed for movement from December 2008 to October 2018 by Aurum Survey Consultants (Appendix B.3), with an anticipated horizontal and vertical variance of ±50mm and ±100mm. The results did not measure evidence of movement on the landslide, but by including the variance over a 10 year survey period, this indicates a potential rate of movement of less than 5mm/year.

The Queenstown Hill landslide was classed by (Stossel, 1999, p.101) as a "classic translational slide, with the toe forming a shallow compressional bulge instead of a toe buckle", with a failure surface inferred at 100-150 m depth. However, based on the results presented in this chapter, the landslide classification can be further refined to include a translational failure by means of a compound rock slide in the main landslide body and a planar block slide in the reactivation zone (Hungr et al., 2014). The upper portion of the landslide body suggests internal deformation, with deep subvertical fractures and large displaced schist blocks travelling along a planar rupture surface. The preconditioning effects of multiple glaciations on a slope consisting of layered schist, oriented unfavourably with the presence of foliation shears is likely to create multiple discrete failure surfaces and exhume along foliation due to dip. Graben type features are expected with multiple shear surfaces in compound rock slides (Hungr et al., 2014). This is further discussed in Chapter 5, as the geomorphology of the landslide forms the basis of the engineering geology ground model.

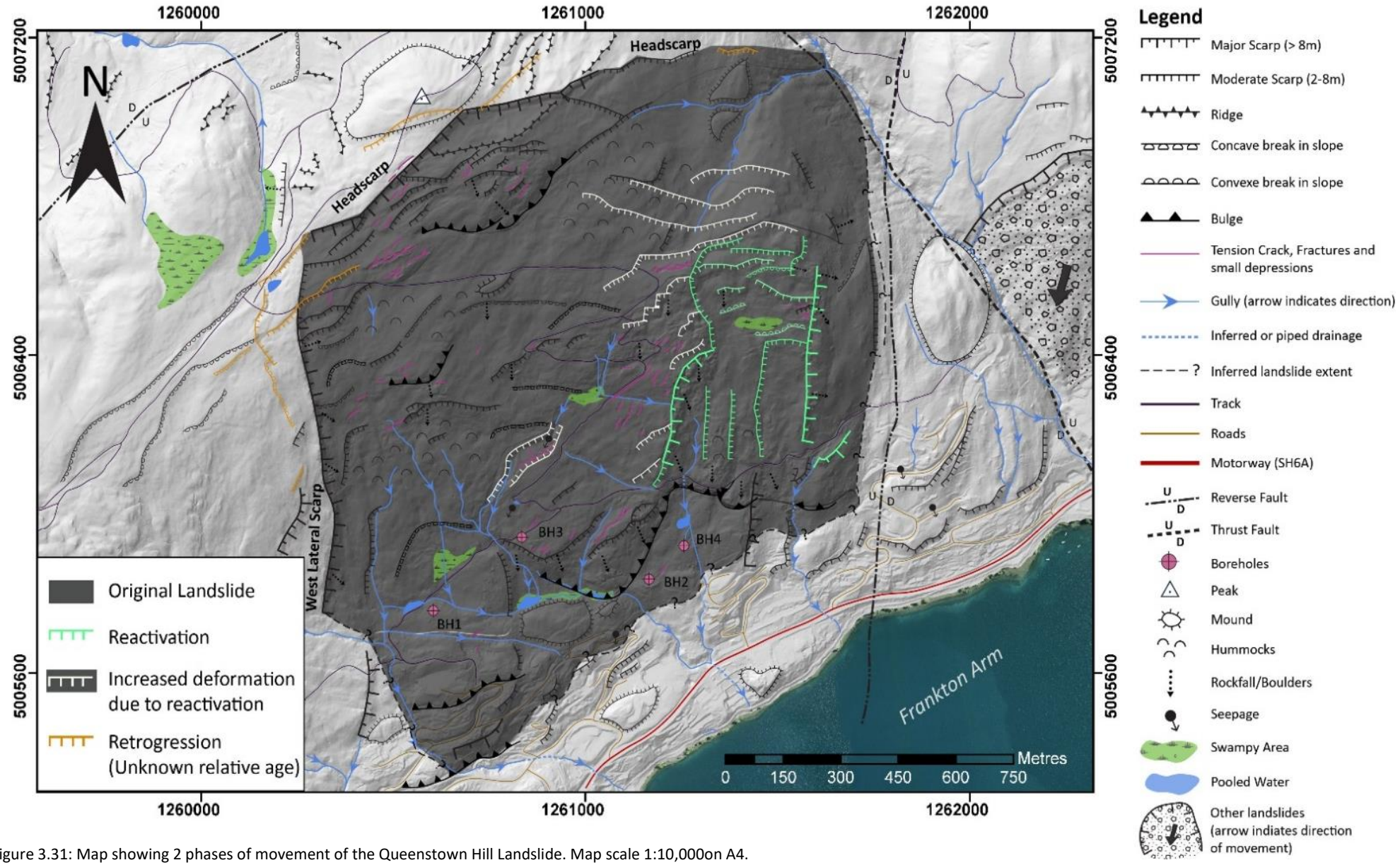

Figure 3.31: Map showing 2 phases of movement of the Queenstown Hill Landslide. Map scale 1:10,000on A4.

Chapter 4: Rock Mechanics

4.1 Introduction

This chapter presents the results derived from laboratory testing of schist samples taken from four boreholes drilled into the Queenstown Hill Landslide. The results are compared with previous engineering geology assessments of schist, from both local (Otago) and international cases. Average values for schist properties recognized from previous work are presented in Section 4.2.

The main objectives of this chapter are to:

1. Present physical and strength parameters derived from laboratory testing. This includes physical parameters: moisture content, density, porosity, sonic velocity and slake durability; and strength parameters: uniaxial compressive strength (UCS), indirect tensile strength, point load strength and triaxial testing.
2. Classify the rock mass (RQD, RMR, ARMR, and GSI) at various locations across the Queenstown Hill Landslide and surrounding area.

All lab testing was carried out on samples at in situ moisture content, as well as oven dried samples. Oven dried samples, in the context of this thesis, are not as applicable as the samples tested at in situ moisture content and will not be further discussed. Tables including raw sample data and results from testing oven-dried samples are included in (Appendix C). The results obtained from samples tested at in situ moisture content presented in this chapter will be used to help inform the behaviour of schist in the ground model and to input parameters into a kinematic analysis in Chapter 5. It is important to note that the use of in situ, in the context of this chapter, refers to the moisture content and not in situ testing methods.

4.2 Previous Geotechnical Characterization of Schist

4.2.1 Previous International Investigations

Many international studies have been undertaken to determine the geo-mechanical properties schist (Andrade and Saraiva, 2010; Behrestaghi et al., 1996; Bell, 2007; Cho et al., 2012; Chu et al., 2013; Loureiro et al., 2015; Mustafa et al., 2015; Nasseri et al., 2003; Papadopoulos and Marinos, 1992; Saroglou et al., 2004; Shrestha and Panthi, 2014; Zhang et al., 2011; Zhang et al., 2016). The reviewed studies include testing results of quartz-mica, quartzofeldspathic and chlorite schists recovered from drillcores. Table 4.1 summarizes the expected average values for schist (González de Vallejo and Ferrer, 2011), with results from a selection from a selection of the international case studies referenced above.

4.2.2 Previous Investigations in Central Otago

Investigations of the geo-mechanical properties of the Haast Schist have been undertaken across Central Otago, including: Macraes Gold Mine (Chapple, 1998), Maniototo: the Paerau Diversion Scheme (Moody, 1985; Paterson, 1979; Paterson et al., 1988), Cromwell Gorge (Clyde Dam) (Macfarlane et al., 1991a; Macfarlane et al., 1991b; Smith and Salt, 1991), Gibbston and Kawarau Valley (Awad et al., 2017; Bell, 1976; Johnson, 1986), Nevis Bluff (Brown et al., 1980) and Lake Lochnagar (Sweeney et al., 2013). A summary of the results from studies across Central Otago is presented in Table 4.2.

	Typical values [1]	Pelitic schist in Portugal [2]	Quartz-Mica schist China [3]	Quartz-Mica Schist in the Himalayas [4,5]	Chlorite Schist Himalayas [5]	Chlorite Schist Himalayas [6]	Athens Schist [7]	Yeoncheon Schist in Korea [8]
Porosity, n (%)	3		1.31	1.70	0.26	0.38-0.67	1.1-5.5 **(2.8)**	2.52
Unit Weight, γ (kN/m³)	25-28	27	27.8	27.2	28.8	27.6	25.38-26.05 **(25.78)**	
Permeability, k (m/s)	10^{-7}-10^{-8}				4.2×10^{-11}			
Durability index, I_{D2}						96.8-98.8		
Compressional wave velocity, V_p (m/s)	4,200-4,900	720-5000 (1000-2000)	Dry: 685-4595.5 **(2494.3)** Saturated: 1867.8-5306.1 **(3575.6)** Ratio sat/dry: 1.15-2.29 **(~1.6)**					
UCS (MPa)	20-160 **(30-60)**	23-77	Dry 13-41 **(27.7)** Saturated 5.3-31.2 **(9.1)**	50	110	17-112	24.7-65.6 **(34.7)**	4.8-157.4 **(63.1)**
MR	250-1100 Mica schist 300-800							
Tensile Strength (MPa)	2-5.5		2.33					
Indirect Tensile Strength (MPa)				12.0	24			2.3-20.1 **(8.1)**
Cohesion, c (MPa)	25 2-15*			15	25			
Basic friction angle, ϕ_b (°)	25-30 20-30*							
Internal Friction Angle, ϕ (°)				50	53			
Static elasticity modulus, E (GPa)	6-39 **(20)**			3.8	12		7.0-22.3	19.2-23.9 **(21.2)**
Poisson Ratio, ν	0.01-0.31 **(0.12)**			0.14	0.2			0.13-0.18 **(0.16)**
Shear Modulus, G (GPa)				2.20	5.7			
Constant m_i for intact rock	12 ± 3						11	
Point Load Strength (MPa)		Pelitic: 0.5-4.1 Quartz-rich: 1.2-7.4		⊥ 4.2 ∥ 1.5	⊥ 10	∥ 2.47-6.58		
Schmidt Hardness (MPa)		16-36						
Anisotropy Index							2.6	3.4

Table 4.1: Summary of typical expected values and results from select international cases. Mean in bolded parenthesis, when available. * in bedding planes or foliation planes. (⊥) perpendicular to foliation (∥) parallel to foliation.
1 González de Vallejo and Ferrer, 2011. 2 Loureiro et al., 2015. 3 Zhang et al., 2011. 4 Behrestaghi et al., 1996. 5 Nasseri et al., 2003. 6 Mustafa et al., 2015. 7 Saroglou et al., 2004. 8 Cho et al., 2012

		Macraes Mine [1]	Maniototo Dam and Canal [2,3]	Cromwell Gorge/Clyde Dam [4,5]	Gibbston and Kawarau Valley [6,7,8]	Nevis Bluff [9]	Lochnagar landslide dam [10]
Porosity, n (%)			1.35-6.61 **(3.3)**				
Unit Weight, γ (kN/m³)		26.8-28.5 **(27.2)**	25.6-27.3 **(26.5)**		27.5	28	
Permeability, k (m/s)		1.0×10^{-7} - 8.4×10^{-8}					
Durability index, I_{D2} (% weight retained after 2 cycles)			77.6-98.2				
UCS (MPa)		∥ 4.8-61.2 **(23.7)**	⊥ 28-86 **(53)** ∥ 9-46 **(29)**	∥ 33-72 **(46.9)** ⊥ 61.4-105.5 **(86)** Mica-rich: 10-50 Quartz-rich: 30-90	20-40	-	⊥ 85* ∥ 18* Sheared Samples: 24
Cohesion, c (MPa)			0-2	10-90	0.34	1.8	
Basic friction angle, ϕ_b (°)		45-55	11-33	23-32	29	27	
Cohesion, c (MPa) Sheared material		0	0	0-9	0	0.26	
Residual friction angle, ϕ_r (°)		6-14	6.6-14 11-27	8-28 14-21	19-32 **(24.5)**	10	
Static elasticity modulus, E (GPa)					7-14	47.3	
Poisson Ratio, v						0.13	
Constant m_i for intact rock						0.26	
Schmidt Hardness (MPa)			16-54 **(30)**				12-22
Point Load Strength Index, $I_{s(50)}$ Perpendicular (MPa)		0.2-3.14 **(1.44)**	0.5-9.4 **(3.0)**	0-3.63			
Point Load Strength Index, $I_{s(50)}$ Parallel (MPa)		0.03-0.58 **(0.26)**	0.3-5.0 **(1.3)**				
Anisotropy Index		1.3-23 **(7.3)**	1.14-3.1 **(2.3)**	3-8			
Residual friction angle, ϕ_r (°)		3.1-6.4 **(5.0)**					
Clays in Shear Zone Material	Dominant mineralogy	Chlorite (Swelling and Non Swelling), Muscovite, Kaolinite, Quartz	Calcium montmorillonite, muscovite, kaolinite, chlorite, illite and quartz	Mica/Smectite	Montmorillonite, Kaolinite and chlorite		Quartz, Clinochlore (Chlorite), Muscovite, Albite and Calcite
% Clay-sized particles in sheared material			2-18	30	20-30		
GSI					21-45		35-45 Sheared Material: 25-35
RQD (Rock Quality Designation)					10-95 %		
Rock Mass Rating					26-50		

Table 4.2: Summary of results from select geotechnical investigations in Otago. Mean in bolded parenthesis, when available. * converted from point load. (⊥) perpendicular to foliation (∥) parallel to foliation.

[1] Chapple, 1998. [2] Moody, 1985. [3] Paterson, 1988. [4] Macfarlane et al, 1992. [5] Stossel, 1999. [6] Johnson, 1986. [7] Awad et al., 2017. [8] Bell, 1976 [9] Brown et al., 1980. [10] Sweeney et al., 2013.

The geotechnical behaviour of schist varies across the Otago region due to differences in protolith (i.e. original parent rock). Expected variations are presented in Table 4.3. Pelitic schist is derived from Rakaia sandstones and mudstones, while psammitic schist is derived from Caples volcaniclastic sandstones. The pelitic schist is more micaceous, weak, and fissile than the blocky quartzofeldspathic psammitic schist. The high mica content in schist has been known to promote failure along mineral cleavage (Bell and Riddolls, 1992). From a practical viewpoint, the high strength of the Caples-derived alluvial gravels (e.g. in glacial till or outwash) makes them eminently suitable for aggregate, unlike the more pelitic schist, which breaks down easily by failure along the foliation and cannot be used for high-quality construction material (Moody, 1985; Watts, 1988).

The stability and engineering properties of individual landslides has historically been assessed by site-specific investigations, including drilling and piezometric monitoring because of the importance of perched water controlling stability (Belcher, 2009; Macfarlane et al., 1991a; Macfarlane, 2009). Inadequate understanding of the behaviour and properties of the schist led to failure at Maniototo (Moody, 1985; Paterson, 1979; Paterson et al., 1983; Paterson et al., 1988) - highlighting the importance of understanding the geotechnical behaviour of schist and especially weak zones, such as foliation shears within the rock mass.

Schist Type	Geotechnical Properties
Pelitic Schist	• Low shear strength • Unweathered strength is weak and the rock is fissile • Compressive strength average range is 5 - 40 MPa, depending on the orientation of foliation. • Highly foliated. Anisotropy and orientation of developed foliations shears control landform development. • Foliation dips at 10°-30°. • Strength varies depending on the orientation of the foliation. • High mica content promotes failure along mineral cleavage. • Defects present: foliation, schistosity, foliation shears, joints, crush and shear zones – all being important on landslide development, movement and control. • Schist fractures on foliation and sub-vertical joint sets. • Permeability is controlled by rock defects. Crush and gouge material often form impermeable barriers. • Relaxed and clay filled foliation shears form potential failure planes and seepage paths.
Psammitic Schist	• Predominantly quartzofeldspathic schist. • Low shear strength. • Compressive strength average range is 15-100 MPa, depending on the orientation of foliation. • Anisotropic, blocky with strongly developed schistosity. • Unweathered strength is stronger than pelitic schist, although it is also dependent on orientation of foliation. • Broadly folded, coarsely foliated, schistosity dipping out of slope at 10°-30°. • Foliation attitude, prominent jointing and shearing of rock mass controls the slope stability.

Table 4.3: Geotechnical properties associated with pelitic and psammitic schist. Adapted from Paterson et al., 1983; Paterson et al., 1988; Gillon et al, 1991; Bell, 1992; Bell and Riddolls, 1992; Willetts, 2000; Awad et al., 2017

4.2.3 Previous Investigations along Frankton Arm

Development in the Queenstown area occurs on both the Rakaia and Caples derived schist, as well as along the boundary between the two terranes. A thesis characterizing the engineering geology of the Frankton Arm, including the Queenstown Hill Landslide, was published by Stossel (1999). The thesis' primary objectives were to develop failure models and stability assessments for seven schist landslides above the residential

developments along Frankton Arm. A combination of field mapping and laboratory testing was undertaken to develop engineering geology and geotechnical failure models. Geological mapping was completed at a scale of 1:5,000 and 1:10,000. Bulk samples were tested to derive point load strength, shear strength, residual strength, mineralogy, and harness of rock defects. A summary of results and collated data, presented in Table 4.4, was then used to create limit-equilibrium sensitivity models.

Stossel (1999) identified three types of schist present along the Frankton Arm: quartzofeldspathic schist, pelitic schist and greenschist. The schist samples were often highly foliated with a low tensile strength resulting in disking and core breakage. Due to the fragile nature of the material, Stossel (1999) was unable to obtain samples large enough to perform uniaxial compressive strength and triaxial testing. As a result, square blocks and irregular lumps were used to derive point load strength and direct shear strength. Generally, the samples are described as fresh to slightly weathered and moderately strong to strong with an average foliation attitude of 15°/197° SW. The schist bedrock dips 20° south-southwest and two to four persistent sub-vertical joint sets were identified along the Frankton Arm (Stossel, 1999).

Further work suggested by Stossel (1999) includes a detailed subsurface investigation to locate the depth and geometry of the failure surface and that engineering geological practices be an integral part of further development.

		Rock Samples	Shear Zone Samples
Cohesion, c (MPa)		0	
Basic friction angle, ϕ_b (degrees)		24°-36° **(29°)**	
(ϕ_b + i)		26°-73° **(49°)**	
Schmidt Hardness (MPa)		21-54 **(39)**	
Point Load Strength Index, $I_{s(50)}$ Perpendicular (MPa)		0.6-3.83 **(2.09)**	
Point Load Strength Index, $I_{s(50)}$ Parallel (MPa)		0.11-0.92 **(0.51)**	
Anisotropy Index		4.1	
Average Foliation (dip/dip direction)		25° ± 5/ 197° ± 30	
Average slope inclination		20° ± 10	
JS1 (dip/direction)		85° ± 5/ 235° SW	
JS2 (dip/direction)		90° ± 5/ 310° NW	
SMR	Summer	67.5	
	Winter	59.5	
Cohesion, c (MPa)			0
Residual friction angle, ϕ_r (degrees)			6°-11° (8°)
X-Ray Diffraction of Shear Zone material (%)	Clinochlore		5-10 (6)
	Albite		3-40 (27)
	Kaolinite		25-60 (39)
	Muscovite		10-25 (20)
	Hornblende		0-15 (3)
	Quartz		5-10 (5)
Dominant clay mineral			Kaolinite
% Clay-sized particles in sheared material			4.5

Table 4.4: Summary of results obtained through laboratory testing of schist along the Frankton Arm (Stossel, 1999).

4.3 Physical Properties

4.3.1 Methodology

4.3.1.1 Sample Selection

Samples were selected for laboratory testing from the four 25 m boreholes drilled into the lower portion of the Queenstown Hill Landslide (Section 2.5.2). Two schist lithotypes were identified in all four boreholes during logging: a dark green-grey semi-pelitic schist (DGy) and a medium grey quartzofeldspathic schist (MGy). The samples selected for testing were separated by lithotype and remained sealed to retain as much of their natural moisture content as possible for testing.

4.3.1.2 Moisture Content and Density

The in situ moisture content, bulk density and dry density of samples were determined using the methods outlined in ISRM (1979). Moisture content was measured using the method for determination of the water content of a rock sample.

4.3.1.3 Porosity

The effective porosity was measured using a Micrometrics AccuPycII1340 gas Pycnometer, with nitrogen gas as a displacement medium. Forty-four schist samples were selected and prepared from the recovered core with twenty-two representative samples selected from each lithotype (DGy and MGy). The samples were cut into rectangular prisms (at least 40 mm in length) to occupy a sufficient volume in the pycnometer chamber to maximize accuracy. A sample was then placed into a sample chamber of a known volume in the pycnometer. Nitrogen gas was introduced into the sample chamber up to a fixed pressure, infiltrating the available pore spaces within the sample. Following this, an opened valve allowed the gas to expand into a reference chamber, also of known volume. The gas pressure before and after this expansion, measured by the pycnometer, along with the known volumes of the sample and reference chambers are used to calculate the solid volume of the sample (V_s). The pycnometer completes 10 cycles per sample. Porosity is then calculated as:

$$V_s = V_{sample} + \left(\frac{V_{chamber}}{1 - \left(\frac{P_1}{P_2} \right)} \right) \quad (1)$$

$$V_v = V - V_s \quad (2)$$

$$n = \frac{V_v}{V} \quad (3)$$

Where,

n= Porosity

V_{sample}= Bulk volume of the sample

$V_{chamber}$= Known chamber volume

V_v= Volume of voids

V_s= Volume of solids

P_1= Fixed chamber pressure

P_2= Filled chamber pressure with sample

4.3.1.4 Sonic Wave Velocities

A Computer-Aided Ultrasonic Velocity Testing System (CATS ULT-100) manufactured by GCTS (Geotechnical Consulting and Testing Systems) was used to determine the compressional (v_p) and shear (v_s) wave sonic velocities of cylindrical core samples (~60 mm diameter). Dry and saturated samples were tested according to the updated suggested methods for determining sound velocity by ultrasonic pulse transmission technique (ISRM, 2015). The core samples were placed between a set of platens with ultrasonic gel and a minor load (1-2 kN) was applied to ensure contact with the platens. A minimum of 100 waveforms were collected for each sample. The orientation of the samples for testing were limited by the drilling orientation. The orientation of foliation (β°) of tested samples varied between 60°-75° to the direction of wave pulses. Wave velocities were then used to derive dynamic elastic constants, Dynamic Young's Modulus (E_d), Dynamic Poisson Ratio (v_d), Dynamic Shear Modulus (G_d), and the Bulk Modulus (K_d) using the following Equations 4-7:

$$E_d=\frac{\rho v_s^2(3v_p^2-4v_s^2)}{(v_p^2-v_s^2)} \quad (4)$$

$$v_d=\frac{v_p^2-2v_s^2}{2(v_p^2-v_s^2)} \quad (5)$$

$$G_d=\rho v_s^2 \quad (6)$$

$$K_d=\frac{\rho(3v_p^2-4v_s^2)}{3} \quad (7)$$

Where,

E_d= Dynamic Young's Modulus
v_d= Dynamic Poisson Ratio
G_d= Dynamic Shear Modulus
K_d= Bulk Modulus
ρ= Density
v_s= S-Wave velocity
v_p= P-Wave velocity

4.3.1.5 Slake Durability

Due to the fissile nature of schist, slake durability testing was undertaken to assess the schists ability to resist alternating cycles of wetting and drying. Four batches of samples from each lithology were prepared and tested in accordance to ASTM D4644 - 16 (2016). As per the standard, the samples underwent three cycles of oven drying and two cycles of soaking/tumbling in distilled water at 19.5-20.5 °C. Due to the schist's high durability index, the samples were tested for an additional 3 cycles (a total of 5 tumbling cycles). The slake durability index (I_D) is calculated using Equations 8 and 9:

$$I_{D1}=\left[\frac{(W_{f1}-C)}{(W_i-C)}\right] \times 100 \quad (8)$$

$$I_{D2}=\left[\frac{(W_{f2}-C)}{(W_i-C)}\right] \times 100 \quad (9)$$

Where,

I_{D1-2}= Slake durability index after first and second cycles

C= mass of drum

W_i= mass of drum plus oven-dried specimen before the first cycle

W_{f1-2}= mass of drum plus oven-dried specimen retained after the first and second cycles

4.3.2 Results: Moisture Content, Density and Porosity

The results have been separated into columns based on lithotype (DGy and MGy) with the addition of a combined column (Table 4.5). The final combined column is simply the MGy and DGy data incorporated together. This column was added because the values obtained from each lithotype showed minor differences with respect to physical properties. The average in situ moisture content measured in the laboratory is 0.9 % with values ranging between 0.6-1.3 %. The average bulk unit weight and dry unit weight derived from the density are 27.2 and 26.9, respectively. The average measured porosity is 2.9 % ranging from 1.0-7.2 %.

		DGy	MGy	Combined
Moisture Content, (%)	Min-Max	0.6-1.3	0.7-1.3	0.6-1.3
	Mean ± Std dev.	**0.9** ± 0.25	**0.9** ± 0.24	**0.9** ± 0.23
	No. of Samples	9	9	18
Bulk Density, ρ_B (kg/m^3)	Min-Max	2550-2830	2640-2890	2550-2890
	Mean ± Std dev.	**2740** ± 47	**2800** ± 44	**2770** ± 55
	No. of Samples	46	40	86
Dry Density, ρ_D (kg/m^3)	Min-Max	2600-2870	2570-2880	2570-2880
	Mean ± Std dev.	**2730** ± 45	**2760** ± 54	**2740** ± 53
	No. of Samples	60	63	123
Bulk Unit Weight, γ (kN/m^3)	Average	26.9	27.4	27.2
Dry Unit Weight, γ_d (kN/m^3)	Average	26.8	27.1	26.9
Porosity, n (%)	Min-Max	2.0-7.2	1.0-6.6	1.0-7.2
	Mean ± Std dev.	**3.1** ± 1.0	**2.8** ± 1.1	**2.9** ± 1.0
	No. of Samples	22	22	44

Table 4.5: Summary of the mean and range values obtained for moisture content, density, unit weight and porosity. The range is expressed as the minimum and maximum value with the mean in bold.

Overall, the results plot within the expected ranges for schist presented in Table 4.1 and are comparable to results obtained during investigations at Maniototo (Table 4.2). The large range in porosity values can be attributed to minor discontinuities, surface weathering, corroded quartz segregations, slaking and fretting of micaceous sample edges. Individual sample results are tabled in Appendix C.1.

4.3.3 Results: P and S Wave Data

The results are presented for each lithotype (DGy and MGy) and combined, as in Section 4.3.2, with the addition of whether the sample was oven dried or saturated (Table 4.6). The P and S wave results share similar values for both lithotypes with an average P wave velocity of 4774 m/s dry and 5529 m/s saturated with a dry to saturated ratio of ~1.2. The average S wave velocity is 2770 m/s dry and 2521 m/s saturated with a dry to saturated ratio of ~0.9. The sonic wave velocity results are comparable to expected values and international cases (see Table 4.1).

The calculated ranges for the Dynamic's Young's Modulus of saturated samples is higher than the dry samples, as expected. The average E_d is ~48-50 GPa calculated for both lithotypes and moisture conditions. The average Dynamic Poisson's ratio is 0.26 for dry samples and 0.36 for saturated samples. The average Bulk modulus is 36.3 GPa for oven dried samples and 61.8 GPa for saturated samples tested.

		DGy		MGy		Combined	
		Dry	Saturated	Dry	Saturated	Dry	Saturated
Number of Samples		6	6	6	6	12	12
P-Wave, V_p (m/s)	Min-Max	4202-5111	5319-5879	4292-5286	5082-5789	4202-5286	5082-5879
	Mean ± Std dev.	**4769** ± 318	**5582** ± 224	**4779** ± 337	**5477** ± 247	**4774** ± 299	**5529** ± 221
S-Wave, V_s (m/s)	Min-Max	2178-2882	2039-2588	2457-3066	2117-2970	2550-2890	2039-2970
	Mean ± Std dev.	**2645** ± 254	**2453** ± 234	**2720** ± 206	**2579** ± 280	**2770** ± 55	**2521** ± 244
Dynamic Young's Modulus, E_d (GPa)	Min-Max	35.9-57.8	33.3-51.7	42.3-59.2	36.1-63.5	35.9-59.2	33.3-63.5
	Mean ± Std dev.	**48.9** ± 8.0	**46.6** ± 7.6	**50.1** ± 6.3	**50.4** ± 9.0	**49.7** ± 6.6	**48.7** ± 318
Dynamic Poisson Ratio, v_d	Min-Max	0.20-0.39	0.35-0.43	0.14-0.33	0.27-0.42	0.14-0.39	0.27-0.43
	Mean ± Std dev.	**0.27** ± 0.06	**0.38** ± 0.03	**0.25** ± 0.07	**0.35** ± 0.05	**0.26** ± 0.06	**0.36** ± 0.04
Dynamic Shear Modulus, G_d (GPa)	Min-Max	48.7-71.1	11.6-18.7	48.1-77.6	12.7-24.9	48.1-77.6	11.6-24.9
	Mean ± Std dev.	**62.7** ± 8.0	**17.0** ± 3.0	**62.9** ± 9.9	**18.8** ± 4.0	**62.8** ± 8.2	**18.0** ± 3.4
Bulk Modulus, K_d (GPa)	Min-Max	24.3-53.9	55.7-77.3	24.9-49.6	43.8-77.9	24.3-53.9	43.8-77.9
	Mean ± Std dev.	**36.9** ± 9.6	**64.9** ± 9.6	**35.8** ± 10.1	**59.2** ± 12.5	**36.3** ± 9.0	**61.8** ± 10.6

Table 4.6: Summary of results derived from the ultrasonic wave velocity testing including dynamic elastic constants. Mean values are bolded.

The increased anisotropy and larger mineral segregations of the DGy lithotype may have increased noise interference during the shear wave testing. As a result, selecting the S-wave arrival proved difficult and may have resulted in lower than expected averages when deriving dynamic constants for saturated samples. Furthermore, the saturated DGy schist may have micro-fractured along foliation planes, as one sample failed during testing in the load frame. Data from that sample was discarded. A table of tested samples is compiled in Appendix C.1.

4.3.4 Results: Slake Durability

Slake durability indices after each cycle are presented in Table 4.7. The average I_D for the DGy after two cycles is 97.9 %, classifying the durability on the boundary between high and very high (González de Vallejo and Ferrer, 2011). After five cycles, the average durability decreases to 95.8 % (high durability). The average I_D for the MGy after two cycles 98.8 % indicating a very high durability and decreasing to 97.3 % (high durability), after five cycles.

Despite both samples indicating high to very high durability, the disintegration of each lithotype was not the same. The DGy schist was more fragmented with murkier water compared to the MGy. The graphed results also indicate more variable fragmentation and slaking of the DGy as it presents a wider range of values than the results obtained with the MGy (Figure 4.1). Sample details, individual results, and photos are presented in Appendix C.1.

		DGy	MGy
No. of Samples		4	4
Slake Durability Index, Cycle 1, I_{D1} (%)	Min-Max	98.0-99.6	99.2-99.3
	Mean ± Std dev.	**98.8** ± 0.01	**99.3** ± 0.00
Slake Durability Index, Cycle 2, I_{D2} (%)	Min-Max	96.8-99.2	98.7-98.9
	Mean ± Std dev.	**97.9** ± 0.01	**98.8** ± 0.00
Slake Durability Index, Cycle 3, I_{D3} (%)	Min-Max	95.8-98.9	98.0-98.5
	Mean ± Std dev.	**97.1** ± 0.01	**98.2** ± 0.00
Slake Durability Index, Cycle 4, I_{D4} (%)	Min-Max	95.0-98.6	97.4-98
	Mean ± Std dev.	**96.4** ± 0.02	**97.8** ± 0.00
Slake Durability Index, Cycle 5, I_{D5} (%)	Min-Max	94.1-98.3	96.9-97.6
	Mean ± Std dev.	**95.8** ± 0.02	**97.3** ± 0.00

Table 4.7: Slake durability index results presented after each cycle.

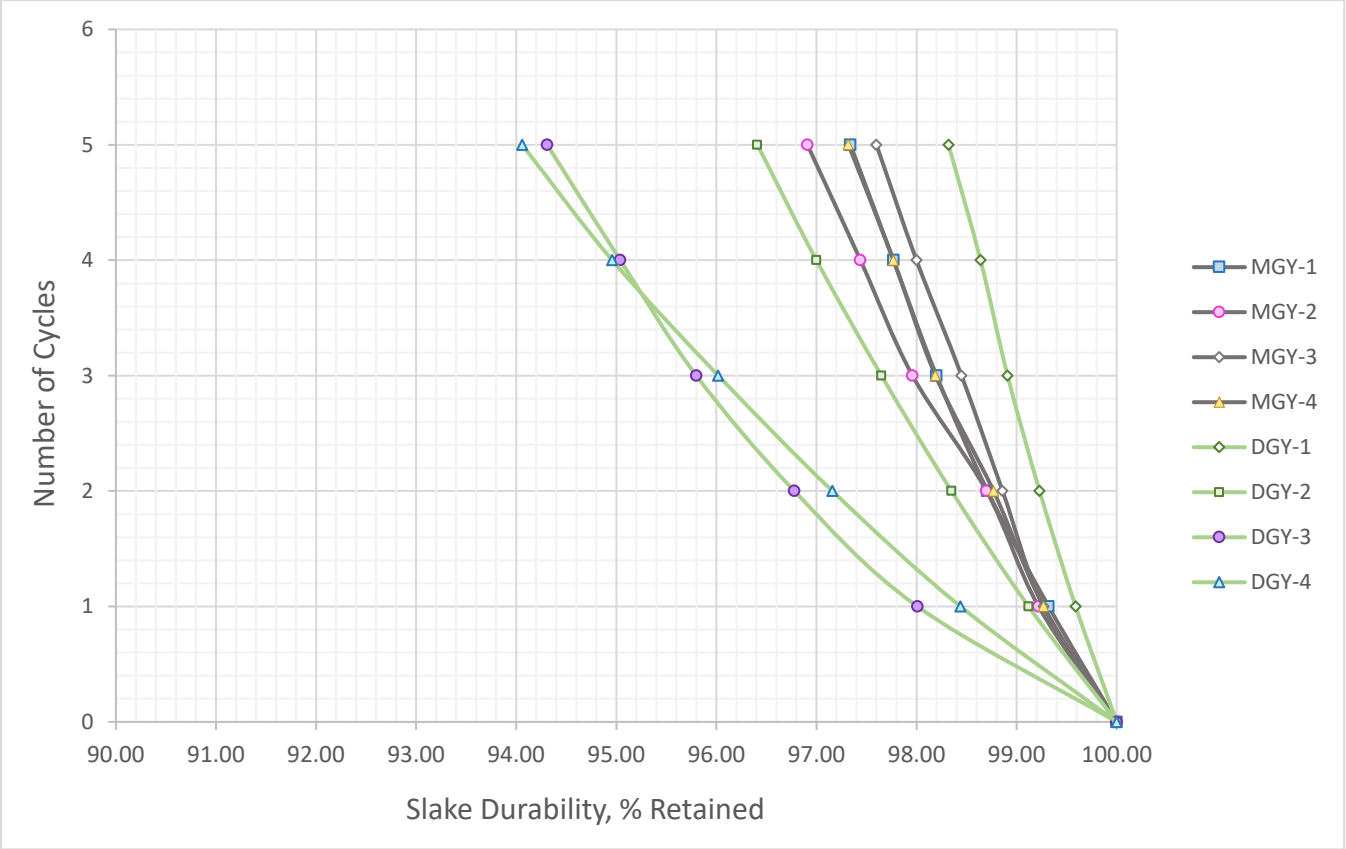

Figure 4.1: Plot showing the influence of the number of slake cycles on each lithotype.

4.4 Mechanical Properties

4.4.1 Methodology

4.4.1.1 Sample Selection and preparation

Samples were selected from the recovered drillcore (Section 2.5.2) and prepared as per the relevant standard for each testing method (Table 4.8). Specimens were separated by lithotype: dark green-grey semi-pelitic schist (DGy) and a medium grey quartzofeldspathic schist (MGy) with the foliation dip angle recorded for each sample. To ensure samples were representative, an even range were selected from each lithotype at varying depths (when possible). Samples lengths were cut evenly, according to the standard.

Standard	Specimen ratios	Test Method
ASTM D4543 (2019)	1.9-2.3 (Length/Diameter)	UCS and Triaxial Testing in a Tecnotest 3000 kN load frame.
ASTM D3967 (2016)	0.5-0.74 (Thickness/Diameter)	Indirect Tensile Strength (Brazilian Test)
ASTM D5731 (2016)	Length/Diameter > 1.0 (Diametral) 0.3 W < D < 1.0 W (Axial and Lumps)	Point Load Strength Test

Table 4.8: Summary of the standards used to prepare specimens for each test method. Specimen ratios column indicates the ratio range measured in the lab.

The foliation dip angle of the tested cores ranges between 10°-40° to horizontal (β= 50°-80°), with an average attitude of 15°-20° (β=70°-75°), which is consistent with the dips measured across Queenstown Hill and recorded in the boreholes. The core orientation was limited by the orientation of the vertical boreholes (Figure 4.2). Samples were not re-cored to avoid parting/breaking along foliation. Attempts made to re-core samples for testing parallel and perpendicular to foliation failed along the foliation meaning large enough samples were not recoverable for testing.

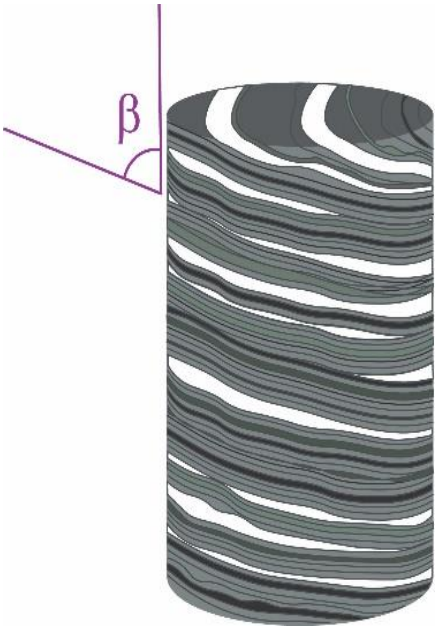

Figure 4.2: Schematic diagram showing the angle from which the foliation was measured prior to testing. β° indicating the measurement from vertical.

Due to the variability in foliation dip recorded, at least 5 samples were selected with a foliation dip of 70°-75° from vertical (or 15°-20° from horizontal) for each test, amongst other orientations. The results from each test method are summarized to reflect the full tested range at various foliation orientations (β= 50°-80°), as well as a separate section presenting samples with a foliation β-angle of 70°-75° (or 15°-20° from horizontal). Both options have been presented to be representative of the average/predominant dips measured in the field and in the boreholes.

4.4.1.2 Strain measurements

Axial strain was generally measured using an extensometer mounted parallel to the loading direction on a Tecnotest 3000 kN load frame, while radial strain was recorded using strain gauges. However, due to technical issues, the extensometer was unavailable for the entire duration of the testing period. When the extensometer became unavailable, strain gauges were used to record both axial and radial deformation.

Tokyo Sokki Kenkyuuja Co. strain gauges were used for both UCS and triaxial compressive strength testing. Two 30 mm radial strain gauges and two 30 mm axial strain gauges (when extensometer unavailable) were positioned based on the configuration used for anisotropic rocks by Read et al. (1985) and Read et al. (1987) (Figure 4.3). This involves mounting the axial and radial strain gauges at 90° from one another rather than diametrically opposite (at 180°). The adjacent configuration allows one strain gauge to be placed along strike of the foliation and one across the dip with preference given to the readings obtained along dip if a discrepancy exists between both strain gauge readings.

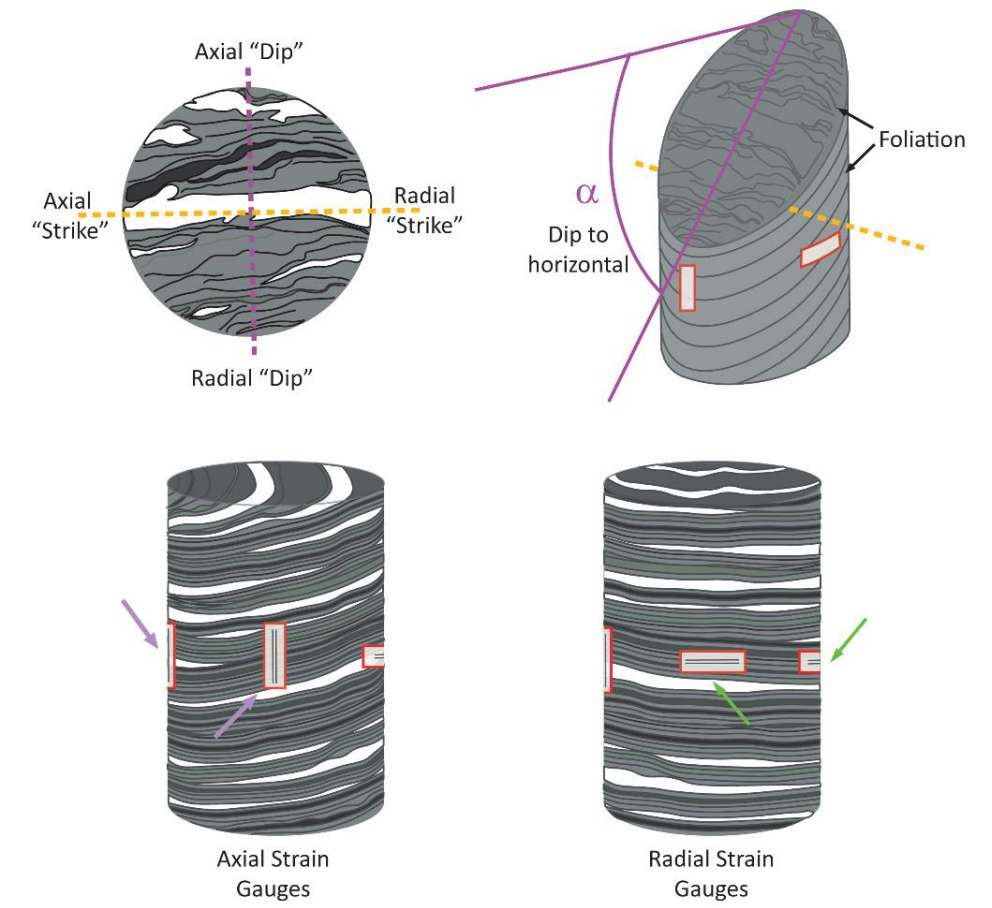

Figure 4.3: Schematic representation showing the orthogonal configuration of the strain gauges used for anisotropic rocks as per Read et al. 1985. The "strike" strain gauge is placed along the strike of the foliation and the "dip" placed along the dip direction. The alpha angle represents the foliation dip from horizontal. The axial strain gauges are configured vertically, and radial/lateral gauges are horizontal.

4.4.1.3 Indirect Tensile Strength (Brazilian Test)

The uniaxial tensile strength was measured indirectly using the method outlined in ASTM D3967 (2016) on 51 samples: 24 at in situ moisture content and 27 oven dried. The samples were separated by lithology and tested in a Technotest 3000 kN load frame using curved platens with a uniform axial load applied at 0.2 MPa/s. As the samples were not re-cored, the orientation of the foliation was measured from vertical (β°), using the same method as UCS and triaxial core samples. However, the specimens were oriented in two directions from the loading direction: either aligned with the dip of the foliation (facing the vertical load applied) or aligned with the foliation strike facing the vertical load (see Figure 4.4).

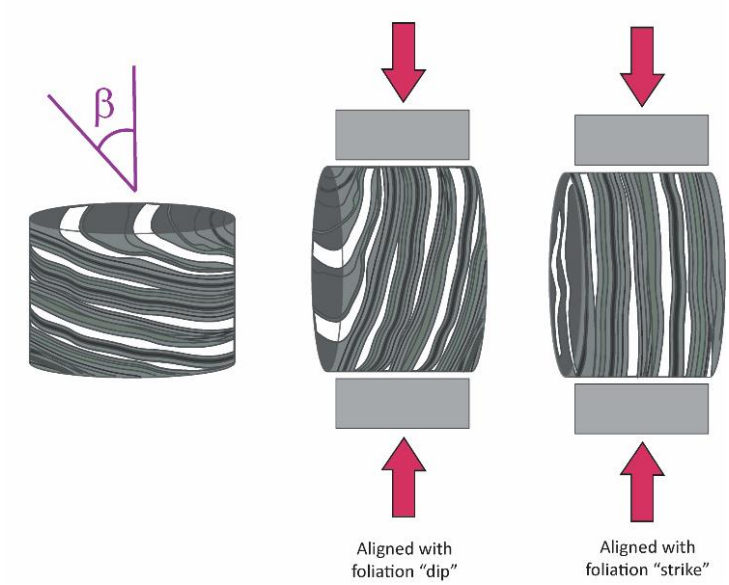

Figure 4.4: Schematic representation of the puck sample orientation for the Brazilian Test. The samples were loaded between the curved platens with either the dip of the foliation facing upward "along dip" or the strike of the foliation "along strike". The beta angle refers to the beta angle measured prior to loading the sample between the platens.

The indirect tensile strength for each sample was calculated using Equation 10 taken from ASTM D3967 (2016) and Equation 11 from ISRM (2007). Both ASTM and ISRM equations were used to compare the values obtained using both standards. When testing with curved platens, the ASTM Standard equation yields lower indirect tensile strength results than the ISRM Standard. As the results obtained through Brazilian tensile strength (BTS) testing tend to be greater than the equivalent direct tensile strength (DTS) values, an estimated DTS can be derived using Equation 12, to improve the correlation between results (Perras and Diederichs, 2014).

$$\sigma_t = 1.272\,\frac{P}{\pi t D} \qquad (20)$$

$$\sigma_t = 0.636\,\frac{P}{Dt} \qquad (11)$$

$$DTS = f \cdot BTS \qquad (12)$$

Where,

σ_t= splitting tensile strength (MPa)
P= maximum load applied (N)
t= sample thickness (mm)
D= sample diameter (mm)

DTS= direct tensile strength (MPa)
f= correlation factor (0.9 for metamorphic rocks)
BTS= Brazilian tensile strength results (MPa)

4.4.1.4 Uniaxial Compressive Strength

A total of thirty-four uniaxial compressive strength (UCS) tests were carried out on in situ moisture content (21 tests) and oven dried (13 tests) cylindrical core samples. Samples were prepared according to ASTM D4543 (2019) (see 4.4.1.1) and tested according to ASTM D7012 (2014) - Method D. The samples were tested in a Tecnotest 3000 kN compression load frame at a rate of 0.2 MPa/s. Axial and radial strain were measured using the methods outlined in Section 4.4.1.2. Due to the variation in test specimen ratio (1.9-2.3), and a sample diameter of 60 mm results were normalized, and a correction was applied using the Equations 13 and 14 proposed by Hoek and Brown (2017):

$$\sigma_c = \frac{\sigma_m}{(0.88+0.222\left(\frac{d}{l}\right))} \quad (33)$$

$$\sigma_{c50} = \frac{\sigma_c}{\left(\frac{50}{d}\right)^{0.18}} \quad (14)$$

Where,

σ_c= UCS corrected for length/ratio
σ_m= measured UCS (MPa)
d= sample diameter (mm)
l= sample length (mm)
σ_{c50}= UCS corrected for 50mm core diameter

The fracture type/failure mode was recorded for each sample. Figure 4.5 summarizes the various end members. Axial and radial deformation from the tangent modulus at 50% of the maximum strength was used to derive Young's Modulus (E) and Poisson ratio (v). Strain was monitored and derived for each strain gauge individually. If both axial strain gauges recorded similar strain, the results were averaged. If not, preference was given to the "dip" position strain gauges as they tend to yield more consistent Poisson ratio values. The same method was applied for the radial strain gauges (Read et al., 1987).

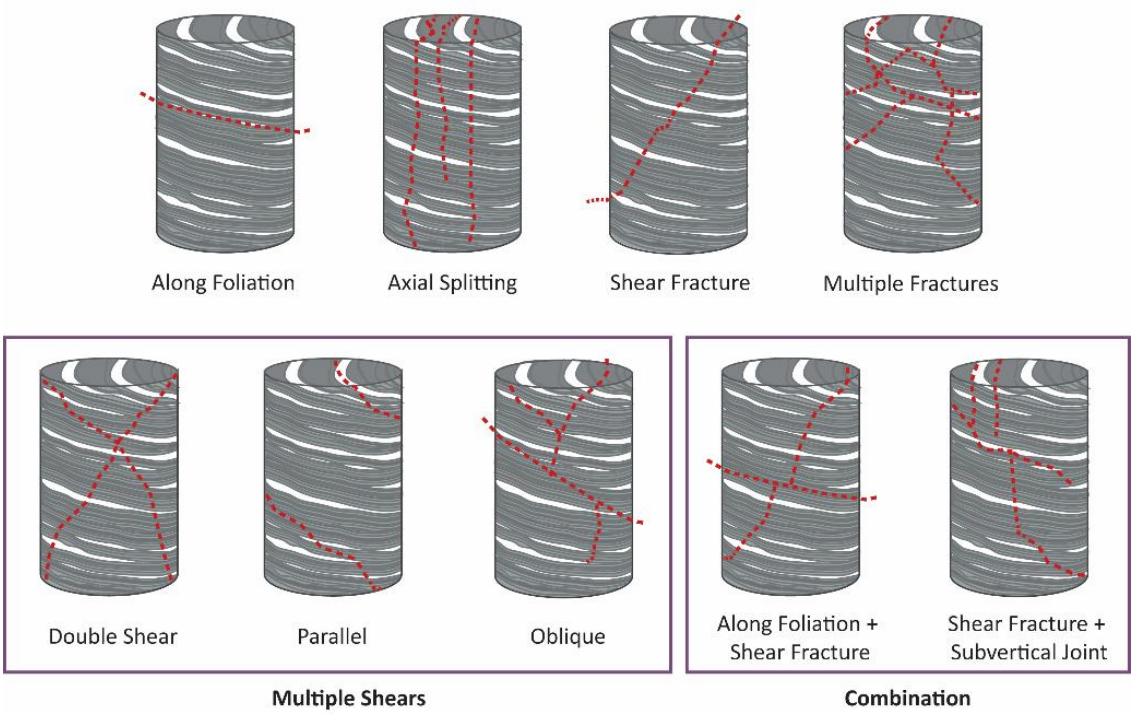

Figure 4.5: Schematic diagram of the failure mode end members recorded after uniaxial compressive strength and triaxial compressive strength testing.

4.4.1.5 Point Load Strength

Point load testing (axial, diametral and lump tests) was carried out on 261 samples at in situ moisture content and 232 oven dried samples (Table 4.9), as per the methods outlined in ASTM D5731 (2016). The samples were separated by lithology (DGy and MGy) and loaded in multiple orientations in the load frame. Samples placed in the test apparatus perpendicular (axial/lump) and parallel (diametral/lump) to foliation conform with the standard. However, in an attempt to correlate point load results with UCS data, specimens were also tested oblique to foliation (orientations ranging between 50°-80° (β°) to foliation). A size correction factor was applied (Equation 15, 16) and estimation of UCS and tensile strength was derived using Equation 17 and 18 from section 10.5 of ASTM D5731 (2016) and Zhang (2016):

$$I_{s(50)}=F\cdot I_s \quad (45) \qquad F=\left(\frac{D_e}{50}\right)^{0.45} \quad (16)$$

$$s_c=K\cdot I_s \quad (17) \qquad \sigma_t=-1.5\cdot I_{s(50)} \quad (18)$$

Where,

$I_{s(50)}$= corrected point load index (for 50 mm)
F = size correction factor "F"
I_s = uncorrected point load index
D_e= equivalent core diameter (mm)
s_c= UCS (MPa)
K= index to strength conversion factor (MPa)

			No. of Samples		
Moisture Content	**Test Type**	**Orientation of foliation**	**DGy**	**MGy**	**Combined**
In Situ	Axial	Perpendicular (⊥)	42	42	84
		β°=50-80	29	37	66
		*β°=70-75	18	23	41
	Diametral	Parallel (‖)	22	29	51
		β°=15-35	42	18	60
		*β°=15-20	16	13	29
Dry	Axial	Perpendicular (⊥)	45	44	89
		β°=50-80	35	28	63
		*β°=70-75	17	19	36
	Diametral	Parallel (‖)	19	19	38
		β°=15-35	23	19	42
		*β°=15-20	17	18	35

Table 4.9: Summary of the number of samples used in each point load test. *samples tested in these orientation ranges are not in addition to the total number of oblique samples. The number is also included within the full oblique range.

4.4.1.6 Triaxial Compressive Strength

Forty-three triaxial compressive strength tests were carried out on in situ moisture content (22 tests) and oven dried (21 tests) cylindrical core samples. Samples were prepared according to ASTM D4543 (2019) (see 4.4.1.1) and tested according to ASTM D7012 (2014) - Method B. The samples were placed in a Roctest Telemac Hoek Cell for testing using a manual hydraulic pump to maintain confining stress, while an axial load was applied using the Tecnotest 3000 kN compression load frame at a uniform rate of 0.2 MPa/s. Three confining stresses were selected: 3 MPa, 5 MPa and 10 MPa. The lowest confining stress was selected to constrain a range of strength values at shallow depths (0-3 MPa), while 5 MPa and 10 MPa were chosen to facilitate comparison with other published work. Axial and radial strain were measured using the same methods outlined in Section 4.4.1.2, and Section 4.4.1.4 was used to calculate Young's Modulus and Poisson ratio.

The intact rock strength parameters were used to assess the Mohr-Coulomb and Hoek-Brown failure criteria. RocData 5.0 (RocScience Inc. 2020) was used for regression analyses of the triaxial data to derive both failure envelopes. Mohr-Coulomb assumes failure of the rock occurs along a plane due to shear stress acting on the plane in a triaxial state of stress (González de Vallejo and Ferrer, 2011). It is plotted as a linear failure envelope that uses normal and shear stresses to derive cohesion (c) and the internal friction angle (ϕ) and can be expressed by Equation 19. The criterion can also be expressed in terms of principal stresses (σ_1 and σ_3) (Equations 20-22) and as a function of principal stresses (Equation 23). By extension, the uniaxial compressive strength ($\sigma_1=\sigma_c$) and tensile strength (σ_t) values can also be derived using Equations 24 and 25:

$$\tau=c+\sigma_n\tan(\phi) \quad (19)$$

$$\sigma_n=\frac{(\sigma_1+\sigma_3)}{2}+\frac{(\sigma_1-\sigma_3)}{2}\cos 2\theta \quad (20)$$

$$\tau=\frac{(\sigma_1-\sigma_3)}{2}\sin(\theta) \quad (21)$$

$$\theta=45°+\frac{\phi}{2} \quad (22)$$

$$\sigma_1=\frac{2c\cos(\phi)+\sigma_3(1+\sin(\phi))}{1-\sin(\phi)} \quad (23)$$

$$\sigma_c=\frac{2c\cos(\phi)}{1-\sin(\phi)} \quad (24)$$

$$\sigma_t=\frac{2c\cos(\phi)}{1+\sin(\phi)} \quad (25)$$

Where,

τ= shear stress on the failure plane (MPa)
σ_n= normal stress on the failure plane (MPa)
ϕ= internal friction angle
c= cohesion (MPa)
θ= critical plane of failure (sometimes noted as β)
σ_c= UCS (MPa)
σ_c= tensile strength (MPa)

The Hoek-Brown failure criterion is a non-linear failure envelope, which allows for a more realistic assessment of rock behaviour and intact rock strength using empirical data (Hoek and Brown, 2017). The failure envelope is drawn using the major and minor principal stresses based on the UCS of the intact rock (σ_{ci}) and the material constant m_i. For intact rock specimens, Equation 26 is the simplified equation used to derive the relationship between the principal stresses at failure and Equations 27-31 are used to manually calculate the strength parameters (Hoek, 2007). The equations are given as:

$$\sigma_1=\sigma_3+\sigma_{ci}\left(m_i\frac{\sigma_3}{\sigma_{ci}}+1\right)^{0.5} \quad (26)$$

$$\sigma_t=\frac{1}{2}\sigma_{ci}\left(m_i-\sqrt{m_i^2+4}\right) \quad (27)$$

$$\sigma_{ci}=\sqrt{\frac{\sum y}{n}-\left[\frac{\sum xy-\left(\frac{\sum x\sum y}{n}\right)}{\sum x^2-\left(\frac{(\sum x)^2}{n}\right)}\right]\frac{\sum x}{n}} \quad (28)$$

$$m_i=\frac{1}{\sigma_{ci}}\left[\frac{\sum xy-\left(\frac{\sum x\sum y}{n}\right)}{\sum x^2-\left(\frac{(\sum x)^2}{n}\right)}\right] \quad (29)$$

$$x=\sigma_3 \quad (30)$$

$$y=(\sigma_1-\sigma_3)^2 \quad (31)$$

Where,

σ_1= maximum principal stress (MPa)
σ_3= minimum principal stress (MPa)
σ_{ci} = intact compressive strength UCS (MPa)
m_i= material constant (characteristic of the rock type)
n= number of triaxial tests

4.4.2 Results: Indirect Tensile Strength

The mean indirect tensile strength values for the DGy and MGy schist samples tested at in situ moisture content are summarized in Table 4.10. Values derived from oven dried test results, individual sample information and detailed tables including range values (min-max) are available in Appendix C.2. The data is presented by lithotype including a column combining both lithotypes due to interlayering, and separates samples with a foliation β-angle of 70°-75° (or 15°-20° from horizontal). Tensile strength values are presented according to the most recently revised ASTM standard (2016) using curved platens, the ISRM standard (2007) and converted to direct tensile strength (Perras and Diederichs, 2014).

In situ moisture %			All Samples	DGy	MGy	Combined	Samples with foliation β° (70-75)	DGy	MGy	Combined
	Loading Direction (Along…)									
Indirect Tensile stress (ASTM), MPa	Strike	Mean ± Std dev.		**3.44 ± 0.98**	**3.81** ± 0.95	**3.59** ± 0.90		3.84 ± 0.86	**3.81** ± 0.95	**3.82** ± 0.86
	Dip	Mean ± Std dev.		**1.57** ± 0.82	**3.50** ± 0.73	**2.37** ± 1.20		1.81 ± 0.84	**3.50** ± 0.73	**2.66** ± 1.16
	Average	Mean ± Std dev.		**2.50** ± 1.26	**3.66** ± 0.78	**2.98** ± 1.22		2.82 ± 1.27	**3.66** ± 0.78	**3.24** ± 1.16
Indirect Tensile Stress (ISRM), MPa	Strike	Mean ± Std dev.		**5.40** ± 1.54	**5.98** ± 1.50	**5.65** ± 1.42		**6.02** ± 1.35	**5.98** ± 1.50	**6.00** ± 1.34
	Dip	Mean ± Std dev.		**2.46** ± 1.29	**5.51** ± 1.15	**3.73** ± 1.88		**2.84** ± 1.31	**5.51** ± 1.15	**4.17** ± 1.83
	Average	Mean ± Std dev.		**3.93** ± 1.97	**5.74** ± 1.22	**4.69** ± 1.92		**4.43** ± 1.99	**5.74** ± 1.22	**5.09** ± 1.82
Conversion to Direct Tensile Stress, MPa	Strike	Mean ± Std dev.		**4.86** ± 1.38	**5.38** ± 1.35	**5.08** ± 1.28		**5.42** ± 1.21	**5.38** ± 1.35	**5.40** ± 1.21
	Dip	Mean ± Std dev.		**2.21** ± 1.16	**4.96** ± 1.04	**3.36** ± 1.69		**2.55** ± 1.18	**4.96** ± 1.04	**3.75** ± 1.64
	Average	Mean ± Std dev.		**3.54** ± 1.78	**5.17** ± 1.10	**4.22** ± 1.73		**3.99** ± 1.79	**5.17** ± 1.10	**4.58** ± 1.64

Table 4.10: Indirect tensile strength results derived from the Brazil test. Results were calculated using ASTM and ISRM standards and the ISRM values were converted to DTS as per Perras and Diederichs (2014).

The average tensile strength measured for DGy, when loaded along the foliation dip and strike was 1.57 MPa and 3.44 MPa, respectively. Tensile strength parameters derived with the load applied along the strike yielded results approximately 2.2 times stronger than the samples tested along dip. Samples with a β° foliation angle between 70°-75° were only marginally (10-15 %) stronger than the full range of orientation tested. The average tensile strength measured for MGy, when loaded along the foliation dip and strike was 3.50 MPa and 3.81 MPa, respectively. Tensile strength parameters derived with the load applied along strike yielded similar results to those tested along dip. Only samples with a β° between 70°-75° were tested, no comparison could be made with other foliation orientations.

When the samples are loaded along strike between the platens, the MGy schist is marginally stronger (10 %) than the DGy samples. When the samples are loaded with the dip between the platens the MGy schist is 2.2 times stronger than the DGy. This is likely due to the strong anisotropy of the DGy samples in comparison to the weaker anisotropy exhibited by the MGy samples. When the results are combined, irrespective of orientation, the MGy schist lithotype is approximately 40 % stronger than the DGy.

The tensile strength results derived through laboratory testing are within the expected values summarized in Table 4.1, no comparable tensile strength results were available from the case studies reviewed in Table 4.2.

4.4.3 Results: Uniaxial Compressive Strength

The uniaxial compressive strength (UCS) and elastic properties of the DGy and MGy schist tested at in situ moisture content are summarized in Figure 4.6 and Table 4.11. Values derived from oven dried samples and individual sample data are available in Appendix C.2. The tabled data is presented by lithotype, including a column combining both lithotypes. Tested samples with a foliation β-angle of 70°-75° (or 15°-20° from horizontal) are presented separately. All maximum stress (UCS) results presented have been corrected for length and to 50mm diameter core.

In situ moisture %			DGy	MGy	Combined		DGy	MGy	Combined
No. of Samples			11	10	21		5	8	13
Maximum Stress, UCS (MPa)	Min-Max	All Samples	11.3-48.0	21.6-61.8	11.3-61.8	Samples with foliation β° (70-75)	12.6-48.0	36.4-61.8	12.6-61.8
	Mean ± Std dev.		**23.4** ± 11.1	**45.4** ± 10.5	**33.8** ± 16.2		**29.9** ± 12.1	**50.6** ± 8.0	**42.6** ± 14.0
Young's Modulus, E (GPa)	Min-Max		5.1-31.7	0.9-41.1	0.9-41.1		2.0-41.1	8.9-31.7	2.0-41.1
	Mean ± Std dev.		**15.7** ± 7.9	**11.7** ± 11.8	**14.5** ± 9.9		**14.0** ± 13.9	**17.8** ± 7.2	**16.3** ± 10.5
Poisson Ratio, v	Min-Max		0.02-0.27	0.02-0.36	0.02-0.36		0.02-0.27	0.02-0.36	0.02-0.36
	Mean ± Std dev.		**0.18** ± 0.09	**0.21** ± 0.12	**0.20** ± 0.10		**0.20** ± 0.11	**0.28** ± 0.13	**0.25** ± 0.13
MR			671	257	429		468	352	383

Table 4.11: Summary of the strength parameters and elastic properties derived from UCS testing. Means are highlighted in bold.

The average strength measured for all DGy samples tested is 23.4 MPa with values ranging between 11.3-48.0 MPa classifying it as weak to moderately strong rock (Zhang, 2016). The average values for Young's modulus and Poisson's ratio derived from the stress-strain graphs are 15.7 GPa and 0.18, respectively. The values for Young's modulus range between 5.1-31.7 GPa and 0.02-0.21 for Poisson's Ratio.

The average strength measured for all MGy samples tested is 45.4 MPa with values ranging between 21.6-61.8 MPa, which is classified as moderately strong to strong rock (Zhang, 2016). The average values for Young's modulus and Poisson's ratio derived from the stress-strain graphs are 11.7 GPa and 0.27, respectively. The values for Young's modulus range between 0.9-41.1 GPa and 0.02-0.36 for Poisson's Ratio. On average, the MGy schist lithotype is approximately 1.9 times stronger than the DGy with similar Young's modulus and a higher Poisson's Ratio.

The samples tested at 70°-75° yielded strength parameters approximately 1.2 times higher than the averaged values for the entire range of orientations (50°-80°). The higher strength value can be attributed to the removal of more oblique (50°-60°) samples. Schist samples are weakest when tested oblique to the foliation planes with strength decreasing as they approach 45° (Ramamurthy, 1993).

The difference in strength values between both lithotypes and the large ranges observed in the data are due to the inherent anisotropic nature of the schist: the β-angle between the foliation and the applied load, the differences in mineralogy and thickness of mineral segregation (González de Vallejo and Ferrer, 2011; Jaeger et al., 2007; Read et al., 1987). The DGy lithotype has a higher degree of anisotropy than the MGy, which is reflected in the increased amount of scatter and variability in the results. The strength values and elastic deformation recorded by Young's Modulus for both lithotypes were plotted against the foliation attitude confirming a relationship between foliation angle and varying strength of the schist. Because of the

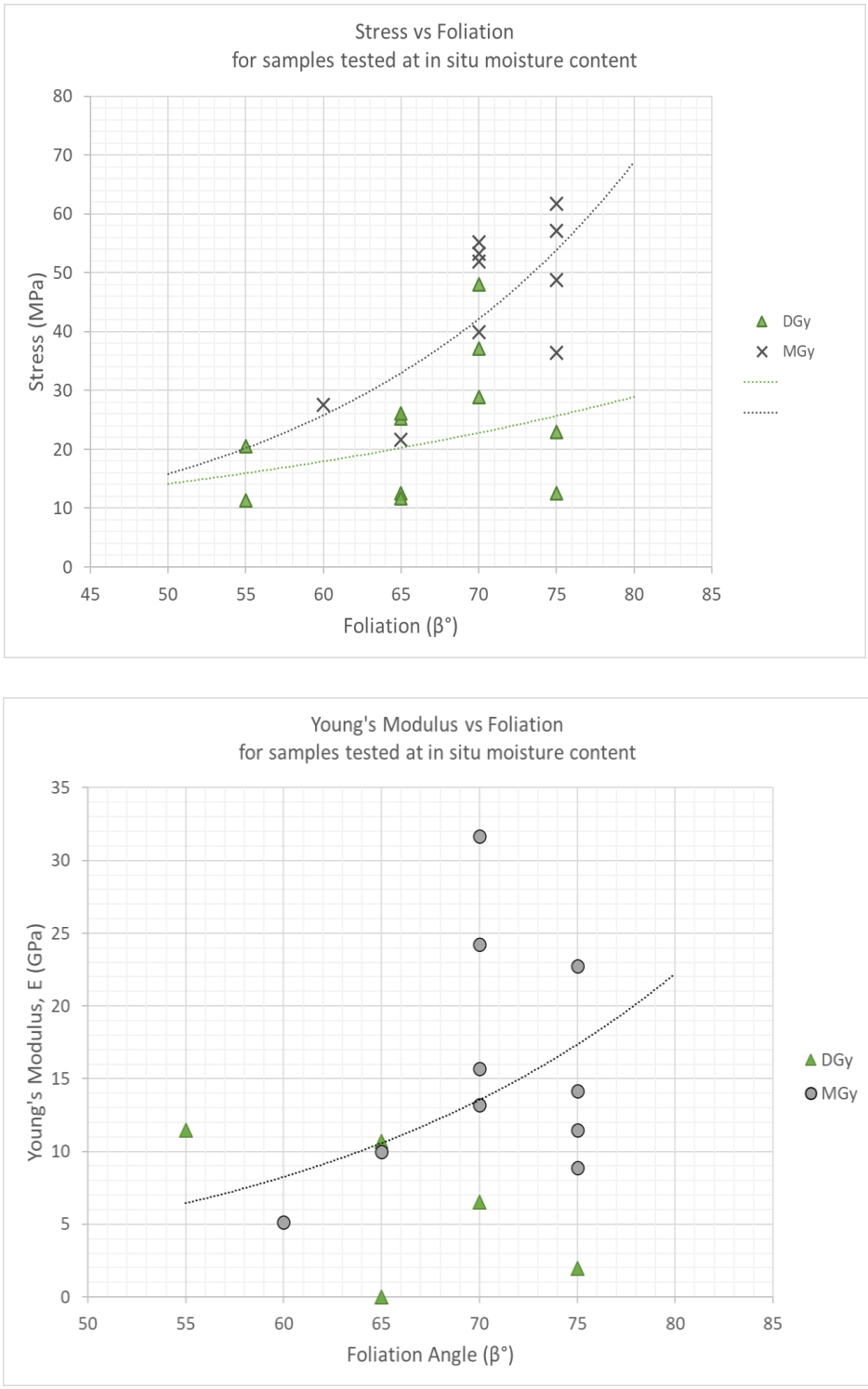

Figure 4.6: Plots showing the relationship between stress and foliation (top); Young's Modulus and Foliation (bottom).

limited availability in foliation orientation for testing, the extent of the anisotropic curve (trend from 0°-90°) is unknown. However, the portion of the strength curve plotted reflects the respective portion of the U-shaped trend (see Figure 4.6) (Kwasniewski, 1993; Ramamurthy, 1993).

A summary of the observed failure modes is included in Figure 4.7. Shear fractures are the predominant mode of failure observed in the lab for both lithotypes with shears occurring at 50°-60°and 60°-70° followed by axial splitting. Fracture patterns and failure modes recorded in the lab mimic the joint angles and stepped roughness measured in the field. The UCS results and elastic parameters obtained for both lithotypes are comparable to results presented in Table 4.1 and Table 4.2. On average the strength results obtained at

Queenstown Hill are slightly weaker than schist tested in the Cromwell Gorge (Macfarlane et al., 1991b) but similar to results from the Kawarau Valley and Maniototo (Moody, 1985; Paterson et al., 1988).

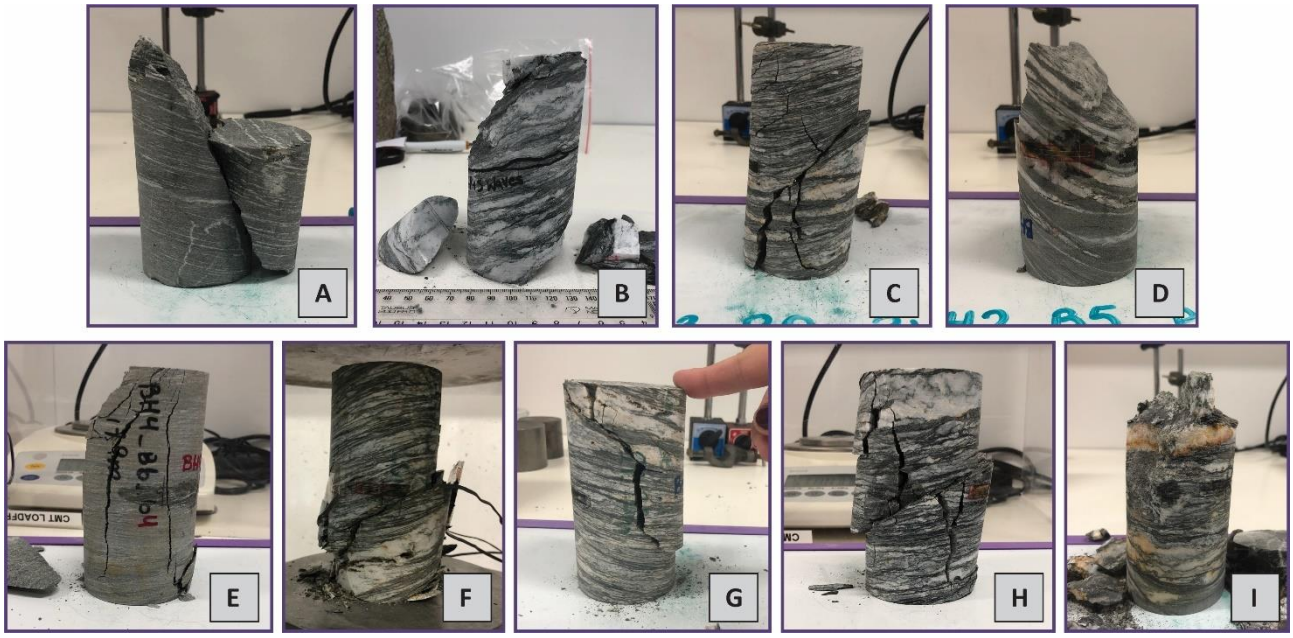

Failure Mode			In situ moisture			Oven Dried		
			DGy	MGy	Total	DGy	MGy	Total
Shear Fracture (A-D)	Shear fracture (A)	Shears occur at 50°-60°, 60°-70° and 40°-50°	2	5	7	0	1	1
	Parallel (B)	Shears occur at 50°-60°	3	0	3	1	1	2
	Oblique (C)	Shears occur at 60°-70° and 45°-55°	0	1	1	1	0	1
	Double Shear (D)	Shears occur at 50°-60°, 60°-70°	1	0	1	1	0	1
Axial splitting (E)		Splitting occurs at 80°-87°	1	2	3	0	2	2
Along Foliation (F)		Fracture occurs along foliation	2	0	2	0	1	1
Combination (G-H)	Shear and Joint (G)	Fractures occur along shears at 50°-60°, and 80°-85° up the centre	1	1	2	2	1	3
	Along foliation and Shear (H)	Fractures along foliation and 40-65° shears	1	0	1	0	1	1
Multiple Fractures (I)		Fractures along multiple orientations	0	1	1	1	0	1

Figure 4.7: Summary of the failure modes observed after UCS testing. Sample photos with the associated failure mode (top). Number of samples recorded for each failure mode (Table).

4.4.4 Results: Point Load Strength

The point load strength index values (corrected for 50 mm) of the DGy and MGy schist and foliation angles tested at in situ moisture content are summarized in Table 4.12 and Figure 4.8. Oven dried specimen test results are presented in Appendix C.2 along with Individual sample information and graphs. The tabled data is presented by lithotype, orientations of the tested specimens and includes a column combining both lithotypes. The β-angle represents the orientation of the foliation relative to the point load platens. These results are presented separately as: 1) samples tested perpendicular and parallel to foliation; 2) an amalgamation of all samples tested oblique to foliation (range: 50°-80° and 10°-35°) and 3) samples tested at 70°-75° and 15°-20° separated out from the amalgamated range. The results were kept separate to allow for consistency when applying conversion factors (such as the UCS conversion factor), as none of the UCS, triaxial strength or indirect tensile strength samples were tested perpendicular or parallel to foliation.

In situ moisture content %		DGy	MGy	Combined
Point Load Strength Index, $I_{s(50)}$ (MPa)	**Perpendicular**	2.40	2.63	2.52
	β = 50°-80°	2.21	2.44	2.32
	β = 70°-75°	2.08	2.18	2.16
	Parallel	0.46	0.46	0.55
	β = 10°-35°		0.61	0.60
	β = 15°-20°		0.40	0.54
Conversion Factor, K (From UCS)	**β = 50°-80°**	10.6	18.6	14.6
	β = 70°-75°	14.4	23.2	19.7
Anisotropy Index, I_a		5.11	5.72	4.85
Tensile Strength, σ_t (MPa)		0.7	0.6-0.9	0.8-0.9

Table 4.12: Point load index strength results including the conversion factor K, anisotropy index and estimated indirect tensile strength.

The average point load strength index values derived from axial testing of the DGy schist range between 2.08-2.40 MPa and mean values derived from diametral testing were 0.46 MPa. A conversion factor (K) for UCS was calculated as K= 10.6 for samples loaded at 50°-80°. However, this increased to 14.4 when only considering samples oriented from 70°-75° (or 15°-20° from horizontal). The average point load strength values measured for the MGy schist were higher than the DGy with means ranging between 2.18-2.63 MPa for axial loading and between 0.40 and 0.61 MPa for diametral loading. Both lithotypes share a similar trend: during axial testing the strength decreases, as the foliation angle decreases from perpendicular towards 40° for diametric testing the strength increases, as the foliation increases from parallel

An overall conversion factor (K) for UCS was calculated as K= 18.6 however, this increased to 23.2 when only considering samples oriented from 70°-75° (or 15°-20° from horizontal). The variability (10.6-23.2) of the UCS correlation factor (K) derived from testing suggests care should be taken when recording the foliation orientation relative to loading direction to convert to UCS and that applying a conversion factor of 23.7 (Broch and Franklin, 1972) may result in overestimation of the UCS.

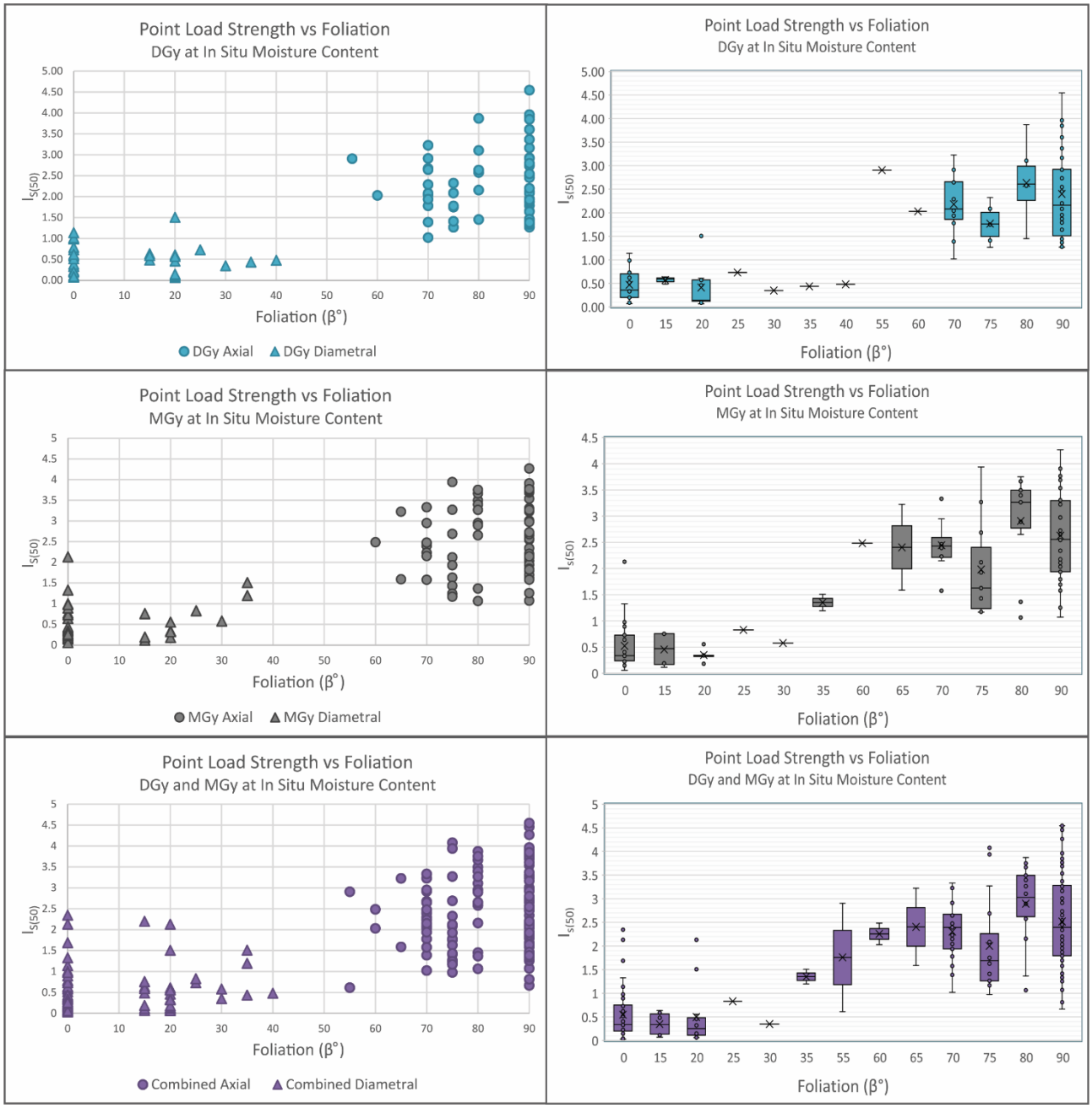

Figure 4.8: Plots showing the relationship between foliation orientation and point load strength for each lithotype (left) and box and whisker plots showing the distribution of the samples (right).

The conversion from diametral point load strength to tensile strength yielded similar results regardless of lithotype between 0.6-0.9 MPa. However, the average tensile strength value derived from point load testing was lower than the average tensile strength derived from the Brazilian test suggesting the conversion from point load strength may result in underestimation of the tensile strength.

The strength anisotropy index calculated from the ratio of mean values perpendicular and parallel to the planes of weakness ranged between 4.85-5.11, indicating a high degree of anisotropy for all lithotypes (ISRM, 2007a).

The DGy and MGy samples were combined, and the two highest and lowest values removed. The average values derived from axial testing range between 2.16-2.52 MPa and diametral testing means range between 0.54-0.60 MPa. Combining the lithotype data resulted in a more consistent conversion factor of K= 14.6 and 19.7. Because previous investigations did not separate out lithotypes, the combined lithotypes tested

perpendicular and parallel to schistosity were then able to be compared with values obtained along Frankton Arm, Macraes and Maniototo. The combined values are very similar to those presented by Stossel (1999) in Table 4.4 (2.09 MPa perpendicular and 0.51 parallel to foliation with an anisotropy index of 4.1) and Macraes, but lower than values derived at Maniototo (Table 4.2)

4.4.5 Results: Triaxial Compressive Strength

The triaxial compressive strength and elastic properties of the DGy and MGy schist tested at in situ moisture content are summarized in Table 4.13, Figure 4.9 and failure modes summarized in Figure 4.10. Values derived from oven dried samples, individual sample data and stress strain curves are available in Appendix C.2. The tabled data is presented by lithotype, including a column combining both lithotypes. Tested samples with a foliation β-angle of 70°-75° (or 15°-20° from horizontal) are presented separately. All maximum differential stress (σ_1-σ_3) results presented have been corrected for length and to 50mm diameter core, along with the samples included to derive parameters for the failure criterion. Samples were tested at 3 confining pressures: 3 MPa, 5 MPa and 10 MPa.

In situ moisture %				DGy	MGy	Combined		DGy	MGy	Combined
No. of Samples				11	11	22		6	8	14
Differential Stress, σ_1-σ_3 (MPa)		Mean ± Std dev.	All Samples	**50.8** ± 15.5	**71.8** ± 29.8	**61.3** ± 25.0	Foliation β° (70-75)	**52.8** ± 16.0	**75.5** ± 28.1	**65.8** ± 25.6
Maximum stress, σ_1 (MPa)	3 MPa	Mean ± Std dev.		**37.4** ± 7.0	**43.1** ± 6.7	**40.3** ± 6.6		**38.7** ± 9.0	**42.9** ± 4.9	**40.8** ± 6.4
	5 MPa	Mean ± Std dev.		**56.2** ± 2.6	**91.7** ± 13.2	**74.0** ± 19.4		**56.2** ± 2.6	**91.7** ± 13.2	**74.0** ± 19.4
	10 MPa	Mean ± Std dev.		**76.8** ± 6.6	**102.4** ± 25.9	**89.6** ± 20.8		**80.0** ± 4.9	**97.9** ± 29.8	**90.7** ± 23.3
Young's Modulus, E (GPa)		Mean ± Std dev		**8.2** ± 2.6	**12.1** ± 6.8	**10.2** ± 5.4		**8.9** ± 2.6	**11.5** ± 7.0	**10.4** ± 5.6
Poisson's Ratio, v		Mean ± Std dev.		**0.18** ± 0.13	**0.16** ± 0.09	**0.17** ± 0.10		**0.22** ± 0.18	**0.13** ± 0.04	**0.16** ± 0.11

Table 4.13: Mean strength results and elastic parameters derived from triaxial compressive strength testing includes: differential stress, the maximum principal stress at each confining stress, Young's Modulus and Poisson's Ratio.

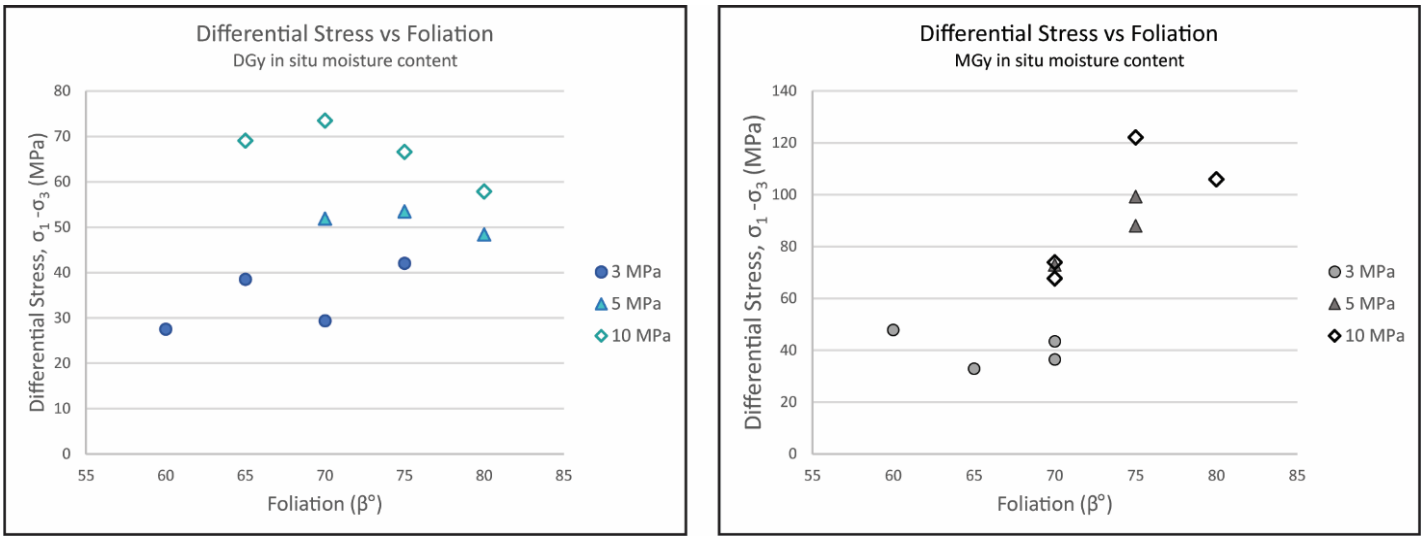

Figure 4.9: Plots showing increasing differential stress as the confining stress is increased.

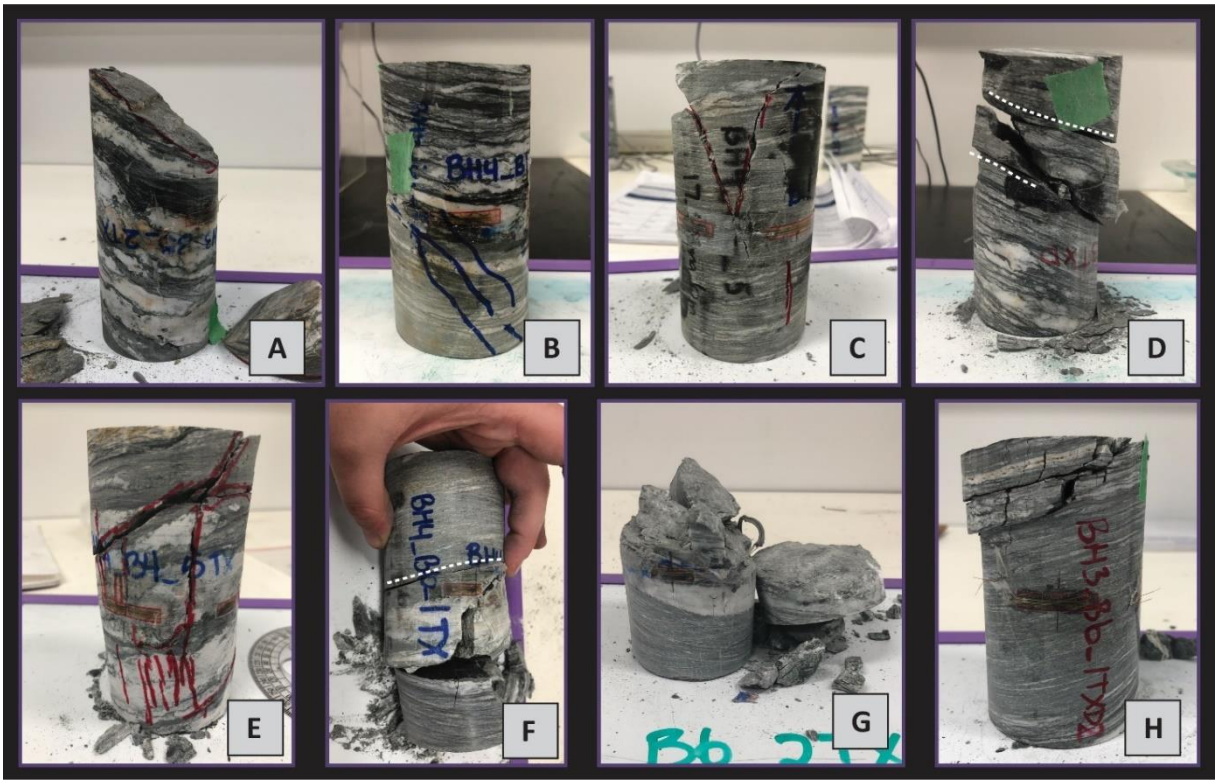

Failure Mode			In situ moisture			Oven Dried		
			DGy	MGy	Total	DGy	MGy	Total
Shear Fracture (A-C)	Shear fracture (A)	Shears occur at 40°-50°, 50°-60° and occasionally 60°-70°	7	2	9	3	7	10
	Parallel (B)	Shears occur at 50°-55°	0	1	1	1	1	2
	Double Shear (C)	Shears occur at 60°-70°	0	2	2	0	0	0
Combination (D-F)	Along foliation and Shear (D)	Fractures occur along foliation and shears at 40°-50° and 50°-60°	1	1	2	3	2	5
	Shear and Joint (E)	Fractures occur along shears at 40°-55°, and 80°-87° up the centre	2	2	4	0	1	1
	Along Foliation and Joint (F)	Fractures along foliation and 80°-87° up the centre	0	1	1	1	0	1
Multiple Fractures (G)		Fractures along multiple orientations	1	2	3	0	0	0
Along Foliation (H)		Fracture occurs along foliation	0	0	0	2	0	2

Figure 4.10: Summary of the failure modes observed after triaxial testing. Sample photos with the associated failure mode (top). Number of samples recorded for each failure mode (Table).

The average differential stress measured for all DGy samples tested at in situ moisture content is 50.8 MPa and 71.8 MPa for MGy. The average values derived for Young's modulus and Poisson's Ratio for both lithotypes are 8.2-12.1 GPa and 0.16-0.22, respectively. On average, the MGy lithotype is approximately 1.2-1.6 times stronger than the DGy lithotype but both share similar elastic properties. The difference in strength values between the lithotypes is likely attributed to their inherent anisotropy. Namely, the thicker (> 1 mm) micaceous and mafic segregations and a coarser grain size of the DGy schist.

The results show that as the confining pressure is increased, the amount of axial load required to fracture the sample increases (Figure 4.9). The results show marginal differences between specimens tested at 70°-75° and the full range of tested samples because most of the tested samples had similar foliation orientation.

The stress-strain curves (included in Appendix C.2) observe a full range of post-peak behaviour from elastic-brittle to elastic-plastic. Strain softening is the most common observed post-peak behaviour in both lithotypes. Suggesting an average overall rock mass quality (Hoek, 2007). In some cases, the samples have multiple peaks as the load increases past the initial failure, while others exhibit elastic-plastic failure at 10 MPa of confining pressure. A summary of the failure modes is included in Figure 10. Shear fractures are the predominant mode of failure recorded for both lithotypes, with shears occurring at 40°-60° followed by a combination of shearing and fracturing along a subvertical joint.

4.4.6 Failure Criteria

The triaxial compressive strength data along with a range of UCS and converted indirect tensile strength results were plotted to derive the Hoek-Brown and Mohr-Coulimb failure criteria (Figure 4.11), with a summary of the resulting parameters in Table 4.14. The intact compressive strength derived for the DGy and MGy schist samples were 25.5 and 44.9 MPa, respectively, indicating the MGy lithotype is approximately 1.7 times stronger than the DGy. The material constant m_i is similar in both lithotypes ranging between 14.2-15.3, which is expected (Hoek, 2007). The average cohesion is 3.6-5.4 MPa, approximately 12-14 % of the average UCS value, with a friction angle (ϕ) of 44.9°-50.4°. The Hoek-Brown and Mohr-Coulomb parameters derived through testing are within the expected ranges presented in Table 4.1 and in Zhang (2016). Cohesion values are similar to ones observed in Maniototo but are lower than values from the Cromwell Gorge (see Table 4.2).

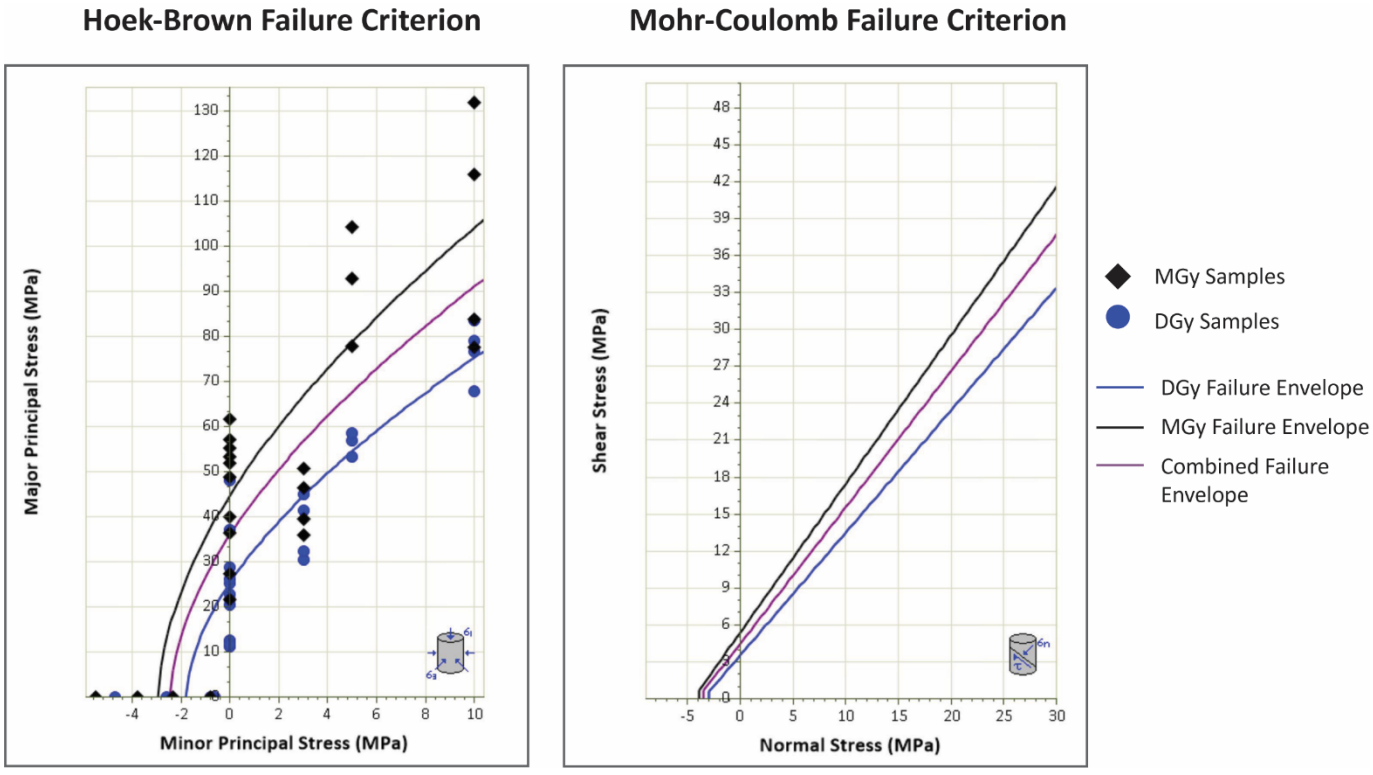

Figure 4.11: UCS, triaxial strength and tensile strength results plotted to derive the Hoek-Brown failure criteria (left) and Mohr-Coulomb failure envelopes (right).

In situ moisture %			DGy	MGy	Combined		DGy	MGy	Combined
No of Samples			11	11	22		6	8	14
UCS range (MPa)		**All Samples**	11.3-48.0	21.6-61.8	11.3-61.8	**Foliation β° (70-75)**	27.4-40.8	36.4-61.8	27.4-61.8
Tensile Strength range (MPa)			-(0.63-4.72)	-(0.80-5.50)	-(0.63-5.50)		-(0.80-4.72)	-(0.80-5.50)	-(0.80-5.50)
Hoek	σ_{ci} (MPa)		25.5	44.9	36.07		30.3	49.5	42.5
Brown	m_i		14.2	15.3	14.6		12.2	12.0	10.9
Mohr	c (MPa)		3.6	5.4	4.5		3.3	5.6	4.6
Coulomb	Φ (°)		44.9	50.4	47.9		45.7	50.9	49.2

Table 4.14: Failure criterion parameters including the range of UCS and tensile strength values used to derive the failure envelopes.

4.5 Geomechanical Classifications

Rock mass classifications can provide quality indices aimed at determining preliminary predictions of slope stability and rock mass suitability in construction practice. The rock-mass classification methods considered in this thesis are: Rock Mass Rating (RMR), Anisotropic Rock Mass Rating (ARMR), Slope Mass Rating (SMR) and Geological Strength Index (GSI).

4.5.1 Methodology

4.5.1.1 Rock Mass Rating (RMR)

The RMR classification was developed by Bienawski (1973) for preliminary assessment of rock mass quality for excavation and tunneling applications. Six main parameters are used to derive the RMR index: uniaxial compressive strength of the intact rock, rock quality designation (RQD), groundwater conditions, and the orientation, spacing and weathering of discontinuities (Bieniawski, 1989). RMR is a widely used classification (Bertuzzi et al., 2016; Hoek, 2007; McKenzie, 1993; Singh et al., 2011) largely due to its simplicity. However, RMR tends to over-estimate strength values when applied to weaker and/or anisotropic materials and was not designed specifically for slopes. A range of RMR values were determined for the landslide using the updated (1989) classification system. The Rock Mass Rating System criteria is presented in Appendix C.3.1.

4.5.1.2 Anisotropic Rock Mass Rating (ARMR)

The ARMR classification developed by Saroglou et al. (2018) is specifically designed for anisotropic rock masses. The main parameters used are: the strength anisotropy index, (R_c), UCS of intact rock, spacing of anisotropy planes on a scale of 5-10m, corrected RQD, condition of anisotropy surfaces and groundwater conditions (Saroglou et al., 2018). However, the ARMR is not recommended in cases where rock mass failure is exclusively controlled by structural features and caution should be used for kinematic instability in highly anisotropic rock masses. “Therefore, it (ARMR) is not directly applicable in slope stability problems, where the anisotropy planes are dipping towards the slope and failure of the rock mass occurs along these planes.” (Saroglou et al., 2018, p. 3623). The Anisotropic Rock Mass Rating System criteria are presented in Appendix C.3.2.

4.5.1.3 Slope Mass Rating (SMR)

The SRM classification was developed by Romana (1985) to assess slope stability by subtracting adjustment factors related to joint and slope orientation, and adding excavation methods to the existing RMR (Singh and Goel, 1999). The four main adjustment factors rely on the orientation between critical joint planes and the slope face, the mode of failure (planar, topple, wedge) including the associated relationships between the

discontinuities, and the excavation method. The Slope Mass Rating System is calculated using Equation 32. The system criteria and all associated equations are presented in Appendix C.3.3.

$$SMR=RMR_{basic}-(F_1 \cdot F_2 \cdot F_3)+F_4 \quad (32)$$

4.5.1.4 Geological Strength Index (GSI)

GSI is a descriptive tool used to qualitatively evaluate rock mass strength by attributing a range of parameters to visible heterogeneities/discontinuities in a rock mass. This method was originally developed by Hoek (1994) and modified to suit various rock types (Hoek, 2007). Hoek and Karzulovic (2000) presented a strength index used to classify schistose metamorphic rocks. The parameters evaluated include the composition, structure, foliation, interlocking of rock pieces and surface conditions of discontinuities (Hoek and Karzulovic, 2000). The Geological Strength Index (GSI) table is presented in Appendix C.3.4 for reference.

4.5.2 Results: Rock Mass Rating

The results derived from the application of the RMR are summarized in Figure 4.12 and criteria selected is tabled in Appendix C.3.1. The values are presented as a range to ensure an accurate representation of variations in rock mass quality has been captured, in multiple locations across the study area. Many parameters affect the ranges presented including: UCS, the condition of the discontinuities, changes in groundwater based on seasonality, and a rating adjustment for discontinuity orientation for slopes.

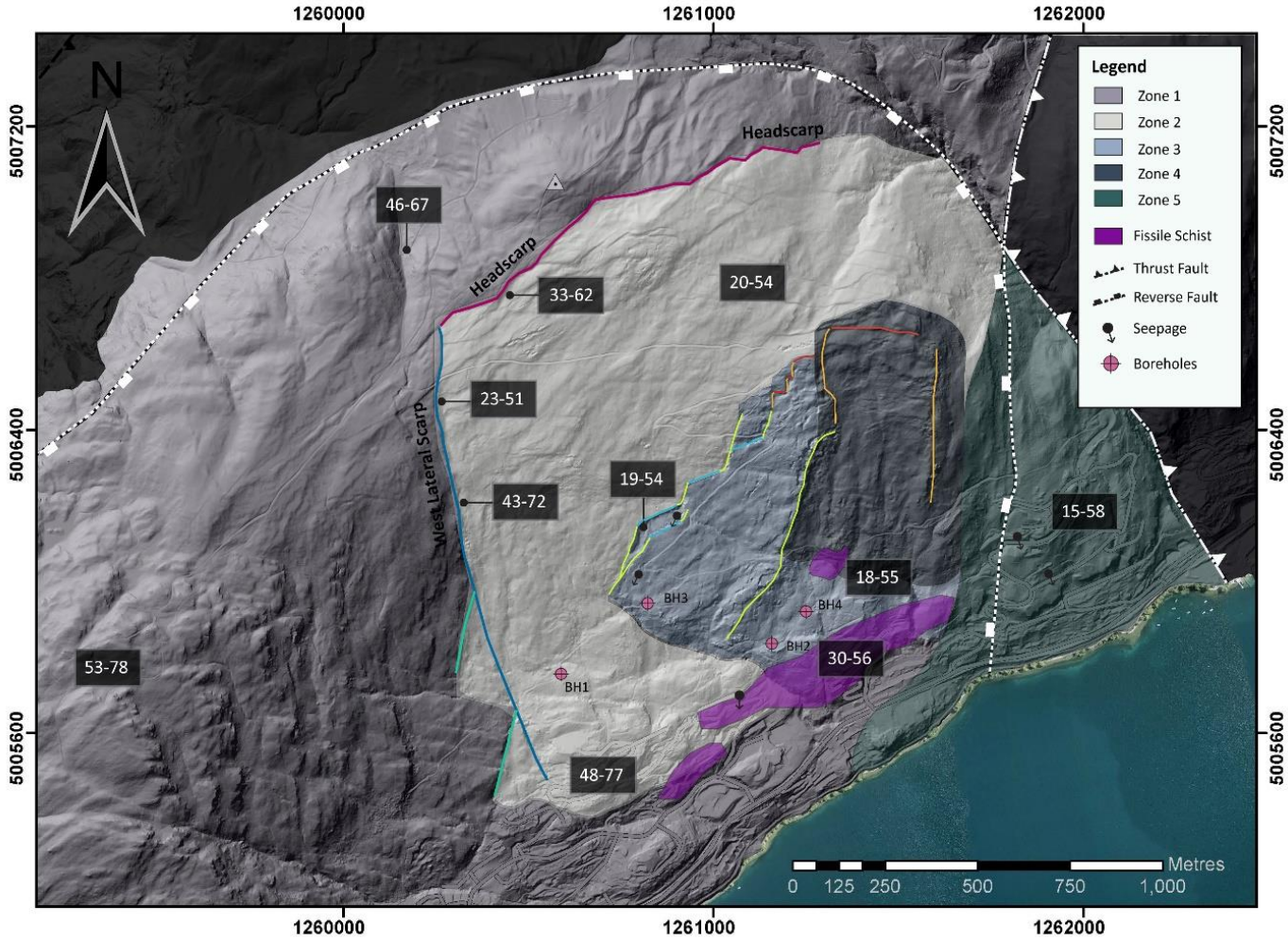

Figure 4.12: 1:12,000 scale map showing the range of RMR values attributed to various areas across Queenstown Hill (in dark grey boxes). Basemap: Structural domain map from Section 2.6.

The RMR values derived from the upper portion of Queenstown Hill yielded the highest results with rock quality ranging from fair to good (RMR=46-78) followed by major scarps on the landslide boundaries. The rock mass quality assessed in the mid to lower portion of the landslide were the most variable. This is largely due to highly weathered, closely fractured, large extensional features and increased seepage occurring within the landslide body. Although not within the landslide body, the kink banded zone (Zone 5: shaded in green) also yielded highly variable results. This is because of inconsistent rock quality observed in outcrops and excavations ranging from unweathered fair quality schist intermixed with foliation shears, fissile kink banded schist and seepage. The ranges provided highlight the need for more site-specific investigations to determine rock mass quality.

4.5.3 Results: Anisotropy Rock Mass Rating

Results derived from the ARMR criteria are summarized in Table 4.15 and selected parameters are included in Appendix C.3.2. The values are presented as a range to account for variability in UCS strength, foliation spacing, weathering profile and seepage for each lithotype. The respective UCS ranges were used for each lithotype, rather than an average value. While the conditions of the discontinuities are similar for both lithotypes, an adjustment was made to reflect the stronger weathering profile recorded in the DGy. An adjustment was also made by providing a range for groundwater to include increased seepages during the winter months.

	DGy		MGy		Combined	
	Min	Max	Min	Max	Min	Max
ARMR	27	43	33	46	27	43
Class	IV		IV		IV	
Description	Highly anisotropic rock mass		Highly anisotropic rock mass		Highly anisotropic rock mass	

Table 4.15: Summary of ARMR values derived for each schist lithotype or if considering the entire rock mass as a whole (combined).

The ARMR values derived from Saroglou et al. (2018) confirm that both lithotypes are highly anisotropic rock masses and that the DGy lithotype is slightly more anisotropic than the MGy. This agrees with results derived from point load strength testing and observations recorded in the field, and hand specimen.

4.5.4 Results: Slope Mass Rating

An assessment of the discontinuity orientations and failure modes are included as part of the Slope Mass Rating classification. As such, field observations were combined with discontinuity data to determine a range of SMR values, within each structural zone (identified in Section 2.6). Prior to the addition of the SMR adjustment values, the RMR value is determined within each zone. When determining RMR ranges, the intact rock strength, spacing of discontinuities, persistence of joints, degree of weathering and seepages (seasonal and non-seasonal) were the most common parameters responsible for variability within each zone. The results derived from the SMR classification are presented in Figure 4.13 and Table 4.16.

According to the range of SMR values derived using Romana (1985), slope stability ranges indicate a poor to good rock mass quality, and a combination of instability and partial stability. The large range in values is attributed to mixed rock quality observed in the field. Many outcrops included “good” and “bad” rock mass qualities. In order to provide representative data for rock mass assessment, the full range recorded in the field was considered when selecting classification parameters.

The highest SMR values were recorded in structural Zone 1, representing the area surrounding the Queenstown Hill Landslide. The rock mass quality observed in the field is well reflected in the SMR values obtained. Structural Zones 2 to 4 are within the landslide margins and have the lowest SMR values. The

"poor" quality index values in Zones 2 and 3 are because of seepages and closely fractured and weathered areas within these zones. Zone 2 includes localized bands of rock mass with high fracture densities and moderate to high weathering profiles in the landslide's main headscarp and lateral scarp. Zone 3 has a higher concentration of extensional features (tension cracks, graben, dilated and released blocks, etc.), seepage, and highly weathered fissile schist in its lower margins - all of which contributed to the lower SMR values. The assessment of Structural Zone 4 was limited to observations gathered along its margins, as there is little to no outcrop exposure within the centre of this zone. Structural Zone 5, located outside of the landslide, received the lowest score from the SMR ranges. The zone comprises the landslides outer margins to the east and is made up of weak kink banded schist. This includes many foliation shears, fissile schist, raveling and seepage from road cuttings. Within each zone, the upper ranges of SMR values are classed within the "good/stable" rock mass quality.

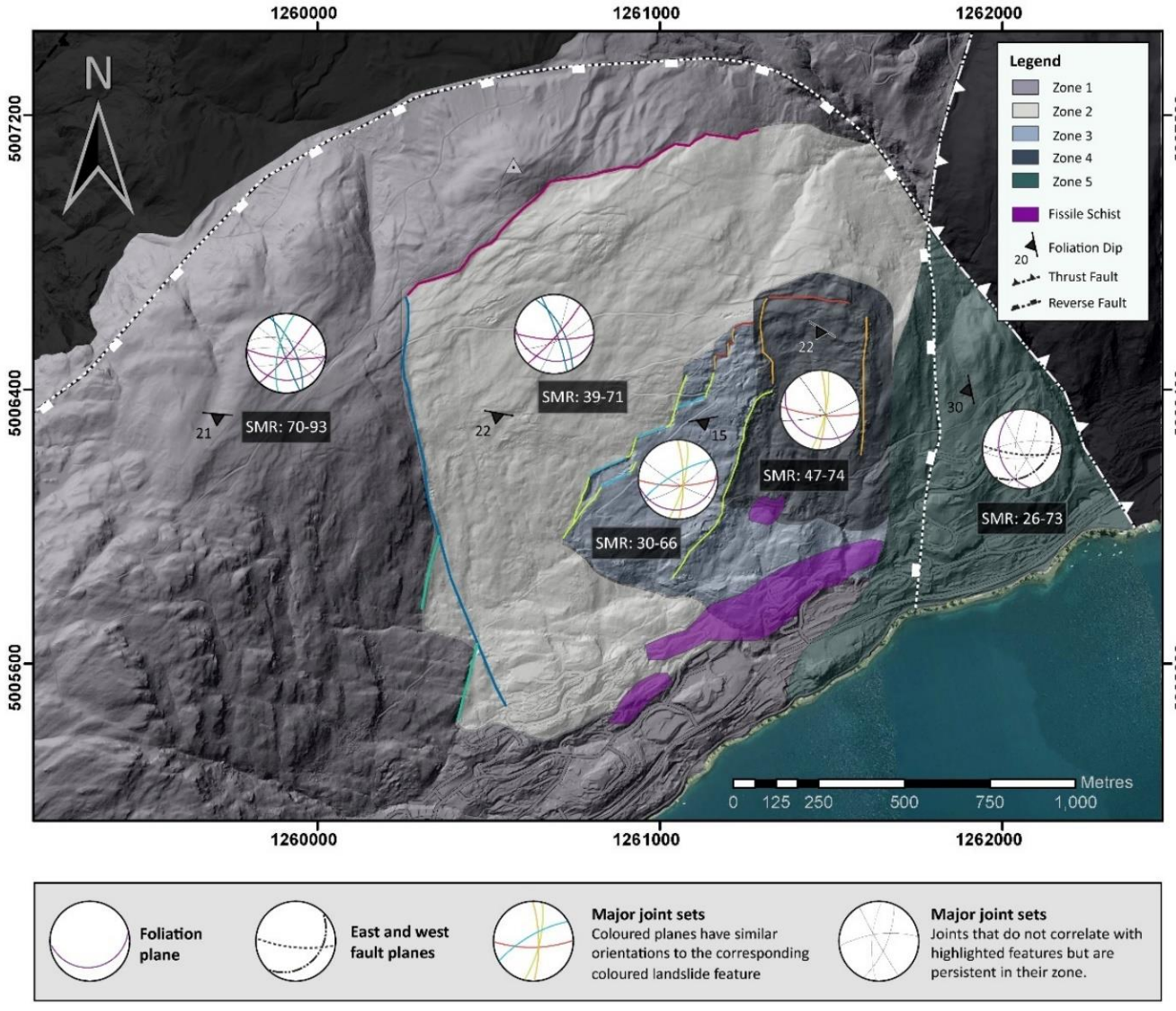

Figure 4.13: SMR ranges derived for each Structural zone (map from Section 2.6, Figure 2.24). Map 1:12,000 scale.

	SMR		Class		Description and stability	
	Min	Max	Min	Max	Min	Max
Zone 1	70	93	II	II	Good, stable. Some block failure.	Good, stable. Some block failure
Zone 2	39	71	IV		Bad, unstable. Planar failures or big wedges	
Zone 3	30	66	IV			
Zone 4	47	74	III		Normal, Partially stable. Planar failures along some joints and many wedges	
Zone 5	26	73	IV		Bad, unstable. Planar failures or big wedges	

Table 4.16: SMR ranges attributed to each zone with the stability class and description per Romana (1985).

4.5.5 Results: Geological Strength Index

A contour map summarizing the geological strength index (GSI) ranges surveyed at 209 locations across the study site are presented in Figure 4.14. The description of the rock mass structure varied between moderately foliation to very foliated with very poor to very good surface quality depending on the location ranges were surveyed. Overall, the GSI values range between 15 and 65.

The highest GSI values were recorded in outcropping in situ schist surrounding the landslide. The rock surfaces were good to very good quality (GSI= 50-65) with slightly weathered rough surfaces with narrow apertures. Degraded scarps surrounding the perimeter of the landslide (i.e headscarp, lateral scarp, etc.) had a more variable rock quality ranging between poor to fair quality (GSI= 30-45). Scarps are generally moderately weathered, rough to smooth, and blocky, with inconsistent intensity of fracturing. Within the main landslide body, variable ranges in GSI can be attributed to variability observed in outcropping material. Schist quality and structure ranged from slightly weathered to highly weathered with high and low fracture density, hard and soft joint fillings with narrow to open apertures. The very poor to poor ranges (GSI= 15-30) derived at the base of the extension and reactivation zones accurately reflects the intense deformation, compressional features, and fissile schist.

While not the focus of this chapter, the qualitative GSI data can be used in conjunction with results presented in this chapter to derive the rock mass constants (m_b, s, a) used in the Generalized Hoek-Brown equation to estimate rock mass strength.

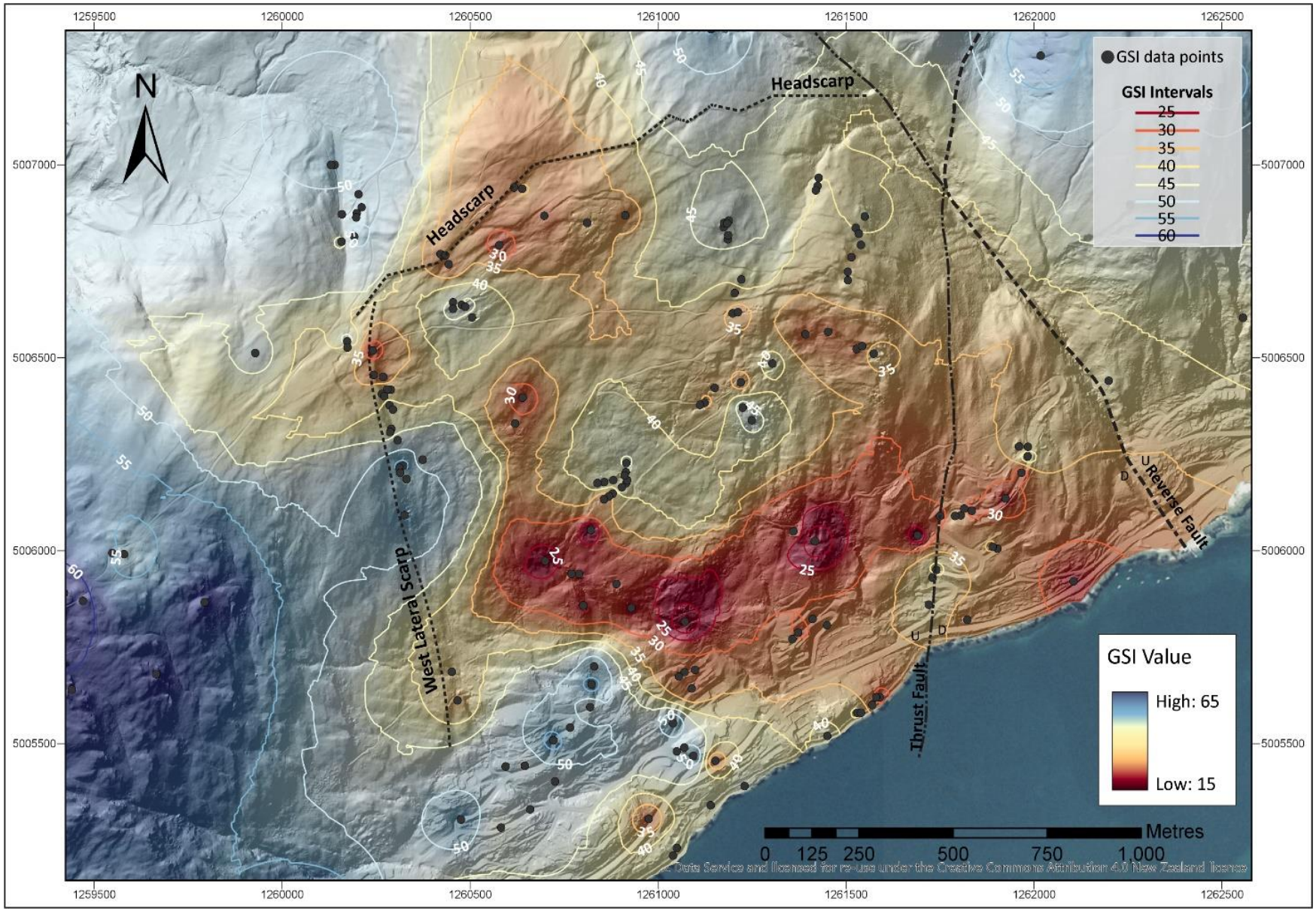

Figure 4.14: GSI contour map (Scale 1:12,000)

4.6 Discussion and Synthesis

A summary of the physical properties and mechanical are presented in Tables 4.17 and 4.18. This includes the mean values for the entire tested range of foliation attitude separated by schist lithotype (DGy and MGy) and a combined column. The decision to maintain the separation of both lithotypes was made due to the significant variations in geotechnical properties demonstrating a clear relationship between mineralogy and texture. Also, a general predominance of the more micaceous dark green-grey schist was recognized in the boreholes; although an uneven distribution was not observed in the field, due to interlayering of both lithotypes.

Due to the inherent anisotropy of schist, samples are typically tested perpendicular, parallel and oblique to foliation to derive the mechanical properties at various orientations. However, the orientation of the samples tested as part of this study were limited by the vertical orientation of the boreholes. The oblique foliation orientations tested in the laboratory are similar to the range of foliation dip measurements obtained in the field (10°-50°); meaning the test results yield representative ranges, which can be implemented in practical applications along Queenstown Hill. However, sampling bias should be considered, especially in schist highly prone to disking meaning the weak and highly fragmented rock could not be tested.

Assessment of the laboratory data shows that although both lithotypes share similar physical properties they show marked differences when comparing their strength parameters (Table 4.18). The strength and stiffness data show variations up to 50 MPa for UCS, 95 MPa for differential stress, up to 40 GPa in Young's Modulus and 0.35 for Poisson's ratio. However, the variability in geo-mechanical properties measured in this research conforms with findings from other international studies characterizing quartz and mica-rich schists (Andrade and Saraiva, 2010; Basu et al., 2013; Behrestaghi et al., 1996; Kundu et al., 2017; Loureiro et al., 2015; Mustafa et al., 2015; Nasseri et al., 2003; Zhang et al., 2011).

On average, the poorly foliated medium grey quartzofeldspathic schist samples (MGy) are 1.5 times (1.2-2.2) stronger than the well foliated dark green-grey semi-pelitic schist (DGy). The strength values and elastic parameters derived from laboratory testing (UCS and triaxial compressive strength testing) confirm a decreasing relationship with the orientation of foliation as the angle approaches 45°, with the exception of a consistent Poisson's ratio.

Analysis of the fracture patterns and failure modes reveal that both lithotypes exhibit shear fractures cross-cutting foliation at 50°-60°. In UCS specimens, this angle sometimes increases to 60°-70°, or decreases to 40°-50° when a confining stress is applied during triaxial testing. The most common brittle failure pattern observed is shear fracturing, with a stepped profile cross-cutting multiple foliations; followed by parallel shears cross-cutting foliation along the top and bottom edges of the core that develop a subvertical (80°-87°) joint along the centre. Stress-strain curves characterizing the post peak behaviour showed a dominance in brittle failure for both schist lithotypes. When confining stresses exceeding 5-10 MPa were applied to the DGy lithotype, it began to display strain hardening and plastic-elastic failure.

Failure criteria (Hoek-Brown and Mohr-Coulomb) were derived for each lithotype using the appropriate corrected strength results (to 50 mm core diameter). The material constant (m_i) was determined as 14.2 for DGy and 15.3 for MGy, with an intact uniaxial compressive strength (σ_{ci}) of 25.5 MPa and 44.9 MPa, respectively. Similar cohesion (c) and friction angles (ϕ) were measured for both lithotypes and ranged between 3.6-5.4 MPa and 45°-50°, respectively. No clear relationship was observed between the orientation of foliation and failure criteria parameters. This does not exclude the possibility of a relationship, but it is likely that the orientation range and number of samples tested were not sufficient to confirm one.

Finally, four rock mass classification methods were applied to the Queenstown Hill Landslide to provide quality indexes, which can be utilized in pre-feasibility design stages: the Rock Mass Rating (RMR) classification, Anisotropic Rock Mass Rating (ARMR) classification, Slope Mass Rating (SMR) classification, and Geological Strength Index (GSI). The RMR classification yielded “fair” values overall, with areas of highly weathered and fissile schist classified as “poor” rock quality. The ARMR classed both schist lithotypes as highly anisotropic rock masses, agreeing with observations recorded in the field and in boreholes. The SMR classification was completed for each structural zone identified in Section 2.6. The results range from bad unstable rock to good stable rock, which was not unreasonable because it includes a range of weathering (slightly to highly weathered areas), and takes into consideration increased seepage observed during the winter months. The results derived from the GSI presented the variable results ranging from 15-65 across the study area. However, the GSI values best reflect the surface morphology, rock mass quality and level of deformation observed across Queesntown Hill. The highest index values were recorded surrounding the landslide, which is to be expected, while the lowest GSI values reflect highly deformed, extensional and compressional zones.

It is important to note that the rock mass classification ranges obtained as part of this study are very large, because they account for variability within a selected zone/area, and can result in overly optimistic or pessimistic values. These ranges are meant to provide an estimate of the overall rock mass quality, and are not representative for site specific investigations. However, from the classification methods presented above, GSI is likely to be the most reliable method. This is largely due to its practical applications developed by Hoek (2007). GSI has been effectively used to estimate strength and deformation characteristics of rock masses for slope stability and foundation design.

The results presented in this chapter are within the published expected ranges (González de Vallejo and Ferrer, 2011; Zhang, 2016) and are comparable to published values elsewhere in Otago, namely Maniototo Dam and Canal (Moody, 1985; Paterson, 1979; Paterson et al., 1988). Along the Frankton Arm, Stossel (1999) undertook preliminary testing and discontinuity surveying as part of her thesis; the combined values from this study correlate well with her previous investigations.

Summary of Physical Properties				
		DGY	MGy	Combined
Moisture Content (%)		**0.9** ± 0.25	**0.9** ± 0.24	**0.9** ± 0.23
Bulk Density, ρ_B (kg/m^3)		**2740** ± 47	**2800** ± 44	**2770** ± 55
Dry Density, ρ_D (kg/m^3)		**2730** ± 45	**2760** ± 54	**2740** ± 53
Bulk Unit Weight, γ (kN/m^3)		26.9	27.4	27.2
Dry Unit Weight, γ_d (kN/m^3)		26.8	27.1	26.9
Porosity, n (%)		**3.1** ± 1.0	**2.8** ± 1.1	**2.9** ± 1.0
P-Wave, V_p (m/s)	Dry	**4769** ± 318	**4779** ± 337	**4774** ± 299
	Saturated	**5582** ± 224	**5477** ± 247	**5529** ± 221
S-Wave, V_s (m/s)	Dry	**2645** ± 254	**2720** ± 206	**2770** ± 55
	Saturated	**2453** ± 234	**2579** ± 280	**2521** ± 244
Dynamic Young's Modulus, E_d (GPa)	Dry	**48.9** ± 8.0	**50.1** ± 6.3	**49.7** ± 6.6
	Saturated	**46.6** ± 7.6	**50.4** ± 9.0	**48.7** ± 318
Dynamic Poisson Ratio, ν_d	Dry	**0.27** ± 0.06	**0.25** ± 0.07	**0.26** ± 0.06
	Saturated	**0.38** ± 0.03	**0.35** ± 0.05	**0.36** ± 0.04
Dynamic Shear Modulus, G_d (GPa)	Dry	**62.7** ± 8.0	**62.9** ± 9.9	**62.8** ± 8.2
	Saturated	**17.0** ± 3.0	**18.8** ± 4.0	**18.0** ± 3.4
Bulk Modulus, K_d (GPa)	Dry	**36.9** ± 9.6	**35.8** ± 10.1	**36.3** ± 9.0
	Saturated	**64.9** ± 9.6	**59.2** ± 12.5	**61.8** ± 10.6
Slake Durability Index, I_D (%)	Cycle 2	**97.9** ± 0.01	**98.8** ± 0.00	-
	Cycle 5	**95.8** ± 0.02	**97.3** ± 0.00	-

Table 4.17: Summary of physical properties derived through laboratory testing. Results are presented as **mean** ± standard deviation.

Summary of Mechanical Properties					
			DGY	MGy	Combined
Uniaxial Compressive Strength, σ_c (MPa)		Mean ± Std dev.	**23.4** ± 11.1	**45.4** ± 10.5	**33.8** ± 16.2
Young's Modulus, E (GPa)	From UCS	Mean ± Std dev.	**15.7** ± 7.9	**11.7** ± 11.8	**14.5** ± 9.9
Poisson Ratio, v	From UCS	Mean ± Std dev.	**0.18** ± 0.09	**0.21** ± 0.12	**0.20** ± 0.10
MR		Mean	671	257	429
Indirect Tensile Stress, σ_t (MPa)	ASTM	Mean ± Std dev.	**2.50** ± 1.26	**3.66** ± 0.78	**2.98** ± 1.22
	ISRM	Mean ± Std dev.	**3.93** ± 1.97	**5.74** ± 1.22	**4.69** ± 1.92
Point Load Strength Index, $I_{s(50)}$ (MPa)	Perpendicular	Mean	2.40	2.63	2.52
	Oblique	Mean	2.21	2.44	2.32
	Parallel	Mean	0.46	0.46	0.55
	Oblique	Mean	0.46	0.61	0.60
Conversion Factor, K		Mean	10.6	18.6	14.6
Anisotropy Index, I_a		Mean	5.11	5.72	4.85
Differential Stress, σ_1-σ_3 (MPa)		Mean ± Std dev.	**50.8** ± 15.5	**71.8** ± 29.8	**61.3** ± 25.0
Young's Modulus, E (GPa)	From Triaxial	Mean ± Std dev.	**8.2** ± 2.6	**12.1** ± 6.8	**10.2** ± 5.4
Poisson Ratio, v	From Triaxial	Mean ± Std dev.	**0.18** ± 0.13	**0.16** ± 0.09	**0.17** ± 0.10
Hoek Brown Failure Criterion	σ_{ci} (MPa)	Mean	25.5	44.9	36.07
	m_i	Mean	14.2	15.3	14.6
Mohr-Coulomb	c (MPa)	Mean	3.6	5.4	4.5
	Φ (°)	Mean	44.9	50.4	47.9

Table 4.18: Summary of mechanical properties derived through laboratory testing. Results are presented as **mean** ± standard deviation.

Chapter 5: Engineering Geology Ground Model

5.1 Introduction

The focus of this chapter is to summarize and interpret results obtained through field mapping and laboratory testing carried out on the Queenstown Hill Landslide. This chapter includes:

- A summary of the landslides surface morphology and geological environment, which was used to create an engineering geological ground model consisting of eight cross sections and a 3D conceptual block model.
- Kinematic analysis of the structural domains identified in Chapter 2.
- A brief discussion on the evolution of the Queenstown Hill Landslide, as it is presently understood.

The surface morphology has been described using historical aerial photos, lidar and field observations. The geological setting comprises a combination of lithotypes, rock mass defects (e.g. foliation shears), structural domains (Section 2.6), borehole data and surficial deposits. The subsurface geology is largely inferred, due to limited subsurface investigations. Four boreholes were drilled along the lower reaches of the Queenstown Hill Landslide, with only one intercepting a potential basal shear. No drilling was undertaken in the upper parts of the slope. Landslides occurring in schist elsewhere were used as an analogue to interpret gaps in the subsurface data.

The integration of the surface and subsurface data allowed for preliminary interpretation of the Queenstown Hill Landslide ground model and failure mechanisms. The ground model was then combined with kinematic analysis to provide a broad understanding of slope stability analysis.

5.2 Engineering Geology Ground Model of the Queenstown Hill Landslide

5.2.1 Overview of the Geology and Geomorphology of the Queenstown Hill Landslide

The Queenstown Hill Landslide is located along the Frankton Arm of Lake Wakatipu with a peak elevation of 870 masl at the crown and ~390 masl. at the base of the toe zone. The landslides headscarp is oriented parallel to the slope, with an average slope angle and direction of 27° ± 12/149° ± 37 (SSE). The landslide measures 1425 m in length (from headscarp to toe), with a maximum width of 1600 m and a vertical elevation range of approximately 500 m. The slide covers an estimated area of 2.28 km^2 with an approximate volume of 1.7 x 10^8 m^3. Failure has occurred along the moderately inclined (25°-35°) dip slope of Queenstown Hill, which has a subparallel orientation to the foliation planes and foliation shears. A conceptual block model summarizing the surface features is presented in Figure 5.1.

The landslide is mapped within the undifferentiated Caples Terrane of the Otago Schist (TZ I-III), approximately 2km west of the Caples-Aspiring Terrane boundary, and is predominantly made up of interlayered medium grey quartzofeldspathic and dark green-grey semi-pelitic schist with an average orientation of 20°/192° (SSW) described as:

Unweathered to moderately weathered medium grey foliated quartzofeldspathic SCHIST; moderately strong to strong (22-62 MPa); poor to moderately developed foliation, planar with thin < 1 mm laminae, laterally continuous 2-25 mm thick quartz segregations, spaced 2-200 mm, occasional pinch and swell structures, foliation dips 10°-30°; quartz veins and discontinuities are very steeply inclined (60°-70°) to sub-vertical (80°-88°). [Otago Schist, Textural Zone III]

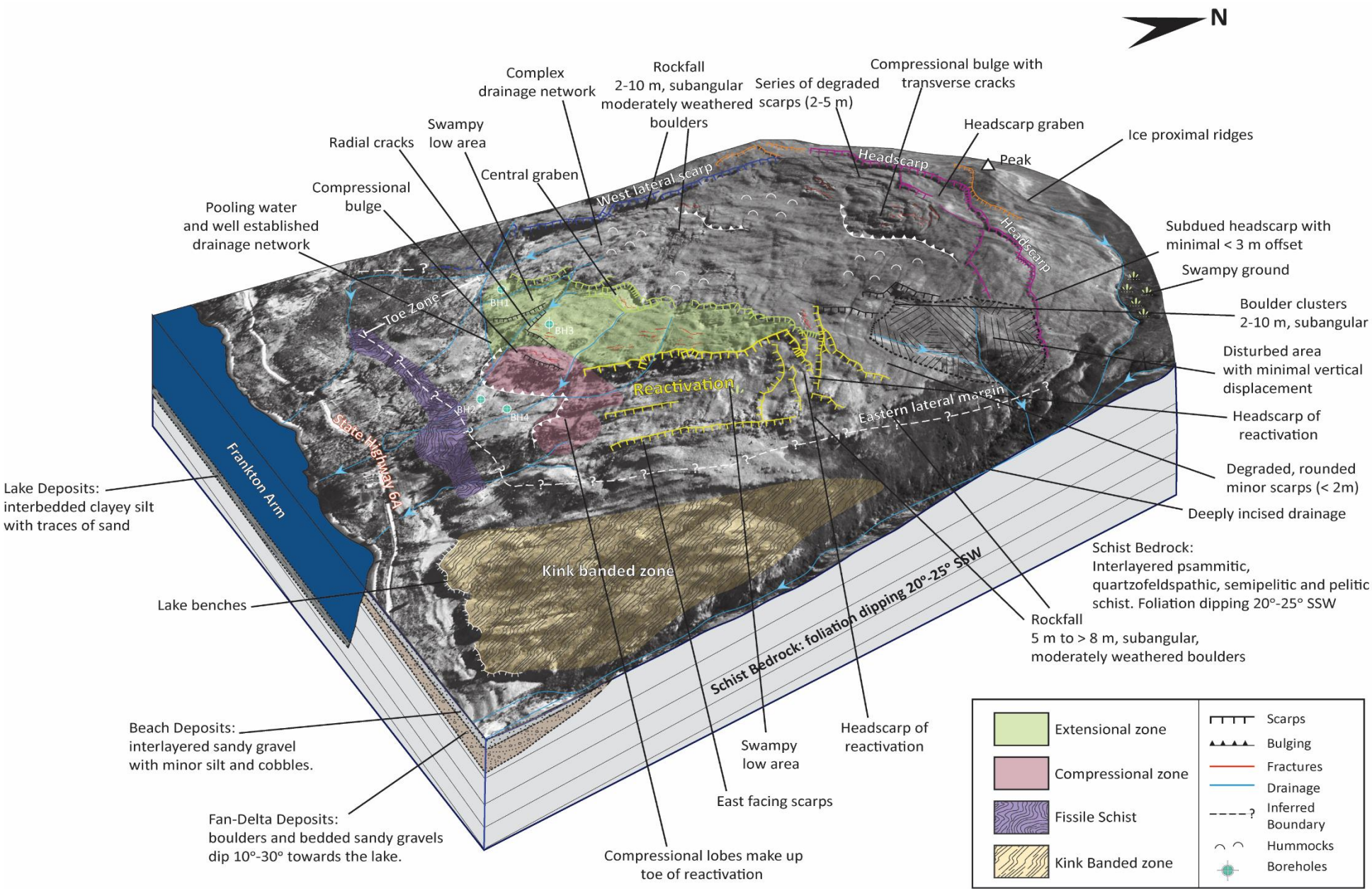

Figure 5.1. Conceptual block model of the Queenstown Hill Landslide with features drawn on the 1956 aerial photo.

Slightly weathered to highly weathered dark green-grey foliated semi-pelitic SCHIST; weak to moderately strong (11-48 MPa); well-developed foliation, planar and undulating with 1-5 mm laminae, laterally continuous 3-40 mm thick quartz segregations, spaced 2-40 mm, pinch and swell as well as folded structures common, foliation dips 10°-40°; discontinuities are very steeply inclined (50°-60°) to sub-vertical (80°-88°). [Otago Schist, Textural Zone IV]

The decision to separate both lithotypes was made due to the significant variations in geotechnical properties, textures, and mineralogy. A general predominance of the more micaceous dark green-grey schist was recognized in the boreholes. However, an uneven distribution was not observed in the field and the lithotypes are interlayered. Due to the variability in interlayering and a lack of lateral persistence, it is unlikely that a detailed distribution of the lithologies is attainable without extensive drilling.

The landslide geometry is defined as rectangular and blocky, with a well-defined joint-controlled crown and west lateral scarp. The eastern boundary is inferred along a deeply incised drainage flowing south towards Frankton Arm and coinciding with a reverse sinistral fault mapped by GNS. It is interpreted that the landslide boundary continues along the trace of the reverse fault mid-slope, as it intersects a separate thrust fault mapped by GNS. The extent of the landslide at the toe is largely unknown, but its farthest possible extent has been drawn as a semi-continuous band made up of fissile schist at 390 masl. Due to the margins being poorly defined to the east and along the toe, they should be treated as broad zones rather than clear boundaries.

Geomorphic mapping has identified five zones characterized by the surface morphology: the headscarp zone, the main landslide body, an extensional zone, a reactivated zone and the toe zone (Section 3.1). The landslide headscarp is largely degraded, with a vertical offset of 10-15 m and minor outcropping schist blocks overlain by glacial material. Towards the centre of the crown, scarps crosscut and offset a series of ice proximal ridges extending down just beneath the headscarp graben and flatten to the east, with < 2 m of vertical offset. The headscarp graben transitions to a compressional bulge made up of large boulders (> 10 m) thrust over the existing ground. To the west, the headscarp intersects a prominent steep dipping (50°-83°) lateral scarp with an estimated 10-25 m of vertical offset. The west lateral scarp becomes poorly defined as it transitions from a scarp with visible offset to an incised gully south towards the toe zone (Figure 5.1).

The upper portion of the landslide hosts a series of eroded vegetated scarps, transverse tension cracks and subdued hummocky topography, with few active drainage gullies at the surface. Fractures in the upper to mid part of the slope allow the water to infiltrate and flow in the subsurface. This rapidly changes to a well-established rectangular drainage network at the surface and is likely following joint sets, and zones of weaker deformed material in the lower half of the landslide. The centre of the landslide then transitions into an extensional zone marked by a NE-SW joint-controlled scarp releasing blocks at the upper end, and forming a graben mid-slope. The zone also includes large (up to 100 m long), deep (> 8 m), NE-SW trending tension cracks and fractures suggesting the rock mass moved downdip towards the lake.

Mid-slope in the east quadrant of the landslide a series of en-echelon scarps (73°/179°) with 2-8 m of vertical offset have been interpreted as the headscarp of the reactivation zone. This zone has been interpreted as a reactivation of the main landslide body, due to a change in scarp orientation from NE-SW to SW-NW, an increased amount of offset measured along scarps (up to 15 m) and a change in surface expression compared to elsewhere within the landslide. The surface expression of the reactivation is rectangular with a prominent joint controlled headscarp and a series of east facing lateral scarps. Subdued hummocky terrain and well-established N-S drainage dominates the central landscape. The reactivation then transitions into a series of compressional lobes defined by bulging and mounds of rotated blocks. Although the reactivation is contained

in the eastern portion of the landslide, it also resulted in an increased intensity of pre-existing fractures and change in scarp orientation along the graben to the west of this area, and a change in orientation of the smaller scarps directly upslope from this zone.

The toe zone is a broad, complex undulating zone defined by bulges, mounds, swampy areas, and subdivision development. Previous investigations undertaken by Cunningham (1994) and Stossel (1999), mapped a tentative toe originating from a NW-SE drainage gully near the west lateral margin, then continuing along the base of the compressional bulges. However, subsurface investigations undertaken as part of this study revealed a crush/shear zone consisting of alternating layers of sandy gravels and silty clay at 10-16.3 m b.g.l (~400-417 masl) in borehole 2 (Section 2.5.2.4). Of note were a series of 100-300 mm thick segments of silty clay coinciding with core loss. Had the soil sequence been fully recovered, it may have extended the total vertical length by up to 3.5 m. The silty clay recorded in the toe zone is described as:

Silty CLAY with minor sand and gravels; silver-grey, homogeneous. Soft to firm; moist; moderate plasticity; gravels subangular to subangular schist fragments.

No surface expression of this shear zone was clearly identified, but a well-established drainage gully, seepage and zones of fissile schist were noted in the vicinity of the borehole. Zones of fissile schist with a thickness ranging from 0.5-5.0 m were mapped along the lower margins of the landslide in compressional lobes and within a laterally continuous band at 390 masl (Section 2.5.1.2). The weak fissile schist material is described as:

Moderately to highly weathered grey-brown to orange-brown foliated SCHIST; extremely weak to weak; well-developed foliation, undulating and/or kink banded with < 1 up to 3 mm laminae, laterally continuous and lensoidal 1-3 mm thick quartz segregations, spaced 2-100 mm, pinch and swell structures common, foliation dips 20°-30°; discontinuities are extremely closely to very closely spaced, moderately inclined (along foliation) to sub-vertical (80°-88°) with narrow to moderately wide apertures infilled with sand to gravel sized schist fragments; moist to wet, seepage common. [Otago Schist, Textural Zone IV].

In addition to the borehole data and zone of fissile schist, a fault mapped by Bell (1985b) was described as a 3m wide exposure in a stream bed that could be traced to the NW for more than 1 km across the lower slopes of Queenstown Hill. The fault was made up of “intensively folded and sheared schist, with clay-rich “pug” zones up to 150 mm wide: considered to form part of the same fault zone, which trends in a general NW-SE direction and controlled stream alignment along the property” (Bell, 1985b, p.3). Analysis of surface mapping, limited subsurface data, and poorly defined landslide “toe morphology” lead to the conclusion that it was more appropriate to delineate a toe zone than to infer a toe at a single location.

5.2.2 Structural controls on surface morphology

Geologic mapping of the rock mass identified foliation, schistosity, foliation shears and jointing as the main defects controlling surface morphology and slope stability. The foliation orientation is highly variable across the landslide, reflecting local deformation and past slope movement. However, the intact schist typically dips downslope at 15°-25°/192° (SSW).

Large-scale joint patterns were identified across the study area (Section 2.6) using lidar images, with the findings supported by field investigations (Figure 5.2). Joint sets are mostly well developed, steeply inclined (40°-60°) or sub-vertical (82°-88°), smooth to stepped, and have a varied persistence (0.5-3 m) throughout outcrops at a local and regional scale. Joints are typically spaced 0.5-2 m apart with narrow to wide apertures. Infill was seldom observed in the field, other than a thin < 2 mm thick weathered veneer. Dilation and relaxation of the rock mass is visible throughout the landslide body, as well as within the “in-situ” schist at

the base of the slope along Frankton Arm. Dilation of the joints has resulted in opposing dip directions within the same joint sets. Discontinuities and joint sets are grouped into five structural domains (Section 2.6) to quantify how rock mass defects influence landslide stability (Figure 5.3).

In addition to jointing, narrow to moderately narrow (0.3-1.5 m thick) foliation shears were recorded at regular intervals in all four boreholes and occasionally recorded in outcrops. Granular shears, clay-rich shears and a combination of both, ranging from 0.1-1.5 m thick (Section 2.5.2.2), were logged parallel and sub-parallel to foliation with granular shears being the most predominant in the subsurface. Clay-rich foliation shears within the Queenstown Hill Landslide exhibit a low residual friction angle, with no cohesion (ϕ_r= 6°-20°, c= 0 kPa) and their shear behaviour has been interpreted as a sliding mode (Stossel, 1999). Despite shears occurring along foliation and sub-parallel to foliation, it was impossible to correlate them between each borehole suggesting that shears may not be laterally extensive.

Based on the results from geologic and geomorphic mapping, the surface morphology and slope evolution of the Queenstown Hill Landslide is influenced by rock mass properties (lithology, structures, discontinuities and geomechanical properties) of the underlying schist bedrock.

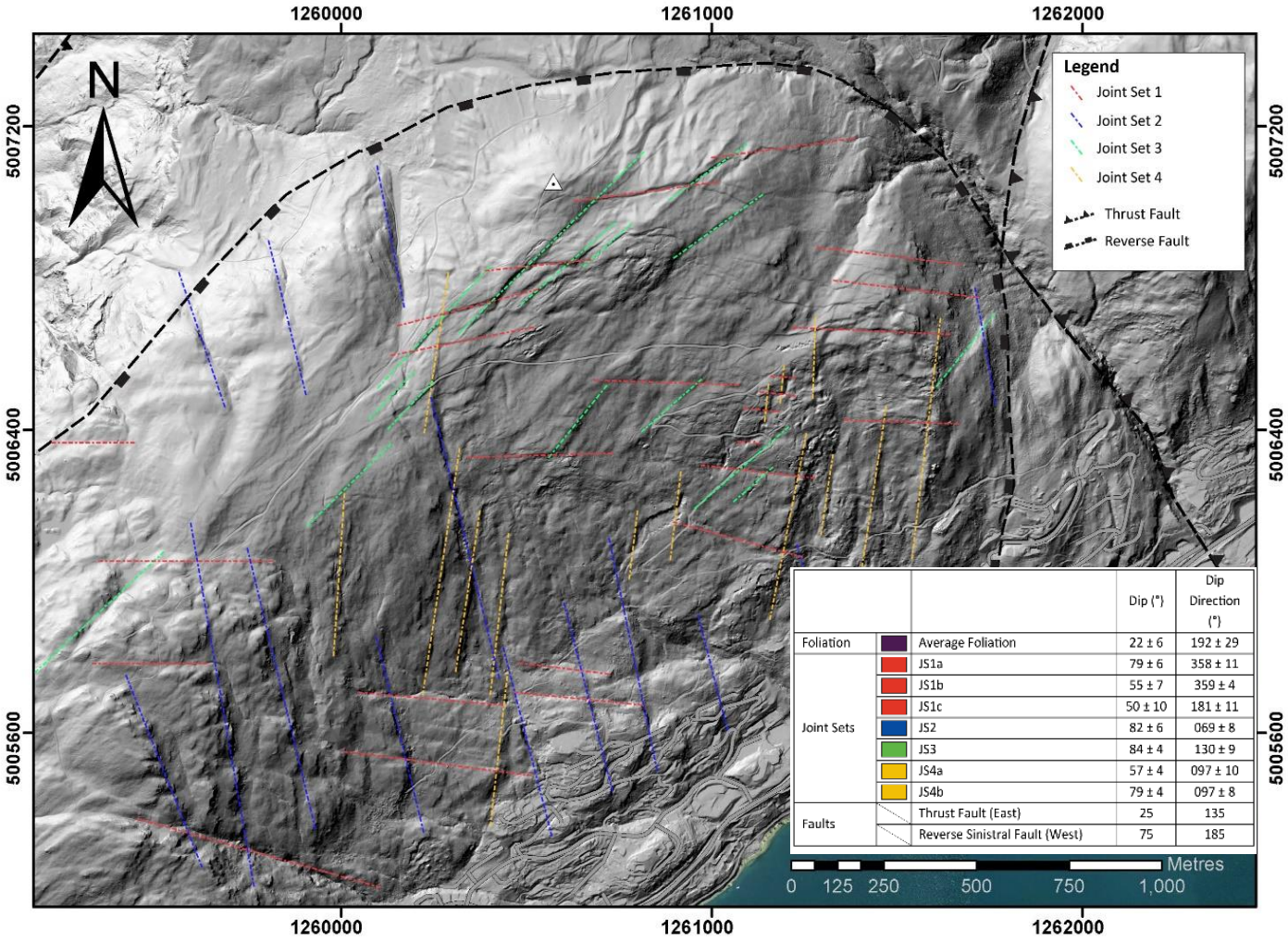

Figure 5.2: Major joint sets mapped across Queenstown Hill

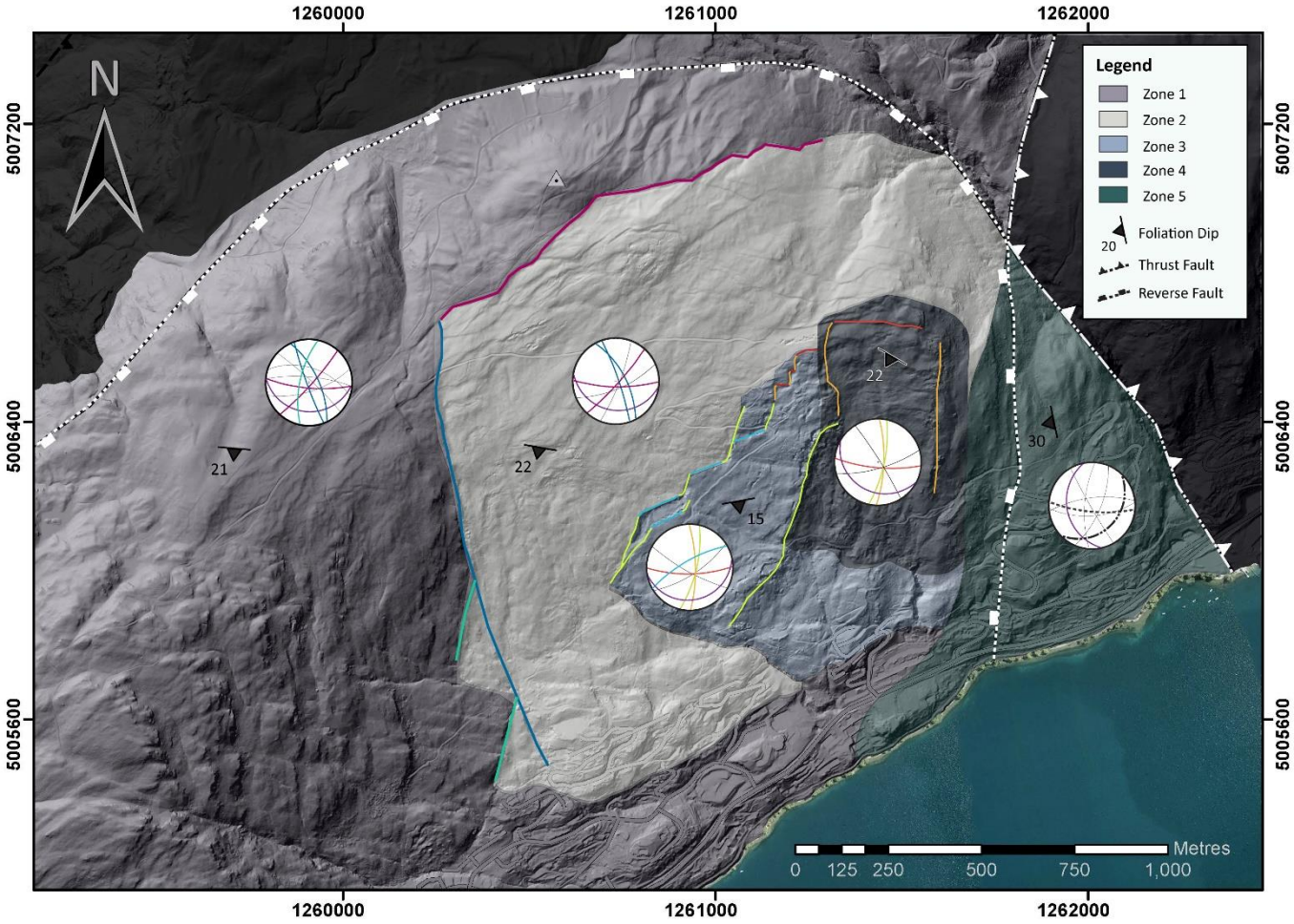

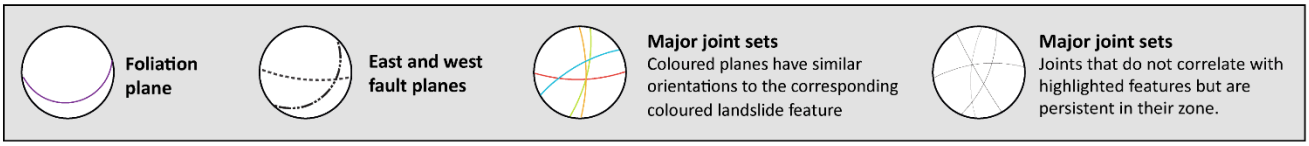

		Zone 1		Zone 2		Zone 3		Zone 4		Zone 5	
		Dip (°)	Dip Direction (°)	Dip (°)	Dip Direction (°)	Dip (°)	Dip Direction (°)	Dip (°)	Dip Direction (°)	Dip (°)	Dip Direction (°)
Foliation	**Average Foliation**	21 ± 5	184 ± 15	22 ± 5	189 ± 15	15 ± 8	169 ± 24	22 ± 4	209 ± 24	30 ± 10	259 ± 14
Joint Sets	**JS1**	84 ± 3	250 ± 8	75 ± 8	181 ± 6	72 ± 4	103 ± 2	74 ± 5	092 ± 4	67 ± 5	113 ± 3
	JS2	65 ± 7	065 ± 10	82 ± 5	071 ± 8	75 ± 5	089 ± 6	75 ± 4	185 ± 2	86 ± 2	240 ± 2
	JS3	83 ± 4	043 ± 7	82 ± 5	132 ± 7	73 ± 3	179 ± 12	73 ± 4	164 ± 3	69 ± 2	353 ± 2
	JS4	66 ± 6	162 ± 6	64 ± 4	062 ± 7	72 ± 10	330 ± 4	73 ± 4	102 ± 3	70 ± 4	274 ± 3
	JS5	75 ± 6	005 ± 14	80 ± 9	111 ± 8	70 ± 8	147 ± 8	84 ± 5	058 ± 8	63 ± 3	176 ± 7
	JS6	66 ± 5	282 ± 8	69 ± 7	157 ± 3	78 ± 8	209 ± 4	-	-	-	-
	JS7	52 ± 3	018 ± 9	-	-	-	-	-	-	-	-
Faults	**Thrust Fault (East)**	-	-	-	-	-	-	-	-	25	135
	Reverse Sinistral Fault (West)	75	185	75	185	-	-	75	185	75	185

Figure 5.3: Structural domain map with discontinuity details

5.2.3 Landslide Classification and Failure Mechanisms

Stossel's (1999) preferred failure model for Queenstown Hill Landslide is a translational rock block slide based on the Varnes (1978) classification. The rock block slide is described as a "classic translational slide, with the toe forming a shallow compressional bulge instead of a toe buckle" (Stossel, 1999, p.101), with a failure surface inferred at 100-150m depth. Based on the results presented in this thesis and using the updated Varnes classification by Hungr et al. (2014), the Queenstown Hill Landslide is interpreted to have undergone two types of movement. The main landslide body is classified as a compound rock slide with a bi-linear rupture surface, while the reactivation zone's geometry suggests a rock planar slide (Figure 5.4). Both movement types describe translational style failure, but with different intensities of internal distorion and surface expression.

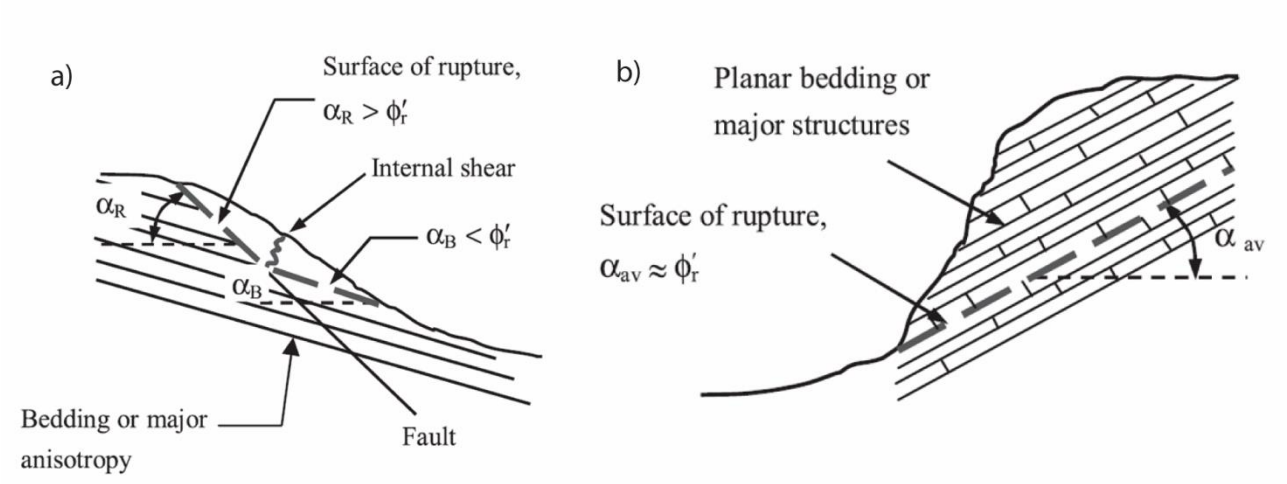

Figure 5.4: Schematic diagram showing the surface of rupture a) compound slide with a bi-linear rupture surface b) rock planar slide failure surface (Glastonbury and Fell, 2010).

The surface expression of the landslide body suggests considerable internal deformation, supported by the morphology mapped in each respective zone. Interpretation of the subsurface geology is presented in Figures 5.5 to 5.11 . Graben structures at the head and centre of the landslide, compressional bulges, hummocks and deep sub-vertical fractures are largely the result of internal sub-parallel shears and large displaced blocks moving along multiple (stepped) rupture surfaces. These internally segmented blocks are overlain by 2-10 m of highly fractured, rotated/displaced, subangular schist blocks within a chaotic schist debris matrix. Pockets of weathered and unweathered glacial deposits have been mapped within the chaotic debris, infilling joints between displaced blocks relaxed fractures.

The failure surface of the landslide body is interpreted as a structurally controlled stepped surface along foliation shears defined by the intersection of steep to subvertical joint sets and pre-sheared foliaiton surfaces. The failure surface is likely sub-parallel to foliation with shears side stepping across the dipslope. The depth of the failure surface is interpreted to be 50-75 m, which is shallower than the 100-150 m proposed by Stossel (1999), due to the amount of offset observed across the landslide and the basal shear zone logged at 10 m depth in borehole 2. In the reactivation zone, the surface morphology (smooth flank, planar scarps and compressional lobes at the toe) and orientation suggests little internal deformation and rapid failure. The failure surface is likely shallow with sliding occuring along a weak internal shear converging with the main landslide failure surface.

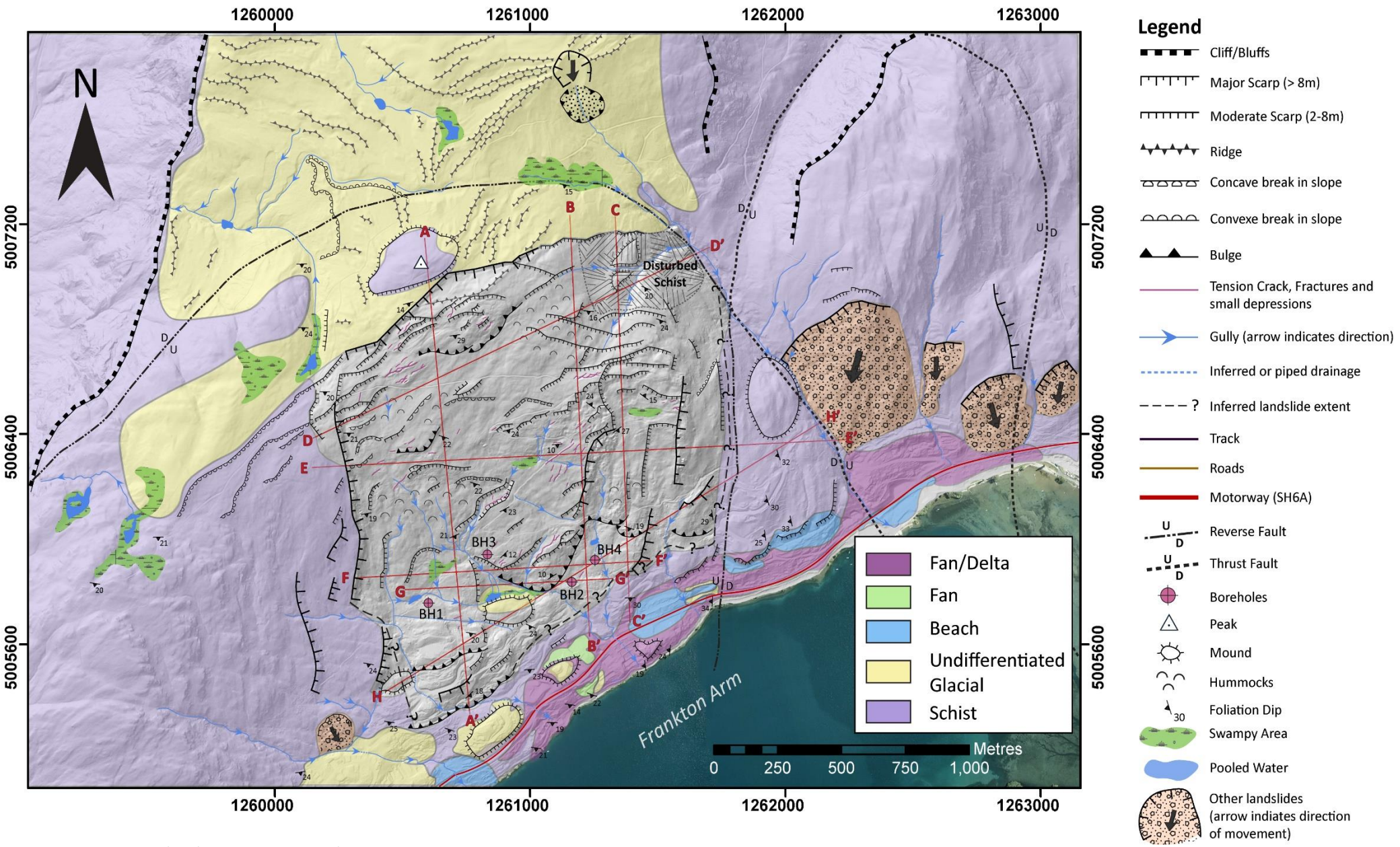

Figure 5.5: 1:15,000 Plan showing cross section locations.

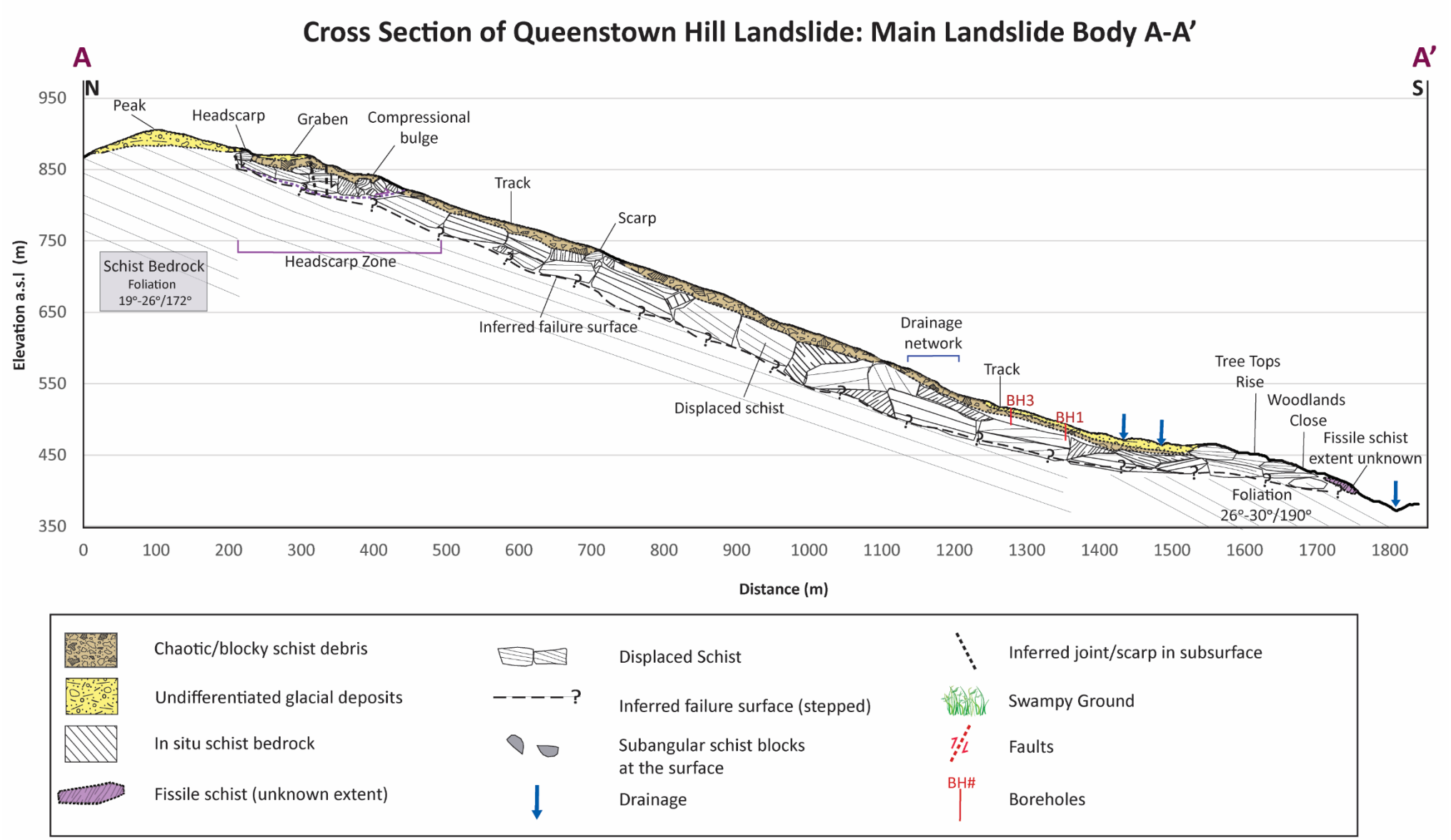

Figure 5.6: Vertical cross section A-A' of the main landslide body (Scale 1V:1H).

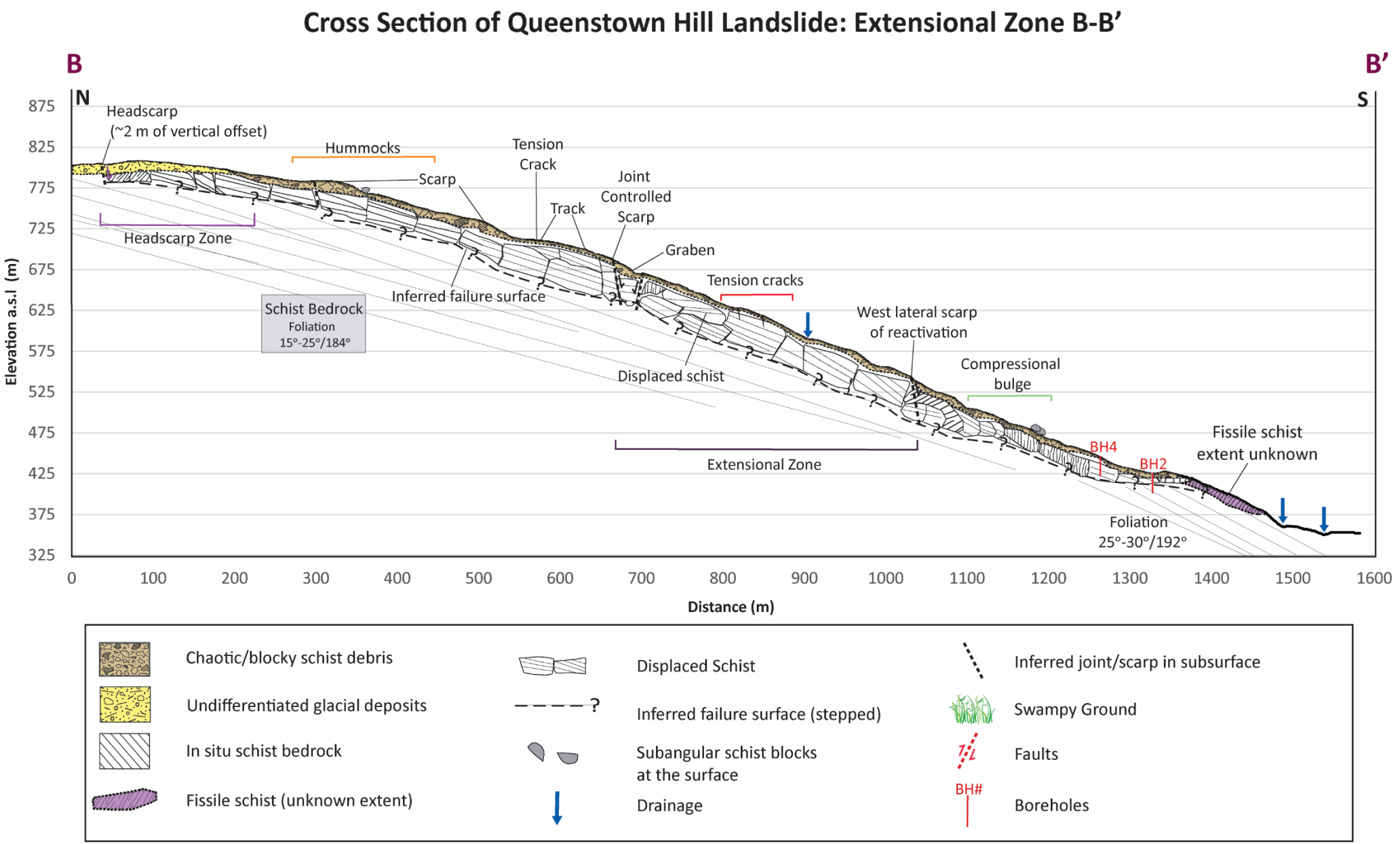

Figure 5.7: Vertical cross section B-B' of the landslide, including the extensional zone (Scale 1V:1H).

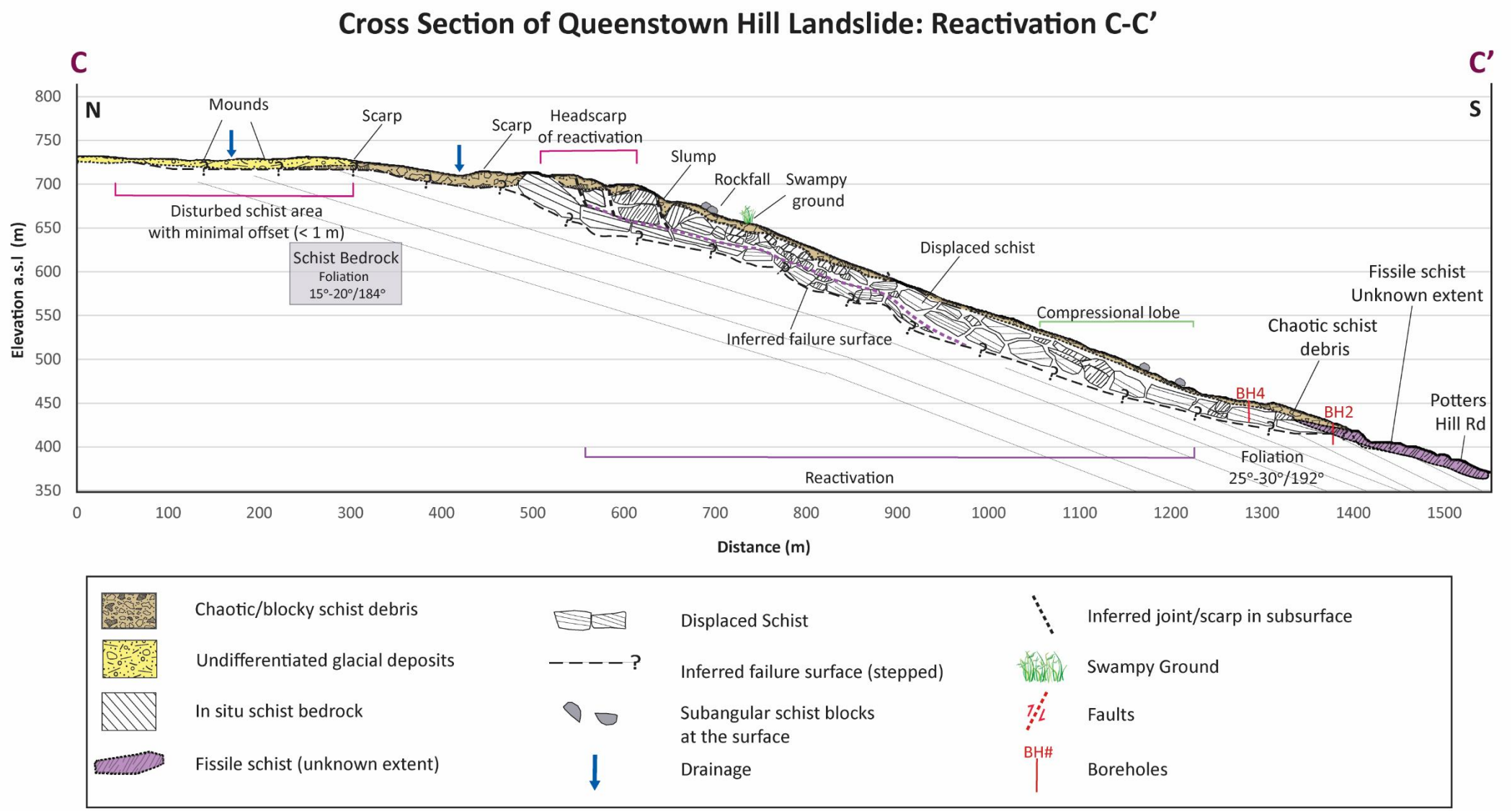

Figure 5.8: Vertical cross section C-C' of the landslide, including the reactivation zone (Scale 1V:1H).

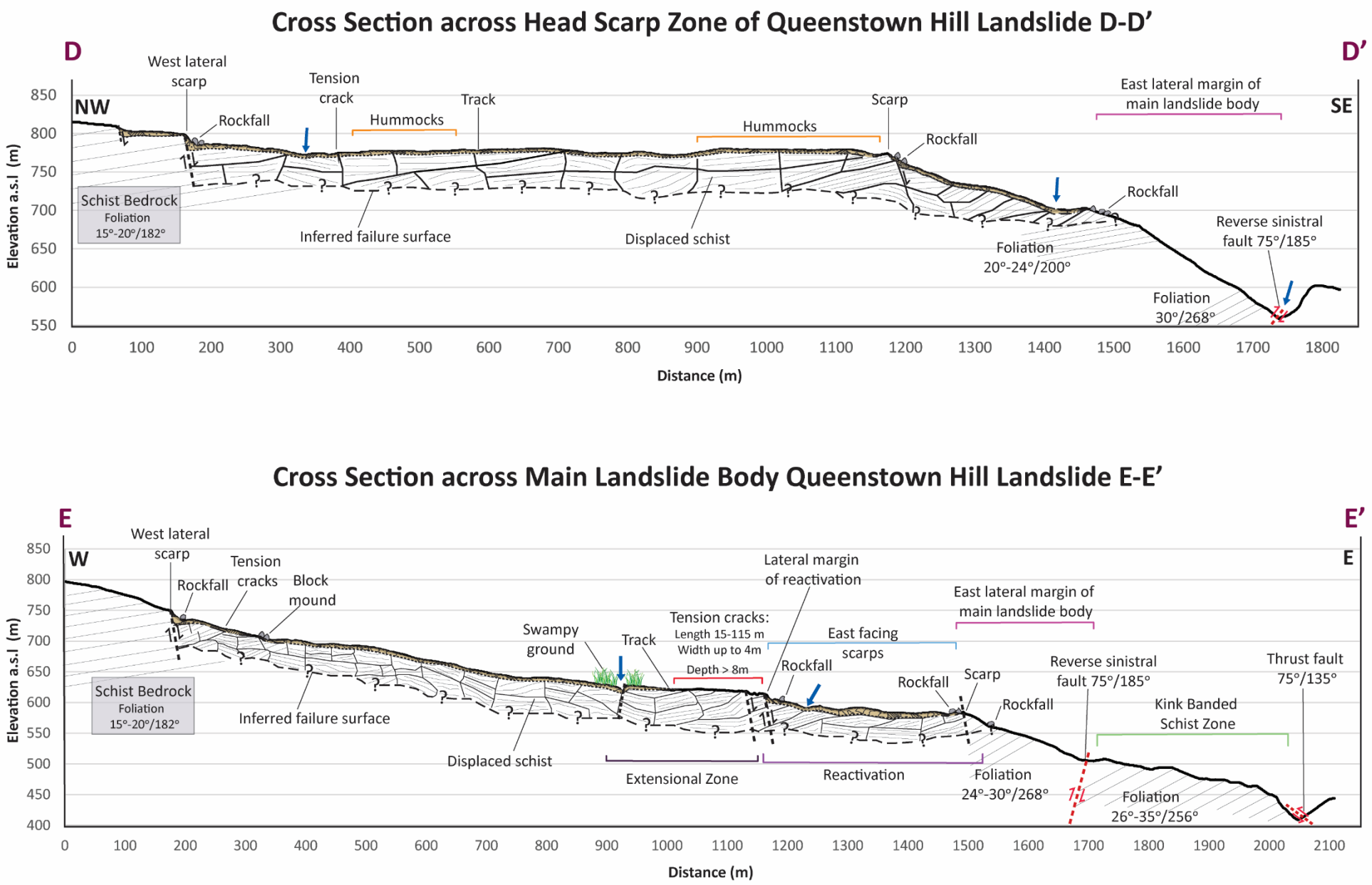

Figure 5.9: Horizontal cross section D-D' across the headscarp zone of the landslide (top). Horizontal cross section E-E' across the main landslide body (Scale 1V:1H)

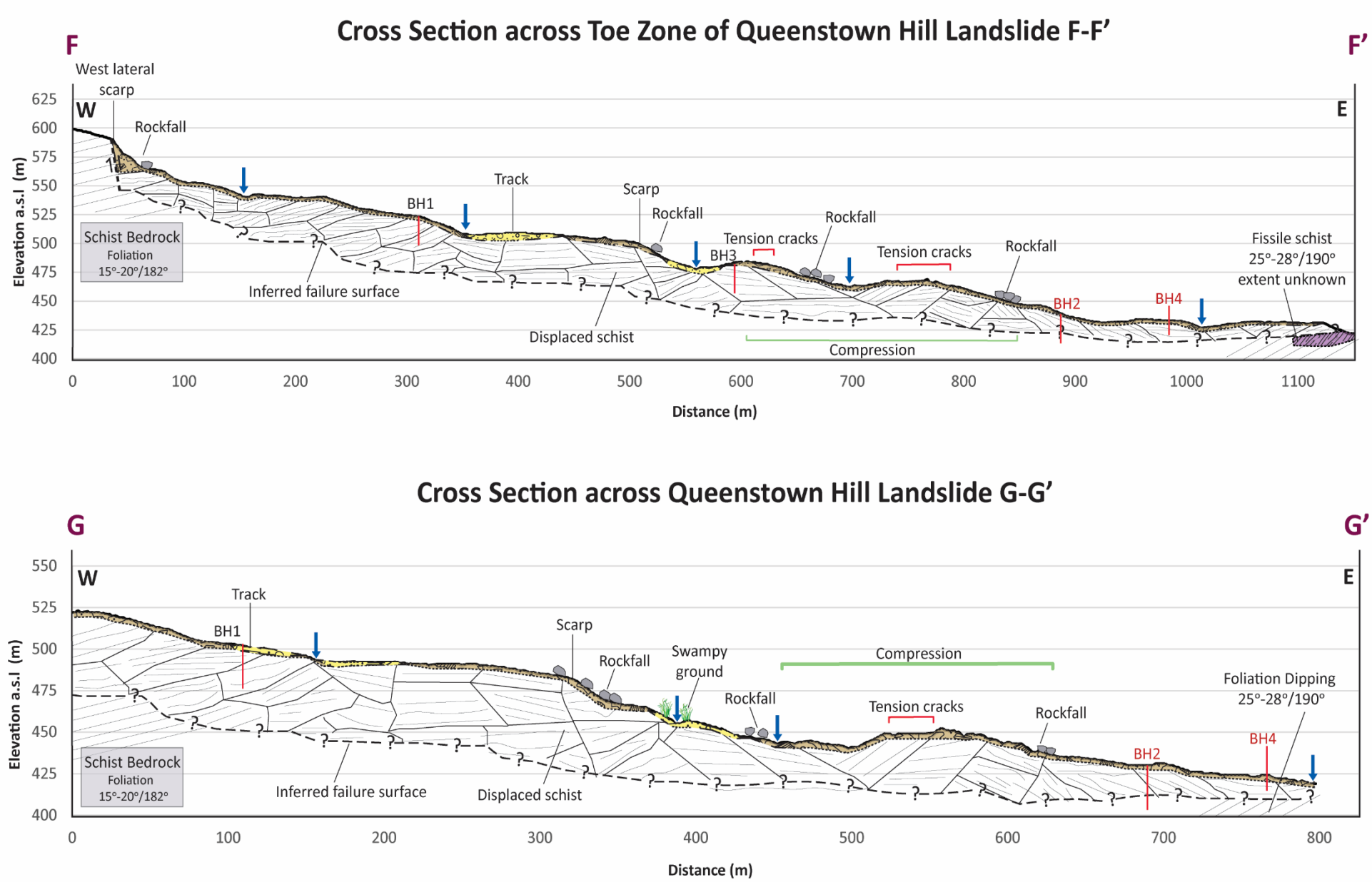

Figure 5.10: Horizontal cross section F-F' across the upper part of the toe zone (top). Horizontal cross section G-G' across the mid-toe zone (bottom). Same key as previous figures.

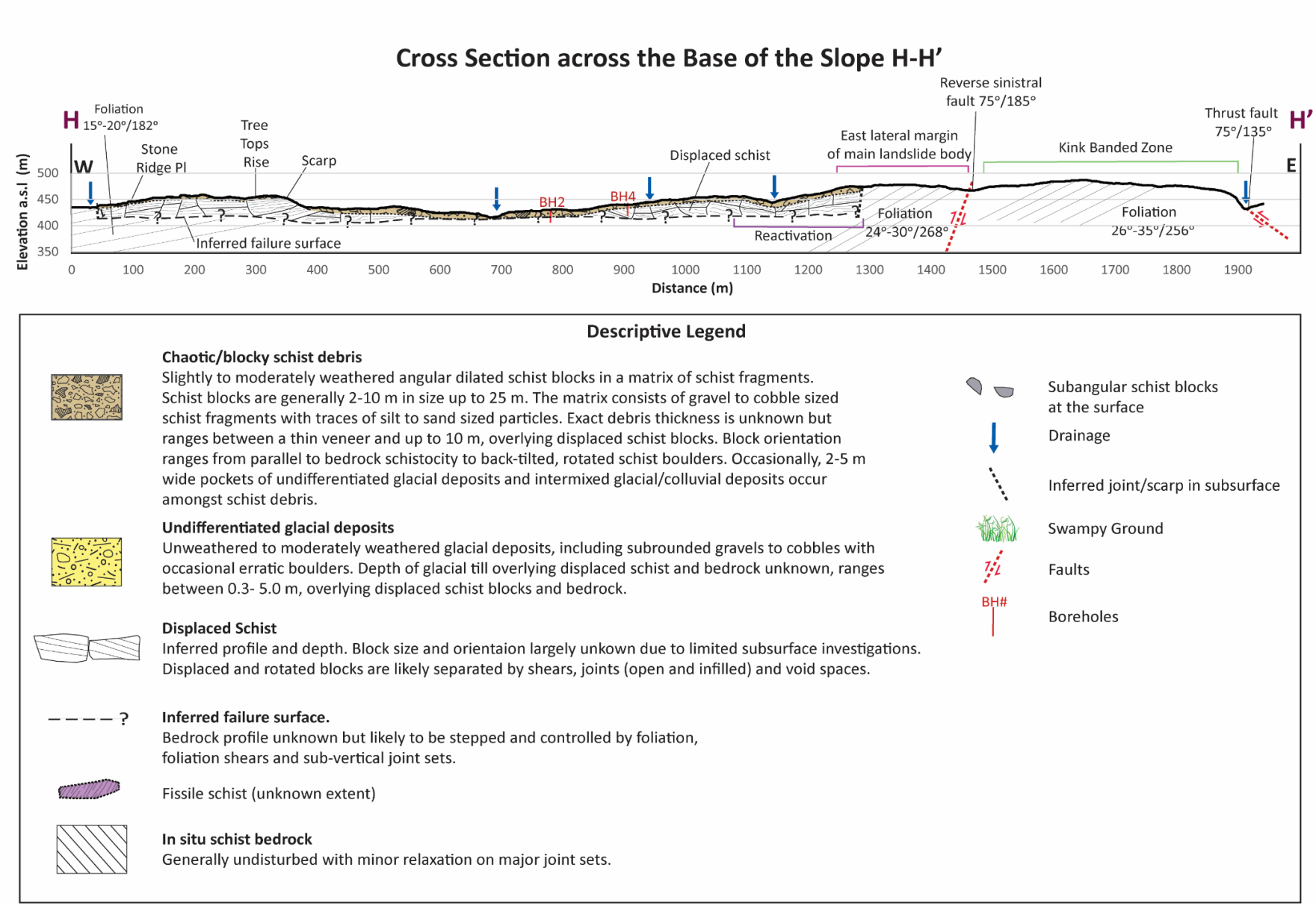

Figure 5.11: Horizontal cross section H-H' across the base of the slope and a descriptive legend of the lithological units. The surficial deposits were originally presented in Chapter 3, Section 3.7. (Scale 1V:1H).

Crush zones and foliation shears can create impermeable barriers (aquitards) allowing water to pool as it percolates along defects and fractures in the slope. Dilation and relaxation of joints increases the permeability of the slope allowing an increased amount of water to infiltrate. This can affect displacement rates by loading the slope and increasing pore pressures, resulting in an increased probability of failure.

The geometry of the failure surface at the toe remains enigmatic. Compressional lobes at the base of the slope indicate a possibility of an overriding wedge of material ploughing into undisplaced material or toe breakout resulting in bulging and overthrusting of landslide material. There is also a possibility the failure surface curves upward crosscutting foliation and outcropping in highly fissile schist with shear zones. However, field investigations and subsurface logs do not suggest any evidence for buckling and oversteepening. Dips measured across the site are consistent with the orientations measured elsewhere on the landslide and within the surrounding in situ bedrock. Additional subsurface investigations are required to ascertain the surface rupture at the toe.

5.2.4 Kinematic analysis

Previous investigations into the overall slope stability and kinematic analysis concluded that the orientation of the foliation, parallel joint defects and orientation of the slope face contribute to the instability of the slope (Stossel, 1999). If failure were to occur, it would most likely be a translational slide parallel to the schist foliation, due to the orientation of foliation and slope angle. Limit equilibrium analyses determined that a friction angle between 20° and 30° and the presence of a perched water were the most likely failure triggering mechanisms of the rock mass (Stossel, 1999).

Stereographic kinematic analysis was performed on the structural domains established in Chapter 2 to obtain quantitative data on the influence that discontinuities exert on slope stability. The analysis was completed using Dips 7.0 (Rocscience 2020) and evaluated the following conditions for failure: planar, wedge, flexural toppling, direct toppling and oblique toppling failure. The analysis does not include all possible discontinuity orientations measured in the field, and limited exposures may not fully capture defect persistence and spacing. Given the absence of multiple boreholes reaching sufficient depths to target the failure surface (at 50-75 m), the friction angles analysed are limited to the ones derived from triaxial testing and results derived from testing elsewhere in Central Otago. No groundwater investiations were undertaken as part of this thesis, therefore the effect of porewater on failure modes cannot be ascertained.

The average natural slope inclination (dip/dip direction) for each domain was derived using statistical analysis in ArcMap 10.7. The lateral limit was set to 25° and two friction angles were considered: (1) 45° was derived from laboratory testing, and (2) 20° is the average angle derived from clay-rich shears tested across Central Otago. However, the results from the 45° friction angle are detailed in this thesis. The slope inclination values were increased for each stereonet from the natural angle to 85°, to account for local variations in foliation attitude, slope angle and as a preliminary evaluatio the slopes response to steepening, especially during construction. The results from each domain and an overall slope analysis are presented in Figures 5.12 to 5.17. The likelihood of failure (%) and plane along which failure is expected to occur (Planes) were tabled for each domain and separated by slope angle. A single likelihood of failure is presented for the natural slope angle and a range of values are presented for slope angles between 50°-85°.

Stereographic analysis of the overall slope (Figure 5.12) indicates that failure is unlikely at the natural slope inclination, using a friction angle of 45°. Direct and oblique toppling are the mostly likely to occur along foliation and at the headscarp. In areas where the overall slope inclination exceeds 50° the number of potential failures begins to increase, and continues to increase as the angle approaches 70°-85°. If the slope angle is steepened to 50°-85°, planar sliding becomes the most common failure mechanism at the headscarp and on JS4.

Kinematic analysis for Zone 1 and Zone 2 (Figure 5.13 and 5.14) indicates a low likelihood of failure at the natural slope angle, with the possibility of oblique toppling along foliation. In steepened areas (from 50°-85°) within Zone 1, planar sliding and wedge sliding at the main headscarp, west lateral scarp and JS4 become the most common failure mechanism with a low probability of toppling (Figure 5.13). When the slope angle is steepened in Zone 2, planar and wedge sliding at the main headscarp and on JS6 are the most common failure types with a low probability of oblique toppling along foliation, JS6 and the headscarp (Figure 5.14). Analysis of Zone 3 and Zone 4, indicates that failure is unlikely at the average natural slope angle, with low probability of oblique and direct toppling along foliation. In Zone 3 if the slope angle is steepened to 50°-80°, planar sliding and wedge failure along foliation, tension cracks and at the reactivation headscarp are most likely to occur with a low probability of toppling (Figure 5.15). In steepened areas within Zone 4, planar sliding and wedge failure are likely to occur at the reactivation headscarp and JS3 with a low probability of toppling failure (Figure 5.16).

Zone 5 is located outside of the Queenstown Hill Landslide boundaries, as it represents the kink banded area (Section 2.6.5). Stereographic analysis of the kink banded area (Figure 5.17) indicates that failure is unlikely at the average natural slope inclination, with a low probability of direct and oblique toppling along foliation and discontinuities that share a similar orientation to the mapped thrust fault (25°/135°). When the slope angle is steepened (to 50°-85°), direct and oblique toppling are likely to occur along foliation, discontinuities oriented similar to the thrust fault and JS5; planar sliding is likely to occur on JS1, JS5 and in discontinuities oriented similarly to the reverse fault (75°/185°).

The kinematic analysis, using the 45° friction angle, confirms that failure is unlikely in moderately inclined (20°-35°) areas. Localized toppling along foliation and subvertical joints acting as a releasing surface was most commonly identified failure type. Once the slope inclination exceeded 50°, the number of potential failure increased in each zone and continued to increase as the angle approached 70-85°. Failures such as planar and wedge sliding were the most common and likely to be controlled by foliation and subvertical joint sets. Individual analysis of each zone identified which major discontinuities were most likely to control large scale geomorphic features (i.e. headscarp, lateral scarp, tension cracks, etc.) within the landslide.

Kinematic analysis, using a 20° friction angle to simulate a continuous clay-rich shear surface confirms an increased likelihood (5-30%) of failure in moderately inclined (20-35°) areas. Failures such as planar and wedge sliding were the most common and likley to be controlled by foliation and subvertical joint sets. Once the slope inclination exceeded 50°, the number of potential failures continued to increase (11-70%). The likelihood of toppling failures did not change using the friction angle for continuous clay-rich shears (20°). Currently, there is insufficient evidence to support a continuous clay-rich shear surface; however, it is possible that localized areas within or at the base of the landslide may contain clay-rich foliation shears.

Field observations of localized planar and wedge failures in steep areas and in road cuttings supports the findings of the kinematic analysis indicating increased failures with steepened slope angles. Localized planar and wedge failures were observed in road cuttings (> 60°) along the subdivisions and blocky rockfall originating from steep scarps (> 60°) releasing small to medium blocks (< 3m) were common within the landslide body. Sliding was observed down dip along foliation, when discontinuities daylight the slope. Subvertical joints often acted as releasing surfaces with basal sliding along foliation. In addition to this, ravelling and undermining was common in moderately to highly weathered schist.

While the moderate inclination (20°-30°) of the natural slope is unlikely to result in large-scale movement, site specific investigations should be undertaken to minimize localized failure during cuts and fills and to determine the appropriate support measures to be implemented.

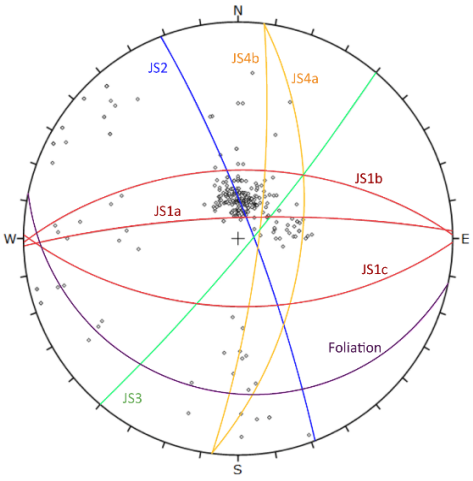

Kinematic Analysis: Overall Slope Stability			Dip (°)	Dip Direction (°)
Foliation		Average Foliation	22 ± 6	192 ± 29
Joint Sets		JS1a	79 ± 6	358 ± 11
		JS1b	55 ± 7	359 ± 4
		JS1c	50 ± 10	181 ± 11
		JS2	82 ± 6	069 ± 8
		JS3	84 ± 4	130 ± 9
		JS4a	57 ± 4	097 ± 10
		JS4b	79 ± 4	097 ± 8
Faults		Thrust Fault (East)	25	135
		Reverse Sinistral Fault (West)	75	185
Slope Inclination			26	148
Lateral Limits			25	
Friction Angle			45	

Kinematic Analysis	Natural Slope	Planes	Slope Angle 50°-85°	Planes
Planar Sliding (All)	0.0%		2.0-15.4%	**JS1c**, **JS4a**, JS3, JS2, JS4b
Planar Sliding (Lateral Limit)	0.0%		0.7-5.0%	**JS1c**, **JS3**
Wedge Sliding	0.0%		0.0-6.8%	
Flexural Toppling	0.0%		0.3-1.3%	**JS1a**, **JS1b**
Direct Toppling	0.1%	Foliation, JS1c	0.3-0.9%	**Foliation**, **JS1c**, **JS3**
Oblique Toppling	1.2%	Foliation, JS1c	1.1-1.2%	**Foliation**, **JS1c**, **JS3**

Figure 5.12: Kinematic analysis of the overall slope.

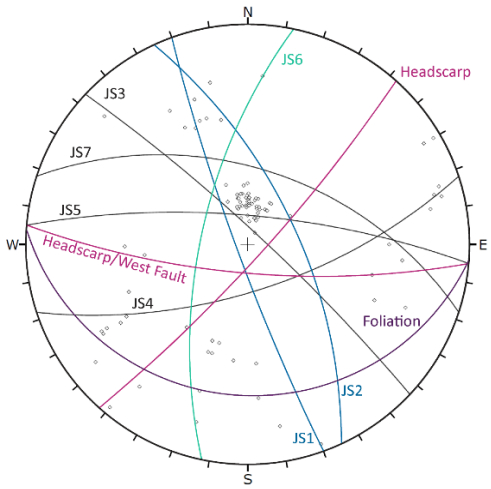

Kinematic Analysis: Zone 1 (In situ schist)			Dip (°)	Dip Direction (°)
Foliation		Average Foliation	21 ± 5	184 ± 15
Joint Sets		JS1 West Lateral Scarp	84 ± 3	250 ± 8
		JS2 West Lateral Scarp	65 ± 7	065 ± 10
		JS3	83 ± 4	043 ± 7
		JS4	66 ± 6	162 ± 6
		JS5	75 ± 6	005 ± 14
		JS6 Lower West Lateral Scarp	66 ± 5	282 ± 8
		JS7	52 ± 3	018 ± 9
		Headscarp	82	132
		Reverse Sinistral Fault (West)	75	185
Slope Inclination			26	160
Lateral Limits			25	
Friction Angle			45	

Kinematic Analysis	Natural Slope	Planes	Slope Angle 50°-85°	Planes
Planar Sliding (All)	0.0%		6.3-17.1%	**JS4**, **Headscarp**, JS1, JS2
Planar Sliding (Lateral Limit)	0.0%		6.3-12.6%	**JS4**, **Headscarp**
Wedge Sliding	0.0%		0.6-16.6%	
Flexural Toppling	0.0%		1.8-3.6%	**JS5**, **JS7**
Direct Toppling	0.7%	Foliation	6.2-7.6%	**Foliation**, **JS4**, **Headscarp**
Oblique Toppling	6.8%	Foliation	3.9%	**Foliation**, **JS4**, **Headscarp**

Figure 5.13: Kinematic analysis of Zone 1.

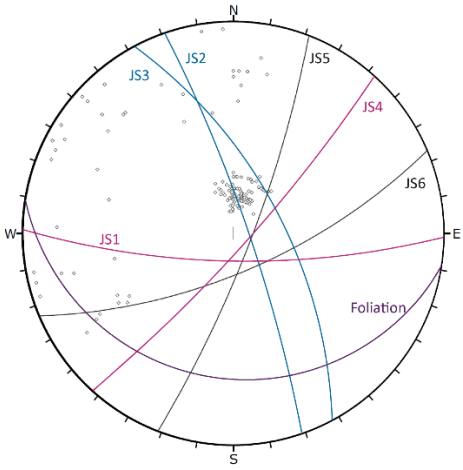

Kinematic Analysis: Zone 2 (Main landslide body)				
			Dip (°)	Dip Direction (°)
Foliation		Average Foliation	21 ± 5	189 ± 15
Joint Sets		JS1 Headscarp	75 ± 8	181 ± 6
		JS2 West Lateral Scarp	82 ± 5	071 ± 8
		JS3 West Lateral Scarp	64 ± 4	062 ± 7
		JS4 Headscarp	82 ± 5	132 ± 7
		JS5	80 ± 9	111 ± 8
		JS6	69 ± 7	157 ± 3
		-		
Faults		Thrust Fault (East)		
		Reverse Sinistral Fault (West)	75	185
Slope Inclination			25	144
Lateral Limits			25	
Friction Angle			45	

Kinematic Analysis	Natural Slope	Planes	Slope Angle 50°-85°	Planes
Planar Sliding (All)	0.0%		1.5-33.3%	**JS1**, **JS6**, JS3, JS4, JS5, JS2
Planar Sliding (Lateral Limit)	0.0%		0.7-9.6%	**JS6**, **JS4**
Wedge Sliding	0.0%		0.4-16.6%	
Flexural Toppling	0.0%		0.0%	
Direct Toppling	0.0%		0.1-0.3%	**Foliation**, **JS6**, **JS4**
Oblique Toppling	1.3%	Foliation	1.3%	**Foliation**, **JS6**, **JS4**

Figure 5.14: Kinematic analysis of Zone 2.

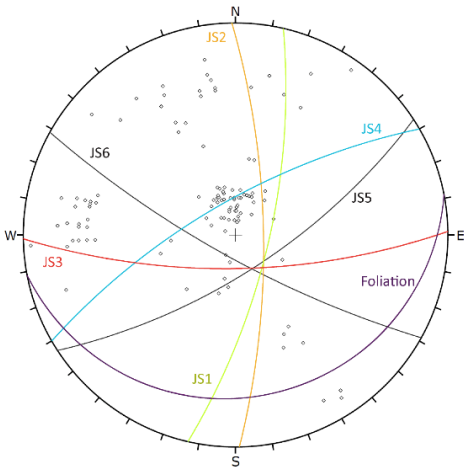

Kinematic Analysis: Zone 3 (Extensional)				
			Dip (°)	Dip Direction (°)
Foliation		Average Foliation	15 ± 8	169 ± 24
Joint Sets		JS1 Lateral Margins	72 ± 4	103 ± 2
		JS2 Reactivation Lateral Scarp	75 ± 5	089 ± 6
		JS3 Reactivation Headscarp	73 ± 3	179 ± 12
		JS4 Graben	72 ± 10	330 ± 4
		JS5 Large Tension Cracks	70 ± 8	147 ± 8
		JS6	78 ± 8	209 ± 4
		-		
		-		
		-		
Slope Inclination			30	162
Lateral Limits			25	
Friction Angle			45	

Kinematic Analysis	Natural Slope	Planes	Slope Angle 50°-85°	Planes
Planar Sliding (All)	0.0%		2.2-37.3%	**Foliation**, **JS5**, **JS3**, **JS6**, **JS1**
Planar Sliding (Lateral Limit)	0.0%		2.2-13.4%	**Foliation**, **JS5**, **JS3**
Wedge Sliding	0.0%		1.2-15.7%	
Flexural Toppling	0.0%		3.7-6.7%	**JS4**
Direct Toppling	0.1%	Foliation	0.2-1.3%	**Foliation**, **JS5**, **JS3**
Oblique Toppling	2.8%	Foliation	2.7%	**Foliation**, **JS5**, **JS3**

Figure 5.15: Kinematic Analysis of Zone 3.

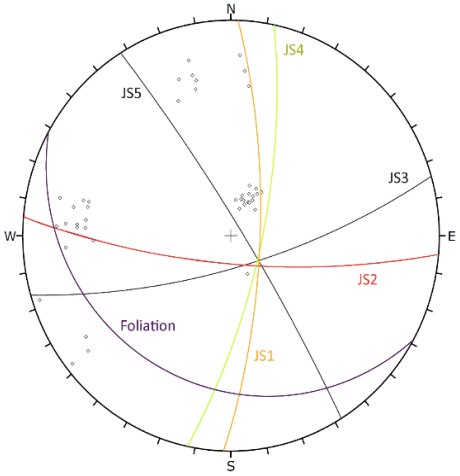

Kinematic Analysis: Zone 4 (Reactivation)				
			Dip (°)	Dip Direction (°)
Foliation		Average Foliation	22 ± 4	209 ± 24
Joint Sets		JS1 Reactivation Lateral Scarp	74 ± 5	092 ± 4
		JS2 Reactivation Headscarp	75 ± 4	185 ± 2
		JS3	73 ± 4	164 ± 3
		JS4 Lower Lateral Margins	73 ± 4	102 ± 3
		JS5	84 ± 5	058 ± 8
		-		
		-		
Faults		Thrust Fault (East)		
		Reverse Sinistral Fault (West)	75	185
Slope Inclination			32	155
Lateral Limits			25	
Friction Angle			45	

Kinematic Analysis	Natural Slope	Planes	Slope Angle 50°-85°	Planes
Planar Sliding (All)	0.0%		0.0-52.2%	**JS2**, **JS3**, JS1, JS4, JS5
Planar Sliding (Lateral Limit)	0.0%		0.0-13.0%	**JS3**
Wedge Sliding	0.0%		1.1-29.0%	
Flexural Toppling	0.0%		0.0%	**JS1a**, **JS1b**
Direct Toppling	0.2%	Foliation	0.2-0.7%	**Foliation, JS3**
Oblique Toppling	1.6%	Foliation	1.6%	**Foliation, JS3**

Figure 5.16: Kinematic analysis of Zone 4.

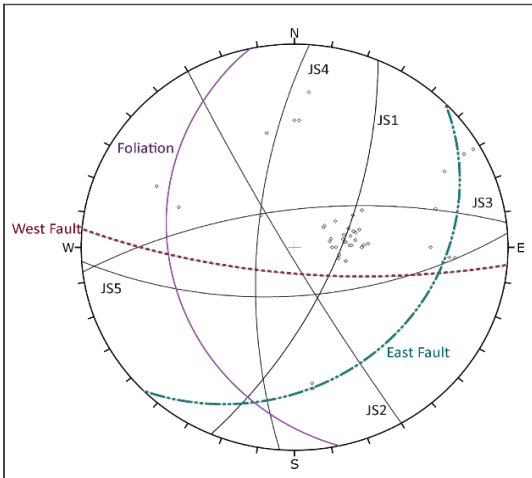

Kinematic Analysis: Zone 5 (Kink banded schist)				
			Dip (°)	Dip Direction (°)
Foliation		Average Foliation	30 ± 10	259 ± 14
Joint Sets		JS1	67 ± 5	113 ± 3
		JS2	86 ± 2	240 ± 2
		JS3	69 ± 2	353 ± 2
		JS4	70 ± 4	274 ± 3
		JS5	63 ± 3	176 ± 7
		-		
		-		
Faults		Thrust Fault (East)	25	135
		Reverse Sinistral Fault (West)	75	185
Slope Inclination			30	143
Lateral Limits			25	
Friction Angle			45	

Kinematic Analysis	Natural Slope	Planes	Slope Angle 50°-85°	Planes
Planar Sliding (All)	0.0%		2.8-9.9%	**JS1**, **JS5**, Reverse fault
Planar Sliding (Lateral Limit)	0.0%		0.0-1.4%	**JS5**
Wedge Sliding	0.0%		0.0-2.9%	
Flexural Toppling	0.0%		0.0%	
Direct Toppling	1.4%	Foliation, Thrust Fault	1.8-25.0%	**Foliation, Thrust Fault, JS5**
Oblique Toppling	0.8%	Foliation, Thrust Fault	1.1-1.2%	**Foliation, Thrust Fault, JS5**

Figure 5.17: Kinematic analysis of Zone 5.

5.3 Evolution of Queenstown Hill Landslide

5.3.1 Glaciation: Preconditioning a slope to failure

Previous studies have identified a variety of factors influencing episodic slope stability during cycles of glaciation and deglaciation: redistribution of stresses, glacial erosion, debuttressing, rock mass strength, geotechnical properties of the basement rock, lithology, weathering, groundwater fluctuations, climate, thermal effects, seismicity, fatigue, and relaxation (Agliardi et al., 2012; Augustinus, 1995; Ballantyne, 2002; Grämiger et al., 2017; McColl, 2012; Millar, 2013).

During cyclical glaciation, changes in the stress regime can occur in response to glacial erosion, unloading at the toe of the slope, oversteepening, and relaxation; this can promote slope movement as joints and microfractures propagate through the rock mass, while pre-existing joints are further exploited. Progressive or redistributed stress release and propagation of discontinuities can increase the extent of zones of weakness (e.g. foliation shears, foliation), permeability, deformability, and decrease overall rock mass strength. These zones of weakness can later be exploited by ice wedging, changing climate, fluvial and/or glacial processes, ultimately resulting in failure, if the slope is no longer in equilibrium (Augustinus, 1995; Ballantyne, 2002; Ballantyne et al., 2014; Fell, 2015; Grämiger et al., 2017; Grämiger et al., 2018; McColl, 2012). Due to the large number of preconditioning factors and interacting geomorphic processes associated with multiple phases of ice advance and retreat, it is often difficult to identify the precise triggering mechanisms leading to slope failure (Augustinus, 1995; Ballantyne, 2002; Glastonbury and Fell, 2010; McColl, 2012).

It is believed that the Queenstown Hill Landslide was initiated sometime during the last glacial maximum. Throughout the Quaternary, repeated periods of ice advance and retreat imply slope modification through erosion and rock slope adjustment, caused by changing stress regimes. Between each period, surviving structures are likely to be weakened, providing zones of closely fractured and jointed bedrock creating favourable paths for subsequent erosion and potential for slope failure (Ballantyne, 2002; Geertsema and Chiarle, 2013).

In turn, rock mass strength plays an important role in controlling slope stability and is influenced by lithology, weathering, and geometry of structural discontinuities. Locally, post-glacial planar rockslides and rockfalls are widespread on foliated psammitic and pelitic schists with failure typically seated on dip slopes at 15°-30°. The stability of closely jointed foliated schist slopes with low to moderate rock mass strength are controlled by the orientation of the foliation and discontinuities in the rock mass such as foliation shears, joints, and shear zones. The depth of many of the features is unknown, however reports by Bell (1989, 2007) and observations recorded while mapping confirm the presence of till injected joints and till pockets in the lower slopes and upper reaches of the Queenstown Hill Landslide.

Continual and rapid slope modification during glacial and interglacial periods is likely as the zones of weakness are more susceptible to erosion (Augustinus, 1995; Bell, 1982; Fell, 2015; Fell et al., 2012). However, this has not been quantitatively determined and other possible triggering mechanisms (e.g. seismic activity, isostatic rebound, progressive stress release, etc.) could be investigated. Determining the trigger of the Queenstown Hill Landslide was beyond the scope of this thesis, but it is important to understand the role glacial cycles may have played in the evolution of the landscape in the Wakatipu basin.

5.3.2 Phases of movement

Geomorphic mapping of the Queenstown Hill Landslide suggests the landslide underwent at least 2 phases of movement, as discussed in Chapter 3. Relative timing and direction of past rock mass movement have been inferred based on orientation, intensity and extent of landscape features mapped within the landslide (Figure 5.18). Timing of events is restricted to relative ages only, as none of the features have been dated.

The first phase of movement encompasses the entire landslide body (Figure 5.18), resulting in approximately 50 m translational movement downslope. The NE-SW orientation of scarps, tension cracks and bulges within the main landslide body suggest the rock mass slid SSE towards the lake. The second phase of movement, reactivated landslide material along the eastern portion of the landslide. The reactivation resulted in an increased intensity of pre-existing fractures in the extensional zone to the west (Figure 5.18) through further dilation of subvertical jointsets, and increased total offset (> 8 m) in the main headscarp and lateral margins of the reactivation. In addition, a change in scarp orientation was observed within the lower scarp of the central landslide graben and in scarps directly above the reactivation (from NE-SW to NW-SE). The orientation of features within the reactivation suggest SW movement in the reactivation, paired with SE movement in the extenstional zone as reactivated material was remobilized. The amount of offset recorded suggests the second phase of movement may have resulted in an additional 25 m of movement downslope.

There are indications of retrogression along the crown of the Queenstown Hill Landslide. Scarps with up to 1-3 m of vertical displacement and dilation were observed extending beyond the main headscarp, predominantly to the west, towards the peak of Queenstown Hill to the north and parallel to the west lateral scarp (Figure 5.18). However, it remains unknown whether retrogression is part of a later reactivation, if it was a caused by a separate event or if it occurred gradually over time.

5.3.3 Queenstown Hill Landslide at present

No significant changes were identified between the 1956 aerial photo and 2016 lidar imagery, and no unweathered fractures, lichen-free scarps or recent scarp and fracture propagation were mapped in the field suggesting there hasn't been any significant movement, in the past 60 years. Minor cracks and voids were identified in Section 3.8, but can be attributed to regular erosional processes and slope evolution. In addition to aerial photos and field observations, the lower portion of the landslide was surveyed for movement from December 2008 to October 2018 by Aurum Survey Consultants (Appendix), with an anticipated horizontal and vertical variance of ±50mm and ±100mm. The results did not measure evidence of movement on the landslide, but by including the variance over a 10 year survey period, this indicates a potential rate of movement of less than 5mm/year.

The block model presented in Figure 5.1 was overlain with a 2008 aerial image (see Figure 5.19) to show landslide at present day. Outcropping landslide material is still visible in major (> 8 m) scarps and fractures but weathering, erosion and vegetation has modfied the appearance of the original structure. Minor scarps (> 2 m) and features are degraded and grassed over giving them a hummocky appearance. The original hummocky surface is now subdued with vegetation re-established across the mid-to lower reaches of the slope. Vegetation consists of tussock and native vegeration at the top of the hill transitioning to douglas fir and larch mid-slope. Sharp defined drainage is likely still reflecting the original landslide boundaries, but new gullies and a complex drainage network are well established within the landslide mass. By definition the landslide is now considered a relict landform, as it resulted from processes that are no longer present or active (Griffiths and Whitworth, 2012).

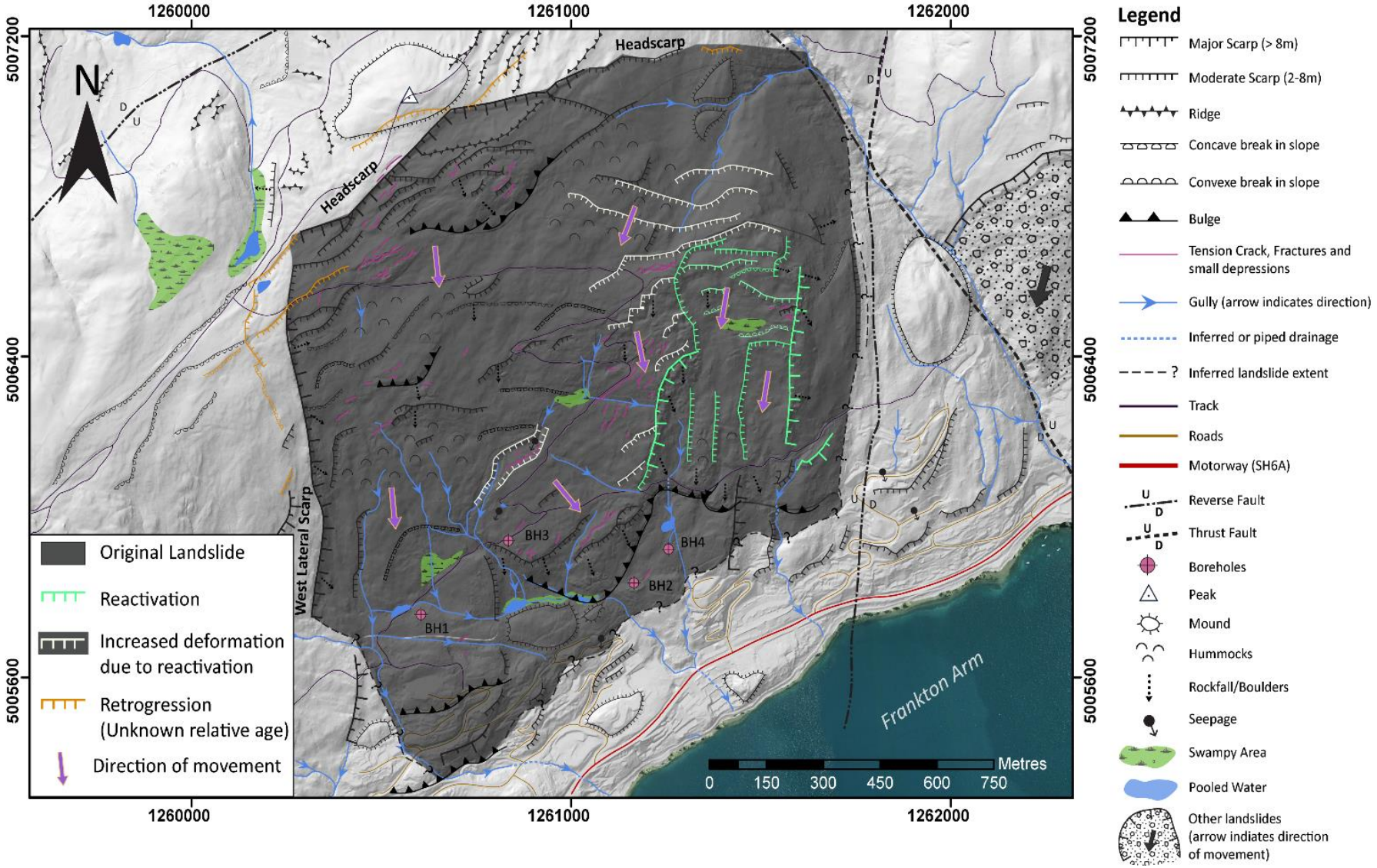

Figure 5.18: Map showing the phases and direction of movement interpreted across the landslide. Dark grey shaded area represents the first phase of movement. Green scarps represent the second phase of movement with increased deformation in the white scarps. Orange scarps possibly linked to retrogression.

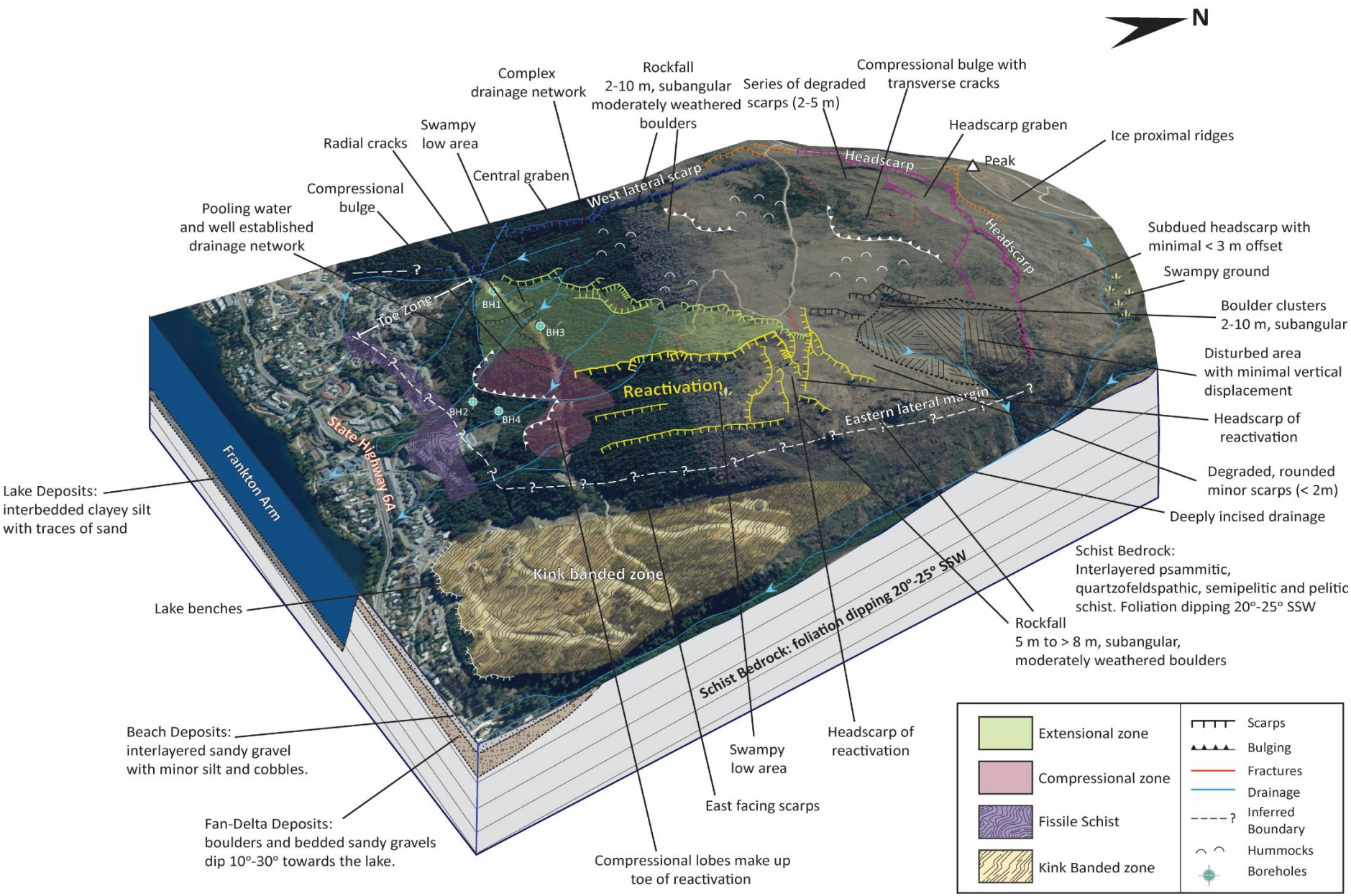

Figure 5.19: Conceptual block model of the Queenstown Hill Landslide overlain by the 2008 NZTA aerial image.

Chapter 6: Conclusion

6.1 Research Summary

The Queenstown Hill Landslide is a large foliation-parallel feature on the northern side of Frankton Arm, Queenstown, having an estimated volume of ~170 Mm^3. The primary aims of this research were to develop a detailed geotechnical characterization and domain profile of the schist in and immediately surrounding the landslide. The methodology was designed to derive geotechnical properties of schist and to parametrize the relationships between topography, geomorphology, geological materials, structure, failure mechanisms and kinematics. Geotechnical and geomorphic field mapping identified local lithological variations (Section 2.5), discontinuities (Section 2.6), and described the surface morphology of the landslide (Section 3.6). Laboratory testing of core samples was used to derive physical and mechanical parameters for the two main lithotypes identified during field mapping (Section 4.3 and 4.4), and the surface and subsurface data was integrated to produce an engineering geology ground model (Section 5.2). The key findings of this thesis address three specific research objectives as detailed below.

6.2 Key findings

6.2.1 Landslide Description

The Queenstown Hill Landslide is interpreted as a deep-seated compound translational rockslide comprising quartzofeldspathic and semi-pelitic schist with an average foliation attitude dipping parallel to the slope at 15-35° SSW. The main landslide body is interpreted as a compound rockslide with a bi-linear rupture surface, while the geometry of the eastern reactivation zone suggests a planar rockslide following the terminology of Hungr et al. (2014). The movement types describe a translational style failure, but with different intensities of internal distortion and surface expression (Section 5.2.3). The failure surface is interpreted at depths of 50-75 m below existing ground, being structurally controlled, and stepped along foliation shears: block release is controlled by the intersection of steep to subvertical joint sets with the pre-sheared foliation surfaces.

The landslide measures approximately 1,425 m from the crown to the toe zone (slope distance), with a maximum width of 1,600 m and a vertical elevation of some 500 m, and an area of approximately 2.28 km^2. Key features of the Queenstown Hill Landslide are summarized in Table 6.1, and the landslide is believed to have been initiated at some stage during the Last Glaciation Maximum (~18-28 ka before present). Repeated periods of ice advance and retreat during the Late Quaternary are thought to have pre-conditioned the slope to failure by a combination of erosion, rock slope adjustment by fracturing, and changing stress regimes.

Coordinates (NZTM 2000)	1,260,804 E, 5,006,653 N
Elevation (high)	890 m
Elevation (low)	380 m
Vertical elevation	510 m
Maximum width (slope distance across)	1,600 m
Length (slope distance from crown to toe)	1,425 m
Depth to failure surface	50-75 m
Area	2.28 km^2
Volume	170 Mm^3
Mean slope angle (dip and dip direction)	26° ± 12/148° ± 051 (SSE)
Mean foliation (dip and dip direction)	22° ± 6/192° ± 29 (SSW)

Table 6.1 Summary of the Queenstown Hill Landslide characteristics

The three research questions addressed in this study are (1) geotechnical properties of the schist rock mass involved in the slope movement; (2) landslide domains and geomorphic relationships; and (3) resultant implications for land development given the residential and commercial pressure in Queenstown.

6.2.2 Schist Properties

Research Question #1: How do the mineralogical and physical properties vary within the different schist types, and is this reflected within the mechanical properties of the different schist types?

Two interlayered schist lithotypes were mapped across the landslide and were logged in four boreholes drilled into the lower part of the Queenstown Hill Landslide (Section 2.5): a medium grey quartzofeldspathic schist and a dark green-grey semi-pelitic schist. Both lithotypes belong to the chlorite zone of the greenschist facies, but exhibit variations in weathering, fabric, and mineral assemblage. Differences expressed in rock defect frequency and type, as well as textural variation, are not immediately obvious at outcrop scale; however, there are significant differences in hand sample and thin section, as summarized in Table 6.2.

Subsurface investigations were unavailable during previous work undertaken along the Frankton Arm. Four 25 m boreholes drilled into the Queenstown Hill Landslide provided an opportunity to characterize recovered rock material and the rock mass within landslide. Geomechanical testing was used to derive and compare the properties of both lithotypes, as summarized in Table 6.2. The decision to separate the lithotypes was made because of significant differences in geotechnical properties, weathering, texture, and mineralogy: strength and weathering variations in both lithotypes are important considerations for construction. Dominance of the more micaceous dark green-grey schist recognized in boreholes was not, however, observed in field outcrops, and further drilling is required due to the interlayering of the two lithotypes.

Physical properties measured included density, porosity, sonic wave velocity and slake durability (Section 4.3). Mechanical testing methods included uniaxial compressive strength (UCS), indirect tensile strength (Brazilian test), point load strength, and triaxial compressive strength (Section 4.4). Review of the laboratory data shows that although both lithotypes share similar physical properties, they show marked differences when comparing strength parameters (Table 6.2). The strength and stiffness data show variations up to 50 MPa for UCS, 95 MPa for differential stress, up to 40 GPa in Young's Modulus and 0.35 for Poisson's ratio. On average the poorly foliated medium grey quartzofeldspathic schist samples (MGy) are 1.5 times (1.2-2.2) stronger than the well foliated dark green-grey semi-pelitic schist (DGy), which is relevant when designing cut slopes and foundations.

6.2.3 Landslide Domains

Research Question #2: What are the main structural domains across the landslide, and how is this reflected in the geomorphology of the landslide?

Five structural domains were identified through geologic mapping across the Frankton Arm side of Queenstown Hill, but only three of the five zones occur within the landslide boundary (Section 2.6). Domains were defined on the basis of average foliation attitude, major joint sets, lithotypes and faults. Across all domains, the schist dips downslope at an average of 15°-25°/192° (SSW), subparallel to the overall slope inclination but with local variations identified in outcrops at the landslide surface. Granular and clay-rich foliation shears 0.3-1.5 m thick, with low residual strength and cohesion (ϕ_r= 6°-11°, c= 0 MPa from Stossel, 1999) were recorded sub-parallel to foliation. Jointing is well developed, sub-vertical (80°-88°), persistent (≤ 8 m), and has narrow to wide aperture with occasional infilling by schist fragments.

Five geomorphic zones were established based on the surface morphology: headscarp, main landslide body, extension, reactivation, and toe zone (Section 3.6). Geologic and geomorphic mapping have identified attitude, foliation shears and joints as the main defects controlling the location and expression of major geomorphic features (e.g. headscarp, west lateral margin, grabens, tension cracks, etc.). As a result, the landslide is interpreted as a joint-controlled feature with steep subvertical joints releasing blocks that slide downslope along foliation. Evidence to support this can be observed in joint sets recorded along the landslide crown, west lateral scarp, east-facing scarps in the reactivation zone, and the orientation of tension cracks. Changes in orientation of scarps in the central graben and NW-SE scarps recorded in the upper east quadrant of the landslide.

The present-day landslide surface expression, and variations in discontinuity orientation across the landslide are attributed to past slope movements. The landslide is interpreted to have undergone at least two phases of movement, with the initial failure encompassing the entire landslide body as a compound rockslide with a bi-linear rupture surface. The NE-SW orientation of scarps, tension cracks and bulges within the main landslide body suggest the rock mass slid downslope in a SSE direction. The second phase of movement, likely reactivated landslide material along the eastern margin of the landslide, and resulted in an increased intensity of fracturing in the extensional zone to the west. This further increased total offset in the main headscarp and lateral margins of the reactivation, and the second phase is interpreted as a planar rockslide.

6.2.4 Land development implications

Research Question #3: How does the improved understanding of geomorphology and geotechnical characterization of the Queenstown Hill Landslide be applied to future land development?

Surface morphology, kinematic analysis and 10-year survey data indicate that the landslide has been stable for the last 60 years. Features such as scarps and fractures within the Queenstown Hill Landslide remain visible but have become poorly defined due to considerable modification by erosion, drainage and other natural process. No unweathered fractures, lichen-free scarps or recent scarp and fracture propagation were mapped in the field. However, some fractures in the extensional zone and densely vegetated areas were less weathered in comparison to those in the rest of the landslide, indicating different time periods over which parts of the landslide have been stable. Minor cracks and voids were identified in Section 3.8 and can be attributed to normal erosional processes (e.g. rainfall, wind) and slope evolution. No significant changes were identified between the 1956 aerial photo and the 2016 images, suggesting there has not been significant movement in the past 60 years. In addition to historical aerial imagery, survey data collected over a 10-year period (2008-2018) did not record evidence of movement within the survey error of < 5 mm/year.

It is concluded that the Queenstown Hill Landslide initially developed in response to glacial and/or periglacial processes that no longer affect the Queenstown area. The lack of these active processes makes reactivation of the entire landslide body currently unlikely, and by definition (Griffiths and Whitworth, 2012) it is now considered a relict landform because it resulted from processes that are no longer present or active.

Kinematic analysis demonstrates that failure is unlikely in moderately inclined (20°-35°) areas, other than localized toppling along foliation with subvertical joints acting as a releasing surface. In areas where the slope angle or cutback exceeds 50°, the number of potential failures increases and continue to increase as the angle approaches 70-85° (Section 5.2.3). Based on the stereographic analysis of the main landslide body, when the slope inclination steepens beyond 50°, planar and wedge sliding along foliation, with joints oriented parallel to the headscarp (82°± 5/132°± 7 SE) acting as a releasing surfaces, are the most common failure types, with a low (10%) probability of toppling. Kinematic analysis indicates that the reactivation and extensional zones of the landslide are most susceptible to failure, especially planar failure along foliation and joint sets

Physical Properties		DGy	MGy	Mechanical Properties		DGy	MGy
Outcrop scale and Hand sample Description	Weathering	SW-HW	UW-MW	Uniaxial Compressive Strength, σ_c (MPa)		23	45
	Colour	Dark green-grey	Medium grey	Indirect Tensile Stress, σ_t (MPa)	ASTM	2.5	3.7
	Fabric	Well-developed foliation	Poorly developed foliation		ISRM	3.9	5.7
	Foliation	• Undulating and planar • Laminae: 1-2 mm, up to 5 mm • Quartz segregations: 3-7 mm, up to 40 mm thick, spaced 2-40 mm. • Occasional 1-2 mm green chlorite/epidote segregations • Dips 10°-30°	• Planar • Laminae: <1 mm • Quartz segregations: 2-5 mm, up to 25 mm thick, spaced 15-200 mm. • 1-3 mm olive green chlorite/epidote segregations throughout • Dips 10°-40°	Point Load Strength Index, $I_{s(50)}$ (MPa)	Perpendicular	2.40	2.63
					Oblique	2.21	2.44
Textural Zone (TZ)		TZ IV	TZIII		Parallel	0.46	0.46
Schist type		semi-pelitic	quartzofeldspathic (psammitic)		Oblique	0.46	0.61
Mineral Composition, (%)	Quartz	23.6	22.0	Conversion Factor, K		10.6	18.6
	Albite	24.2	20.6	Anisotropy Index, I_a		5.11	5.72
	Muscovite	19.0	11.2	Differential Stress, σ_1-σ_3 (MPa)		51	72
	Chlorite	13.3	17.8	Hoek-Brown Failure Criterion	σ_{ci} (MPa)	26	45
	Epidote	9.1	21.1		m_i	14.2	15.3
	Calcite	3.5	1.9	Mohr-Coulomb Failure Criterion	c (MPa)	3.6	5.4
	Titanite	0.6	2.6		Φ (°)	45	50
	Stilpnomelane	0.3	0.1	Young's Modulus, E (GPa)	UCS	16	12
	Garnet	0.1	0.0		Triaxial	8	12
	Opaques	6.4	2.7	Poisson Ratio, v	UCS	0.18	0.21
Moisture Content (%)		1	1		Triaxial	0.18	0.16
Dry Density, ρ_D (kg/m³)		2730	2760	MR		671	257
Dry Unit Weight, γ_d (kN/m³)		26.8	27.1	Dynamic Young's Modulus, E_d (GPa)	Dry	49	50
Porosity, n (%)		3	3		Saturated	47	50
P-Wave, V_p (m/s)	Dry	4769	4779	Dynamic Poisson's Ratio, v_d	Dry	0.27	0.25
	Saturated	5582	5477		Saturated	0.38	0.35
S-Wave, V_s (m/s)	Dry	2645	2720	Dynamic Shear Modulus, G_d (GPa)	Dry	63	63
	Saturated	2453	2579		Saturated	17	19
Slake Durability Index, I_D (%)	Cycle 2	97.9	98.8	Bulk Modulus, K_d (GPa)	Dry	37	36
	Cycle 5	95.8	97.3		Saturated	65	59

Table 6.2: Summary of physical and mechanical properties of the dark green-grey semi-pelitic schist (DGy) and medium grey quartzofeldspathic schist (MGy). Mean values presented in table.

orientated parallel to the reactivation headscarp (75°± 4/185°± 2 S). This evidence is also supported through the various methods of geomechanical classification undertaken as part of this research in Section 4.5.

Preliminary slope stability classification methods included RMR, SMR, ARMR and GSI, with a common aim to derive quality indexes at various locations across the slope. Each method used identified fair to good quality rock mass within the main landslide body, and identified poor rock mass qualities in the compressional lobes/bulges and extensional zone. The low values derived from each stability indexes indicate poor ground conditions adequately reflecting the highly deformed and degraded rock mass in these zones.

Although the evidence suggests present movement within the Queenstown Hill Landslide is unlikely, the complexity of the landslide warrants site-specific geotechnical investigations to avoid or minimise localized failures during construction. Future development within/surrounding the extension and reactivation zones should be avoided until further surface and subsurface investigations are undertaken to refine our current understanding of stability. Kinematic analysis has identified that steeper topographic areas may provide constraints and attention must be paid to the orientation of rock mass defects on which planar or wedge failures could be initiated. Rock fall analysis should be considered in areas with steep scarps and bluffs up-slope, to assess the likelihood of subvertical joint sets releasing large blocks. Lastly, particular attention should be paid to any groundwater seepage, surface drainage and stormwater runoff to ensure long term stability of the slope.

6.3 Further Research

Future research should develop the proposed engineering geology ground model and confirm the findings presented in this thesis by dating landslide features, locating the basal shear surface upslope, conducting groundwater investigations, monitoring movement and assessing slope stability through numerical modelling.

Currently, there is no clear consensus defining ice extents and deposit ages in the Wakatipu Basin. Deposit ages have largely been inferred from geomorphic correlation with dated sequences and the timing of events on Queenstown Hill are restricted to relative ages only, as none of the features have been dated. Further research should include augering ponded, swampy ground, and/or till injected fractures on the upper and mid-slope of Queenstown Hill to recover materials suitable for dating, to help reconstruct the geomorphic evolution of the landslide (e.g. to obtain long-term rates of motion and to determine when/how the landslide initiated).

Additional boreholes are recommended in the mid to upper reaches of the Queenstown Hill Landslide, to determine the depth and geometry of the failure surface and to gain a better understanding of the lateral continuity of features in the subsurface. In addition to providing additional subsurface data, drillholes can be used to install inclinometers and piezometers for monitoring. Although the survey data collected over a 10-year period, from December 2008 to October 2018, did not measure evidence of movement within a survey error of < 5 mm/year, monitoring was only placed along the lower portion of the landslide. Prior to 2018 land development was confined to the lower margins of the landslide but pressure to expand urban development has led to more intensive development proposals further onto the landslide. As a result, it is strongly recommended that surface movement monitoring should be re-established across the landslide. Installation of continuous GPS, inclinometers and extensometers along fractures would record any changes in vertical and horizontal displacements or any increasing internal deformation, as development continues upslope.

Groundwater investigations were not included within the scope of this thesis and very little has been published on the groundwater conditions in the study area. Knowledge of groundwater conditions are important because of the potential influence on the landslide behaviour. When available, groundwater data should be included when evaluating slope stability (Gillon et al., 1991; Gillon and Hancox, 1991). Identification of any additional seepages and installation of piezometers would provide a better understanding of the groundwater conditions at depth and identify perched aquifers. This data could then be integrated with the presented ground model to carry out sensitivity analysis across the study site.

Finally, the engineering geology ground model and geotechnical characterization of schist presented in this thesis provides parameters required to carry out limit equilibrium analysis to factor of safety, and numerical modelling (continuum and discontinuum).

References

Adams, C. J., Campbell, H. J., and Griffin, W. L., 2009, Tracing the Caples Terrane through New Zealand using detrital zircon age patterns and radiogenic isotope signatures: New Zealand Journal of Geology and Geophysics, v. 52, no. 3, p. 223-245.

Adams, C. J., and Graham, I. J., 1996, Metamorphic and tectonic geochronology of the Torlesse Terrane, Wellington, New Zealand: New Zealand Journal of Geology and Geophysics, v. 39, no. 2, p. 157-180.

-, 1997, Age of metamorphism of Otago Schist in eastern Otago and determination of protoliths from initial strontium isotope characteristics: New Zealand Journal of Geology and Geophysics, v. 40, no. 3, p. 275-286.

Agliardi, F., Crosta, G. B., and Frattini, P., 2012, Slow rock-slope deformation, Cambridge University Press, p. 207-221.

Agliardi, F., Zanchetta, S., and Crosta, G. B., 2014, Fabric controls on the brittle failure of folded gneiss and schist: Tectonophysics, v. 637, p. 150-162.

Andrade, P. S., and Saraiva, A. A., 2010, Physical and mechanical characterization of phyllites and metagreywackes in central Portugal: Bulletin of Engineering Geology and the Environment, v. 69, no. 2, p. 207-214.

ASTM International, 2016a, ASTM D4644 Standard Test Method for Slake Durability of Shales and Similar Weak Rocks: West Conshohocken, PA, American Society for Testing and Materials, 4pp.

-, 2016b, ASTM D5731: Standard Test Method for Determination of the Point Load Strength Index of Rock and Application to Rock Strength Classifications, Volume ASTM D5731-16: West Conshohocken, PA, ASTM, 11p.

-, 2019, ASTM D4543 Standard Practices for Preparing Rock Core as Cylindrical Test Specimens and Verifying Conformance to Dimensional and Shape Tolerances: West Conshohocken, PA, American Society for Testing Materials, 13pp.

Augustinus, P. C., 1995, Glacial valley cross-profile development: the influence of in situ rock stress and rock mass strength, with examples from the Southern Alps, New Zealand: Geomorphology (Amsterdam, Netherlands), v. 14, no. 2, p. 87-97.

Awad, A. S., Antonopoulos, I., and Sadeghian, M., 2017, Case Study: Geotechnical design of bored piles in rock for the Kawarau Falls Bridge, *in* Alexander, G. J. C., C.Y, ed., 20th NZGS Geotechnical Symposium.

Ballantyne, C. K., 2002, Paraglacial geomorphology: Quaternary Science Reviews, v. 21, no. 18, p. 1935-2017.

Ballantyne, C. K., Wilson, P., Gheorghiu, D., and Rodés, À., 2014, Enhanced rock-slope failure following ice-sheet deglaciation: timing and causes: Earth Surface Processes and Landforms, v. 39, no. 7, p. 900-913.

Barker, A. J. P. D., 1998, Introduction to metamorphic textures and microstructures, Cheltenham [England], Stanley Thornes

Barrell, D. J. A., 2011, Quaternary Glaciers of New Zealand, Elsevier Science & Technology, p. 1047-1064.

Barrell, D. J. A., Riddolls, B. W., Riddolls, P. M., and Thomson, R., 1994, Surficial geology of the Wakatipu Basin, Central Otago, New Zealand: Institute of Geological & Nuclear Sciences.

Basu, A., Mishra, D. A., and Roychowdhury, K., 2013, Rock failure modes under uniaxial compression, Brazilian, and point load tests: Bulletin of engineering geology and the environment, v. 72, no. 3-4, p. 457-475.

Beetham, R. D., Smith, G., Jennings, D. N., and Newton, C. J., The geology of Nine Mile Creek schist landslide complex, *in* Proceedings 6th International Symposium on Landslides, Christchurch, 1991, A.A.Balkema, v.1, p. 25-32.

Behrestaghi, M. H. N., Seshagiri Rao, K., and Ramamurthy, T., 1996, Engineering geological and geotechnical responses of schistose rocks from dam project areas in India: Engineering geology, v. 44, no. 1-4, p. 183-201.

Belcher, D. M., 2009, The stable isotopic variations and the hydrogeology of the Coronet Peak Skifield, Queenstown: a thesis submitted in partial fulfilment of the requirements for the degree of Master of Science in Engineering Geology in the University of Canterbury, MSc.: University of Canterbury.

Bell, D. H., 1976, Slope evolution and slope stability, Kawarau valley, Central Otago, New Zealand: Bulletin of the International Association of Engineering Geology - Bulletin de l'Association Internationale de Géologie de l'Ingénieur, v. 13, no. 1, p. 5-16.

-, 1982, Geomorphic Evolution of a Valley System: The Kawarau Valley, Central Otago, *in* Soons, J. M., and Selby, M. J., eds., Landforms of New Zealand: Auckland, New Zealand, p. 317-341.

-, 1985a, Engineering geology report on proposed subdivision Bishop property - Frankton.: Unpublished report to Clark Bewster McDonald & Associates.

-, 1985b, Engineering geology report on proposed subdivision Newman property - Frankton road Queenstown.: Unpublished report to P. Newman.

-, 1989, Engineering geology assessment of Goldfields stage IV Development, Queenstown.: Unpublished report to Woodlot Villas Ltd.

-, 1992, Geomorphic Evolution of a Valley System: The Kawarau Valley, Central Otago, *in* Soons, J. M., and Selby, M. J., eds., Landforms of New Zealand: Auckland, New Zealand, Longman Paul, p. 456-481.

-, 1994, Mike Stone Subdivision – Frankton Road – Queenstown.: Canterprise.

-, 1995, Maurice Jamieson Property – Larch Hill Place – Queenstown.: Canterprise.

-, 1996a, Building on Marginal Land - Some New Zealand Experiences, *in* Proceedings 7th Australia New Zealand Conference on Geomechanics, Adelaide, July 1996 1996a, p. 273-281.

-, 1996b, D Broomfield Development - Mt. Dewar - Queenstown: New Zealand, Canterprise Report to Clark Fortune McDonald & Associates, p. 5p + 2 figs.

-, 1997a, Engineering geology report on proposed Remarkables View subdivision P& G Hensman - Frankton Arm.: Unpublished report to Clark Fortune McDonald Associates.

-, 1997b, Engineering geology report on proposed subdivision Kremer & Associates Frankton Road property - Queenstown.: Unpublished report to Clark Fortune McDonald & Associates.

-, 2007a, Rocky Gully Snowmaking Reservoir - Summary Review: New Zealand, BGL Report to Hadley Consultants Ltd., p. 3p.

-, 2007b, Sarah-Sue Snowmaking Reservoir - Summary Review: New Zealand, BGL Report to Hadley Consultants Ltd, p. 6p.

-, 2007c, Woodlot Properties Ltd - Andrews Road Building Site: Bell Geoconsulting Limited.

-, 2008a, Coronet Peak - Water Resources for Snowmaking: New Zealand, BGL Report to Hadley Consultants Ltd, p. 4p + 1 table.

-, 2008b, Elephant Pit Snowmaking Reservoir - Summary Review: New Zealand, BGL Report to Hadley Consultants Ltd, p. 4p.

-, 2009, Design Philosophy - Coronet Snowmaking Reservoirs: New Zealand, BGL Report to Hadley Consultants Ltd, p. 3p.

-, 2018, Initial Geotechnical Report - Middleton Block - Goldfield Heights Development, Queenstown: Bell Geoconsulting Limited.

Bell, D. H., and Pettinga, J. R., 1985, Engineering geology and subdivision planning in New Zealand: Engineering Geology, v. 22, no. 1, p. 45-59.

Bell, D. H., and Riddolls, B. W., 1992, Slope Instability and Residential Development in the Queenstown Area, 6th International Symposium on Landslides, p. 16p.

Bell, F. G., 2007, Engineering geology, Amsterdam;Boston;, Butterworth-Heinemann.

Bertuzzi, R., Douglas, K., and Mostyn, G., 2016, Comparison of quantified and chart GSI for four rock masses: Engineering Geology, v. 202, p. 24-35.

Bieniawski, Z. T., 1989, Engineering rock mass classifications: a complete manual for engineers and geologists in mining, civil, and petroleum engineering, New York, Wiley.

Bishop, D. G., 1994, Extent and regional deformation of the Otago peneplain: Institute of Geological & Nuclear Sciences.

Bishop, D. G., 1972, Progressive Metamorphism from Prehnite-Pumpellyite to Greenschist Facies in the Dansey Pass Area, Otago, New Zealand: Geological Society of America bulletin, v. 83, no. 11.

Bishop, D. G., Bradshaw, J. D., Landis, C. A., and Turnbull, I. M., 1976, Lithostratigraphy and structure of the Caples terrane of the Humboldt Mountains, New Zealand: New Zealand Journal of Geology and Geophysics, v. 19, no. 6, p. 827-848.

Braathen, A., Blikra, L., Berg, S., and Karlsen, F., 2004, Rock-slope failures in Norway; type, geometry, deformation mechanisms and stability: Norwegian Journal of Geology, v. 84, p. 67-88.

Broch, E., and Franklin, J. A., 1972, The point-load strength test: International Journal of Rock Mechanics and Mining Sciences & Geomechanics Abstracts, v. 9, no. 6, p. 669-676.

Brown, E. H., 1963, The geology of the Mt Stoker area, Eastern Otago: New Zealand journal of geology and geophysics, v. 6, no. 5, p. 847-871.

-, 1967, The greenschist facies in part of eastern Otago, New Zealand: Contributions to mineralogy and petrology, v. 14, no. 4, p. 259-292.

Brown, I., Hittinger, M., and Goodman, R., 1980, Finite element study of the Nevis Bluff (New Zealand) rock slope failure: Rock Mechanics Felsmechanik Mecanique des Roches, v. 12, no. 3-4, p. 231-245.

Chapple, A. P., 1998, An engineering geological investigation into pit slope stability at Macraes Gold Mine, Macraes Flat, Otago, New Zealand: a thesis submitted in partial fulfilment of the requirements for the degree of Master of Science in Engineering Geology at the University of Canterbury.

Cho, J.-W., Kim, H., Jeon, S., and Min, K.-B., 2012, Deformation and strength anisotropy of Asan gneiss, Boryeong shale, and Yeoncheon schist: International journal of rock mechanics and mining sciences (Oxford, England : 1997), v. 50, p. 158-169.

Chu, W. J., Zhang, C. S., and Hou, J., 2013, Numerical simulation of deformation and strength anisotropy of Danba Schist: HydroChina.

Coates, G., and Cox, G. J., 2002, The rise and fall of the Southern Alps, Christchurch, N.Z, Canterbury University Press.

Cooper, E. K., 1995, Petrofabric studies across the Caples/Torlesse terrane boundary Otago schist, New Zealand: a thesis submitted in partial fulfilment of the requirements for the degree of Master of Science in Geology in the University of Canterbury.

Cotton, R., Christie, A. B., Geology, D., and Geophysics, 1991, Sheet QM398, Queenstown: geological resource map of New Zealand, 1:250 000: DSIR Geology & Geophysics.

Cox, S. C., 1991, The Caples/Aspiring terrane boundary-the translation surface of an early nappe structure in the Otago Schist: New Zealand Journal of Geology and Geophysics, v. 34, no. 1, p. 73-82.

Craw, D., 1984, Lithologic variations in Otago Schist, Mt Aspiring area, northwest Otago, New Zealand: New Zealand Journal of Geology and Geophysics, v. 27, no. 2, p. 151-166.

Cunningham, V., 1994, Land use planning and development suitability in Queenstown, New Zealand: a thesis submitted in partial fulfilment of the requirements for the degree of Masters of Engineering Geology at the University of Canterbury.

Fell, R., 2015, Geotechnical engineering of dams, Boca Raton, CRC Press, Taylor & Francis Group.

Fell, R., Stapledon, D., and MacGregor, P., 2012, Landslides and geologic environments, Cambridge University Press, p. 134-143.

Forster, M. A., and Lister, G. S., 2003, Cretaceous metamorphic core complexes in the Otago Schist, New Zealand: Australian journal of earth sciences, v. 50, no. 2, p. 181-198.

Geertsema, M., and Chiarle, M., 2013, 7.22 Mass-Movement Causes: Glacier Thinning, Elsevier Inc, p. 217-222.

Gillon, M., Denton, B. N., and Macfarlane, D. F., Field Investigation of the Cromwell Gorge landslides, *in* Proceedings 6th International Symposium on Landslides, Christchurch, 1991, v.1, A.A Balkema, p. 111-118

Gillon, M., Foster, P. F., Jennings, D. N., and Graham, C. J., Stability analysis applications: Cromwell Gorge landslides, *in* Proceedings 6th International Symposium on Landslides, Christchurch, 1991a, v.1, A.A Balkema, p. 423-428.

Gillon, M., Foster, P. F., Proffitt, G. T., and Smits, A. P., Monitoring of the Cromwell Gorge landslides, *in* Proceedings 6th International Symposium on Landslides, Christchurch, 1991b, v.2, A.A.Balkema, p. 1135-1140.

Gillon, M., Graham, C. J., and Grocott, G. G., Low level drainage works at the Brewery Creek Slide, *in* Proceedings 6th International Symposium on Landslides, Christchurch, 1991c, v.1, A.A.Balkema, p. 715-720.

Gillon, M., and Hancox, G. T., Cromwell Gorge landslides — a general overview, *in* Proceedings 6th International Symposium on Landslides, Christchurch, 1991, v.1, p. 83-102.

Glastonbury, J., and Fell, R., 2010, Geotechnical characteristics of large rapid rock slides: Canadian Geotechnical Journal, v.47, p. 116-132.

Glueer, F., Loew, S., and Manconi, A., 2020, Paraglacial history and structure of the Moosfluh Landslide (1850–2016), Switzerland: Geomorphology (Amsterdam, Netherlands), v. 355.

Glueer, F., Loew, S., Manconi, A., and Aaron, J., 2019, From Toppling to Sliding: Progressive Evolution of the Moosfluh Landslide, Switzerland: Journal of Geophysical Research: Earth Surface, v. 124, no. 12, p. 2899-2919.

GNS Science, 2018, New Zealand Geology Web Map, Lower Hutt, NZ, https://data.gns.cri.nz/geology/ (accessed January 2020)

González de Vallejo, L. I., and Ferrer, M., 2011, Geological engineering, Leiden, The Netherlands, CRC Press/Balkema.

Graham, I. J., and Mortimer, N., 1992, Terrane characterisation and timing of metamorphism in the Otago Schist, New Zealand, using Rb-Sr and K-Ar geochronology: New Zealand Journal of Geology and Geophysics, v. 35, no. 4, p. 391-401.

Grämiger, L. M., Moore, J. R., Gischig, V. S., Ivy-Ochs, S., and Loew, S., 2017, Beyond debuttressing: Mechanics of paraglacial rock slope damage during repeat glacial cycles, v.122, p. 1004-1036.

Grämiger, L. M., Moore, J. R., Gischig, V. S., and Loew, S., 2018, Thermomechanical Stresses Drive Damage of Alpine Valley Rock Walls During Repeat Glacial Cycles, v.123, p. 2620-2646.

Gray, D. R., and Foster, D. A., 2004, 40Ar/ 39Ar thermochronologic constraints on deformation, metamorphism and cooling/exhumation of a Mesozoic accretionary wedge, Otago Schist, New Zealand: Tectonophysics, v. 385, no. 1, p. 181-210.

Griffiths, J. S., and Whitworth, M., 2012, Engineering geomorphology of landslides, Cambridge University Press, p. 172-186.

Halliday, G. S., 2010, Large-scale toppling of schist in North-West Otago, Southern Alps, NZ; a precursor to rockslides and rock avalanches: Tonkin & Taylor Ltd.

Hector, J., 1863, Geological expedition to the west coast of Otago, New Zealand : report / by James Hector, Dunedin, N.Z., Dunedin, N.Z. : Printed for the Provincial Government by Daniel Campbell.

Higgins, M. D., 2006, Quantitative textural measurements in igneous and metamorphic petrology, Cambridge, UK;New York;, Cambridge University Press.

Hoek, E., 2007, Practical Rock Engineering, North Vancouver, B.C.

Hoek, E., and Brown, E. T., 2017, Underground Excavations in Rock, Boca Raton;Florence;, CRC Press LLC.

Hoek, E., and Karzulovic, A., 2000, Rock mass properties for surface mines: Rock mass properties for surface mines, p. 59-70.

Hollocher, K., 2014, A pictorial guide to metamorphic rocks in the field, Leiden, The Netherlands, CRC Press/Balkema.

Hungr, O., Leroueil, S., and Picarelli, L., 2014, The Varnes classification of landslide types, an update: Landslides, v. 11, no. 2, p. 167-194.

Hutchinson, J. N., 2001, The Fourth Glossop Lecture: Reading the Ground: Morphology and Geology in Site Appraisal: Quarterly Journal of Engineering Geology & Hydrogeology, v. 34, no. 1, p. 7-50.

Hutton, C. O., and Turner, F. J., 1936, Metamorphic Zones in North-west Otago: University of Otago.

Imrie, A. S., Moore, D. P., and Enegren, E. G., Performance and maintenance of the drainage system at Downie Slide, *in* Proceedings 6th International Symposium on Landslides, Christchurch, 1991, v.1, A.A.Balkema, p. 751-758.

ISRM, 2007a, Determining Point Load Strength, Part 2: Laboratory Testing: Ankara, Turkey, ISRM Turkish National Group, p. 12.

-, 2007b, Suggested Methods for Determining Indirect Tensile Strength by the Brazil Test, Part 2: Laboratory testing: Ankara, Turkey, ISRM Turkish National Group, p. 3

-, 2015, The ISRM suggested methods for rock characterization, testing and monitoring: 2007-2014, Upgraded ISRM Suggested Method for Determining Sound Velocity by Ultrasonic Pulse Transmission Technique: Cham, Springer.

Jaeger, J. C., Cook, N. G. W., and Zimmerman, R., 2007, Fundamentals of rock mechanics, Oxford;Malden, Mass;, Blackwell.

Jennings, D. N., Newton, C. J., Beetham, D., and Smith, G., Stabilization of the Nine Mile Creek schist landslide complex, *in* Proceedings 6th International Symposium on Landslides, Christchurch, 1991, v.1, A.A.Balkema, p. 759-764.

Johnson, J. D., 1986, The Gibbston slide, Kawarau Valley, Central Otago: a thesis submitted in partial fulfillment of the requirements for a degree of Master of Science in Engineering Geology in the University of Canterbury.

Johnson, S. E., 1990, Deformation history of the Otago schists, New Zealand, from progressively developed porphyroblast-matrix microstructures: uplift-collapse orogenesis and its implications: Journal of Structural Geology, v. 12, no. 5, p. 727-746.

Kalenchuk, K. S., Hutchinson, D. J., Diederichs, M., and Moore, D., 2012, Downie Slide, British Columbia, Canada, Cambridge University Press, p. 345-358.

Kawachi, Y., 1974, Geology and petrochemistry of weakly metamorphosed rocks in the upper Wakatipu district, southern New Zealand: New Zealand Journal of Geology and Geophysics, v. 17, no. 1, p. 169-208.

Kundu, J., Mahanta, B., Sarkar, K., and Singh, T. N., 2017, The Effect of Lineation on Anisotropy in Dry and Saturated Himalayan Schistose Rock Under Brazilian Test Conditions: Rock mechanics and rock engineering, v. 51, no. 1, p. 5-21.

Kwasniewski, M. A., 1993, Mechanical Behaviour of Anisotropic Rocks, *in* Hudson, J. A., ed., Comprehensive Rock Engineering: Principles, Practice & Projects, Volume 1: Oxford, England, Pergamon Press Ltd., p. 285-312.

Land Information New Zealand, 2019, Map Chooser, Topo50 maps, New Zealand, https://www.linz.govt.nz/land/maps/linz-topographic-maps/map-chooser (accessed January 2020).

Landis, C. A., Campbell, H. J., Begg, J. G., Mildenhall, D. C., Paterson, A. M., and Trewick, S. A., 2008, The Waipounamu Erosion Surface: questioning the antiquity of the New Zealand land surface and terrestrial fauna and flora: Geological Magazine, v. 145, no. 2, p. 173-197.

Leser, H., and Stäblein, G., 1985, Legend of the geomorphological map 1:25.000 (GMK 25) - fifth version in the GMK priority programm of the Deutsche Forschungsgemeinschaft: Berliner Geographische Abhandlingen.

Loew, S., Gischig, V., Willenberg, h., Alpiger, A., and Moore, J. R., 2012, Randa: Kinematics and driving mechanisms of a large complex rockslide, Cambridge University Press, p. 297-309.

Loureiro, F., Fernandes, I., Ribeiro, M. A., Neves, J., and Quinta-Ferreira, M., 2015, CHARACTERIZATION OF A SCHIST USING LABORATORY TESTS: International Multidisciplinary Scientific GeoConference : SGEM : Surveying Geology & mining Ecology Management, v. 2, p. 171.

Macfarlane, D., Pattle, A. D., and Salt, G., Nature and identification of Cromwell Gorge landslides groundwater systems, *in* Proceedings 6th International Symposium on Landslides, Christchurch, 1991a, v.1, A.ABalkema, p. 509-518.

Macfarlane, D. F., 2009, Observations and predictions of the behaviour of large, slow-moving landslides in schist, Clyde Dam reservoir, New Zealand: Engineering Geology, v. 109, no. 1, p. 5-15.

Macfarlane, D. F., Riddolls, B. W., Crampton, N. A., and Foley, M. R., Engineering geology of schist landslides, Cromwell, New Zealand, *in* Proceedings 6th International Symposium on Landslides, Christchurch, 1991b, v.3: Rotterdam, A.A.Balkema, p. 2137-2144.

Mackenzie, D. J., and Craw, D., 2005, Structural and lithological continuity and discontinuity in the Otago Schist, Central Otago, New Zealand: New Zealand Journal of Geology and Geophysics, v. 48, no. 2, p. 279-293.

Malone, A. W., Hansen, A., Hencher, S. R., and Fletcher, C. J. N., 2008, Post-failure movements of a large slow rock slide in schist near Pos Selim, Malaysia, CRC Press, p. 479-484.

Martin, A. P., S Rattenbury, M., and Cox, S., 2013, Geophysics-aided geological interpretation of the Otago Schist: new insights for mineral exploration and geological mapping.

McColl, S. T., 2012, Paraglacial rock-slope stability: Geomorphology, v. 153-154, p. 1-16.

McKenzie, M. J., 1993, An evaluation of the rock mass rating (RMR) system and its potential applicability in the prediction of the stability of natural slopes: a thesis submitted in partial fulfilment of the requirements for the degree of Master of Science in Engineering Geology in the University of Canterbury.

McSaveney, M. J., and Stirling, M., 1992, Central Otago: Basin and Range Country, *in* Soons, J. M., and Selby, M. J., eds., Landforms of New Zealand: Auckland, Longman Paul Limited, p. 482-504.

McSaveney, M. J., Thomson, R., and Turnbull, I. M., Timing of relief and landslides in central Otago, New Zealand, *in* Proceedings 6th International Symposium on Landslides, Christchurch, 01/01 1992, v.2, p. 1451-1456.

Millar, S., 2013, 8.23 Mass Movement Processes in the Periglacial Environment, Elsevier Inc, p. 374-391.

Moody, K. E., 1985, Engineering geology assessment of batter stability, Paerau diversion works, Maniototo, Central Otago.

Mortimer, N., 1993, Jurassic tectonic history of the Otago Schist, New Zealand: Tectonics, v. 12, no. 1, p. 237-244.

Mortimer, N., 2000, Metamorphic discontinuities in orogenic belts: example of the garnet–biotite–albite zone in the Otago Schist, New Zealand: International Journal of Earth Sciences, v. 89, no. 2, p. 295-306.

Mortimer, N., 2003, A provisional structural thickness map of the Otago Schist, New Zealand: American Journal of Science, v. 303, no. 7, p. 603-621.

Mortimer, N., 2004, New Zealand's Geological Foundations: Gondwana Research, v. 7, no. 1, p. 261-272.

Mortimer, N., Reay, M. B., and Mercury, W., 1993, Geology of the Otago schist and adjacent rocks: Institute of Geological and Nuclear Sciences.

Mortimer, N., and Roser, B. P., 1992, Geochemical evidence for the position of the Caples–Torlesse boundary in the Otago Schist, New Zealand: Journal of the Geological Society, v. 149, no. 6, p. 967-977.

Mortimer, N., Sutherland, R., and Nathan, S., 2001, Torlesse greywacke and Haast Schist source for Pliocene conglomerates near Reefton, New Zealand: New Zealand Journal of Geology and Geophysics, v. 44, no. 1, p. 105-111.

Mustafa, S., Khan, M. A., Khan, M. R., Hameed, F., Mughal, M. S., Asghar, A., and Niaz, A., 2015, Geotechnical study of marble, schist, and granite as dimension stone: a case study from parts of Lesser Himalaya, Neelum Valley Area, Azad Kashmir, Pakistan: Bulletin of Engineering Geology and the Environment, v. 74, no. 4, p. 1475-1487.

Nasseri, M. H. B., Rao, K. S., and Ramamurthy, T., 2003, Anisotropic strength and deformational behavior of Himalayan schists: International journal of rock mechanics and mining sciences (Oxford, England : 1997), v. 40, no. 1, p. 3-23.

Newton, C. J., and Smith, G., Dewatering of the Nine Mile Creek Landslide, *in* Proceedings 6th International Symposium on Landslides, Christchurch, 1991, v.1, A.A.Balkema, p. 797-804.

Norris, R. J., and Bishop, D. G., 1990, Deformed conglomerates and textural zones in the Otago Schists, South Island, New Zealand: Tectonophysics, v. 174, no. 3, p. 331-349.

Otago Regional Council, 2018, Otago Regional Council Long Term Plan 2018-2028: Otago Regional Council.

-, 2020, Otago Natural Hazards Database, Otago Regional Council, https://www.orc.govt.nz/managing-our-environment/natural-hazards/otago-natural-hazards-database (accessed January 2020).

Papadopoulos, Z., and Marinos, P., 1992, On the anisotropy of the athenian schist and its relation to weathering: Bulletin of the International Association of Engineering Geology - Bulletin de l'Association Internationale de Géologie de l'Ingénieur, v. 45, no. 1, p. 111-116.

Park, J., 1906, The geology of the area covered by the Alexandra sheet, Central Otago division, (including the survey districts of Leaning Rock, Tiger Hill, and Poolburn): N.Z. Govt. Printer.

-, 1908, The geology of the Cromwell subdivision, Western Otago division, Wellington, New Zealand Geological Survey Bulletin, Dept. of Mines, vol.5.

-, 1909, The geology of the Queenstown subdivision. Western Otago division, Wellington, New Zealand Geological Survey Bulletin, Dept. of Mines, vol.7.

Paterson, B. R., 1979, Engineering geological investigations of the Maniototo combined irrigation and power scheme: New Zealand Geological Survey.

Paterson, B. R., Hancox, G. T., Thomson, R., and Thompson, B. N., Part I - Philosophy and Methods of Investigation used in New Zealand, *in* Proceedings Symposium on Engineering for Dams and Canals, Wellington, 1983, v.9, p. 5.1-5.35.

Paterson, B. R., Ramsay, G., and Jennings, D. N., Design and Construction Aspects of the Maniototo Scheme Paerau Diversion, *in* Proceedings Fifth Australia-New Zealand Conference on Geomechanics, Sydney, August 1988 1988, p. 591-597.

Perras, M. A., and Diederichs, M. S., 2014, A Review of the Tensile Strength of Rock: Concepts and Testing: Geotechnical and geological engineering, v. 32, no. 2, p. 525-546.

Philp, M., 2011, Have snow, will ski: Engineering insight, v. 12/3, p. 26-29.

Queenstown Lakes District Council, 2018, Queenstown Lakes District Population Projections (December 2018): Queenstown Lake District Council.

-, 2019, Planning & Consents, New Zealand, https://www.qldc.govt.nz/services/resource-consents (accessed August 2019)

Ramamurthy, T., 1993, Strength and Modulus Responses of Anisotropic Rocks, *in* Hudson, J. A., ed., Comprehensive Rock Engineering: Principles, Practice & Projects, v.1: Oxford, England, Pergamon Press Ltd., p. 313-329.

Raymond, L. A., 1995, Petrology: the study of igneous, sedimentary, metamorphic rocks, Dubuque, Iowa, W.C. Brown.

Read, S. A. L., Perrin, N. D., and Brown, I. R., 1987, Measurement And Analysis Of Laboratory Strength And Deformability Characteristics Of Schistose Rock, 6th ISRM Congress: Montreal, Canada, International Society for Rock Mechanics and Rock Engineering, p. 6.

Read, S. A. L., Perrin, N. D., and Wong, D., 1985, Uniaxial compression testing and determination of modulus of elasticity and poisson's ratio of highly anisotropic (schistose) rocks.

Salt, G., and Yetton, M. D., 1985, An engineering geological appraisal of the proposed subdivision of part section 50-51, block xx-xxi, Shotover Survey District, Lake County.: Soils and Foundations (1973) Limited.

Saroglou, C., Qi, S., Guo, S., and Wu, F., 2018, ARMR, a new classification system for the rating of anisotropic rock masses: Bulletin of engineering geology and the environment, v. 78, no. 5, p. 3611-3626.

Saroglou, H., Marinos, and Tsiambaos, G., 2004, Applicability of the Hoek-Brown failure criterion and the effect of anisotropy on intact rock samples from Athens Schist: Journal- South African Institute of Mining and Metallurgy, v. 104, p. 209-215.

Shrestha, P. K., and Panthi, K. K., 2014, Analysis of the plastic deformation behavior of schist and schistose mica gneiss at Khimti headrace tunnel, Nepal: Bulletin of Engineering Geology and the Environment, v. 73, no. 3, p. 759-773.

Singh, B., and Goel, R. K., 1999, Rock mass classification: a practical approach in civil engineering, New York;Amsterdam, Elsevier.

Singh, B. and Goel, R. K., 2011, Engineering rock mass classification: tunneling, foundations, and landslides, Waltham, MA, Butterworth-Heinemann,.

Smith, A., and Salt, G., 1991, Clyde Power Station Reservoir. General report on geotechnical materials involved in landsliding: mineralogical, shear strength and related properties.: New Zealand Geological Survey: Department of Scientific and Industrial Research: Geology & Geophysics

Stahl, T., 2014, Active tectonics and geomorphology of the central South Island, New Zealand: earthquake hazards of reverse faults : a thesis submitted in partial fulfilment of the requirements for the degree of Doctor of Philosophy in Geology at the University of Canterbury.

Stossel, D. L., 1999, The engineering geology of Frankton Arm, Master of Science, University of Canterbury.

Sweeney, C. G., Brideau, M.-A., Augustinus, P., and Fink, D., 2013, Lochnagar landslide dam, Central Otago, New Zealand: Geomechanics and timing of the event, 19th NZGS Geotechnical Symposium: Queenstown, p. 1-9.

Turnbull, I. M., 1979a, Petrography of the Caples terrane of the Thomson Mountains, northern Southland, New Zealand: New Zealand Journal of Geology and Geophysics, v. 22, no. 6, p. 709-727.
-, 1979b, Stratigraphy and sedimentology of the Caples terrane of the Thomson Mountains, northern Southland, New Zealand: New Zealand Journal of Geology and Geophysics, v. 22, no. 5, p. 555-574.
-, 1980, Structure and interpretation of the Caples terrane of the Thomson Mountains, northern Southland, New Zealand: New Zealand Journal of Geology and Geophysics, v. 23, no. 1, p. 43-62.
-, 1981, Contortions in the schists of the Cromwell district, Central Otago, New Zealand: New Zealand Journal of Geology and Geophysics, v. 24, no. 1, p. 65-86.
-, 2000a, Geology of the Wakatipu area, *in* Science, G. N. S., ed., v.18, Lower Hutt, N.Z GNS Science.
-, 2000b, Geology of the Wakatipu area.: Institute of Geological & Nuclear Sciences, Institute of Geological & Nuclear Sciences 1:250,000 Geological Map, scale 1:250,000.

Turnbull, I. M., Barry, J. M., Carter, R. M., and Norris, R. J., 1975, The Bobs Cove Beds and their relationship to the Moonlight Fault Zone: Journal of the Royal Society of New Zealand, v. 5, no. 4, p. 355-394.

Turnbull, I. M., and Forsyth, P. J., 1988, Queenstown: a geological guide, Lower Hutt [N.Z.], Geological Society of New Zealand.

Turnbull, I. M., Mortimer, N., and Craw, D., 2001, Textural zones in the Haast Schist-a reappraisal: New Zealand Journal of Geology and Geophysics, v. 44, no. 1, p. 171-183.

van Woerden, T. H., 2018, Quaternary geology and landslide dam hazard assessment of the Shotover Gorge, Otago: a thesis submitted in partial fulfilment of the requirements for the degree of Master of Science in Disaster, Risk and Resilience at the University of Canterbury: Christchurch, New Zealand, University of Canterbury.

Varnes, D., 1978, Slope Movement Types and Processes: Transportation Research Board.

Watts, C. R., 1988, Engineering geological roading aggregate investigations of the Wakatipu basin: a thesis submitted in partial fulfillment of the requirements for the degree of Master of Science in Engineering Geology in the University of Canterbury.

Weinberger, R., Eyal, Y., and Mortimer, N., 2010, Formation of systematic joints in metamorphic rocks due to release of residual elastic strain energy, Otago Schist, New Zealand: Journal of Structural Geology, v. 32, no. 3, p. 288-305.

Willetts, A. J., 2000, The geology and geomorphology of the Coronet Peak and Arthurs Point landslide complexes, Master of Science, University of Canterbury.

Wood, B. L., 1963, Structure of the Otago schists: New Zealand Journal of Geology and Geophysics, v. 6, no. 5, p. 641-680.

-, 1978, The Otago schist megaculmination: Its possible origins and tectonic significance in the Rangitata orogen of New Zealand: Tectonophysics, v. 47, no. 3, p. 339-368.

Yardley, B. W. D., 1989, An introduction to metamorphic petrology, Harlow, Essex, England;New York;, Longman Scientific & Technical.

Zhang, L., 2016, Engineering Properties of Rocks, Oxford, Elsevier Science & Technology.

Zhang, X.-P., Wong, L. N. Y., Wang, S.-J., and Han, G.-Y., 2011, Engineering properties of quartz mica schist: Engineering Geology, v. 121, no. 3, p. 135-149.

Zhang, X.-P., Wu, S., Afolagboye, L. O., Wang, S., and Han, G., 2016, Using the Point Load Test to Analyze the Strength Anisotropy of Quartz Mica Schist Along an Exploration Adit: Rock Mechanics and Rock Engineering, v. 49, no. 5, p. 1967-1975.

APPENDICES

Appendix A

Appendix A: Contents

Appendix A: Geology of Queenstown Hill

A.1 Table of Revised Textural Zones Definitions and Field Identification Methods

	Textural Zone (TZ)	Metamorphic white mica thickness, length, habit	Hand specimen foliation features	Hand specimen quartz vein/segregation features	Thin section textures	Special Otago Schist features	Applicable rock names
	I	< 5 µm thick, < 75 µm long. Naked eye and hand lens reveal only coarse detrital micas	None, or only a spaced fracture cleavage	Local veins	Detrital textures only; no preferred orientation of metamorphic mica	-	Sandstone, mudstone, greywacke, argillite
	IIA	< 5 µm thick, < 75 µm long. Pelites have a matte black colour and can be slaty. Naked eye and hand lens reveal only coarse detrital micas	Weak-mod, anastomosing, penetrative, stronger in fine-grained rocks. Bedding still dominates over cleavage. Hand samples break into wedge-shaped blocks.	Local Veins	Detrital quartz grains have undulose extinction. Weak preferred orientation of metamorphic micas	-	Foliated greywacke, semi-schist, slate
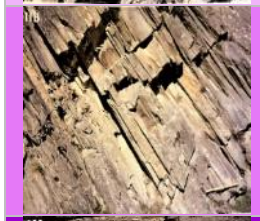	IIB	5-15 µm thick, < 75 µm long. Individual micas not visible through a hand lens. Pelites black but with distinct sheen, psammites grey	Strong, penetrative. Cleavage dominates over bedding which is transposed. Psammite-pelite contrasts sill easily resolved through colour differences. Hand specimens break into parallel-sided slabs	Appearance of flattened detrital grains may be enhanced but there is no foliation-parallel segregation. Veins locally common but these cut foliation at an angle	Detrital quartz grains still recognizable but mainly composed of subgrains. Strong preferred orientation of mica in anastomosing folia	F2 folds may develop and veins may be locally important. Pumpellyite-out isograd is within TZIIB	Psammitic or pelitic semi-schist, phyllite, slate
	III	15-25 µm thick, < 75-125 µm long (very fine sand size). Individual mica grains visible through hand lens, both pelites and psammites are silvery grey	Strong and penetrative but undulating on mm scale, less perfect than IIB. Where seen, psammitic-pelitic contacts are still sharp at mm scale	Distributed foliation-parallel quartz lenses <1 mm thick, throughout rock. Different generations of mm-cm thick veins ubiquitous	Detrital quartz and mica unrecognizable; quartz and mica in rock are approximately equigranular and form sub-mm segregations	Maximum textural grade of volcaniclastic Caples psammites. F2 folds can start to dominate. Garnet-biotite isograd is within TZIII	Quartzofeldspathic schist, greyschist
	IV	25-50 µm thick, < 125-500 µm long (fine-medium sand size). Individual mica grains clearly visible to naked eye	Strong and penetrative, undulating on mm-cm scale. Psammitic-pelitic contacts blurred at mm scale, but resolvable at cm scale	Essential and widespread quartz veins/segregations >1 mm thick, mainly polydeformed quartz veins	Adjacent quartz and mica grains merge into segregations and folia of variable thickness and length	Main foliation is S2	Quartzofeldspathic schist, greyschist, gneiss

Table 1:Revised definitions and features of psammitic and pelitic schist protoliths at different textural grades (Turnbull et al, 2001) Photos taken from Turnbull, 2000.

A.2 Core Box Photos

Borehole 1

Box 1/8

Borehole 1

Box 2/8

Borehole 1

Box 3/8

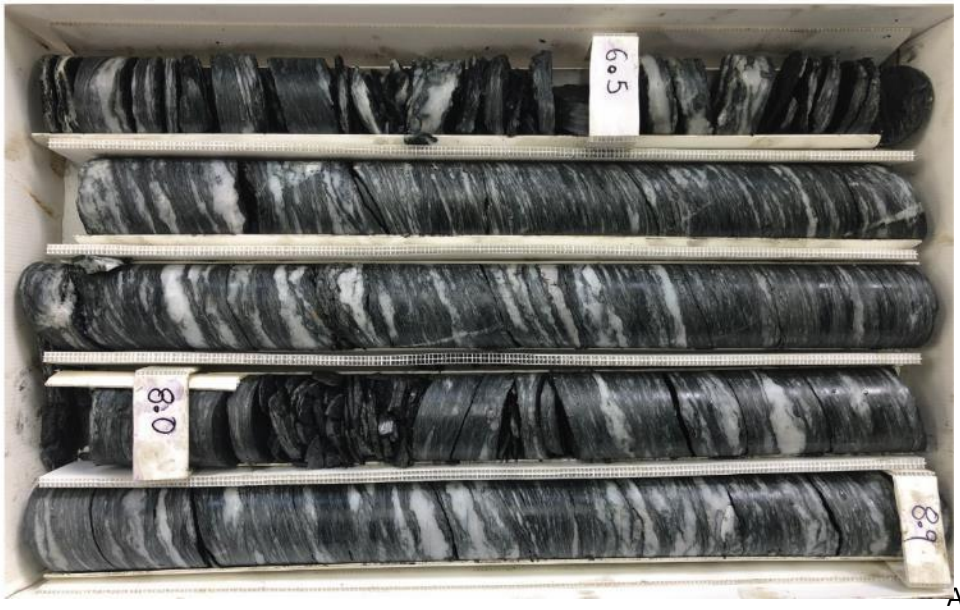

Borehole 1

Box 4/8

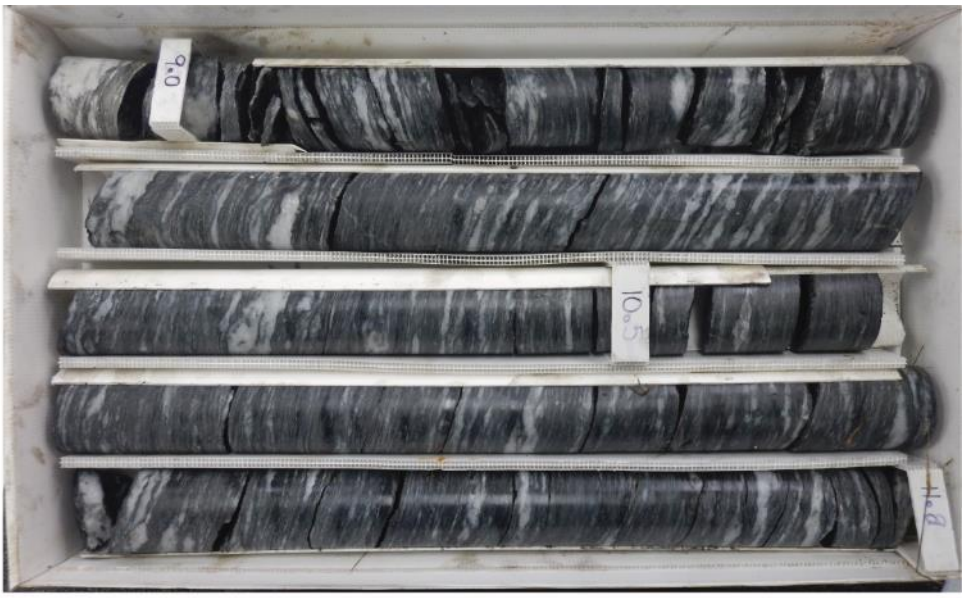

Borehole 1

Box 5/8

Borehole 1

Box 6/8

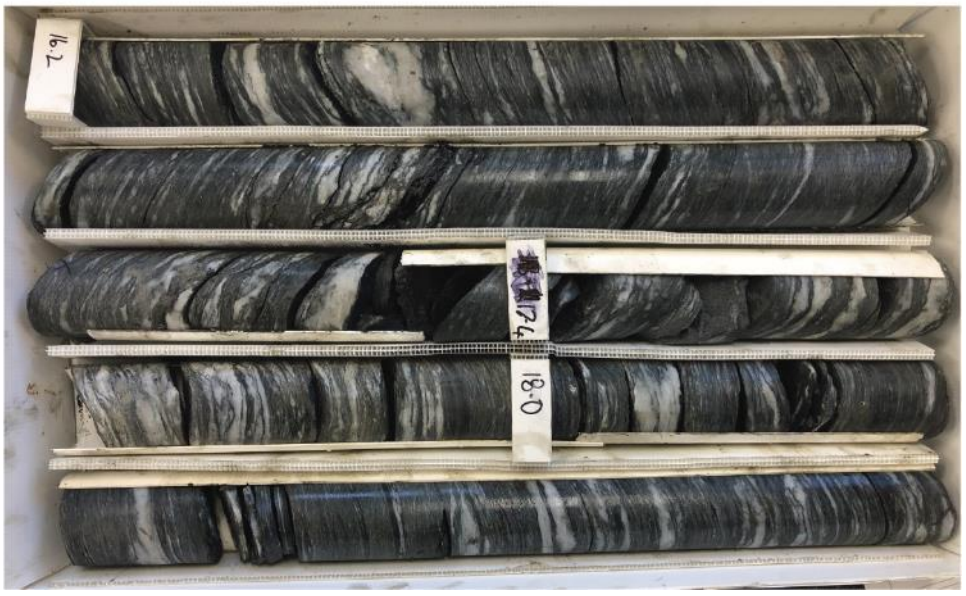

Borehole 1

Box 7/8

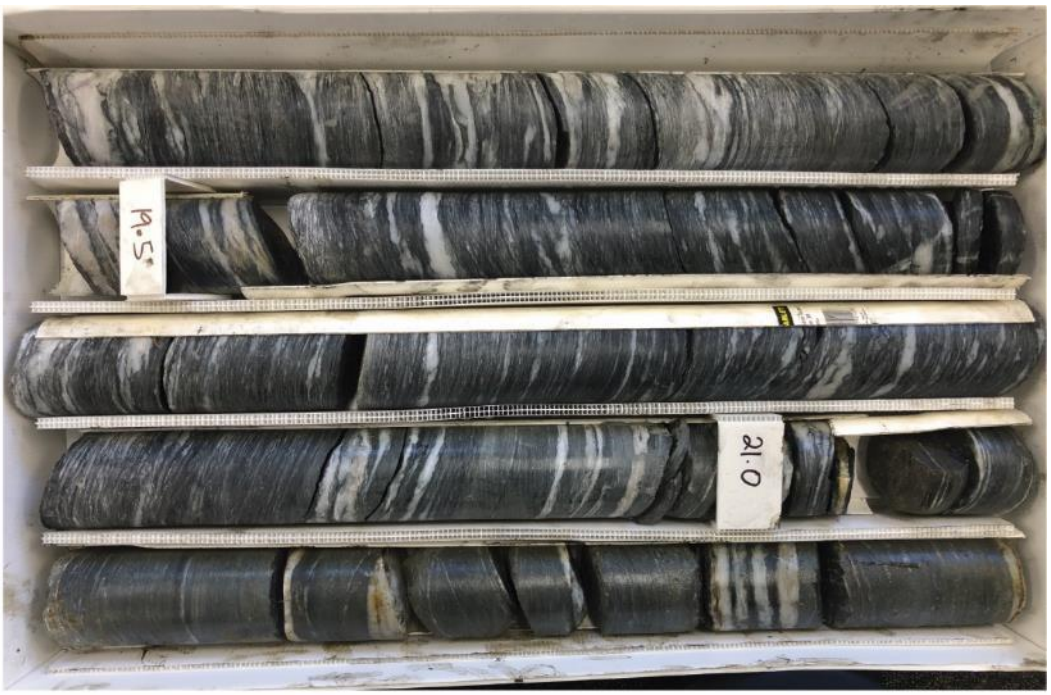

Borehole 1

Box 8/8

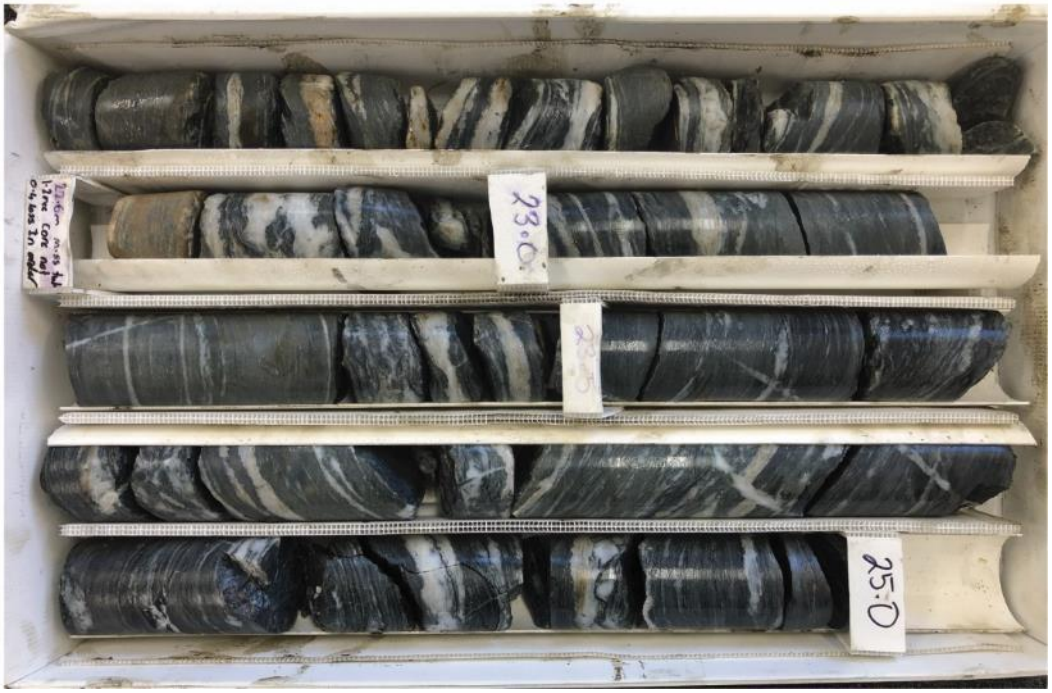

Borehole 2

Box 1/8

Borehole 2

Box 2/8

Borehole 2

Box 3/8

Borehole 2

Box 4/8

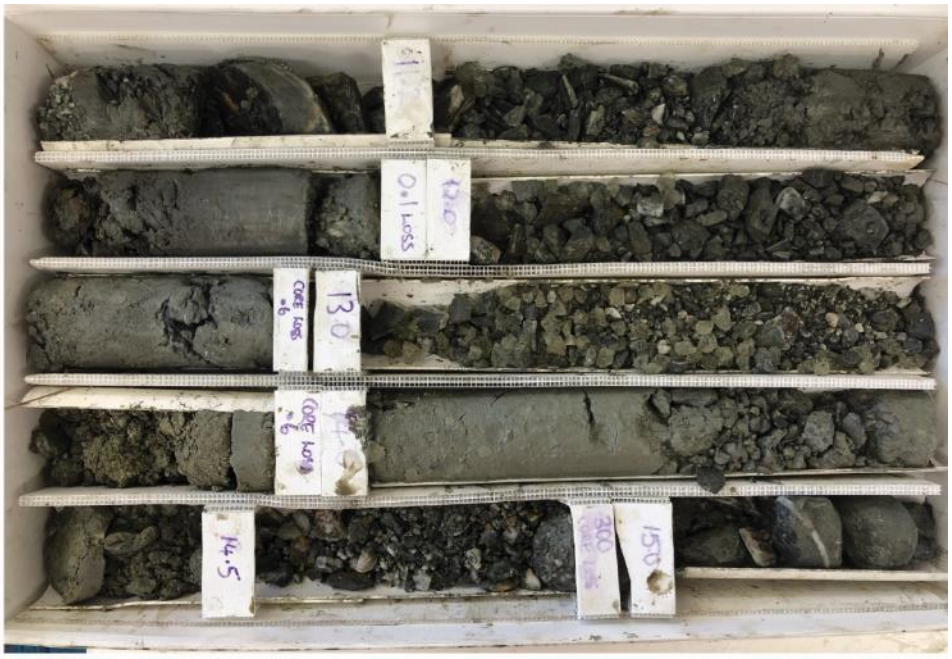

Borehole 2

Box 5/8

Borehole 2

Box 6/8

Borehole 2

Box 7/8

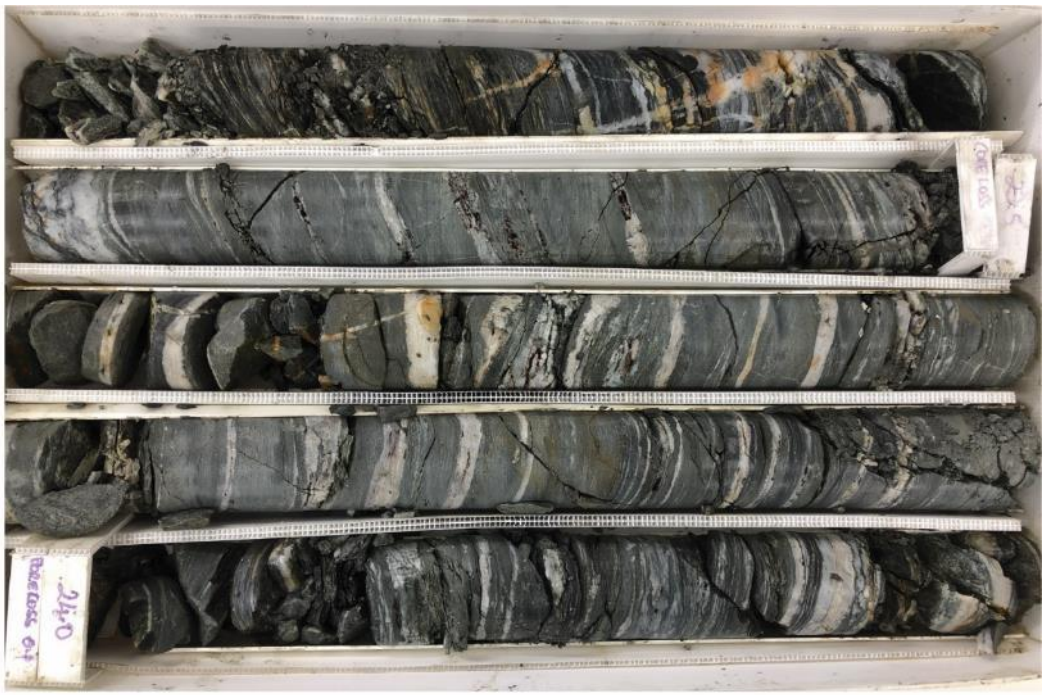

Borehole 2

Box 8/8

Borehole 3

Box 1/9

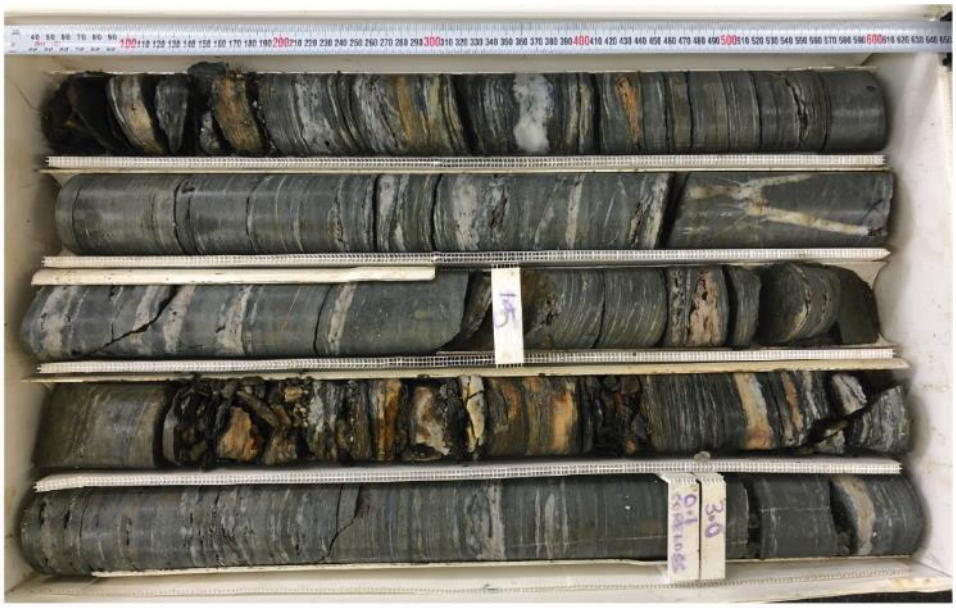

Borehole 3

Box 2/9

Borehole 3

Box 3/9

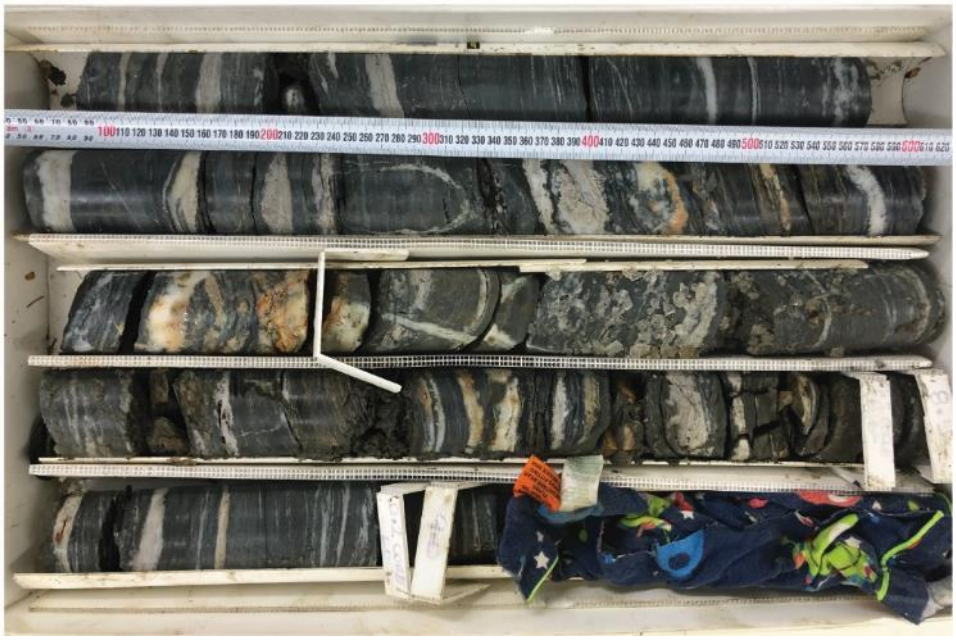

Borehole 3

Box 4/9

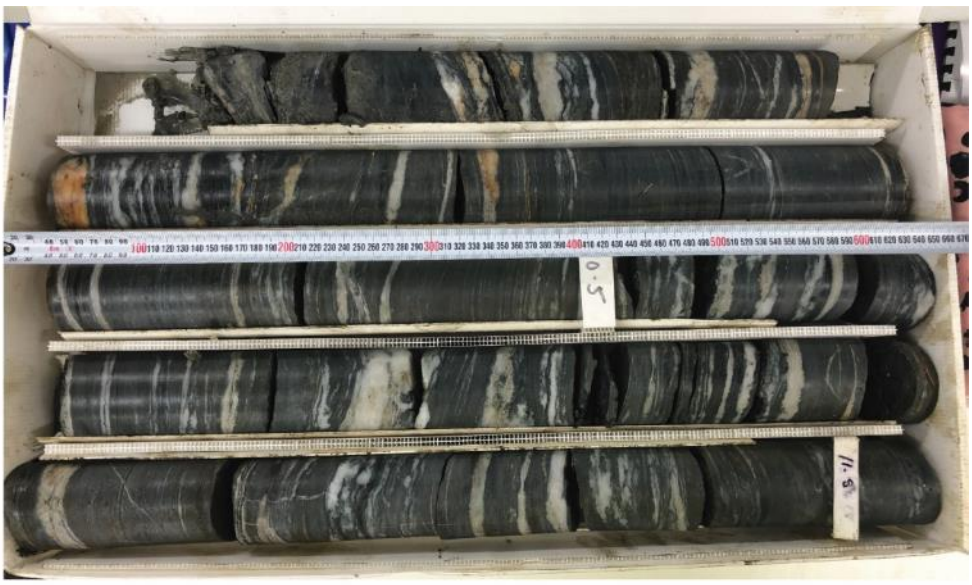

Borehole 3

Box 5/9

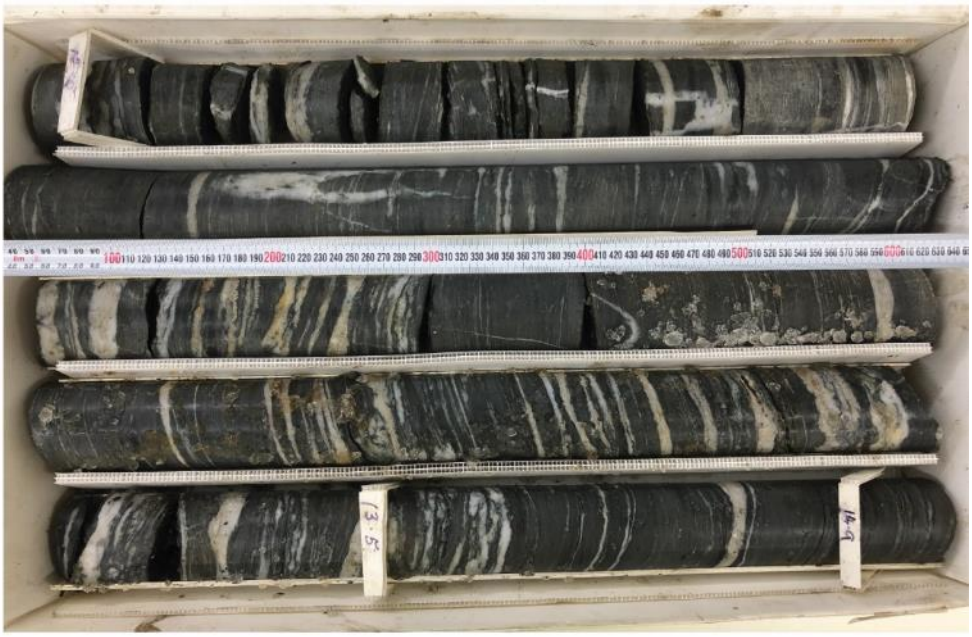

Borehole 3

Box 6/9

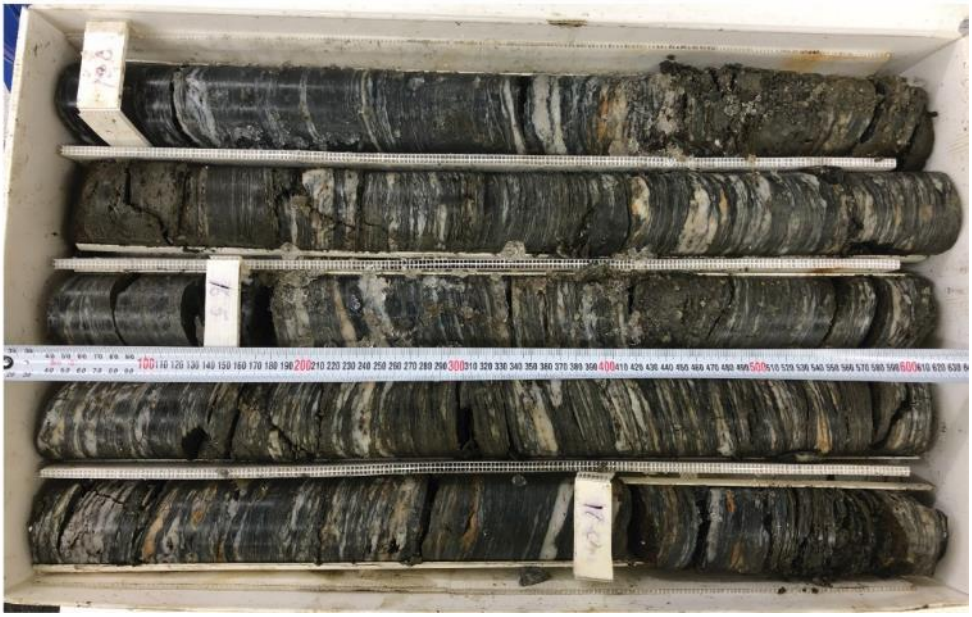

Borehole 3

Box 7/9

Borehole 3

Box 8/9

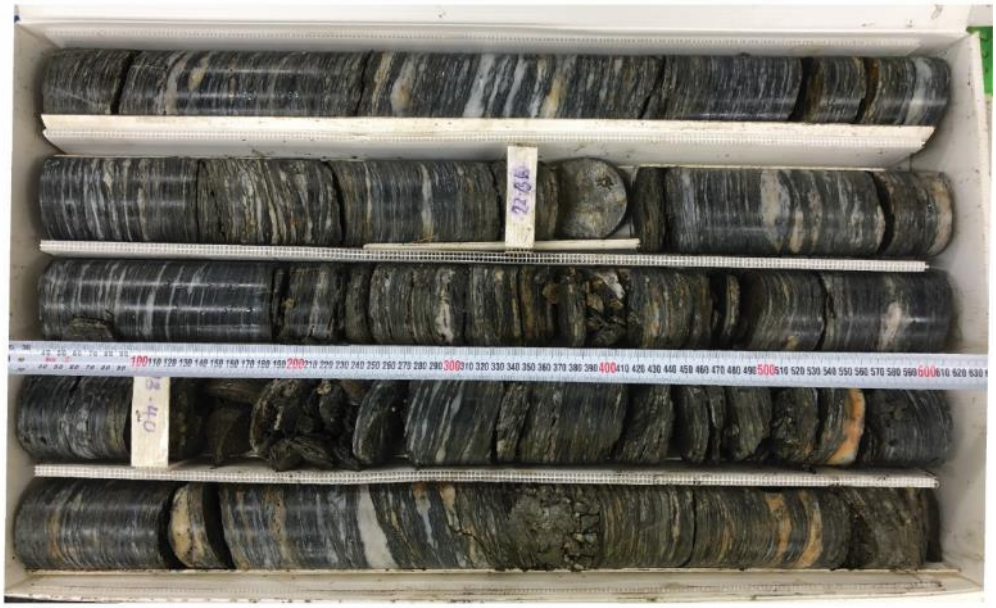

Borehole 3

Box 9/9

Borehole 4

Box 1/9

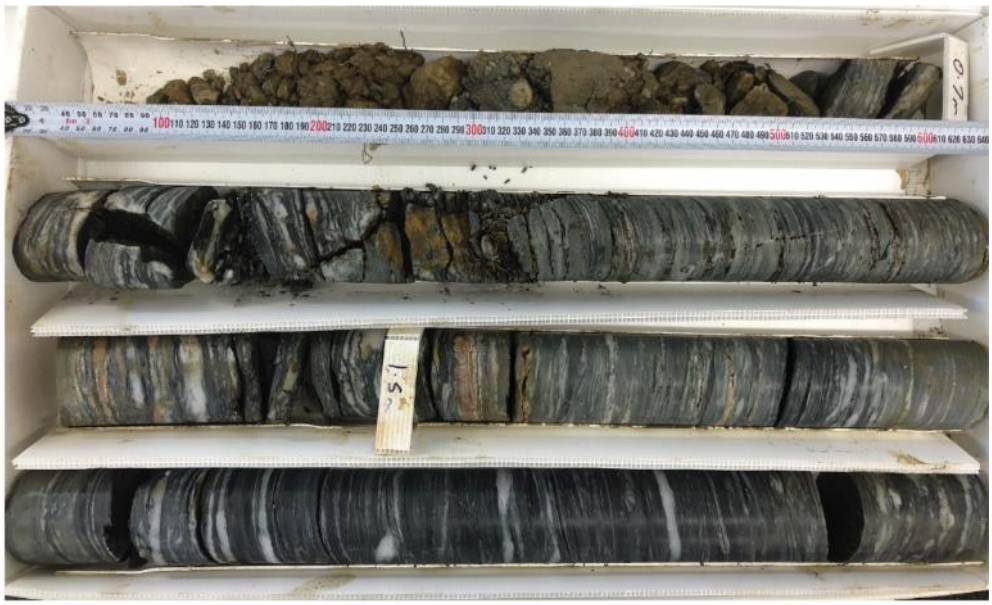

Borehole 4

Box 2/9

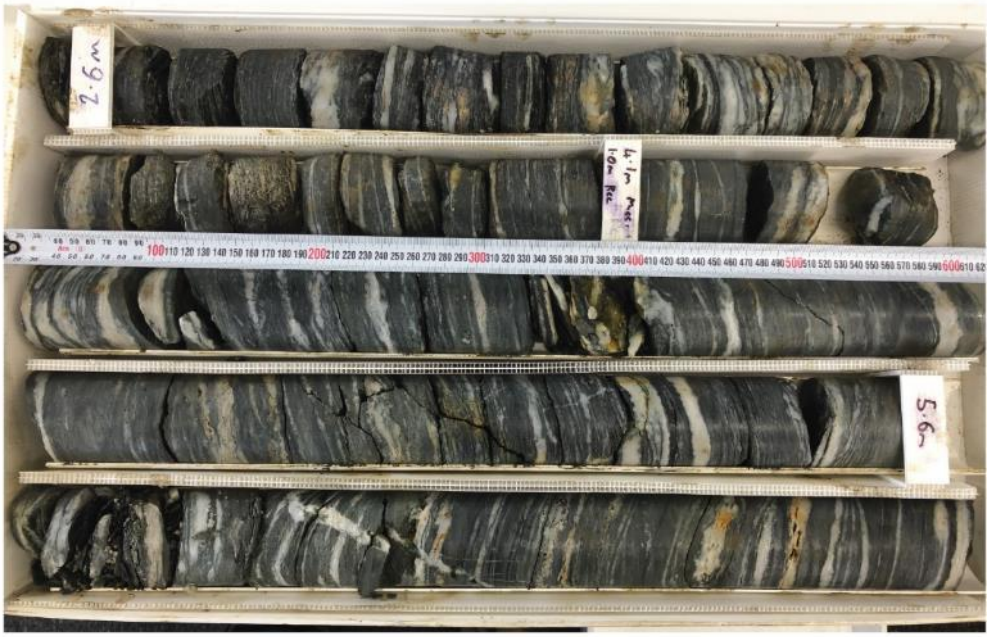

Borehole 4

Box 3/9

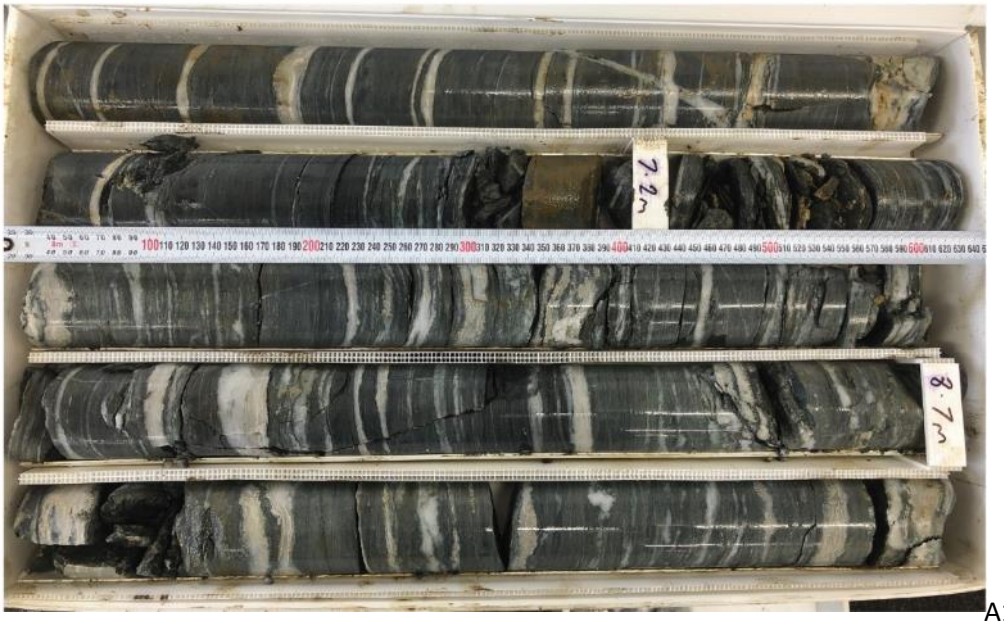

Borehole 4

Box 4/9

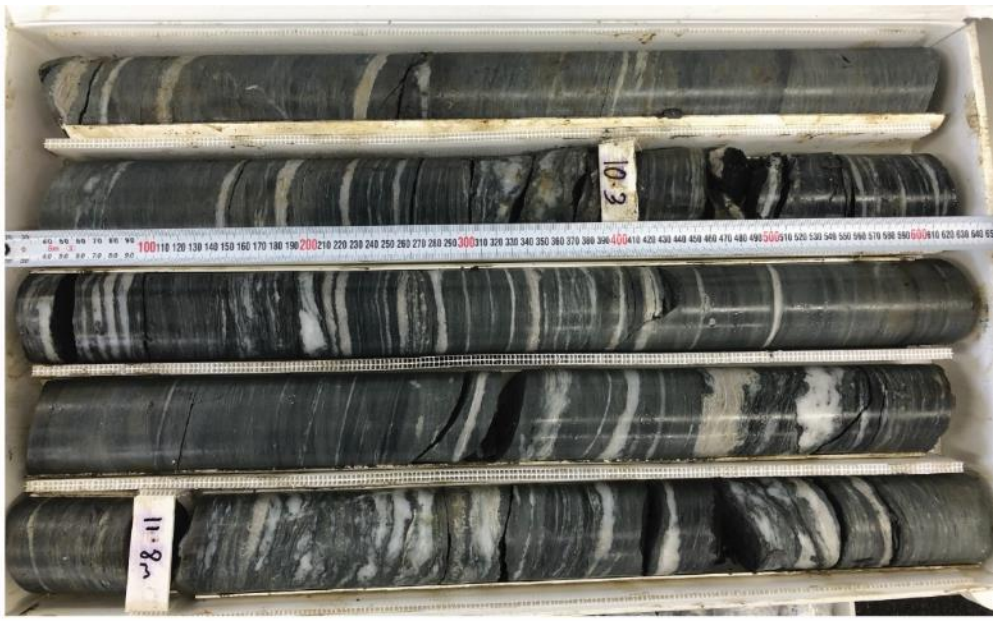

Borehole 4

Box 5/9

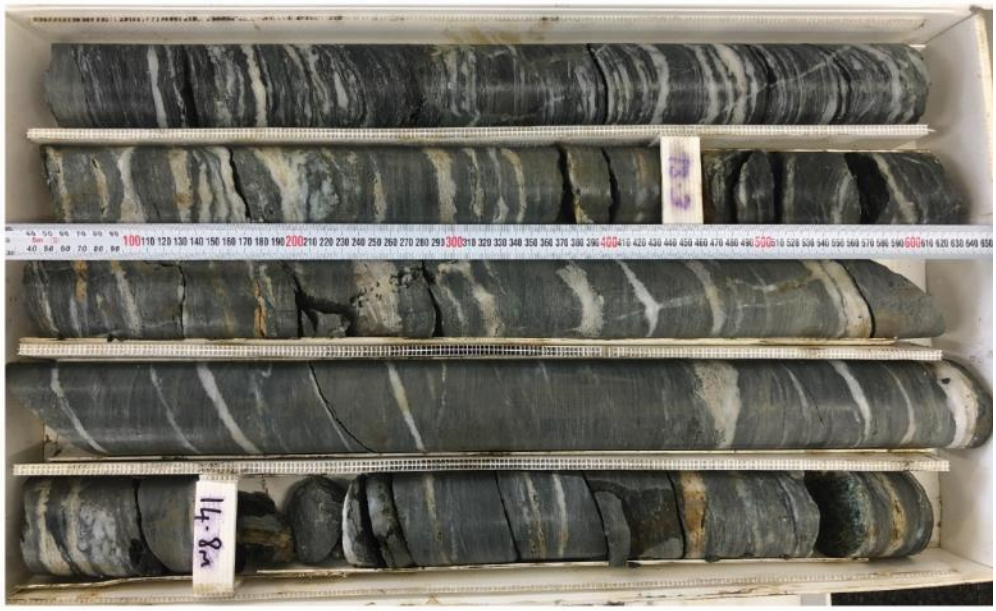

Borehole 4

Box 6/9

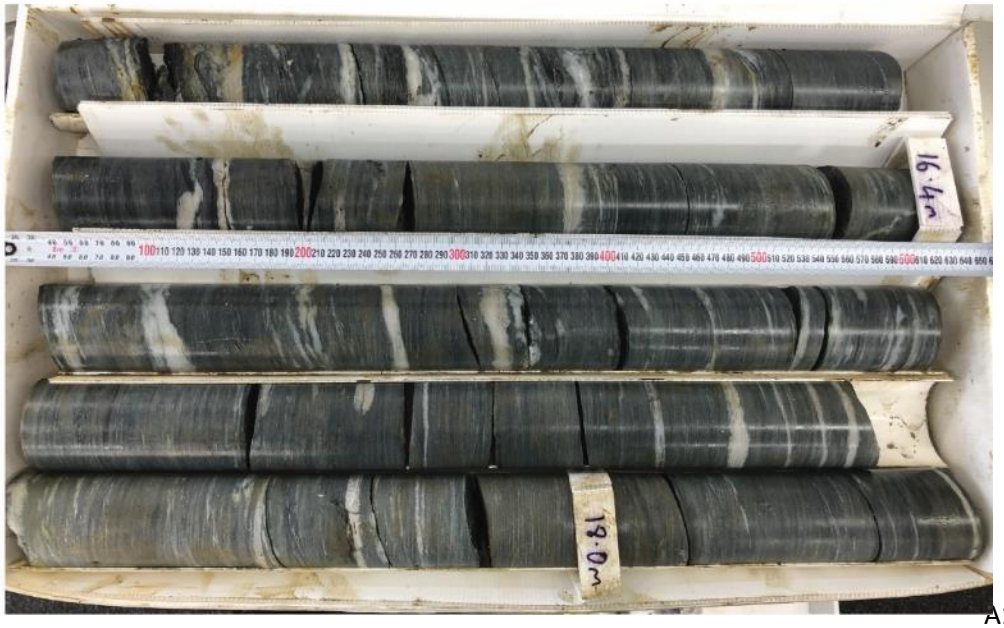

Borehole 4

Box 7/9

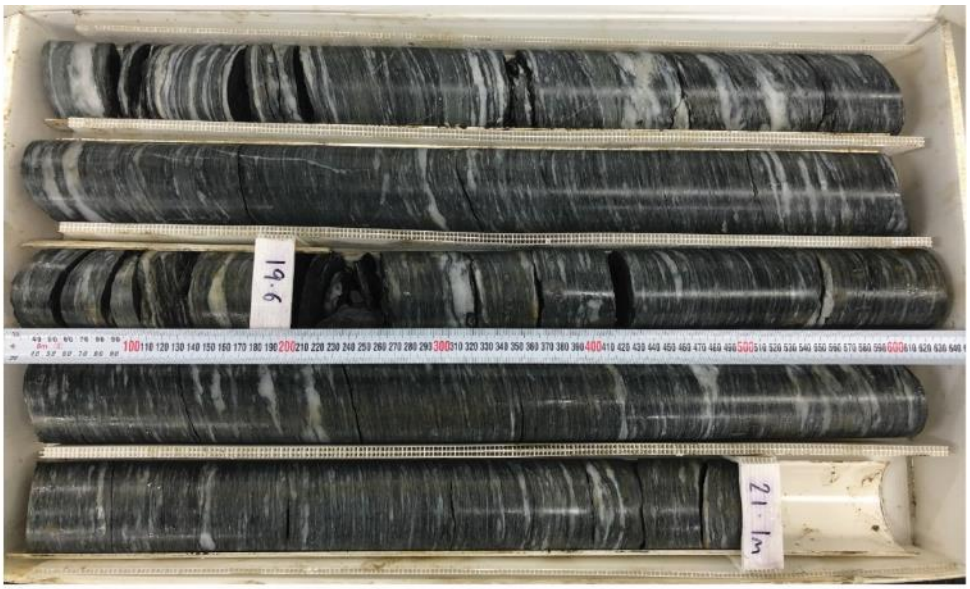

Borehole 4

Box 8/9

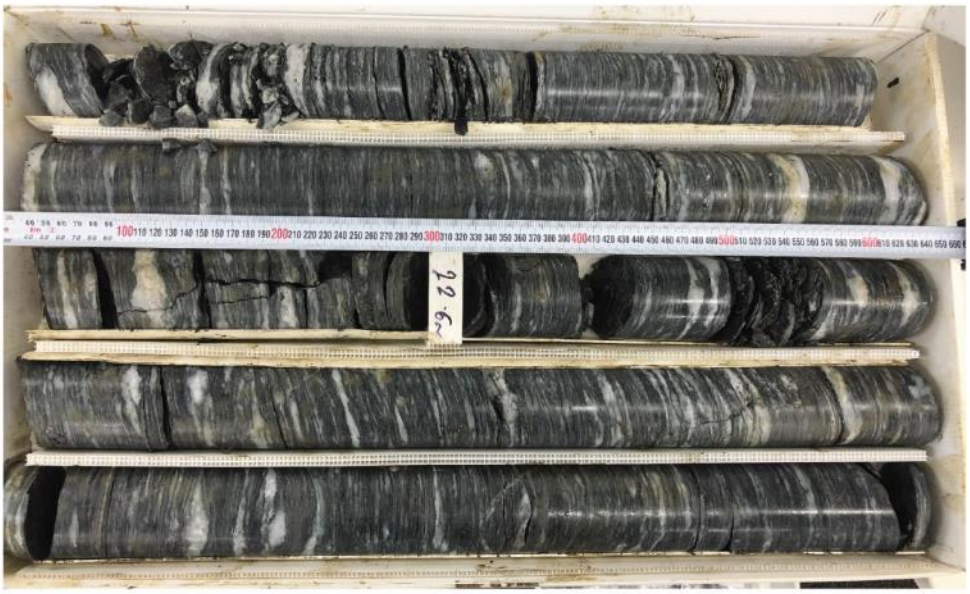

Borehole 4

Box 9/9

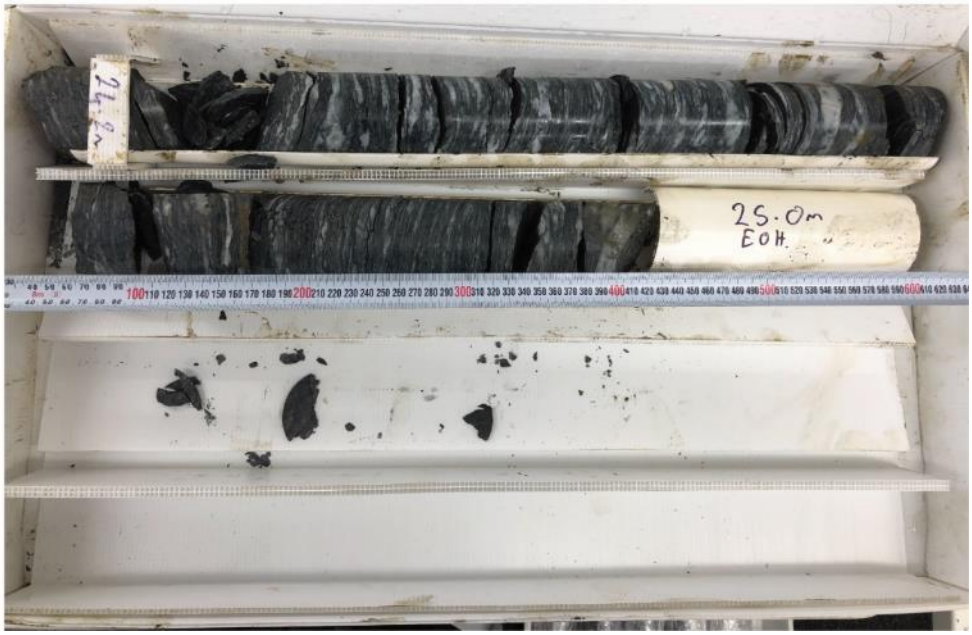

A.3 Borehole Logs: Full detailed logs

A.3.1 Borehole 1

Geotechnical Borehole Log

Project:	Queenstown Hill Landslide - GCL	**Borehole No.:**	BH1	**Box No.:**	1 to 8
Address:	Middleton Block - Goldfield Heights	**Coordinates:**	1260602.934, 5005756.898	**Sheet No.:**	1 to 10
Logged by:	Laura Gnesko	**Date Logged:**	29/04/2019	**Drilling Method:**	Rotary drilling
Meterage:	0.0 to 25.0m	**Coordinate System:**	NZTM2000	**Direction:**	Vertical
Date Drilled:	15/04/2019-16/04/2019	**Elevation:**	499.266m (a.s.l)	**Core diameter:**	63mm
		Angle from Horizontal:	90°		

Comments:

Box 1:	0.0 to 3.0m	Increased Qtz vein frequency and more intact material at 2.5m. Thin section samples can be recovered from this box if needed.
Box 2:	3.0 to 6.0m	Acceptable UCS size in this box.
Box 3:	6.0 to 8.9m	Increased presence of mm-scale chlorite laminae
Box 4:	8.9 to 11.8m	
Box 5:	11.8 to 16.2m	Markers in box. 1) 12.5m 2) 13.4m 3) 1.2m lost core 4) 14.9m 5) 0.4m lost core 6) 15.4m 7) 15.9m Interesting chlorite foliation in this box. Lots of samples left that can be point loaded if needed
Box 6:	16.2 to 18.9m	15.2m written on the top of the box, but last box terminated at 16.2 and the first placecard in box indicates 16.2m - 16.2m will be used. I suspect an error in the meterage stated in the corebox between block 16.2m and 17.4m. Cards indicate 1.2m of core. I measured 1.5m of core. I logged the box as per the cards in the box at 1.2m, but do not agree.
Box 7:	18.9 to 21.8m	Lithological change noted at ~21m mark.
Box 8:	21.8 to 25.0m	22.6m misstube, 1.2m core loss and 0.4m not in order.

Page 1 of 10

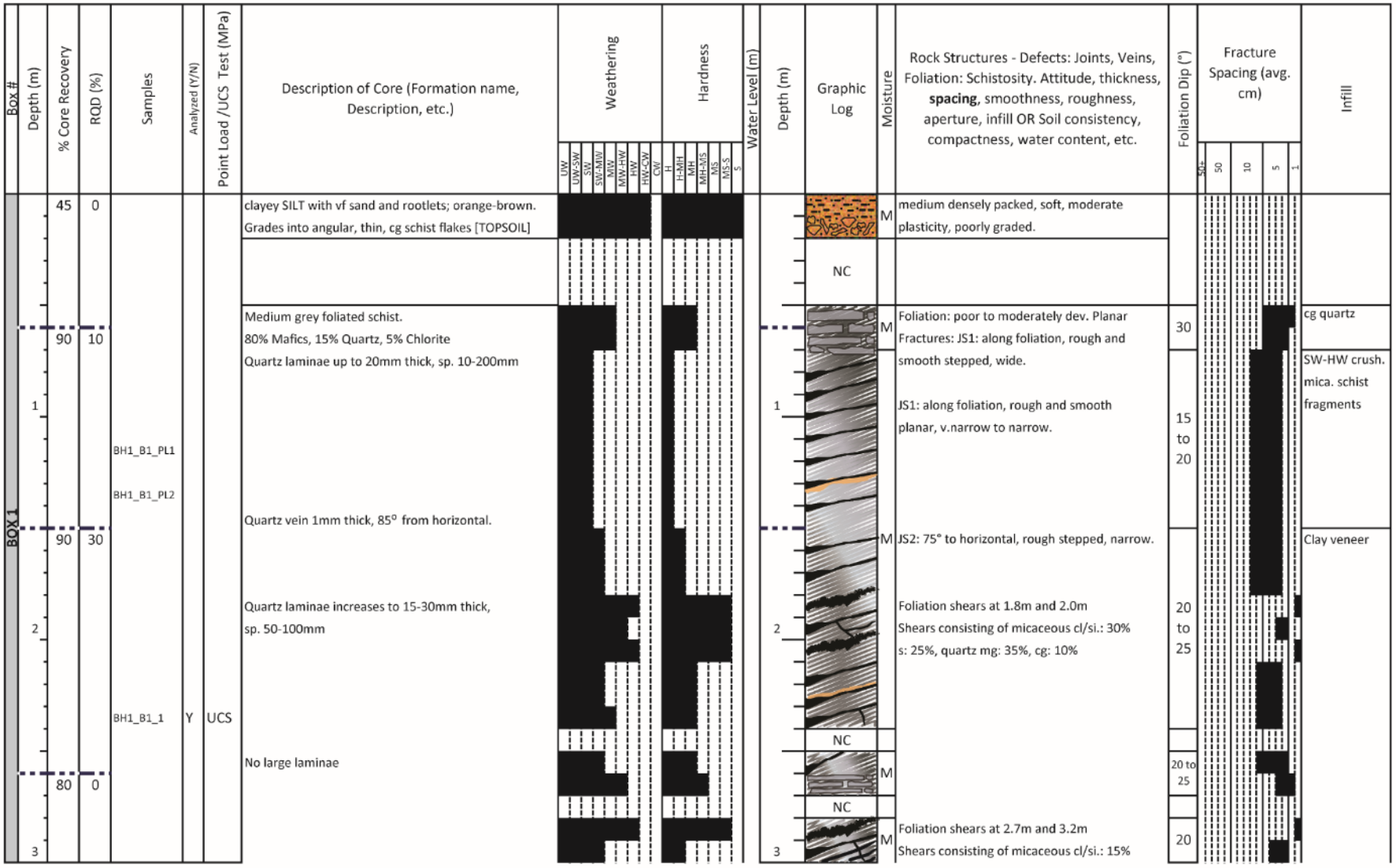
Box #
Depth (m)
% Core Recovery
RQD (%)
Samples
Analyzed (Y/N)
Point Load /UCS Test (MPa)
Description of Core (Formation name, Description, etc.)
Weathering
UW
UW-SW
SW
SW-MW
MW
MW-HW
HW
HW-CW
CW
Hardness
H
H-MH
MH
MH-MS
MS
MS-S
S
Water Level (m)
Depth (m)
Graphic Log
Moisture
Rock Structures - Defects: Joints, Veins, Foliation: Schistosity. Attitude, thickness, spacing, smoothness, roughness, aperture, infill OR Soil consistency, compactness, water content, etc.
Foliation Dip (°)
Fracture Spacing (avg. cm)
50
10
5
1
Infill
BOX 1
45
0
clayey SILT with vf sand and rootlets; orange-brown.
Grades into angular, thin, cg schist flakes [TOPSOIL]
M
medium densely packed, soft, moderate plasticity, poorly graded.
NC
90
10
Medium grey foliated schist.
80% Mafics, 15% Quartz, 5% Chlorite
Quartz laminae up to 20mm thick, sp. 10-200mm
M
Foliation: poor to moderately dev. Planar
Fractures: JS1: along foliation, rough and smooth stepped, wide.
30
cg quartz
JS1: along foliation, rough and smooth planar, v.narrow to narrow.
15 to 20
SW-HW crush. mica. schist fragments
BH1_B1_PL1
BH1_B1_PL2
Quartz vein 1mm thick, 85° from horizontal.
90
30
M
JS2: 75° to horizontal, rough stepped, narrow.
Clay veneer
Quartz laminae increases to 15-30mm thick, sp. 50-100mm
Foliation shears at 1.8m and 2.0m
Shears consisting of micaceous cl/si.: 30%
s: 25%, quartz mg: 35%, cg: 10%
20 to 25
BH1_B1_1
Y
UCS
NC
No large laminae
M
20 to 25
NC
80
0
Foliation shears at 2.7m and 3.2m
Shears consisting of micaceous cl/si.: 15%
M
20
1
2
3

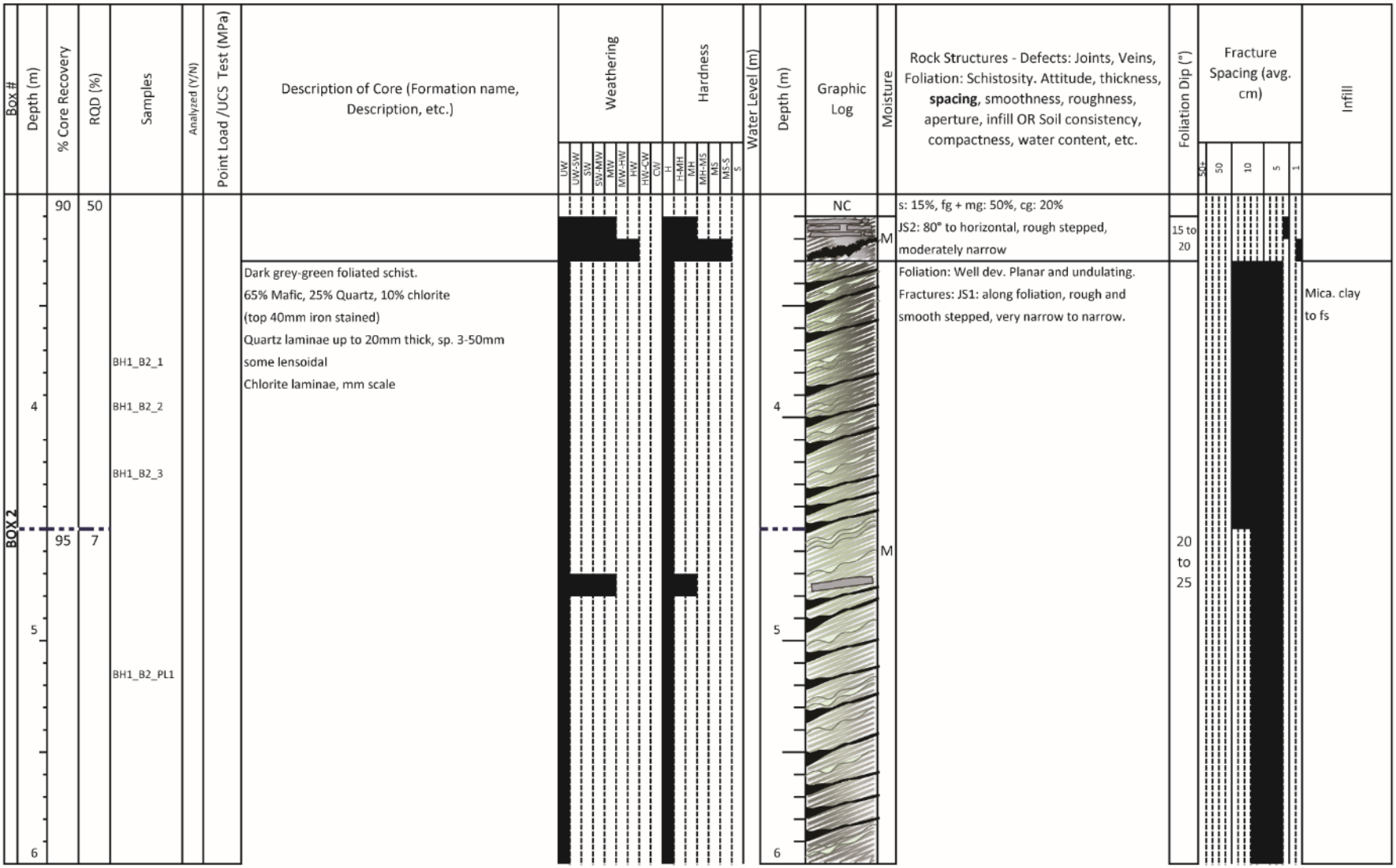
Box #
Depth (m)
% Core Recovery
RQD (%)
Samples
Analyzed (Y/N)
Point Load /UCS Test (MPa)
Description of Core (Formation name, Description, etc.)
Weathering
UW
UW-SW
SW
SW-MW
MW
MW-HW
HW
HW-CW
CW
Hardness
H
H-MH
MH
MH-MS
MS
MS-S
S
Water Level (m)
Depth (m)
Graphic Log
Moisture
Rock Structures - Defects: Joints, Veins, Foliation: Schistosity. Attitude, thickness, spacing, smoothness, roughness, aperture, infill OR Soil consistency, compactness, water content, etc.
Foliation Dip (°)
Fracture Spacing (avg. cm)
Infill
90
50
95
7
BOX 2
BH1_B2_1
BH1_B2_2
BH1_B2_3
BH1_B2_PL1
4
5
6
Dark grey-green foliated schist.
65% Mafic, 25% Quartz, 10% chlorite
(top 40mm iron stained)
Quartz laminae up to 20mm thick, sp. 3-50mm
some lensoidal
Chlorite laminae, mm scale
NC
M
M
s: 15%, fg + mg: 50%, cg: 20%
JS2: 80° to horizontal, rough stepped, moderately narrow
Foliation: Well dev. Planar and undulating.
Fractures: JS1: along foliation, rough and smooth stepped, very narrow to narrow.
15 to 20
20 to 25
50
10
5
1
Mica. clay to fs

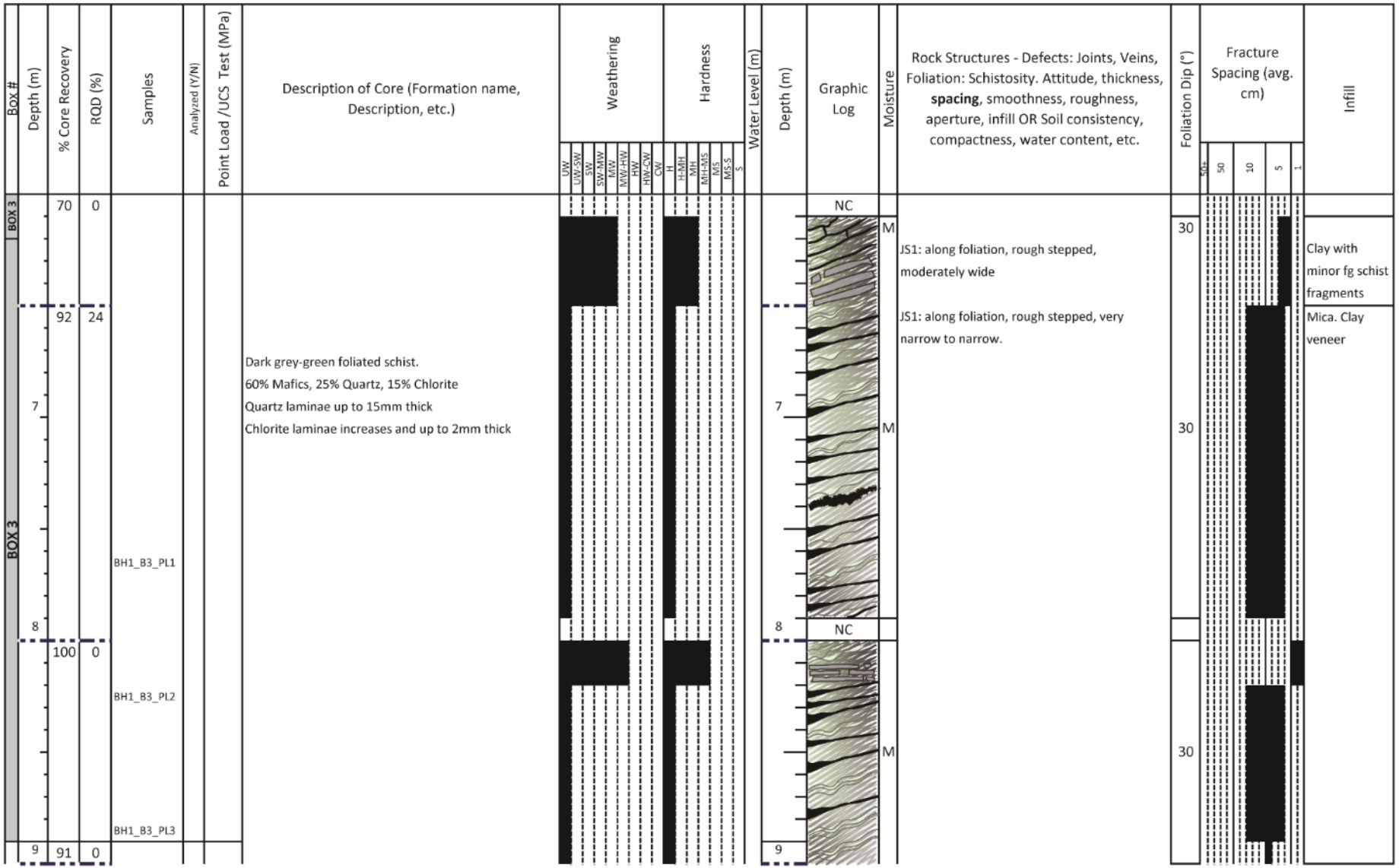
Box #
Depth (m)
% Core Recovery
RQD (%)
Samples
Analyzed (Y/N)
Point Load /UCS Test (MPa)
Description of Core (Formation name, Description, etc.)
Weathering
UW
UW-SW
SW
SW-MW
MW
MW-HW
HW
HW-CW
CW
Hardness
H
H-MH
MH
MH-MS
MS
MS-S
S
Water Level (m)
Depth (m)
Graphic Log
Moisture
Rock Structures - Defects: Joints, Veins, Foliation: Schistosity. Attitude, thickness, spacing, smoothness, roughness, aperture, infill OR Soil consistency, compactness, water content, etc.
Foliation Dip (°)
Fracture Spacing (avg. cm)
50+
50
10
5
1
Infill
BOX 3
70
0
92
24
100
0
91
0
7
8
9
BH1_B3_PL1
BH1_B3_PL2
BH1_B3_PL3
Dark grey-green foliated schist.
60% Mafics, 25% Quartz, 15% Chlorite
Quartz laminae up to 15mm thick
Chlorite laminae increases and up to 2mm thick
NC
M
JS1: along foliation, rough stepped, moderately wide
JS1: along foliation, rough stepped, very narrow to narrow.
30
Clay with minor fg schist fragments
Mica. Clay veneer

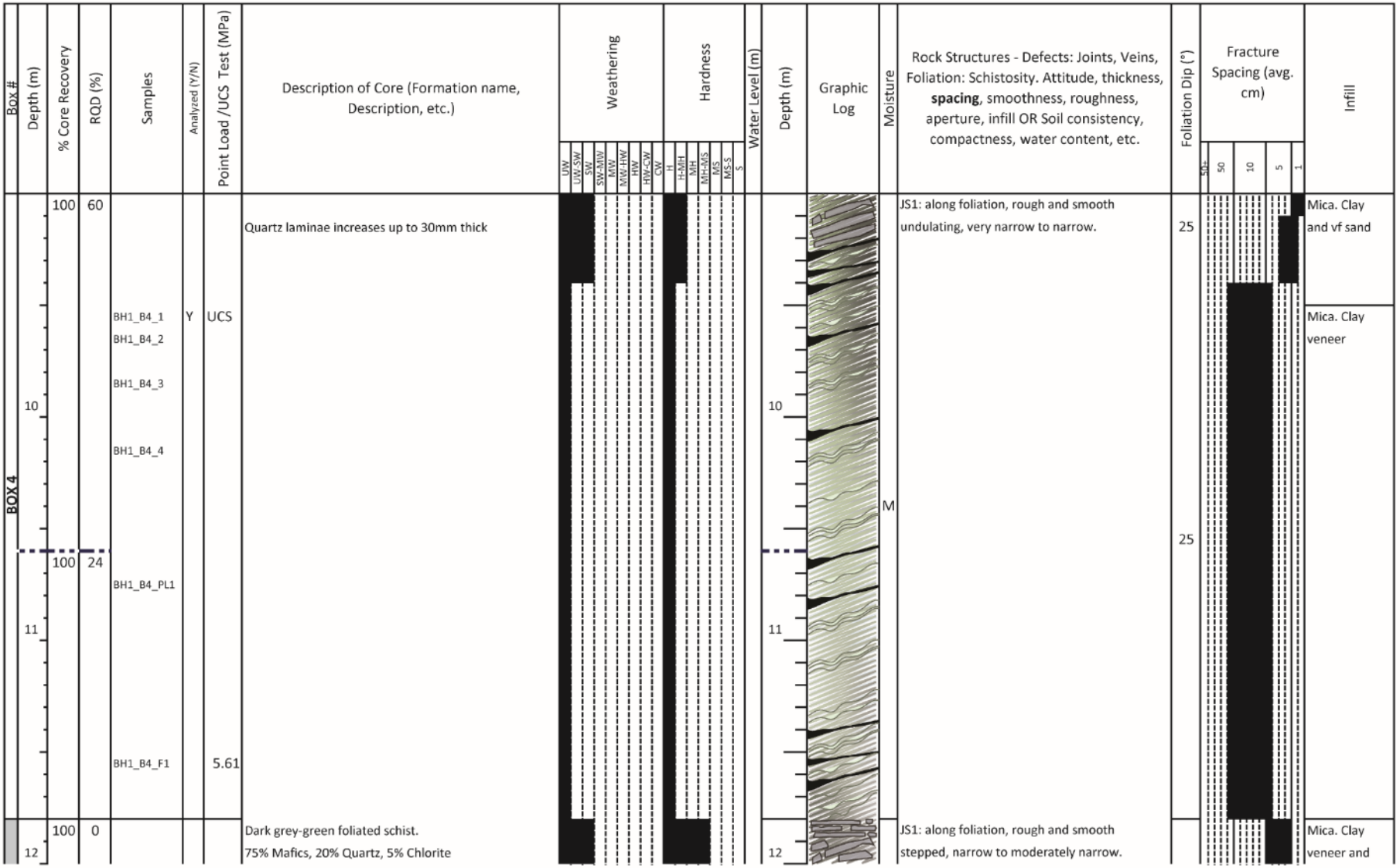
Box #
Depth (m)
% Core Recovery
RQD (%)
Samples
Analyzed (Y/N)
Point Load /UCS Test (MPa)
Description of Core (Formation name, Description, etc.)
Weathering
UW
UW-SW
SW
SW-MW
MW
MW-HW
HW
HW-CW
CW
Hardness
H
H-MH
MH
MH-MS
MS
MS-S
S
Water Level (m)
Depth (m)
Graphic Log
Moisture
Rock Structures - Defects: Joints, Veins, Foliation: Schistosity. Attitude, thickness, spacing, smoothness, roughness, aperture, infill OR Soil consistency, compactness, water content, etc.
Foliation Dip (°)
Fracture Spacing (avg. cm)
50+
50
10
5
1
Infill
BOX 4
100
60
Quartz laminae increases up to 30mm thick
BH1_B4_1
BH1_B4_2
BH1_B4_3
BH1_B4_4
Y
UCS
JS1: along foliation, rough and smooth undulating, very narrow to narrow.
25
Mica. Clay and vf sand
Mica. Clay veneer
10
M
100
24
BH1_B4_PL1
25
11
BH1_B4_F1
5.61
100
0
Dark grey-green foliated schist.
75% Mafics, 20% Quartz, 5% Chlorite
JS1: along foliation, rough and smooth stepped, narrow to moderately narrow.
Mica. Clay veneer and
12

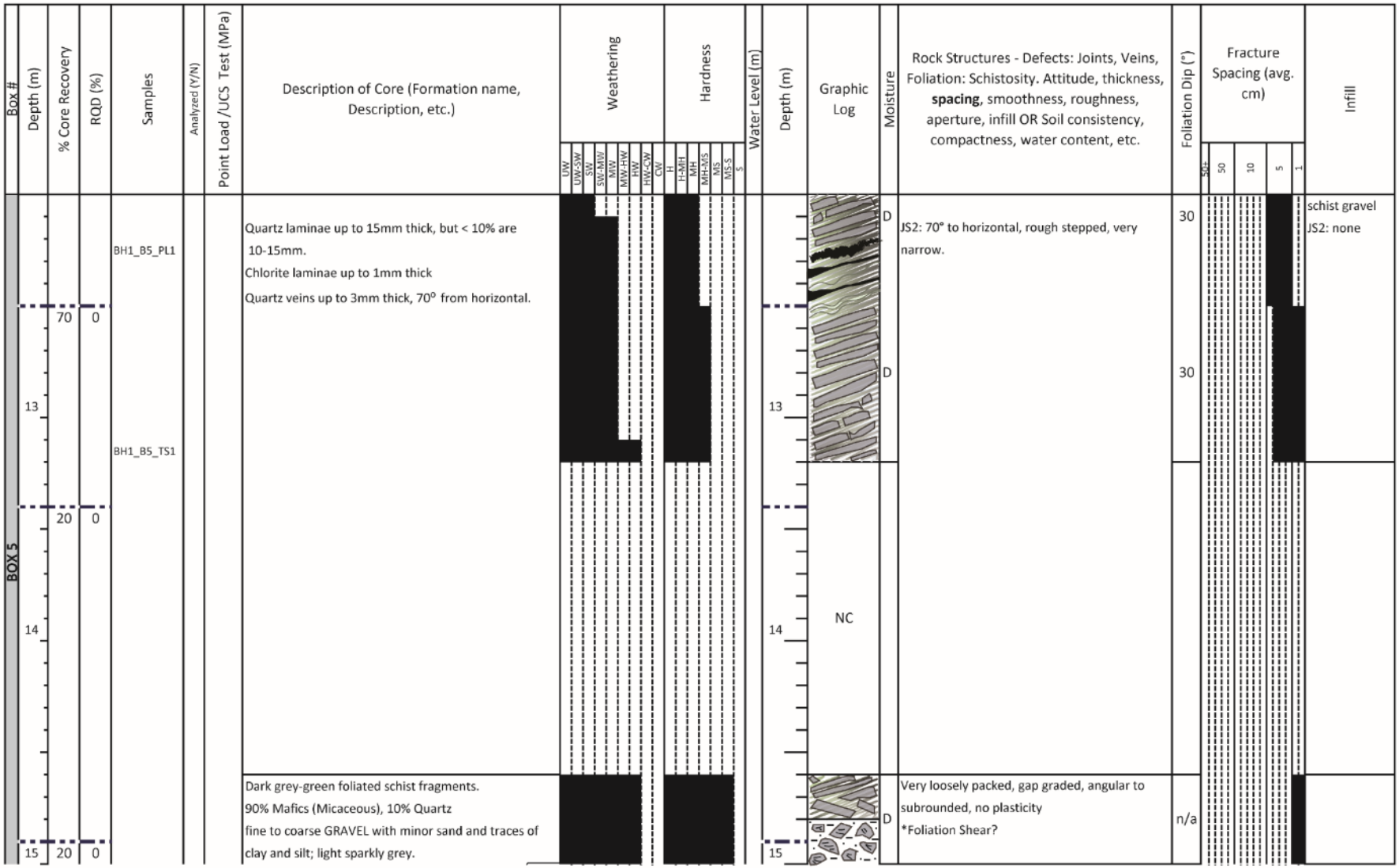
Box #
Depth (m)
% Core Recovery
RQD (%)
Samples
Analyzed (Y/N)
Point Load /UCS Test (MPa)
Description of Core (Formation name, Description, etc.)
Weathering
UW
UW-SW
SW
SW-MW
MW
MW-HW
HW
HW-CW
CW
Hardness
H
H-MH
MH
MH-MS
MS
MS-S
S
Water Level (m)
Depth (m)
Graphic Log
Moisture
Rock Structures - Defects: Joints, Veins, Foliation: Schistosity. Attitude, thickness, spacing, smoothness, roughness, aperture, infill OR Soil consistency, compactness, water content, etc.
Foliation Dip (°)
Fracture Spacing (avg. cm)
Infill
BOX 5
70
0
20
0
20
0
BH1_B5_PL1
BH1_B5_TS1
Quartz laminae up to 15mm thick, but < 10% are 10-15mm.
Chlorite laminae up to 1mm thick
Quartz veins up to 3mm thick, 70° from horizontal.
Dark grey-green foliated schist fragments.
90% Mafics (Micaceous), 10% Quartz
fine to coarse GRAVEL with minor sand and traces of clay and silt; light sparkly grey.
13
14
15
NC
D
D
D
JS2: 70° to horizontal, rough stepped, very narrow.
Very loosely packed, gap graded, angular to subrounded, no plasticity
*Foliation Shear?
30
30
n/a
schist gravel
JS2: none

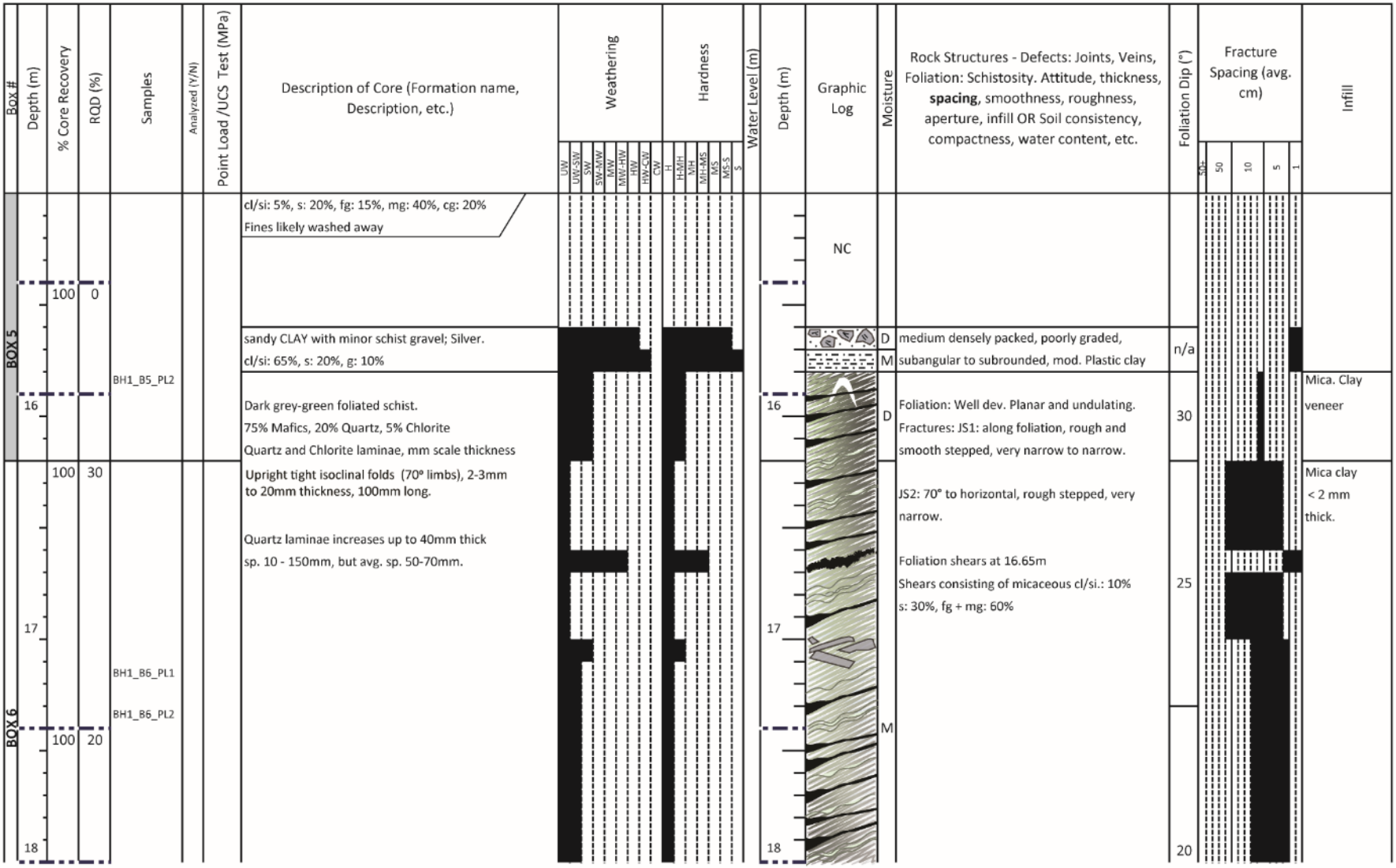
Box #
Depth (m)
% Core Recovery
RQD (%)
Samples
Analyzed (Y/N)
Point Load /UCS Test (MPa)
Description of Core (Formation name, Description, etc.)
Weathering
UW
UW-SW
SW
SW-MW
MW
MW-HW
HW
HW-CW
CW
Hardness
H
H-MH
MH
MH-MS
MS
MS-S
S
Water Level (m)
Depth (m)
Graphic Log
Moisture
Rock Structures - Defects: Joints, Veins, Foliation: Schistosity. Attitude, thickness, spacing, smoothness, roughness, aperture, infill OR Soil consistency, compactness, water content, etc.
Foliation Dip (°)
Fracture Spacing (avg. cm)
50
10
5
1
Infill
BOX 5
BOX 6
100
0
16
BH1_B5_PL2
100
30
17
BH1_B6_PL1
BH1_B6_PL2
100
20
18
cl/si: 5%, s: 20%, fg: 15%, mg: 40%, cg: 20%
Fines likely washed away
NC
sandy CLAY with minor schist gravel; Silver.
cl/si: 65%, s: 20%, g: 10%
D
M
medium densely packed, poorly graded, subangular to subrounded, mod. Plastic clay
n/a
Dark grey-green foliated schist.
75% Mafics, 20% Quartz, 5% Chlorite
Quartz and Chlorite laminae, mm scale thickness
Foliation: Well dev. Planar and undulating.
Fractures: JS1: along foliation, rough and smooth stepped, very narrow to narrow.
30
Mica. Clay veneer
Upright tight isoclinal folds (70° limbs), 2-3mm to 20mm thickness, 100mm long.
Quartz laminae increases up to 40mm thick
sp. 10 - 150mm, but avg. sp. 50-70mm.
JS2: 70° to horizontal, rough stepped, very narrow.
Foliation shears at 16.65m
Shears consisting of micaceous cl/si.: 10%
s: 30%, fg + mg: 60%
25
Mica clay < 2 mm thick.
20

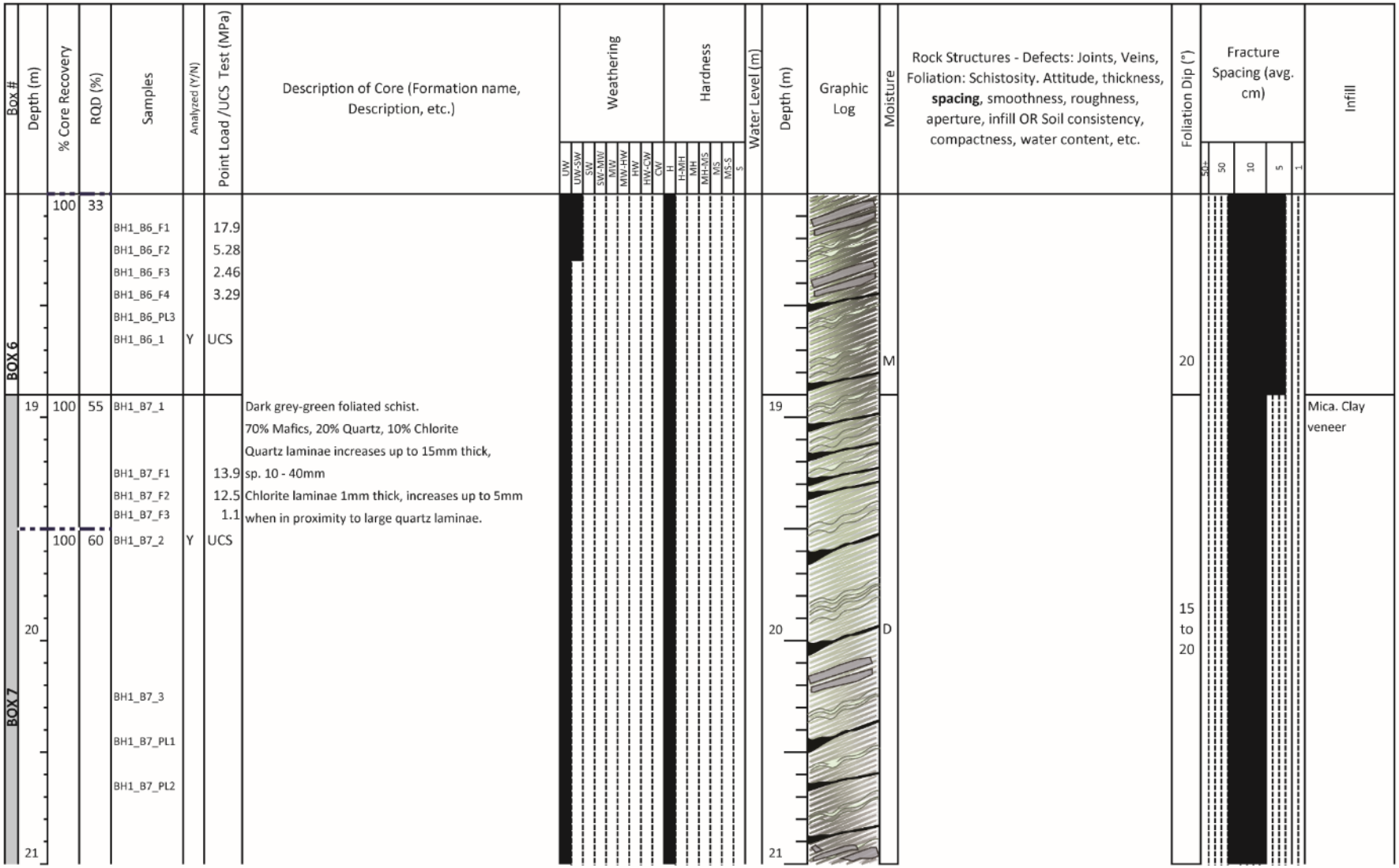
Box #
Depth (m)
% Core Recovery
RQD (%)
Samples
Analyzed (Y/N)
Point Load /UCS Test (MPa)
Description of Core (Formation name, Description, etc.)
Weathering
UW
UW-SW
SW
SW-MW
MW
MW-HW
HW
HW-CW
CW
Hardness
H
H-MH
MH
MH-MS
MS
MS-S
S
Water Level (m)
Depth (m)
Graphic Log
Moisture
Rock Structures - Defects: Joints, Veins, Foliation: Schistosity. Attitude, thickness, spacing, smoothness, roughness, aperture, infill OR Soil consistency, compactness, water content, etc.
Foliation Dip (°)
Fracture Spacing (avg. cm)
50+
50
10
5
1
Infill
BOX 6
100
33
BH1_B6_F1
17.9
BH1_B6_F2
5.28
BH1_B6_F3
2.46
BH1_B6_F4
3.29
BH1_B6_PL3
BH1_B6_1
Y
UCS
M
20
BOX 7
19
100
55
BH1_B7_1
Dark grey-green foliated schist.
70% Mafics, 20% Quartz, 10% Chlorite
Quartz laminae increases up to 15mm thick,
BH1_B7_F1
13.9
sp. 10 - 40mm
BH1_B7_F2
12.5
Chlorite laminae 1mm thick, increases up to 5mm
BH1_B7_F3
1.1
when in proximity to large quartz laminae.
Mica. Clay veneer
100
60
BH1_B7_2
Y
UCS
20
BH1_B7_3
BH1_B7_PL1
BH1_B7_PL2
21
19
20
21
D
15 to 20

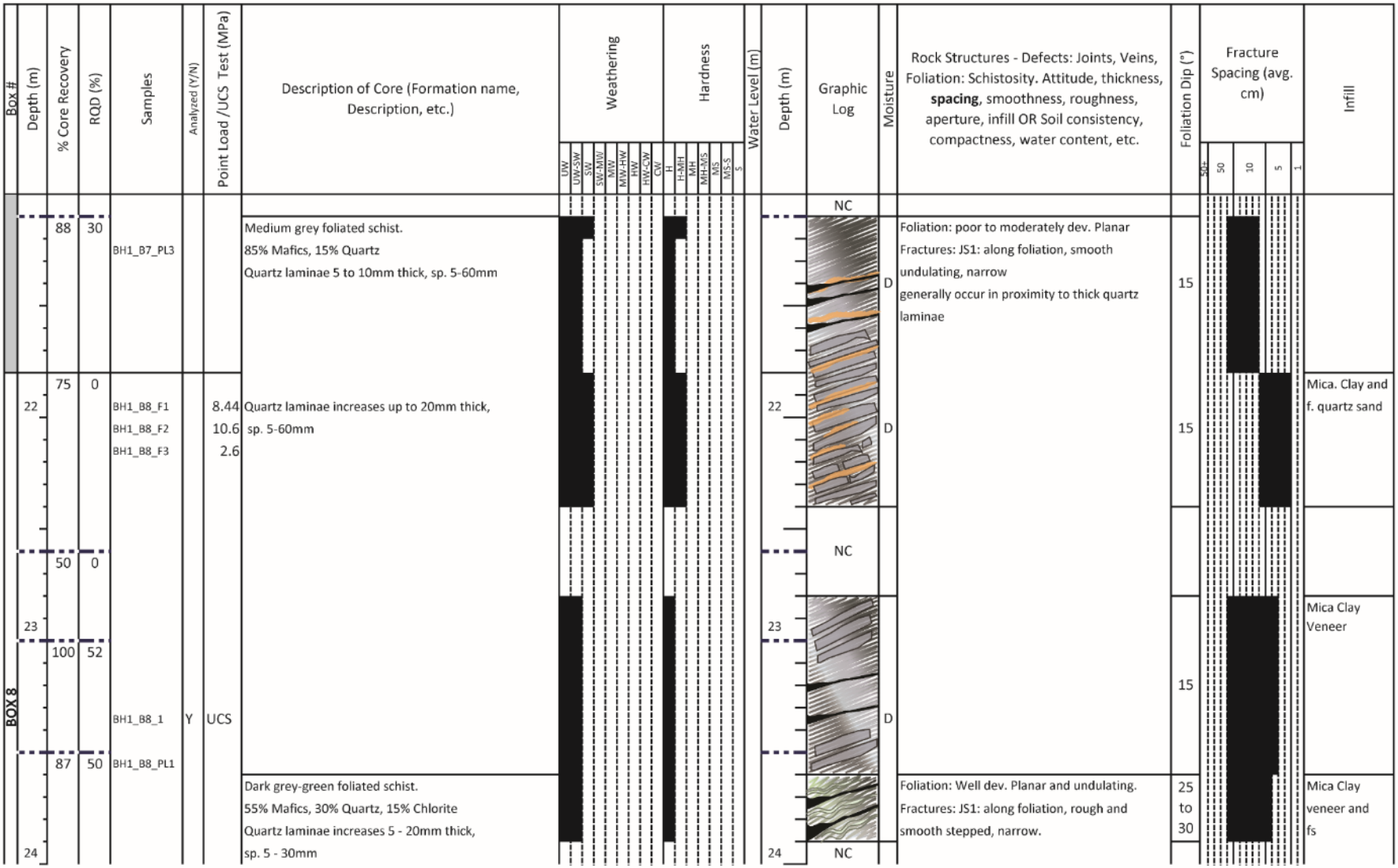
Box #
Depth (m)
% Core Recovery
RQD (%)
Samples
Analyzed (Y/N)
Point Load /UCS Test (MPa)
Description of Core (Formation name, Description, etc.)
Weathering
UW
UW-SW
SW
SW-MW
MW
MW-HW
HW
HW-CW
CW
Hardness
H
H-MH
MH
MH-MS
MS
MS-S
S
Water Level (m)
Depth (m)
Graphic Log
Moisture
Rock Structures - Defects: Joints, Veins, Foliation: Schistosity. Attitude, thickness, spacing, smoothness, roughness, aperture, infill OR Soil consistency, compactness, water content, etc.
Foliation Dip (°)
Fracture Spacing (avg. cm)
50+
50
10
5
1
Infill
BOX 8
88
30
BH1_B7_PL3
Medium grey foliated schist.
85% Mafics, 15% Quartz
Quartz laminae 5 to 10mm thick, sp. 5-60mm
NC
D
Foliation: poor to moderately dev. Planar
Fractures: JS1: along foliation, smooth undulating, narrow
generally occur in proximity to thick quartz laminae
15
75
0
22
BH1_B8_F1
BH1_B8_F2
BH1_B8_F3
8.44
10.6
2.6
Quartz laminae increases up to 20mm thick, sp. 5-60mm
22
D
15
Mica. Clay and f. quartz sand
50
0
NC
23
Mica Clay Veneer
100
52
BH1_B8_1
Y
UCS
23
D
15
87
50
BH1_B8_PL1
Dark grey-green foliated schist.
55% Mafics, 30% Quartz, 15% Chlorite
Quartz laminae increases 5 - 20mm thick, sp. 5 - 30mm
Foliation: Well dev. Planar and undulating.
Fractures: JS1: along foliation, rough and smooth stepped, narrow.
25 to 30
Mica Clay veneer and fs
24
24
NC

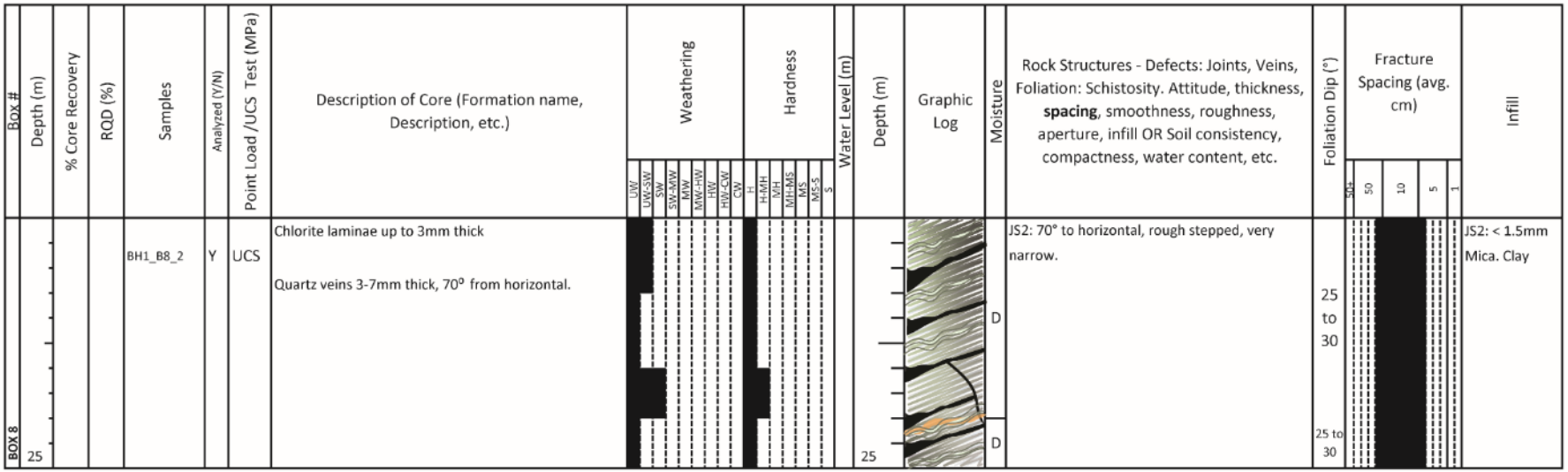

Legend

UW-MW, foliated dark grey-green SCHIST; strong; foliation dips 15-30° to horizontal, well developed, planar and undulating. Joints are steep to sub-vertically inclined and moderately wide spaced. [Mapped as Caples Terrane, Textural Zone 3 Schist]

UW-MW, foliated medium grey SCHIST; strong; foliation dips 15-25° to horizontal, poorly to moderately developed, planar. Joints are steep to sub-vertically inclined and moderately wide spaced. [Mapped as Caples Terrane, Textural Zone 3 Schist]

Clayey SILT with vf sand and rootlets; orange-brown.

Fine to coarse GRAVEL schist fragments with minor sand and traces of clay and silt; light sparkly grey.

sandy CLAY with traces of schist gravel; silver.

Cobble sized schist fragments

Coarse Gravel sized schist fragments

Gravels

Sand

Clay/Silt

Fracture or Joint

Iron Staining/ Weathering

Foliation Shear

Upright tight isoclinal folds (70° limbs)

Weathering
UW: Unweathered
SW: Slightly Weathered
MW: Moderately Weathered
HW: Highly Weathered
CW: Completely Weathered

Hardness
H: Hard
MH: Moderately Hard
MS: Moderately Soft
S: Soft

Moisture
D: Dry
M: Moist
W: Wet

Grain Size
cl/si: Clay/Silt
vfs: Very fine sand
fs: Fine sand
ms: Medium sand
cs: Coarse sand
s: Sand
fg: Fine gravel
mg: Medium gravel
cg: Coarse gravel
g: Gravel
cb: Cobble

NC Core loss/No Recovery

A.3.2 Borehole 2

Geotechnical Borehole Log

Project: Queenstown Hill Landslide - GCL
Borehole No.: BH2
Box No.: 1 to 8
Sheet No.: 1 to 10

Address: Middleton Block - Goldfield Heights
Coordinates: 1261164.975, 5005835.904
Drilling Method: Rotary drilling

Logged by: Laura Gnesko
Date Logged: 30/04/2019
Coordinate System: NZTM2000
Direction: Vertical

Core diameter: 63mm

Meterage: 0.0 to 26.5m
Elevation: 427.832m (a.s.l)

Date Drilled: 17/04/2019
Angle from Horizontal: 90°

Comments:

Box 1:	0.0 to 4.0m	Can point load this box, if needed.
Box 2:	4.2 to 7.4m	Prev. box ended at 4.0m unsure what happened. Recorded as core loss on the log (blank) but need to check drillers log. More samples available to be tested in this box Remaining samples can be point loaded as lumps. Possible change in lithology at the 6.0m mark. From 6.0 to 7.25m poorly developed foliations noted, and more mafics/mica.
Box 3:	7.4 to 11.2m	0.1m of core loss indicated at 8.8m . Additional point load samples available in this box, if needed.
Box 4:	11.2 to 15.2m	The assumption was made that all schist fragments in this box are derived from the schist described in previous and subsequent boxes. A lot of core loss indicated in this box. Markers in box are 1) 11.2m 2) 0.1m core loss 3) 12.0m 4) 0.6m core loss 5) 13.0m 6) 0.6m core loss 7) 14.0m 8) 14.5m 9) 300 core loss 10)15.0m **11.2m marker was not placed at the start of the box - this is a mystery - need to check drillers log. Drillers mud: 11 -12m (4-5cm of drillers mud moved to side), 12-13m (5cm of drillers mud moved to side), 13-14m (9cm of drillers mud moved to the side) A mystery section (from beginning of box to 11.2 marker) is logged here separately as 0.2m very dark grey foliated schist. Mod well dev. Foliations at 50°. One 5cm coherent piece in the section and the rest is sand, clay and gravel sized quartz. Fractures in the coherent piece are along foliation. Sample is moist, and there are approximately 35% dark schist pieces.
Box 5:	15.2 to 17.8m	Core loss and drillers mud present in box. As marked in box. 1) 15.2m 2) Core loss 0.1m 3)15.6m (Drillers mud) 4) 15.8m (Drillers Mud) 5) 16.2m 6) 17.1m (Drillers Mud)
Box 6:	17.8 to 12.2m	
Box 7:	21.2 to 24.5m	Core loss indicated. Markers in box - 1) 0.1m Core loss (marker washed off - need to confirm with drillers log) 2) 22.5m 3) 0.1m Core loss (check log, marker is bleeding) 4) 24.0m Can point load this box, if needed.
Box 8:	24.5 to 26.5m	Box was poorly packaged. A lot of broken core and last bit no longer in order. This box can be point loaded on site, if needed.

Page 1 of 10

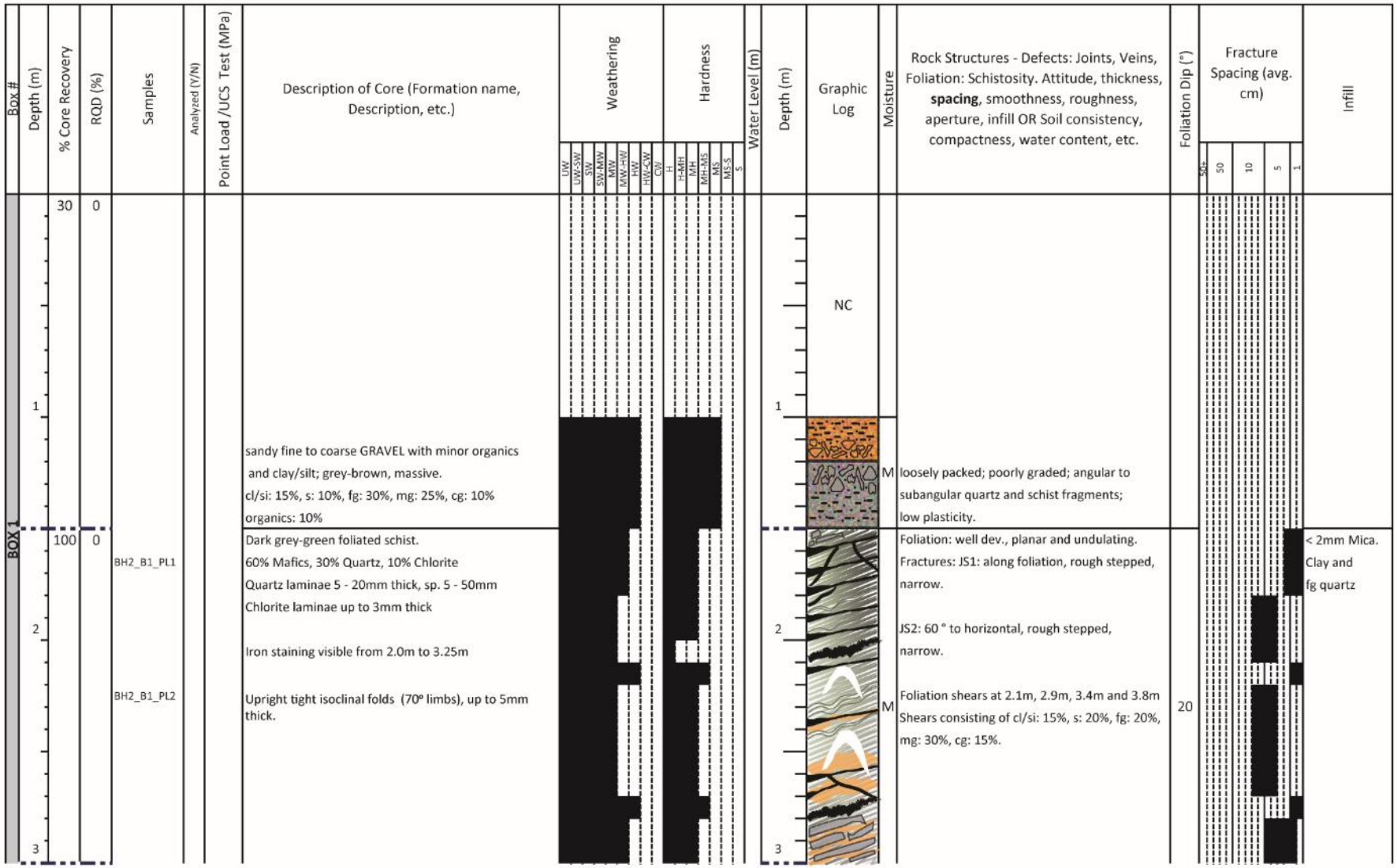
Box #
Depth (m)
% Core Recovery
RQD (%)
Samples
Analyzed (Y/N)
Point Load /UCS Test (MPa)
Description of Core (Formation name, Description, etc.)
Weathering
UW
UW-SW
SW
SW-MW
MW
MW-HW
HW
HW-CW
CW
Hardness
H
H-MH
MH
MH-MS
MS
MS-S
S
Water Level (m)
Depth (m)
Graphic Log
Moisture
Rock Structures - Defects: Joints, Veins, Foliation: Schistosity. Attitude, thickness, spacing, smoothness, roughness, aperture, infill OR Soil consistency, compactness, water content, etc.
Foliation Dip (°)
Fracture Spacing (avg. cm)
50+
50
10
5
1
Infill
BOX 1
30
0
100
0
BH2_B1_PL1
BH2_B1_PL2
NC
M
M
1
2
3
sandy fine to coarse GRAVEL with minor organics and clay/silt; grey-brown, massive.
cl/si: 15%, s: 10%, fg: 30%, mg: 25%, cg: 10%
organics: 10%
loosely packed; poorly graded; angular to subangular quartz and schist fragments; low plasticity.
Dark grey-green foliated schist.
60% Mafics, 30% Quartz, 10% Chlorite
Quartz laminae 5 - 20mm thick, sp. 5 - 50mm
Chlorite laminae up to 3mm thick
Iron staining visible from 2.0m to 3.25m
Upright tight isoclinal folds (70° limbs), up to 5mm thick.
Foliation: well dev., planar and undulating.
Fractures: JS1: along foliation, rough stepped, narrow.
JS2: 60 ° to horizontal, rough stepped, narrow.
Foliation shears at 2.1m, 2.9m, 3.4m and 3.8m
Shears consisting of cl/si: 15%, s: 20%, fg: 20%, mg: 30%, cg: 15%.
20
< 2mm Mica. Clay and fg quartz

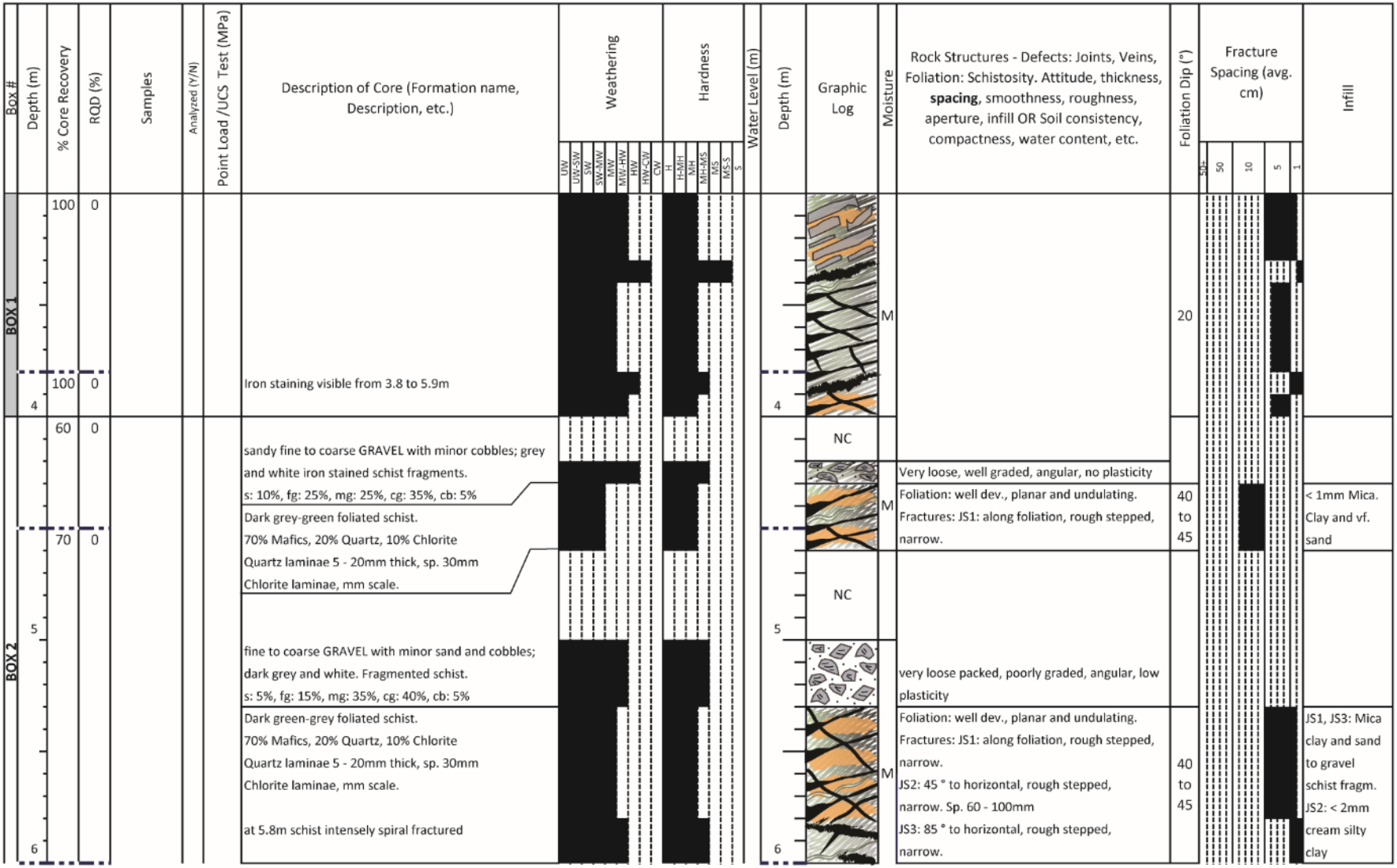
Box #
Depth (m)
% Core Recovery
RQD (%)
Samples
Analyzed (Y/N)
Point Load /UCS Test (MPa)
Description of Core (Formation name, Description, etc.)
Weathering
UW
UW-SW
SW
SW-MW
MW
MW-HW
HW
HW-CW
CW
Hardness
H
H-MH
MH
MH-MS
MS
MS-S
S
Water Level (m)
Depth (m)
Graphic Log
Moisture
Rock Structures - Defects: Joints, Veins, Foliation: Schistosity. Attitude, thickness, spacing, smoothness, roughness, aperture, infill OR Soil consistency, compactness, water content, etc.
Foliation Dip (°)
Fracture Spacing (avg. cm)
50+
50
10
5
1
Infill
BOX 1
100
0
100
0
4
Iron staining visible from 3.8 to 5.9m
M
20
BOX 2
60
0
sandy fine to coarse GRAVEL with minor cobbles; grey and white iron stained schist fragments.
s: 10%, fg: 25%, mg: 25%, cg: 35%, cb: 5%
Dark grey-green foliated schist.
70% Mafics, 20% Quartz, 10% Chlorite
Quartz laminae 5 - 20mm thick, sp. 30mm
Chlorite laminae, mm scale.
NC
Very loose, well graded, angular, no plasticity
Foliation: well dev., planar and undulating.
Fractures: JS1: along foliation, rough stepped, narrow.
M
40 to 45
< 1mm Mica. Clay and vf. sand
70
0
5
NC
fine to coarse GRAVEL with minor sand and cobbles; dark grey and white. Fragmented schist.
s: 5%, fg: 15%, mg: 35%, cg: 40%, cb: 5%
very loose packed, poorly graded, angular, low plasticity
Dark green-grey foliated schist.
70% Mafics, 20% Quartz, 10% Chlorite
Quartz laminae 5 - 20mm thick, sp. 30mm
Chlorite laminae, mm scale.
at 5.8m schist intensely spiral fractured
Foliation: well dev., planar and undulating.
Fractures: JS1: along foliation, rough stepped, narrow.
JS2: 45 ° to horizontal, rough stepped, narrow. Sp. 60 - 100mm
JS3: 85 ° to horizontal, rough stepped, narrow.
M
40 to 45
JS1, JS3: Mica clay and sand to gravel schist fragm.
JS2: < 2mm cream silty clay
6

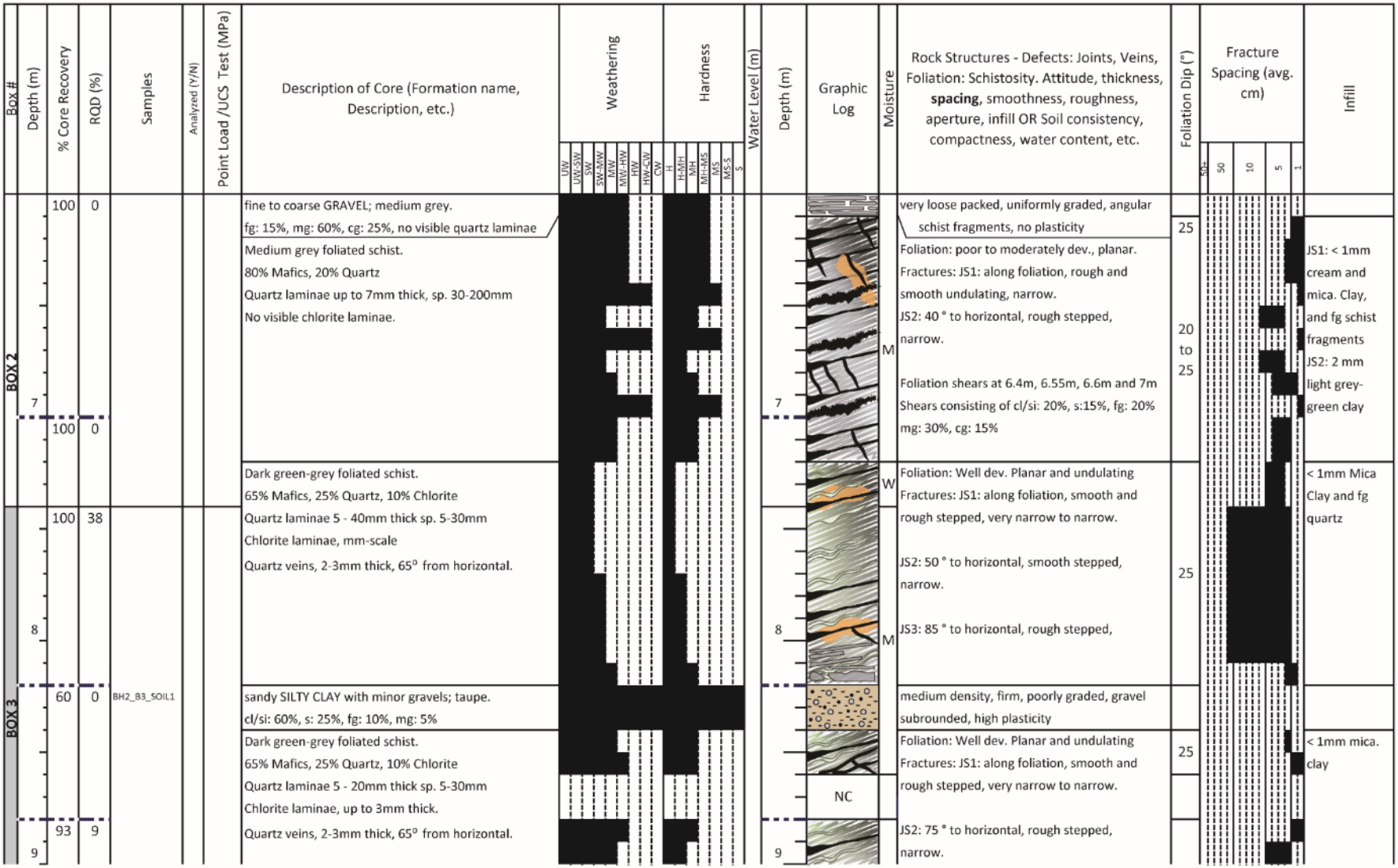
Box #
Depth (m)
% Core Recovery
RQD (%)
Samples
Analyzed (Y/N)
Point Load /UCS Test (MPa)
Description of Core (Formation name, Description, etc.)
Weathering
UW
UW-SW
SW
SW-MW
MW
MW-HW
HW
HW-CW
CW
Hardness
H
H-MH
MH
MH-MS
MS
MS-S
S
Water Level (m)
Depth (m)
Graphic Log
Moisture
Rock Structures - Defects: Joints, Veins, Foliation: Schistosity. Attitude, thickness, spacing, smoothness, roughness, aperture, infill OR Soil consistency, compactness, water content, etc.
Foliation Dip (°)
Fracture Spacing (avg. cm)
50
10
5
1
Infill
BOX 2
BOX 3
100
0
fine to coarse GRAVEL; medium grey.
fg: 15%, mg: 60%, cg: 25%, no visible quartz laminae
very loose packed, uniformly graded, angular schist fragments, no plasticity
25
7
Medium grey foliated schist.
80% Mafics, 20% Quartz
Quartz laminae up to 7mm thick, sp. 30-200mm
No visible chlorite laminae.
Foliation: poor to moderately dev., planar.
Fractures: JS1: along foliation, rough and smooth undulating, narrow.
JS2: 40 ° to horizontal, rough stepped, narrow.
M
20 to 25
Foliation shears at 6.4m, 6.55m, 6.6m and 7m
Shears consisting of cl/si: 20%, s:15%, fg: 20% mg: 30%, cg: 15%
JS1: < 1mm cream and mica. Clay, and fg schist fragments
JS2: 2 mm light grey-green clay
100
0
Dark green-grey foliated schist.
65% Mafics, 25% Quartz, 10% Chlorite
Quartz laminae 5 - 40mm thick sp. 5-30mm
Chlorite laminae, mm-scale
Quartz veins, 2-3mm thick, 65° from horizontal.
W
Foliation: Well dev. Planar and undulating
Fractures: JS1: along foliation, smooth and rough stepped, very narrow to narrow.
JS2: 50 ° to horizontal, smooth stepped, narrow.
JS3: 85 ° to horizontal, rough stepped,
25
< 1mm Mica Clay and fg quartz
100
38
8
M
60
0
BH2_B3_SOIL1
sandy SILTY CLAY with minor gravels; taupe.
cl/si: 60%, s: 25%, fg: 10%, mg: 5%
medium density, firm, poorly graded, gravel subrounded, high plasticity
Dark green-grey foliated schist.
65% Mafics, 25% Quartz, 10% Chlorite
Quartz laminae 5 - 20mm thick sp. 5-30mm
Chlorite laminae, up to 3mm thick.
Quartz veins, 2-3mm thick, 65° from horizontal.
Foliation: Well dev. Planar and undulating
Fractures: JS1: along foliation, smooth and rough stepped, very narrow to narrow.
25
< 1mm mica. clay
NC
93
9
9
JS2: 75 ° to horizontal, rough stepped, narrow.

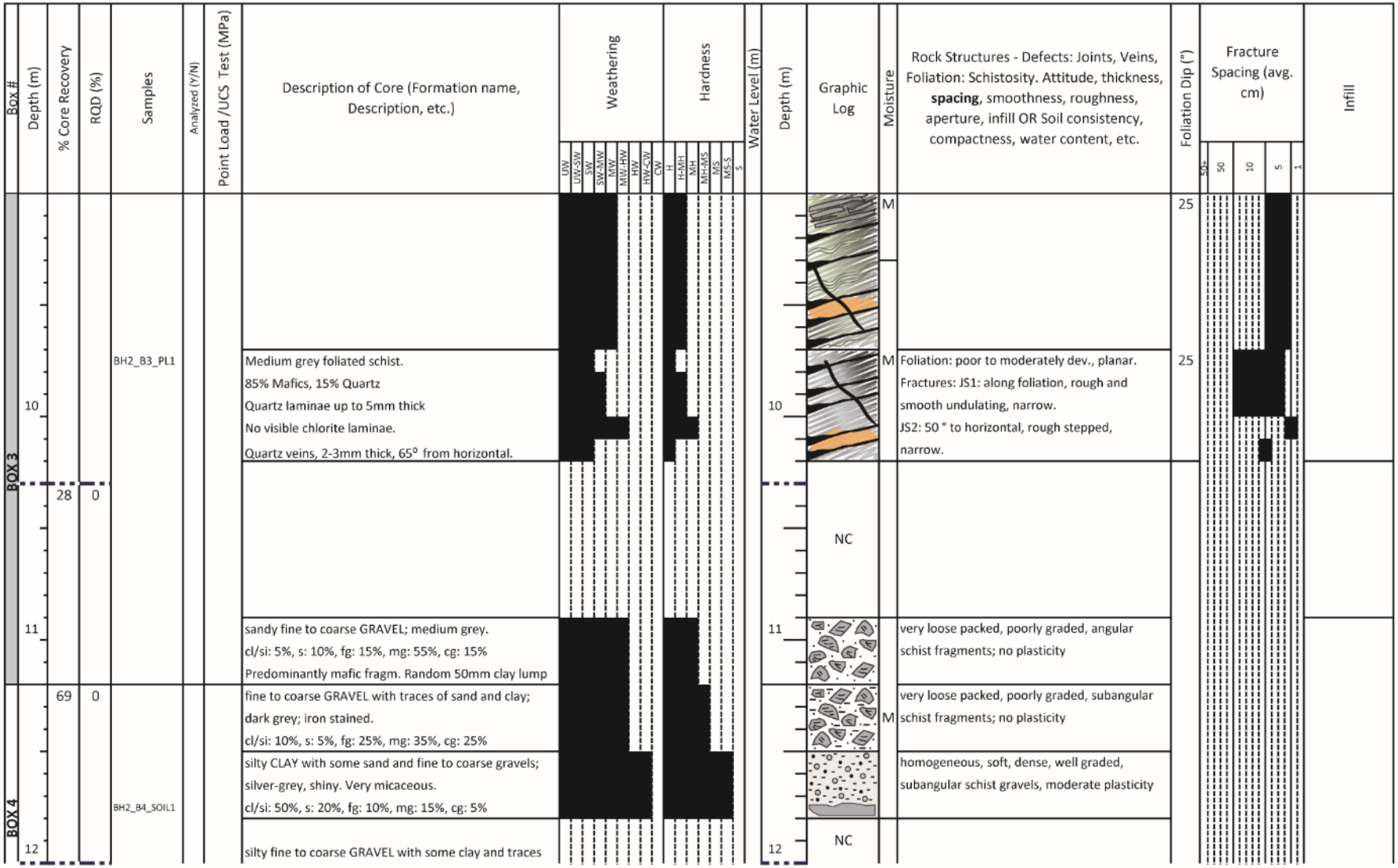
Box #
Depth (m)
% Core Recovery
RQD (%)
Samples
Analyzed (Y/N)
Point Load /UCS Test (MPa)
Description of Core (Formation name, Description, etc.)
Weathering
UW
UW-SW
SW
SW-MW
MW
MW-HW
HW
HW-CW
CW
Hardness
H
H-MH
MH
MH-MS
MS
MS-S
S
Water Level (m)
Depth (m)
Graphic Log
Moisture
Rock Structures - Defects: Joints, Veins, Foliation: Schistosity. Attitude, thickness, spacing, smoothness, roughness, aperture, infill OR Soil consistency, compactness, water content, etc.
Foliation Dip (°)
Fracture Spacing (avg. cm)
50+
50
10
5
1
Infill
BOX 3
BOX 4
10
11
12
28
0
69
0
BH2_B3_PL1
BH2_B4_SOIL1
Medium grey foliated schist.
85% Mafics, 15% Quartz
Quartz laminae up to 5mm thick
No visible chlorite laminae.
Quartz veins, 2-3mm thick, 65° from horizontal.
sandy fine to coarse GRAVEL; medium grey.
cl/si: 5%, s: 10%, fg: 15%, mg: 55%, cg: 15%
Predominantly mafic fragm. Random 50mm clay lump
fine to coarse GRAVEL with traces of sand and clay;
dark grey; iron stained.
cl/si: 10%, s: 5%, fg: 25%, mg: 35%, cg: 25%
silty CLAY with some sand and fine to coarse gravels;
silver-grey, shiny. Very micaceous.
cl/si: 50%, s: 20%, fg: 10%, mg: 15%, cg: 5%
silty fine to coarse GRAVEL with some clay and traces
M
M
NC
M
NC
Foliation: poor to moderately dev., planar.
Fractures: JS1: along foliation, rough and smooth undulating, narrow.
JS2: 50 ° to horizontal, rough stepped, narrow.
very loose packed, poorly graded, angular schist fragments; no plasticity
very loose packed, poorly graded, subangular schist fragments; no plasticity
homogeneous, soft, dense, well graded, subangular schist gravels, moderate plasticity
25
25

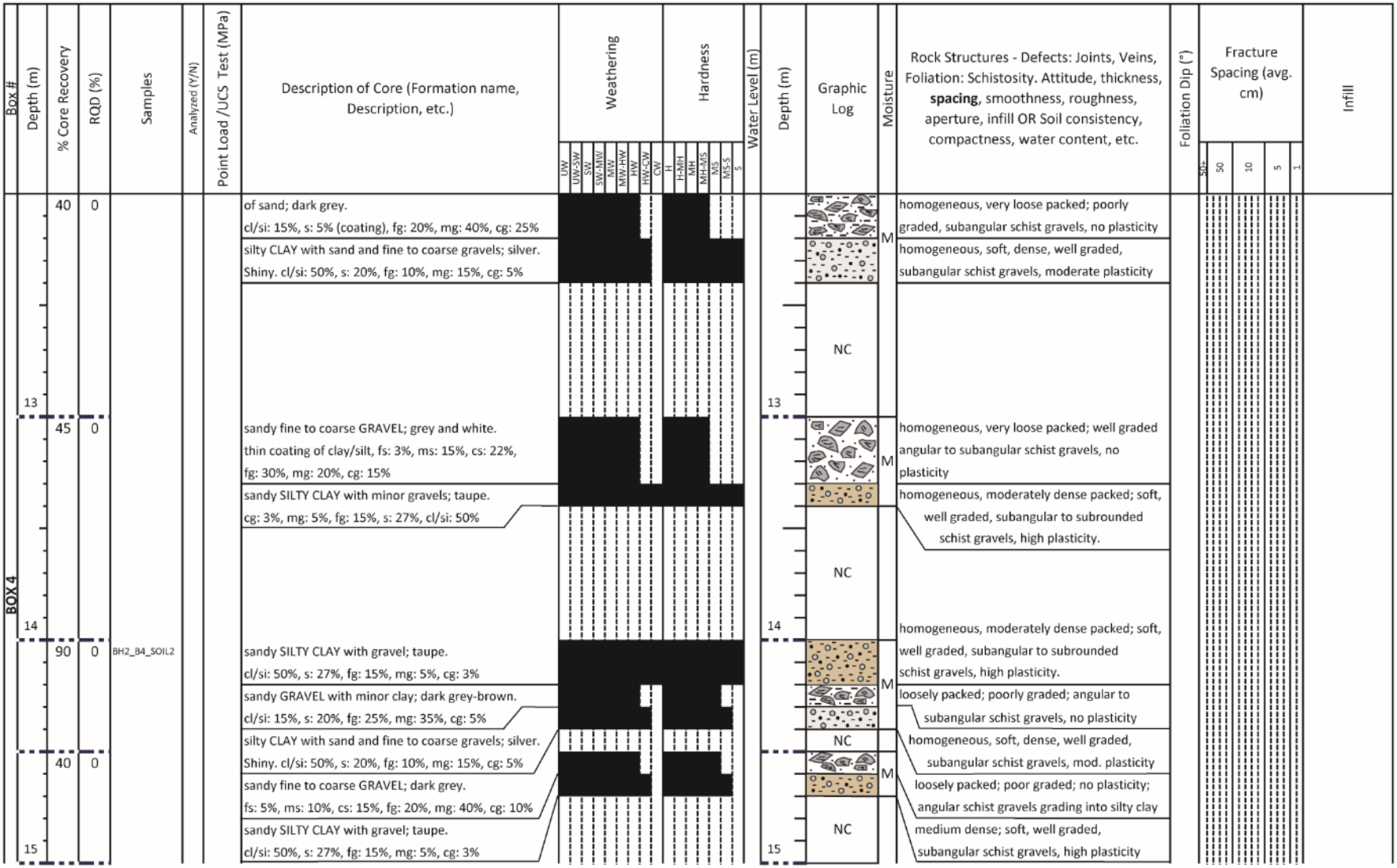
Box #
Depth (m)
% Core Recovery
RQD (%)
Samples
Analyzed (Y/N)
Point Load /UCS Test (MPa)
Description of Core (Formation name, Description, etc.)
Weathering
UW
UW-SW
SW
SW-MW
MW
MW-HW
HW
HW-CW
CW
Hardness
H
H-MH
MH
MH-MS
MS
MS-S
S
Water Level (m)
Depth (m)
Graphic Log
Moisture
Rock Structures - Defects: Joints, Veins, Foliation: Schistosity. Attitude, thickness, spacing, smoothness, roughness, aperture, infill OR Soil consistency, compactness, water content, etc.
Foliation Dip (°)
Fracture Spacing (avg. cm)
50+
50
10
5
1
Infill
BOX 4
40
0
of sand; dark grey.
cl/si: 15%, s: 5% (coating), fg: 20%, mg: 40%, cg: 25%
homogeneous, very loose packed; poorly graded, subangular schist gravels, no plasticity
silty CLAY with sand and fine to coarse gravels; silver.
Shiny. cl/si: 50%, s: 20%, fg: 10%, mg: 15%, cg: 5%
M
homogeneous, soft, dense, well graded, subangular schist gravels, moderate plasticity
NC
13
13
45
0
sandy fine to coarse GRAVEL; grey and white.
thin coating of clay/silt, fs: 3%, ms: 15%, cs: 22%,
fg: 30%, mg: 20%, cg: 15%
M
homogeneous, very loose packed; well graded angular to subangular schist gravels, no plasticity
sandy SILTY CLAY with minor gravels; taupe.
cg: 3%, mg: 5%, fg: 15%, s: 27%, cl/si: 50%
homogeneous, moderately dense packed; soft, well graded, subangular to subrounded schist gravels, high plasticity.
NC
14
14
homogeneous, moderately dense packed; soft, well graded, subangular to subrounded schist gravels, high plasticity.
90
0
BH2_B4_SOIL2
sandy SILTY CLAY with gravel; taupe.
cl/si: 50%, s: 27%, fg: 15%, mg: 5%, cg: 3%
M
sandy GRAVEL with minor clay; dark grey-brown.
cl/si: 15%, s: 20%, fg: 25%, mg: 35%, cg: 5%
loosely packed; poorly graded; angular to subangular schist gravels, no plasticity
silty CLAY with sand and fine to coarse gravels; silver.
Shiny. cl/si: 50%, s: 20%, fg: 10%, mg: 15%, cg: 5%
NC
homogeneous, soft, dense, well graded, subangular schist gravels, mod. plasticity
40
0
M
sandy fine to coarse GRAVEL; dark grey.
fs: 5%, ms: 10%, cs: 15%, fg: 20%, mg: 40%, cg: 10%
loosely packed; poor graded; no plasticity; angular schist gravels grading into silty clay
sandy SILTY CLAY with gravel; taupe.
cl/si: 50%, s: 27%, fg: 15%, mg: 5%, cg: 3%
NC
medium dense; soft, well graded, subangular schist gravels, high plasticity
15
15

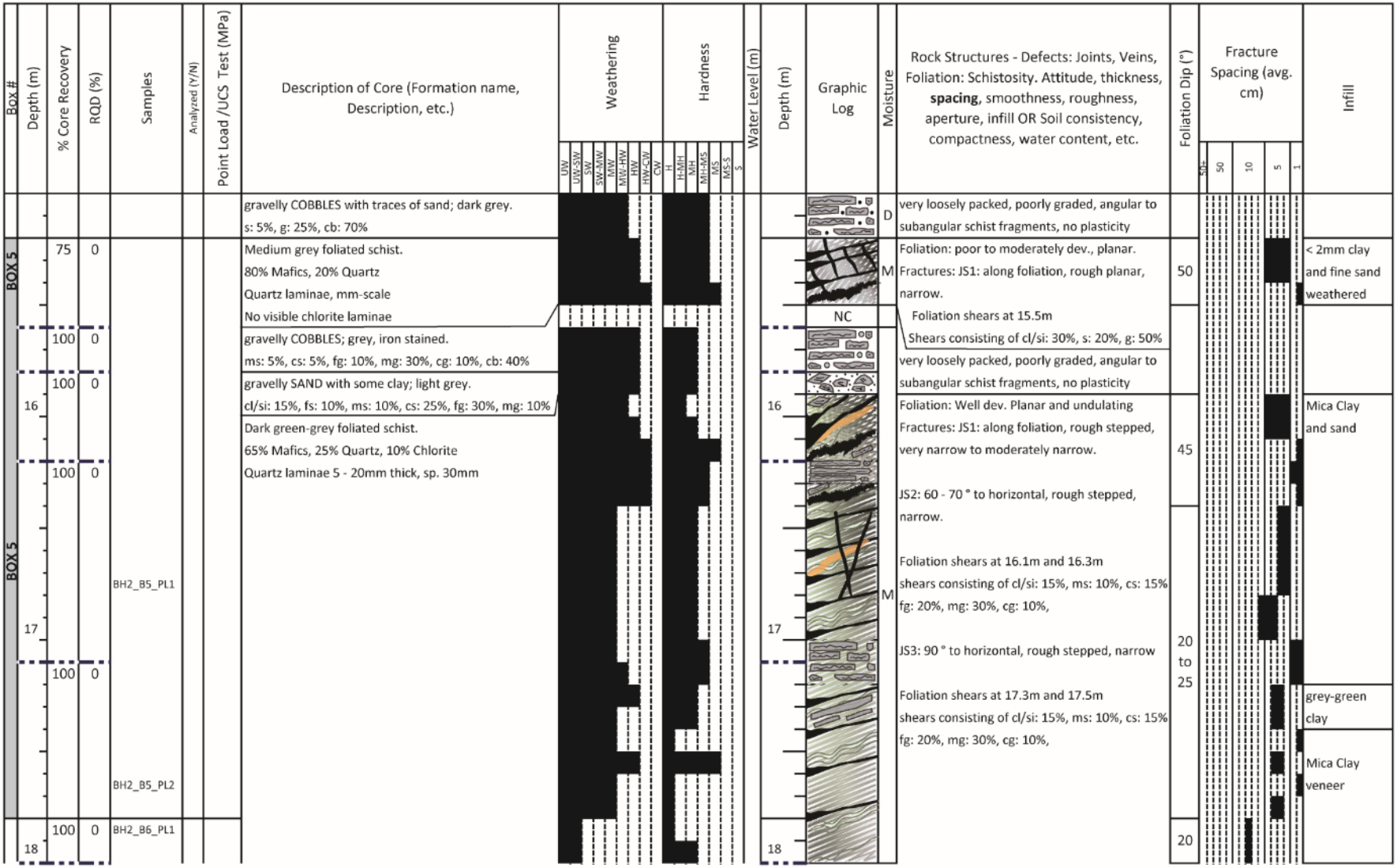
Box #
Depth (m)
% Core Recovery
RQD (%)
Samples
Analyzed (Y/N)
Point Load /UCS Test (MPa)
Description of Core (Formation name, Description, etc.)
Weathering
UW
UW-SW
SW
SW-MW
MW
MW-HW
HW
HW-CW
CW
Hardness
H
H-MH
MH
MH-MS
MS
MS-S
S
Water Level (m)
Depth (m)
Graphic Log
Moisture
Rock Structures - Defects: Joints, Veins, Foliation: Schistosity. Attitude, thickness, spacing, smoothness, roughness, aperture, infill OR Soil consistency, compactness, water content, etc.
Foliation Dip (°)
Fracture Spacing (avg. cm)
50+
50
10
5
1
Infill
gravelly COBBLES with traces of sand; dark grey.
s: 5%, g: 25%, cb: 70%
D
very loosely packed, poorly graded, angular to subangular schist fragments, no plasticity
BOX 5
75
0
Medium grey foliated schist.
80% Mafics, 20% Quartz
Quartz laminae, mm-scale
No visible chlorite laminae
M
Foliation: poor to moderately dev., planar.
Fractures: JS1: along foliation, rough planar, narrow.
50
< 2mm clay and fine sand weathered
NC
Foliation shears at 15.5m
Shears consisting of cl/si: 30%, s: 20%, g: 50%
100
0
gravelly COBBLES; grey, iron stained.
ms: 5%, cs: 5%, fg: 10%, mg: 30%, cg: 10%, cb: 40%
very loosely packed, poorly graded, angular to subangular schist fragments, no plasticity
100
0
gravelly SAND with some clay; light grey.
cl/si: 15%, fs: 10%, ms: 10%, cs: 25%, fg: 30%, mg: 10%
16
16
Foliation: Well dev. Planar and undulating
Fractures: JS1: along foliation, rough stepped, very narrow to moderately narrow.
45
Mica Clay and sand
Dark green-grey foliated schist.
65% Mafics, 25% Quartz, 10% Chlorite
Quartz laminae 5 - 20mm thick, sp. 30mm
100
0
JS2: 60 - 70 ° to horizontal, rough stepped, narrow.
Foliation shears at 16.1m and 16.3m
shears consisting of cl/si: 15%, ms: 10%, cs: 15%
fg: 20%, mg: 30%, cg: 10%,
BOX 5
BH2_B5_PL1
M
17
17
JS3: 90 ° to horizontal, rough stepped, narrow
20 to 25
100
0
Foliation shears at 17.3m and 17.5m
shears consisting of cl/si: 15%, ms: 10%, cs: 15%
fg: 20%, mg: 30%, cg: 10%,
grey-green clay
Mica Clay veneer
BH2_B5_PL2
100
0
BH2_B6_PL1
18
18
20

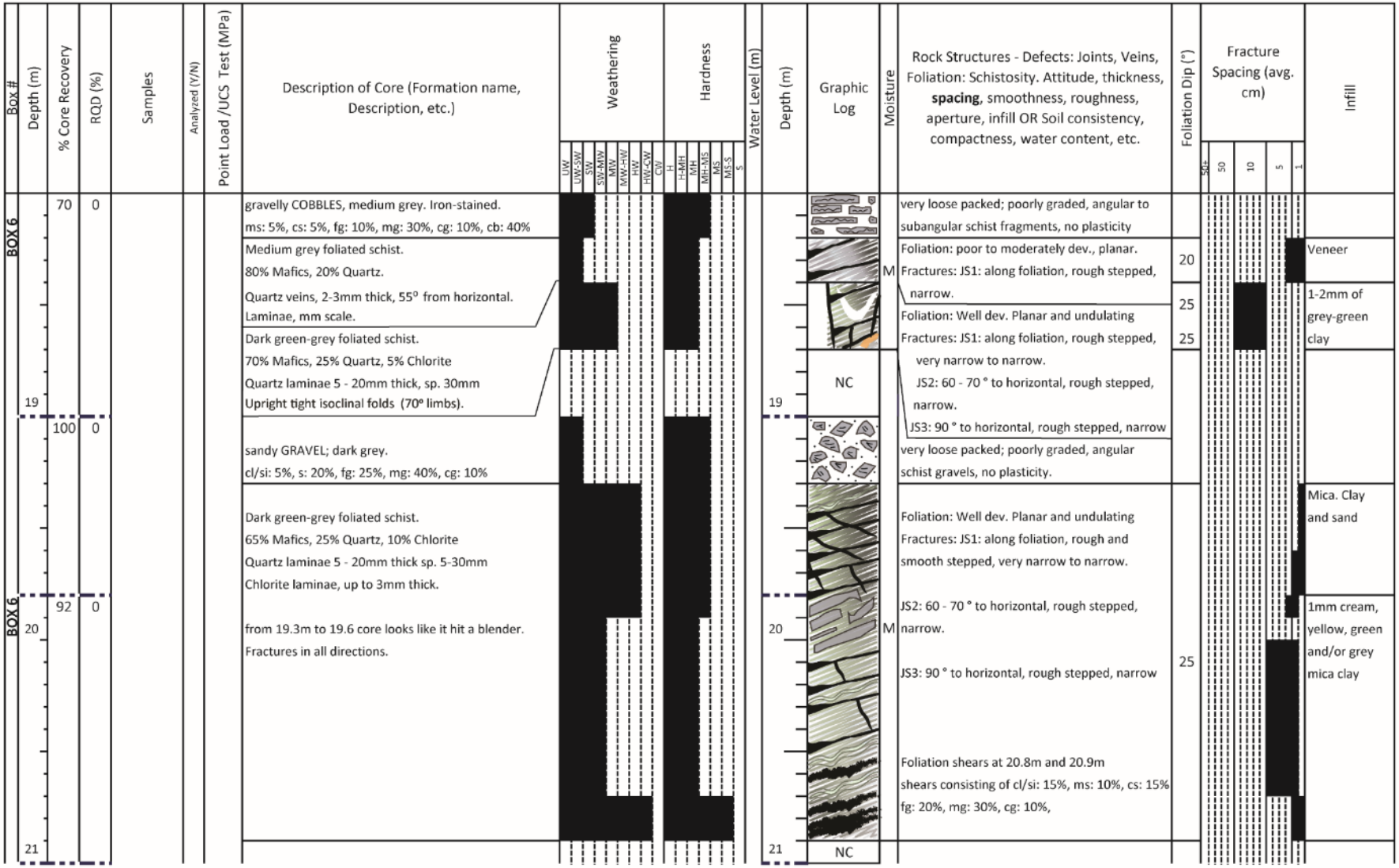
Box #
Depth (m)
% Core Recovery
RQD (%)
Samples
Analyzed (Y/N)
Point Load /UCS Test (MPa)
Description of Core (Formation name, Description, etc.)
Weathering
UW
UW-SW
SW
SW-MW
MW
MW-HW
HW
HW-CW
CW
Hardness
H
H-MH
MH
MH-MS
MS
MS-S
S
Water Level (m)
Depth (m)
Graphic Log
Moisture
Rock Structures - Defects: Joints, Veins, Foliation: Schistosity. Attitude, thickness, spacing, smoothness, roughness, aperture, infill OR Soil consistency, compactness, water content, etc.
Foliation Dip (°)
Fracture Spacing (avg. cm)
50
10
5
1
Infill
BOX 6
70
0
gravelly COBBLES, medium grey. Iron-stained.
ms: 5%, cs: 5%, fg: 10%, mg: 30%, cg: 10%, cb: 40%
very loose packed; poorly graded, angular to subangular schist fragments, no plasticity
Medium grey foliated schist.
80% Mafics, 20% Quartz.
Quartz veins, 2-3mm thick, 55° from horizontal.
Laminae, mm scale.
Foliation: poor to moderately dev., planar.
Fractures: JS1: along foliation, rough stepped, narrow.
M
20
Veneer
25
1-2mm of grey-green clay
Dark green-grey foliated schist.
70% Mafics, 25% Quartz, 5% Chlorite
Quartz laminae 5 - 20mm thick, sp. 30mm
Upright tight isoclinal folds (70° limbs).
Foliation: Well dev. Planar and undulating
Fractures: JS1: along foliation, rough stepped, very narrow to narrow.
JS2: 60 - 70 ° to horizontal, rough stepped, narrow.
JS3: 90 ° to horizontal, rough stepped, narrow
25
19
NC
19
100
0
sandy GRAVEL; dark grey.
cl/si: 5%, s: 20%, fg: 25%, mg: 40%, cg: 10%
very loose packed; poorly graded, angular schist gravels, no plasticity.
Dark green-grey foliated schist.
65% Mafics, 25% Quartz, 10% Chlorite
Quartz laminae 5 - 20mm thick sp. 5-30mm
Chlorite laminae, up to 3mm thick.
Foliation: Well dev. Planar and undulating
Fractures: JS1: along foliation, rough and smooth stepped, very narrow to narrow.
Mica. Clay and sand
BOX 6
92
0
from 19.3m to 19.6 core looks like it hit a blender.
Fractures in all directions.
JS2: 60 - 70 ° to horizontal, rough stepped, narrow.
JS3: 90 ° to horizontal, rough stepped, narrow
Foliation shears at 20.8m and 20.9m
shears consisting of cl/si: 15%, ms: 10%, cs: 15%
fg: 20%, mg: 30%, cg: 10%,
M
20
20
25
1mm cream, yellow, green and/or grey mica clay
21
NC
21

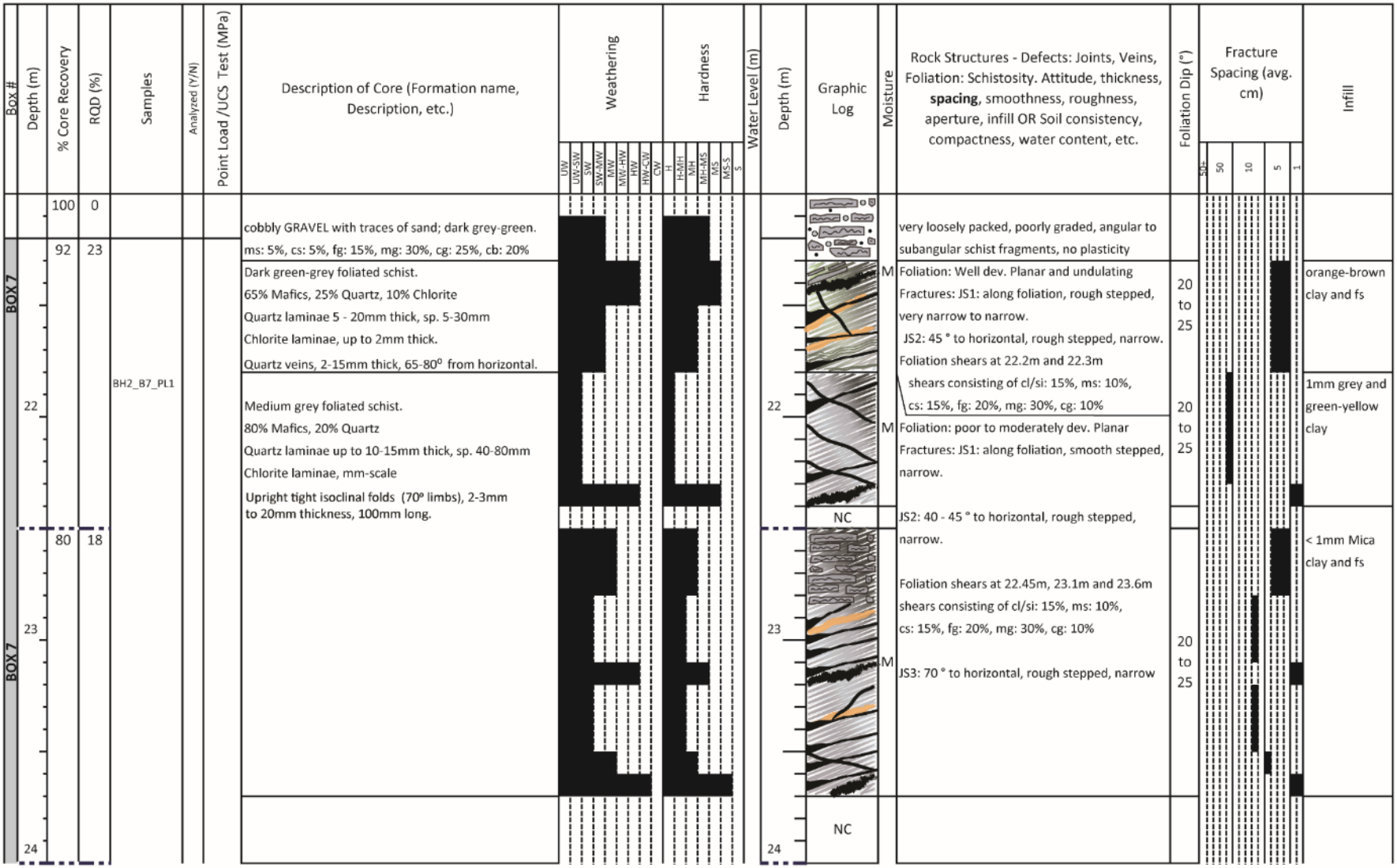
Box #
Depth (m)
% Core Recovery
RQD (%)
Samples
Analyzed (Y/N)
Point Load /UCS Test (MPa)
Description of Core (Formation name, Description, etc.)
Weathering
UW
UW-SW
SW
SW-MW
MW
MW-HW
HW
HW-CW
CW
Hardness
H
H-MH
MH
MH-MS
MS
MS-S
S
Water Level (m)
Depth (m)
Graphic Log
Moisture
Rock Structures - Defects: Joints, Veins, Foliation: Schistosity. Attitude, thickness, spacing, smoothness, roughness, aperture, infill OR Soil consistency, compactness, water content, etc.
Foliation Dip (°)
Fracture Spacing (avg. cm)
50
10
5
1
Infill
100
0
cobbly GRAVEL with traces of sand; dark grey-green.
ms: 5%, cs: 5%, fg: 15%, mg: 30%, cg: 25%, cb: 20%
very loosely packed, poorly graded, angular to subangular schist fragments, no plasticity
BOX 7
92
23
BH2_B7_PL1
Dark green-grey foliated schist.
65% Mafics, 25% Quartz, 10% Chlorite
Quartz laminae 5 - 20mm thick, sp. 5-30mm
Chlorite laminae, up to 2mm thick.
Quartz veins, 2-15mm thick, 65-80° from horizontal.
M
Foliation: Well dev. Planar and undulating
Fractures: JS1: along foliation, rough stepped, very narrow to narrow.
JS2: 45 ° to horizontal, rough stepped, narrow.
Foliation shears at 22.2m and 22.3m
shears consisting of cl/si: 15%, ms: 10%, cs: 15%, fg: 20%, mg: 30%, cg: 10%
20 to 25
orange-brown clay and fs
22
Medium grey foliated schist.
80% Mafics, 20% Quartz
Quartz laminae up to 10-15mm thick, sp. 40-80mm
Chlorite laminae, mm-scale
Upright tight isoclinal folds (70° limbs), 2-3mm to 20mm thickness, 100mm long.
M
Foliation: poor to moderately dev. Planar
Fractures: JS1: along foliation, smooth stepped, narrow.
20 to 25
1mm grey and green-yellow clay
NC
JS2: 40 - 45 ° to horizontal, rough stepped, narrow.
80
18
BOX 7
23
Foliation shears at 22.45m, 23.1m and 23.6m
shears consisting of cl/si: 15%, ms: 10%, cs: 15%, fg: 20%, mg: 30%, cg: 10%
M
JS3: 70 ° to horizontal, rough stepped, narrow
20 to 25
< 1mm Mica clay and fs
24
NC

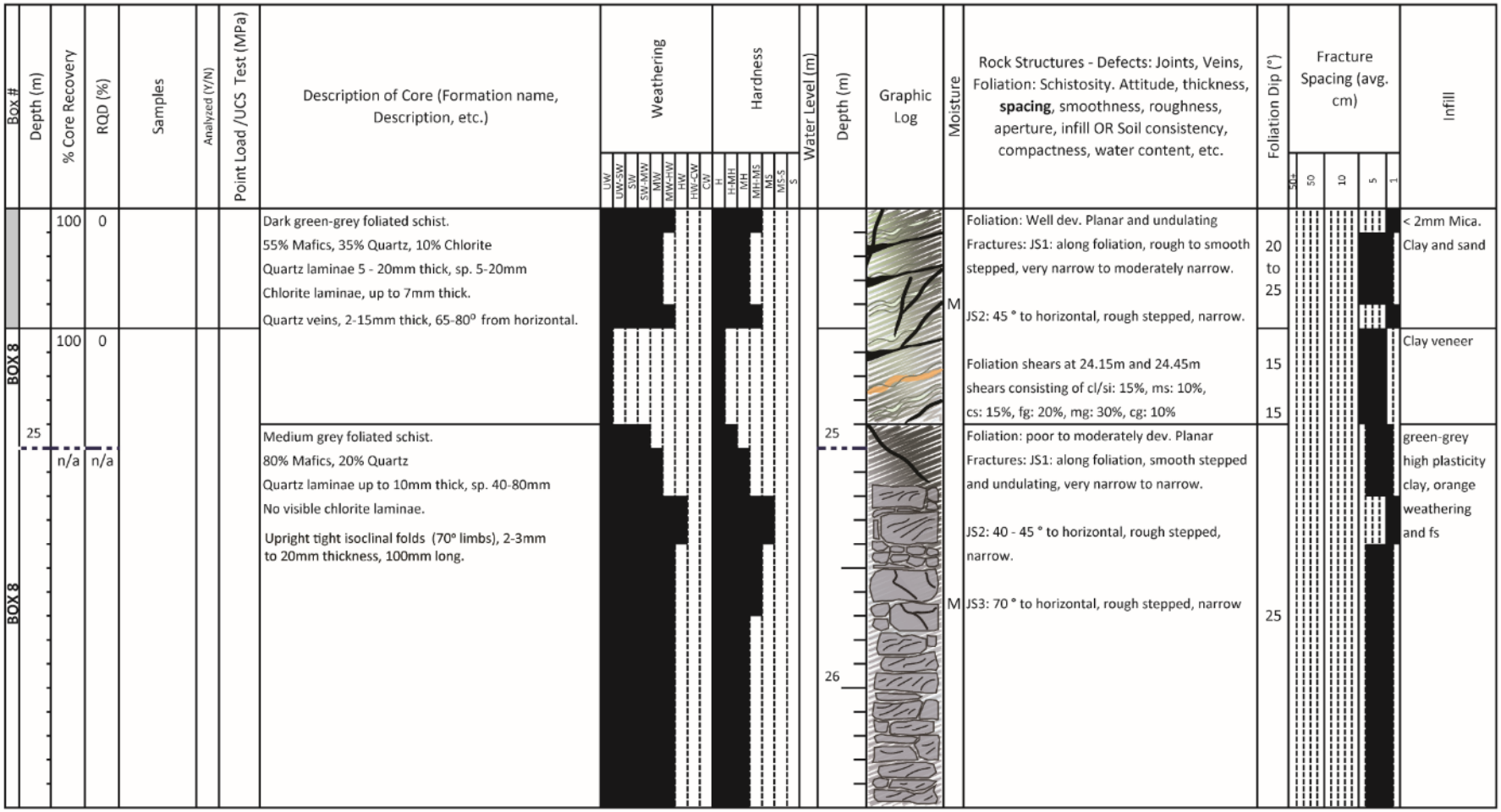
Box #
Depth (m)
% Core Recovery
RQD (%)
Samples
Analyzed (Y/N)
Point Load /UCS Test (MPa)
Description of Core (Formation name, Description, etc.)
Weathering
UW
UW-SW
SW
SW-MW
MW
MW-HW
HW
HW-CW
CW
Hardness
H
H-MH
MH
MH-MS
MS
MS-S
S
Water Level (m)
Depth (m)
Graphic Log
Moisture
Rock Structures - Defects: Joints, Veins, Foliation: Schistosity. Attitude, thickness, spacing, smoothness, roughness, aperture, infill OR Soil consistency, compactness, water content, etc.
Foliation Dip (°)
Fracture Spacing (avg. cm)
Infill
100
0
Dark green-grey foliated schist.
55% Mafics, 35% Quartz, 10% Chlorite
Quartz laminae 5 - 20mm thick, sp. 5-20mm
Chlorite laminae, up to 7mm thick.
Quartz veins, 2-15mm thick, 65-80° from horizontal.
Foliation: Well dev. Planar and undulating
Fractures: JS1: along foliation, rough to smooth stepped, very narrow to moderately narrow.
JS2: 45 ° to horizontal, rough stepped, narrow.
20 to 25
< 2mm Mica. Clay and sand
BOX 8
100
0
Foliation shears at 24.15m and 24.45m shears consisting of cl/si: 15%, ms: 10%, cs: 15%, fg: 20%, mg: 30%, cg: 10%
15
15
Clay veneer
25
n/a
n/a
Medium grey foliated schist.
80% Mafics, 20% Quartz
Quartz laminae up to 10mm thick, sp. 40-80mm
No visible chlorite laminae.
Upright tight isoclinal folds (70° limbs), 2-3mm to 20mm thickness, 100mm long.
Foliation: poor to moderately dev. Planar
Fractures: JS1: along foliation, smooth stepped and undulating, very narrow to narrow.
JS2: 40 - 45 ° to horizontal, rough stepped, narrow.
JS3: 70 ° to horizontal, rough stepped, narrow
25
green-grey high plasticity clay, orange weathering and fs
M
M
25
26

Legend

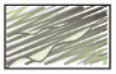
UW-MW, foliated dark grey-green SCHIST; strong; foliation dips 15-50° to horizontal, well developed, planar and undulating. Joints are steep to sub-vertically inclined and moderately wide spaced.
[Mapped as Caples Terrane, Textural Zone 3 Schist]

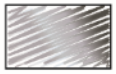
UW-MW, foliated medium grey SCHIST; strong; foliation dips 20-25° to horizontal, poorly to moderately developed, planar. Joints are steep to sub-vertically inclined and moderately wide spaced.
[Mapped as Caples Terrane, Textural Zone 3 Schist]


Clayey SILT with vf sand, f gravels and rootlets; orange-brown.


Sandy fine to coarse GRAVEL with minor organics and clay/silt; grey-brown.


Fine to coarse GRAVEL schist fragments with minor sand and traces of clay and silt; light sparkly grey.


sandy SILTY CLAY with minor schist gravel; silver.


Cobble sized schist fragments


Coarse Gravel sized schist fragments


Gravels


Sand


Clay/Silt


Fracture or Joint

Iron Staining/ Weathering


Foliation Shear

Upright tight isoclinal folds (70° limbs)

Weathering
UW: Unweathered
SW: Slightly Weathered
MW: Moderately Weathered
HW: Highly Weathered
CW: Completely Weathered

Hardness
H: Hard
MH: Moderately Hard
MS: Moderately Soft
S: Soft

Moisture
D: Dry
M: Moist
W: Wet

Grain Size
cl/si: Clay/Silt
vfs: Very fine sand
fs: Fine sand
ms: Medium sand
cs: Coarse sand
s: Sand
fg: Fine gravel
mg: Medium gravel
cg: Coarse gravel
g: Gravel
cb: Cobble

NC Core loss/No Recovery

A.3.3 Borehole 3

Geotechnical Borehole Log

Project: Queenstown Hill Landslide - GCL
Borehole No.: BH3
Box No.: 1 to 9
Sheet No.: 1 to 10

Address: Middleton Block - Goldfield Heights
Coordinates: 1260833.914, 5005941.35
Drilling Method: Rotary drilling

Logged by: Laura Gnesko
Date Logged: 01/05/2019
Coordinate System: NZTM2000
Direction: Vertical

Core diameter: 63mm

Meterage: 0.0 to 25.0m
Elevation: 517.732m (a.s.l)

Date Drilled: 18/04/2019 - 29/04/2019
Angle from Horizontal: 90°

Comments:

Box 1:	0.0 to 3.1m	Core loss indicated. Markers 1) 1.5m 2) 0.1m core loss 3) 3.0m (drillers mud)
Box 2	3.1 to 6.0m	UCS Samples in this box. Drillers mud up to 3.7m
Box 3:	6.0 to 9.0m	unsure about 9.0m being the end up. Assuming based on next box. Core loss indicated in box. UCS samples in box Markers in box 1) 7.4m 2) 0.2m core loss (drillers mud) 3) 8.5m (drillers mud) 4) 0.2m core loss 5) 9.0m
Box 4:	9.0 to 11.94m	UCS in this box.
Box 5:	11.94 to 14.9m	Huge UCS pieces. Drillers mud from 13.5 - 14.5m. Drillers markers were not in the correct place. Meterage says 11.94 to 14.9m ~300m. There is 300m of core in the box, but the 13.5m marker is not in the correct place. It was likely moved during transport and was loose in the box. - I moved the marker to the assumed correct location.
Box 6:	14.9 to 18.2m	Point load from this box would be ideal. UCS may be possible. Drillers mud from 15-16.8m
Box 7:	18.2 to 21.44m	Core loss indicated. Markers 1) 19.2m, 2) 0.3m core loss 3) 20.8m (drillers mud) 4) 21.44m
Box 8:	21.44 to 24.5m	UCS in this box.
Box 9:	24.5 to 25.0m	only 0.12m in box. This box was point loaded

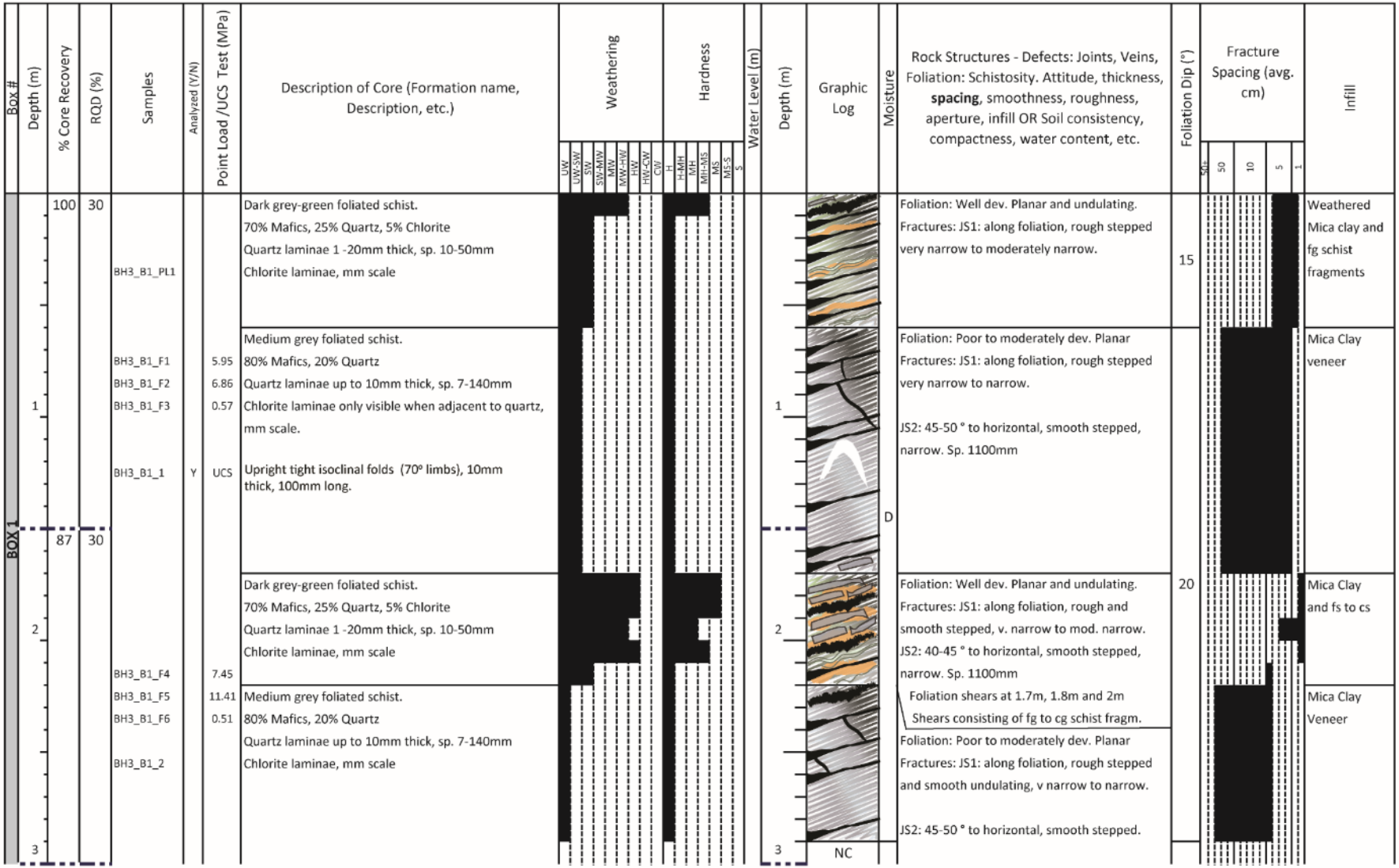
Box #
Depth (m)
% Core Recovery
RQD (%)
Samples
Analyzed (Y/N)
Point Load /UCS Test (MPa)
Description of Core (Formation name, Description, etc.)
Weathering
UW
UW-SW
SW
SW-MW
MW
MW-HW
HW
HW-CW
CW
Hardness
H
H-MH
MH
MH-MS
MS
MS-S
S
Water Level (m)
Depth (m)
Graphic Log
Moisture
Rock Structures - Defects: Joints, Veins, Foliation: Schistosity. Attitude, thickness, spacing, smoothness, roughness, aperture, infill OR Soil consistency, compactness, water content, etc.
Foliation Dip (°)
Fracture Spacing (avg. cm)
Infill
BOX 1
100
30
BH3_B1_PL1
Dark grey-green foliated schist.
70% Mafics, 25% Quartz, 5% Chlorite
Quartz laminae 1 -20mm thick, sp. 10-50mm
Chlorite laminae, mm scale
Foliation: Well dev. Planar and undulating.
Fractures: JS1: along foliation, rough stepped very narrow to moderately narrow.
15
Weathered Mica clay and fg schist fragments
BH3_B1_F1
BH3_B1_F2
BH3_B1_F3
5.95
6.86
0.57
Medium grey foliated schist.
80% Mafics, 20% Quartz
Quartz laminae up to 10mm thick, sp. 7-140mm
Chlorite laminae only visible when adjacent to quartz, mm scale.
Foliation: Poor to moderately dev. Planar
Fractures: JS1: along foliation, rough stepped very narrow to narrow.
JS2: 45-50 ° to horizontal, smooth stepped, narrow. Sp. 1100mm
Mica Clay veneer
BH3_B1_1
Y
UCS
Upright tight isoclinal folds (70° limbs), 10mm thick, 100mm long.
D
87
30
Dark grey-green foliated schist.
70% Mafics, 25% Quartz, 5% Chlorite
Quartz laminae 1 -20mm thick, sp. 10-50mm
Chlorite laminae, mm scale
Foliation: Well dev. Planar and undulating.
Fractures: JS1: along foliation, rough and smooth stepped, v. narrow to mod. narrow.
JS2: 40-45 ° to horizontal, smooth stepped, narrow. Sp. 1100mm
Foliation shears at 1.7m, 1.8m and 2m
Shears consisting of fg to cg schist fragm.
20
Mica Clay and fs to cs
BH3_B1_F4
BH3_B1_F5
BH3_B1_F6
7.45
11.41
0.51
Medium grey foliated schist.
80% Mafics, 20% Quartz
Quartz laminae up to 10mm thick, sp. 7-140mm
Chlorite laminae, mm scale
Foliation: Poor to moderately dev. Planar
Fractures: JS1: along foliation, rough stepped and smooth undulating, v narrow to narrow.
JS2: 45-50 ° to horizontal, smooth stepped.
Mica Clay Veneer
BH3_B1_2
NC
1
2
3

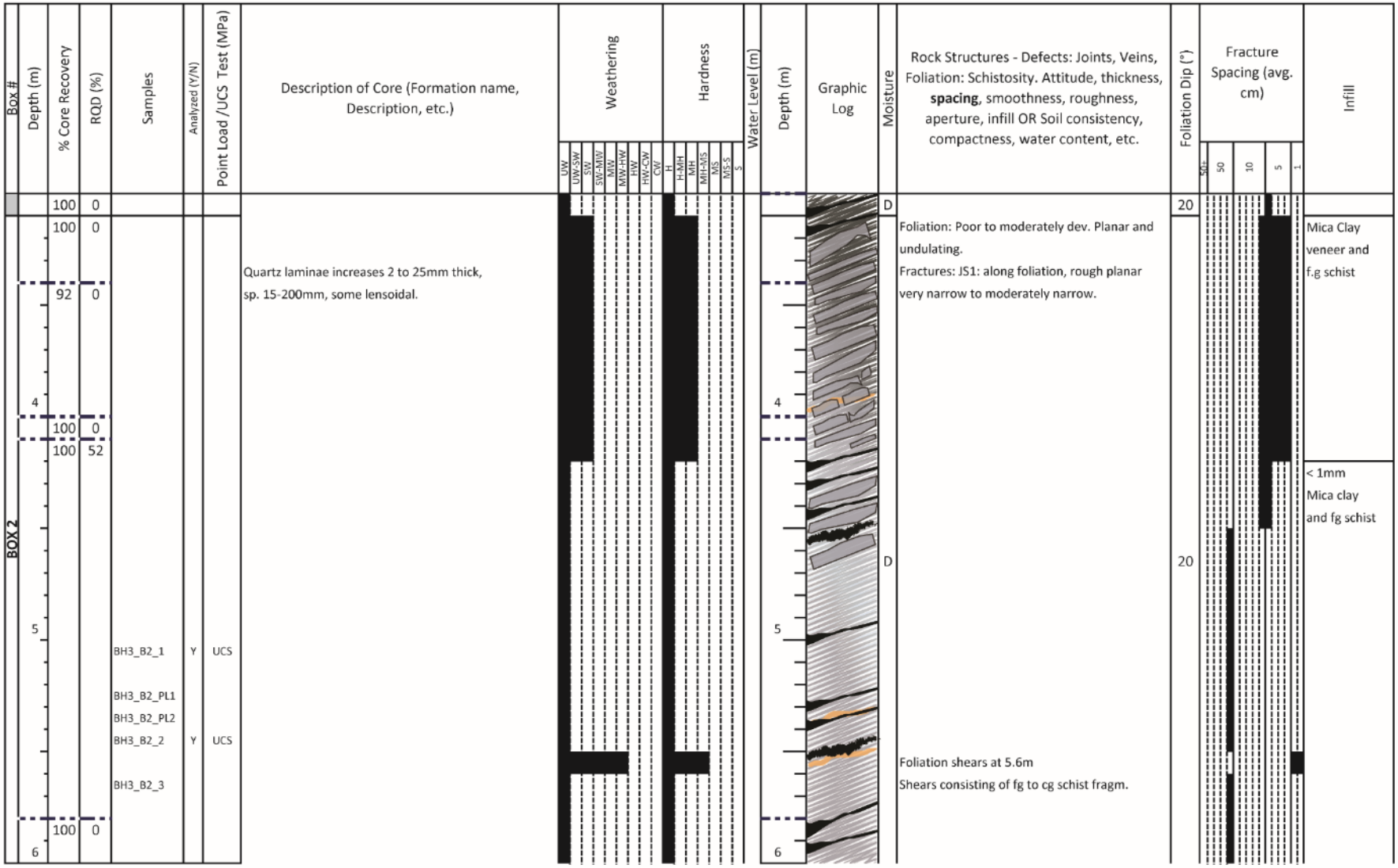
Box #
Depth (m)
% Core Recovery
RQD (%)
Samples
Analyzed (Y/N)
Point Load /UCS Test (MPa)
Description of Core (Formation name, Description, etc.)
Weathering
UW
UW-SW
SW
SW-MW
MW
MW-HW
HW
HW-CW
CW
Hardness
H
H-MH
MH
MH-MS
MS
MS-S
S
Water Level (m)
Depth (m)
Graphic Log
Moisture
Rock Structures - Defects: Joints, Veins, Foliation: Schistosity. Attitude, thickness, spacing, smoothness, roughness, aperture, infill OR Soil consistency, compactness, water content, etc.
Foliation Dip (°)
Fracture Spacing (avg. cm)
Infill
BOX 2
100 0
100 0
92 0
100 0
100 52
100 0
Quartz laminae increases 2 to 25mm thick, sp. 15-200mm, some lensoidal.
BH3_B2_1 Y UCS
BH3_B2_PL1
BH3_B2_PL2
BH3_B2_2 Y UCS
BH3_B2_3
D
D
Foliation: Poor to moderately dev. Planar and undulating.
Fractures: JS1: along foliation, rough planar very narrow to moderately narrow.
Foliation shears at 5.6m
Shears consisting of fg to cg schist fragm.
20
20
Mica Clay veneer and f.g schist
< 1mm Mica clay and fg schist

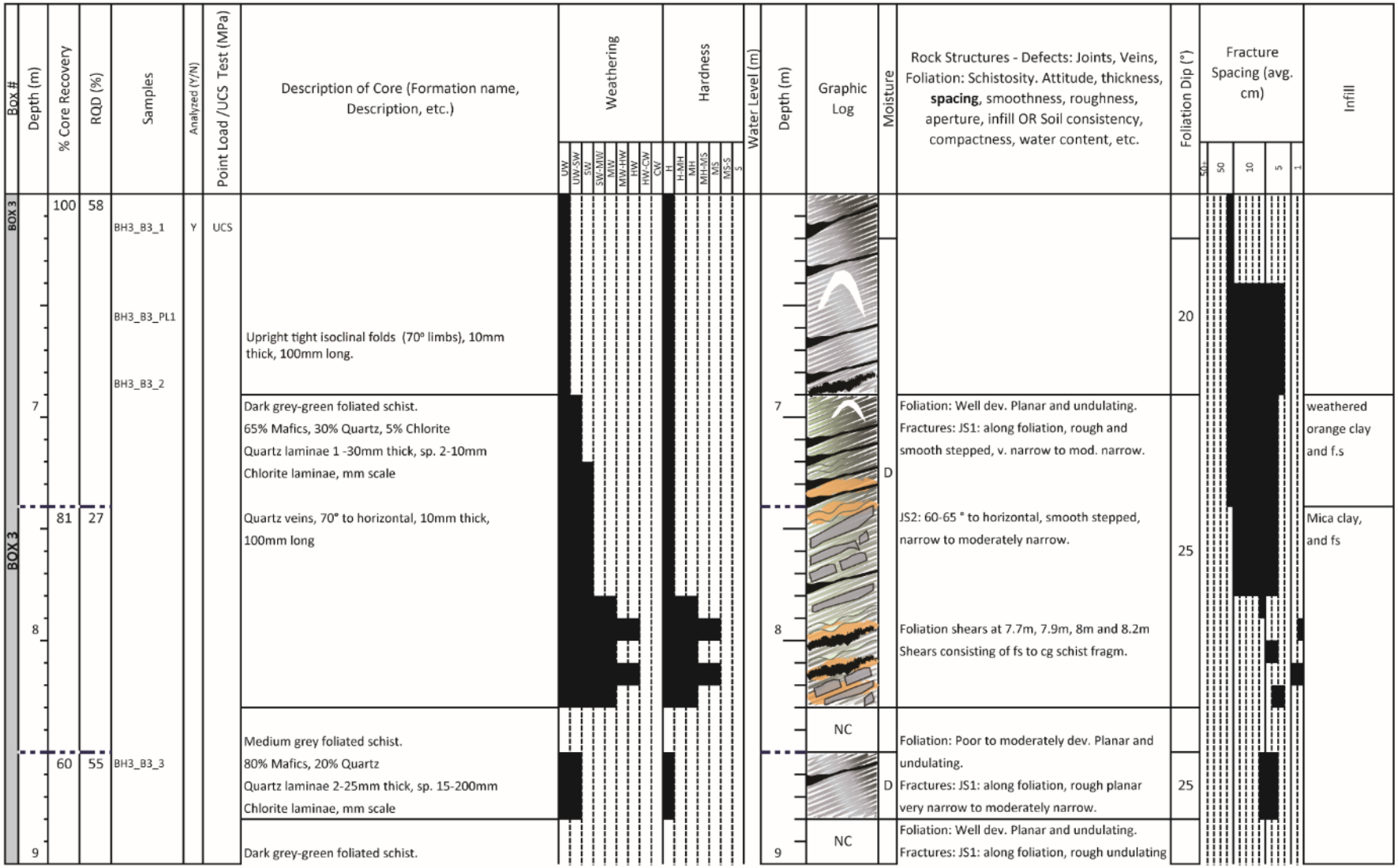
Box #
Depth (m)
% Core Recovery
RQD (%)
Samples
Analyzed (Y/N)
Point Load /UCS Test (MPa)
Description of Core (Formation name, Description, etc.)
Weathering
UW
UW-SW
SW
SW-MW
MW
MW-HW
HW
HW-CW
CW
Hardness
H
H-MH
MH
MH-MS
MS
MS-S
S
Water Level (m)
Depth (m)
Graphic Log
Moisture
Rock Structures - Defects: Joints, Veins, Foliation: Schistosity. Attitude, thickness, spacing, smoothness, roughness, aperture, infill OR Soil consistency, compactness, water content, etc.
Foliation Dip (°)
Fracture Spacing (avg. cm)
50
10
5
1
Infill
BOX 3
100
58
BH3_B3_1
Y
UCS
BH3_B3_PL1
BH3_B3_2
Upright tight isoclinal folds (70° limbs), 10mm thick, 100mm long.
20
7
Dark grey-green foliated schist.
65% Mafics, 30% Quartz, 5% Chlorite
Quartz laminae 1 -30mm thick, sp. 2-10mm
Chlorite laminae, mm scale
Foliation: Well dev. Planar and undulating.
Fractures: JS1: along foliation, rough and smooth stepped, v. narrow to mod. narrow.
D
weathered orange clay and f.s
81
27
Quartz veins, 70° to horizontal, 10mm thick, 100mm long
JS2: 60-65 ° to horizontal, smooth stepped, narrow to moderately narrow.
25
Mica clay, and fs
8
Foliation shears at 7.7m, 7.9m, 8m and 8.2m
Shears consisting of fs to cg schist fragm.
NC
Medium grey foliated schist.
80% Mafics, 20% Quartz
Quartz laminae 2-25mm thick, sp. 15-200mm
Chlorite laminae, mm scale
Foliation: Poor to moderately dev. Planar and undulating.
60
55
BH3_B3_3
D
Fractures: JS1: along foliation, rough planar very narrow to moderately narrow.
25
9
NC
Dark grey-green foliated schist.
Foliation: Well dev. Planar and undulating.
Fractures: JS1: along foliation, rough undulating

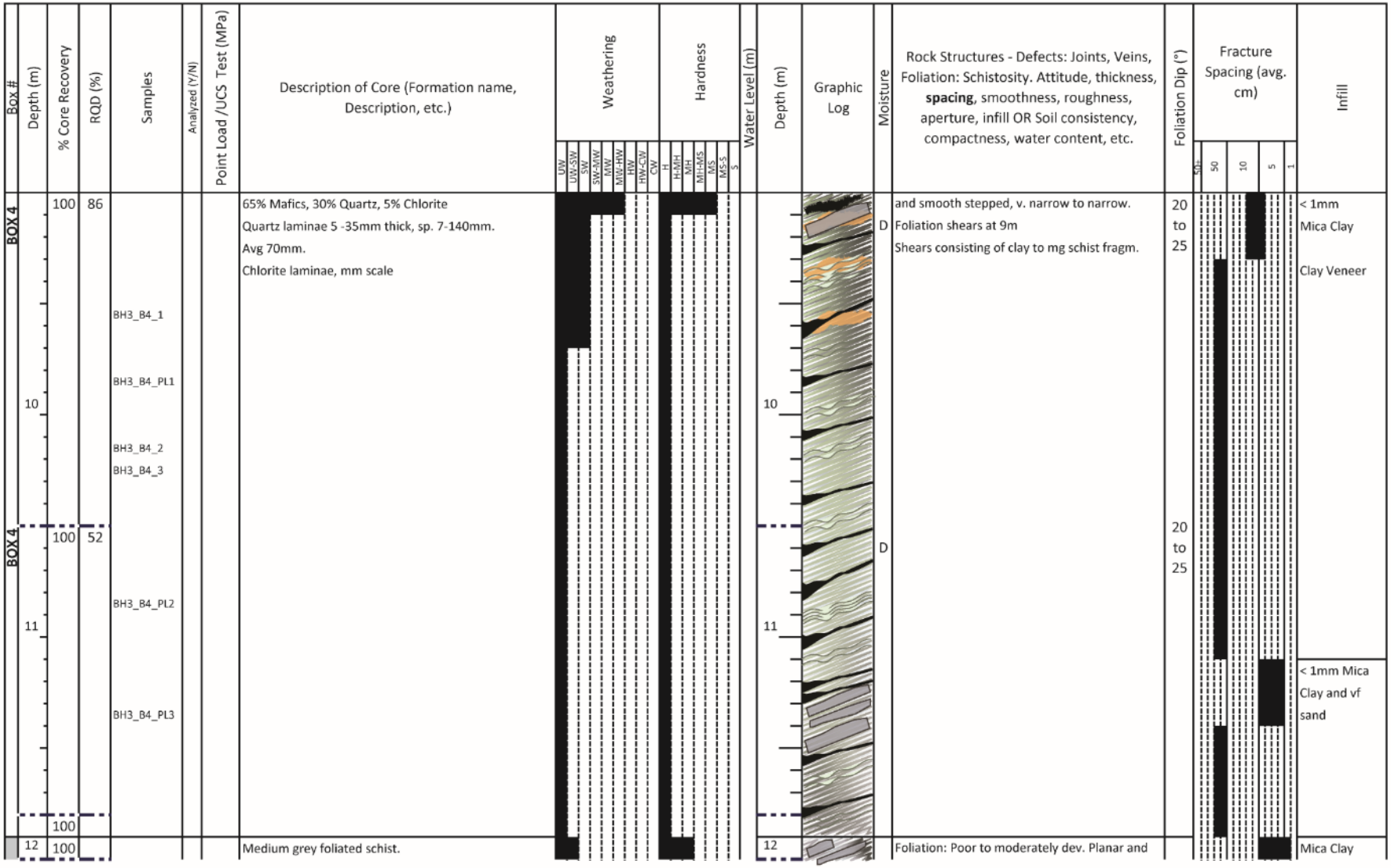
Box #
Depth (m)
% Core Recovery
RQD (%)
Samples
Analyzed (Y/N)
Point Load /UCS Test (MPa)
Description of Core (Formation name, Description, etc.)
Weathering
UW
UW-SW
SW
SW-MW
MW
MW-HW
HW
HW-CW
CW
Hardness
H
H-MH
MH
MH-MS
MS
MS-S
S
Water Level (m)
Depth (m)
Graphic Log
Moisture
Rock Structures - Defects: Joints, Veins, Foliation: Schistosity. Attitude, thickness, spacing, smoothness, roughness, aperture, infill OR Soil consistency, compactness, water content, etc.
Foliation Dip (°)
Fracture Spacing (avg. cm)
50+
50
10
5
1
Infill
BOX 4
100
86
65% Mafics, 30% Quartz, 5% Chlorite
Quartz laminae 5 -35mm thick, sp. 7-140mm.
Avg 70mm.
Chlorite laminae, mm scale
BH3_B4_1
BH3_B4_PL1
BH3_B4_2
BH3_B4_3
BH3_B4_PL2
BH3_B4_PL3
10
11
D
and smooth stepped, v. narrow to narrow.
Foliation shears at 9m
Shears consisting of clay to mg schist fragm.
20 to 25
< 1mm Mica Clay
Clay Veneer
BOX 4
100
52
100
12
100
Medium grey foliated schist.
Foliation: Poor to moderately dev. Planar and
< 1mm Mica Clay and vf sand
Mica Clay

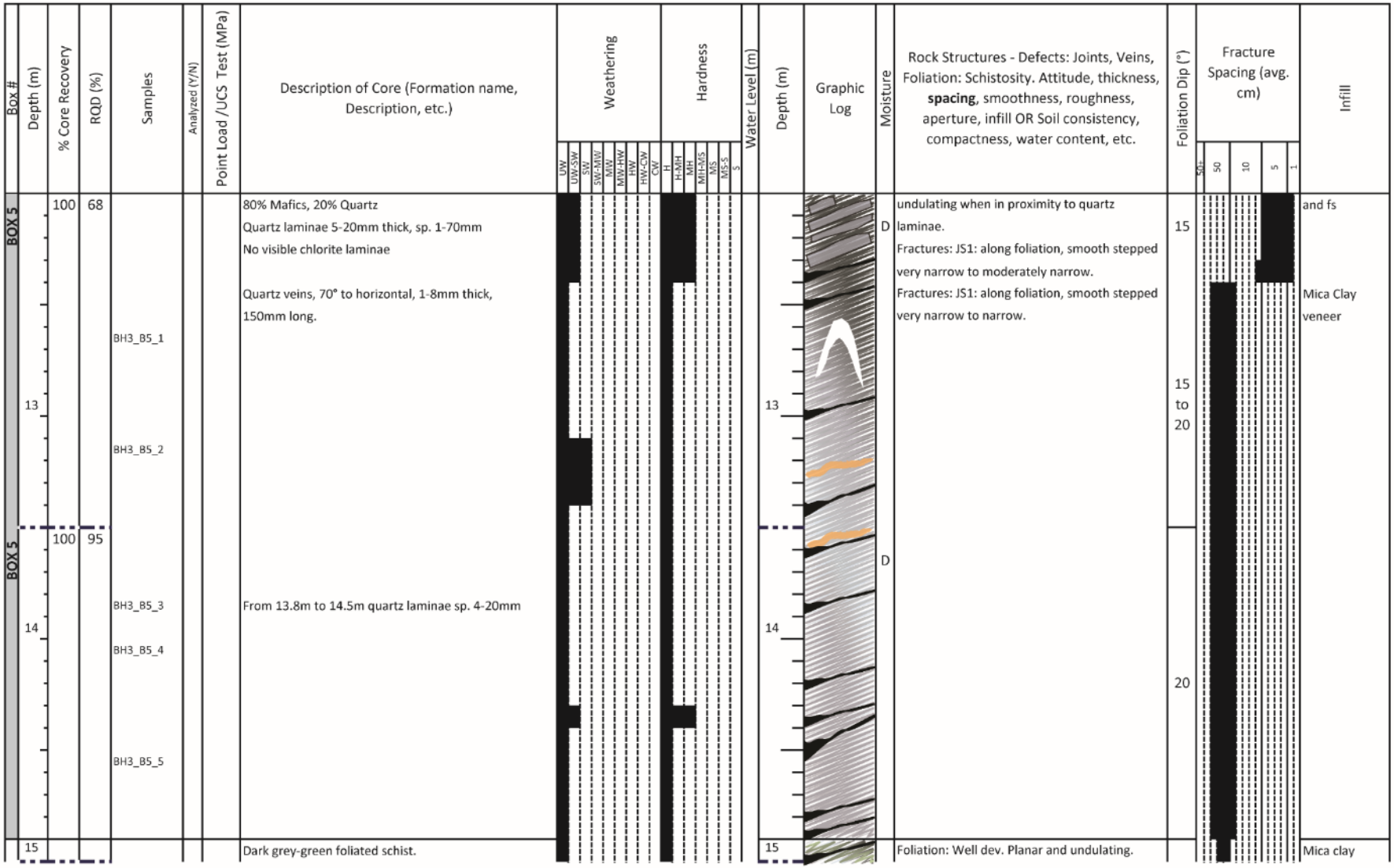
Box #
Depth (m)
% Core Recovery
RQD (%)
Samples
Analyzed (Y/N)
Point Load /UCS Test (MPa)
Description of Core (Formation name, Description, etc.)
Weathering
UW
UW-SW
SW
SW-MW
MW
MW-HW
HW
HW-CW
CW
Hardness
H
H-MH
MH
MH-MS
MS
MS-S
S
Water Level (m)
Depth (m)
Graphic Log
Moisture
Rock Structures - Defects: Joints, Veins, Foliation: Schistosity. Attitude, thickness, spacing, smoothness, roughness, aperture, infill OR Soil consistency, compactness, water content, etc.
Foliation Dip (°)
Fracture Spacing (avg. cm)
50+
50
10
5
1
Infill
BOX 5
100
68
80% Mafics, 20% Quartz
Quartz laminae 5-20mm thick, sp. 1-70mm
No visible chlorite laminae
Quartz veins, 70° to horizontal, 1-8mm thick, 150mm long.
BH3_B5_1
BH3_B5_2
13
D
undulating when in proximity to quartz laminae.
Fractures: JS1: along foliation, smooth stepped very narrow to moderately narrow.
Fractures: JS1: along foliation, smooth stepped very narrow to narrow.
15
15 to 20
and fs
Mica Clay veneer
BOX 5
100
95
BH3_B5_3
BH3_B5_4
BH3_B5_5
From 13.8m to 14.5m quartz laminae sp. 4-20mm
14
D
20
15
Dark grey-green foliated schist.
Foliation: Well dev. Planar and undulating.
Mica clay

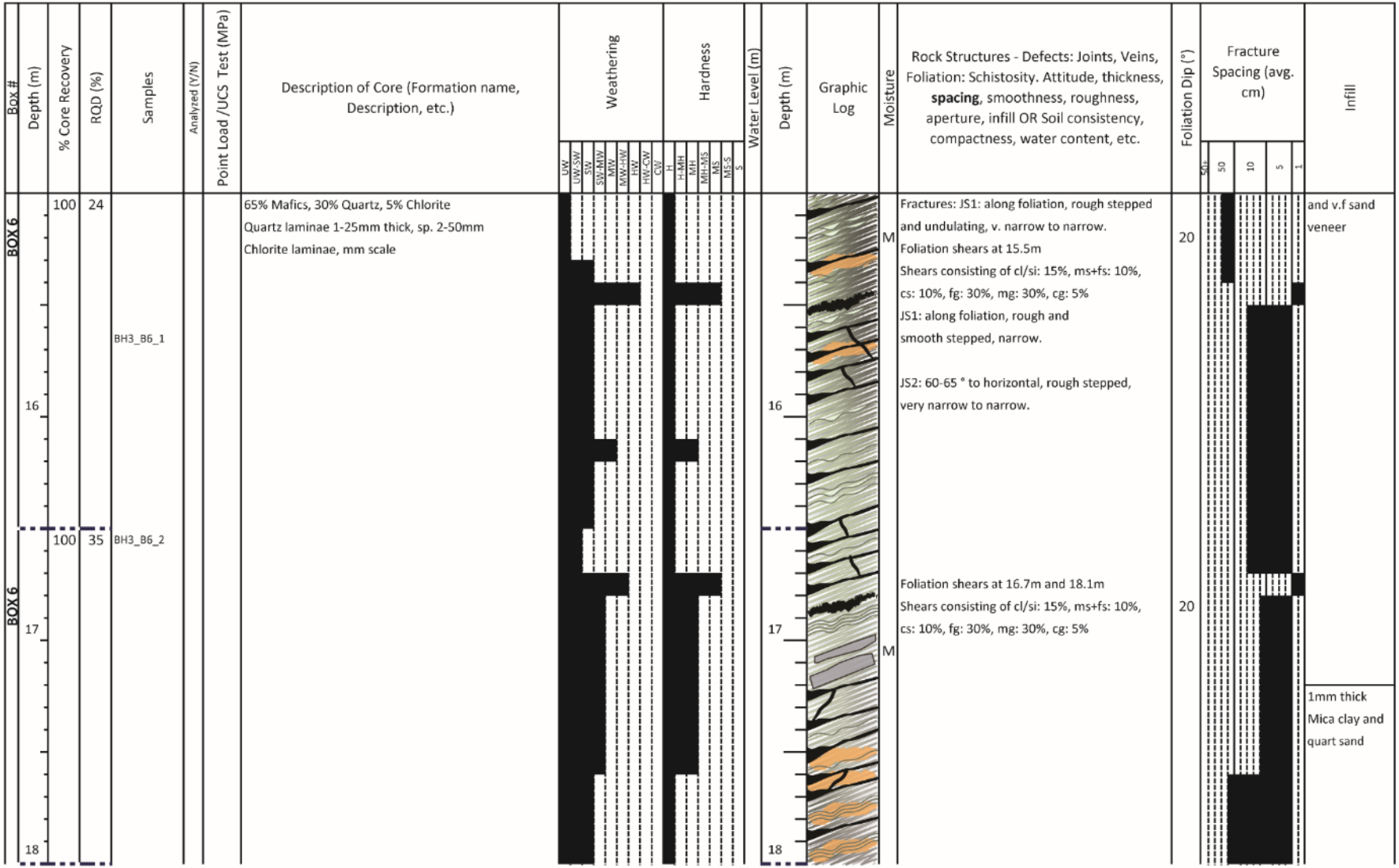
Box #
Depth (m)
% Core Recovery
RQD (%)
Samples
Analyzed (Y/N)
Point Load /UCS Test (MPa)
Description of Core (Formation name, Description, etc.)
Weathering
UW
UW-SW
SW
SW-MW
MW
MW-HW
HW
HW-CW
CW
Hardness
H
H-MH
MH
MH-MS
MS
MS-S
S
Water Level (m)
Depth (m)
Graphic Log
Moisture
Rock Structures - Defects: Joints, Veins, Foliation: Schistosity. Attitude, thickness, spacing, smoothness, roughness, aperture, infill OR Soil consistency, compactness, water content, etc.
Foliation Dip (°)
Fracture Spacing (avg. cm)
50
10
5
1
Infill
BOX 6
100
24
BH3_B6_1
65% Mafics, 30% Quartz, 5% Chlorite
Quartz laminae 1-25mm thick, sp. 2-50mm
Chlorite laminae, mm scale
16
M
Fractures: JS1: along foliation, rough stepped and undulating, v. narrow to narrow.
Foliation shears at 15.5m
Shears consisting of cl/si: 15%, ms+fs: 10%, cs: 10%, fg: 30%, mg: 30%, cg: 5%
JS1: along foliation, rough and smooth stepped, narrow.
JS2: 60-65 ° to horizontal, rough stepped, very narrow to narrow.
20
and v.f sand veneer
BOX 6
100
35
BH3_B6_2
17
M
Foliation shears at 16.7m and 18.1m
Shears consisting of cl/si: 15%, ms+fs: 10%, cs: 10%, fg: 30%, mg: 30%, cg: 5%
20
1mm thick Mica clay and quart sand
18

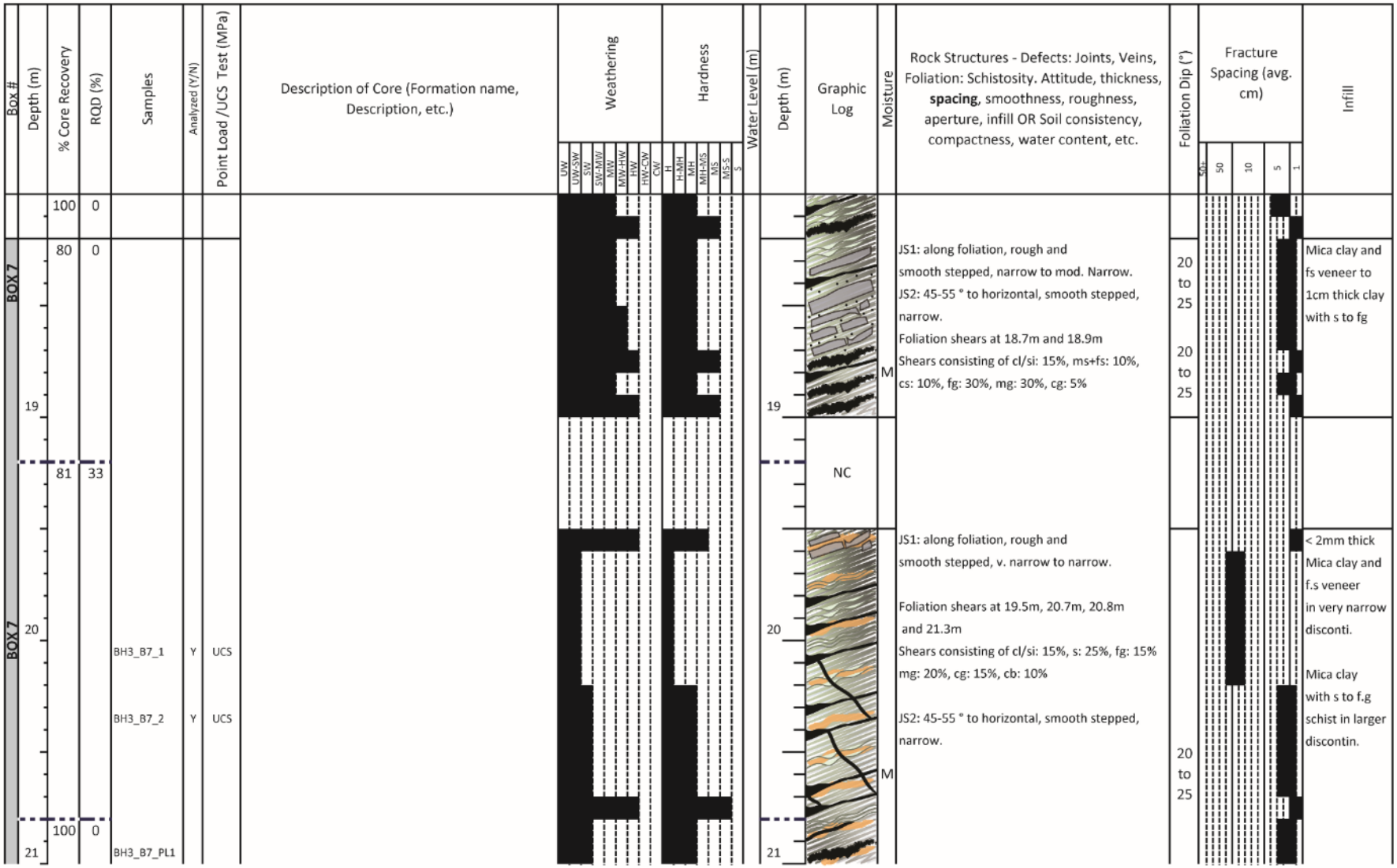
Box #
Depth (m)
% Core Recovery
RQD (%)
Samples
Analyzed (Y/N)
Point Load /UCS Test (MPa)
Description of Core (Formation name, Description, etc.)
Weathering
UW
UW-SW
SW
SW-MW
MW
MW-HW
HW
HW-CW
CW
Hardness
H
H-MH
MH
MH-MS
MS
MS-S
S
Water Level (m)
Depth (m)
Graphic Log
Moisture
Rock Structures - Defects: Joints, Veins, Foliation: Schistosity. Attitude, thickness, spacing, smoothness, roughness, aperture, infill OR Soil consistency, compactness, water content, etc.
Foliation Dip (°)
Fracture Spacing (avg. cm)
50
10
5
1
Infill
100 0
80 0
BOX 7
19
JS1: along foliation, rough and smooth stepped, narrow to mod. Narrow.
JS2: 45-55 ° to horizontal, smooth stepped, narrow.
Foliation shears at 18.7m and 18.9m
Shears consisting of cl/si: 15%, ms+fs: 10%, cs: 10%, fg: 30%, mg: 30%, cg: 5%
M
20 to 25
20 to 25
Mica clay and fs veneer to 1cm thick clay with s to fg
81 33
NC
BOX 7
20
BH3_B7_1 Y UCS
BH3_B7_2 Y UCS
JS1: along foliation, rough and smooth stepped, v. narrow to narrow.
Foliation shears at 19.5m, 20.7m, 20.8m and 21.3m
Shears consisting of cl/si: 15%, s: 25%, fg: 15% mg: 20%, cg: 15%, cb: 10%
JS2: 45-55 ° to horizontal, smooth stepped, narrow.
M
20 to 25
< 2mm thick Mica clay and f.s veneer in very narrow disconti.
Mica clay with s to f.g schist in larger discontin.
100 0
21
BH3_B7_PL1

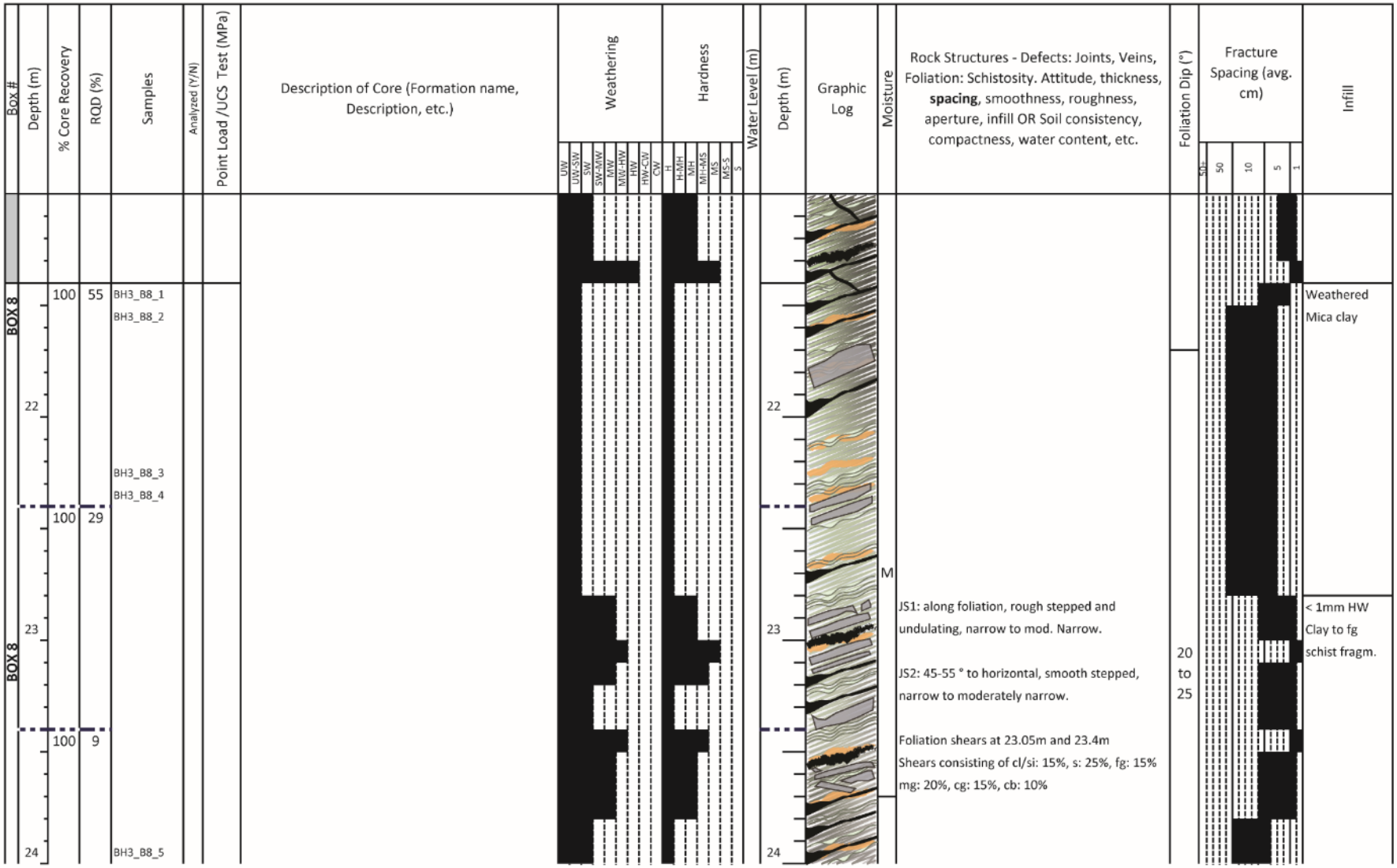
Box #
Depth (m)
% Core Recovery
RQD (%)
Samples
Analyzed (Y/N)
Point Load /UCS Test (MPa)
Description of Core (Formation name, Description, etc.)
Weathering
UW
UW-SW
SW
SW-MW
MW
MW-HW
HW
HW-CW
CW
Hardness
H
H-MH
MH
MH-MS
MS
MS-S
S
Water Level (m)
Depth (m)
Graphic Log
Moisture
Rock Structures - Defects: Joints, Veins, Foliation: Schistosity. Attitude, thickness, spacing, smoothness, roughness, aperture, infill OR Soil consistency, compactness, water content, etc.
Foliation Dip (°)
Fracture Spacing (avg. cm)
50
10
5
1
Infill
BOX 8
100
55
BH3_B8_1
BH3_B8_2
22
BH3_B8_3
BH3_B8_4
100
29
23
100
9
24
BH3_B8_5
M
JS1: along foliation, rough stepped and undulating, narrow to mod. Narrow.
JS2: 45-55 ° to horizontal, smooth stepped, narrow to moderately narrow.
Foliation shears at 23.05m and 23.4m
Shears consisting of cl/si: 15%, s: 25%, fg: 15% mg: 20%, cg: 15%, cb: 10%
20 to 25
Weathered Mica clay
< 1mm HW Clay to fg schist fragm.

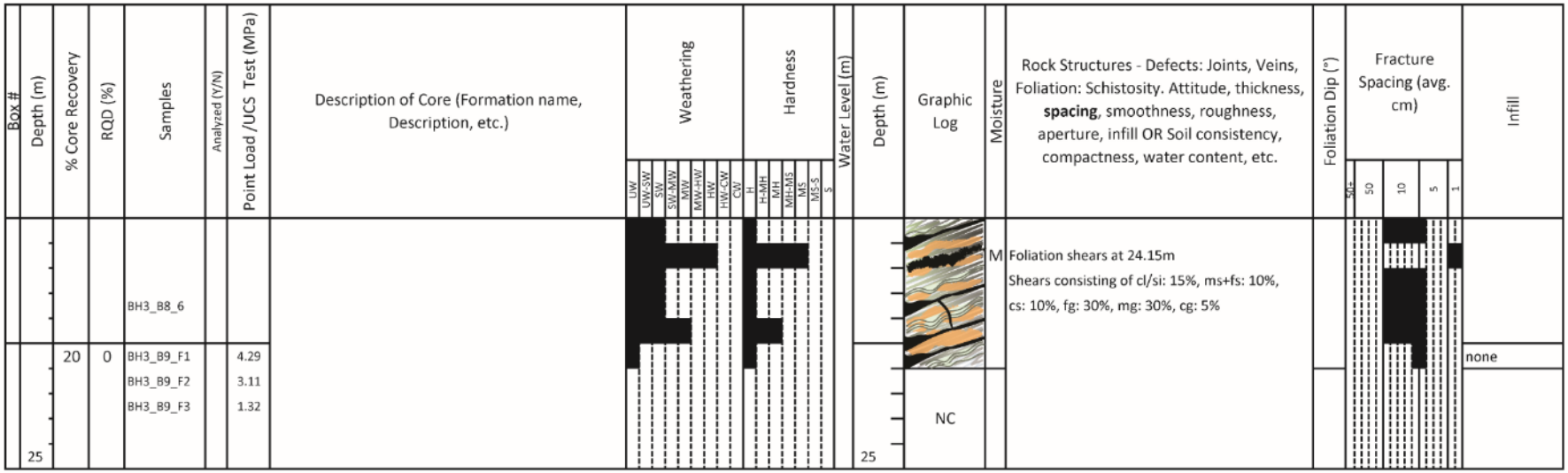

Legend

UW-MW, foliated dark grey-green SCHIST; strong; foliation dips 10-30° to horizontal, well developed, planar and undulating. Joints are steep to sub-vertically inclined and moderately wide spaced.
[Mapped as Caples Terrane, Textural Zone 3 Schist]

UW-MW, foliated medium grey SCHIST; strong; foliation dips 10-30° to horizontal, poorly to moderately developed, planar. Joints are steep to sub-vertically inclined and moderately wide spaced.
[Mapped as Caples Terrane, Textural Zone 3 Schist]

Cobble sized schist fragments

Coarse Gravel sized schist fragments

Gravels

Sand

Clay/Silt

Fracture or Joint

Iron Staining/ Weathering

Foliation Shear

Upright tight isoclinal folds (70° limbs)

Weathering
UW: Unweathered
SW: Slightly Weathered
MW: Moderately Weathered
HW: Highly Weathered
CW: Completely Weathered

Hardness
H: Hard
MH: Moderately Hard
MS: Moderately Soft
S: Soft

Moisture
D: Dry
M: Moist
W: Wet

Grain Size
cl/si: Clay/Silt
vfs: Very fine sand
fs: Fine sand
ms: Medium sand
cs: Coarse sand
s: Sand
fg: Fine gravel
mg: Medium gravel
cg: Coarse gravel
g: Gravel
cb: Cobble

NC Core loss/No Recovery

A.3.4 Borehole 4

Geotechnical Borehole Log

Project: Queenstown Hill Landslide - GCL
Borehole No.: BH4
Box No.: 1 to 9
Sheet No.: 1 to 10

Address: Middleton Block - Goldfield Heights
Coordinates: 1261255.897, 5005919.899
Drilling Method: Rotary drilling

Logged by: Laura Gnesko
Date Logged: 19/06/2019
Coordinate System: NZTM2000
Direction: Vertical

Core diameter: 63mm

Meterage: 0.0 to 25.0m
Elevation: 432m (a.s.l)

Date Drilled: 23/05/2019 - 24/05/2019
Angle from Horizontal: 90°

Comments:

Box 1: 0.0 to 2.55m
Box 2: 2.55 to 6.2m Markers in box at 1) 2.6m 2) 4.1m *Miss tube 1.0m recovered 3) 5.6m - Disking and signs of core rotating a barrel
Box 3: 6.2 to 9.3m
Box 4: 9.3 to 12.3m
Box 5: 12.3 to 15.3m
Box 6: 15.3 to 18.2m
Box 7: 18.2 to 21.1m
Box 8: 21.1 to 24.1m
Box 9: 24.1 to 25.0m

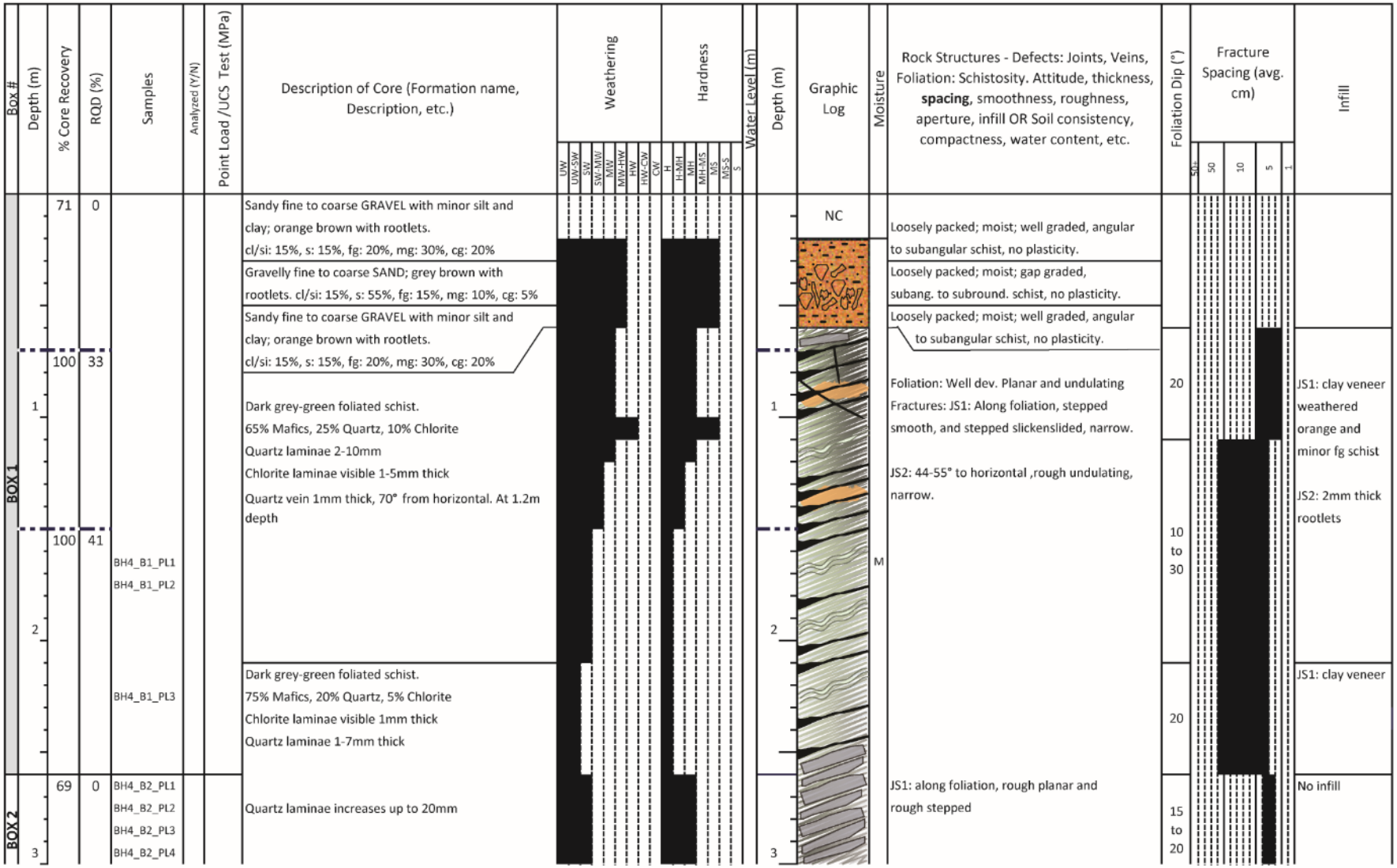
Box #
Depth (m)
% Core Recovery
RQD (%)
Samples
Analyzed (Y/N)
Point Load /UCS Test (MPa)
Description of Core (Formation name, Description, etc.)
Weathering
UW
UW-SW
SW
SW-MW
MW
MW-HW
HW
HW-CW
CW
Hardness
H
H-MH
MH
MH-MS
MS
MS-S
S
Water Level (m)
Depth (m)
Graphic Log
Moisture
Rock Structures - Defects: Joints, Veins, Foliation: Schistosity. Attitude, thickness, spacing, smoothness, roughness, aperture, infill OR Soil consistency, compactness, water content, etc.
Foliation Dip (°)
Fracture Spacing (avg. cm)
50
10
5
1
Infill
BOX 1
BOX 2
71
0
Sandy fine to coarse GRAVEL with minor silt and clay; orange brown with rootlets.
cl/si: 15%, s: 15%, fg: 20%, mg: 30%, cg: 20%
NC
Loosely packed; moist; well graded, angular to subangular schist, no plasticity.
Gravelly fine to coarse SAND; grey brown with rootlets. cl/si: 15%, s: 55%, fg: 15%, mg: 10%, cg: 5%
Loosely packed; moist; gap graded, subang. to subround. schist, no plasticity.
Sandy fine to coarse GRAVEL with minor silt and clay; orange brown with rootlets.
cl/si: 15%, s: 15%, fg: 20%, mg: 30%, cg: 20%
Loosely packed; moist; well graded, angular to subangular schist, no plasticity.
100
33
1
Dark grey-green foliated schist.
65% Mafics, 25% Quartz, 10% Chlorite
Quartz laminae 2-10mm
Chlorite laminae visible 1-5mm thick
Quartz vein 1mm thick, 70° from horizontal. At 1.2m depth
Foliation: Well dev. Planar and undulating
Fractures: JS1: Along foliation, stepped smooth, and stepped slickenslided, narrow.
JS2: 44-55° to horizontal ,rough undulating, narrow.
20
JS1: clay veneer weathered orange and minor fg schist
JS2: 2mm thick rootlets
100
41
BH4_B1_PL1
BH4_B1_PL2
2
M
10 to 30
BH4_B1_PL3
Dark grey-green foliated schist.
75% Mafics, 20% Quartz, 5% Chlorite
Chlorite laminae visible 1mm thick
Quartz laminae 1-7mm thick
20
JS1: clay veneer
69
0
BH4_B2_PL1
BH4_B2_PL2
BH4_B2_PL3
BH4_B2_PL4
3
Quartz laminae increases up to 20mm
JS1: along foliation, rough planar and rough stepped
15 to 20
No infill

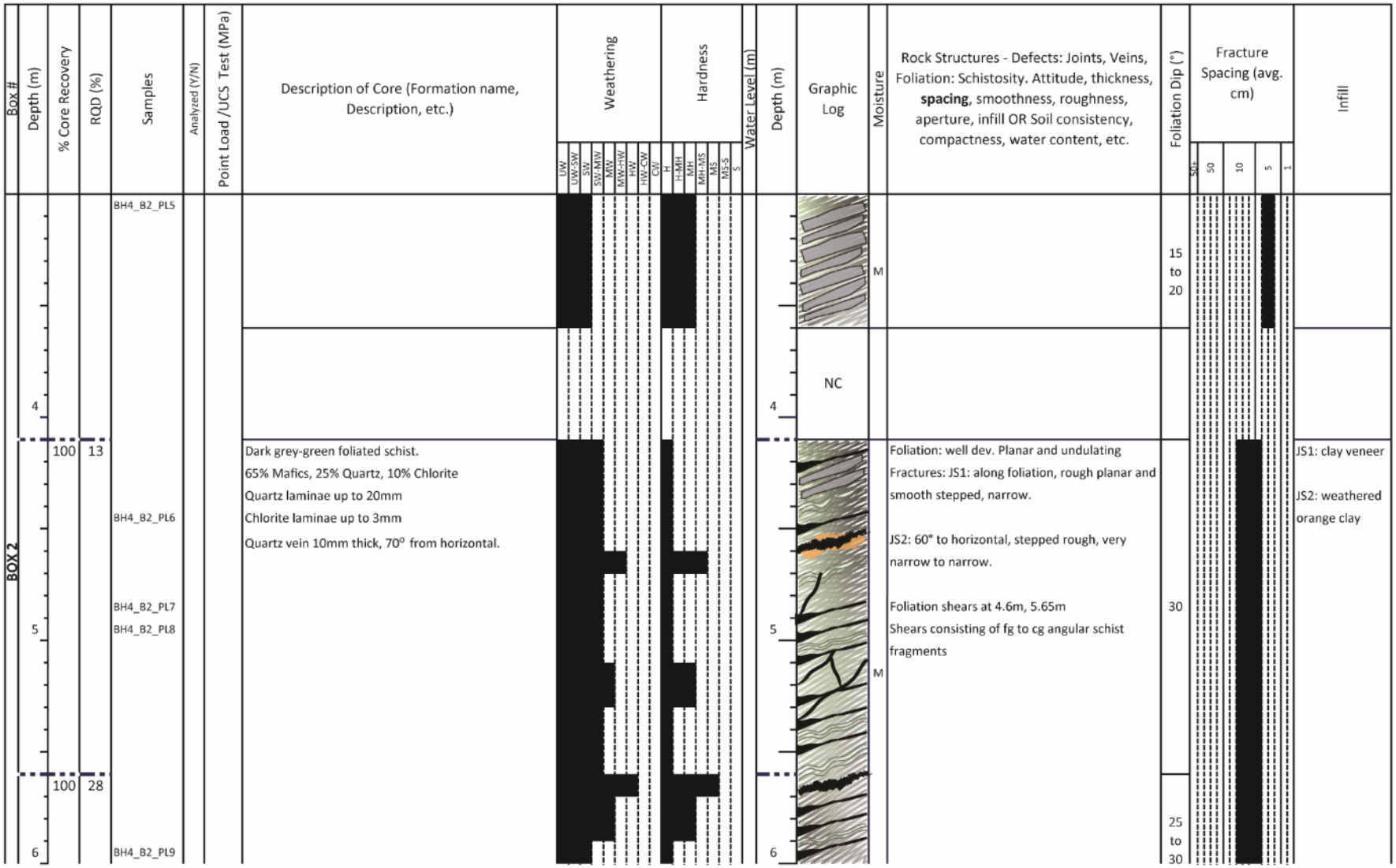
Box #
Depth (m)
% Core Recovery
RQD (%)
Samples
Analyzed (Y/N)
Point Load /UCS Test (MPa)
Description of Core (Formation name, Description, etc.)
Weathering
UW
UW-SW
SW
SW-MW
MW
MW-HW
HW
HW-CW
CW
Hardness
H
H-MH
MH
MH-MS
MS
MS-S
S
Water Level (m)
Depth (m)
Graphic Log
Moisture
Rock Structures - Defects: Joints, Veins, Foliation: Schistosity. Attitude, thickness, spacing, smoothness, roughness, aperture, infill OR Soil consistency, compactness, water content, etc.
Foliation Dip (°)
Fracture Spacing (avg. cm)
50
10
5
1
Infill
BOX 2
4
5
6
100
13
100
28
BH4_B2_PL5
BH4_B2_PL6
BH4_B2_PL7
BH4_B2_PL8
BH4_B2_PL9
Dark grey-green foliated schist.
65% Mafics, 25% Quartz, 10% Chlorite
Quartz laminae up to 20mm
Chlorite laminae up to 3mm
Quartz vein 10mm thick, 70° from horizontal.
NC
M
M
15 to 20
30
25 to 30
Foliation: well dev. Planar and undulating
Fractures: JS1: along foliation, rough planar and smooth stepped, narrow.
JS2: 60° to horizontal, stepped rough, very narrow to narrow.
Foliation shears at 4.6m, 5.65m
Shears consisting of fg to cg angular schist fragments
JS1: clay veneer
JS2: weathered orange clay

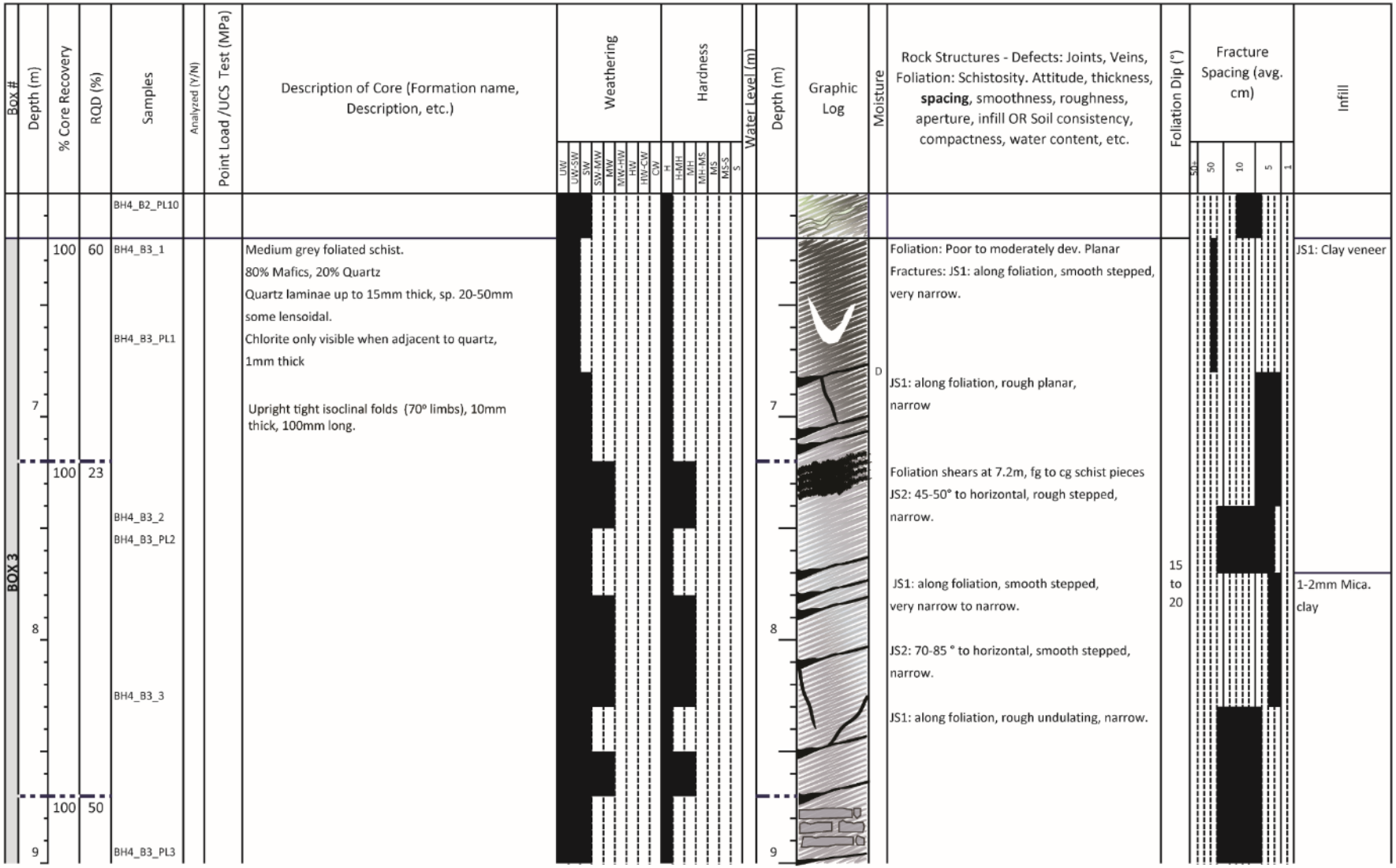
Box #
Depth (m)
% Core Recovery
RQD (%)
Samples
Analyzed (Y/N)
Point Load /UCS Test (MPa)
Description of Core (Formation name, Description, etc.)
Weathering
UW
UW-SW
SW
SW-MW
MW
MW-HW
HW
HW-CW
CW
Hardness
H
H-MH
MH
MH-MS
MS
MS-S
S
Water Level (m)
Depth (m)
Graphic Log
Moisture
Rock Structures - Defects: Joints, Veins, Foliation: Schistosity. Attitude, thickness, spacing, smoothness, roughness, aperture, infill OR Soil consistency, compactness, water content, etc.
Foliation Dip (°)
Fracture Spacing (avg. cm)
50+
50
10
5
1
Infill
BOX 3
BH4_B2_PL10
100
60
BH4_B3_1
BH4_B3_PL1
Medium grey foliated schist.
80% Mafics, 20% Quartz
Quartz laminae up to 15mm thick, sp. 20-50mm some lensoidal.
Chlorite only visible when adjacent to quartz, 1mm thick
Upright tight isoclinal folds (70° limbs), 10mm thick, 100mm long.
Foliation: Poor to moderately dev. Planar
Fractures: JS1: along foliation, smooth stepped, very narrow.
JS1: along foliation, rough planar, narrow
JS1: Clay veneer
7
D
100
23
BH4_B3_2
BH4_B3_PL2
Foliation shears at 7.2m, fg to cg schist pieces
JS2: 45-50° to horizontal, rough stepped, narrow.
15 to 20
JS1: along foliation, smooth stepped, very narrow to narrow.
1-2mm Mica. clay
8
JS2: 70-85 ° to horizontal, smooth stepped, narrow.
BH4_B3_3
JS1: along foliation, rough undulating, narrow.
100
50
9
BH4_B3_PL3

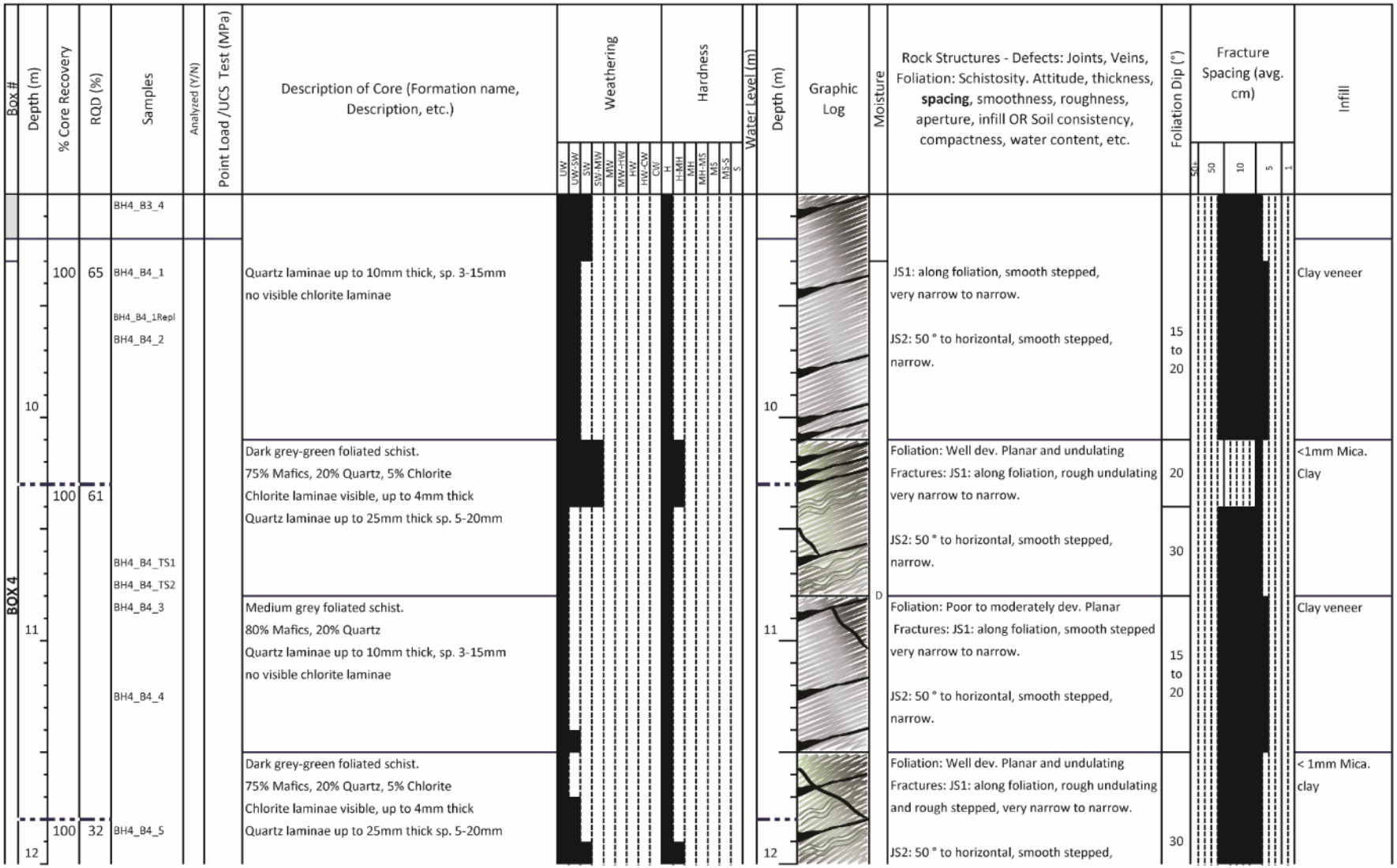
Box #
Depth (m)
% Core Recovery
RQD (%)
Samples
Analyzed (Y/N)
Point Load /UCS Test (MPa)
Description of Core (Formation name, Description, etc.)
Weathering
UW
UW-SW
SW
SW-MW
MW
MW-HW
HW
HW-CW
CW
Hardness
H
H-MH
MH
MH-MS
MS
MS-S
S
Water Level (m)
Depth (m)
Graphic Log
Moisture
Rock Structures - Defects: Joints, Veins, Foliation: Schistosity. Attitude, thickness, spacing, smoothness, roughness, aperture, infill OR Soil consistency, compactness, water content, etc.
Foliation Dip (°)
Fracture Spacing (avg. cm)
50+
50
10
5
1
Infill
BOX 4
BH4_B3_4
100
65
BH4_B4_1
BH4_B4_1Repl
BH4_B4_2
Quartz laminae up to 10mm thick, sp. 3-15mm
no visible chlorite laminae
JS1: along foliation, smooth stepped, very narrow to narrow.
JS2: 50 ° to horizontal, smooth stepped, narrow.
15 to 20
Clay veneer
10
100
61
Dark grey-green foliated schist.
75% Mafics, 20% Quartz, 5% Chlorite
Chlorite laminae visible, up to 4mm thick
Quartz laminae up to 25mm thick sp. 5-20mm
Foliation: Well dev. Planar and undulating
Fractures: JS1: along foliation, rough undulating very narrow to narrow.
JS2: 50 ° to horizontal, smooth stepped, narrow.
20
30
<1mm Mica.
Clay
BH4_B4_TS1
BH4_B4_TS2
BH4_B4_3
BH4_B4_4
11
D
Medium grey foliated schist.
80% Mafics, 20% Quartz
Quartz laminae up to 10mm thick, sp. 3-15mm
no visible chlorite laminae
Foliation: Poor to moderately dev. Planar
Fractures: JS1: along foliation, smooth stepped very narrow to narrow.
JS2: 50 ° to horizontal, smooth stepped, narrow.
15 to 20
Clay veneer
Dark grey-green foliated schist.
75% Mafics, 20% Quartz, 5% Chlorite
Chlorite laminae visible, up to 4mm thick
Quartz laminae up to 25mm thick sp. 5-20mm
Foliation: Well dev. Planar and undulating
Fractures: JS1: along foliation, rough undulating and rough stepped, very narrow to narrow.
JS2: 50 ° to horizontal, smooth stepped,
30
< 1mm Mica.
clay
100
32
BH4_B4_5
12

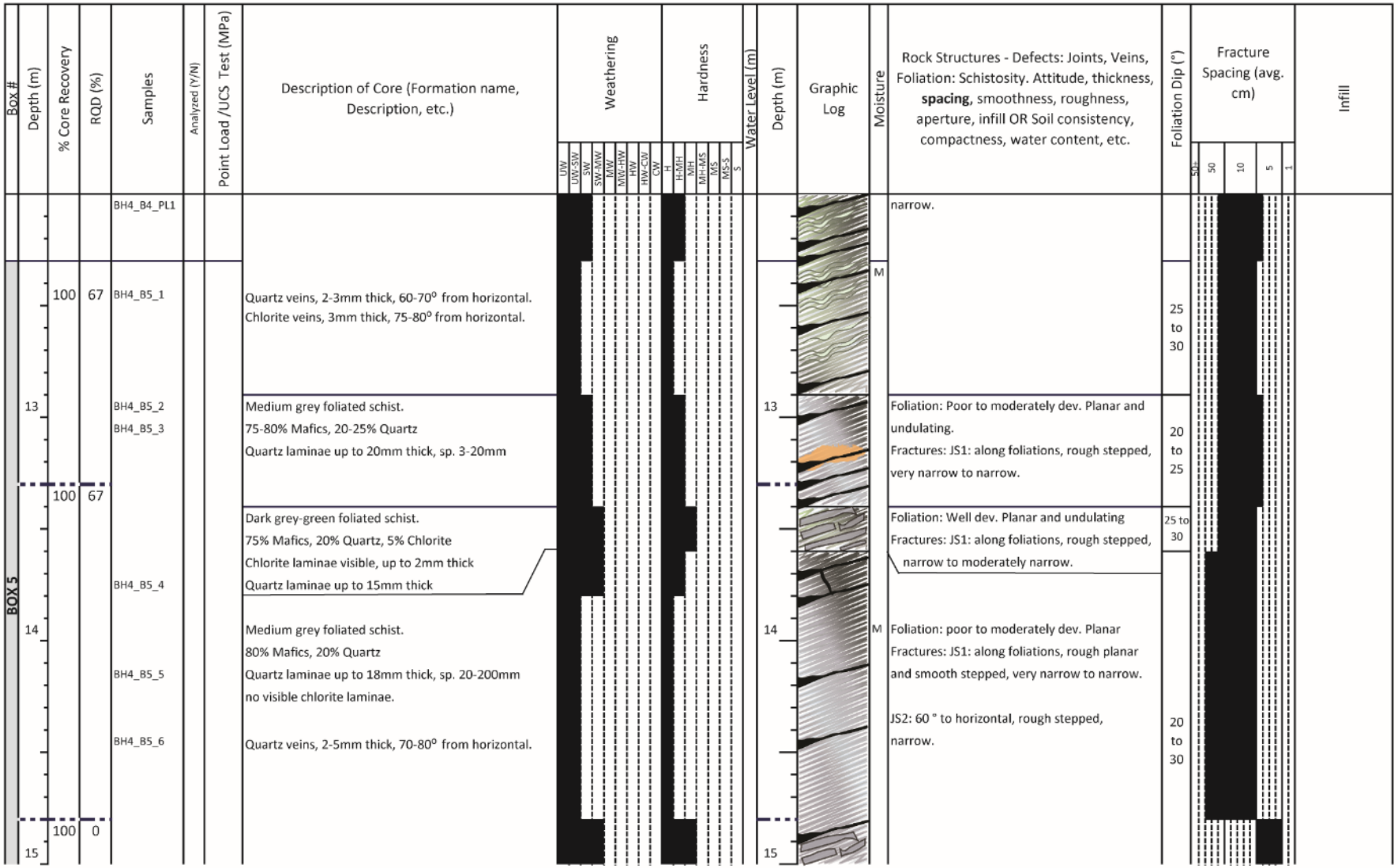
Box #
Depth (m)
% Core Recovery
RQD (%)
Samples
Analyzed (Y/N)
Point Load /UCS Test (MPa)
Description of Core (Formation name, Description, etc.)
Weathering
UW
UW-SW
SW
SW-MW
MW
MW-HW
HW
HW-CW
CW
Hardness
H
H-MH
MH
MH-MS
MS
MS-S
S
Water Level (m)
Depth (m)
Graphic Log
Moisture
Rock Structures - Defects: Joints, Veins, Foliation: Schistosity. Attitude, thickness, spacing, smoothness, roughness, aperture, infill OR Soil consistency, compactness, water content, etc.
Foliation Dip (°)
Fracture Spacing (avg. cm)
Infill
BOX 5
BH4_B4_PL1
BH4_B5_1
BH4_B5_2
BH4_B5_3
BH4_B5_4
BH4_B5_5
BH4_B5_6
100
67
100
67
100
0
13
14
15
Quartz veins, 2-3mm thick, 60-70° from horizontal.
Chlorite veins, 3mm thick, 75-80° from horizontal.
Medium grey foliated schist.
75-80% Mafics, 20-25% Quartz
Quartz laminae up to 20mm thick, sp. 3-20mm
Dark grey-green foliated schist.
75% Mafics, 20% Quartz, 5% Chlorite
Chlorite laminae visible, up to 2mm thick
Quartz laminae up to 15mm thick
Medium grey foliated schist.
80% Mafics, 20% Quartz
Quartz laminae up to 18mm thick, sp. 20-200mm
no visible chlorite laminae.
Quartz veins, 2-5mm thick, 70-80° from horizontal.
M
narrow.
25 to 30
Foliation: Poor to moderately dev. Planar and undulating.
Fractures: JS1: along foliations, rough stepped, very narrow to narrow.
20 to 25
Foliation: Well dev. Planar and undulating
Fractures: JS1: along foliations, rough stepped, narrow to moderately narrow.
25 to 30
Foliation: poor to moderately dev. Planar
Fractures: JS1: along foliations, rough planar and smooth stepped, very narrow to narrow.
JS2: 60 ° to horizontal, rough stepped, narrow.
20 to 30
Sh
50
10
5
1

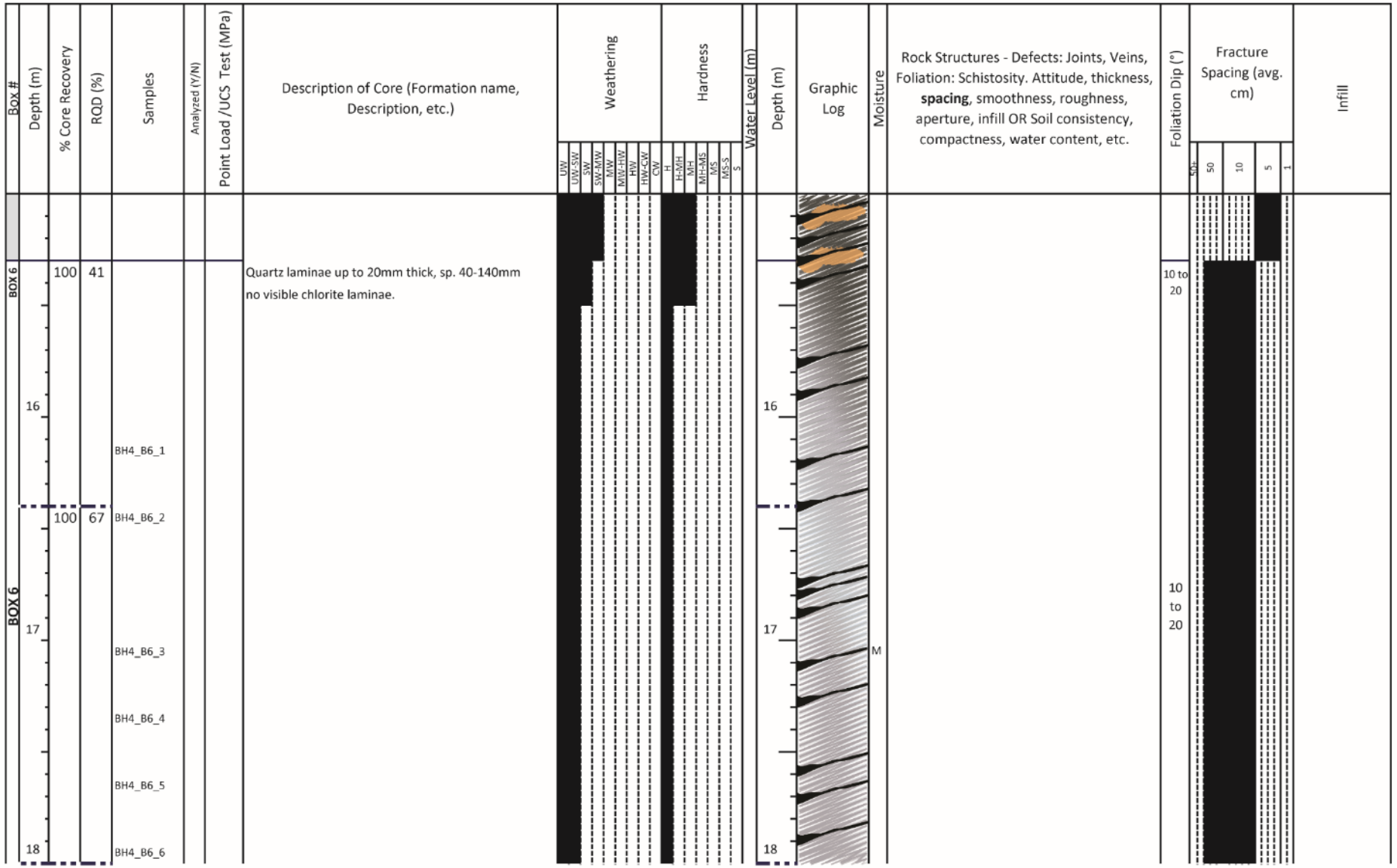
Box #
Depth (m)
% Core Recovery
RQD (%)
Samples
Analyzed (Y/N)
Point Load /UCS Test (MPa)
Description of Core (Formation name, Description, etc.)
Weathering
UW
UW-SW
SW
SW-MW
MW
MW-HW
HW
HW-CW
CW
Hardness
H
H-MH
MH
MH-MS
MS
MS-S
S
Water Level (m)
Depth (m)
Graphic Log
Moisture
Rock Structures - Defects: Joints, Veins, Foliation: Schistosity. Attitude, thickness, spacing, smoothness, roughness, aperture, infill OR Soil consistency, compactness, water content, etc.
Foliation Dip (°)
Fracture Spacing (avg. cm)
Infill
BOX 6
100
41
Quartz laminae up to 20mm thick, sp. 40-140mm
no visible chlorite laminae.
10 to 20
16
BH4_B6_1
100
67
BH4_B6_2
17
BH4_B6_3
BH4_B6_4
BH4_B6_5
M
10 to 20
18
BH4_B6_6

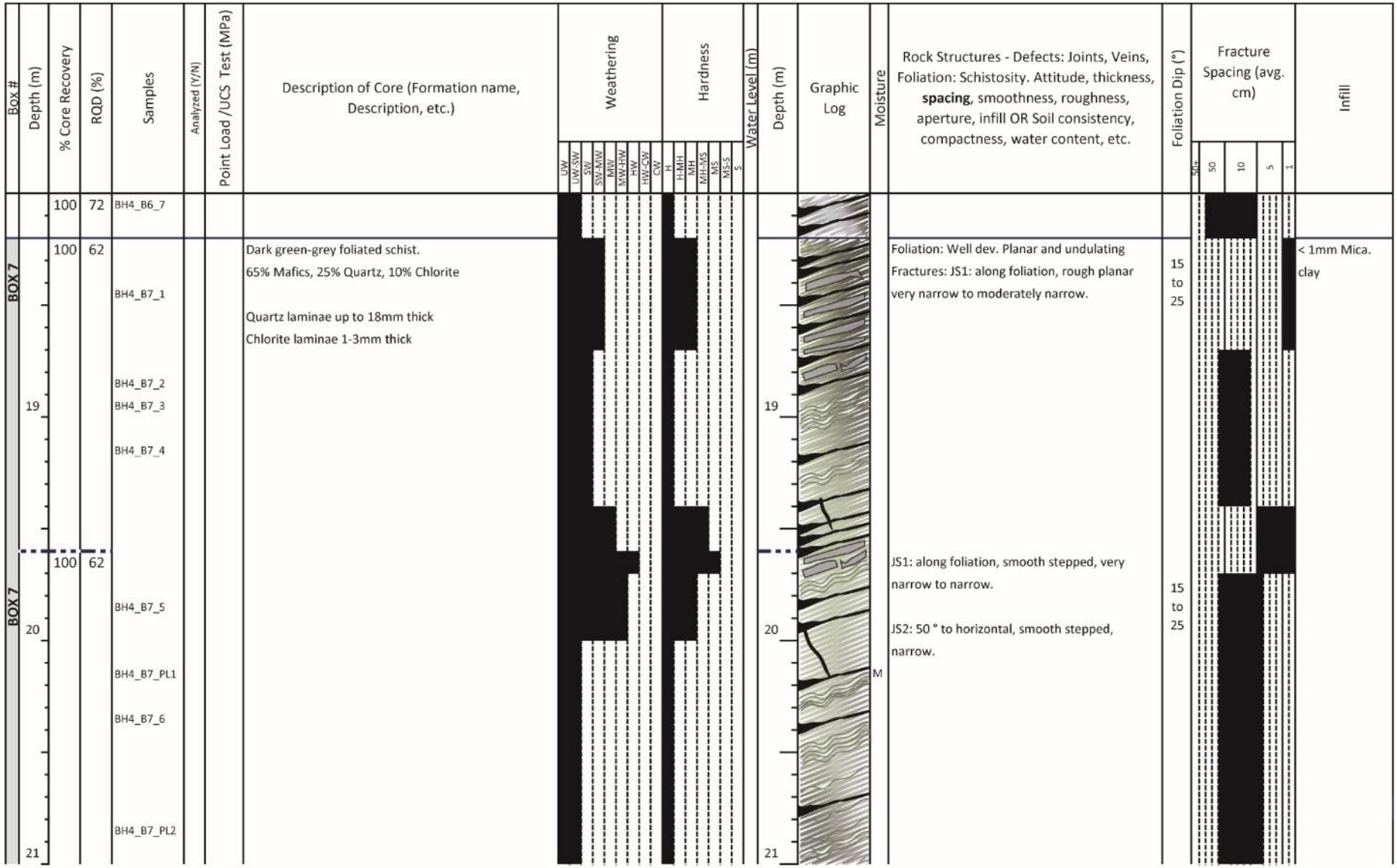
Box #
Depth (m)
% Core Recovery
RQD (%)
Samples
Analyzed (Y/N)
Point Load /UCS Test (MPa)
Description of Core (Formation name, Description, etc.)
Weathering
UW
UW-SW
SW
SW-MW
MW
MW-HW
HW
HW-CW
CW
Hardness
H
H-MH
MH
MH-MS
MS
MS-S
S
Water Level (m)
Depth (m)
Graphic Log
Moisture
Rock Structures - Defects: Joints, Veins, Foliation: Schistosity. Attitude, thickness, spacing, smoothness, roughness, aperture, infill OR Soil consistency, compactness, water content, etc.
Foliation Dip (°)
Fracture Spacing (avg. cm)
Sd+
50
10
5
1
Infill
100 72 BH4_B6_7
BOX 7
100 62
Dark green-grey foliated schist.
65% Mafics, 25% Quartz, 10% Chlorite
Quartz laminae up to 18mm thick
Chlorite laminae 1-3mm thick
BH4_B7_1
BH4_B7_2
BH4_B7_3
BH4_B7_4
19
Foliation: Well dev. Planar and undulating
Fractures: JS1: along foliation, rough planar very narrow to moderately narrow.
15 to 25
< 1mm Mica. clay
BOX 7
100 62
BH4_B7_5
BH4_B7_PL1
BH4_B7_6
20
JS1: along foliation, smooth stepped, very narrow to narrow.
JS2: 50 ° to horizontal, smooth stepped, narrow.
15 to 25
M
BH4_B7_PL2
21

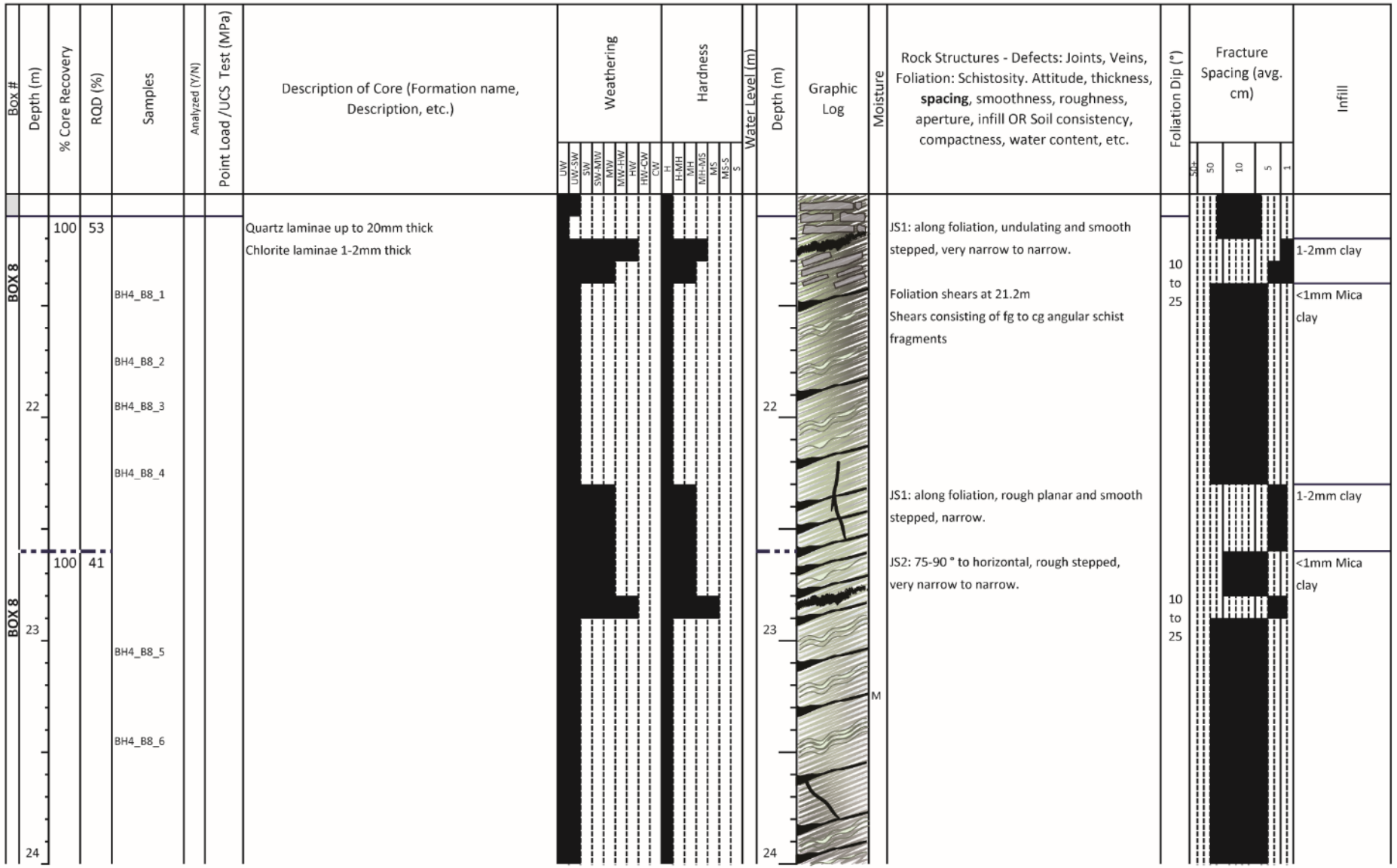
Box #
Depth (m)
% Core Recovery
RQD (%)
Samples
Analyzed (Y/N)
Point Load /UCS Test (MPa)
Description of Core (Formation name, Description, etc.)
Weathering
UW
UW-SW
SW
SW-MW
MW
MW-HW
HW
HW-CW
CW
Hardness
H
H-MH
MH
MH-MS
MS
MS-S
S
Water Level (m)
Depth (m)
Graphic Log
Moisture
Rock Structures - Defects: Joints, Veins, Foliation: Schistosity. Attitude, thickness, spacing, smoothness, roughness, aperture, infill OR Soil consistency, compactness, water content, etc.
Foliation Dip (°)
Fracture Spacing (avg. cm)
Sd+
50
10
5
1
Infill
BOX 8
100
53
Quartz laminae up to 20mm thick
Chlorite laminae 1-2mm thick
BH4_B8_1
BH4_B8_2
BH4_B8_3
BH4_B8_4
22
JS1: along foliation, undulating and smooth stepped, very narrow to narrow.
Foliation shears at 21.2m
Shears consisting of fg to cg angular schist fragments
10 to 25
1-2mm clay
<1mm Mica clay
JS1: along foliation, rough planar and smooth stepped, narrow.
1-2mm clay
BOX 8
100
41
JS2: 75-90 ° to horizontal, rough stepped, very narrow to narrow.
<1mm Mica clay
23
BH4_B8_5
M
10 to 25
BH4_B8_6
24

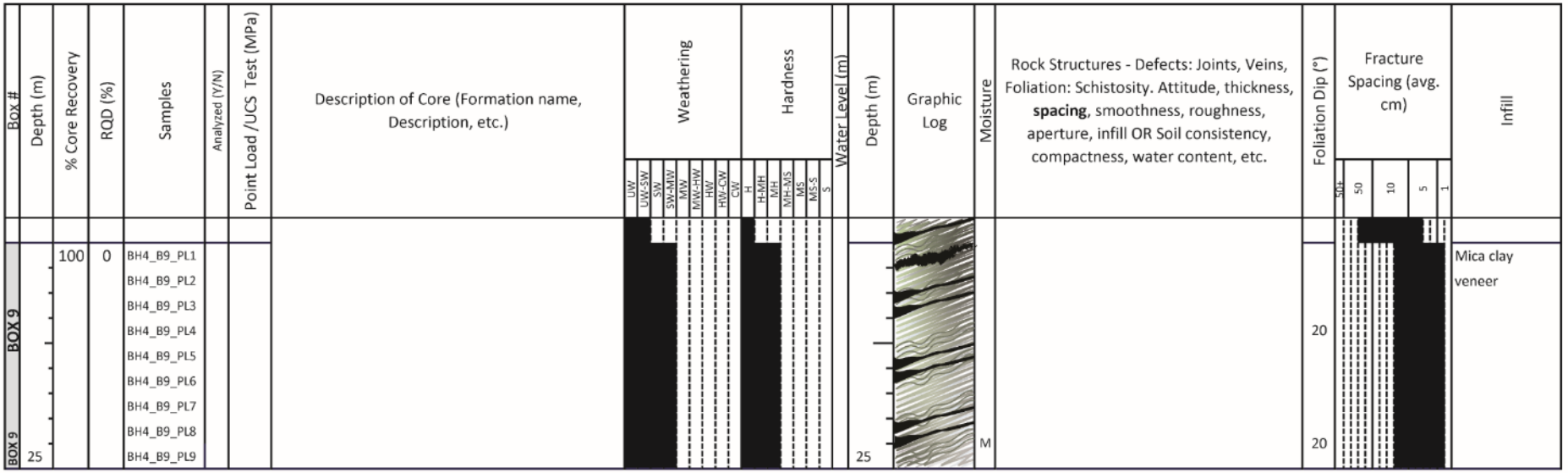

Legend

BH4_B9_PL10

UW-MW, foliated dark grey-green SCHIST; strong; foliation dips 15-30° to horizontal, well developed, planar and undulating. Joints are steep to sub-vertically inclined and moderately wide spaced.
[Mapped as Caples Terrane, Textural Zone 3 Schist]

UW-MW, foliated medium grey SCHIST; strong; foliation dips 15-25° to horizontal, poorly to moderately developed, planar. Joints are steep to sub-vertically inclined and moderately wide spaced.
[Mapped as Caples Terrane, Textural Zone 3 Schist]

Clayey SILT with vf sand and rootlets; orange-brown.

Cobble sized schist fragments

Coarse Gravel sized schist fragments

Gravels

Sand

Clay/Silt

Fracture or Joint

Iron Staining/ Weathering

Foliation Shear

Upright tight isoclinal folds (70° limbs)

Weathering
UW: Unweathered
SW: Slightly Weathered
MW: Moderately Weathered
HW: Highly Weathered
CW: Completely Weathered

Hardness
H: Hard
MH: Moderately Hard
MS: Moderately Soft
S: Soft

Moisture
D: Dry
M: Moist
W: Wet

Grain Size
cl/si: Clay/Silt
vfs: Very fine sand
fs: Fine sand
ms: Medium sand
cs: Coarse sand
s: Sand
fg: Fine gravel
mg: Medium gravel
cg: Coarse gravel
g: Gravel
cb: Cobble

NC Core loss/No Recovery

Appendix B

Appendix B: Contents

Appendix B: Geomorphology of Queenstown Hill

B.1 Mapped Ice Extents in the Wakatipu Area

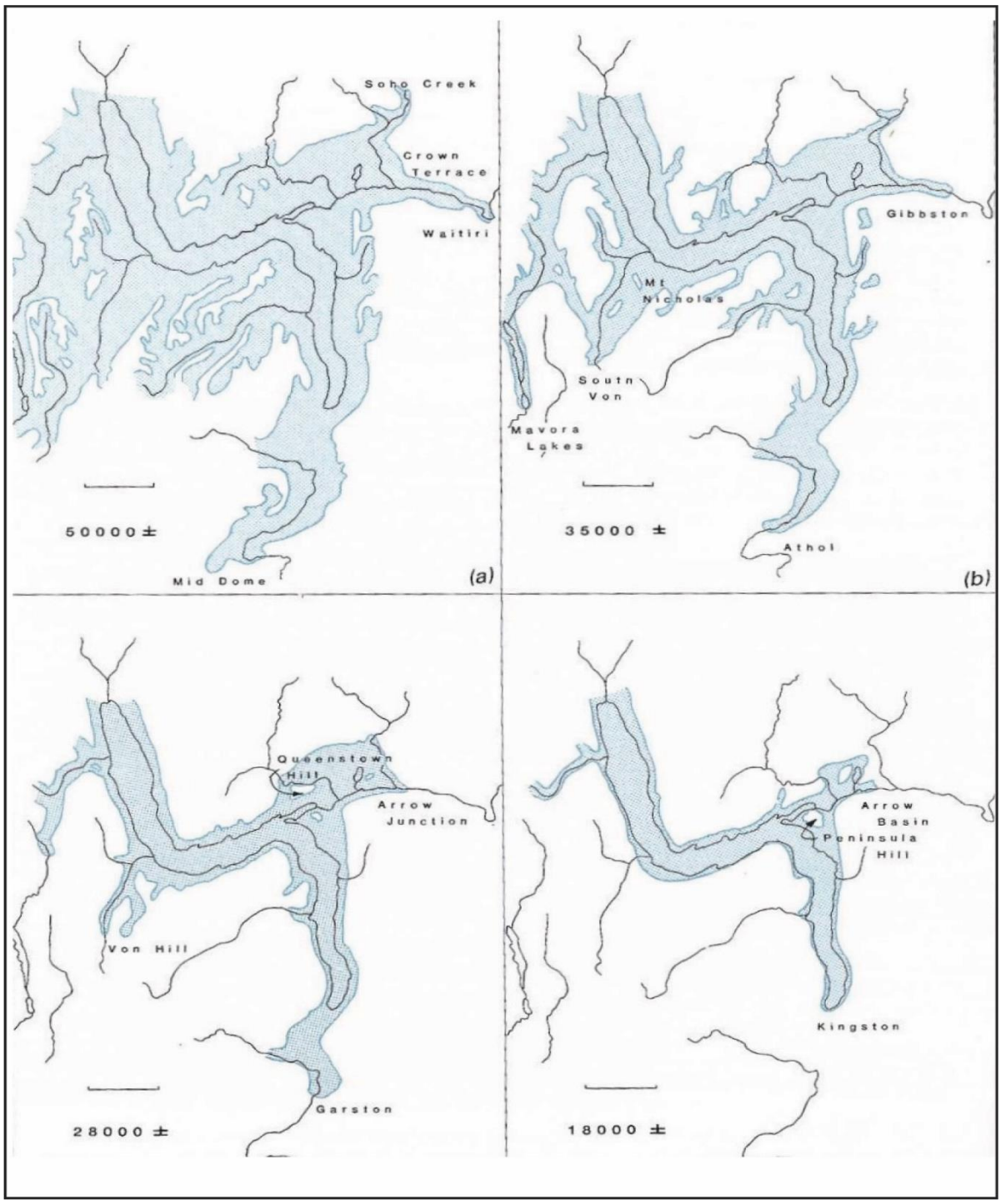

Figure B1: Maps of Lake Wakatipu area, showing limits of ice advances over the last 50,000 years (approximately). Scale is 10km in each map.
a) 50,000 years BP (before present). Ice extended down the Oreti and Mararoa valleys beyond Mavora Lakes, down the Mataura Valley to near Mid Dome, down the Kawarau Valley to Waitiri, over the Crown Terrace, and up the Arrow River.
b) 35,000 years BP. Following an interglacial retreat at ca. 40,000 years BP, ice again pushed into the Von as far as the South Von area, down the Kawarau to Gibbston, and as far as Athol in the Mataura catchment. Mt Nicholas emerged from the ice as a nunatak.
c) The next advance at 28,000 years BP. Ice terminated near Garston and at the entrance to the Kawarau Gorge. Ice tongues reached into the Von valley, and Queenstown and Peninsula hills emerged as nunataks.
d) The last advance, 18,000 years ago. Ice covered most of the Arrow Basin, but only reached as far as Kingston. (Turnbull and Forsyth, 1988).

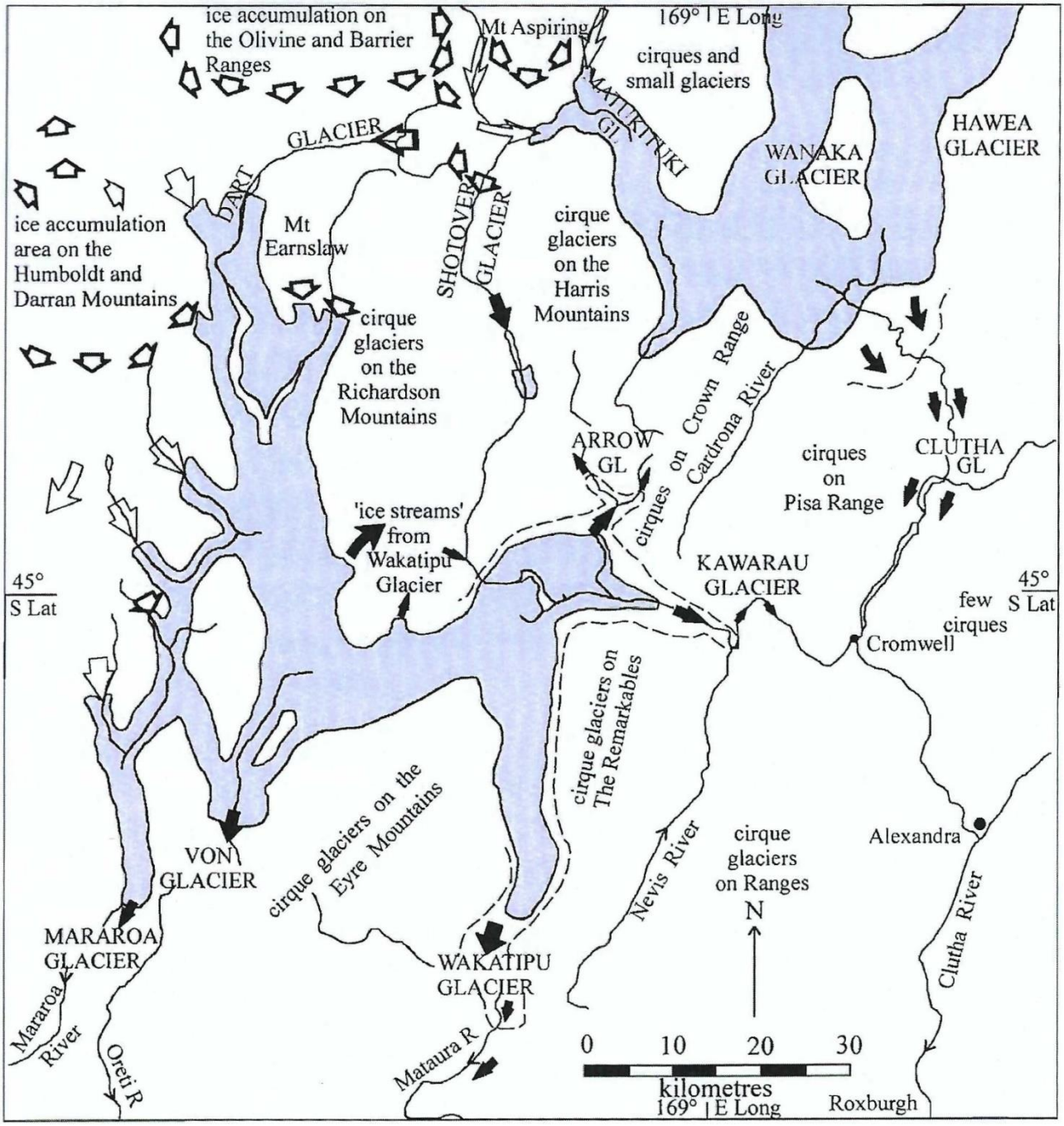

Figure B2: Map showing maximum ice limits for the Last (light blue) and Penultimate (dashed) Glaciations in the Wakatipu and Clutha catchments. Open arrows show the approximate directions of ice movement away from the snow accumulation areas, and the infilled arrows indicate the resultant glacier patterns (Bell, 1992).

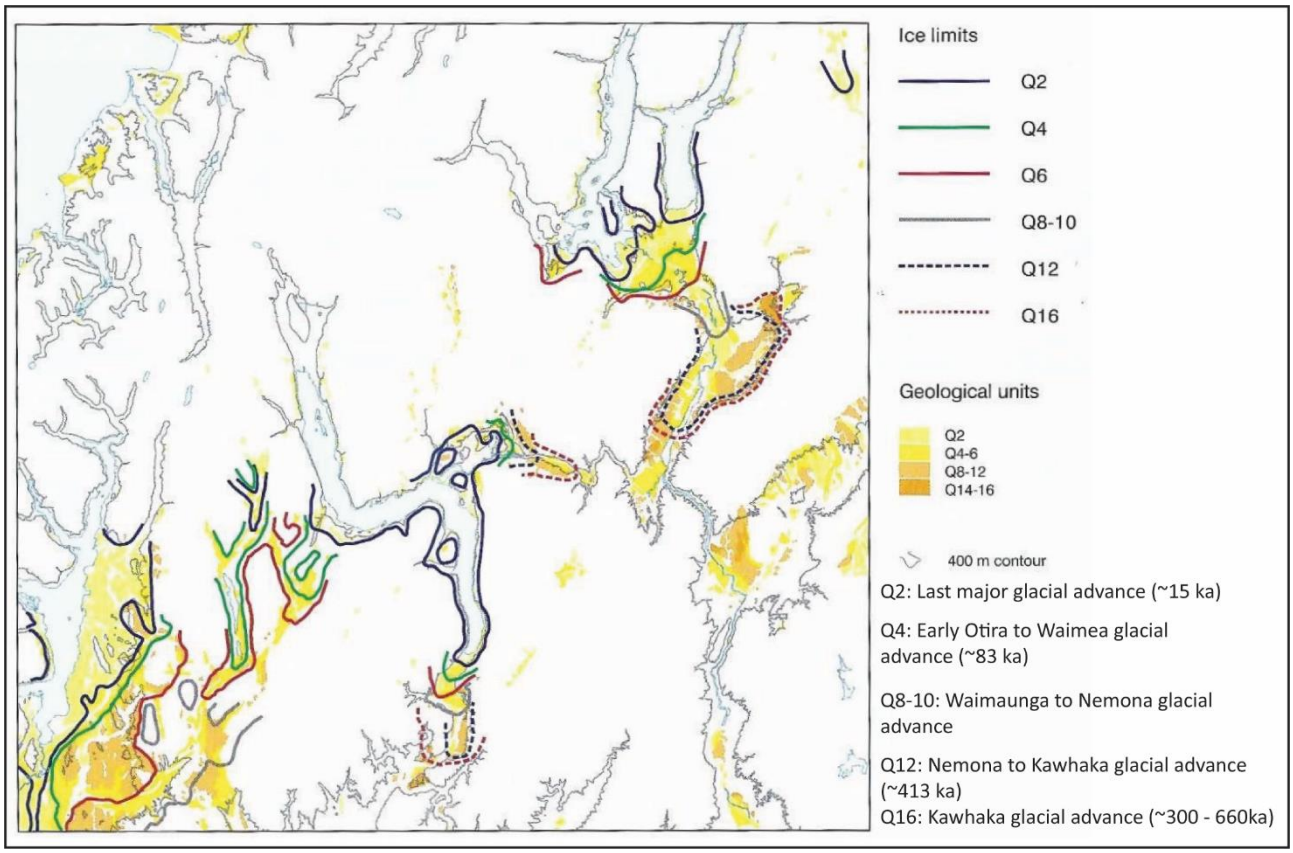

Figure B3: Down-valley limits of ice advances in major catchments, and extent of main Quaternary deposits. Early Quaternary ice limits and South Westland floating ice are not shown. (Turnbull, 2000).

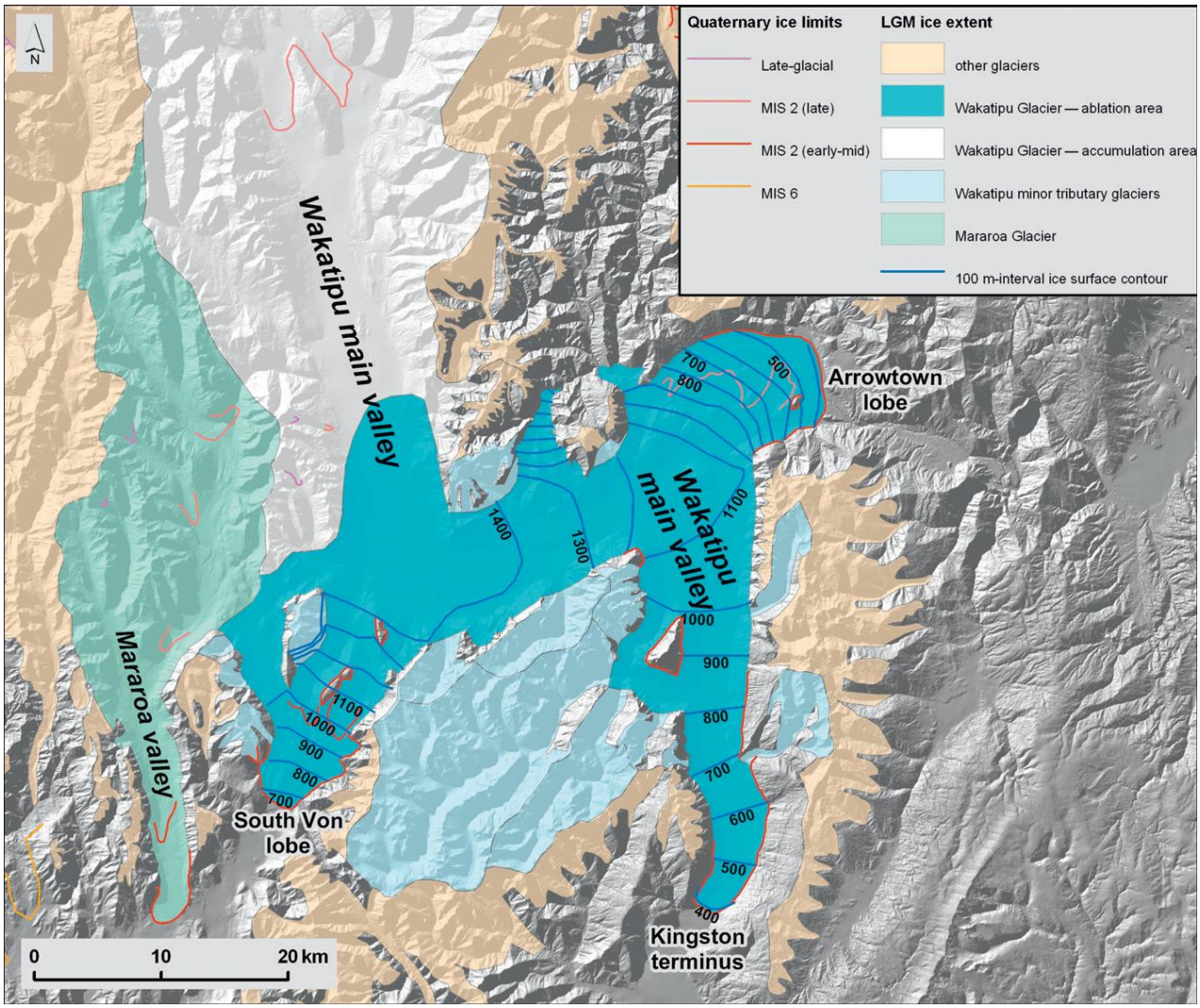

Figure B4: A reconstruction of the LGM glacier of the Lake Wakatipu area (Barrell, 2011).

Appendix B: Geomorphology of Queenstown Hill

B.2 Surficial Deposit Maps

B.2.1 Cunningham (1994)

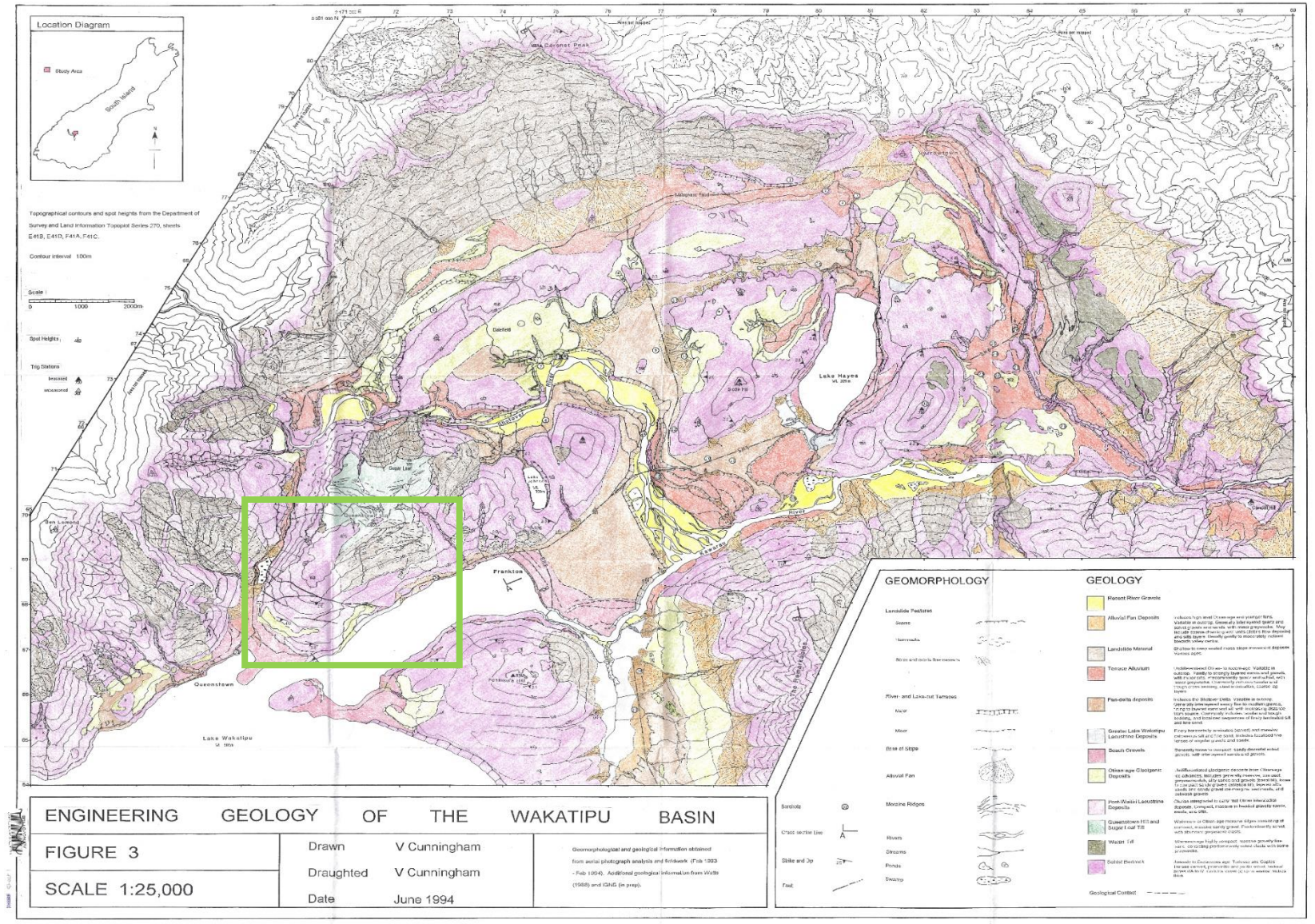

Figure B5.1: Engineering Geological Map of the Wakatipu Basin 1:25,000. Field area is highlighted in Green. Zoomed in view in Figure 5.2 (Cunningham, 1994).

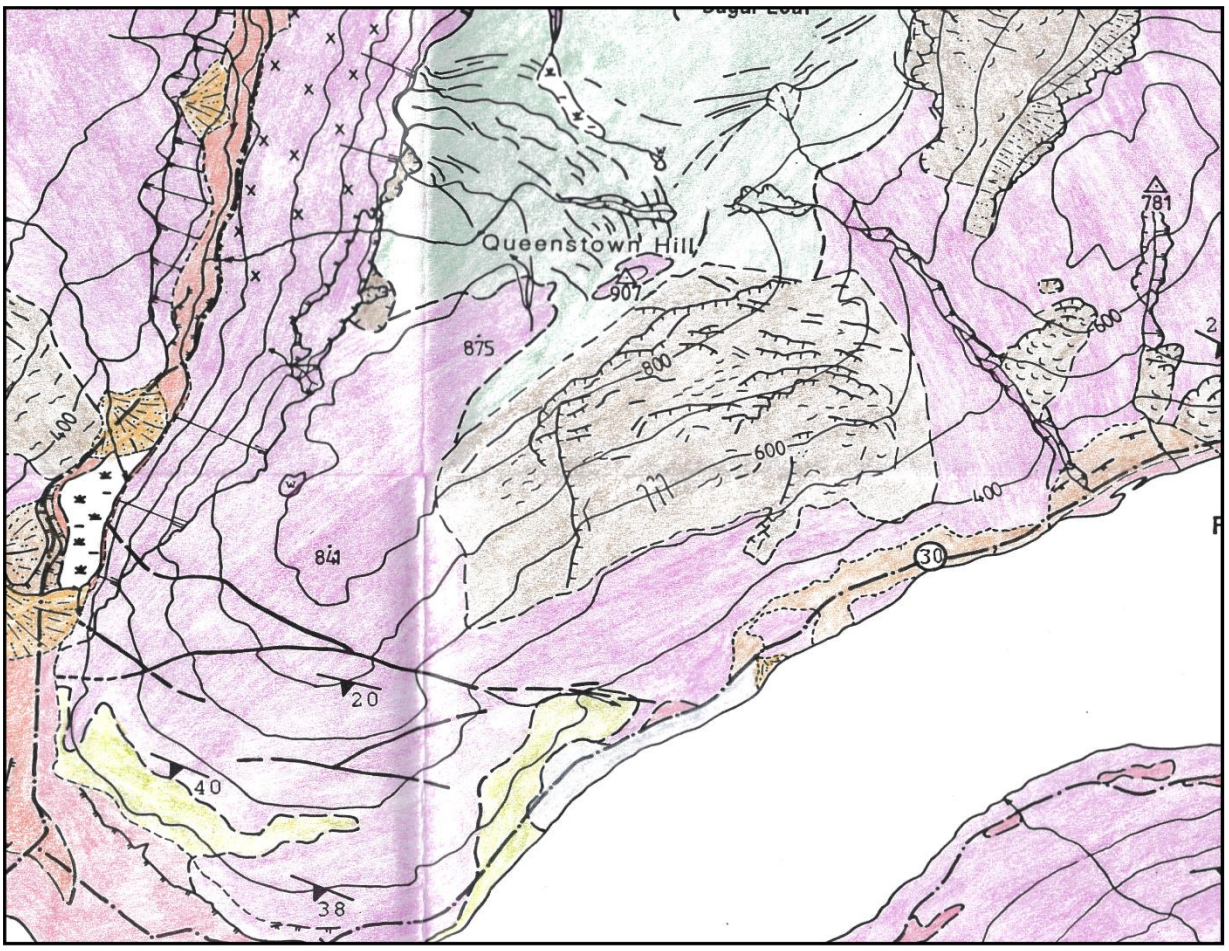

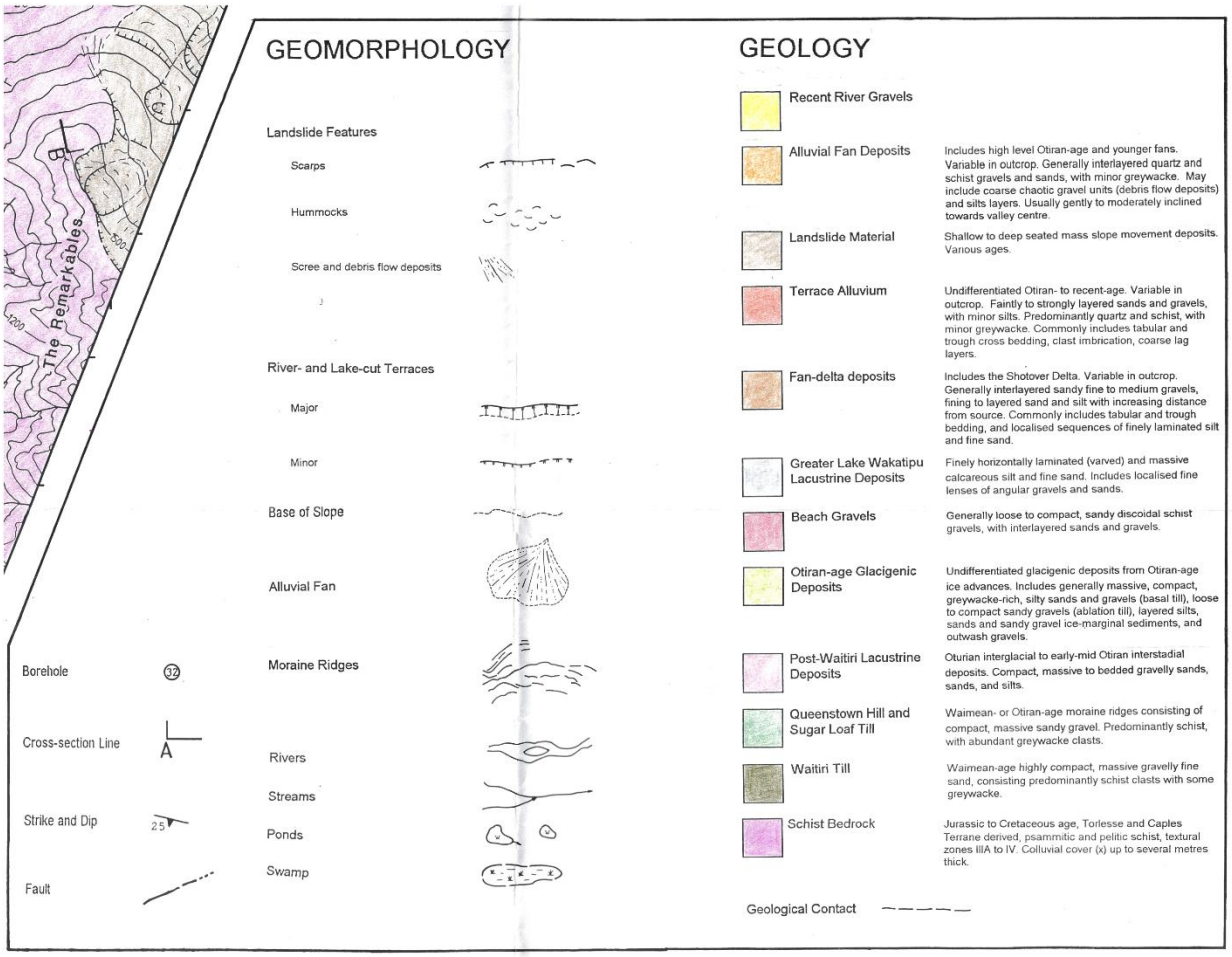

Figure B5.2: Zoomed in view of Queenstown Hill from the 1:25,000 map (Cunningham,1994).

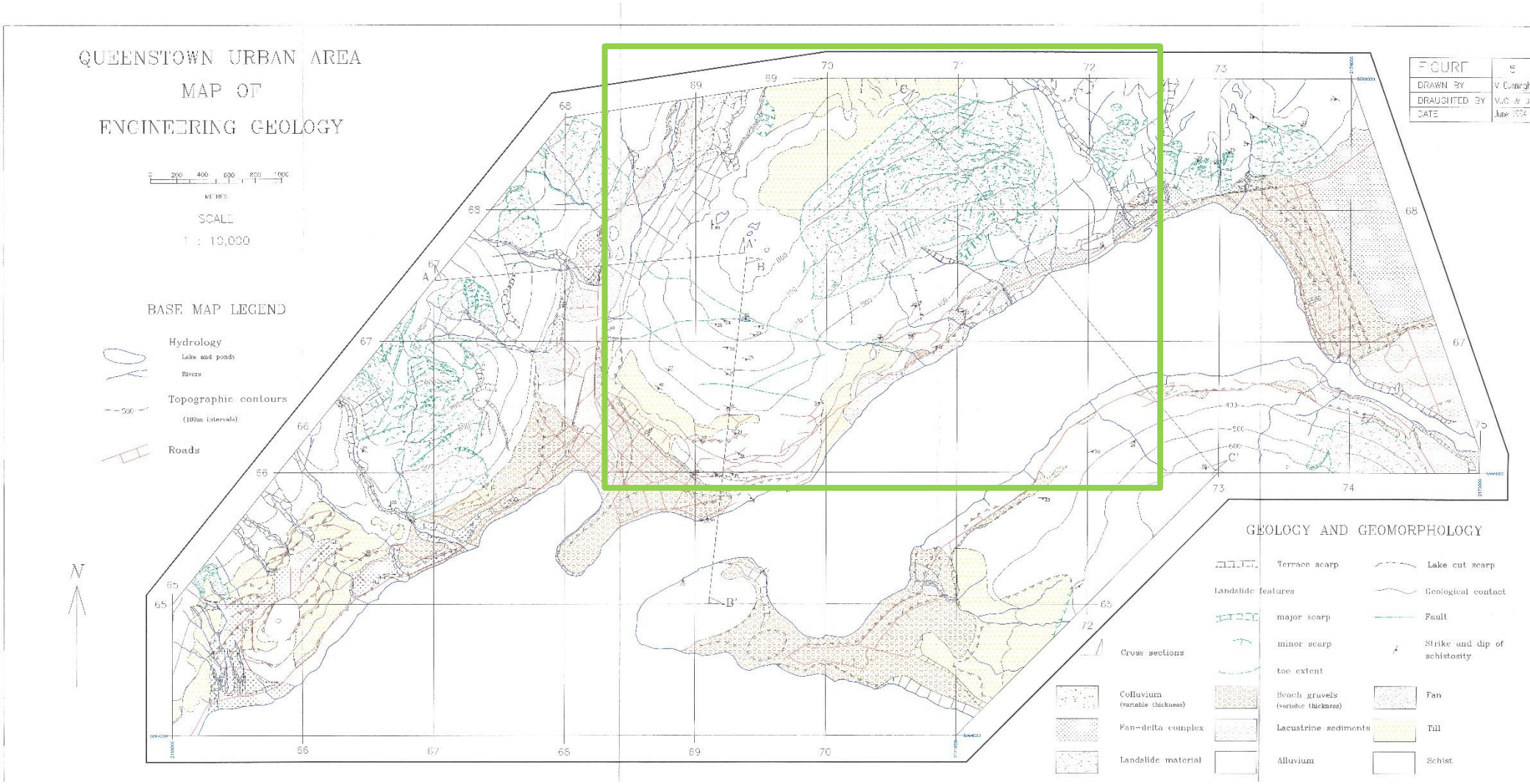

Figure B6.1: Engineering Geological Map of the Queenstown Urban Area, 1:10,000. Field area highlighted in green. Zoomed in view in Figure 6.2 (Cunningham, 1994).

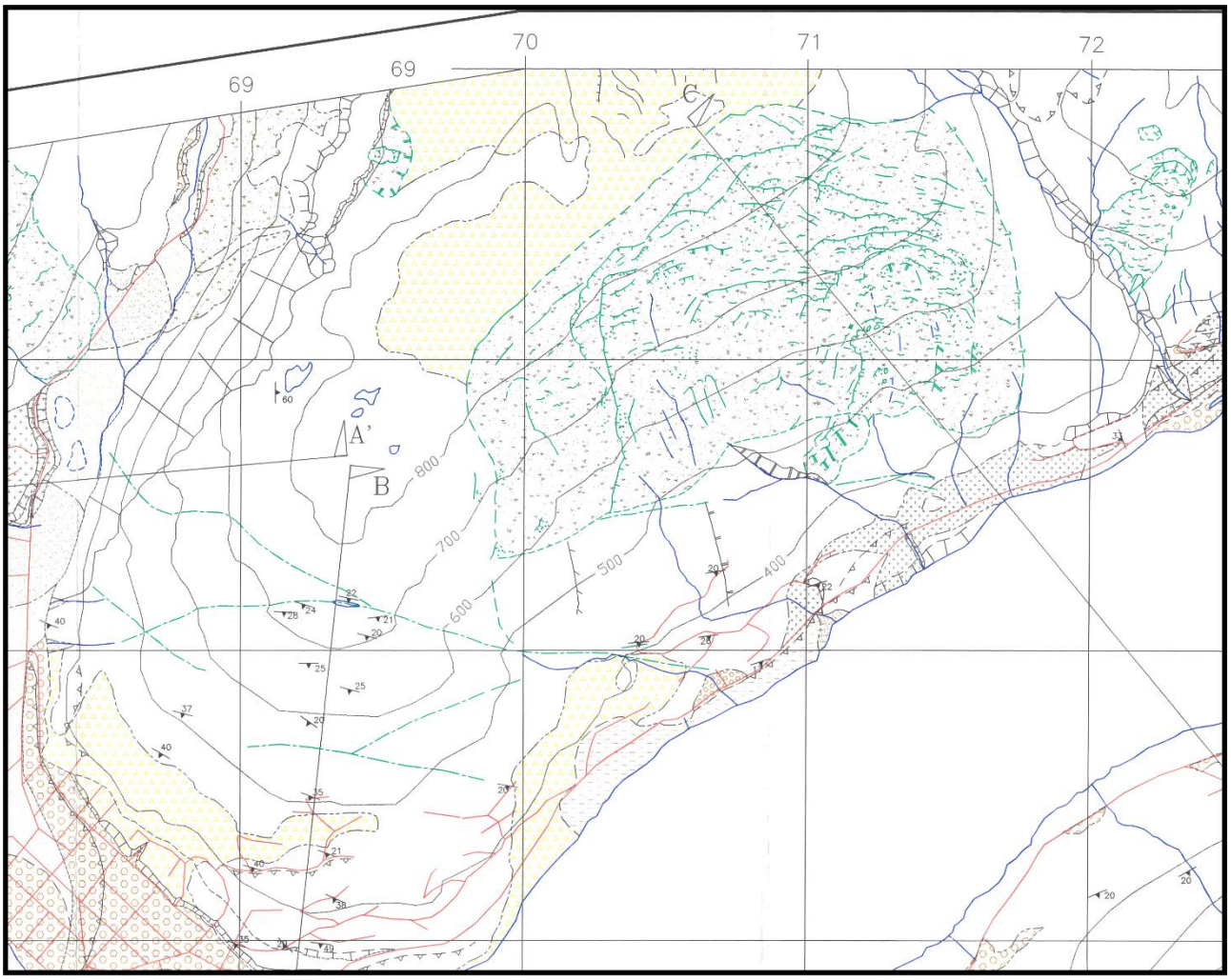

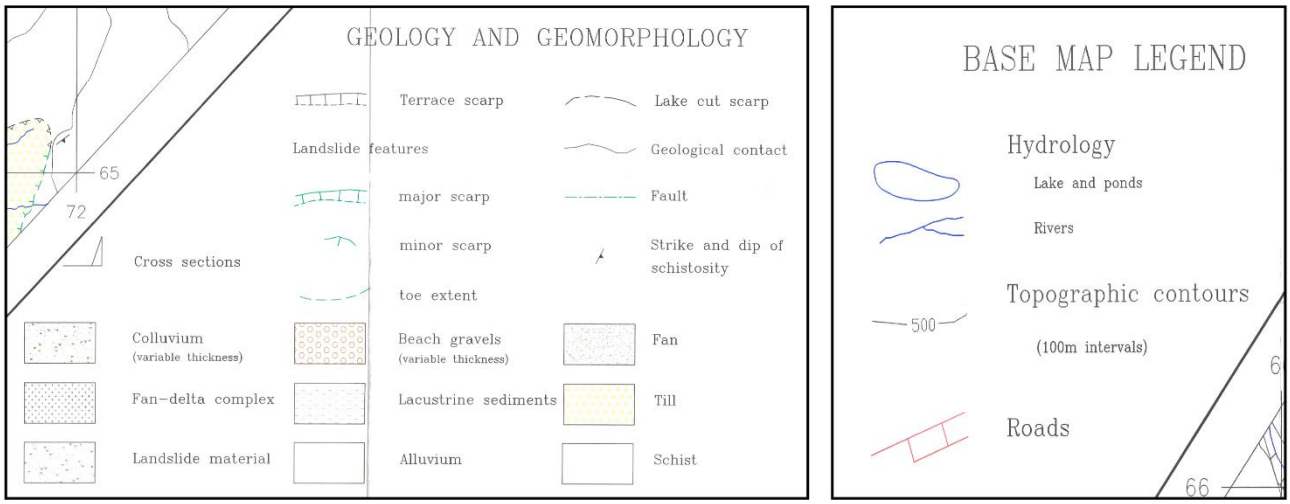

Figure B6.2: Zoomed in view of Queenstown Hill from the 1:10,000 map (Cunningham,1994).

B.2.2 Barrell et al. (1994)

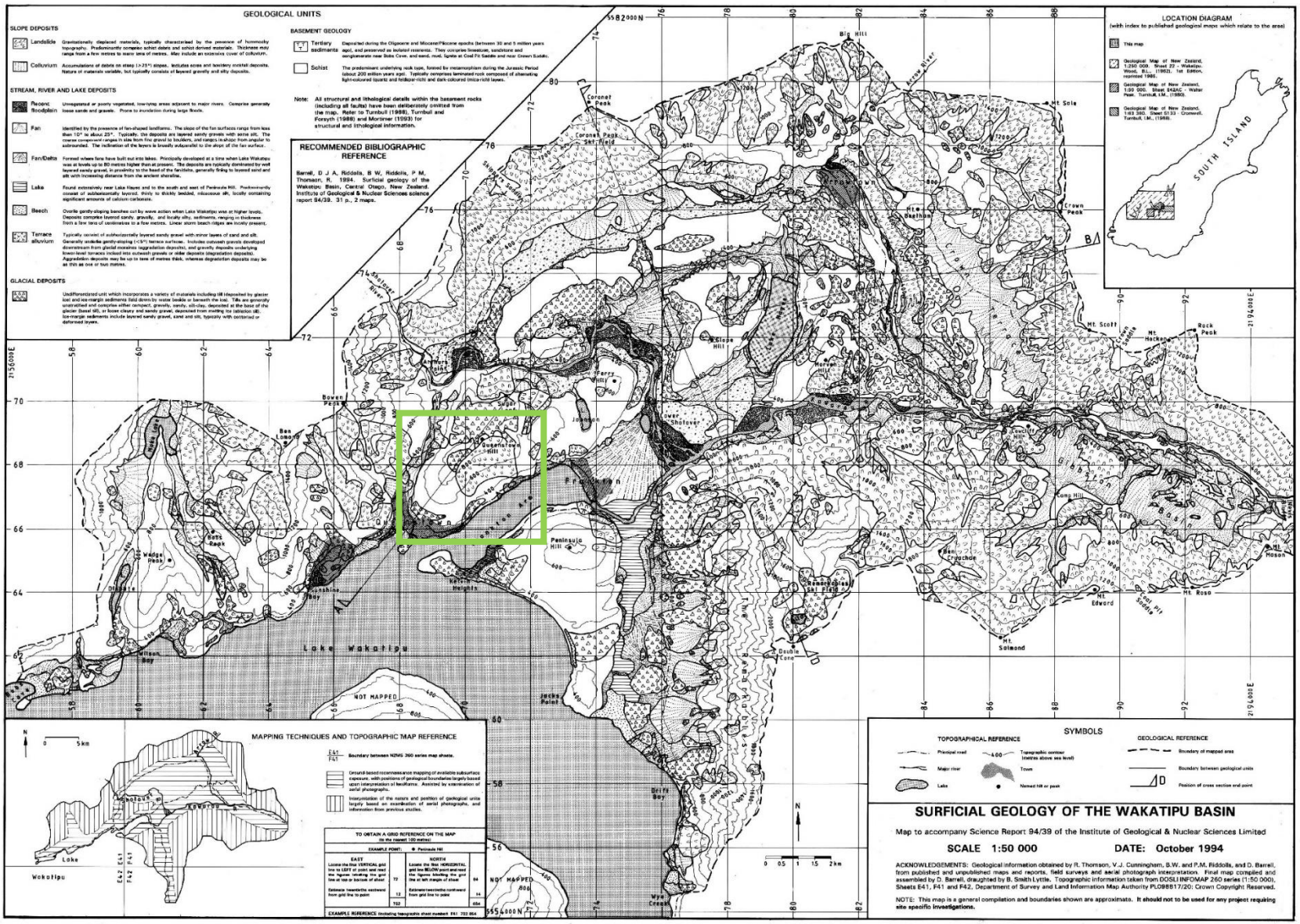

Figure B7.1: Surficial Geology of the Wakatipu Basin, 1:50,000. Field area highlighted in green. Zoomed in view in Figure 7.2 (Barrell et al., 1994).

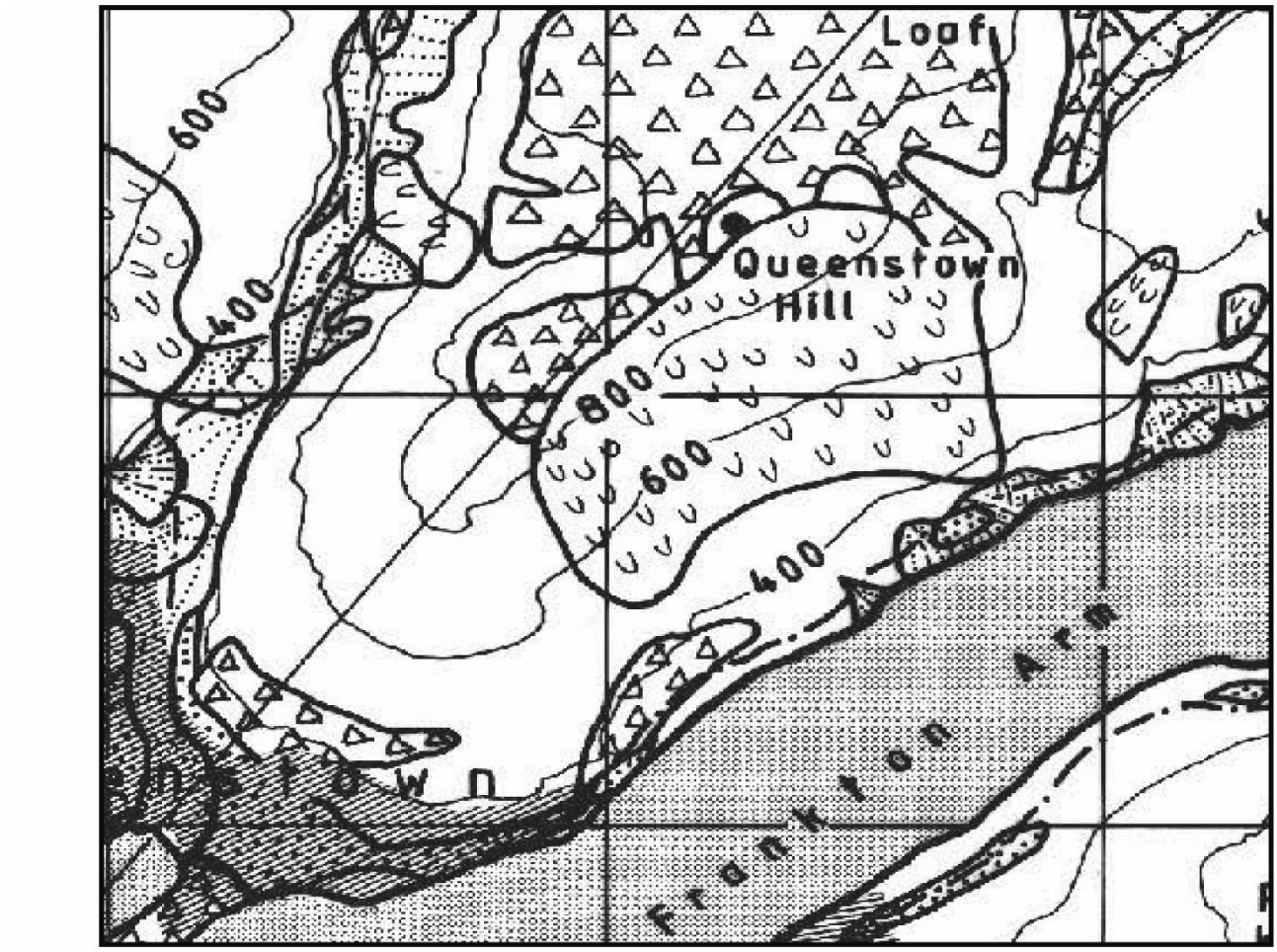

GEOLOGICAL UNITS

SLOPE DEPOSITS

Landslide — Gravitationally displaced materials, typically characterised by the presence of hummocky topography. Predominantly comprise schist debris and schist-derived materials. Thickness may range from a few metres to many tens of metres. May include an extensive cover of colluvium.

Colluvium — Accumulations of debris on steep (>25°) slopes. Includes scree and bouldery rockfall deposits. Nature of materials variable, but typically consists of layered gravelly and silty deposits.

STREAM, RIVER AND LAKE DEPOSITS

Recent floodplain — Unvegetated or poorly vegetated, low-lying areas adjacent to major rivers. Comprise generally loose sands and gravels. Prone to inundation during large floods.

Fan — Identified by the presence of fan-shaped landforms. The slope of the fan surfaces range from less than 10° to about 25°. Typically, the deposits are layered sandy gravels with some silt. The coarse component ranges in size from fine gravel to boulders, and ranges in shape from angular to subrounded. The inclination of the layers is broadly subparallel to the slope of the fan surface.

Fan/Delta — Formed where fans have built out into lakes. Principally developed at a time when Lake Wakatipu was at levels up to 80 metres higher than at present. The deposits are typically dominated by well layered sandy gravel, in proximity to the head of the fan/delta, generally fining to layered sand and silt with increasing distance from the ancient shoreline.

Lake — Found extensively near Lake Hayes and to the south and east of Peninsula Hill. Predominantly consist of subhorizontally layered, thinly to thickly bedded, micaceous silt, locally containing significant amounts of calcium carbonate.

Beach — Overlie gently-sloping benches cut by wave action when Lake Wakatipu was at higher levels. Deposits comprise layered sandy, gravelly, and locally silty, sediments, ranging in thickness from a few tens of centimetres to a few metres. Linear storm beach ridges are locally present.

Terrace alluvium — Typically consist of subhorizontally layered sandy gravel with minor layers of sand and silt. Generally underlie gently-sloping (<5°) terrace surfaces. Includes outwash gravels developed downstream from glacial moraines (aggradation deposits), and gravelly deposits underlying lower-level terraces incised into outwash gravels or older deposits (degradation deposits). Aggradation deposits may be up to tens of metres thick, whereas degradation deposits may be as thin as one or two metres.

GLACIAL DEPOSITS

Undifferentiated unit which incorporates a variety of materials including till (deposited by glacier ice) and ice-margin sediments (laid down by water beside or beneath the ice). Tills are generally unstratified and comprise either compact, gravelly, sandy, silt-clay, deposited at the base of the glacier (basal till), or loose clayey and sandy gravel, deposited from melting ice (ablation till). Ice-margin sediments include layered sandy gravel, sand and silt, typically with contorted or deformed layers.

BASEMENT GEOLOGY

Tertiary sediments — Deposited during the Oligocene and Miocene/Pliocene epochs (between 30 and 5 million years ago), and preserved as isolated remnants. They comprise limestone, sandstone and conglomerate near Bobs Cove, and sand, mud, lignite at Coal Pit Saddle and near Crown Saddle.

Schist — The predominant underlying rock type, formed by metamorphism during the Jurassic Period (about 200 million years ago). Typically comprises laminated rock composed of alternating light-coloured (quartz and feldspar-rich) and dark-coloured (mica-rich) layers.

Note: All structural and lithological details within the basement rocks (including all faults) have been deliberately omitted from the map. Refer to Turnbull (1988), Turnbull and Forsyth (1988) and Mortimer (1993) for structural and lithological information.

RECOMMENDED BIBLIOGRAPHIC REFERENCE

Barrell, D J A, Riddolls, B W, Riddolls, P M, Thomson, R, 1994. Surficial geology of the Wakatipu Basin, Central Otago, New Zealand. Institute of Geological & Nuclear Sciences science report 94/39. 31 p., 2 maps.

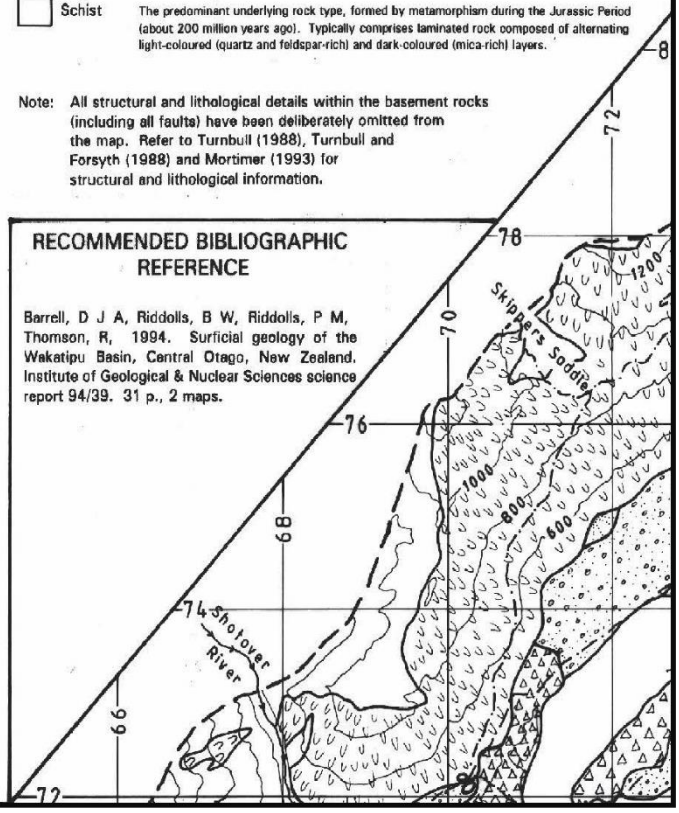

Figure B7.2: Zoomed in view of Queenstown Hill from the 1:50,000 map (Barrell et al.,1994).

B.2.3 Stossel, (1999)

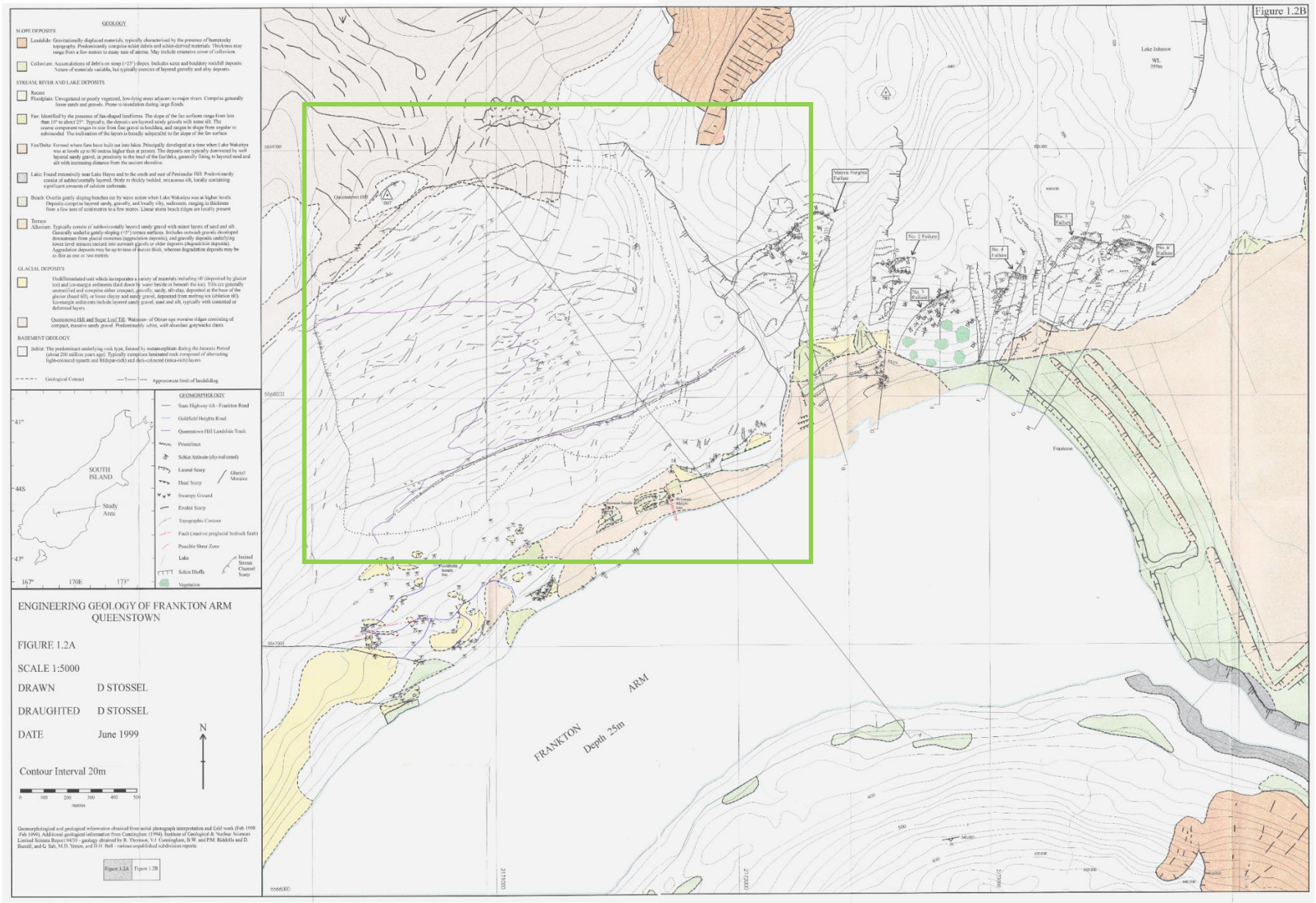

Figure B8: Engineering Geology of Frankton Arm Queenstown 1:5000 scale (Stossel, 1999).

Appendix B: Geomorphology of Queenstown Hill

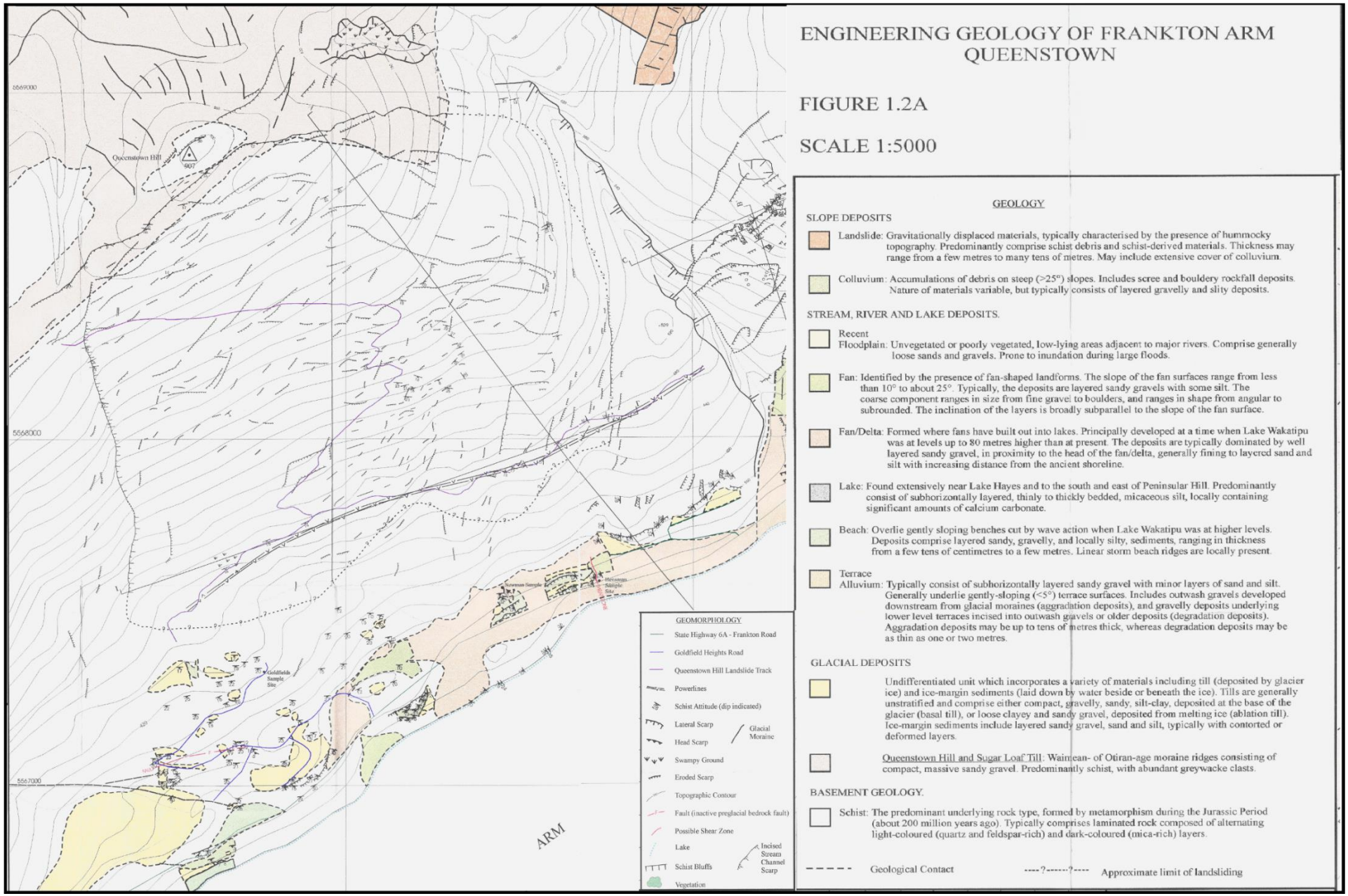

Figure B8.2: Zoomed in view of Queenstown Hill from the 1:5000 map (Stossel, 1999).

B.2.4 Turnbull (2000)

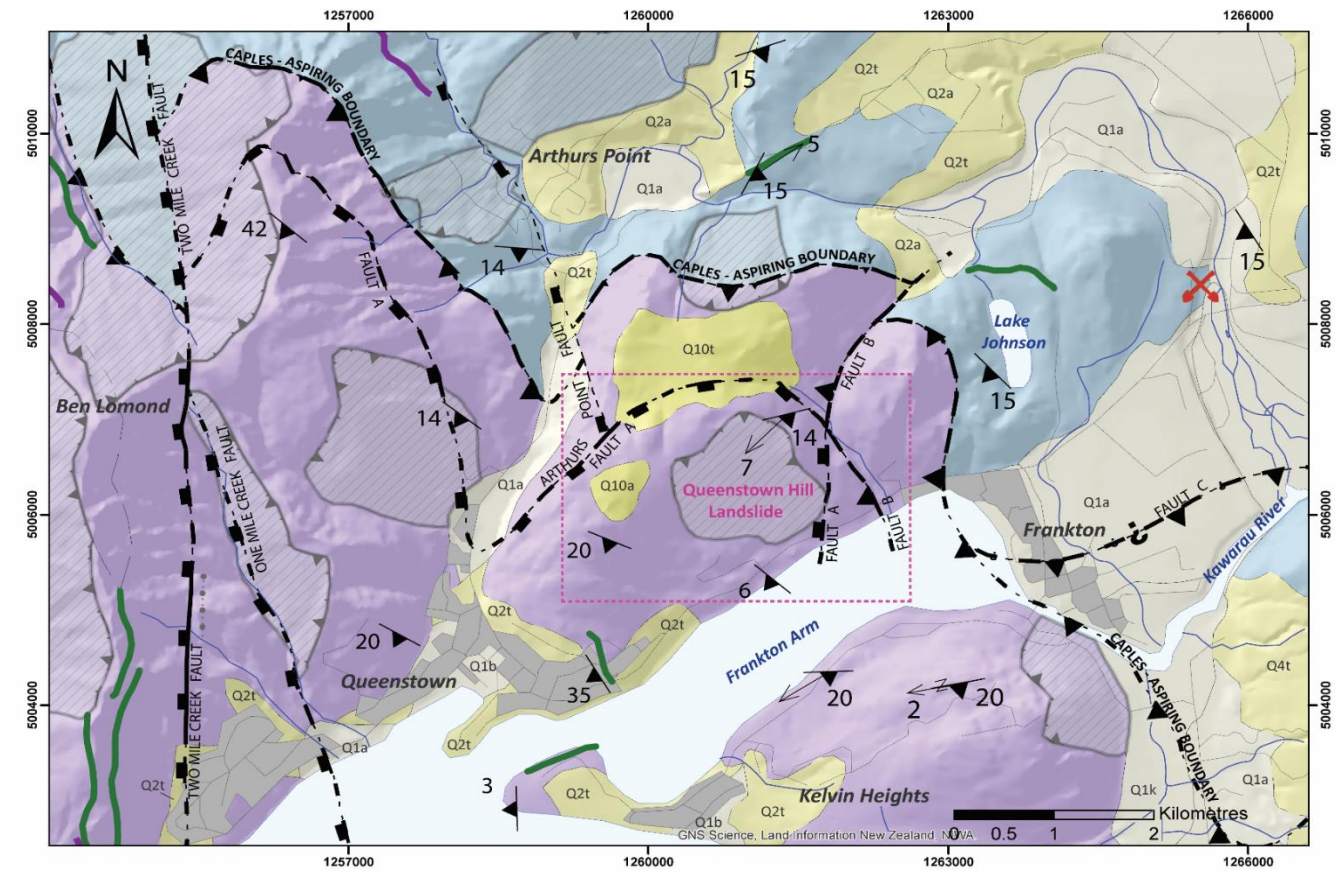

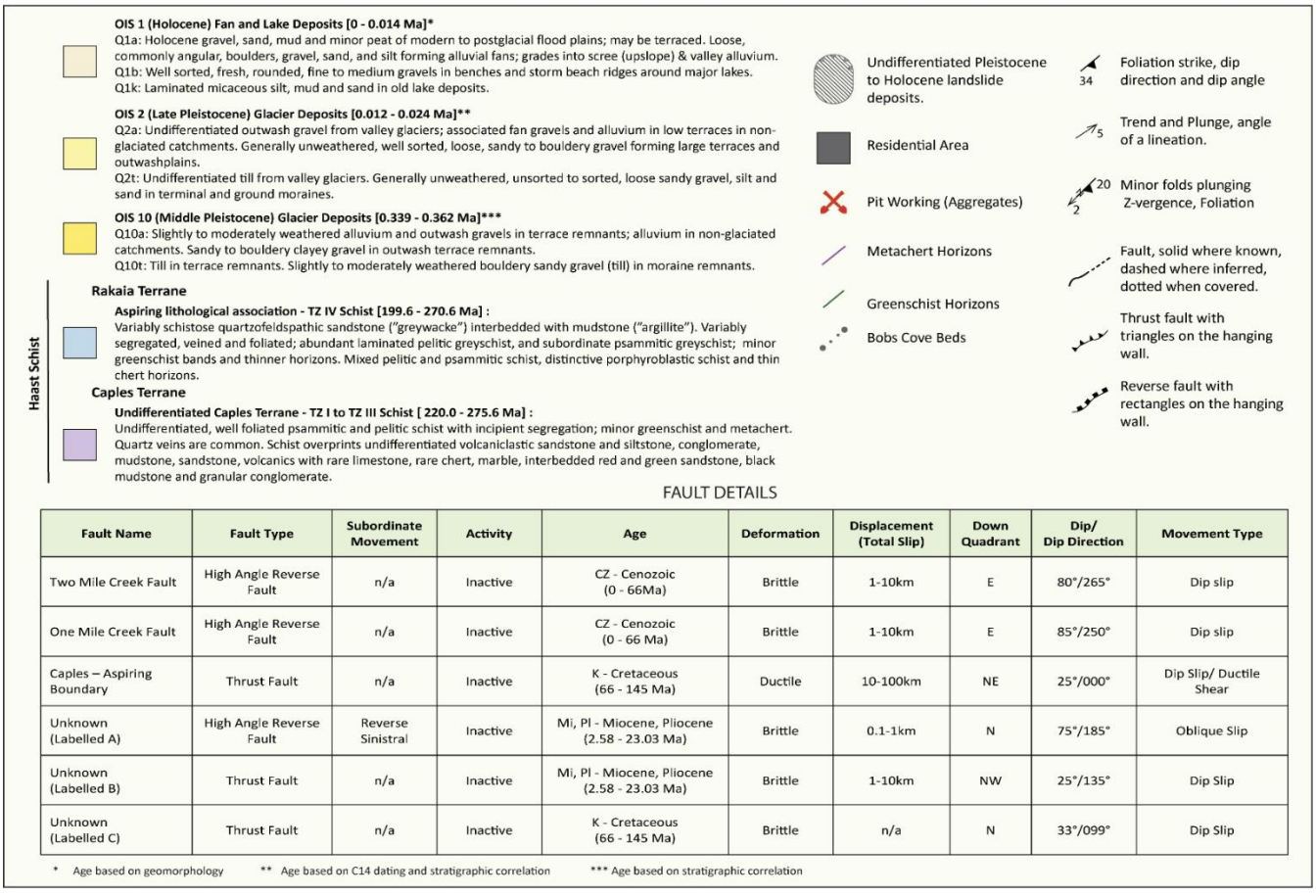

FAULT DETAILS

Fault Name	Fault Type	Subordinate Movement	Activity	Age	Deformation	Displacement (Total Slip)	Down Quadrant	Dip/ Dip Direction	Movement Type
Two Mile Creek Fault	High Angle Reverse Fault	n/a	Inactive	CZ - Cenozoic (0 - 66Ma)	Brittle	1-10km	E	80°/265°	Dip slip
One Mile Creek Fault	High Angle Reverse Fault	n/a	Inactive	CZ - Cenozoic (0 - 66 Ma)	Brittle	1-10km	E	85°/250°	Dip slip
Caples – Aspiring Boundary	Thrust Fault	n/a	Inactive	K - Cretaceous (66 - 145 Ma)	Ductile	10-100km	NE	25°/000°	Dip Slip/ Ductile Shear
Unknown (Labelled A)	High Angle Reverse Fault	Reverse Sinistral	Inactive	Mi, Pl - Miocene, Pliocene (2.58 - 23.03 Ma)	Brittle	0.1-1km	N	75°/185°	Oblique Slip
Unknown (Labelled B)	Thrust Fault	n/a	Inactive	Mi, Pl - Miocene, Pliocene (2.58 - 23.03 Ma)	Brittle	1-10km	NW	25°/135°	Dip Slip
Unknown (Labelled C)	Thrust Fault	n/a	Inactive	K - Cretaceous (66 - 145 Ma)	Brittle	n/a	N	33°/099°	Dip Slip

* Age based on geomorphology ** Age based on C14 dating and stratigraphic correlation *** Age based on stratigraphic correlation

Figure B9: Surficial deposits mapped on a redrawn QMap (Turnbull, 2000).

B.3 10-year Survey Data from Aurum Survey

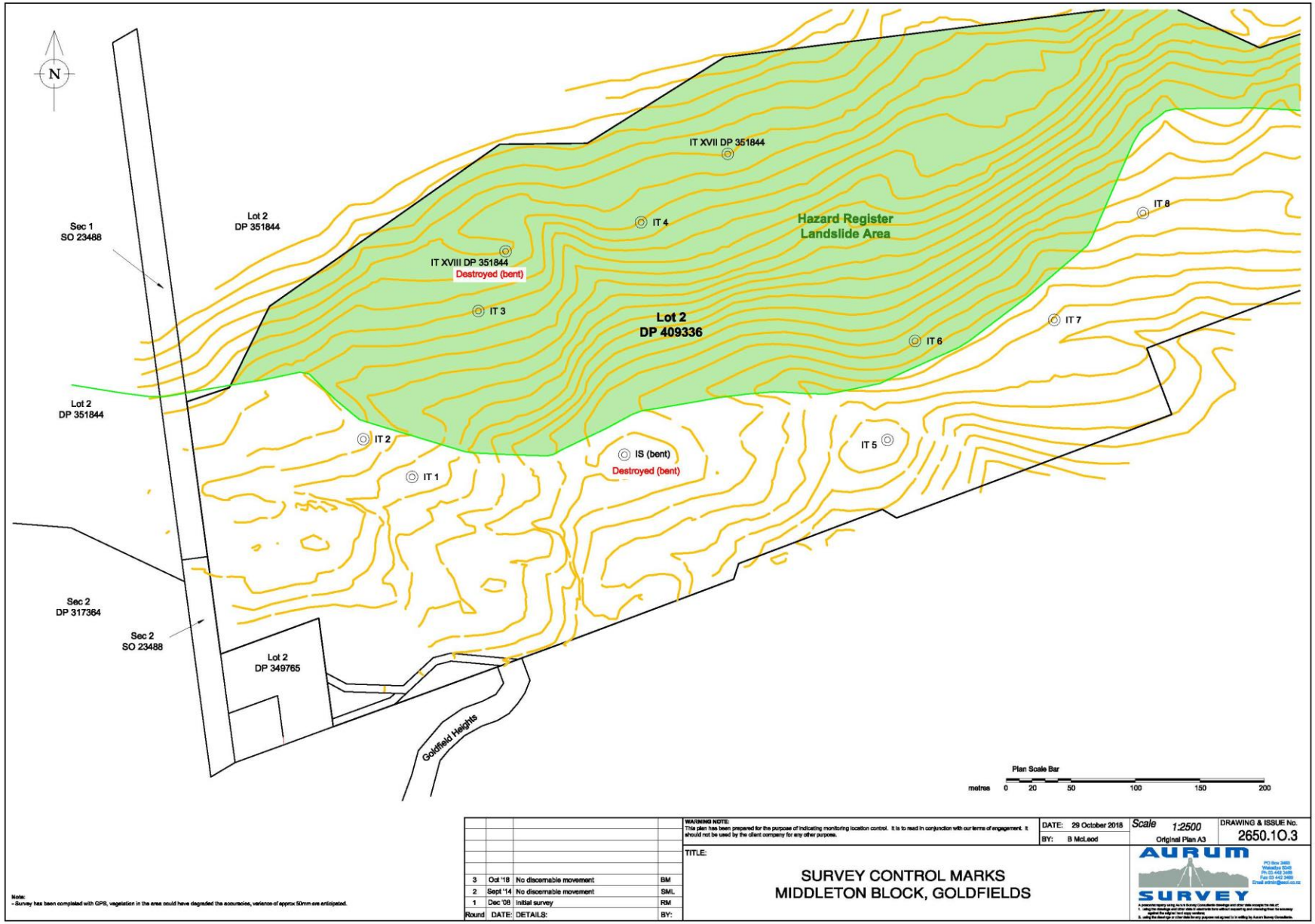

Figure B10: Survey data of the lower portion of Queenstown Hill. Surveyed by Aurum Survey from 2008 to 2018.

Appendix C

Appendix C: Contents

C.1 Sample Data: Physical Properties (Moisture Content, Density, and Porosity)

C.1.1 Moisture Content Samples

Individual moisture content sample results.

Moisture Content Data							
Sample	Lithotype	Depth (m)	In situ mass (g)	Dry mass (g)	Bulk density (kg/m^3)	Dry density (kg/m^3)	Moisture Content
BH3_B1_2	MGy	2.50	1106.20	1097.40	2829.3	2806.8	0.80
BH3_B5_4	MGy	14.00	1085.90	1078.10	2812.2	2792.0	0.72
BH3_B5_4	MGy	14.00	1018.30	1006.50	2771.0	2738.8	1.16
BH4_B3_2	MGy	7.40	920.30	914.30	2771.5	2753.4	0.65
BH4_B3_PL1	MGy	6.67	841.30	830.00	2644.2	2608.7	1.34
BH4_B3_PL2	MGy	7.55	513.10	509.30	2736.8	2716.5	0.74
BH4_B3_PL3	MGy	8.80	564.50	560.70	2817.3	2798.3	0.67
BH4_B5_2	MGy	12.89	481.80	478.30	2797.1	2776.7	0.73
BH4_B6_7	MGy	18.05	607.50	601.70	2804.7	2777.9	0.95
BH1_B4_3	DGy	9.85	1074.60	1067.30	2767.8	2749.0	0.68
BH3_B6_2	DGy	16.50	963.20	956.40	2725.4	2706.1	0.71
BH4_B1_PL1	DGy	1.60	749.10	743.30	2781.0	2759.5	0.77
BH4_B1_PL3	DGy	2.25	585.30	581.70	2754.4	2737.5	0.62
BH4_B2_PL10	DGy	6.03	660.00	652.10	2757.1	2724.1	1.20
BH4_B2_PL7	DGy	4.80	456.30	450.50	2834.3	2798.3	1.27
BH4_B7_PL1	DGy	20.15	467.30	462.60	2748.2	2720.6	1.01
BH4_B7_PL2	DGy	20.80	363.30	359.70	2774.7	2747.2	0.99
BH4_B8_3	DGy	21.97	984.00	977.80	2766.5	2749.0	0.63

C.1.2 Porosity Samples

Individual sample results obtained from the gas pycnometer to derive porosity.

Porosity Data							
Sample	Lithotype	Density (kg/m^3)	Cube volume (cm^3)	Pycnometer volume (cm^3)	Pycnometer Standard Deviation	Pore Volume (cm^3)	Porosity (%)
BH4_B3_2	MGy	2694.0	40.20	38.91	0.02	1.29	3.22
BH4_B3_2PP	MGy	2720.9	38.15	37.41	0.01	0.73	1.93
BH4_B3_2PR	MGy	2747.6	24.28	23.41	0.04	0.86	3.56
BH4_B3_PL1	MGy	2573.1	46.05	43.03	0.05	3.02	6.57
BH4_B3_PL2	MGy	2687.3	40.97	39.72	0.02	1.25	3.04
BH4_B3_PL2P	MGy	2701.2	16.07	15.73	0.04	0.33	2.07
BH4_B3_PL2R	MGy	2691.8	16.57	16.16	0.03	0.41	2.49
BH4_B3_PL3	MGy	2763.7	48.01	46.87	0.05	1.15	2.39
BH4_B3_PR1	MGy	2682.5	33.18	32.27	0.05	0.91	2.75
BH4_B5_2	MGy	2794.4	33.42	32.35	0.04	1.08	3.23
BH4_B5_2P	MGy	2724.6	12.37	11.98	0.02	0.39	3.18
BH4_B6_7	MGy	2707.2	25.71	24.95	0.06	0.75	2.94
BH3_B5_1A	MGy	2793.4	22.78	22.05	0.01	0.73	3.19
BH3_B5_1B	MGy	2786.1	22.83	22.60	0.03	0.23	1.02
BH3_B5_5A	MGy	2686.0	22.31	21.68	0.03	0.63	2.84
BH3_B5_1C	MGy	2751.4	24.62	24.15	0.03	0.47	1.91
BH3_B5_5B	MGy	2831.2	35.06	34.10	0.02	0.97	2.75
BH1_B8_A3A	MGy	2712.1	23.42	22.76	0.03	0.66	2.81
BH1_B8_A3A2	MGy	2767.7	22.98	22.69	0.02	0.29	1.27
BH4_B6_5	MGy	2686.7	22.60	21.82	0.03	0.78	3.47
BH4_B5_4B	MGy	2803.4	19.94	19.49	0.02	0.44	2.23
BH4_B5_4A	MGy	2755.8	16.99	16.63	0.03	0.36	2.09
BH4_B1_PL1	DGy	2752.6	35.24	34.31	0.02	0.93	2.63
BH4_B1_PL3	DGy	2772.6	18.65	18.04	0.02	0.61	3.27
BH4_B1_PL3P	DGy	2718.0	21.01	20.60	0.01	0.41	1.96
BH4_B1_PR1	DGy	2752.9	39.45	38.23	0.06	1.22	3.09
BH4_B1_PR2	DGy	2733.1	31.80	30.99	0.06	0.81	2.54
BH4_B2_PL10	DGy	2657.6	51.14	47.46	0.02	3.67	7.18
BH4_B2_PL7	DGy	2756.5	50.17	48.75	0.03	1.42	2.83
BH4_B2_PLP	DGy	2710.9	49.36	47.49	0.01	1.87	3.78
BH4_B7_PL1	DGy	2713.0	59.23	57.73	0.02	1.50	2.53
BH4_B7_PL2	DGy	2699.2	45.01	43.71	0.02	1.30	2.89
BH1_B2_AB	DGy	2714.7	23.07	22.32	0.02	0.76	3.28
BH1_B2_A27	DGy	2679.5	28.42	27.52	0.04	0.90	3.17

Appendix C: Rock Mechanics

Porosity Data							
Sample	Lithotype	Density (kg/m³)	Cube volume (cm³)	Pycnometer volume (cm³)	Pycnometer Standard Deviation	Pore Volume (cm³)	Porosity (%)
BH1_B2_A3	DGy	2698.7	22.09	21.44	0.03	0.65	2.92
BH1_B2_A4	DGy	2756.7	16.14	15.81	0.03	0.33	2.04
BH1_B7_A11A	DGy	2706.3	21.37	20.70	0.05	0.67	3.13
BH1_B7_A11	DGy	2667.5	27.00	26.05	0.04	0.95	3.53
BH1_B2_A35	DGy	2705.2	20.85	20.27	0.02	0.58	2.79
BH1_B7_A5	DGy	2702.4	22.03	21.44	0.03	0.59	2.69
BH1_B7_A8	DGy	2664.4	25.52	24.72	0.03	0.81	3.16
BH1_B2_A11	DGy	2691.9	21.96	21.30	0.03	0.67	3.03
BH1_B2_A38A	DGy	2752.5	12.76	12.43	0.02	0.33	2.58
BH1_B2_A38B	DGy	2768.2	10.56	10.31	0.02	0.26	2.43

C.1.3 P and S Wave Samples

Individual sample results obtained from ultrasonic pulse velocity testing used to derive dynamic elastic constants.

Wave Velocity data												
Sample	Lithotype	Foliation (ß°)	Condition	Density (kg/m^3)	P-Wave (m/s)	S-Wave (m/s)	E_d (GPa)	ν_d	G_d (GPa)	K_d (GPa)	P Wave Ratio Sat/Dry	S Wave Ratio Sat/Dry
BH4_B3_2	MGy	25	Dry	2753.4	4756	3066	59.2	0.14	62.3	27.8	1.12	0.97
BH4_B3_PL1	MGy	25	Dry	2608.7	4292	2583	42.3	0.22	48.1	24.8	1.18	1.04
BH4_B3_PL2	MGy	30	Dry	2716.5	4853	2689	50.2	0.28	64.0	37.8	1.13	0.93
BH4_B3_PL3	MGy	30	Dry	2798.3	4921	2457	45.1	0.33	67.8	45.2	1.14	1.03
BH4_B5_2	MGy	20	Dry	2776.7	5286	2748	55.1	0.31	77.6	49.6	1.10	0.77
BH4_B6_7	MGy	15	Dry	2777.9	4564	2776	51.7	0.21	57.9	29.3	1.21	0.96
BH4_B1_PL1	DGy	15	Dry	2759.5	4202	2579	44.0	0.20	48.7	24.3	1.27	0.97
BH4_B1_PL3	DGy	20	Dry	2737.5	4785	2723	51.2	0.26	62.7	35.6	1.18	0.95
BH4_B2_PL10	DGy	25	Dry	2724.1	4912	2838	54.8	0.25	65.7	36.5	1.20	0.91
BH4_B2_PL7	DGy	30	Dry	2798.3	4955	2882	57.8	0.24	68.7	37.7	1.12	
BH4_B7_PL1	DGy	15	Dry	2720.6	5111	2178	35.9	0.39	71.1	53.9	1.13	0.94
BH4_B7_PL2	DGy	20	Dry	2747.2	4651	2675	49.3	0.25	59.4	33.2	1.15	0.95
BH4_B3_2	MGy	25	Saturated	2826.6	5318	2970	63.5	0.27	24.9	46.7	1.12	0.97
BH4_B3_PL1	MGy	25	Saturated	2697.1	5082	2680	50.7	0.31	19.4	43.8	1.18	1.04
BH4_B3_PL2	MGy	30	Saturated	2759.5	5507	2511	47.6	0.37	17.4	60.5	1.13	0.93
BH4_B3_PL3	MGy	30	Saturated	2834.3	5620	2529	49.8	0.37	18.1	65.3	1.14	1.03
BH4_B5_2	MGy	20	Saturated	2829.8	5789	2117	36.1	0.42	12.7	77.9	1.10	0.77
BH4_B6_7	MGy	15	Saturated	2860.8	5543	2665	54.8	0.35	20.3	60.8	1.21	0.96
BH4_B1_PL1	DGy	15	Saturated	2795.9	5319	2506	47.7	0.36	17.6	55.7	1.27	0.97
BH4_B1_PL3	DGy	20	Saturated	2789.7	5625	2582	50.8	0.37	18.6	63.5	1.18	0.95
BH4_B2_PL10	DGy	25	Saturated	2797.6	5879	2588	51.7	0.38	18.7	71.7	1.20	0.91
BH4_B2_PL7	DGy	30	Saturated	2859.2	5574	-	-	-	-	-	1.12	
BH4_B7_PL1	DGy	15	Saturated	2800.5	5758	2039	33.3	0.43	11.6	77.3	1.13	0.94
BH4_B7_PL2	DGy	20	Saturated	2829.0	5338	2550	49.7	0.35	18.4	56.1	1.15	0.95

C.1.4 Slake Durability

Individual lithotype slake durability index results are tabled below, with sample photos after the 2nd and 5th cycles followed by a table, which includes descriptions of the fragments retained in the drum and of the material passing through the drum.

C.1.4.1 Dark green-grey schist (DGy)

Slake Durability - DGy				
Sample	**QHL_GREEN_1**	**QHL_GREEN_2**	**QHL_GREEN_3**	**QHL_GREEN_4**
Dry mass of specimen for testing (10 samples) (g)	530.9	524.2	502.4	488.0
Drum name	Left 3,4	Left 1,2	Right 1,2	Right 3,4
Dry mass of drum + sample (initial) (g)	2782.5	2693.6	2681.1	2740.3
Dry mass of drum + sample (1st Cycle) (g)	2780.3	2689.0	2671.1	2732.7
Dry mass of drum + sample (2nd Cycle) (g)	2778.5	2685.1	2665.1	2726.5
New Dry mass of drum + sample (2nd Cycle) (g)	2778.3	2684.8	2664.7	2726.4
Average Dry mass of drum + sample (2nd Cycle) (g)	2778.4	2685.0	2664.9	2726.5
Dry mass of drum + sample (3rd Cycle) (g)	2776.7	2681.3	2660.0	2720.9
Dry mass of drum + sample (4th Cycle) (g)	2775.3	2677.9	2656.2	2715.7
Dry mass of drum + sample (5th Cycle) (g)	2773.6	2674.8	2652.5	2711.3
Dry mass of empty drum (g)	2251.6	2169.4	2178.7	2252.3
Amount of sediment settled to bottom of tank after test (1st Cycle) (g)	2.2	4.6	10.0	7.6
Amount of sediment settled to bottom of tank after test (2nd Cycle) (g)	1.8	3.9	6.0	6.2
Slake-Durability Index (1st Cycle) Id1 (%)	99.59%	99.12%	98.01%	98.44%
Slake-Durability Index (2nd Cycle) Id2 (%)	99.23%	98.35%	96.78%	97.16%
Slake-Durability Index (3rd Cycle) Id3 (%)	98.91%	97.65%	95.80%	96.02%
Slake-Durability Index (4th Cycle) Id4 (%)	98.64%	97.00%	95.04%	94.96%
Slake-Durability Index (5th Cycle) Id5 (%)	98.32%	96.41%	94.31%	94.06%

C.1.4.2 Medium grey schist (MGy)

Slake Durability - MGy				
Sample	**QHL_GREY_1**	**QHL_GREY_2**	**QHL_GREY_3**	**QHL_GREY_4**
Dry mass of specimen for testing (10 samples) (g)	512.2	539.6	496.2	492.8
Drum name	Left 3,4	Left 1,2	Right 1,2	Right 3,4
Dry mass of drum + sample (initial) (g)	2763.8	2709.0	2674.9	2745.1
Dry mass of drum + sample (1st Cycle) (g)	2760.3	2704.8	2671.3	2741.5
Dry mass of drum + sample (2nd Cycle) (g)	2757.4	2702.3	2669.5	2739.3
New Dry mass of drum + sample (2nd Cycle) (g)	2757.0	2701.7	2669.0	2738.8
Average Dry mass of drum + sample (2nd Cycle) (g)	2757.2	2702.0	2669.3	2739.1
Dry mass of drum + sample (3rd Cycle) (g)	2754.6	2698.0	2667.2	2736.2
Dry mass of drum + sample (4th Cycle) (g)	2752.4	2695.2	2665.0	2734.1
Dry mass of drum + sample (5th Cycle) (g)	2750.2	2692.3	2663.0	2731.9
Dry mass of empty drum (g)	2251.6	2169.4	2178.7	2252.3
Amount of sediment settled to bottom of tank after test (1st Cycle) (g)	3.5	4.2	3.6	3.6
Amount of sediment settled to bottom of tank after test (2nd Cycle) (g)	2.9	2.5	1.8	2.2
Slake-Durability Index (1st Cycle) Id1 (%)	99.32%	99.22%	99.27%	99.27%
Slake-Durability Index (2nd Cycle) Id2 (%)	98.71%	98.70%	98.86%	98.77%
Slake-Durability Index (3rd Cycle) Id3 (%)	98.20%	97.96%	98.45%	98.19%
Slake-Durability Index (4th Cycle) Id4 (%)	97.77%	97.44%	98.00%	97.77%
Slake-Durability Index (5th Cycle) Id5 (%)	97.34%	96.91%	97.60%	97.32%

C.1.4.3 DGy Photos

C.1.4.4 MGy Photos

C.1.4.5 Slake Material Description

Descriptions	DGy	MGy
Fragments retained in drum	• After the 1st and 2nd cycles more than 70% of the fragments were coarse gravel sized (> 20mm) and 25% fine to medium gravel. • Fragments were subrounded to subangular • Fragmenting usually occurred along foliation or adjacent to quartz veins • The larger ~30-40mm fragments were most likely to split in half.	• Fragments occasionally split in half along foliation. • Rare/minimal fretting. • Fragments remained largely unchanged.
Appearance of material passing through the drum	• During the test, the water was murkier for DGy than MGy. • Silt sized mica and very fine to fine sand sized material • Variable amounts of accumulated material settled in the bottom ranging from a veneer of fines to a 0.5-1.5mm thick accumulation.	• Water was mildly to moderately murky. Not as cloudy as the DGy. • Silt sized mica and very fine sand sized material • A veneer of fines settled to the bottom with the occasional 0.5-1mm fragment.

C.2 Sample Data: Mechanical Parameters (ITS, UCS, Point Load Strength, Triaxial Strength)

C.2.1 Indirect Tensile Strength Samples

C.2.1.1 In Situ Sample Data

Brazilian Test Data		In situ									
Sample	Depth (m)	Lithotype	Loading Direction (Along…)	Foliation (ß°)	Density (kg/m³)	Thickness (mm)	Diameter (mm)	Max Load (kN)	Max Stress - ASTM (MPa)	Max Stress - ISRM (MPa)	Corrected Max Stress - ISRM (MPa)
BH1_B6_PL1B1	17.16	DGy	Strike	60	2670	45.17	60.84	15.35	2.26	3.55	3.20
BH1_B6_PL3B2	18.30	DGy	Strike	70	2680	37.91	60.85	24.97	4.38	6.88	6.20
BH1_B7_A10BS	19.70	DGy	Strike	70	2730	36.24	60.8	24.19	4.45	6.98	6.28
BH1_B7_A2BS	19.17	DGy	Strike	75	2640	34.97	60.65	23.84	4.55	7.15	6.43
BH3_B1_PL1B1	0.30	DGy	Strike	70	2710	34.82	60.85	15.42	2.95	4.63	4.17
BH4_B8_6B1	23.47	DGy	Strike	65	2750	35.94	60.98	14.31	2.64	4.15	3.74
BH4_B9_PL4B	24.40	DGy	Strike	70	2550	30.49	60.71	13.03	2.85	4.48	4.03
BH4_B9_PL7BD	24.65	DGy	Dip	75	2700	35.40	60.9	13.34	2.51	3.94	3.54
BH1_B6_PL1B2	17.16	DGy	Dip	60	2680	34.17	60.8	6.82	1.33	2.09	1.88
BH1_B6_PL3B1	18.30	DGy	Dip	70	2720	39.67	60.68	6.7	1.13	1.77	1.59
BH1_B7_A9BD	19.46	DGy	Dip	70	2720	36.83	60.81	15.15	2.74	4.30	3.87
BH1_B7_A15BD	20.38	DGy	Dip	70	2760	36.28	60.8	4.45	0.82	1.28	1.15
BH4_B7_4B	18.40	DGy	Dip	65	2720	41.29	60.80	3.75	0.60	0.95	0.86
BH4_B8_6B2	23.47	DGy	Dip	75	2750	35.33	60.96	9.79	1.84	2.89	2.60
BH1_B1_PL1B	1.17	MGy	Strike	75	2750	40.94	60.87	17.73	2.88	4.52	4.07
BH3_B2_PL1B1	5.20	MGy	Strike	75	2890	36.21	60.82	28.88	5.31	8.34	7.51
BH3_B2_PL2B2	5.20	MGy	Strike	70	2890	37.50	60.8	23.32	4.14	6.51	5.85
BH3_B4_2B2	10.10	MGy	Strike	70	2780	36.67	60.81	18.24	3.31	5.20	4.68
BH4_B5_6B2	14.40	MGy	Strike	75	2850	35.49	60.85	18.14	3.40	5.34	4.81
BH1_B1_PL2B	1.30	MGy	Dip	70	2750	34.49	60.85	11.63	2.24	3.52	3.17
BH3_B2_PL1B2	5.20	MGy	Dip	75	2890	35.5	60.82	19.26	3.61	5.67	5.11
BH3_B2_PL2B1	5.30	MGy	Dip	70	2780	38.90	60.8	22.41	3.84	6.03	5.42
BH3_B4_2B1	10.10	MGy	Dip	75	2800	35.72	60.81	19.81	3.69	5.80	5.22
BH4_B5_6B1	14.40	MGy	Dip	70	2880	35.87	60.85	22.32	4.14	6.50	5.85

Detailed summary of in situ indirect tensile strength data

In situ moisture		DGy			MGy			Combined		
Loading Direction (Along…)		Strike	Dip	Averaged	Strike	Dip	Averaged	Strike	Dip	Averaged
All Samples										
No of Samples		7	7	14	5	5	10	12	12	24
Indirect Tensile stress (ASTM), MPa	Min-Max	2.26-4.55	0.60-2.74	0.6-4.55	2.88-5.31	2.24-4.14	2.24-5.31	2.26-5.31	0.60-4.14	0.60-5.31
	Mean ± Std dev.	**3.44** ± 0.98	**1.57** ± 0.82	**2.50** ± 1.26	**3.81** ± 0.95	**3.50** ± 0.73	**3.66** ± 0.78	**3.59** ± 0.90	**2.37** ± 1.20	**2.98** ± 1.22
Indirect Tensile Stress (ISRM), MPa	Min-Max	3.55-7.15	0.95-4.30	0.95-7.15	4.52-8.34	3.52-6.50	3.52-8.34	3.55-8.34	0.95-6.50	0.95-8.34
	Mean ± Std dev.	**5.40** ± 1.54	**2.46** ± 1.29	**3.93** ± 1.97	**5.98** ± 1.50	**5.51** ± 1.15	**5.74** ± 1.22	**5.65** ± 1.42	**3.73** ± 1.88	**4.69** ± 1.92
Conversion to Direct Tensile Stress, MPa	Min-Max	3.20-6.43	0.86-3.87	0.86-6.43	4.07-7.51	3.17-5.85	3.17-7.51	3.20-7.51	0.86-5.85	0.86-7.51
	Mean ± Std dev.	**4.86** ± 1.38	**2.21** ± 1.16	**3.54** ± 1.78	**5.38** ± 1.35	**4.96** ± 1.04	**5.17** ± 1.10	**5.08** ± 1.28	**3.36** ± 1.69	**4.22** ± 1.73
Samples with foliation β° (70-75)										
No of Samples		5	5	10	5	5	10	10	10	20
Indirect Tensile stress (ASTM), MPa	Min-Max	2.85-4.55	0.82-2.74	0.82-4.55	2.88-5.31	2.24-4.14	2.24-5.31	2.85-5.31	0.82-4.14	0.82-5.31
	Mean ± Std dev.	**3.84** ± 0.86	**1.81** ± 0.84	**2.82** ± 1.27	**3.81** ± 0.95	**3.50** ± 0.73	**3.66** ± 0.78	**3.82** ± 0.86	**2.66** ± 1.16	**3.24** ± 1.16
Indirect Tensile Stress (ISRM), MPa	Min-Max	4.48-7.15	1.28-4.30	1.28-7.15	4.52-8.34	3.52-6.50	3.52-8.34	4.48-8.34	1.28-6.50	1.28-8.34
	Mean ± Std dev.	**6.02** ± 1.35	**2.84** ± 1.31	**4.43** ± 1.99	**5.98** ± 1.50	**5.51** ± 1.15	**5.74** ± 1.22	**6.00** ± 1.34	**4.17** ± 1.83	**5.09** ± 1.82
Conversion to Direct Tensile Stress, MPa	Min-Max	4.03-6.43	1.15-3.87	1.15-6.43	4.07-7.51	3.17-5.85	3.17-7.51	4.03-7.51	1.15-5.85	1.15-7.51
	Mean ± Std dev.	**5.42** ± 1.21	**2.55** ± 1.18	**3.99** ± 1.79	**5.38** ± 1.35	**4.96** ± 1.04	**5.17** ± 1.10	**5.40** ± 1.21	**3.75** ± 1.64	**4.58** ± 1.64

C.2.1.2 Oven-Dried Sample Data

Brazilian Test Data		Oven-Dried									
Sample	Depth (m)	Lithotype	Loading Direction (Along…)	Foliation (ß°)	Density (kg/m³)	Thickness (mm)	Diameter (mm)	Max Load (kN)	Max Stress - ASTM (MPa)	Max Stress - ISRM (MPa)	Corrected Max Stress - ISRM (MPa)
BH1_B5_PL2BD	15.60	DGy	Strike	70	2650	35.60	60.8	23.7	4.43	6.96	6.27
BH4_B2_PL5BD	2.80	DGy	Strike	75	2720	39.09	60.5	24.86	4.26	6.69	6.02
BH4_B2_PL8BD1	4.90	DGy	Strike	75	2870	35.12	60.75	34.9	6.62	10.40	9.36
BH4_B2_PL9BD	5.93	DGy	Strike	70	2740	35.98	60.74	25	4.63	7.28	6.55
BH1_B2_A13BS	4.06	DGy	Strike	70	2770	36.05	60.75	21.96	4.06	6.38	5.74
BH4_B7_2BD2	18.80	DGy	Strike	65	2660	38.85	60.81	30.86	5.29	8.31	7.48
BH1_B6_PL2BD	17.30	DGy	Dip	60	2740	36.85	60.79	14.91	2.69	4.23	3.81
BH3_B1_PL1B2	0.30	DGy	Dip	75	2610	35.01	60.84	39.28	7.47	11.73	10.56
BH1_B7_A13BD	19.86	DGy	Dip	70	2790	33.05	60.83	24.84	5.00	7.86	7.07
BH1_B2_A13BD	4.06	DGy	Dip	70	2630	33.81	60.77	16.45	3.24	5.09	4.58
BH4_B2_PL6BD	4.40	DGy	Dip	70	2770	36.50	60.85	17	3.10	4.87	4.38
BH4_B2_PL8BD2	4.90	DGy	Dip	75	2760	31.05	60.75	28.38	6.09	9.57	8.61
BH4_B7_2BD1	18.80	DGy	Dip	65	2670	35.82	60.9	1.59	0.30	0.46	0.42
BH2_B7_PL1BD1	21.80	MGy	Strike	65	2800	31.03	60.64	21.06	4.53	7.12	6.41
BH3_B1_2BD2	2.50	MGy	Strike	80	2790	36.80	60.85	30.63	5.54	8.70	7.83
BH3_B5_1BS1	12.65	MGy	Strike	75	2800	44.47	60.89	22.33	3.34	5.24	4.72
BH3_B5_1BS2	12.65	MGy	Strike	75	2770	34.94	60.89	30.61	5.83	9.15	8.24
BH3_B3_PL1BD1	6.50	MGy	Strike	75	2740	38.21	60.76	31	5.41	8.49	7.64
BH3_B4_3BD1	10.17	MGy	Strike	70	2810	34.68	60.85	32.95	6.32	9.93	8.94
BH4_B4_1BD1	9.52	MGy	Strike	70	2790	35.67	60.83	46.49	8.68	13.63	12.26
BH2_B7_PL1BD2	21.80	MGy	Dip	55	2680	35.79	60.62	15.09	2.82	4.42	3.98
BH3_B1_2BD1	2.50	MGy	Dip	80	2780	35.63	60.85	34.47	6.44	10.11	9.10
BH3_B3_PL1BD2	6.50	MGy	Dip	75	2750	36.22	60.8	26.2	4.82	7.57	6.81
BH3_B4_3BD2	10.17	MGy	Dip	70	2740	34.30	60.85	32.03	6.21	9.76	8.78
BH3_B5_1BD1	12.65	MGy	Dip	75	2790	41.47	60.89	22.07	3.54	5.56	5.00
BH3_B5_1BD2	12.65	MGy	Dip	75	2830	40.44	60.89	31.18	5.13	8.05	7.25
BH4_B4_1BD2	9.52	MGy	Dip	70	2820	35.78	60.83	30.45	5.66	8.90	8.01

Detailed summary of oven-dried indirect tensile strength data

Oven Dried		DGy			MGy			Combined		
Loading Direction (Along…)		Strike	Dip	Averaged	Strike	Dip	Averaged	Strike	Dip	Averaged
All Samples										
No of Samples		6	7	13	7	7	14	13	14	27
Indirect Tensile stress (ASTM), MPa	Min-Max	4.06-6.62	0.30-7.47	0.30-7.47	3.34-8.68	2.82-6.44	2.82-8.68	3.34-8.68	0.30-7.47	0.30-8.68
	Mean ± Std dev.	**4.88** ± 0.95	**3.98** ± 2.39	**4.40** ± 1.78	**5.66** ± 1.65	**4.94** ± 1.35	**5.30** ± 1.44	**5.30** ± 1.32	**4.46** ± 1.86	**4.87** ± 1.68
Indirect Tensile Stress (ISRM), MPa	Min-Max	6.38-10.40	0.46-11.73	0.46-11.73	5.24-13.63	4.42-10.11	4.42-13.63	5.24-13.63	0.46-11.73	0.46-13.63
	Mean ± Std dev.	**7.67** ± 1.49	**6.26** ± 3.75	**6.91** ± 2.80	**8.89** ± 2.59	**7.77** ± 2.12	**8.33** ± 2.26	**8.33** ± 2.08	**7.01** ± 2.92	**7.65** ± 2.63
Conversion to Direct Tensile Stress, MPa	Min-Max	5.74-9.36	0.42-10.56	0.42-10.56	4.72-12.26	3.98-9.10	3.98-12.26	4.72-12.26	0.42-10.56	0.42-12.26
	Mean ± Std dev.	**6.90** ± 1.35	**5.63** ± 3.38	**6.22** ± 2.52	**8.01** ± 2.33	**6.99** ± 1.91	**7.50** ± 2.04	**7.50** ± 1.87	**6.31** ± 2.63	**6.88** ± 2.37
Samples with foliation β° (70-75)										
No of Samples		5	5	10	5	5	10	10	10	20
Indirect Tensile stress (ASTM), MPa	Min-Max	4.06-6.62	3.10-7.47	3.10-7.47	3.34-8.68	3.54-6.21	3.34-8.68	3.34-8.68	3.10-7.47	3.10-8.68
	Mean ± Std dev.	**4.80** ± 1.04	**4.98** ± 1.87	**4.89** ± 1.43	**5.91** ± 1.92	**5.07** ± 1.01	**5.49** ± 1.51	**5.36** ±1.57	**5.03** ± 1.42	**5.19** ± 1.43
Indirect Tensile Stress (ISRM), MPa	Min-Max	6.38-10.40	4.87-11.73	4.87-11.73	5.24-13.63	5.56-9.76	5.24-13.63	5.24-13.63	4.87-11.73	4.87-13.63
	Mean ± Std dev.	**7.54** ± 1.63	**7.82** ± 2.94	**7.68** ± 2.25	**9.29** ± 3.01	**7.97** ± 1.59	**8.63** ± 2.37	**8.42** ± 2.46	**7.90** ± 2.23	**8.16** ± 2.24
Conversion to Direct Tensile Stress, MPa	Min-Max	5.74-9.36	4.38-10.56	4.38-10.56	4.72-12.26	5.00-8.78	4.72-12.26	4.72-12.26	4.38-10.56	4.38-12.26
	Mean ± Std dev.	**6.79** ± 1.47	**7.04** ± 2.64	**6.91** ± 2.02	**8.36** ± 2.71	**7.17** ± 1.43	**7.77** ± 2.14	**7.57** ± 2.22	**7.11** ± 2.00	**7.34** ± 2.02

C.2.2 UCS Samples

C.2.2.1 In Situ Sample Data

Individual sample results obtained from UCS testing to derive strength and elastic properties of DGy and MGy schist. The table 1 summarizes specimen data followed by stress strain curves for tested samples.

UCS Data		In situ Moisture content										
Sample	Depth (m)	Lithotype	Foliation (ß°)	Density (kg/m³)	Max Load (kN)	Max Stress (MPa) Uncorrected	Max Stress (MPa) Corrected	E (GPa)	Radial 1, v	Radial 2, v	Averaged Radials, v	Failure Mode (α°)
BH1_B4_1U	9.50	DGy	65	2740	34.60	12.0	12.5	-	-	-	-	Multiple Shear Fractures: Parallel Shears (50-60°)
BH1_B6_1U	18.65	DGy	70	2740	101.81	35.1	37.1	41.1	0.32	0.21	0.26	Multiple Shear Fractures: Parallel Shears (60°)
BH1_B7_2U	19.50	DGy	65	2750	69.51	24.0	25.2	-	-	-	-	Axial Splitting (85°-87°)
BH1_B7_PL1U	20.45	DGy	75	2780	34.89	12.0	12.6	2.0	0.02	0.02	0.02	Shear Fracture (40°-50°)
BH1_B8_2U	24.15	DGy	55	2780	31.22	10.7	11.3	11.5	0.17	0.18	0.17	Multiple Fractures: Shear (60°) + Joint (80°)
BH3_B7_1U	20.00	DGy	65	2720	71.91	24.8	26.1	10.7	0.15	0.14	0.14	Along Foliation (20°)
BH3_B7_2U	20.30	DGy	70	2760	79.55	27.3	28.9	6.6	0.25	0.26	0.26	Shear Fracture (50°-65°)
BH3_B8_2U	21.55	DGy	70	2650	132.30	45.5	48.0	12.2	0.24	0.30	0.27	Double Shear (50°-65°)
BH4_B5_1U	12.40	DGy	55	2770	57.60	19.8	20.5	-	-	-	-	Along Foliation (40°-45°)
BH4_B7_5U	19.85	DGy	65	2740	32.40	11.1	11.7	0.9	0.11	-	0.11	Multiple Shear Fractures: Parallel Shears (50°-60°)
BH4_B8_6U	23.47	DGy	75	2750	64.10	22.0	22.9	8.3	-	-	-	Multiple Fractures: Along foliation (15°-20°) + Shear (75°-80°)
BH1_B1_1U	2.35	MGy	65	2740	59.29	20.4	21.6	10.0	0.51	0.34	0.34	Multiple Fractures
BH1_B8_1U	23.35	MGy	70	2770	147.25	50.7	53.3	24.2	0.17	0.69	0.40	Shear Fracture (65°-70°)
BH3_B1_1U	1.20	MGy	70	2780	111.30	38.2	39.9	13.2	0.29	-	0.29	Axial Splitting (80°-85°)
BH3_B2_1U	5.00	MGy	70	2820	152.94	52.6	55.2	31.7	0.38	0.21	0.29	Shear Fracture (65°-70°)
BH3_B2_2U	5.38	MGy	75	2810	169.81	58.4	61.8	22.7	0.37	0.34	0.35	Multiple Fractures: Shear (60°-65°) + Joint (80°-85°)
BH3_B3_1U	6.35	MGy	75	2820	156.34	53.7	57.1	11.5	0.55	0.36	0.46	Shear Fracture (65°-70°)
BH4_B3_4U	9.00	MGy	70	2850	143.50	49.3	51.9	15.7	0.41	0.12	0.26	Shear Fracture (65°)
BH4_B4_3U	10.81	MGy	75	2830	134.10	46.1	48.8	14.2	0.25	0.02	0.13	Shear Fracture (60°)
BH4_B5_3U	13.00	MGy	60	2860	75.70	26.1	27.5	5.1	0.20	-	0.20	Multiple Shear Fractures: Oblique Shears (50°-55°), (65°-75°)
BH4_B6_6U	17.90	MGy	75	2790	101.60	35.0	36.4	8.9	0.03	0.02	0.02	Axial Splitting (80°-85°)

C.2.2.2 In Situ Stress vs Strain Curves

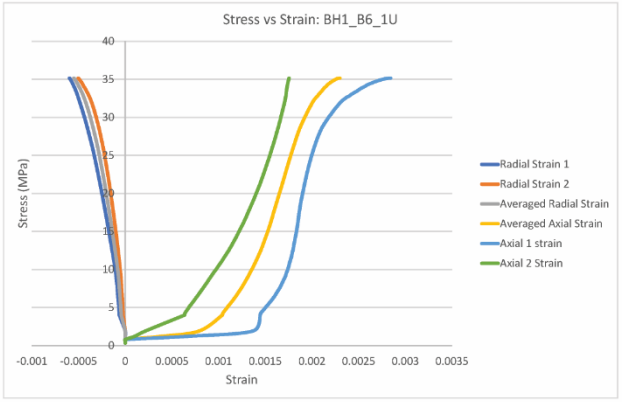

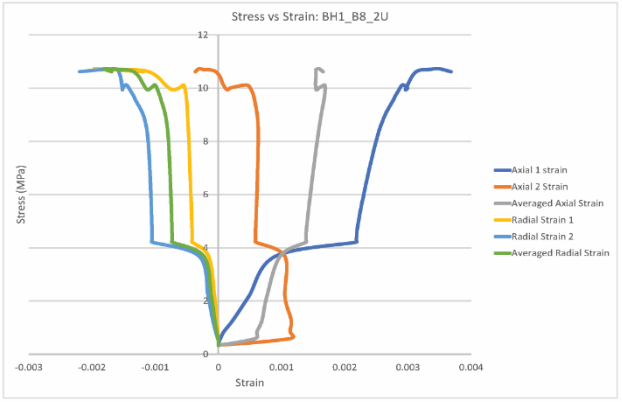

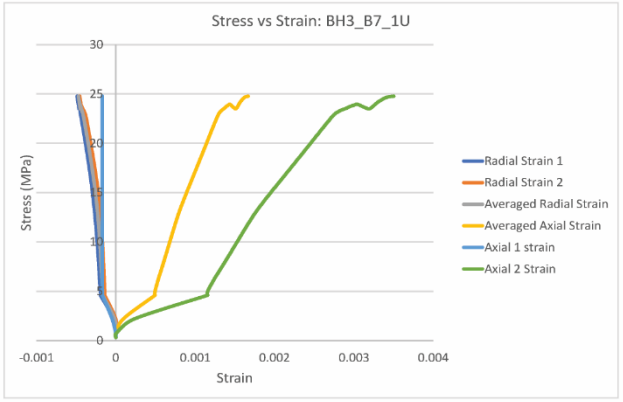

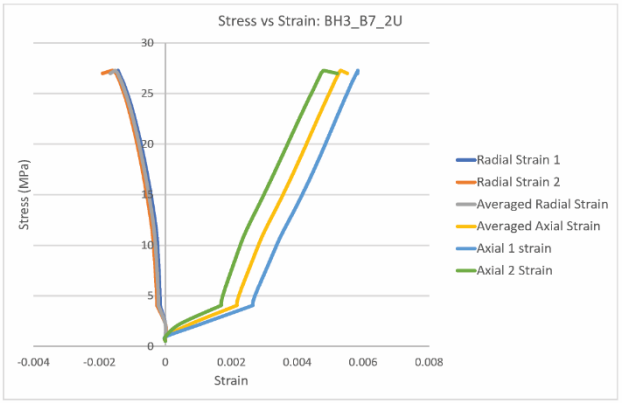

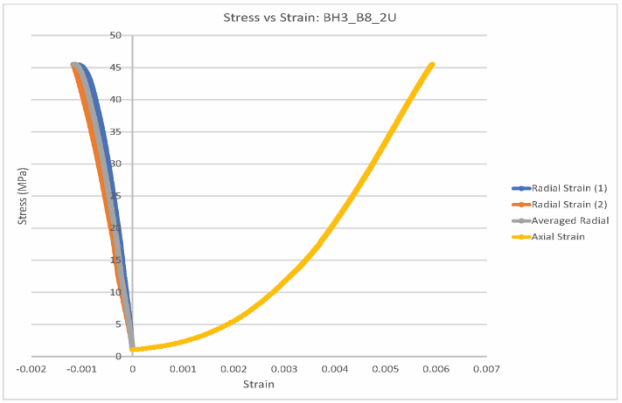

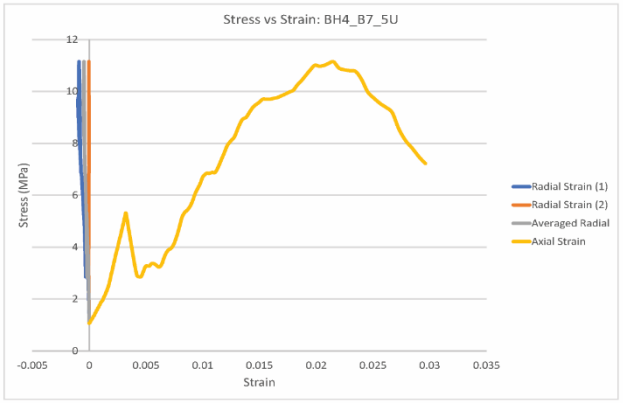

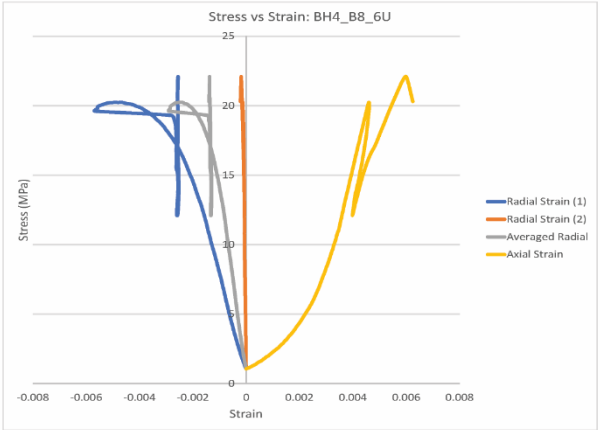

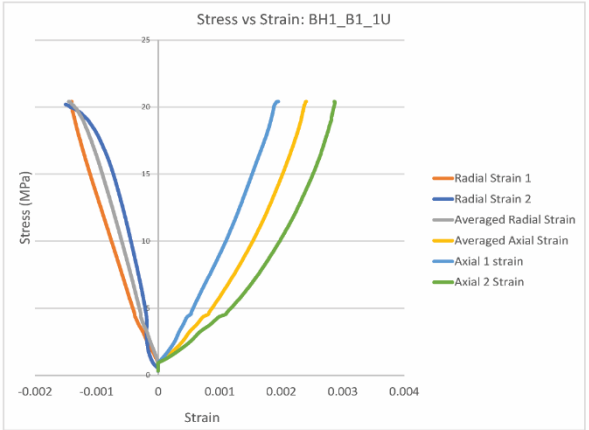

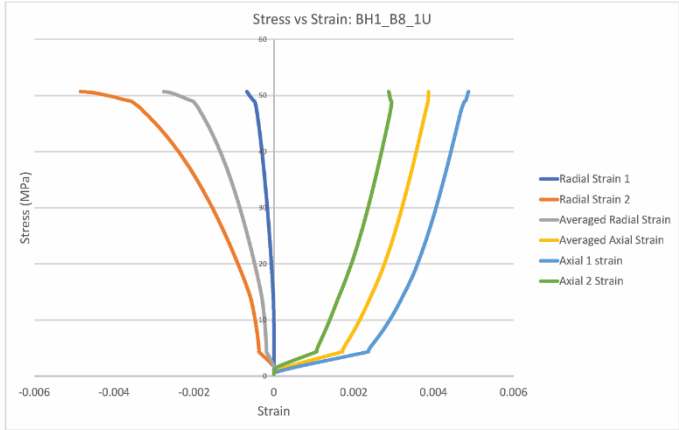

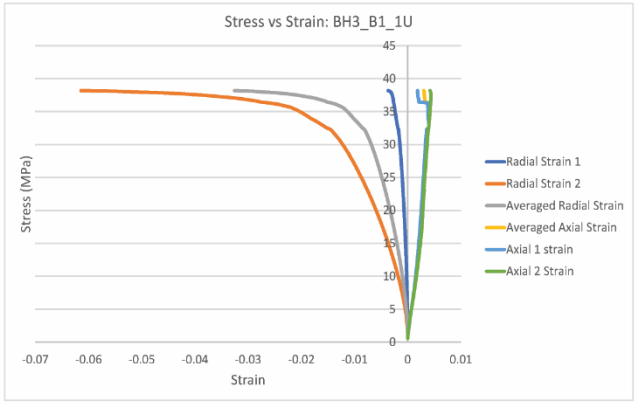
Stress vs Strain: BH3_B1_1U
Stress (MPa)
Strain
Radial Strain 1
Radial Strain 2
Averaged Radial Strain
Averaged Axial Strain
Axial 1 strain
Axial 2 Strain

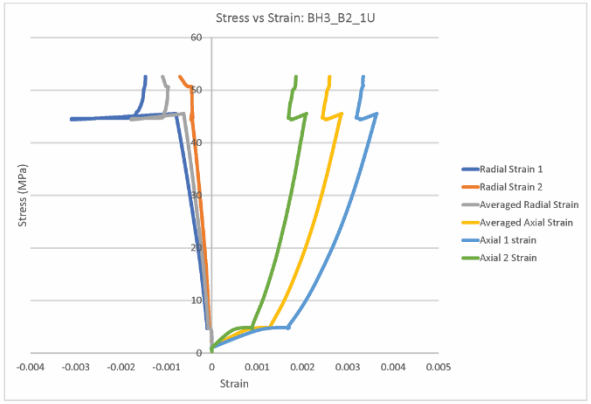
Stress vs Strain: BH3_B2_1U
Stress (MPa)
Strain
Radial Strain 1
Radial Strain 2
Averaged Radial Strain
Averaged Axial Strain
Axial 1 strain
Axial 2 Strain

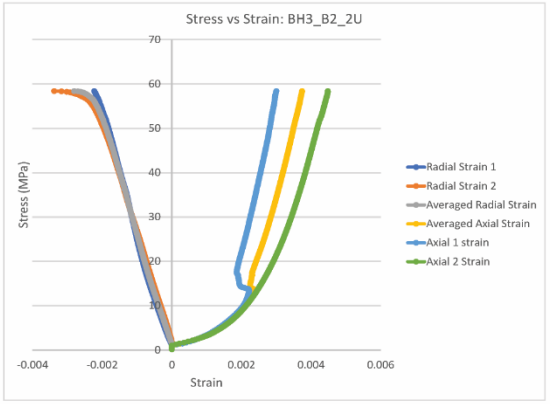
Stress vs Strain: BH3_B2_2U
Stress (MPa)
Strain
Radial Strain 1
Radial Strain 2
Averaged Radial Strain
Averaged Axial Strain
Axial 1 strain
Axial 2 Strain

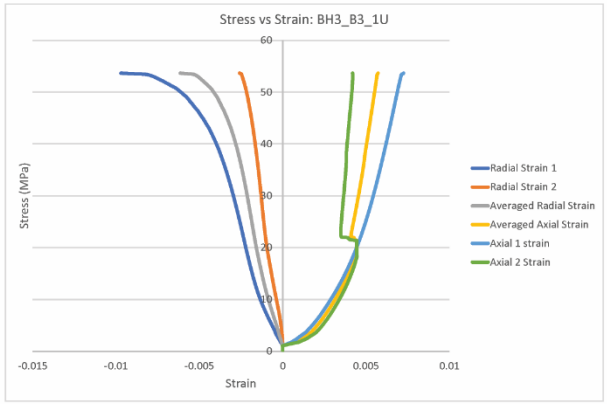
Stress vs Strain: BH3_B3_1U
Stress (MPa)
Strain
Radial Strain 1
Radial Strain 2
Averaged Radial Strain
Averaged Axial Strain
Axial 1 strain
Axial 2 Strain

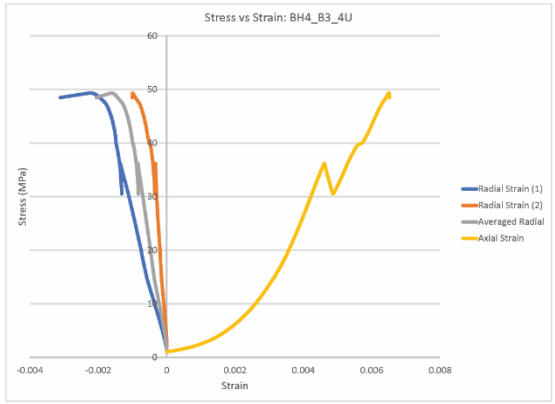
Stress vs Strain: BH4_B3_4U
Stress (MPa)
Strain
Radial Strain (1)
Radial Strain (2)
Averaged Radial
Axial Strain

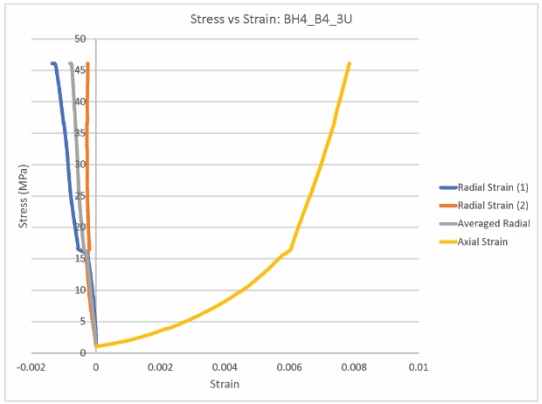
Stress vs Strain: BH4_B4_3U
Stress (MPa)
Strain
Radial Strain (1)
Radial Strain (2)
Averaged Radial
Axial Strain

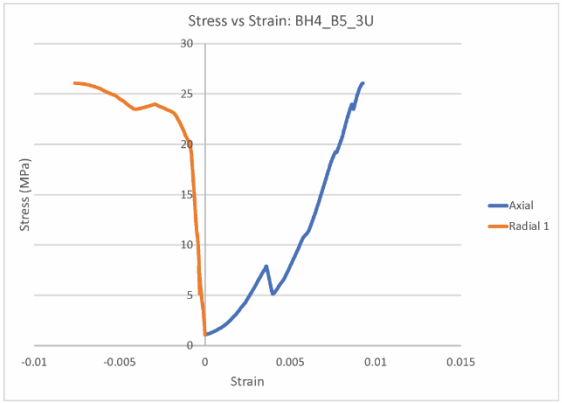
Stress vs Strain: BH4_B5_3U
Stress (MPa)
Strain
Axial
Radial 1

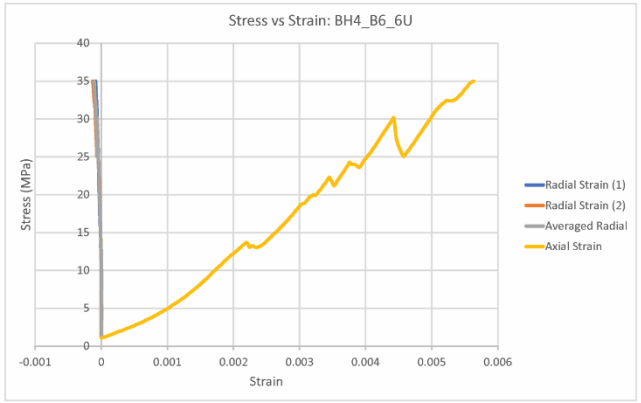
Stress vs Strain: BH4_B6_6U
Stress (MPa)
Strain
Radial Strain (1)
Radial Strain (2)
Averaged Radial
Axial Strain

C.2.2.3 Oven-Dried Sample Data

UCS Data		Oven Dried										
Sample	Depth (m)	Lithotype	Foliation (ß°)	Density (kg/m³)	Max Load (kN)	Max Stress (MPa) Uncorrected	Max Stress (MPa) Corrected	E (GPa)	Radial 1, ν	Radial 2, ν	Averaged Radials, ν	Failure Mode (α°)
BH3_B8_3U	22.20	DGy	75	2730	111.85	38.4	40.6	9.6	0.56	0.05	0.31	Multiple Shear Fractures: Oblique Shears (45°), (60°-70°)
BH1_B7_3U	20.20	DGy	70	2770	75.25	26.0	27.4	9.2	0.16	0.00	0.08	Multiple Shear Fractures: Parallel Shears (45°-50°)
BH1_B7_A1U	19.07	DGy	70	2700	87.60	30.3	31.4	5.4	0.12	0.01	0.07	Multiple Fractures: Shear (45°-50°) + Joint (85°)
BH2_B5_PL2U	17.60	DGy	50	2770	51.16	17.7	18.5	-	-	-	-	Double Shear (60°-70°)
BH3_B4_1NU	9.50	DGy	75	2730	111.48	38.4	40.8	-	-	-	-	Multiple Fractures
BH3_B8_1U	21.40	DGy	70	2680	105.86	36.4	38.1	6.0	0.17	0.04	0.11	Multiple Fractures: Shear (45°-50°) + Joint (82°-87°)
BH4_B3_1U	6.20	MGy	70	2730	77.62	26.7	27.9	6.0	0.04	0.29	0.16	Multiple Shear Fractures: Parallel Shears (55°-60°)
BH1_B7_A27U	21.58	MGy	70	2700	133.23	45.8	47.6	12.1	0.07	0.07	0.07	Multiple Fractures: Along foliation (15°-20°) + Shear (40°-45°)
BH1_B7_PL3U	21.20	MGy	70	2780	239.61	82.6	86.7	19.0	0.08	0.16	0.12	Shear Fracture (60°-70°)
BH1_B8_PL1U	23.55	MGy	65	2800	143.32	49.4	51.6	8.8	0.11	0.09	0.10	Multiple Fractures: Shear (45°-55°) + Joint (85°-87°)
BH3_B4_1YU	9.50	MGy	75	2740	119.99	41.3	43.5	7.8	0.01	0.13	0.07	Along Foliation (15°-20°)
BH3_B4_3U	10.17	MGy	70	2780	112.94	38.8	41.1	14.0	0.00	0.11	0.06	Axial Splitting (83°-85°)
BH3_B5_5U	14.50	MGy	70	2750	129.50	44.5	46.6	-	-	-	-	Axial Splitting (82°-87°)

Oven dried			DGy	MGy	Combined		DGy	MGy	Combined
No. of Samples			6	7	13		5	6	11
Maximum Stress, UCS (MPa)	Min-Max	All Samples	18.5-40.8	27.9-86.7	18.5-86.7	Samples with foliation β° (70-75)	27.4-40.8	27.9-51.6	27.4-51.6
	Mean ± Std dev.		**32.8** ± 8.1	**49.3** ± 16.8	**41.7** ± 15.8		**35.7** ± 5.3	**43.1** ± 7.5	**39.7** ± 7.6
Young's Modulus, E (GPa)	Min-Max		5.4-9.6	6.0-19.0	5.4-19.0		5.4-9.6	6.0-14.0	5.4-14.0
	Mean ± Std dev.		**7.5** ± 1.9	**11.3** ± 4.3	**9.8** ± 4.0		**7.5** ± 1.8	**9.7** ± 2.9	**8.8** ± 2.7
Poisson Ratio, v	Min-Max		0.07-0.31	0.06-0.16	0.06-0.31		0.07-0.31	0.06-0.16	0.06-0.31
	Mean ± Std dev.		**0.14** ± 0.10	**0.10** ± 0.04	**0.11** ± 0.07		**0.14** ± 0.10	**0.09** ± 0.04	**0.11** ± 0.07

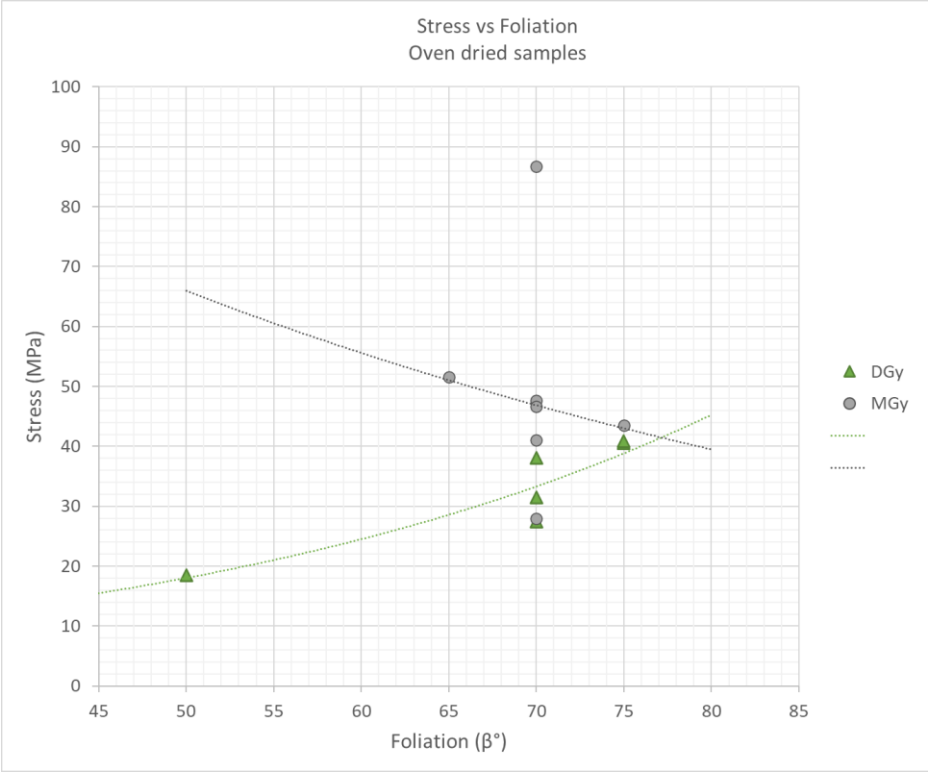

C.2.2.4 Oven Dried Stress vs Strain Curves

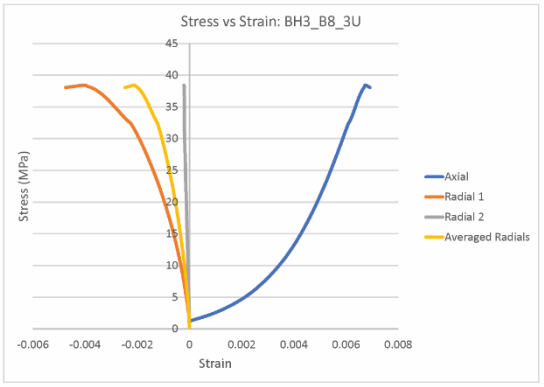

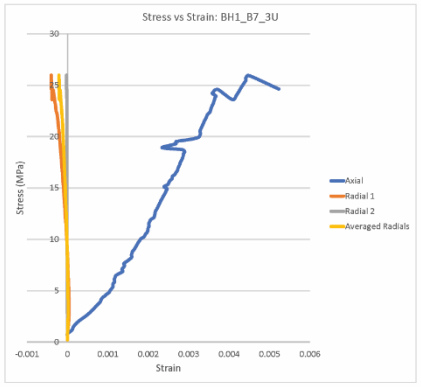

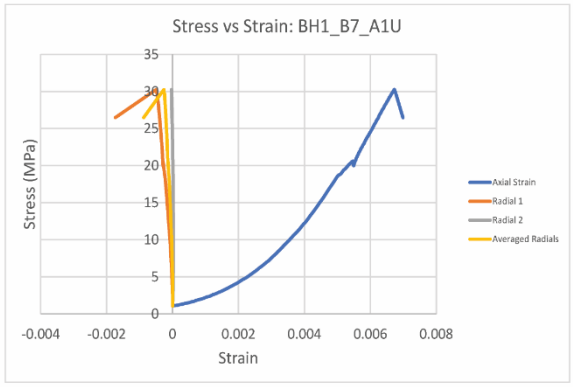

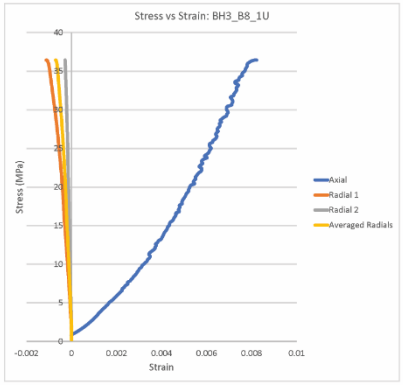

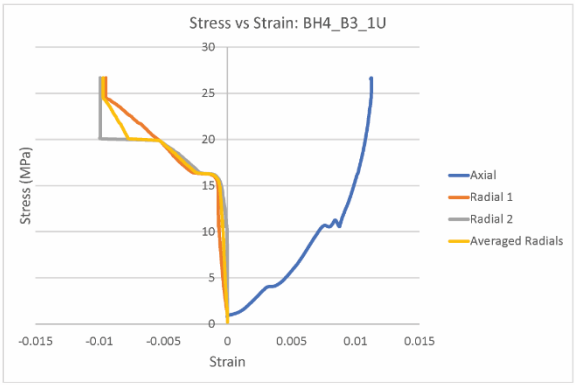

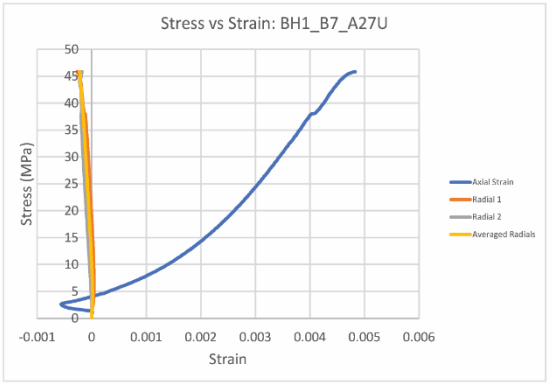

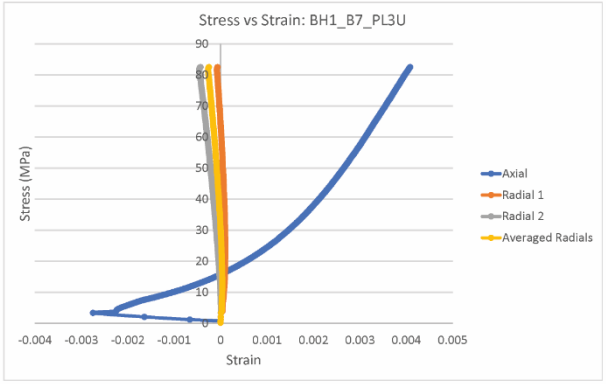

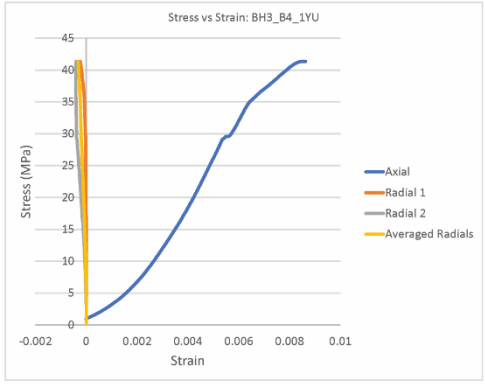

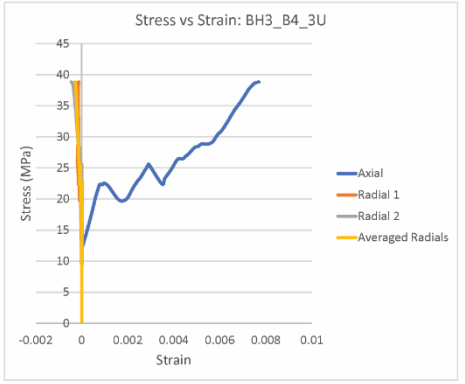

C.2.3 Point Load Strength Samples

Sample Inventory Breakdown			No. of Samples		
Moisture Content	Test Type	Orientation of foliation	DGy	MGy	Combined
In Situ	Axial	Perpendicular (⊥)	42	42	84
		β°=50-80	29	37	66
		*β°=70-75	18	23	41
	Diametral	Parallel (‖)	22	29	51
		β°=15-35	42	18	60
		*β°=15-20	16	13	29
Dry	Axial	Perpendicular (⊥)	45	44	89
		β°=50-80	35	28	63
		*β°=70-75	17	19	36
	Diametral	Parallel (‖)	19	19	38
		β°=15-35	23	19	42
		*β°=15-20	17	18	35

C.2.3.1 In Situ Dark Green-Grey Samples

DGY: In Situ - Tests Performed Parallel and Perpendicular to Foliation											
Sample	Depth (m)	Type		Width (W), mm	Diameter (D), mm	Load (P), kN	D_e^2, mm²	D_e, mm	I_s, MPa	F	$I_{s(50)}$, MPa
BH1_B8_A34A	24.78	A	⊥	60.89	24.65	2.59	1911	43.7	1.36	0.94	1.28
BH1_B4_F1		A	⊥	61.00	38.55	5.61	2994	54.7	1.87	1.04	1.95
BH1_B6_F1		A	⊥	60.60	37.20	17.91	2870	53.6	6.24	1.03	6.44
BH1_B6_F2		A	⊥	60.93	39.89	5.28	3095	55.6	1.71	1.05	1.79
BH1_B7_F1		A	⊥	60.56	41.98	13.88	3237	56.9	4.29	1.06	4.54
BH1_B7_F2		A	⊥	60.45	44.46	12.45	3422	58.5	3.64	1.07	3.90
BH3_B1_F4		A	⊥	60.72	35.75	7.45	2764	52.6	2.70	1.02	2.76
BH3_B9_F1		A	⊥	60.85	39.52	4.29	3062	55.3	1.40	1.05	1.47
BH3_B9_F2		A	⊥	61.76	30.94	3.11	2433	49.3	1.28	0.99	1.27
BH1_B2_2PD1	3.95	A	⊥	60.80	21.39	6.99	1656	40.7	4.22	0.91	3.85
BH1_B4_PL1PD	10.70	A	⊥	60.75	46.15	13.05	3570	59.7	3.66	1.08	3.96
BH1_B4_PL1P2	10.70	A	⊥	60.60	31.18	6.65	2406	49.0	2.76	0.99	2.74
BH1_B2_1PD1	3.70	A	⊥	60.86	35.51	7.88	2752	52.5	2.86	1.02	2.93
BH1_B2_1PD2	3.70	A	⊥	60.82	30.18	8.56	2337	48.3	3.66	0.98	3.61
BH4_B7_4	19.10	A	⊥	60.57	20.11	4.32	1551	39.4	2.79	0.90	2.50
BH4_B9_PL8	24.10	A	⊥	60.95	37.12	5.27	2881	53.7	1.83	1.03	1.89
BH4_B7_1PD1	18.40	A	⊥	60.79	36.33	5.81	2812	53.0	2.07	1.03	2.12
BH4_B2_PL1P	1.60	A	⊥	60.46	37.04	4.58	2851	53.4	1.61	1.03	1.65
BH4_B9_PL9	24.10	A	⊥	60.90	35.54	3.60	2756	52.5	1.31	1.02	1.34
BH4_B2_PL2P1	2.6	A	⊥	60.51	38.57	4.69	2972	54.5	1.58	1.04	1.64
BH4_B8_4PD	22.20	A	⊥	60.71	41.94	7.50	3242	56.9	2.31	1.06	2.45
BH4_B7_1PD2	18.40	A	⊥	60.92	31.52	3.55	2445	49.4	1.45	0.99	1.44
BH1_B4_2PL1	9.68	A	⊥	60.68	30.73	3.40	2374	48.7	1.43	0.99	1.42
BH4_B2_PL2P1	2.6	A	⊥	60.91	40.95	5.63	3176	56.4	1.77	1.06	1.87
BH2_B6_PL1P1	17.80	A	⊥	61.08	35.91	8.62	2793	52.8	3.09	1.03	3.16
BH1_B8_A24D1	23.81	A	⊥	60.87	26.80	1.44	2077	45.6	0.69	0.96	0.66
BH4_B7_1PP1B	18.40	A	⊥	60.87	18.48	2.22	1432	37.8	1.55	0.88	1.37
BH1_B8_A25B	23.89	A	⊥	60.97	40.48	4.36	3142	56.1	1.39	1.05	1.46
BH1_B8_A23B	23.75	A	⊥	60.58	29.82	3.14	2300	48.0	1.37	0.98	1.34
BH1_B2_1D1	3.70	A	⊥	60.77	26.08	5.79	2018	44.9	2.87	0.95	2.73
BH1_B4_PL1D	10.70	A	⊥	60.75	23.12	5.62	1788	42.3	3.14	0.93	2.91
BH3_B7_2X2	20.30	A	⊥	60.73	23.25	1.57	1798	42.4	0.87	0.93	0.81
BH1_B4_3DG	9.85	A	⊥	60.72	31.92	5.15	2468	49.7	2.09	1.00	2.08
BH2_B6_PL1DP1	17.80	A	⊥	60.81	20.48	2.43	1586	39.8	1.53	0.90	1.38
BH2_B6_PL1DP2	17.80	A	⊥	60.81	26.52	4.13	2053	45.3	2.01	0.96	1.92
BH4_B4_TS1D1	10.67	A	⊥	60.96	27.94	7.54	2169	46.6	3.48	0.97	3.37

DGY: In Situ - Tests Performed Parallel and Perpendicular to Foliation											
Sample	Depth (m)	Type		Width (W), mm	Diameter (D), mm	Load (P), kN	D_e^2, mm²	D_e, mm	I_s, MPa	F	$I_{s(50)}$, MPa
BH1_B7_2PDG1	19.50	A	⊥	61.06	24.08	5.59	1872	43.3	2.99	0.94	2.80
BH1_B7_2PDG2	19.50	A	⊥	61.06	18.55	3.59	1442	38.0	2.49	0.88	2.20
BH1_B2_A28B	5.26	A	⊥	61.16	23.53	7.08	1832	42.8	3.86	0.93	3.60
BH1_B6_PL2	17.30	A	⊥	55.75	23.04	8.18	1635	40.4	5.00	0.91	4.55
BH1_B4_3LX1	9.85	L	⊥	38.65	27.59	5.99	1358	36.8	4.41	0.87	3.85
BH1_B8_A32B4	24.63	L	⊥	38.28	25.82	3.74	1258	35.5	2.97	0.86	2.55
BH4_B7_1PP1	18.40	D	‖	-	61.28	0.11	3755	-	0.03	1.10	0.03
BH1_B7_2PDG	19.50	D	‖	-	61.06	0.79	3728	-	0.21	1.09	0.23
BH1_B4_PL1D	10.70	D	‖	-	60.75	1.13	3691	-	0.31	1.09	0.33
BH1_B6_F3		D	‖	-	60.64	2.46	3677	-	0.67	1.09	0.73
BH1_B6_F4		D	‖	-	60.20	3.29	3624	-	0.91	1.09	0.99
BH1_B7_F3		D	‖	-	60.41	1.10	3649	-	0.30	1.09	0.33
BH3_B9_F3		D	‖	-	61.36	1.32	3765	-	0.35	1.10	0.38
BH1_B2_1D1	3.70	D	‖	-	60.82	0.67	3699	-	0.18	1.09	0.20
BH4_B9_PL2D	24.10	D	‖	-	61.00	1.98	3721	-	0.53	1.09	0.58
BH4_B2_PL4P	2.6	D	‖	-	60.49	2.65	3659	-	0.72	1.09	0.79
BH4_B9_PL1P	24.10	D	‖	-	60.92	0.24	3711	-	0.06	1.09	0.07
BH1_B4_3DG	9.85	D	‖	-	60.72	2.09	3687	-	0.57	1.09	0.62
BH4_B9_PL7	24.10	D	‖	-	60.87	0.39	3705	-	0.11	1.09	0.12
BH1_B5_PL2S	15.60	D	‖	-	61.40	0.40	3770	-	0.11	1.10	0.12
BH1_B5_PL2X	15.66	D	‖	-	60.90	0.70	3709	-	0.19	1.09	0.21
BH1_B3_PL1D	7.64	D	‖	-	60.71	5.70	3686	-	1.55	1.09	1.69
BH2_B6_PL1DP	17.80	D	‖	-	60.81	0.14	3698	-	0.04	1.09	0.04
BH4_B4_TS1D	10.67	D	‖	-	60.96	3.87	3716	-	1.04	1.09	1.14
BH4_B9_PL3D	24.30	D	‖	-	61.34	0.31	3763	-	0.08	1.10	0.09
BH1_B8_A32A	24.63	L	‖	-	33.19	6.80	1102	-	6.17	0.83	5.13
BH1_B8_A32B	24.63	L	‖	-	28.61	1.07	819	-	1.31	0.78	1.02
BH1_B8_A32B3	24.63	L	‖	-	41.59	0.97	1730	-	0.56	0.92	0.52
A = Axial											
D = Diametral											
L = Lump											
						No. Samples	42	Mean $I_{s(50)}$, (⊥)		2.40	± 0.92
						No. Samples	22	Mean $I_{s(50)}$ (‖)		0.47	± 0.34
								Mean $I_{s(50)}$ (‖)		5.11	

DGY: In Situ - Tests Performed Oblique to Foliation											
Sample	Depth (m)	Type		Width (W), mm	Diameter (D), mm	Load (P), kN	D_e^2, mm²	D_e, mm	I_s, MPa	F	$I_{s(50)}$, MPa
BH2_B1_PL2C	2.20	A	55	60.60	48.38	2.09	3733	61.1	0.56	1.09	0.61
BH1_B5_TS1A2	13.10	A	55	60.68	31.82	7.17	2458	49.6	2.92	1.00	2.91
BH1_B4_2PL2	9.68	A	60	60.80	39.93	5.98	3091	55.6	1.93	1.05	2.03
BH1_B3_PL2CA	8.27	A	60	60.69	31.40	1.88	2426	49.3	0.77	0.99	0.77
BH4_B8_3LP	21.97	A	70	61.73	30.01	3.32	2359	48.6	1.41	0.99	1.39
BH1_B2_PL1D1	5.10	A	70	60.88	26.74	4.95	2073	45.5	2.39	0.96	2.29
BH1_B7_3LP1	20.20	A	70	61.11	27.55	5.93	2144	46.3	2.77	0.97	2.67
BH4_B8_4PL1	22.20	A	70	60.90	31.40	5.00	2435	49.3	2.05	0.99	2.04
BH4_B8_4PL2	22.20	A	70	60.84	26.51	2.19	2054	45.3	1.07	0.96	1.02

DGY: In Situ - Tests Performed Oblique to Foliation											
Sample	Depth (m)	Type		Width (W), mm	Diameter (D), mm	Load (P), kN	D_e^2, mm²	D_e, mm	I_s, MPa	F	$I_{s(50)}$, MPa
BH1_B2_2PL01	3.95	A	70	60.89	29.06	7.44	2253	47.5	3.30	0.98	3.23
BH1_B6_1P1	18.65	A	70	60.71	38.90	6.00	3007	54.8	2.00	1.04	2.08
BH4_B9_PL10	24.93	A	70	60.94	25.10	6.00	1948	44.1	3.08	0.95	2.91
BH1_B2_2D1A	3.95	A	70	60.71	23.44	5.15	1812	42.6	2.84	0.93	2.64
BH1_B2_2D1B	3.95	A	70	60.71	24.44	3.58	1889	43.5	1.90	0.94	1.78
BH4_B2_PL6L	4.40	A	75	60.94	33.88	3.29	2629	51.3	1.25	1.01	1.27
BH3_B3_2XL	6.80	A	75	60.15	32.49	3.51	2488	49.9	1.41	1.00	1.41
BH1_B5_PL1LA	12.27	A	75	60.93	26.52	4.48	2057	45.4	2.18	0.96	2.08
BH1_B5_PL2CA	15.60	A	75	61.13	23.99	3.49	1867	43.2	1.87	0.94	1.75
BH1_B2_PL1A1	5.10	A	75	60.72	36.46	6.37	2819	53.1	2.26	1.03	2.32
BH4_B4_TS1	10.67	A	75	60.89	37.74	11.51	2926	54.1	3.93	1.04	4.08
BH1_B2_A28A	5.26	A	80	61.16	25.89	6.57	2016	44.9	3.26	0.95	3.10
BH4_B8_3LX	21.97	A	80	60.03	25.77	4.48	1970	44.4	2.27	0.95	2.16
BH1_B4_1X	9.50	A	80	60.17	23.57	2.82	1806	42.5	1.56	0.93	1.45
BH4_B2_PL3	2.6	A	80	60.60	47.47	8.66	3663	60.5	2.36	1.09	2.58
BH4_B4_TS1D2	10.67	A	80	60.96	19.21	6.48	1491	38.6	4.35	0.89	3.87
BH4_B8_6GA	23.47	A	80	60.94	21.01	4.73	1630	40.4	2.90	0.91	2.64
BH4_B8_4L	22.20	L	70	48.97	45.45	5.34	2834	53.2	1.88	1.03	1.94
BH1_B5_PL2LX	15.60	L	75	59.00	23.02	3.34	1729	41.6	1.93	0.92	1.78
BH1_B4_1_Top	9.50	L	80	59.52	17.91	8.02	1357	36.8	5.91	0.87	5.15
BH1_B8_A23	23.75	D	15	-	60.98	2.17	3719	-	0.58	1.09	0.64
BH1_B8_A23B	23.75	D	15	-	60.98	2.01	3719	-	0.54	1.09	0.59
BH1_B8_A21	23.67	D	15	-	61.56	8.10	3790	-	2.14	1.10	2.35
BH1_B2_2D1	3.95	D	20	-	60.77	0.22	3693	-	0.06	1.09	0.07
BH1_B2_PL1D1	5.10	D	20	-	60.88	0.31	3706	-	0.08	1.09	0.09
BH3_B7_PL1D1	20.90	D	20	-	61.36	0.10	3765	-	0.03	1.10	0.03
BH4_B7_2XD	18.80	D	20	-	60.88	0.21	3706	-	0.06	1.09	0.06
BH1_B8_A34D	24.78	D	20	-	60.80	0.47	3697	-	0.13	1.09	0.14
BH1_B8_A22	23.71	D	20	-	61.59	5.20	3793	-	1.37	1.10	1.51
BH1_B2_A28	5.26	D	20	-	61.16	0.50	3741	-	0.13	1.09	0.15
BH1_B2_A39	5.77	D	20	-	60.77	7.21	3693	-	1.95	1.09	2.13
BH1_B2_A24	4.85	D	25	-	60.75	2.47	3691	-	0.67	1.09	0.73
BH1_B8_A24D	23.81	D	30	-	60.83	1.18	3700	-	0.32	1.09	0.35
BH1_B8_A25	23.89	D	35	-	61.04	1.49	3726	-	0.40	1.09	0.44
BH1_B8_2D1	24.15	D	40	-	61.00	1.63	3721	-	0.44	1.09	0.48
BH1_B8_A32B2	24.63	D	15	-	28.61	0.51	819	-	0.62	0.78	0.48
BH1_B8_A30C	24.44	D	20	-	39.31	1.05	1545	-	0.68	0.90	0.61
BH1_B8_A30C2	24.44	D	20	-	38.69	0.77	1497	-	0.51	0.89	0.46
BH1_B8_A30C3	24.44	D	20	-	38.37	0.95	1472	-	0.65	0.89	0.57
BH1_B8_A31	24.57	D	20	-	37.06	0.19	1373	-	0.14	0.87	0.12
A = Axial											
D = Diametral											
L = Lump											
				No. Samples	29	Axial		Mean $I_{s(50)}$, (50°-80°)		2.21	± 0.67
				No Samples	18	Axial		Mean $I_{s(50)}$ (70°-75°)		2.08	± 0.46
				No. Samples	20	Diametral		Mean $I_{s(50)}$, (10°-40°)		0.46	± 0.34
				No Samples	16	Diametral		Mean $I_{s(50)}$ (15°-20°)		0.45	± 0.40

C.2.3.2 In Situ Medium Grey Samples

MGY: In Situ - Tests Performed Parallel and Perpendicular to Foliation											
Sample	Depth (m)	Type		Width (W), mm	Diameter (D), mm	Load (P), kN	D_e^2, mm^2	D_e, mm	I_s, MPa	F	$I_{s(50)}$, MPa
BH4_B4_TS2PD	10.76	A	⊥	60.94	32.57	4.55	2527	50.3	1.80	1.00	1.80
BH4_B5_6	14.40	A	⊥	62.90	21.92	6.72	1756	41.9	3.83	0.92	3.54
BH1_B8_F1		A	⊥	60.71	37.59	8.44	2906	53.9	2.90	1.03	3.00
BH1_B8_F2		A	⊥	60.51	38.21	10.63	2944	54.3	3.61	1.04	3.75
BH3_B1_F1		A	⊥	61.39	36.49	5.95	2852	53.4	2.09	1.03	2.15
BH3_B1_F2		A	⊥	60.53	45.60	6.86	3514	59.3	1.95	1.08	2.11
BH3_B1_F5		A	⊥	61.18	42.26	11.41	3292	57.4	3.47	1.06	3.69
BH3_B3_PL1	6.50	A	⊥	61.01	22.56	4.83	1752	41.9	2.76	0.92	2.54
BH3_B4_2PA	10.10	A	⊥	60.64	28.31	5.97	2186	46.8	2.73	0.97	2.65
BH4_B6_1TX1	16.15	A	⊥	60.98	21.69	6.84	1684	41.0	4.06	0.91	3.72
BH1_B8_1PG	23.35	A	⊥	60.92	19.46	6.32	1509	38.9	4.19	0.89	3.74
BH3_B5_2D2	13.10	A	⊥	60.96	29.94	7.74	2324	48.2	3.33	0.98	3.28
BH1_B8_A19A	22.73	A	⊥	60.89	41.04	9.72	3182	56.4	3.05	1.06	3.23
BH1_B8_A1	21.80	A	⊥	61.00	30.65	4.32	2381	48.8	1.81	0.99	1.79
BH1_B8_A4	21.94	A	⊥	60.58	36.16	8.99	2789	52.8	3.22	1.02	3.30
BH1_B1_A16	1.41	A	⊥	60.90	32.84	4.11	2546	50.5	1.61	1.00	1.62
BH1_B1_A20	1.56	A	⊥	60.74	36.50	5.34	2823	53.1	1.89	1.03	1.94
BH1_B1_A33B	2.61	A	⊥	60.95	22.23	4.08	1725	41.5	2.37	0.92	2.18
BH1_B1_A33C	2.61	A	⊥	60.95	22.16	3.45	1720	41.5	2.01	0.92	1.84
BH1_B1_A6A	0.74	A	⊥	61.07	24.05	5.13	1870	43.2	2.74	0.94	2.57
BH1_B1_A12C	1.25	A	⊥	60.89	24.94	3.47	1934	44.0	1.79	0.94	1.69
BH1_B1_A13C	1.29	A	⊥	60.91	32.28	5.52	2503	50.0	2.20	1.00	2.21
BH1_B8_A14B	22.35	A	⊥	60.80	26.67	5.77	2065	45.4	2.79	0.96	2.68
BH1_B8_A14C	22.35	A	⊥	60.86	25.36	6.17	1965	44.3	3.14	0.95	2.97
BH1_B1_PL1XA	1.17	A	⊥	60.86	19.61	4.63	1520	39.0	3.05	0.89	2.72
BH1_B8_A13	22.30	A	⊥	60.76	32.62	11.22	2524	50.2	4.45	1.00	4.46
BH1_B8_A19D	22.73	A	⊥	60.67	24.62	7.90	1902	43.6	4.15	0.94	3.91
BH1_B1_A35	2.68	A	⊥	61.90	21.41	0.97	1687	41.1	0.57	0.92	0.53
BH1_B8_A15	22.40	A	⊥	61.02	29.48	5.00	2290	47.9	2.18	0.98	2.14
BH1_B1_A4A	0.67	A	⊥	60.80	23.13	6.30	1791	42.3	3.52	0.93	3.26
BH4_B3_1DC	6.20	A	⊥	61.19	29.96	0.62	2334	48.3	0.27	0.98	0.26
BH1_B1_A11	0.93	A	⊥	60.84	25.89	2.26	2006	44.8	1.13	0.95	1.07
BH1_B1_A11	0.93	A	⊥	60.84	22.92	3.03	1775	42.1	1.71	0.93	1.58
BH1_B1_A10A	0.89	A	⊥	60.72	22.05	2.33	1705	41.3	1.37	0.92	1.25
BH3_B4_2PD	10.10	A	⊥	60.82	21.84	3.36	1691	41.1	1.99	0.92	1.82
BH1_B1_A5	0.71	A	⊥	60.89	28.61	9.72	2218	47.1	4.38	0.97	4.27
BH4_B4_1DA	9.36	A	⊥	61.31	32.01	9.41	2499	50.0	3.77	1.00	3.77
BH1_B8_A9	22.13	L	⊥	45.24	42.99	5.05	2476	49.8	2.04	1.00	2.04
BH4_B3_1LDB	6.20	L	⊥	42.63	20.44	2.58	1109	33.3	2.33	0.83	1.94
BH4_B4_1L1D	9.36	L	⊥	37.40	25.24	5.38	1202	34.7	4.48	0.85	3.80
BH4_B4_1L1A	9.36	L	⊥	50.23	27.40	4.44	1752	41.9	2.53	0.92	2.34
BH4_B4_1R1	9.52	L	⊥	62.41	31.50	13.77	2503	50.0	5.50	1.00	5.50
BH4_B6_4D1	17.35	D	∥	-	61.39	2.20	3769	-	0.58	1.10	0.64
BH3_B4_2PD	10.10	D	∥	-	60.82	0.81	3699	-	0.22	1.09	0.24
BH1_B1_A4A	0.67	D	∥	-	60.80	1.14	3697	-	0.31	1.09	0.34
BH4_B5_6D1	14.40	D	∥	-	61.15	3.40	3739	-	0.91	1.09	1.00
BH1_B1_PL1X	1.17	D	∥	-	60.85	0.67	3703	-	0.18	1.09	0.20
BH1_B8_F3		D	∥	-	60.55	2.60	3666	-	0.71	1.09	0.77
BH3_B1_F3		D	∥	-	60.85	0.57	3703	-	0.15	1.09	0.17
BH3_B1_F6		D	∥	-	61.45	0.51	3776	-	0.14	1.10	0.15
BH1_B1_A11D	0.93	D	∥	-	60.84	0.60	3702	-	0.16	1.09	0.18
BH1_B8_A18D	22.63	D	∥	-	60.74	0.20	3689	-	0.05	1.09	0.06

MGY: In Situ - Tests Performed Parallel and Perpendicular to Foliation											
Sample	Depth (m)	Type		Width (W), mm	Diameter (D), mm	Load (P), kN	D_e^2, mm^2	D_e, mm	I_s, MPa	F	$I_{s(50)}$, MPa
BH1_B8_A19D	22.73	D	‖	-	60.67	0.97	3681	-	0.26	1.09	0.29
BH1_B8_A17D	22.54	D	‖	-	60.91	1.26	3710	-	0.34	1.09	0.37
BH1_B8_A15	22.40	D	‖	-	61.02	8.04	3723	-	2.16	1.09	2.36
BH1_B8_A15A	22.40	D	‖	-	60.32	2.44	3639	-	0.67	1.09	0.73
BH1_B1_A5	0.71	D	‖	-	60.89	3.03	3708	-	0.82	1.09	0.89
BH1_B1_A6D	0.74	D	‖	-	61.07	7.99	3730	-	2.14	1.09	2.34
BH1_B1_A9	0.85	D	‖	-	60.79	0.95	3695	-	0.26	1.09	0.28
BH1_B1_A33	2.61	D	‖	-	60.81	0.04	3698	-	0.01	1.09	0.01
BH1_B1_A26	1.94	D	‖	-	61.75	4.60	3813	-	1.21	1.10	1.33
BH1_B1_A26A	1.94	D	‖	-	61.75	7.39	3813	-	1.94	1.10	2.13
BH1_B1_A27	1.99	D	‖	-	60.79	0.02	3695	-	0.01	1.09	0.01
BH3_B4_PL2PD	10.85	D	‖	-	60.76	1.37	3692	-	0.37	1.09	0.41
BH1_B1_A10A	0.89	D	‖	-	60.72	1.48	3687	-	0.40	1.09	0.44
BH4_B4_1DA	9.36	D	‖	-	61.31	1.14	3759	-	0.30	1.10	0.33
BH4_B3_1LD	6.20	D	‖	-	45.43	0.56	2064	-	0.27	0.96	0.26
BH4_B4_1L1D	9.36	D	‖	-	38.22	1.61	1461	-	1.10	0.89	0.98
BH4_B3_3L2	8.25	L	‖	-	45.05	0.71	2030	-	0.35	0.95	0.33
BH4_B3_3DL	8.25	L	‖	-	39.32	0.60	1546	-	0.39	0.90	0.35
BH4_B4_1L1	9.36	L	‖	-	39.28	0.39	1543	-	0.25	0.90	0.23
A = Axial											
D = Diametral											
L = Lump											
						No. Samples	42	Mean $I_{s(50)}$, (⊥)		2.63	± 0.84
						No. Samples	29	Mean $I_{s(50)}$ (‖)		0.46	± 0.45
								Mean $I_{s(50)}$ (‖)		5.72	

MGY: In Situ - Tests Performed Oblique to Foliation											
Sample	Depth (m)	Type		Width (W), mm	Diameter (D), mm	Load (P), kN	D_e^2, mm^2	D_e, mm	I_s, MPa	F	$I_{s(50)}$, MPa
BH1_B8_A17A	22.54	A	65	60.82	31.52	7.91	2441	49.4	3.24	0.99	3.22
BH4_B4_1A1	9.36	A	65	54.88	26.79	3.17	1872	43.3	1.69	0.94	1.59
BH1_B1_A13B	1.29	A	70	60.89	30.25	3.75	2345	48.4	1.60	0.99	1.58
BH1_B8_A18A	22.63	A	70	60.77	33.60	6.35	2600	51.0	2.44	1.01	2.46
BH3_B5_3YA	13.80	A	70	60.84	21.52	4.37	1667	40.8	2.62	0.91	2.39
BH1_B8_A15C	22.40	A	70	60.86	24.96	6.04	1934	44.0	3.12	0.94	2.95
BH1_B8_A15D	22.40	A	70	60.86	23.90	6.60	1852	43.0	3.56	0.93	3.33
BH1_B1_1A	2.35	A	70	58.81	26.69	4.69	1999	44.7	2.35	0.95	2.23
BH4_B4_3P1	10.81	A	70	60.86	41.22	7.48	3194	56.5	2.34	1.06	2.47
BH3_B4_3	10.17	A	70	60.85	33.19	10.86	2571	50.7	4.22	1.01	4.25
BH4_B5_4LX	13.76	A	70	60.64	27.40	4.72	2116	46.0	2.23	0.96	2.15
BH1_B8_A2A1	21.83	A	75	60.82	30.05	2.91	2327	48.2	1.25	0.98	1.23
BH1_B8_A2A2	21.83	A	75	60.79	19.21	1.28	1487	38.6	0.86	0.89	0.77
BH4_B4_TS2P	10.76	A	75	60.89	44.71	5.24	3466	58.9	1.51	1.08	1.63
BH3_B4_PL2P2	10.85	A	75	60.83	38.17	7.65	2956	54.4	2.59	1.04	2.69
BH4_B5_6P1	14.40	A	75	60.97	25.89	2.48	2010	44.8	1.23	0.95	1.17
BH1_B1_A12B	1.25	A	75	60.85	20.12	2.48	1559	39.5	1.59	0.90	1.43
BH1_B1_A10AX	0.89	A	75	60.72	26.95	2.12	2084	45.6	1.02	0.96	0.98
BH4_B5_6A	14.40	A	75	60.80	29.51	4.94	2284	47.8	2.16	0.98	2.12
BH3_B2_PL1	5.20	A	75	60.89	23.46	9.38	1819	42.6	5.16	0.93	4.80

MGY: In Situ - Tests Performed Oblique to Foliation											
Sample	Depth (m)	Type		Width (W), mm	Diameter (D), mm	Load (P), kN	D_e^2, mm^2	D_e, mm	I_s, MPa	F	$I_{s(50)}$, MPa
BH1_B8_A15AX	22.40	A	75	60.13	24.64	3.87	1886	43.4	2.05	0.94	1.93
BH4_B6_4D1X	17.35	A	75	61.30	18.21	2.00	1421	37.7	1.41	0.88	1.24
BH4_B6_4D1Y	17.35	A	75	61.30	19.43	1.98	1517	38.9	1.31	0.89	1.17
BH3_B4_PL2P	10.85	A	80	60.74	34.64	9.22	2679	51.8	3.44	1.02	3.50
BH3_B1_2L1	2.50	A	80	61.30	22.57	6.66	1762	42.0	3.78	0.92	3.49
BH4_B5_6D1A	14.40	A	80	61.10	21.67	6.75	1686	41.1	4.00	0.92	3.66
BH4_B5_6D1B	14.40	A	80	61.10	20.40	5.74	1587	39.8	3.62	0.90	3.27
BH3_B5_3	13.80	A	80	60.79	26.87	8.13	2080	45.6	3.91	0.96	3.75
BH4_B3_3DL1	8.25	L	60	47.85	33.56	5.31	2044	45.2	2.60	0.96	2.48
BH4_B4_TS2L	10.76	L	75	51.96	33.41	7.43	2210	47.0	3.36	0.97	3.27
BH4_B4_3L1A1	10.81	L	75	53.07	32.34	8.87	2185	46.7	4.06	0.97	3.94
BH4_B4_3L1	10.81	L	80	39.96	44.98	6.19	2288	47.8	2.71	0.98	2.65
BH3_B1_1LN	1.20	L	80	59.82	19.84	2.31	1511	38.9	1.53	0.89	1.36
BH1_B8_A18D	22.63	L	80	62.76	25.25	7.19	2018	44.9	3.56	0.95	3.40
BH4_B3_3L2A	8.25	L	80	47.84	22.46	4.62	1368	37.0	3.38	0.87	2.95
BH4_B3_3L2B	8.25	L	80	50.27	23.52	4.88	1505	38.8	3.24	0.89	2.89
BH4_B3_1LDA	6.20	L	80	47.13	20.94	1.56	1256	35.4	1.24	0.86	1.06
BH3_B5_3	13.80	D	15	-	60.43	2.53	3652	-	0.69	1.09	0.75
BH4_B4_1D	9.36	D	15	-	61.31	7.54	3759	-	2.01	1.10	2.20
BH1_B8_A14	22.35	D	15	-	60.94	2.58	3714	-	0.69	1.09	0.76
BH1_B1_A10	0.89	D	15	-	60.72	0.24	3687	-	0.07	1.09	0.07
BH1_B1_A11	0.93	D	15	-	60.84	0.39	3702	-	0.11	1.09	0.12
BH1_B1_A12	1.25	D	15	-	62.57	0.67	3915	-	0.17	1.11	0.19
BH1_B1_PL2D	1.30	D	20	-	60.91	0.09	3710	-	0.02	1.09	0.03
BH4_B3_1DC	6.20	D	20	-	61.19	0.62	3744	-	0.17	1.10	0.18
BH1_B8_A13	22.30	D	20	-	60.52	1.15	3663	-	0.31	1.09	0.34
BH1_B8_A15B	22.40	D	20	-	60.86	9.82	3704	-	2.65	1.09	2.90
BH1_B1_A4	0.67	D	20	-	60.80	1.16	3697	-	0.31	1.09	0.34
BH1_B1_A13	1.29	D	20	-	61.72	1.92	3809	-	0.50	1.10	0.55
BH1_B1_A35	2.68	D	20	-	61.90	1.12	3832	-	0.29	1.10	0.32
BH1_B8_A12	22.23	D	25	-	60.75	2.80	3691	-	0.76	1.09	0.83
BH1_B1_1L2	2.35	D	30	-	60.56	1.95	3668	-	0.53	1.09	0.58
BH1_B8_A8	22.07	D	35	-	60.75	5.10	3691	-	1.38	1.09	1.51
BH4_B4_TS2LD	10.76	L	25	-	42.99	1.64	1848	-	0.89	0.93	0.83
BH4_B5_5LP	14.10	L	35	-	37.33	1.90	1394	-	1.36	0.88	1.20
A = Axial											
D = Diametral											
L = Lump											
				No. Samples	37	Axial		Mean $I_{s(50)}$, (50°-80°)		2.44	± 0.87
				No Samples	23	Axial		Mean $I_{s(50)}$ (70°-75°)		2.17	± 0.81
				No. Samples	18	Diametral		Mean $I_{s(50)}$, (10°-40°)		0.61	± 0.39
				No Samples	13	Diametral		Mean $I_{s(50)}$ (15°-20°)		0.40	± 0.24

C.2.3.3 Oven-Dried Dark Green-Grey Samples

DGY: Oven-Dried - Tests Performed Parallel and Perpendicular to Foliation											
Sample	Depth (m)	Type		Width (W), mm	Diameter (D), mm	Load (P), kN	D_e^2, mm²	D_e, mm	I_s, MPa	F	$I_{s(50)}$, MPa
BH1_B2_A7	3.20	A	⊥	60.81	25.74	10.04	1993	44.6	5.04	0.95	4.79
BH1_B2_A7	3.20	A	⊥	60.81	24.27	12.24	1879	43.3	6.51	0.94	6.11
BH1_B8_A28A	24.09	A	⊥	60.84	24.17	6.51	1872	43.3	3.48	0.94	3.26
BH1_B2_A33P	5.44	A	⊥	61.00	24.89	7.36	1933	44.0	3.81	0.94	3.59
BH3_B3_2A	6.80	A	⊥	60.68	23.23	7.71	1795	42.4	4.30	0.93	3.99
BH1_B2_A32B	5.41	A	⊥	61.00	18.99	6.94	1475	38.4	4.71	0.89	4.18
BH1_B2_A37C	5.67	A	⊥	60.74	24.00	11.01	1856	43.1	5.93	0.94	5.55
BH1_B2_A33A	5.44	A	⊥	60.81	18.91	7.80	1464	38.3	5.33	0.89	4.72
BH1_B2_A33B	5.44	A	⊥	60.81	20.00	5.21	1549	39.4	3.36	0.90	3.02
BH1_B2_A36B1	5.59	A	⊥	60.83	21.68	8.72	1679	41.0	5.19	0.91	4.75
BH1_B2_A36B2	5.59	A	⊥	60.83	21.45	11.32	1661	40.8	6.81	0.91	6.22
BH2_B3_PL1A	9.70	A	⊥	60.91	28.48	9.15	2209	47.0	4.14	0.97	4.03
BH1_B7_A15PL	20.38	A	⊥	61.72	24.51	5.76	1926	43.9	2.99	0.94	2.82
BH1_B7_PL1	20.45	A	⊥	66.00	27.16	10.57	2282	47.8	4.63	0.98	4.54
BH4_B4_4PL	11.30	A	⊥	58.30	22.87	7.56	1698	41.2	4.45	0.92	4.08
BH1_B2_AAX	3.00	A	⊥	60.56	23.64	7.70	1823	42.7	4.22	0.93	3.93
BH1_B2_A12BXN	3.81	A	⊥	60.83	34.15	8.04	2645	51.4	3.04	1.01	3.08
BH1_B2_A14BXN	4.33	A	⊥	61.01	31.85	15.30	2474	49.7	6.18	1.00	6.17
BH1_B2_A18XN	4.56	A	⊥	60.19	24.99	8.04	1915	43.8	4.20	0.94	3.95
BH1_B2_A18XN2	4.56	A	⊥	60.67	25.81	10.71	1994	44.7	5.37	0.95	5.11
BH1_B2_A23XN	4.82	A	⊥	61.00	27.34	8.28	2123	46.1	3.90	0.96	3.76
BH4_B2_PL6XN	4.40	A	⊥	60.85	22.73	8.78	1761	42.0	4.99	0.92	4.61
BH2_B3_PL1B	9.70	A	⊥	60.91	19.07	3.44	1479	38.5	2.33	0.89	2.07
BH1_B2_A19A	4.62	A	⊥	60.83	24.36	7.43	1887	43.4	3.94	0.94	3.70
BH1_B2_A5A	3.13	A	⊥	60.94	20.06	8.42	1556	39.5	5.41	0.90	4.86
BH1_B2_A5B	3.13	A	⊥	60.94	26.66	8.87	2069	45.5	4.29	0.96	4.11
BH1_B2_A5C	3.13	A	⊥	60.94	20.82	3.92	1615	40.2	2.43	0.91	2.20
BH1_B2_A20	4.70	A	⊥	60.81	28.70	9.23	2222	47.1	4.15	0.97	4.05
BH1_B2_A18	4.56	A	⊥	60.82	30.08	15.51	2329	48.3	6.66	0.98	6.55
BH1_B7_3P1A	20.20	A	⊥	61.77	30.75	10.93	2418	49.2	4.52	0.99	4.49
BH4_B7_4S	19.10	A	⊥	60.84	27.30	15.42	2115	46.0	7.29	0.96	7.02
BH4_B8_5PD1	23.07	A	⊥	60.92	28.40	11.01	2203	46.9	5.00	0.97	4.86
BH4_B2_PL9	5.93	A	⊥	60.85	32.10	5.40	2487	49.9	2.17	1.00	2.17
BH4_B9_PL4P2	24.40	A	⊥	60.97	22.15	7.57	1719	41.5	4.40	0.92	4.05
BH3_B3_2P	6.80	A	⊥	60.78	18.68	7.01	1446	38.0	4.85	0.88	4.29
BH1_B5_PL1D1	12.20	A	⊥	60.66	22.64	7.63	1749	41.8	4.36	0.92	4.03
BH1_B5_PL1D2	12.20	A	⊥	61.11	20.52	8.75	1597	40.0	5.48	0.90	4.95
BH1_B3_PL1X	7.64	A	⊥	60.81	26.05	12.41	2017	44.9	6.15	0.95	5.86
BH1_B3_PL1X1	7.64	A	⊥	60.48	22.96	4.44	1768	42.0	2.51	0.93	2.32
BH1_B5_PL2L	15.60	A	⊥	60.85	18.61	7.62	1442	38.0	5.28	0.88	4.67
BH4_B9_PL3P	24.30	A	⊥	60.96	32.80	7.10	2546	50.5	2.79	1.00	2.80
BH2_B1_PL2PD	2.20	A	⊥	61.19	39.81	2.94	3102	55.7	0.95	1.05	1.00
BH2_B1_PL1	1.60	A	⊥	60.78	30.98	5.56	2397	49.0	2.32	0.99	2.30
BH1_B6_PL2LA	17.30	L	⊥	55.92	29.38	12.13	2092	45.7	5.80	0.96	5.57
BH1_B8_A27L	23.98	L	⊥	56.72	29.98	12.78	2165	46.5	5.90	0.97	5.71
BH2_B3_PL1	9.70	D	‖	-	61.46	0.63	3777	-	0.17	1.10	0.18
BH1_B8_A28	24.09	D	‖	-	60.43	9.89	3652	-	2.71	1.09	2.95
BH1_B2_A23	4.82	D	‖	-	60.61	1.50	3674	-	0.41	1.09	0.45
BH1_B2_A5	3.13	D	‖	-	60.94	3.30	3714	-	0.89	1.09	0.97
BH1_B2_A16	4.47	D	‖	-	60.66	5.24	3680	-	1.42	1.09	1.55
BH1_B2_A18	4.56	D	‖	-	60.78	4.95	3694	-	1.34	1.09	1.46
BH1_B2_A36A2	5.59	D	‖	-	60.83	0.81	3700	-	0.22	1.09	0.24

DGY: Oven-Dried - Tests Performed Parallel and Perpendicular to Foliation											
Sample	Depth (m)	Type		Width (W), mm	Diameter (D), mm	Load (P), kN	D_e^2, mm²	D_e, mm	I_s, MPa	F	$I_{s(50)}$, MPa
BH1_B2_A33P	5.44	D	‖		61.01	0.37	3722	-	0.10	1.09	0.11
BH1_B2_A33	5.44	D	‖		60.85	0.63	3703	-	0.17	1.09	0.19
BH1_B2_A15	4.44	D	‖		60.79	1.84	3695	-	0.50	1.09	0.54
BH1_B2_A31	5.38	D	‖	-	60.96	1.95	3716	-	0.52	1.09	0.57
BH1_B2_A21	4.73	D	‖	-	62.24	0.50	3874	-	0.13	1.10	0.14
BH1_B2_A10	3.31	D	‖	-	60.94	0.04	3714	-	0.01	1.09	0.01
BH1_B2_A17	4.52	D	‖	-	60.82	4.05	3699	-	1.09	1.09	1.20
BH1_B2_A40	5.81	D	‖	-	60.87	0.99	3705	-	0.27	1.09	0.29
BH1_B2_A9A	3.27	D	‖	-	60.83	0.16	3700	-	0.04	1.09	0.05
BH1_B2_A5D	3.13	D	‖	-	60.94	3.61	3714	-	0.97	1.09	1.06
BH1_B2_A18	4.56	D	‖	-	60.78	1.58	3694	-	0.43	1.09	0.47
BH3_B8_2D1	21.55	L	‖	-	25.36	0.81	643	-	1.26	0.74	0.93
A = Axial											
D = Diametral											
L = Lump											
						No. Samples	45	Mean $I_{s(50)}$, (⊥)		4.22	± 1.08
						No. Samples	19	Mean $I_{s(50)}$ (‖)		0.58	± 0.42
								Mean $I_{s(50)}$ (‖)		7.28	

DGY: Oven-Dried - Tests Performed Oblique to Foliation											
Sample	Depth (m)	Type		Width (W), mm	Diameter (D), mm	Load (P), kN	D_e^2, mm²	D_e, mm	I_s, MPa	F	$I_{s(50)}$, MPa
BH1_B8_A26B	23.98	A	65	60.87	25.47	10.21	1974	44.4	5.17	0.95	4.90
BH1_B8_A26	23.94	A	50	60.90	26.31	4.32	2040	45.2	2.12	0.96	2.02
BH1_B3_PL2DA	8.27	A	60	60.40	24.21	7.28	1862	43.1	3.91	0.94	3.66
BH1_B8_A24A	23.81	A	60	60.85	26.19	3.12	2029	45.0	1.54	0.95	1.47
BH1_B3_PL31	8.85	A	65	60.63	34.12	8.46	2634	51.3	3.21	1.01	3.25
BH1_B8_A33	24.73	A	65	60.62	40.56	6.84	3131	56.0	2.18	1.05	2.30
BH1_B8_A29A	24.33	A	65	60.81	31.67	5.06	2452	49.5	2.06	1.00	2.05
BH1_B8_A29A1	24.33	A	65	60.79	30.95	8.23	2396	48.9	3.44	0.99	3.40
BH1_B2_A25	4.92	A	65	60.87	34.37	11.80	2664	51.6	4.43	1.01	4.49
BH1_B7_A4	19.36	A	75	60.70	22.88	5.20	1768	42.1	2.94	0.93	2.72
BH1_B7_A12	19.81	A	70	60.69	24.61	8.28	1902	43.6	4.35	0.94	4.09
BH1_B2_A13	4.06	A	75	60.39	33.20	8.16	2553	50.5	3.20	1.00	3.21
BH3_B8_A5A	23.90	A	70	60.81	30.91	6.86	2393	48.9	2.87	0.99	2.84
BH3_B8_A5B	23.90	A	75	60.89	23.87	3.85	1851	43.0	2.08	0.93	1.94
BH3_B8_A5C	23.90	A	70	60.67	20.50	3.30	1584	39.8	2.08	0.90	1.88
BH3_B8_A8A	23.00	A	70	60.77	24.75	4.01	1915	43.8	2.09	0.94	1.97
BH3_B8_A8B	23.00	A	70	60.75	26.48	4.61	2048	45.3	2.25	0.96	2.15
BH3_B8_A8C	23.00	A	70	60.77	20.53	2.99	1589	39.9	1.88	0.90	1.70
BH1_B3_PL3D	8.85	A	70	61.60	24.85	7.60	1949	44.1	3.90	0.95	3.69
BH1_B8_A20	23.51	A	70	60.61	35.93	11.53	2773	52.7	4.16	1.02	4.26
BH1_B2_A29	5.31	A	70	60.67	29.40	6.67	2271	47.7	2.94	0.98	2.87
BH1_B8_A30A	24.44	A	75	6.71	29.63	4.04	253	15.9	15.96	0.60	9.53
BH1_B8_A30B	24.44	A	75	60.69	25.67	1.26	1984	44.5	0.64	0.95	0.60
BH1_B2_A22	4.76	A	75	60.89	37.77	14.62	2928	54.1	4.99	1.04	5.17
BH1_B2_A26	5.19	A	75	60.68	31.53	13.64	2436	49.4	5.60	0.99	5.57
BH1_B6_PL1LA	17.16	A	80	56.65	22.56	7.62	1627	40.3	4.68	0.91	4.25
BH1_B8_A35	24.85	A	80	60.92	22.73	6.05	1763	42.0	3.43	0.92	3.17

DGY: Oven-Dried - Tests Performed Oblique to Foliation											
Sample	Depth (m)	Type		Width (W), mm	Diameter (D), mm	Load (P), kN	D_e^2, mm^2	D_e, mm	I_s, MPa	F	$I_{s(50)}$, MPa
BH2_B3_PL1AL	9.70	A	80	61.06	43.13	6.71	3353	57.9	2.00	1.07	2.14
BH3_B7_PL1LA	20.90	A	80	60.77	23.83	6.00	1844	42.9	3.25	0.93	3.04
BH4_B2_PL6LA	4.40	A	80	61.12	22.12	8.07	1721	41.5	4.69	0.92	4.31
BH1_B4_4LP	10.10	A	80	60.68	24.77	4.41	1914	43.7	2.30	0.94	2.17
BH1_B2_A32A	5.41	A	80	61.00	28.15	9.34	2186	46.8	4.27	0.97	4.15
BH1_B2_A37B	5.67	A	80	60.74	25.80	10.11	1995	44.7	5.07	0.95	4.82
BH1_B6_PL2LA	17.30	L	65	62.81	33.01	6.04	2640	51.4	2.29	1.01	2.32
BH3_B8_2L1	21.55	L	70	44.84	27.99	5.88	1598	40.0	3.68	0.90	3.33
BH1_B2_A12A	3.81	D	20	-	60.72	1.73	3687	-	0.47	1.09	0.51
BH1_B2_A12B	3.81	D	20	-	60.78	3.13	3694	-	0.85	1.09	0.93
BH1_B2_A14	4.33	D	20	-	60.78	2.31	3694	-	0.63	1.09	0.68
BH1_B2_A14DM	4.33	D	15	-	60.70	1.87	3684	-	0.51	1.09	0.55
BH4_B9_PL1PD	24.10	D	15	-	60.32	1.37	3639	-	0.38	1.09	0.41
BH1_B2_A16DN	4.47	D	15	-	61.16	1.83	3741	-	0.49	1.09	0.54
BH1_B2_A24DN	4.85	D	15	-	60.89	3.24	3708	-	0.87	1.09	0.95
BH1_B2_A12ADN	3.81	D	20	-	62.57	1.76	3915	-	0.45	1.11	0.50
BH1_B2_A34DN	5.52	D	20	-	61.76	0.96	3814	-	0.25	1.10	0.28
BH1_B2_A37BDN	5.67	D	20	-	60.84	3.36	3702	-	0.91	1.09	0.99
BH1_B2_A19BDN	4.62	D	20	-	61.15	1.32	3739	-	0.35	1.09	0.39
BH1_B8_A34DDN	24.78	D	20	-	61.66	1.60	3802	-	0.42	1.10	0.46
BH1_B2_A1	3.00	D	20	-	60.72	1.15	3687	-	0.31	1.09	0.34
BH1_B2_A7	3.20	D	20	-	61.02	1.30	3723	-	0.35	1.09	0.38
BH1_B2_A20	4.70	D	20	-	60.81	0.55	3698	-	0.15	1.09	0.16
BH1_B2_A34	5.52	D	20	-	60.79	2.45	3695	-	0.66	1.09	0.72
BH1_B2_A37B	5.67	D	20	-	60.73	0.50	3688	-	0.14	1.09	0.15
BH1_B2_A9	3.27	D	25	-	60.83	1.33	3700	-	0.36	1.09	0.39
BH1_B2_A37	5.67	D	25	-	60.74	0.40	3689	-	0.11	1.09	0.12
BH1_B2_A19A	4.62	D	25	-	60.66	4.32	3680	-	1.17	1.09	1.28
BH1_B2_A19B	4.62	D	25	-	60.68	0.89	3682	-	0.24	1.09	0.26
BH1_B2_A32	5.41	D	30	-	61.00	2.21	3721	-	0.59	1.09	0.65
BH1_B2_A14B	4.33	D	30	-	60.94	2.75	3714	-	0.74	1.09	0.81
A = Axial											
D = Diametral											
L = Lump											
				No. Samples	35	Axial		Mean $I_{s(50)}$, (50°-80°)		3.13	± 1.01
				No Samples	17	Axial		Mean $I_{s(50)}$ (70°-75°)		3.09	± 1.01
				No. Samples	23	Diametral		Mean $I_{s(50)}$, (10°-40°)		0.52	± 0.21
				No Samples	17	Diametral		Mean $I_{s(50)}$ (15°-20°)		0.51	± 0.18

C.2.3.4 Oven-Dried Medium Grey Samples

MGY: Oven-Dried - Tests Performed Parallel and Perpendicular to Foliation											
Sample	Depth (m)	Type		Width (W), mm	Diameter (D), mm	Load (P), kN	D_e^2, mm²	D_e, mm	I_s, MPa	F	$I_{s(50)}$, MPa
BH1_B1_A18A	1.49	A	⊥	60.84	26.75	10.04	2072	45.5	4.85	0.96	4.64
BH1_B1_A18B	1.49	A	⊥	60.84	26.31	8.74	2038	45.1	4.29	0.96	4.10
BH1_B1_A17A	1.44	A	⊥	60.94	22.18	6.36	1721	41.5	3.70	0.92	3.40
BH1_B1_A17B	1.44	A	⊥	60.94	31.11	10.32	2414	49.1	4.28	0.99	4.24
BH3_B5_5	14.50	A	⊥	58.50	29.93	9.09	2229	47.2	4.08	0.97	3.97
BH3_B5_1	12.65	A	⊥	60.62	24.85	10.65	1918	43.8	5.55	0.94	5.23
BH1_B8_A27XN1	5.24	A	⊥	59.40	39.29	12.33	2972	54.5	4.15	1.04	4.31
BH1_B8_A27XN2	5.24	A	⊥	59.11	24.83	13.58	1869	43.2	7.27	0.94	6.81
BH1_B1_A21D	1.60	A	⊥	60.82	22.10	8.16	1711	41.4	4.77	0.92	4.38
BH1_B1_A37A	2.74	A	⊥	61.01	21.53	6.65	1672	40.9	3.98	0.91	3.63
BH1_B1_A21G	1.60	A	⊥	61.04	20.91	7.22	1625	40.3	4.44	0.91	4.03
BH1_B7_A22A	20.87	A	⊥	61.42	25.47	11.62	1992	44.6	5.83	0.95	5.54
BH1_B1_A6A	0.74	A	⊥	60.71	18.50	4.36	1430	37.8	3.05	0.88	2.69
BH1_B1_A23A	1.76	A	⊥	60.55	22.70	3.91	1750	41.8	2.23	0.92	2.06
BH1_B1_A23B	1.76	A	⊥	60.55	25.23	4.08	1945	44.1	2.10	0.95	1.98
BH1_B1_A22A1	1.69	A	⊥	60.91	19.51	6.44	1513	38.9	4.26	0.89	3.80
BH1_B1_A22A2	1.69	A	⊥	60.91	21.80	6.38	1691	41.1	3.77	0.92	3.46
BH1_B1_A22A3	1.69	A	⊥	60.91	29.34	8.61	2275	47.7	3.78	0.98	3.70
BH1_B8_A12B1	22.23	A	⊥	60.75	29.22	10.53	2260	47.5	4.66	0.98	4.55
BH1_B8_A12B2	22.23	A	⊥	60.75	23.45	15.76	1814	42.6	8.69	0.93	8.08
BH1_B8_A8A	22.07	A	⊥	60.80	36.36	9.42	2815	53.1	3.35	1.03	3.44
BH1_B1_A7	0.80	A	⊥	60.80	31.34	10.30	2426	49.3	4.25	0.99	4.22
BH1_B1_A8	0.83	A	⊥	61.04	21.03	4.51	1634	40.4	2.76	0.91	2.51
BH1_B1_A14	1.37	A	⊥	61.25	18.39	4.12	1434	37.9	2.87	0.88	2.54
BH1_B1_A34	2.66	A	⊥	60.70	20.89	3.93	1614	40.2	2.43	0.91	2.21
BH1_B1_A32	2.59	A	⊥	61.68	18.72	4.91	1470	38.3	3.34	0.89	2.96
BH1_B1_A28	2.04	A	⊥	61.05	18.53	3.00	1440	38.0	2.08	0.88	1.84
BH1_B1_A25A	1.86	A	⊥	60.90	37.15	11.94	2881	53.7	4.14	1.03	4.28
BH1_B1_A36	2.72	A	⊥	61.03	23.76	4.18	1846	43.0	2.26	0.93	2.11
BH1_B1_A38	2.78	A	⊥	20.90	19.64	8.61	523	22.9	16.47	0.70	11.58
BH1_B7_A17	20.72	A	⊥	60.84	38.23	10.23	2961	54.4	3.45	1.04	3.59
BH1_B7_A19	20.80	A	⊥	60.60	22.59	7.06	1743	41.7	4.05	0.92	3.73
BH1_B7_A20	20.82	A	⊥	60.71	29.14	11.86	2252	47.5	5.27	0.98	5.14
BH1_B7_A27C	21.58	A	⊥	60.76	25.87	9.42	2001	44.7	4.71	0.95	4.48
BH4_B4_2A1	9.66	A	⊥	60.74	26.36	4.71	2039	45.2	2.31	0.96	2.21
BH4_B4_2A2	9.66	A	⊥	60.80	22.41	8.90	1735	41.7	5.13	0.92	4.73
BH4_B4_2C1	9.66	A	⊥	60.82	23.64	10.73	1831	42.8	5.86	0.93	5.46
BH1_B7_A28D1	21.58	A	⊥	60.44	19.70	4.44	1516	38.9	2.93	0.89	2.62
BH1_B1_A3	0.64	L	⊥	45.84	27.70	7.55	1617	40.2	4.67	0.91	4.23
BH1_B7_A21	20.84	L	⊥	46.04	33.12	11.03	1941	44.1	5.68	0.94	5.37
BH4_B4_2L1	9.66	L	⊥	47.92	34.88	7.96	2128	46.1	3.74	0.96	3.61
BH1_B8_A5L	21.98	L	⊥	47.30	38.45	21.76	2315	48.1	9.40	0.98	9.24
BH3_B3_3D1C	8.55	L	⊥	52.16	19.49	6.13	1294	36.0	4.74	0.86	4.08
BH3_B3_3D1D	8.55	L	⊥	52.16	23.88	9.26	1586	39.8	5.84	0.90	5.27
BH1_B1_A22C	1.69	D	∥	-	60.91	1.06	3710	-	0.29	1.09	0.31
BH1_B1_A22	1.69	D	∥	-	60.91	1.59	3710	-	0.43	1.09	0.47
BH1_B1_A19	1.54	D	∥	-	61.08	2.29	3731	-	0.61	1.09	0.67
BH1_B1_A37	2.74	D	∥	-	61.01	1.35	3722	-	0.36	1.09	0.40
BH1_B7_A22	20.87	D	∥	-	61.15	1.67	3739	-	0.45	1.09	0.49
BH1_B7_A24	21.41	D	∥	-	60.80	2.96	3697	-	0.80	1.09	0.87
BH1_B7_A24B	21.41	D	∥	-	60.80	4.00	3697	-	1.08	1.09	1.18
BH1_B7_A24C	22.00	D	∥	-	60.86	2.33	3704	-	0.63	1.09	0.69

MGY: Oven-Dried - Tests Performed Parallel and Perpendicular to Foliation											
Sample	Depth (m)	Type		Width (W), mm	Diameter (D), mm	Load (P), kN	D_e^2, mm^2	D_e, mm	I_s, MPa	F	$I_{s(50)}$, MPa
BH4_B4_2D1	9.66	D	‖	-	61.53	4.65	3786	-	1.23	1.10	1.35
		D	‖	-				-			
BH4_B4_2D	9.66	D	‖	-	60.79	10.17	3695	-	2.75	1.09	3.01
BH3_B3_3A	8.55	D	‖	-	60.71	3.07	3686	-	0.83	1.09	0.91
BH1_B8_A27	23.98	D	‖	-	60.94	1.93	3714	-	0.52	1.09	0.57
BH1_B8_A15A	22.40	D	‖	-	60.54	5.99	3665	-	1.63	1.09	1.78
BH1_B1_A27D	1.99	D	‖	-	61.75	0.92	3813	-	0.24	1.10	0.27
BH1_B8_A8	22.07	D	‖	-	60.80	11.47	3697	-	3.10	1.09	3.39
BH1_B8_A12B	22.23	D	‖	-	60.75	4.79	3691	-	1.30	1.09	1.42
BH1_B8_A8A	22.07	D	‖	-	60.80	9.12	3697	-	2.47	1.09	2.69
BH1_B1_A29	2.06	L	‖	-	32.81	0.17	1076	-	0.16	0.83	0.13
BH1_B1_A31	2.55	L	‖	-	29.84	0.48	890	-	0.54	0.79	0.43
A = Axial											
D = Diametral											
L = Lump											
						No. Samples	44	Mean $I_{s(50)}$, (⊥)		4.03	± 1.24
						No. Samples	19	Mean $I_{s(50)}$ (‖)		0.95	± 0.06
								Mean $I_{s(50)}$ (‖)		4.24	

MGY: Oven-Dried - Tests Performed Oblique to Foliation											
Sample	Depth (m)	Type		Width (W), mm	Diameter (D), mm	Load (P), kN	D_e^2, mm^2	D_e, mm	I_s, MPa	F	$I_{s(50)}$, MPa
BH1_B7_A23B	21.34	A	65	60.70	22.63	3.89	1749	41.8	2.22	0.92	2.05
BH1_B7_A23	21.34	A	70	60.83	26.32	8.88	2039	45.1	4.36	0.96	4.16
BH1_B1_A21E	1.60	A	70	60.31	21.42	3.92	1645	40.6	2.38	0.91	2.17
BH1_B1_A21F	1.60	A	70	61.04	20.14	4.79	1565	39.6	3.06	0.90	2.75
BH2_B3_PL1DC1	9.70	A	70	60.91	23.80	8.14	1846	43.0	4.41	0.93	4.12
BH2_B3_PL1DC2	9.70	A	70	60.88	21.43	5.29	1661	40.8	3.18	0.91	2.90
BH1_B7_A25A	21.47	A	70	60.86	28.51	16.10	2209	47.0	7.29	0.97	7.09
BH1_B7_A23C	21.34	A	70	60.75	23.44	5.30	1813	42.6	2.92	0.93	2.72
BH1_B7_A26	21.51	A	70	60.84	22.16	6.14	1717	41.4	3.58	0.92	3.29
BH1_B7_A26B	21.51	A	70	60.91	27.35	8.34	2121	46.1	3.93	0.96	3.79
BH1_B7_A27	21.58	A	70	60.95	27.60	9.55	2142	46.3	4.46	0.97	4.31
BH1_B7_A28C	21.58	A	70	60.71	30.52	9.09	2359	48.6	3.85	0.99	3.80
BH1_B1_A6A2	0.74	A	75	60.71	32.62	8.42	2521	50.2	3.34	1.00	3.35
BH1_B7_A27B	21.58	A	75	60.67	23.38	4.53	1806	42.5	2.51	0.93	2.33
BH1_B7_A28B	21.58	A	75	60.73	25.31	6.19	1957	44.2	3.16	0.95	2.99
BH4_B4_2B1	9.66	A	75	60.76	22.17	8.86	1715	41.4	5.17	0.92	4.75
BH1_B7_A28D2	21.58	A	75	60.46	20.95	9.01	1613	40.2	5.59	0.91	5.06
BH1_B7_A28	21.58	A	75	60.70	23.86	9.52	1844	42.9	5.16	0.93	4.82
BH4_B4_2D	9.66	A	80	60.79	32.56	12.70	2520	50.2	5.04	1.00	5.05
BH3_B3_3A1	8.55	A	80	50.60	28.12	11.29	1812	42.6	6.23	0.93	5.80
BH3_B3_3A2	8.55	A	80	50.60	21.33	6.20	1374	37.1	4.51	0.87	3.94
BH3_B3_3B1	8.55	A	80	48.49	31.52	8.52	1946	44.1	4.38	0.95	4.14
BH3_B3_3B2	8.55	A	80	56.92	18.08	3.66	1310	36.2	2.79	0.86	2.42
BH4_B4_2B2	9.66	A	80	60.84	21.40	4.31	1658	40.7	2.60	0.91	2.37
BH1_B1_A24	1.81	L	60	35.12	31.84	4.26	1424	37.7	2.99	0.88	2.64

MGY: Oven-Dried - Tests Performed Oblique to Foliation											
Sample	Depth (m)	Type		Width (W), mm	Diameter (D), mm	Load (P), kN	D_e^2, mm^2	D_e, mm	I_s, MPa	F	$I_{s(50)}$, MPa
BH1_B1_A25B	1.86	L	70	53.48	34.75	3.79	2366	48.6	1.60	0.99	1.58
BH1_B1_A2	0.62	L	75	59.68	22.04	5.06	1675	40.9	3.02	0.91	2.76
BH1_B1_A15	1.39	L	80	41.41	27.06	5.19	1427	37.8	3.64	0.88	3.21
BH1_B1_A23	1.76	D	10	-	60.48	0.16	3658	-	0.04	1.09	0.05
BH1_B1_A17	1.44	D	15	-	61.09	2.75	3732	-	0.74	1.09	0.81
BH1_B8_A5D	21.98	D	15	-	60.47	0.63	3657	-	0.17	1.09	0.19
BH1_B1_A6	0.74	D	15	-	60.76	1.06	3692	-	0.29	1.09	0.31
BH1_B1_A6B	0.74	D	15	-	60.76	2.01	3692	-	0.54	1.09	0.59
BH1_B8_A5D	21.98	D	15	-	60.47	0.86	3657	-	0.24	1.09	0.26
BH1_B7_A28D	21.58	D	15	-	60.58	0.75	3670	-	0.20	1.09	0.22
BH1_B1_A18	1.49	D	15	-	61.14	1.38	3738	-	0.37	1.09	0.40
BH1_B1_A21A	1.60	D	20	-	60.73	3.39	3688	-	0.92	1.09	1.00
BH1_B1_A21B	1.60	D	20	-	61.02	2.16	3723	-	0.58	1.09	0.63
BH1_B1_A21C	1.60	D	20	-	60.73	3.66	3688	-	0.99	1.09	1.08
BH3_B3_3B	8.55	D	20	-	60.68	0.62	3682	-	0.17	1.09	0.18
BH2_B3_PL1DC	9.70	D	20	-	61.15	4.29	3739	-	1.15	1.09	1.26
BH1_B7_A25	21.47	D	20	-	60.67	0.55	3681	-	0.15	1.09	0.16
BH1_B1_A30	2.51	L	20	-	28.15	1.34	792	-	1.69	0.77	1.31
BH1_B7_A18	20.75	L	20	-	36.95	3.57	1365	-	2.61	0.87	2.28
BH3_B3_3D1	8.55	L	20	-	52.16	6.54	2721	-	2.40	1.02	2.45
BH3_B3_3D1A	8.55	L	20	-	52.16	6.12	2721	-	2.25	1.02	2.29
BH3_B3_3D1B	8.55	L	20	-	52.16	4.70	2721	-	1.73	1.02	1.76
A = Axial											
D = Diametral											
L = Lump											
				No. Samples	28	Axial		Mean $I_{s(50)}$, (50°-80°)		3.49	± 0.89
				No Samples	19	Axial		Mean $I_{s(50)}$ (70°-75°)		3.52	± 0.79
				No. Samples	19	Diametral		Mean $I_{s(50)}$, (10°-40°)		0.82	± 0.61
				No Samples	18	Diametral		Mean $I_{s(50)}$ (15°-20°)		0.87	± 0.63

C.2.3.5 Detailed In Situ Point Load Strength Summary

In situ moisture content							
		DGy		MGy		Combined	
Point Load Strength Index, I_s (MPa)	Perpendicular	2.44	± 0.95	2.74	± 0.89	2.60	± 1.01
	β = 50°-80°	2.29	± 0.74	2.57	± 0.92	2.42	± 0.91
	β = 70°-75°	2.14	± 0.49	2.25	± 0.83	2.22	± 0.78
	Parallel	0.46	± 0.35	0.43	± 0.42	0.52	± 0.48
	β = 10°-35°	0.46	± 0.32	0.58	± 0.40	0.58	± 0.50
	β = 15°-20°	0.46	± 0.38	0.36	± 0.22	0.51	± 0.54
Point Load Strength Index, $I_{s(50)}$ (MPa)	Perpendicular	2.40	± 0.92	2.63	± 0.84	2.52	± 0.96
	β = 50°-80°	2.21	± 0.67	2.44	± 0.87	2.32	± 0.86
	β = 70°-75°	2.08	± 0.46	2.18	± 0.81	2.16	± 0.77
	Parallel	0.46	± 0.34	0.46	± 0.45	0.55	± 0.51
	β = 10°-35°		± 0.34	0.61	± 0.39	0.60	± 0.54
	β = 15°-20°		± 0.40	0.40	± 0.24	0.54	± 0.59
Conversion Factor, K (From UCS)	β = 50°-80°	10.6		18.6		14.6	
	β = 70°-75°	14.4		23.2		19.7	
Anisotropy Index, I_a		5.11		5.72		4.85	
Tensile Strength, σ_t (MPa)		0.7		0.6-0.9		0.8-0.9	

C.2.3.6 Detailed Oven-Dried Point Load Strength Summary

Oven Dried Samples							
		DGy		MGy		Combined	
Point Load Strength Index, I_s (MPa)	Perpendicular	4.50	1.17	4.28	1.32	4.40	1.32
	β = 50°-80°	3.25	1.05	3.75	0.92	3.49	1.18
	β = 70°-75°	3.19	0.96	3.74	0.82	3.29	0.91
	Parallel	0.56	0.42	0.88	0.57	0.77	0.62
	β = 10°-35°	0.48	0.20	0.83	0.69	0.63	0.51
	β = 15°-20°	0.47	0.16	0.87	0.72	0.66	0.54
Point Load Strength Index, $I_{s(50)}$ (MPa)	Perpendicular	4.22	1.08	3.49	0.89	4.14	1.25
	β = 50°-80°	3.13	1.01	4.04	1.24	3.31	1.13
	β = 70°-75°	3.09	1.01	3.52	0.79	3.12	0.89
	Parallel	0.58	0.42	0.95	0.63	0.82	0.67
	β = 10°-35°	0.52	0.21	0.82	0.61	0.65	0.46
	β = 15°-20°	0.51	0.18	0.87	0.63	0.68	0.48
Conversion Factor, K (From UCS)	β = 50°-80°	10.5		14.1		12.6	
	β = 70°-75°	11.6		12.2		12.7	
Anisotropy Index, I_a		7.28		4.24		5.38	
Tensile Strength, σ_t (MPa)		0.8-0.9		1.2-1.4		1.0-1.2	

Appendix C: Rock Mechanics

Point Load Strength Distribution for Oven-Dried Samples

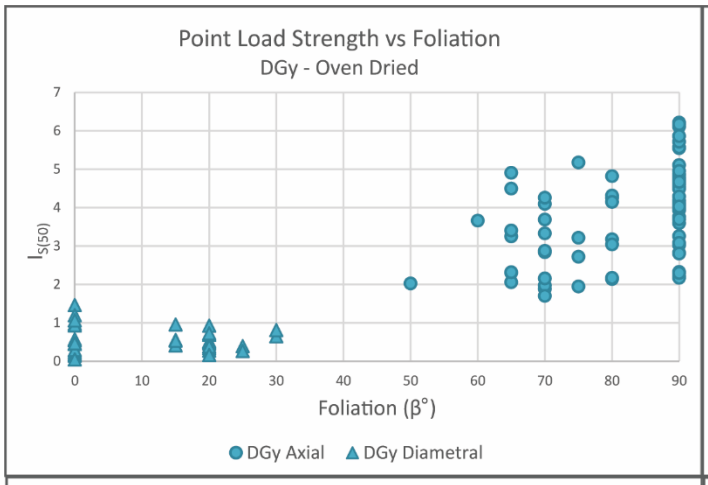

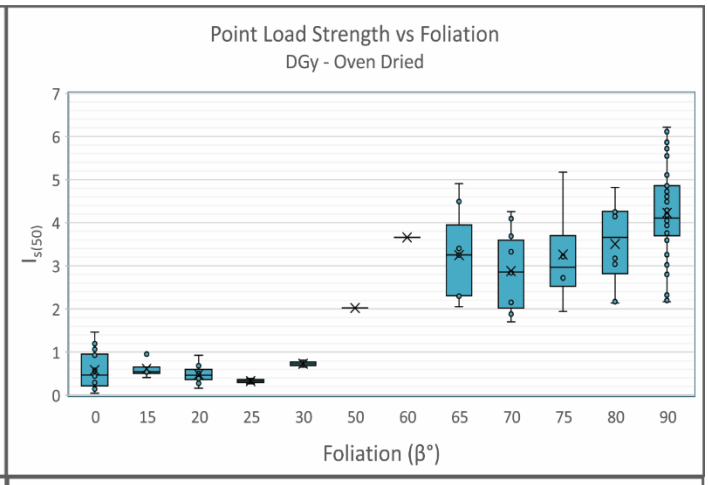

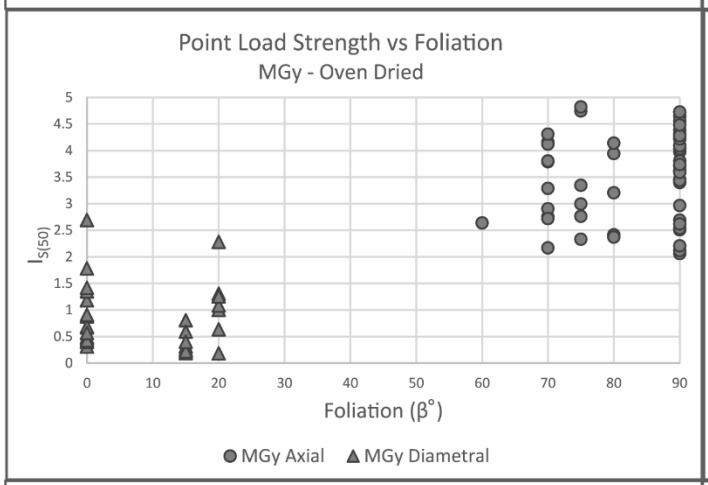

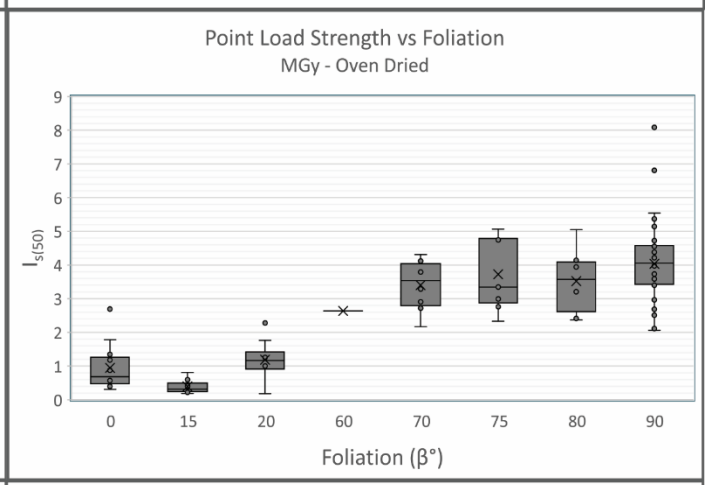

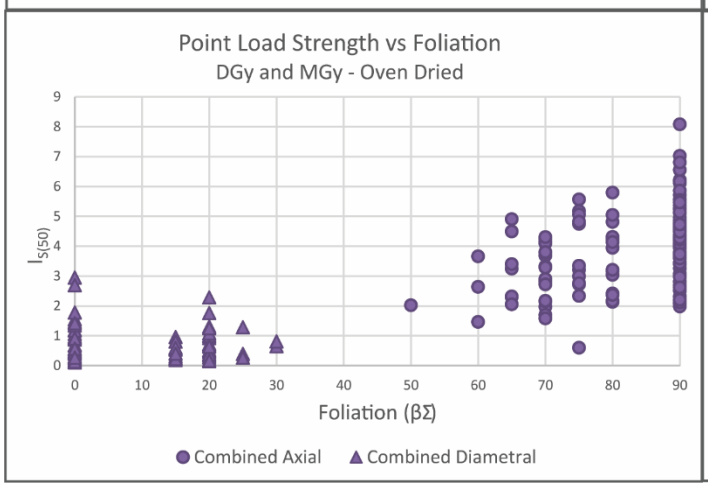

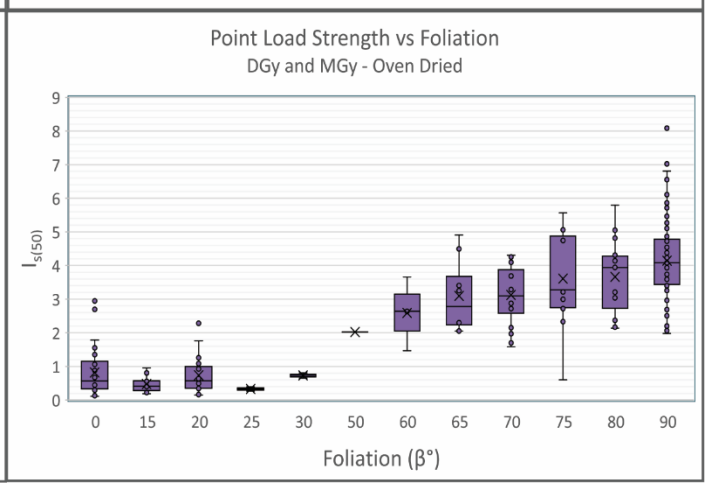

C.2.4 Triaxial Strength Samples

C.2.4.1 In Situ Sample Data

In Situ Triaxial Strength Sample Data														
Sample	Depth (m)	Lithotype	Foliation (ß°)	Density (kg/m³)	Confining Stress (MPa)	Max Load (kN)	Max Stress (MPa) Uncorrected	Max Stress (MPa) Corrected	Corrected Differential Stress (MPa)	E (GPa)	Radial 1, ν	Radial 2, ν	Averaged Radials, ν	Failure Mode
BH3_B3_2TX	6.80	DGy	60	2790	3	83.20	28.6	30.5	27.5	4.7	0.05	0.17	0.11	Shear Fractures (40°)
BH4_B4_5TX	11.80	DGy	65	2775	3	115.50	39.7	41.5	38.5	5.7	0.11	0.15	0.13	Multiple Fractures: Shear (40°) + Joint (85°-87°)
BH4_B4_4TX	11.30	DGy	70	2830	3	89.67	30.9	32.4	29.4	10.1	0.03	0.42	0.22	Multiple Fractures: Shear (50°-55°)+ Joint (85°-87°)
BH4_B8_2TX1	21.70	DGy	75	2760	3	124.60	42.9	45.1	42.1	5.5	0.00	0.07	0.03	Shear Fractures (30°, 50°-65°)
BH1_B4_4TX	10.10	DGy	70	2760	5	155.00	53.6	56.9	51.9	9.7	-	0.05	-	Shear Fractures (50°)
BH4_B8_1TX	21.45	DGy	75	2743	5	163.00	56.2	58.5	53.5	7.7	0.27	0.02	0.14	Shear Fractures (55°-65°)
BH4_B7_6TX2	20.37	DGy	80	2749	5	148.40	51.0	53.4	48.4	10.5	0.36	0.05	0.21	Shear Fractures (50°-60°)
BH1_B7_1TX	18.90	DGy	70	2770	10	227.00	78.2	83.5	73.5	7.5	0.12	-	-	Shear Fractures (45°-50°)
BH4_B7_6TX1	20.37	DGy	75	2711	10	215.70	74.1	76.6	66.6	13.0	0.81	0.13	0.47	Multiple Fractures: Along Foliation (15°) + Shear (50°-55°)
BH4_B8_2TX2	21.70	DGy	80	2743	10	190.60	65.5	67.9	57.9	7.4	0.16	0.02	0.10	Shear Fractures (50°-55°)
BH1_B7_A16	20.45	DGy	65	2750	10	221.80	76.5	79.1	69.1	-	-	-	-	Multiple Fractures

In Situ Triaxial Strength Sample Data														
Sample	Depth (m)	Lithotype	Foliation (ß°)	Density (kg/m³)	Confining Stress (MPa)	Max Load (kN)	Max Stress (MPa) Uncorrected	Max Stress (MPa) Corrected	Corrected Differential Stress (MPa)	E (GPa)	Radial 1, v	Radial 2, v	Averaged Radials, v	Failure Mode
BH4_B6_1TX	16.15	MGy	70	2848	3	127.40	43.9	46.4	43.4	6.3	0.28	0.08	0.18	Multiple Fractures: Along Foliation (20°) + Joint (80°)
BH4_B5_5TX	14.10	MGy	60	2843	3	140.90	48.3	50.8	47.8	11.3	0.59	0.14	0.37	Shear Fractures (75°)
BH3_B5_5TX	14.50	MGy	70	2770	3	109.64	37.7	39.5	36.5	4.6	0.15	0.08	0.12	Multiple Fractures: Shear (40°-50°) + Joint (85°-87°)
BH4_B5_4TX	13.76	MGy	65	2839	3	100.00	34.4	35.9	32.9	7.4	-	0.06	-	Multiple Fractures: Shear (65°-70°) + Joint (88°)
BH4_B6_5TX	17.60	MGy	75	2810	5	257.00	88.4	93.0	88.0	16.3	0.07	0.14	0.11	Double Shear (60°)
BH4_B6_2TX1	16.40	MGy	70	2800	5	215.90	74.2	77.9	72.9	13.9	0.14	0.23	0.18	Shear Fractures (40°)
BH4_B6_3TX	17.00	MGy	75	2811	5	289.50	99.3	104.3	99.3	22.0	0.06	0.18	0.12	Double Shear (60°-70°)
BH3_B5_2TX	13.10	MGy	70	2810	10	230.50	79.2	83.9	73.9	5.7	0.26	0.01	0.12	Multiple Fractures: Along Foliation (20°-30°) + Shear (65°-70°)
BH3_B5_1TX	12.65	MGy	75	2810	10	364.60	125.2	132.0	122.0	18.6	0.09	0.18	0.14	Multiple Shear Fractures: Parallel (60°-70°)
BH4_B6_4TX	17.35	MGy	80	2780	10	319.20	109.5	115.9	105.9	21.9	-	-	-	Multiple Fractures
BH4_B6_2TX2	16.40	MGy	70	2789	10	219.10	75.3	77.7	67.7	4.6	0.14	0.01	0.07	Multiple Fractures

C.2.4.2 In Situ Stress vs Strain Curves

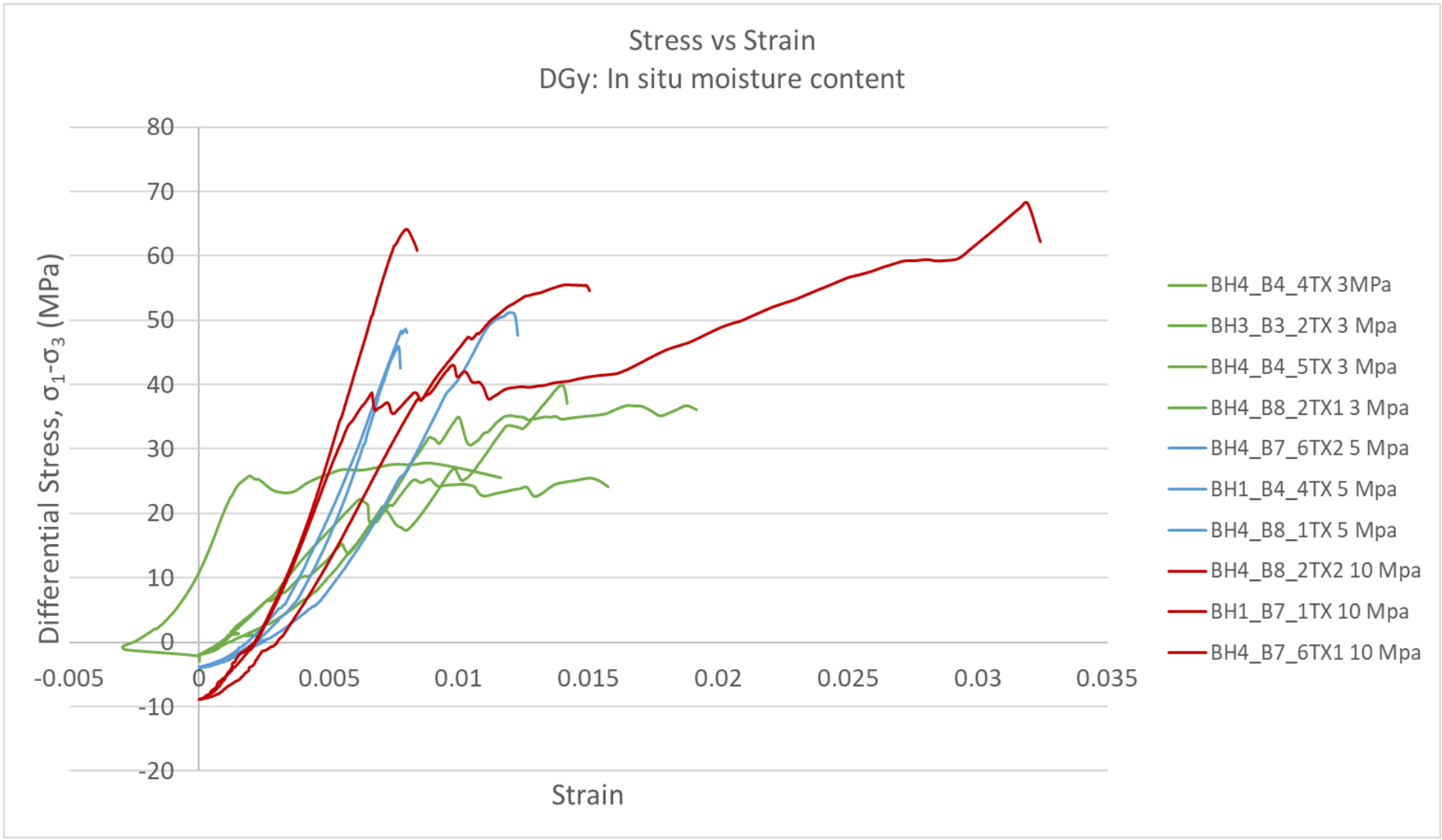

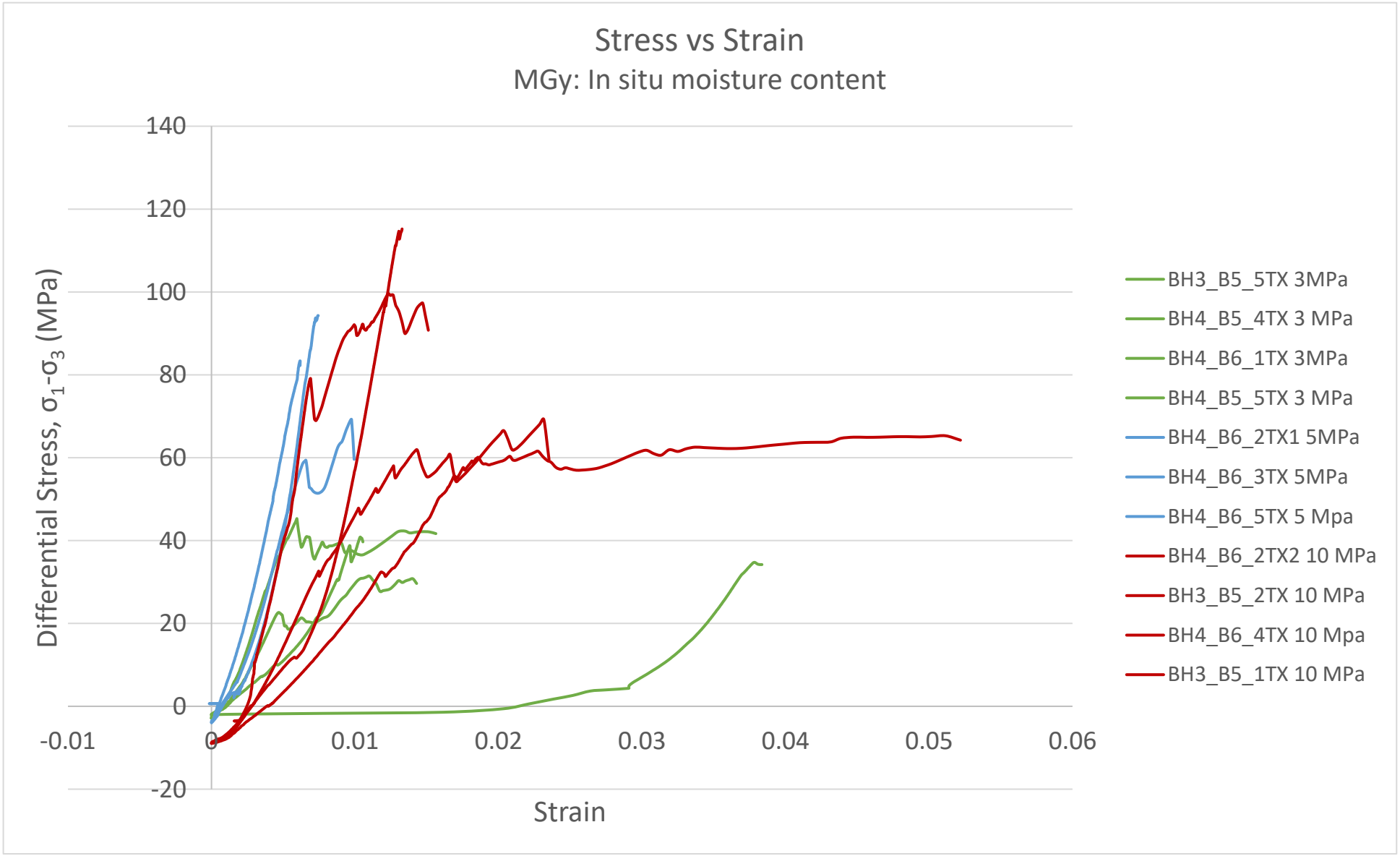
Stress vs Strain
MGy: In situ moisture content
Differential Stress, σ_1-σ_3 (MPa)
Strain
140
120
100
80
60
40
20
0
-20
-0.01
0
0.01
0.02
0.03
0.04
0.05
0.06
BH3_B5_5TX 3MPa
BH4_B5_4TX 3 MPa
BH4_B6_1TX 3MPa
BH4_B5_5TX 3 MPa
BH4_B6_2TX1 5MPa
BH4_B6_3TX 5MPa
BH4_B6_5TX 5 Mpa
BH4_B6_2TX2 10 MPa
BH3_B5_2TX 10 MPa
BH4_B6_4TX 10 Mpa
BH3_B5_1TX 10 MPa

C.2.4.3 In Situ Failure Criteria

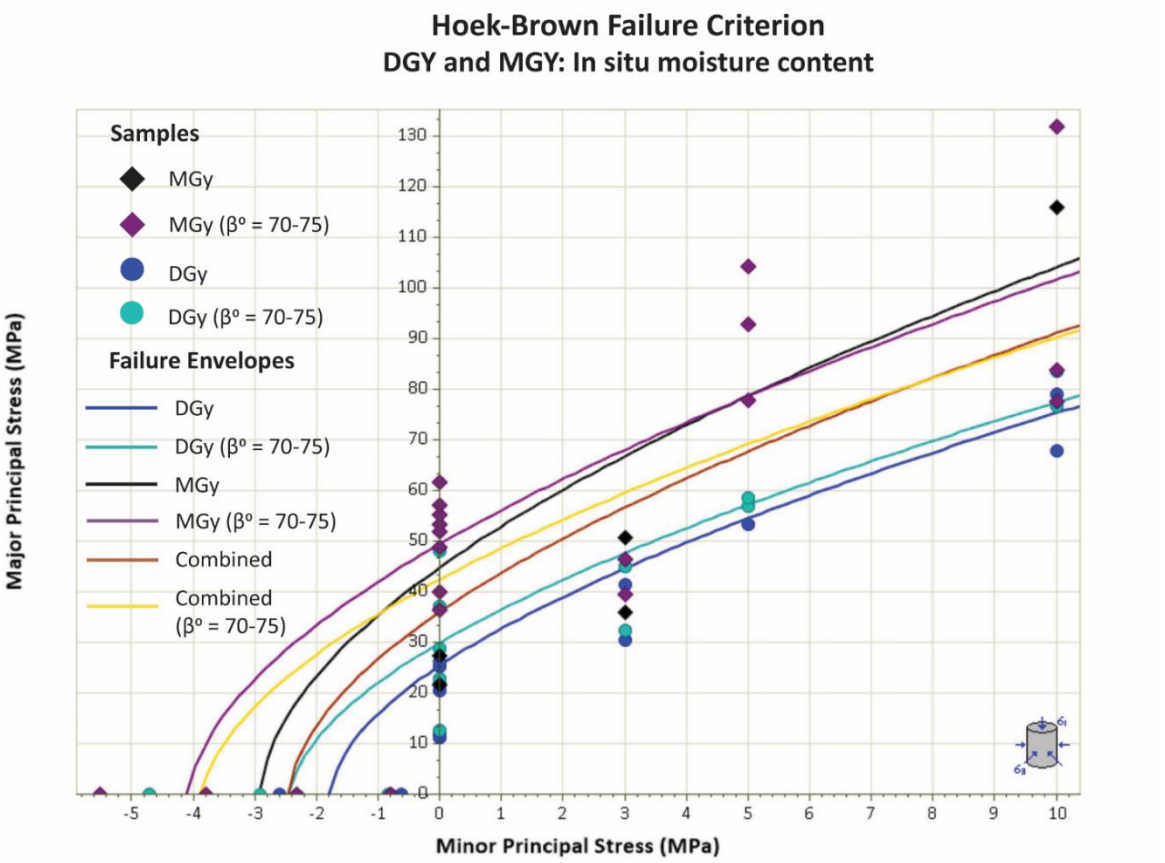

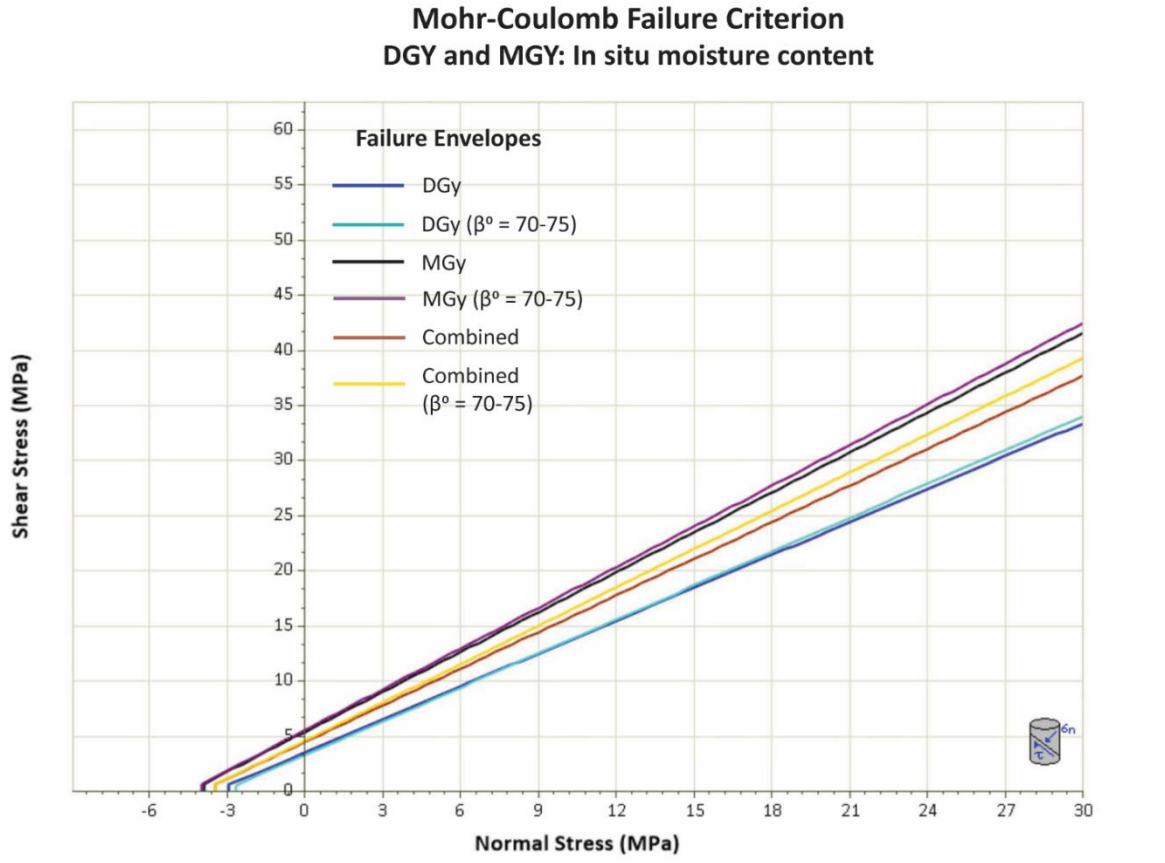

C.2.4.4 Oven-Dried Sample Data

In Situ Triaxial Strength Sample Data														
Sample	Depth (m)	Lithotype	Foliation (ß°)	Density (kg/m³)	Confining Stress (MPa)	Max Load (kN)	Max Stress (MPa) Uncorrected	Max Stress (MPa) Corrected	Corrected Differential Stress (MPa)	E (GPa)	Radial 1, ν	Radial 2, ν	Averaged Radials, ν	Failure Mode
BH1_B4_3TXD	9.85	DGy	60	2760	3	140.90	48.7	51.4	48.4	10.0	0.02	0.03	0.03	Shear Fractures (50°-60°)
BH3_B6_1TXD2	15.60	DGy	70	2660	3	180.50	62.1	64.2	61.2	4.8	0.08	0.07	0.08	Along Foliation (20°-30°)
BH1_B2_3TXD	4.20	DGy	70	2760	3	174.87	60.2	63.3	60.3	23.0	0.58	0.03	0.31	Multiple Fractures: Along Foliation (20°) + Shear (40°)
BH4_B7_3TXD	18.95	DGy	65	2740	5	152.30	52.3	54.7	49.7	9.3	0.27	0.07	0.17	Shear Fractures (40°-50°)
BH4_B8_3TXD	21.97	DGy	70	2760	5	265.30	91.3	95.5	90.5	17.6	0.18	0.06	0.12	Shear Fractures (55°-60°)
BH1_B7_A14TXD	19.95	DGy	70	2730	5	134.60	46.6	47.9	42.9	10.6	0.11	0.03	0.07	Multiple Fractures: Along Foliation (20°) + Shear (40°-50°)
BH3_B8_4TXD	22.37	DGy	80	2760	5	281.92	96.9	102.6	97.6	28.7	0.22	0.30	0.26	Multiple Fractures: Along Foliation (20°) + Shear (40°-50°)
BH3_B6_2TXD	16.50	DGy	65	2700	10	309.00	106.0	110.8	100.8	13.9	0.16	0.13	0.14	Along Foliation (25°-35°)
BH3_B6_1TXD1	15.60	DGy	70	2690	10	349.70	120.3	124.5	114.5	13.9	-	0.07	-	Multiple Fractures: Along Foliation (20°-25°) + Joint (75°-85°)
BH4_B1_PL2TXD	1.78	DGy	75	2740	10	322.40	112.4	117.1	107.1	43.5	0.26	-	0.26	Multiple Shear Fractures: Parallel (50°-55°)
BH3_B1_2TXD	2.50	MGy	75	2810	3	292.00	100.3	106.0	103.0	14.6	0.06	0.07	0.06	Multiple Fractures: Along Foliation (15°) + Shear (40°-45°, 60°-65°)
BH4_B3_3TXD	8.25	MGy	75	2840	3	290.20	100.0	105.1	102.1	20.6	-	0.03	-	Shear Fractures (40°)
BH3_B5_5TXD3	14.50	MGy	70	2780	3	103.84	35.7	37.7	34.7	8.4	0.09	0.13	0.11	Multiple Fractures: Shear (50°-55°) + Joint (85°-87°)
BH4_B3_1TXD	6.20	MGy	70	2740	3	142.55	49.1	51.7	48.7	28.4	0.60	0.17	0.38	Shear Fractures (40°-45°)
BH3_B5_3TXD	13.80	MGy	70	2810	5	290.10	99.6	105.1	100.1	15.1	-	-	-	Shear Fractures (65°-70°)

Appendix C: Rock Mechanics

In Situ Triaxial Strength Sample Data														
Sample	**Depth (m)**	**Lithotype**	**Foliation (ß°)**	**Density (kg/m³)**	**Confining Stress (MPa)**	**Max Load (kN)**	**Max Stress (MPa) Uncorrected**	**Max Stress (MPa) Corrected**	**Corrected Differential Stress (MPa)**	**E (GPa)**	**Radial 1, ν**	**Radial 2, ν**	**Averaged Radials, ν**	**Failure Mode**
BH3_B5_4TXD1	14.00	MGy	70	2760	5	224.70	77.1	81.4	76.4	18.9	0.13	0.17	0.15	Multiple Fractures: Along Foliation (20°) + Shear (45°-50°, 60°)
BH3_B2_3TXD	5.65	MGy	70	2860	5	265.79	92.1	95.8	90.8	-	-	-	-	Shear Fractures (50°-55°)
BH3_B5_4TXD2	14.00	MGy	70	2800	10	296.10	101.7	106.7	96.7	15.0	0.25	0.12	0.19	Shear Fractures (60°-70°)
BH4_B4_2TXD	9.66	MGy	75	2870	10	450.90	155.5	163.5	153.5	24.1	-	0.11	-	Shear Fractures (60°-70°)
BH3_B5_1TXD	12.65	MGy	75	2790	10	388.70	133.5	139.6	129.6	17.4	0.16	0.07	0.11	Multiple Shear Fractures: Parallel (40°-45°, 55°-60°)
BH3_B4_PL3TXD	11.30	MGy	80	2740	10	374.80	129.1	135.5	125.5	29.9	0.24	0.23	0.23	Shear Fractures (60°)

Oven Dried				DGy	MGy	Combined		DGy	MGy	Combined
No. of Samples				10	11	21		6	10	16
Differential Stress, σ_1-σ_3 (MPa)		Mean ± Std dev.	All Samples	**77.3** ± 27.4	**89.6** ± 34.4	87.3 ± 31.2	foliation β° (70-75)	**79.4** ± 28.8	**93.6** ± 34.8	**88.3** ± 32.5
Maximum stress, σ_1 (MPa)	3 MPa	Mean ± Std dev		**59.6** ± 7.1	**75.1** ± 35.6	**68.5** ± 24.8		**63.7** ± 0.6	**75.1** ± 35.6	**71.3** ± 28.2
	5 MPa	Mean ± Std dev		**75.1** ± 27.8	**94.1** ± 11.9	**83.3** ± 21.5		**71.71** ± 33.6	**94.1** ± 11.9	**85.1** ± 22.5
	10 MPa	Mean ± Std dev		117.5 ± 6.9	**136.3** ± 23.3	**128.2** ± 18.3		120.8 ± 5.3	**136.6** ± 28.5	**130.3** ± 22.1
Young's Modulus, E (GPa)		Mean ± Std dev		**17.5** ± 11.5	**18.1** ± 6.3	**18.4** ± 9.0		**18.9** ± 13.5	**18.1** ± 5.9	**18.4** ± 9.2
Poisson Ratio, v		Mean ± Std dev.		**0.16** ± 0.10	**0.18** ± 0.12	**0.17** ± 0.10		**0.17** ± 0.11	**0.17** ± 0.11	**0.17** ± 0.11

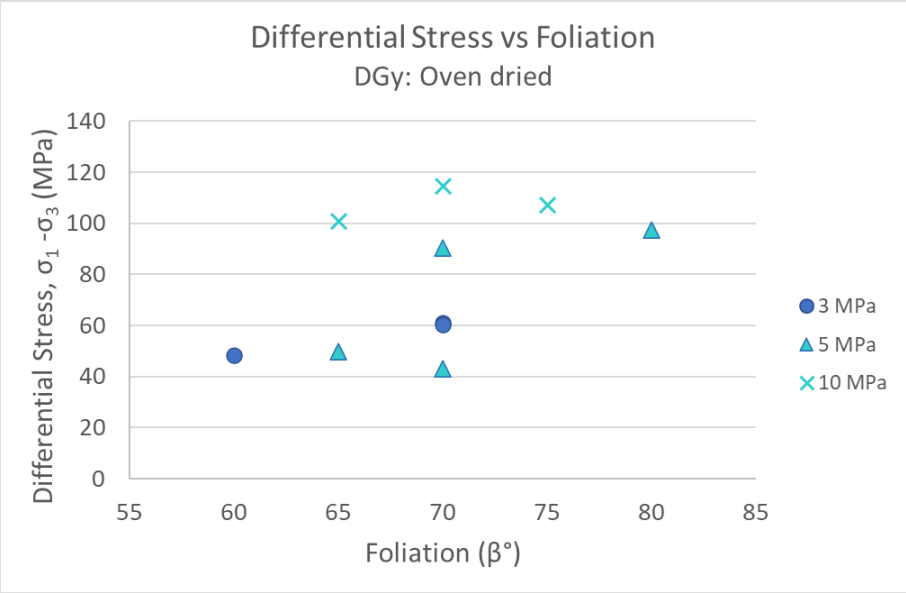

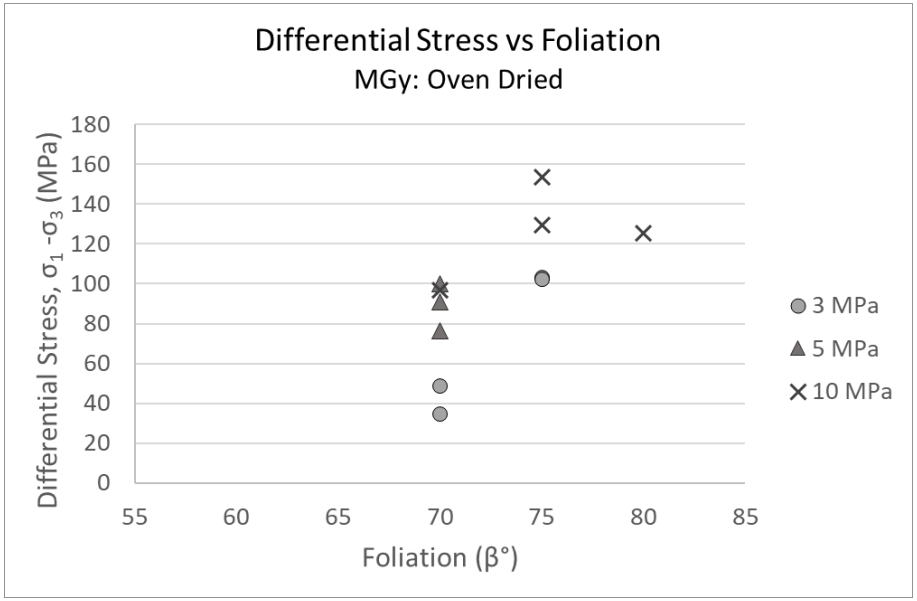

C.2.4.5 In Situ Stress vs Strain Curves

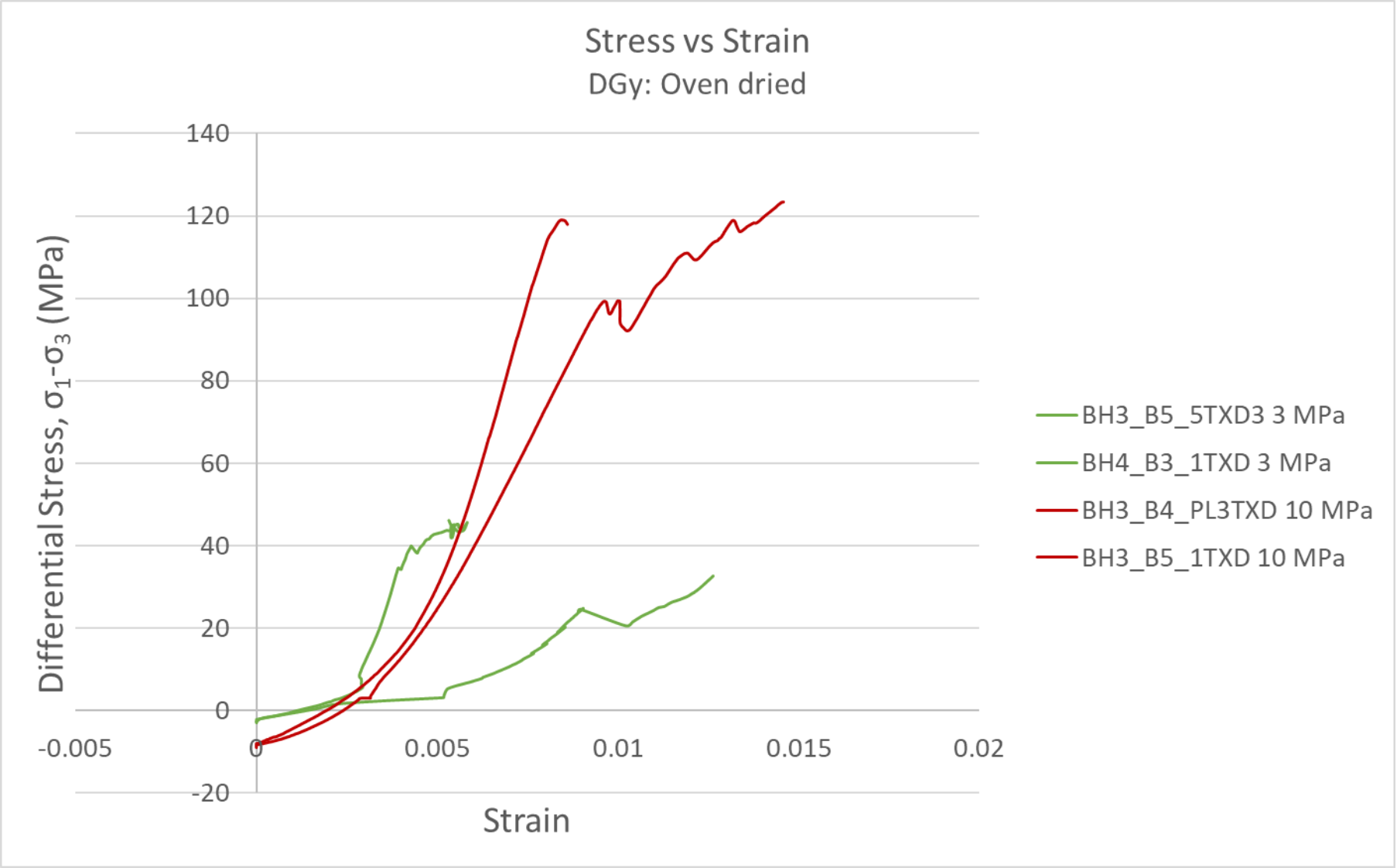

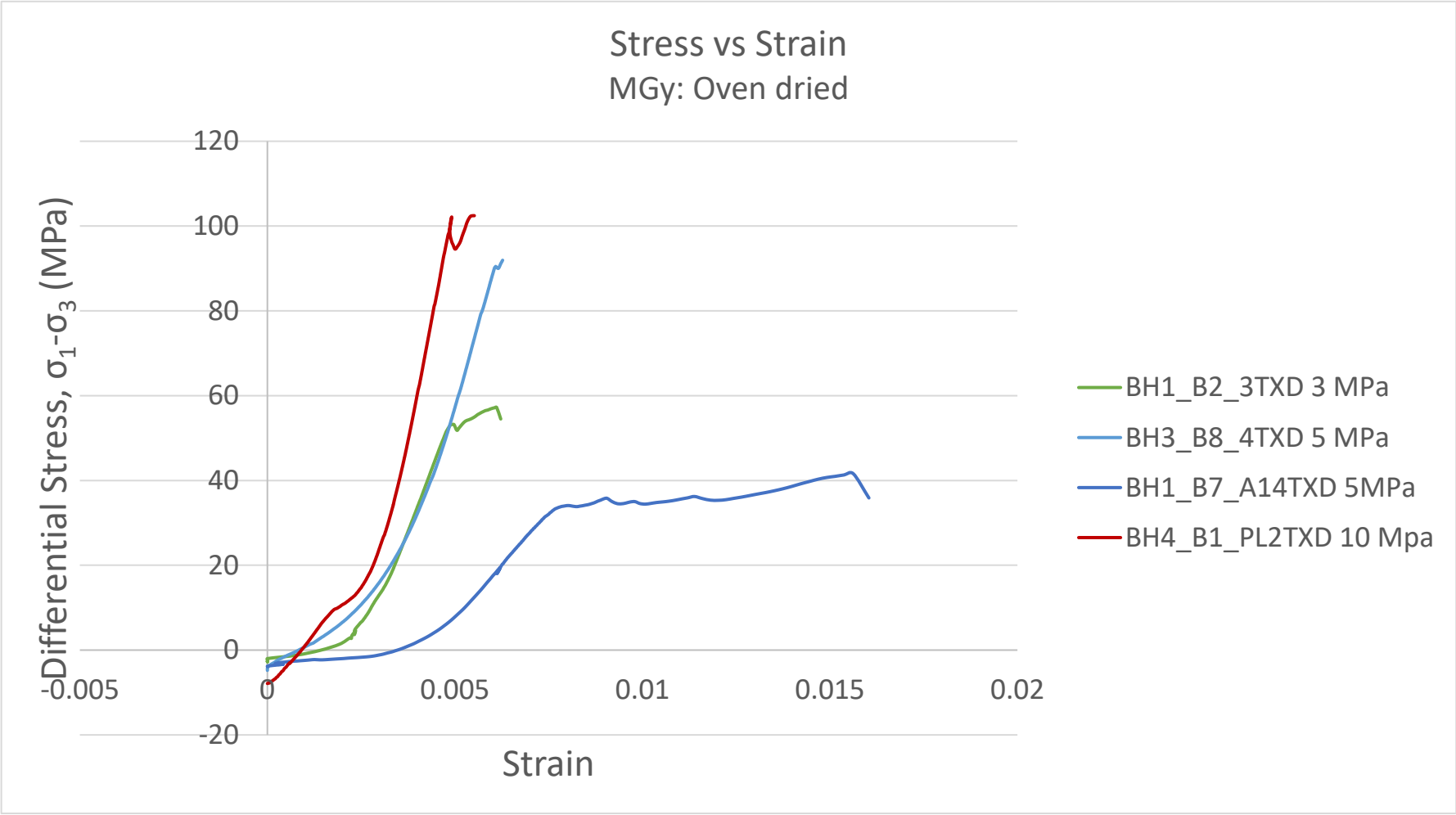
Stress vs Strain
MGy: Oven dried
Differential Stress, σ_1-σ_3 (MPa)
120
100
80
60
40
20
0
-20
-0.005
0
0.005
0.01
0.015
0.02
Strain
BH1_B2_3TXD 3 MPa
BH3_B8_4TXD 5 MPa
BH1_B7_A14TXD 5MPa
BH4_B1_PL2TXD 10 Mpa

C.2.4.6 Oven-Dried Failure Criteria

Oven dried			DGy	MGy	Combined		DGy	MGy	Combined
No of Samples		All Samples	10	11	21	foliation β° (70-75)	6	10	16
UCS range (MPa)			18.5-40.8	27.9-86.7	18.5-86.7		27.4-40.8	27.9-51.6	27.4-51.6
Tensile Strength range (MPa)			-(0.31-7.74)	-(0.80-8.99)	-(0.31-8.99)		-(0.70-7.74)	-(0.80-8.99)	-(0.70-8.99)
Hoek Brown	σ_{ci} (MPa)		43.2	60.9	53.0		47.7	59.4	54.9
	m_i		18.2	17.3	17.7		15.7	17.4	16.9
Mohr Coulomb	c (MPa)		3.5	5.0	4.3		3.5	4.2	3.9
	Φ_b (°)		52.4	54.8	53.6		52.5	55.8	54.6

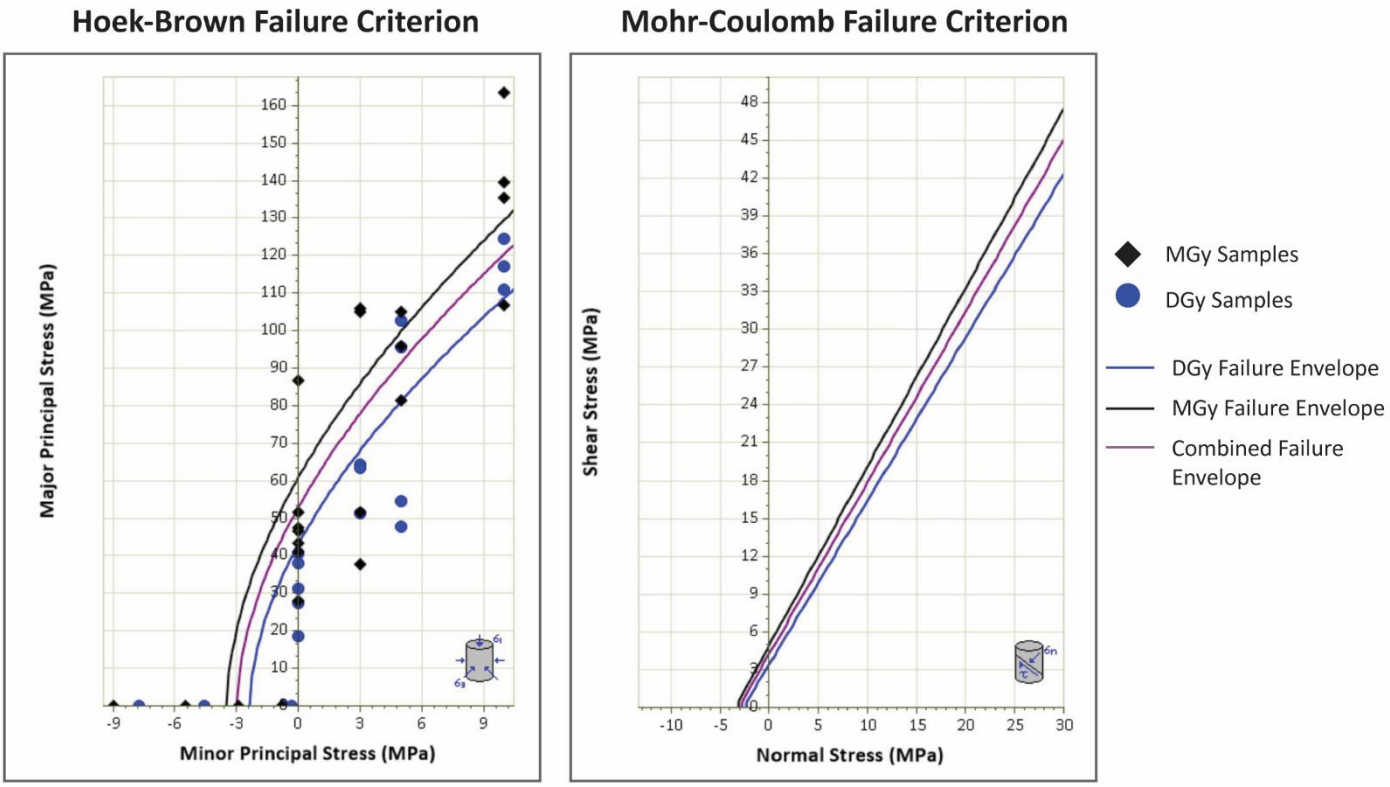

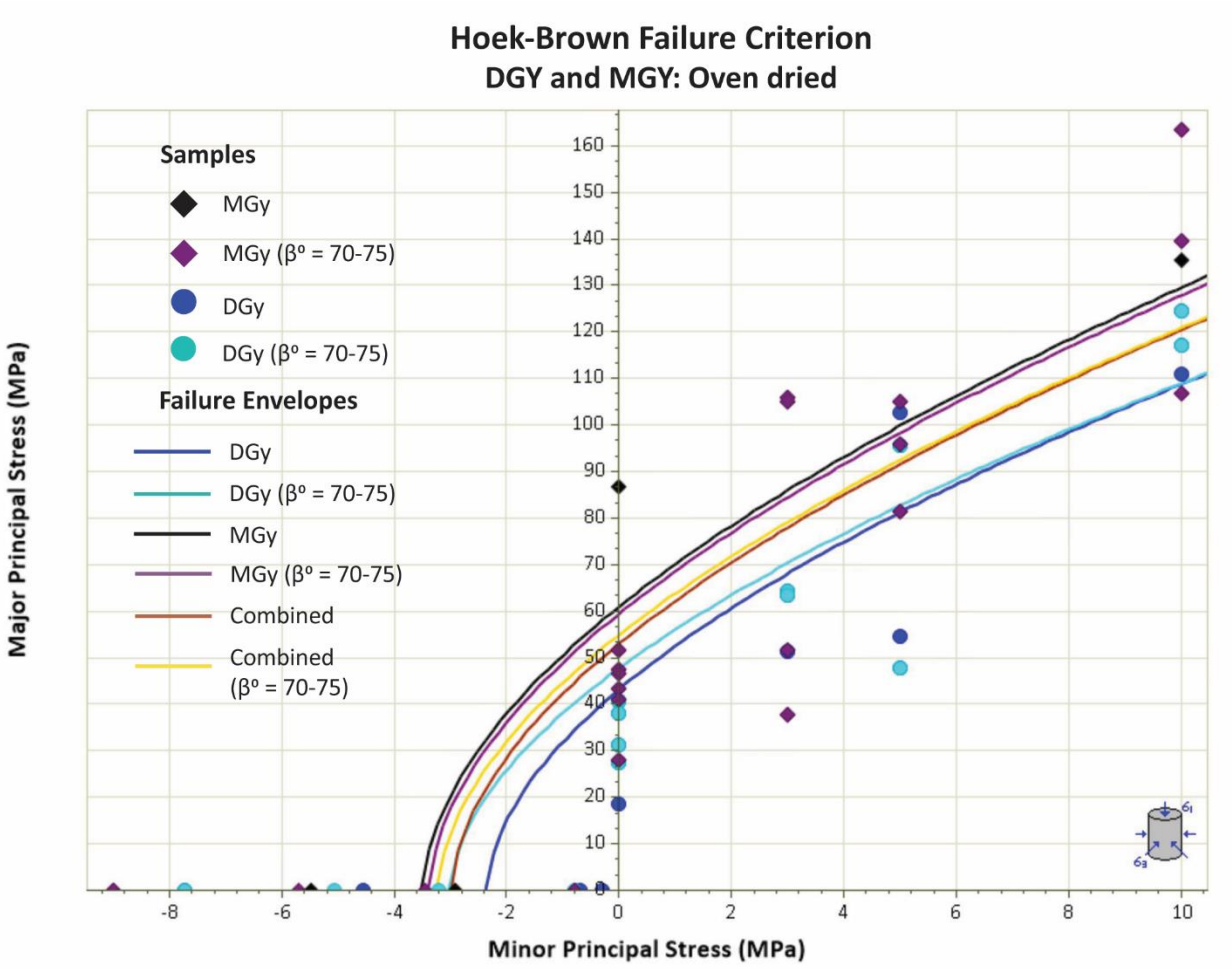
Hoek-Brown Failure Criterion
DGY and MGY: Oven dried
Samples
MGy
MGy (βº = 70-75)
DGy
DGy (βº = 70-75)
Failure Envelopes
DGy
DGy (βº = 70-75)
MGy
MGy (βº = 70-75)
Combined
Combined (βº = 70-75)
Major Principal Stress (MPa)
Minor Principal Stress (MPa)

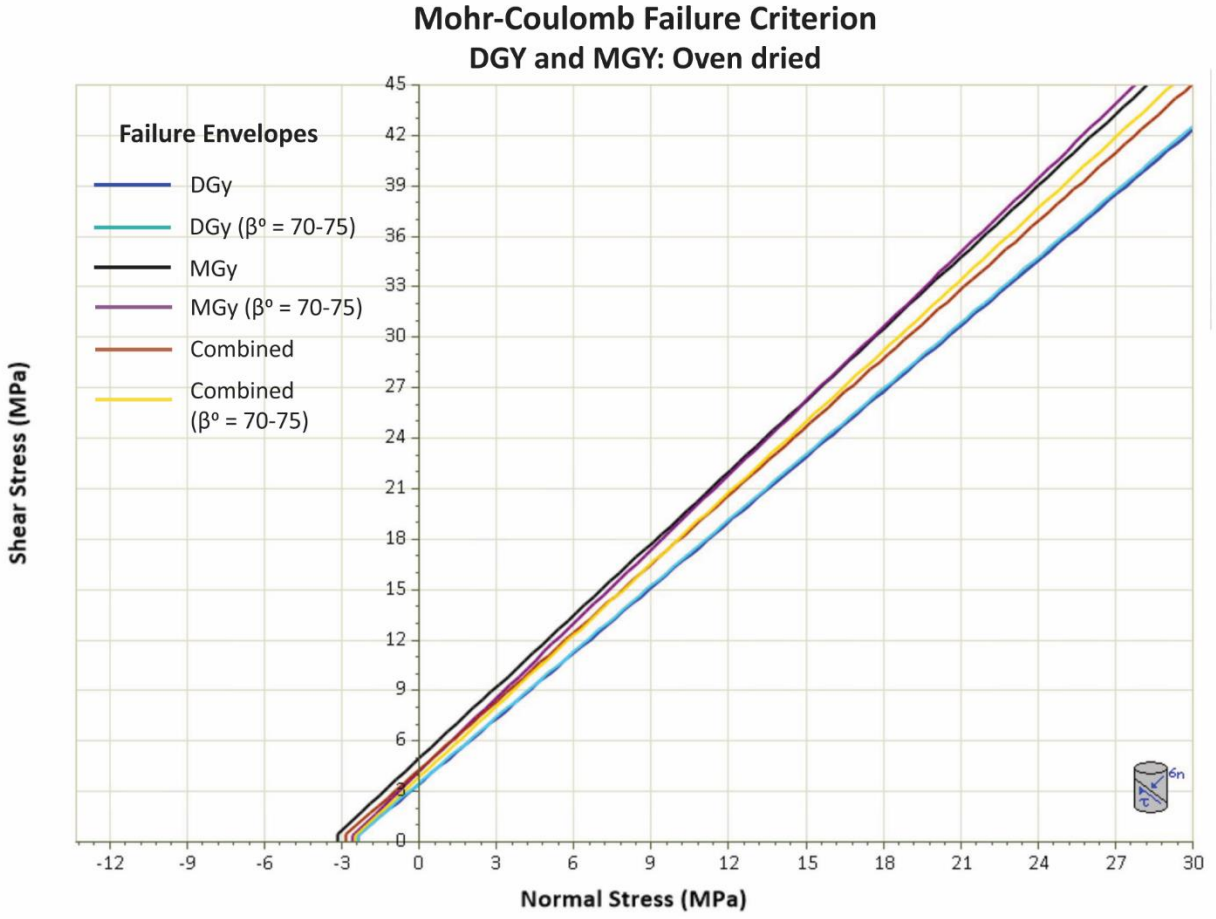
Mohr-Coulomb Failure Criterion
DGY and MGY: Oven dried
Failure Envelopes
DGy
DGy (βº = 70-75)
MGy
MGy (βº = 70-75)
Combined
Combined (βº = 70-75)
Shear Stress (MPa)
Normal Stress (MPa)

C.3 Rock Mass Classification

C.3.1 RMR Classification

ROCK MASS RATING SYSTEM (RMR) (Bieniawski, 1989)									
A. CLASSIFICATION PARAMETERS AND THEIR RATINGS									
1	Strength of intact rock material	Point-load strength index	> 10 MPa	4-10 MPa	2-4 MPa	1-2 MPa	For this low range - UCS test is preferred		
		UCS	> 250 MPa	100-250 MPa	50-100 MPa	25-50 MPa	5-25 MPa	1-5 MPa	< 1 MPa
	Rating		15	12	7	4	2	1	0
2	Drill core Quality (RQD)		90-100%	75-90%	50-75%	25-50%	< 25%		
	Rating		20	17	13	8	3		
3	Spacing of discontinuities		> 2 m	0.6-2 m	0.2-0.6 m	60 mm-200 mm	< 60 mm		
	Rating		20	15	10	8	5		
4	Condition of Discontinuities (see E)		Very rough surfaces. Not continuous. No separation. Unweathered wall rock.	Slightly rough surfaces. Separation < 1mm. Slightly weathered walls.	Slightly rough surfaces. Separation < 1 mm. Highly weathered walls.	Slickensided surfaces or Gouge < 5 mm thick or Separation 1-5mm Continuous	Soft gouge > 5mm thick or Separations > 5mm Continuous		
	Rating		30	25	20	10	0		
5	Groundwater	Inflow per 10m tunnel length	None	< 10 litres/min	10-25 litres/min	25-125 litres/min	> 125 litres/min		
		(Joint water press)/(Major principal stress, σ_1)	0	< 0.1	0.1-0.2	0.2-0.5	> 0.5		
		General Conditions	Completely Dry	Damp	Wet	Dripping	Flowing		
	Rating		15	10	7	4	0		
B. RATING ADJUSTMENT FOR DISCONTINUITY ORIENTATIONS (See F)									
Strike and dip orientations			Very favourable	Favourable	Fair	Unfavourable	Very Unfavourable		
Ratings		Tunnels and mines	0	-2	-5	-10	-12		
		Foundations	0	-2	-7	-15	-25		
		Slopes	0	-5	-25	-50			
C. ROCK MASS CLASSES DETERMINED FROM TOTAL RATINGS									
Rating			100 ← 81	80 ← 61	60 ← 41	40 ← 21	< 21		
Class Number			I	II	III	IV	V		
Description			Very good rock	Good rock	Fair rock	Poor rock	Very poor rock		
D. MEANING OF ROCK CLASSES									
Class Number			I	II	III	IV	V		
Average stand-up time			20 yrs for 15 m span	1 yr for 10 m span	1 week for 5m span	10 hrs for 2.5 m span	30 min for 1 m span		
Cohesion of rock mass, c			> 400 kPa	300-400 kPa	200-300 kPa	100-200 kPa	< 100 kPa		
Friction angle of rock mass (°)			> 45°	35°-45°	25°-35°	15°-25°	< 15°		
E. GUIDELINES FOR CLASSIFICATION OF DISCONTINUITY CONDITIONS									
Discontinuity length (persistence)			< 1m	1-3 m	3-10 m	10-20 m	> 20 m		
Rating			6	4	2	1	0		
Separation (aperture)			None	< 0.1 mm	0.1-1.0 mm	1-5 mm	> 5 mm		
Rating			6	5	4	1	0		
Roughness			Very rough	Rough	Slightly rough	Smooth	Slickensided		
Rating			6	5	3	1	0		
Infilling (gouge)			None	Hard filling < 5 mm	Hard filling > 5 mm	Soft filling < 5 mm	Soft filling > 5 mm		
Rating			6	4	2	2	0		
Weathering			Unweathered	Slightly weathered	Moderately weathered	Highly weathered	Decomposed		
Rating			6	5	3	1	0		
F. EFFECT OF DISCONTINUITY STRIKE AND DIP ORIENTATION IN TUNNELLING									
Strike perpendicular to tunnel axis				Strike parallel to tunnel axis			Dip 0°-20° Irrespective of strike		
Drive with dip		Drive against dip							
Dip 45°-90°	Dip 20°-45°	Dip 45°-90°	Dip 20°-45°	Dip 45°-90°		Dip 20°-45°			
Very favourable	Favourable	Very favourable	Favourable	Very Favourable		Fair	Fair		
ROCK MASS QUALITY ACCORDING TO THE RMR INDEX									
Class		Quality	RMR Rating	Cohesion (MPa)		Friction Angle			
I		Very good	81-100	> 0.4 MPa		> 45°			
II		Good	61-80	0.3-0.4		35°-45°			
III		Fair	41-61	0.2-0.3		25°-35°			
IV		Poor	21-41	0.1-0.2		15°-25°			
V		Very poor	< 20	< 0.1		< 15°			

C.3.1.1 RMR Results Summary

Area Assessed	RMR		Classification	
	Low	High	Low	High
Queenstown Hill Track	53	78	Fair	Good
Above headscarp	46	67	Fair	Good
Headscarp area	33	62	Poor	Good
Upper west lateral scarp	23	51	Poor	Fair
Mid west lateral scarp	43	72	Fair	Good
Main landslide body	20	54	Very poor	Fair
Graben Feature	19	54	Very poor	Fair
Subdivisions - west	48	77	Fair	Good
Subdivisions - east	30	56	Fair	Fair
Toe/Compressional area	18	55	Very poor	Fair
Kink Banded Area	15	58	Very poor	Fair

C.3.2 ARMR Classification

ANISOTROPIC ROCK MASS RATING SYSTEM (ARMR) (Saroglou et al., 2018)							
1. CLASSIFICATION PARAMETERS AND THEIR RATINGS							
Strength anisotropy degree, R_c	≤ 1.1	1.1-2.0	2.0-3.0	3.0-5.0	≥ 5.0		
Description	Isotropic	Low	Moderate	High	Very high		
Rating	20	17	13	8	3		
Uniaxial compressive strength (MPa)	> 250 MPa	100-250 MPa	50-100 MPa	25-50 MPa	5-25 MPa	1-5 MPa	< 1 MPa
Point-load strength (MPa)	> 10 MPa	4-10 MPa	2-4 MPa	1-2 MPa	For this low range, UCS is preferred		
Rating	15	12	7	4	2	1	0
Spacing of anisotropic structure	> 1.2 m	0.6-1.2 m	200-600 mm	40-200 mm	< 40 mm		
Rating	20	15	10	8	5		
Rock quality designation, RQD (%)	90-100%	75-90%	50-75%	25-50%	< 25%		
Rating	15	10	7	4	2		
Condition of surfaces	Very rough surfaces. Not continuous. No separation. Unweathered rock wall.	Rough Surfaces. Separation < 1 mm. Slightly weathered rock.	Slightly rough surfaces. Separation < 1 mm. Highly weathered rock.	Slickensided Surfaces or Gouge < 5 mm thick or Separation 1-5 mm. Continuous	Soft gouge > 5 mm thick or Separation > 5 mm. Continuous		
Rating	15	10	7	4	0		
Groundwater	Completely dry	Damp	Wet	Dripping	Flowing		
Rating	15	10	7	4	0		
2. ADJUSTMENT OF TOTAL RATING BASED ON CONFINING STRESS RANGE							
Stress		σ_1/σ_c	Adjustment				
Low in-situ stress		< 0.15	No change to rating				
Intermediate in-situ stress		0.15-0.4	Move one cell towards left in the strength anisotropy degree (+ 5, +4, or +3)				
High in-situ stress		> 0.4	Move two cells towards left in the strength anisotropy degree				
3. ROCK MASS QUALITY CLASSES ACCORDING TO ARMR VALUES							
Rating	100-81	80-61	60-41	40-21	< 20		
Class No.	I	II	III	IV	V		
Description	Massive or isotropic rock mass	Slightly anisotropic rock mass	Moderately anisotropic rock mass	Highly anisotropic rock mass	Very highly anisotropic to sheared rock mass		
Spacing of anisotropic structure, S	> 1.2 m	0.6-1.2 m	0.2-0.6 m	0.04-0.2 m	< 0.04 m		
Proposed approach of analysis	Continuum (FEM, FDM)	Discontinuum (DEM) or anisotropic continuum		Discontinuum (DEM) and anisotropic continuum	Anisotropic continuum		
GSI Sketches from Hoek and Karzulovic (2000)	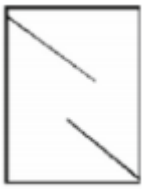						

C.3.2.1 ARMR Results

ANISOTROPIC ROCK MASS RATING SYSTEM (ARMR) (Saroglou et al., 2018)							
1. CLASSIFICATION PARAMETERS AND THEIR RATINGS							
Strength anisotropy degree, R_c	≤ 1.1	1.1-2.0	2.0-3.0	3.0-5.0	≥ 5.0		
Description	Isotropic	Low	Moderate	High	Very high		
Rating	20	17	13	8	3		
Uniaxial compressive strength (MPa)	> 250 MPa	100-250 MPa	50-100 MPa	25-50 MPa	5-25 MPa	1-5 MPa	< 1 MPa
Point-load strength (MPa)	> 10 MPa	4-10 MPa	2-4 MPa	1-2 MPa	For this low range, UCS is preferred		
Rating	15	12	7	4	2	1	0
Spacing of anisotropic structure	> 1.2 m	0.6-1.2 m	200-600 mm	40-200 mm	< 40 mm		
Rating	20	15	10	8	5		
Rock quality designation, RQD (%)	90-100%	75-90%	50-75%	25-50%	< 25%		
Rating	15	10	7	4	2		
Condition of surfaces	Very rough surfaces. Not continuous. No separation. Unweathered rock wall.	Rough Surfaces. Separation < 1 mm. Slightly weathered rock.	Slightly rough surfaces. Separation < 1 mm. Highly weathered rock.	Slickensided Surfaces or Gouge < 5 mm thick or Separation 1-5 mm. Continuous	Soft gouge > 5 mm thick or Separation > 5 mm. Continuous		
Rating	15	10	7	4	0		
Groundwater	Completely dry	Damp	Wet	Dripping	Flowing		
Rating	15	10	7	4	0		

2. ADJUSTMENT OF TOTAL RATING BASED ON CONFINING STRESS RANGE		
Stress	σ_1/σ_c	Adjustment
Low in-situ stress	< 0.15	No change to rating
Intermediate in-situ stress	0.15-0.4	Move one cell towards left in the strength anisotropy degree (+ 5, +4, or +3)
High in-situ stress	> 0.4	Move two cells towards left in the strength anisotropy degree

3. ROCK MASS QUALITY CLASSES ACCORDING TO ARMR VALUES					
Rating	100-81	80-61	60-41	40-21	< 20
Class No.	I	II	III	IV	V
Description	Massive or isotropic rock mass	Slightly anisotropic rock mass	Moderately anisotropic rock mass	Highly anisotropic rock mass	Very highly anisotropic to sheared rock mass
Spacing of anisotropic structure, S	> 1.2 m	0.6-1.2 m	0.2-0.6 m	0.04-0.2 m	< 0.04 m
Proposed approach of analysis	Continuum (FEM, FDM)	Discontinuum (DEM) or anisotropic continuum		Discontinuum (DEM) and anisotropic continuum	Anisotropic continuum
GSI Sketches from Hoek and Karzulovic (2000)	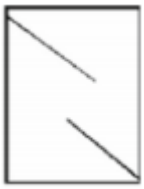				

C.3.3 SMR Classification

Slope Mass Rating System (SMR) (Singh and Goel, 1999)		
Adjustment Factor	**Equation**	**Description**
F_1	$F_1=(1-\sin(A))^2$	Degree of parallelism between joints and slope face strikes. Where, A = refers to the angle between the strike of the slope face and joints $A = (\alpha_s - \alpha_j)$ * for planar and wedge failure $A= (\alpha_s - \alpha_j - 180°)$ ***for toppling failure** Where, α_j: Refers to the strike of the discontinuity/the slope face α_s: Refers to the slope strike/joint Adjustment factor values range from 0.15-1.0. 0.15: When the angle between the critical joint plane and the slope face is more than 30° (failure probability low) 1.0: When they are both near parallel
F_2	$F_2=\tan(\beta_j)$	For planar or wedge failures (* for toppling failure F_2 = 1.0) β_j : Refers to the joint dip angle associated with the planar failure mode. β_i: Refers to the plunge or angle of the line of intersection with the horizontal in wedge failure Adjustment factor values range from 0.15-1.0. 0.15: When the dip of the critical joint is < 20° 1.0: for joints with a dip greater > 45°
F_3	$\sum \beta_j+\beta_s$	Relationship between the slope face and joint dips. For planar failure: Refers to the probability of a joint "daylighting" the slope. Fair: when the slope face and the joints are parallel Very unfavourable: when the slope dips 10° more than the joints For toppling failure: Unfavourable: depends on the sum of joint dips and the slope $B_j+\beta_s$
F_4		Method of excavation (includes natural or cut slope) F_4 Values: Natural slope: **+15** Pre-splitting: **+10** Smooth blasting: **+8** Normal blasting or mechanical excavation: **0** Poor blasting: **-8**

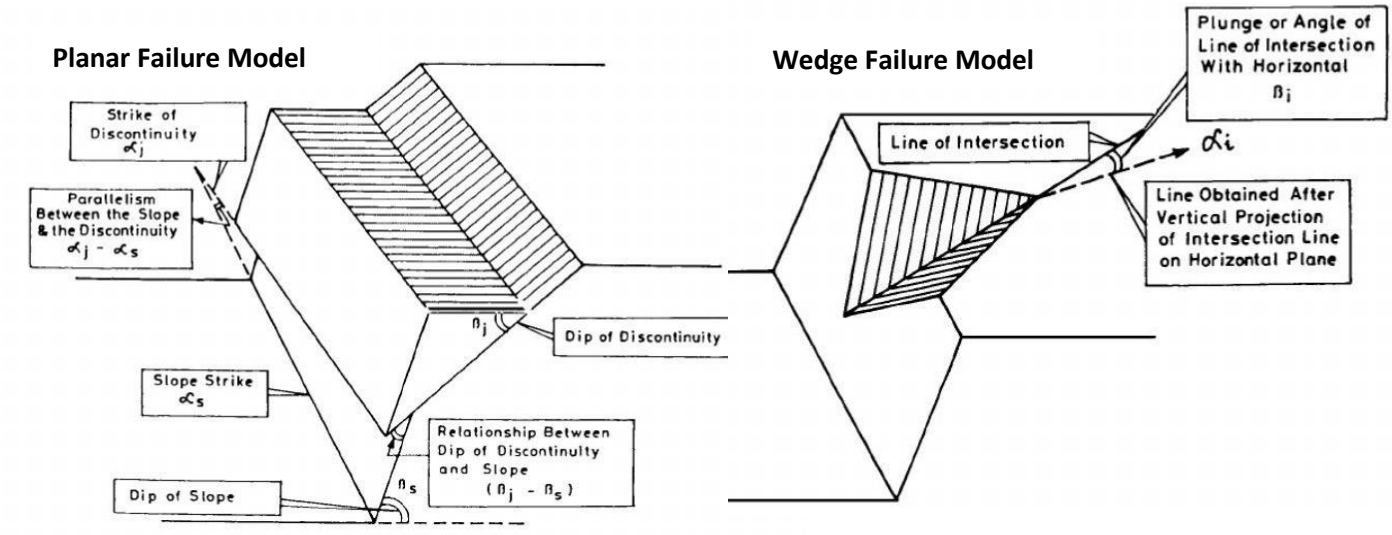

Slope Mass Rating System (SMR) (Singh and Goel, 1999)						
VALUES OF ADJUSTMENT FACTORS FOR DIFFERENT JOINT ORIENTATIONS						
Mode of Failure		Very favourable	Favourable	Fair	Unfavourable	Very Unfavourable
F_1 Adjustment Factor						
Planar	$(\alpha_s - \alpha_j)$	> 30°	20-30°	10-20°	5-10°	< 5°
Topple	$(\alpha_s - \alpha_j - 180°)$					
Wedge	$(\alpha_s - \alpha_j)$					
F_1 Rating		0.15	0.40	0.70	0.85	1.00
F_2 Adjustment Factor						
Planar	β_j	< 20°	20-30°	30-35°	35-40°	> 45°
Wedge	β_i					
F_2 Rating *(1.0 for Topple)		0.15	0.4	0.70	0.85	1.00
F_3 Adjustment Factor						
Planar	Bj-βs	> 10°	0-10°	0°	0°- (-10°)	< -10°
Wedge	$\beta_i - \beta_s$					
Topple	$B_j + \beta_s$	< 110°	110-120°	> 120°	-	-
F_3 Rating		0	-6	-25	-50	-60
F_4 Adjustment Factor						
Method of Excavation		Natural slope	Pre-splitting	Smooth blasting	Normal blasting or Mechanical Excavation	Poor Blasting
F_4 Rating		15	10	8	0	-8
STABILITY CLASSES AS PER SMR VALUES						
SMR Value		0-20	21-40	41-60	61-80	81-100
Class		V	IV	III	II	I
Rock mass Description		Very bad	Bad	Normal	Good	Very Good
Stability		Completely unstable	Unstable	Partially stable	Stable	Completely Stable
Failures		Big planar or soil like circular	Planar or big wedges	Planar along some joints and many wedges	Some block failure	No failure
Probability of Failure		0.9	0.6	0.4	0.2	0

C.3.3.1 SMR Results

	F_1			F_2		F_3		F_4
	$A=\alpha_s-\alpha_j$	Adjustment value from Table	Empirical Formula	β_j	Adjustment value from Table	$\beta_j - \beta_s$	Adjustement value from table	Natural slope
Zone 1	102	0.15	0.0005	66	1	40	0	15
Zone 2	16	0.70	0.5247	84	1	58	0	15
Zone 3	45	0.15	0.0858	70	1	44	0	15
Zone 4	37	0.15	0.1586	75	1	49	0	15
Zone 5	35	0.15	0.1818	67	1	41	0	15

C.3.4 GSI Classification

Characterization of schist rock mass based on foliation and discontinuity condition (Hoek and Karzulovic, 2000)